



**US Army Corps
of Engineers®**
Engineer Research and
Development Center

Great Lakes Coastal Flood Study, 2012 Federal Inter-Agency Initiative

Lake Michigan Storm: Wave and Water Level Modeling

Robert E. Jensen, Mary A. Cialone, Raymond S. Chapman,
Bruce A. Ebersole, Mary Anderson, and Leonette Thomas

November 2012

Modeling of Lake Michigan Storm Waves and Water Levels

Robert E. Jensen, Mary A. Cialone, Raymond S. Chapman, Bruce A. Ebersole,
Mary Anderson, and Leonette Thomas

*Coastal and Hydraulics Laboratory
U.S. Army Engineer Research and Development Center
3909 Halls Ferry Road
Vicksburg, MS 39180-6199*



Final report

Approved for public release; distribution is unlimited.

Abstract

This report documents the methodologies used, procedures followed to generate wind, wave, and storm surge estimates for 150 pre-selected extreme storm events along the Lake Michigan coastline. These simulations provide a storm climatology spanning 60-years (1960 through 2009). Two methodologies are used to generate the wind and pressure fields for the Lake Michigan region. The NOAA/NCEP Climate Forecast System Reanalysis, a 30-year (1979 through 2009) archive data set providing gridded wind speed, direction and sea level surface pressure fields. The second being the Natural Neighbor Method developing necessary fields from point source meteorological stations on a fixed grid system (1960 though 1978). Archived ice concentration fields were applied to the extreme storm events occurring during the winter months. The WAM model and STWAVE are used to describe the wave climate; ADCIRC is used to estimate the surge. The models are rigorously evaluated for a pre-selected storm population, using both wind field methodologies and compared to existing data sources (winds, waves and water levels). Upon completion of this evaluation phase, the 150-extreme storm events are simulated and evaluated at gage sites, for the entire coastline of Lake Michigan.

DISCLAIMER: The contents of this report are not to be used for advertising, publication, or promotional purposes. Citation of trade names does not constitute an official endorsement or approval of the use of such commercial products. All product names and trademarks cited are the property of their respective owners. The findings of this report are not to be construed as an official Department of the Army position unless so designated by other authorized documents.

DESTROY THIS REPORT WHEN NO LONGER NEEDED. DO NOT RETURN IT TO THE ORIGINATOR.

Contents

Abstract.....	ii
Figures and Tables.....	vi
Preface	xvi
Unit Conversion Factors.....	xvii
1 Wind and Pressure Field Generation	1
1.1 Introduction.....	1
1.2 Mining wind data bases	3
1.2.1 <i>The Global Integrated Surface Hourly database: ISH</i>	3
1.2.2 <i>Additional meteorological stations (NDBC/NOS/NWS/GLERL)</i>	7
1.2.3 <i>Data mining summary</i>	10
1.3 Natural Neighbor Method (NNM): Wind and pressure fields	10
1.3.1 <i>MET-EDIT: Building of meteorological station information</i>	10
1.3.2 <i>Application of Natural Neighbor Method: Building of model-ready wind and pressure fields.</i>	15
1.3.3 <i>NNM summary</i>	18
1.4 NCEP Climate Forecast System Re-analysis (CFSR): Wind and pressure fields	20
2 Ice Field Generation.....	26
2.1 Introduction.....	26
2.2 Composition of ice fields.....	28
2.2.1 <i>Ice Concentration Data Base, 1960 to 1979</i>	29
2.2.2 <i>Digital Ice Atlas, 1973 to 2002</i>	29
2.2.3 <i>Recent digital ice data, 2003 to 2009</i>	30
2.2.4 <i>Addendum to the ice field evaluation</i>	32
3 Wave Modeling.....	33
3.1 Previous Great Lakes wave hindcasts.....	33
3.2 Wave modeling approach	34
3.3 WAM wave model	35
3.3.1 <i>WAM Cycle 4.5.1C description</i>	36
3.3.2 <i>Model domain</i>	38
3.3.3 <i>Bathymetry and grid resolution</i>	38
3.3.4 <i>Frequency resolution</i>	40
3.3.5 <i>Directional resolution</i>	41
3.4 Initial wind-wave growth tests: Constant winds	41
3.5 Point-source wave measurements for model validation	43
3.6 Storm event simulations	49
3.6.1 <i>December 1990 storm</i>	51
3.6.2 <i>September 1989 storm</i>	60

3.6.3	<i>November 1992 storm</i>	68
3.6.4	<i>March 1985 storm</i>	75
3.6.5	<i>December 2009 storm</i>	82
3.6.6	<i>October 1993 storm</i>	93
3.6.7	<i>May 1998 storm</i>	99
3.6.8	<i>Examination of negative bias in modeled wave periods</i>	104
3.6.9	<i>Statistical comparison of model results and measurements</i>	108
3.7	Summary of observations and recommendations	115
3.7.1	<i>Observations: Winds</i>	115
3.7.2	<i>Observations: Ice fields</i>	116
3.7.3	<i>Observations: Wave measurements</i>	116
3.7.4	<i>Observations: Wave model and modeling effort</i>	116
3.7.5	<i>Recommendations: Winds</i>	117
3.7.6	<i>Recommendations: Ice fields</i>	117
3.7.7	<i>Recommendations: Wave measurements</i>	117
3.7.8	<i>Recommendations: Wave model and modeling effort</i>	117
4	Water Level Modeling	119
4.1	<i>Introduction</i>	119
4.2	<i>The ADCIRC model</i>	119
4.2.1	<i>Model description</i>	119
4.2.2	<i>Storm surge modeling approach</i>	120
4.2.3	<i>Treatment of ice cover – method for specifying the coefficient of drag</i>	120
4.2.4	<i>Initial grid mesh development</i>	121
4.3	<i>Validation for Lake Michigan/Green Bay only storm simulations</i>	123
4.3.1	<i>December 1990 storm</i>	123
4.3.2	<i>December 2009 storm</i>	130
4.3.3	<i>May 1998 storm</i>	132
4.3.4	<i>October 1993 storm</i>	134
4.3.5	<i>November 1992 storm</i>	136
4.3.6	<i>September 1989 storm</i>	140
4.3.7	<i>March 1985 storm</i>	141
4.4	<i>Systematic low bias in simulated water levels</i>	145
4.5	<i>Model sensitivity testing</i>	149
4.5.1	<i>Sensitivity to wind speed</i>	149
4.5.2	<i>Sensitivity to bottom friction</i>	149
4.5.3	<i>Sensitivity to presence of ice cover</i>	149
4.6	<i>ADCIRC mesh expansions</i>	152
4.7	<i>Expansion of the ADCIRC mesh to Lake Michigan-Lake Huron</i>	153
4.8	<i>Expansion of the ADCIRC grid to Lake Michigan harbors</i>	158
4.9	<i>Final validation: Lake Michigan-Lake Huron Mesh with harbors</i>	160
4.9.1	<i>December 2009 storm</i>	163
4.9.2	<i>May 1998 storm</i>	163
4.9.3	<i>October 1993 storm</i>	167
4.9.4	<i>November 1992 storm</i>	167
4.9.5	<i>March 1985 storm</i>	170

4.9.6	<i>Statistical analysis</i>	173
4.10	Summary of findings from Lake Michigan storm surge modeling	173
5	Nearshore Wave Modeling	175
5.1	Introduction.....	175
5.2	STWAVE Version 6.0.....	175
5.2.1	<i>Governing equations and description</i>	175
5.2.2	<i>Grid geometry and bathymetry</i>	177
5.2.3	<i>Boundary spectra</i>	180
5.2.4	<i>Save points</i>	183
5.2.5	<i>Model parameters</i>	185
5.2.6	<i>CSTORM-MS coupler</i>	186
6	Lake Michigan Storm Production.....	189
6.1	Introduction.....	189
6.2	Wind field production	194
6.3	Ice field analyses	195
6.4	Ice field production.....	202
6.5	Offshore wave production	203
6.5.1	<i>Post-processing QA/QC</i>	208
6.5.2	<i>Summary of Lake Michigan offshore wave model production</i>	218
6.6	Water level production.....	245
6.6.1	<i>Post-processing QA/QC</i>	250
6.6.2	<i>Synopsis of Lake Michigan water level modeling</i>	250
6.7	Statistics	273
6.8	Nearshore wave production.....	287
6.8.1	<i>QA/QC for all storms</i>	288
6.8.2	<i>Evaluation to wave measurements</i>	291
7	Summary and Conclusions.....	300
References.....		309
Report Documentation Page		

Figures and Tables

Figures

Figure 1-1. Time variation of active airways stations found in the NCDC ISH data archive.....	8
Figure 1-2. Available meteorological station locations accessed and preprocessed for Storm 6W.....	12
Figure 1-3. Comparison of input wind speed, direction and temporally smoothed (1:1:1) for Storm 6W at Milwaukee, WI.....	13
Figure 1-4. Example of general input file for <i>Metedit.f</i>	13
Figure 1-5. Comparison of input wind speed, direction and barometric pressure and output from <i>Metedit.f</i> for Storm 6W.....	14
Figure 1-6. Snapshot of wind speed isotac color contour (m/sec) and wind directions (arrows) using the NNM for Storm 6W.....	17
Figure 1-7. Increase NNM target domain and added four new meteorological sites for Storm 6W.....	19
Figure 1-8. Snapshot of extended grid domain wind speed isotac color contour (m/sec) and wind directions (arrows) using the NNM for Storm 6W.....	20
Figure 1-9. Comparison of easterly and westerly meteorological stations for Storm 6W.....	23
Figure 1-10. Comparison of NDBC Buoy 45002 and 45007 wind speed and direction during Storm 6W.....	23
Figure 1-11. Snapshot of wind speed isotac color contour (m/sec) and wind directions (arrows) using the CFSR for Storm 6W.....	24
Figure 2-1. Example of ice coverage graphic for 1 February 1990. Accompanying data file (901631.dat).....	30
Figure 2-2. Interpolated ice field output for 1 February 1990.....	31
Figure 3-1. Domain and bathymetry for the Lake Michigan WAM model.....	39
Figure 3-2. Difference between 5-deg and 15-deg directional resolutions for the Northeasterly wind wave growth test.....	43
Figure 3-3. Active point-source wave measurement sites in Lake Michigan.....	45
Figure 3-4. Available meteorological station locations accessed and preprocessed for the December 1990 storm.....	52
Figure 3-5. Maximum wind speed envelope for the December 1990 storm derived from the NNM wind field generation routine.....	53
Figure 3-6. Maximum wind speed envelope for the December 1990 storm derived from the CFSR wind field.....	54
Figure 3-7. Maximum significant wave height envelope for the December 1990 storm derived from the NNM wind field generation routine.....	55
Figure 3-8. Maximum significant wave height envelope for the December 1990 storm derived from the CFSR wind field.....	56
Figure 3-9. Time plots of significant wave height, peak and mean wave period, vector mean wave direction wind speed and direction at NDBC 45002 for the December 1990 storm.....	58

Figure 3-10. Time plots of significant wave height, peak and mean wave period, vector mean wave direction wind speed and direction at a WAM save location in lower Green Bay for the December 1990 storm.....	61
Figure 3-11. Available meteorological station locations accessed and preprocessed for the September 1989 storm.....	62
Figure 3-12. Maximum wind speed envelope for the September 1989 storm derived from the NNM wind field generation routine.....	63
Figure 3-13. Maximum wind speed envelope for the September 1989 storm derived from the CFSR wind fields.....	64
Figure 3-14. Time plots of significant wave height, peak and mean wave period, vector mean wave direction wind speed and direction at NDBC 45002 for the September 1989 storm.....	65
Figure 3-15. Time plots of significant wave height, peak and mean wave period, vector mean wave direction wind speed and direction at NDBC 45007 for the September 1989 storm.....	66
Figure 3-16. Time plots of significant wave height, peak and mean wave period, vector mean wave direction wind speed and direction at a WAM save location offshore from Calumet, IL for the September 1989 storm.....	69
Figure 3-17. Maximum wind speed envelope for the November 1992 storm derived from the NNM wind field generation routine.....	70
Figure 3-18. Maximum wind speed envelope for the November 1992 storm derived from the CFSR wind fields.....	71
Figure 3-19. Time plots of significant wave height, peak and mean wave period, vector mean wave direction wind speed and direction at NDBC 45002 for the November 1992 storm.....	72
Figure 3-20. Time plots of significant wave height, peak and mean wave period, vector mean wave direction wind speed and direction at NDBC 45007 for the November 1992 storm.....	74
Figure 3-21. Time plots of significant wave height, peak and mean wave period, vector mean wave direction wind speed and direction at a WAM save location offshore of Kewaunee, WI for the November 1992 storm.....	76
Figure 3-22. Available meteorological station locations accessed and preprocessed for the March 1985 storm.....	77
Figure 3-23. Maximum wind speed envelope for the March 1985 storm derived from the NNM wind field generation routine.....	79
Figure 3-24. Time plot of winds at Muskegon (726360) and Milwaukee (726400) Airways Stations for the March 1985 storm.....	80
Figure 3-25. Maximum wind speed envelope for the March 1985 storm derived from the CFSR wind field generation routine.....	80
Figure 3-26. Ice concentration level for 16 February 1985 (Assel 2005).	81
Figure 3-27. Ice concentration level for 23 February 1985 (Assel 2005).	82
Figure 3-28. Ice concentration level for 2 March 1985 (Assel 2005).	83
Figure 3-29. Ice concentration level for 9 March 1985 (Assel 2005).	84
Figure 3-30. Time plots of significant wave height, peak and mean wave period, vector mean wave direction wind speed and direction at a WAM save location offshore of Ludington, MI for the March 1985 storm.	85
Figure 3-31. Available meteorological station locations accessed and preprocessed for the December 2009 storm.....	86
Figure 3-32. Maximum wind speed envelope for the December 2009 storm derived from the NNM wind field generation routine.....	88

Figure 3-33. Maximum wind speed envelope for the December 2009 storm derived from the CFSR wind field generation routine	89
Figure 3-34. Ice concentration estimates for 14 December 2009, from the Canadian Ice Service.....	90
Figure 3-35. Time plots of significant wave height, peak and mean wave period, vector mean wave direction wind speed and direction at a WAM save location offshore of Green Bay, WI, for the December 2009 storm.	91
Figure 3-36. Time plot of wind speed and direction from four meteorological stations in the mid- and southern portions of Green Bay, used in the NNM wind field generation for the December 2009 storm.	92
Figure 3-37. Time plots of significant wave height, peak and mean wave period, vector mean wave direction wind speed and direction at a WAM save location offshore of Holland, MI, for the December 2009 storm.	94
Figure 3-38. Time plots of significant wave height, peak and mean wave period, vector mean wave direction wind speed and direction at NDBC 45002 for the October 1993 storm.....	96
Figure 3-39. Time plots of significant wave height, peak and mean wave period, vector mean wave direction wind speed and direction at NDBC 45007 for the October 1993 storm.....	97
Figure 3-40. Time plots of significant wave height, peak and mean wave period, vector mean wave direction wind speed and direction at NDBC 45010 for the October 1993 storm.....	98
Figure 3-41. Time plots of raw non-adjusted wind speed, wind direction and sea-level pressure at six selected point-source measurement sites surrounding Lake Michigan for the May 1998 storm.	101
Figure 3-42. Time plots of significant wave height, peak and mean wave period, vector mean wave direction wind speed and direction at NDBC 45002 for the May 1998 storm.	102
Figure 3-43. Time plots of significant wave height, peak and mean wave period, vector mean wave direction wind speed and direction at NDBC 45007 for the May 1998 storm.	103
Figure 3-44. Time plots of significant wave height, peak and mean wave period, vector mean wave direction wind speed and direction at a WAM save location off shore of Calumet, IL, for the May 1998 storm.	105
Figure 3-45. Time paired comparison differences in the frequency spectra (Buoy minus Model) at NDBC 45002 for the October 1993 storm.....	107
Figure 3-46. Time paired comparison differences in the frequency spectra (Buoy minus Model) at NDBC 45007 for the October 1993 storm.....	107
Figure 3-47. Time paired comparison differences in the frequency spectra (Buoy minus Model) at NDBC 45010 for the October 1993 storm.....	108
Figure 3-48. Time-paired scatter plot of at NDBC 45002 and WAM wave height results using NNM and CFSR forced winds for all storm simulations.	110
Figure 3-49. Time-paired scatter plot of at NDBC 45007 and WAM wave height results using NNM and CFSR forced winds for all storm simulations.	111
Figure 3-50. Time-paired scatter plot of at NDBC 45007 and WAM wave height results using NNM and CFSR forced winds for ONLY the October 1993 storm	112
Figure 3-51. Peak to peak analysis of all seven storm simulations at NDBC 45002.	114
Figure 3-52. Peak to peak analysis of all seven storm simulations at NDBC 45007.	114
Figure 4-1. Feature map adopted for ADCIRC grid mesh generation.....	122
Figure 4-2. ADCIRC grid of Lake Michigan and Green Bay.	124
Figure 4-3. Refined grid in the vicinity of Sturgeon Bay Canal.....	124

Figure 4-4. Refined grid in the vicinity of Calumet Harbor.....	125
Figure 4-5. Refined grid in the vicinity of Chicago Harbor.....	125
Figure 4-6. Refined grid in the vicinity of Green Bay.....	126
Figure 4-7. Comparison of observed and model-generated water levels at Green Bay, WI, December 1990 event	126
Figure 4-8. Comparison of observed and model-generated water levels at Holland, MI, December 1990 event	128
Figure 4-9. Comparison of observed and model-generated water levels at Calumet Harbor, IL, December 1990 event	129
Figure 4-10. Comparison of observed and model-generated water levels at Milwaukee, WI December 1990 event	129
Figure 4-11. Comparison of simulated and observed water surface elevations at Green Bay, WI, December 2009 event	130
Figure 4-12. Comparison of simulated and observed water surface elevations at Calumet Harbor, IL, December 2009 event.....	131
Figure 4-13. Comparison of simulated and observed water surface elevations at Menominee, MI, December 2009 event	132
Figure 4-14. Comparison of simulated and observed water surface elevations at Holland, MI December 2009 event.....	133
Figure 4-15. Comparison of simulated and observed water surface elevations at Calumet Harbor, IL May 1998 event.....	133
Figure 4-16. Comparison of simulated and observed water surface elevations at Green Bay, WI May 1998 event.....	134
Figure 4-17. Comparison of simulated and observed water surface elevations at Calumet Harbor, IL October 1993 event	135
Figure 4-18. Comparison of simulated and observed water surface elevations at Green Bay, WI October 1993 event	135
Figure 4-19. Comparison of simulated and observed water surface elevations at Kewaunee, WI November 1992 event	137
Figure 4-20. Comparison of simulated and observed water surface elevations at Ludington, MI November 1992 event	137
Figure 4-21. Comparison of simulated and observed water surface elevations at Sturgeon Bay Canal, WI November 1992 event	138
Figure 4-22. Comparison of simulated and observed water surface elevations at Calumet Harbor, IL November 1992 event	138
Figure 4-23. Comparison of simulated and observed water surface elevations at Green Bay, WI November 1992 event	139
Figure 4-24. Comparison of simulated and observed water surface elevations at Calumet Harbor, WI September 1989 event	140
Figure 4-25. Comparison of simulated and observed water surface elevations at Green Bay, WI September 1989 event	141
Figure 4-26. Comparison of simulated and observed water surface elevations at Ludington, MI March 1985 event	142
Figure 4-27. Comparison of simulated and observed water surface elevations at Kewaunee, WI March 1985 event	142

Figure 4-28. Comparison of simulated and observed water surface elevations at Port Inland, MI March 1985 event	144
Figure 4-29. Comparison of simulated and observed water surface elevations at Calumet Harbor, IL March 1985 event.....	144
Figure 4-30. December 2009 storm event, minimum modeled pressure.....	146
Figure 4-31. December 2009 storm event, observed (symbols) and modeled CFSR atmospheric pressure at Chicago, Milwaukee, Mackinaw and Muskegon.....	146
Figure 4-32. March 1985 storm event, minimum modeled pressure.....	147
Figure 4-33. March 1985 Storm, observed atmospheric pressure throughout Lake Michigan.....	148
Figure 4-34. A comparison of simulated and observed water-surface elevation at the Green Bay, WI December 2009 event, with a 12-percent increase in wind speed.....	150
Figure 4-35. Comparison of simulated and observed water-surface elevations at the Calumet Harbor, IL December 2009 event, with a 12-percent increase in wind speed.....	150
Figure 4-36. Comparison of simulated and observed water-surface elevations at the Menominee, MI, December 2009 event, with a 12-percent increase in wind speed.....	151
Figure 4-37. Comparison of Manning's n.....	151
Figure 4-38. Comparison of with- and without-ice conditions.....	152
Figure 4-39. NOAA water level stations.....	155
Figure 4-40. Dec 1990 Green Bay modeled and observed water level time series.....	156
Figure 4-41. Dec 1990 Holland modeled and observed water level time series.....	156
Figure 4-42. Dec 1990 Calumet Harbor modeled and observed water level time series.....	157
Figure 4-43. Dec 1990 Milwaukee modeled and observed water level time series.....	157
Figure 4-44. ADCIRC mesh boundary with 48 harbors.....	158
Figure 4-45. Original ADCIRC mesh in the vicinity of Lake Betsie (top panel), Lake Betsie shoreline and idealized bathymetry added to ADICRC mesh (middle panel); and Lake Betsie bathymetry and refined mesh (bottom panel).....	159
Figure 4-46. Dec 1990 Green Bay final modeled and observed water level time series.....	161
Figure 4-47. Dec 1990 Holland final modeled and observed water level time series.....	161
Figure 4-48. Dec 1990 Calumet Harbor final modeled and observed water level time series.....	162
Figure 4-49. Dec 1990 Milwaukee final modeled and observed water level time series.....	162
Figure 4-50. Dec 2009 Green Bay final modeled and observed water level time series.....	164
Figure 4-51. Dec 2009 Calumet final modeled and observed water level time series.....	164
Figure 4-52. Dec 2009 Menominee final modeled and observed water level time series.....	165
Figure 4-53. Dec 2009 Holland final modeled and observed water level time series.....	165
Figure 4-54. May 1998 Calumet final modeled and observed water level time series.....	166
Figure 4-55. May 1998 Green Bay final modeled and observed water level time series.....	166
Figure 4-56. October 1993 Calumet final modeled and observed water level time series.....	168
Figure 4-57. October 1993 Green Bay final modeled and observed water level time series.....	168
Figure 4-58. November 1992 Kewaunee final modeled and observed water level time series.....	169

Figure 4-59. November 1992 Ludington final modeled and observed water level time series.....	169
Figure 4-60. November 1992 Sturgeon Bay Canal final modeled and observed water level time series.....	170
Figure 4-61. November 1992 Calumet Harbor final modeled and observed water level time series.....	171
Figure 4-62. March 1985 Ludington final modeled and observed water level time series.....	171
Figure 4-63. March 1985 Kewaunee final modeled and observed water level time series.....	172
Figure 4-64. March 1985 Port Inland final modeled and observed water level time series.....	172
Figure 4-65. March 1985 Calumet Harbor final modeled and observed water level time series.....	173
Figure 5-1. STWAVE grid locations.....	178
Figure 5-2. STWAVE Chicago grid bathymetry.....	179
Figure 5-3. STWAVE Kenosha grid bathymetry.....	179
Figure 5-4. STWAVE Green Bay grid bathymetry.	180
Figure 5-5. WAM spectra save points for Chicago.....	181
Figure 5-6. WAM spectra save points for Kenosha.....	182
Figure 5-7. WAM spectra save points for Green Bay.	182
Figure 5-8. Save points for Chicago.....	183
Figure 5-9. Save points for Kenosha.....	184
Figure 5-10. Save points for Green Bay.....	184
Figure 5-11. Diagram of timing between ADCIRC and STWAVE.	187
Figure 6-1. Location of wave measurement (red dots) and water level sites (blue dots).....	189
Figure 6-2. Maximum wave height color contour for February 1999, with ice coverage (grey shaded), selecting 70-percent concentration threshold.....	197
Figure 6-3. Wave height, peak, mean wave period, wind speed and direction time plot evaluation for WAMCY4.5.1C and NDBC Buoy 45002, February 1991	198
Figure 6-4. Wave height comparison at Burns Harbor (45900), and Chicago Harbor (45901) for December 2002 and WAMCY4.5.1C.....	199
Figure 6-5. Wave height comparison at Burns Harbor (45900), and WAMCY451C for March 2003.....	200
Figure 6-6. Ice concentration levels for 1 March (top left), 5 March (top right), 10 March (bottom left) and 15 March (bottom right) 2003, from http://www.natice.noaa.gov/products/great_lakes.html	201
Figure 6-7. Wave height time paired comparison at Burns Harbor (45900) and WAMCY4.5.1C.....	202
Figure 6-8. Wave height time paired comparison at Chicago Harbor (45901) and WAMCY4.5.1C.....	203
Figure 6-9. Special output locations for the WAM simulations.....	205
Figure 6-10. Zoom of the Green Bay area. The STWAVE boundary is identified by the red circle.	206
Figure 6-11. Zoom view of the southwestern domain of Lake Michigan, red and green ovals identify the two boundary input locations for STWAVE simulations.	207
Figure 6-12. Maximum wind speed envelope for ST0127.....	209

Figure 6-13. Maximum significant wave height envelope for ST0127.....	210
Figure 6-14. Maximum wind speed envelope for ST0048.....	211
Figure 6-15. Maximum significant wave height envelope for ST0048.....	212
Figure 6-16. Time plot of WAM (blue line) versus measurements at 45007 for Storm 118.....	214
Figure 6-17. Scatter and Q-Q plots of WAM versus measurements at 45007 for Storm 118.....	215
Figure 6-18. Scatter and Q-Q plots of WAM versus measurements at 45007 for Storm 118.....	216
Figure 6-19. Compendium plot of significant wave height comparisons to all available measurement sites for Storm 118.....	217
Figure 6-20. Overall maximum wind speed and significant wave height locations for the 150 extreme storm event population.....	220
Figure 6-21. Magnitudes of the maximum wind speed (upper panel) and significant wave height (lower panel) for the 150 extreme storm events.....	221
Figure 6-22. Measurement availability for the five buoy sites during the 150 extreme storm event simulation. Location of wave measurement sites found in Figure 6-1.....	224
Figure 6-23. Color contour of time paired significant wave heights, buoy to WAM for NDBC 45002.....	225
Figure 6-24. Color contour of time paired equivalent neutral stable 10-m wind speeds, buoy to CFSR for NDBC 45002.....	225
Figure 6-25. Color contour of time paired significant wave heights, buoy to WAM for NDBC 45007.....	227
Figure 6-26. Color contour of time paired equivalent neutral stable 10-m wind speeds, buoy to CFSR for NDBC 45007.....	227
Figure 6-27. Color contour of time paired significant wave heights, buoy to WAM for NDBC 45010.....	229
Figure 6-28. Color contour of time paired equivalent neutral stable 10-m wind speeds, buoy to CFSR for NDBC 45010.....	230
Figure 6-29. Color contour of time paired significant wave heights, buoy to WAM for Burns Harbor ST 45900.....	231
Figure 6-30. Color contour of time paired significant wave heights, buoy to WAM for Chicago Harbor ST 45901.....	232
Figure 6-31. Quartile-Quartile graphic for WAM versus buoy data at NDBC 45002.....	233
Figure 6-32. Quartile-Quartile graphic for WAM versus buoy data at NDBC 45002.....	234
Figure 6-33. Quartile-Quartile graphic for WAM versus buoy data at Burns Harbor, 45900.....	235
Figure 6-34. Quartile-Quartile graphic for WAM versus buoy data at Chicago Harbor, 45901.....	235
Figure 6-35. Peak-to-peak analysis, at NDBC 45002.....	238
Figure 6-36. Peak-to-peak analysis, at NDBC 45007.....	238
Figure 6-37. Peak-to-peak analysis, at NDBC 45010.....	239
Figure 6-38. Peak-to-peak analysis, at Chicago Harbor (ST 45901).....	239
Figure 6-39. Peak-to-peak analysis, at Burns Harbor (ST 45900).....	241
Figure 6-40. ADCIRC Save point locations for Lake Michigan and Green Bay. The color indicates the water depth at the save point location.....	247
Figure 6-41. ADCIRC save point locations and numbers for lower Lake Michigan. The color indicates the water depth at the save point location.....	248

Figure 6-42. ADCIRC save point locations and numbers for lower Green Bay. The color indicates the water depth at the save point location.....	248
Figure 6-43. ADCIRC maximum water level envelope for Storm099 (December 1990) indicating highest water levels in Green Bay.	251
Figure 6-44. ADCIRC maximum water level envelope for Storm048 (January 1975) indicating highest water levels in northern Lake Michigan and Green Bay.....	251
Figure 6-45. Time series of water levels for Storm099 (December 1990); Ludington.....	253
Figure 6-46. Time series of water levels for Storm099 (December 1990); Holland.	253
Figure 6-47. Time series of water levels for Storm099 (December 1990); Calumet.....	254
Figure 6-48. Time series of water levels for Storm099 (December 1990); Milwaukee.....	254
Figure 6-49. Time series of water levels for Storm099 (December 1990); Kewaunee.	255
Figure 6-50. Time series of water levels for Storm099 (December 1990); Sturgeon Bay Canal.....	255
Figure 6-51. Time series of water levels for Storm099 (December 1990); Green Bay.	256
Figure 6-52. Time series of water levels for Storm099 (December 1990); Port Inland.....	256
Figure 6-53. Time series of water levels for Storm099 (December 1990); Mackinaw City.	257
Figure 6-54. Time series of water levels for Storm048 (January 1975); Ludington.	258
Figure 6-55. Time series of water levels for Storm048 (January 1975); Holland.	258
Figure 6-56. Time series of water levels for Storm048 (January 1975); Calumet Harbor.	259
Figure 6-57. Time series of water levels for Storm048 (January 1975); Milwaukee.	259
Figure 6-58. Time series of water levels for Storm048 (January 1975); Kewaunee.	260
Figure 6-59. Time series of water levels for Storm048 (January 1975); Sturgeon Bay Canal.....	260
Figure 6-60. Time series of water levels for Storm048 (January 1975); Port Inland.	261
Figure 6-61. Time series of water levels for Storm048 (January 1975); Mackinaw City.	261
Figure 6-62. Time series of water levels for Storm061 (December 1979); Ludington.....	263
Figure 6-63. Time series of water levels for Storm061 (December 1979); Holland.	263
Figure 6-64. Time series of water levels for Storm061 (December 1979); Calumet Harbor.	264
Figure 6-65. Time series of water levels for Storm061 (December 1979); Milwaukee.	264
Figure 6-66. Time series of water levels for Storm061 (December 1979); Kewaunee.	265
Figure 6-67. Time series of water levels for Storm061 (December 1979); Sturgeon Bay Canal.....	265
Figure 6-68. Time series of water levels for Storm061 (December 1979); Green Bay.	266
Figure 6-69. Time series of water levels for Storm061 (December 1979); Port Inland.	266
Figure 6-70. Time series of water levels for Storm061 (December 1979); Mackinaw City.....	267
Figure 6-71. Time series of water levels for Storm129 (November 1998); Ludington.	268
Figure 6-72. Time series of water levels for Storm129 (November 1998); Holland.	268
Figure 6-73. Time series of water levels for Storm129 (November 1998); Calumet Harbor.	269
Figure 6-74. Time series of water levels for Storm129 (November 1998); Milwaukee.	269
Figure 6-75. Time series of water levels for Storm129 (November 1998); Kewaunee.	270

Figure 6-76. Time series of water levels for Storm129 (November 1998); Sturgeon Bay Canal.....	270
Figure 6-77. Time series of water levels for Storm129 (November 1998); Green Bay.....	271
Figure 6-78. Time series of water levels for Storm129 (November 1998); Port Inland.....	271
Figure 6-79. Time series of water levels for Storm129 (November 1998); Mackinaw City.....	272
Figure 6-80. Water level bias for all storm and all gages.	281
Figure 6-81. Water level bias at Station 9075080 (Mackinaw City).	282
Figure 6-82. Water level bias at Station 9087096 (Port Inland).	282
Figure 6-83. Water level bias at Station 9087023 (Ludington).	283
Figure 6-84. Water level bias at Station 9087031 (Holland).	283
Figure 6-85. Water level bias at station 9087044 (Calumet Harbor).	284
Figure 6-86. Water level bias at station 9087057 (Milwaukee).	284
Figure 6-87. Water level bias at station 9087068 (Kewaunee).	285
Figure 6-88. Water level bias at station 9087072 (Sturgeon Bay Canal).	285
Figure 6-89. Water level bias at station 9087079 (Green Bay).	286
Figure 6-90. Water level bias at station 9087088 (Menominee).	286
Figure 6-91. Water level RMSE for all storm and all gages.	287
Figure 6-92. Maximum wave heights for ST0127 for Chicago.	289
Figure 6-93. Maximum wave heights for ST0127 for Kenosha.	289
Figure 6-94. Maximum wave heights for ST0099 for Green Bay.	290
Figure 6-95. Location of Burns (45900) and Chicago Harbor (45901) indicated by filled circles.	291
Figure 6-96. Time and scatter plot of STWAVE versus measurements at 45900 for ST0115.....	292
Figure 6-97. Color contour of time paired significant wave heights for 45900.	293
Figure 6-98. Color contour of time paired significant wave heights for 45901.	293
Figure 6-99. Quartile-Quartile analysis for 45900.	295
Figure 6-100. Quartile-quartile analysis for 45901.	296
Figure 6-101. Peak-to-peak analysis at 45900.	297
Figure 6-102. Peak-to-peak analysis at 45901.	298

Tables

Table 1-1. List of airways stations (2009).	5
Table 1-2. Additional meteorological station information.	9
Table 2-1. Ice atlas database archives.	28
Table 3-1. Grid and model characteristics.	39
Table 3-2. Growth tests for constant winds of 20 m/sec.	42
Table 3-3. Available wave measurements.	44
Table 3-4. NDBC 45002 extreme wave conditions list.	46
Table 3-5. NDBC 45007 extreme wave conditions list.	47
Table 3-6. NDBC 45010 extreme wave conditions list.	48

Table 3-7. NDBC 45011 extreme wave conditions list.	49
Table 3-8. List of extreme events, locations and times.	50
Table 3-9. Statistics for seven Lake Michigan test storms H_{Mo} (m).....	112
Table 3-10. Statistics for seven Lake Michigan test storms T_p	113
Table 3-11. Statistics for seven Lake Michigan test storms T_{mean}	113
Table 5-1. Grid geometry.	180
Table 5-2. Location of boundary points.....	181
Table 5-3. Full-plane and serial execution parameters.....	186
Table 5-4. Timing between ADCIRC and STWAVE in terms of ADCIRC time-steps.	187
Table 6-1. Extreme storm event list.	190
Table 6-2. Peak-to-peak analysis results.....	223
Table 6-3. Summary statistics for all storm simulations wind speed (m/sec).	243
Table 6-4. Summary statistics for all storm simulations significant wave height (m).....	244
Table 6-5. Summary statistics for all storm simulations parabolic fit peak wave period.	244
Table 6-6. Summary statistics for all storm simulations mean wave period (sec).....	245
Table 6-7. Water level bias for all storms and all gages, meters.	274
Table 6-8. Water level root mean square error for all storms and all gages, meters.	277
Table 6-9. Peak-to-peak analysis results.....	297
Table 6-10. Summary statistics for significant wave height (m).	299

Preface

The study summarized in this report was conducted at the request of the Detroit District (LRE), USACE. Greg Mausolf was the primary engineering point of contact, and Mary Weidel was the primary project management point of contact at LRE. The study was funded by the Federal Emergency Management Agency (FEMA) through LRE and conducted at the Engineering Research and Development Center (ERDC), Coastal and Hydraulics Laboratory (CHL), Vicksburg, MS, during the period Nov 2009 – Sep 2010. The FEMA Lead was Ken Hinterlong, Chief, Risk Analysis Branch, Mitigation Division, FEMA Region V. Julie Tochor, Accenture, was the Program Management Lead for FEMA Region V.

The work performed at CHL was under the general supervision of Dr. Ty V. Wamsley, Chief, Coastal Processes Branch and Bruce A. Ebersole, Chief, Coastal Flood and Storm Protection Division. The Director of the Coastal and Hydraulics Laboratory was Dr. William D. Martin.

COL Kevin J. Wilson was Commander and Executive Director of ERDC. Dr. Jeffery P. Holland was Director.

The authors would like to acknowledge Dr. David Schwab, National Oceanic and Atmospheric Administration's Great Lakes Environmental Research Laboratory for providing the Natural Neighbor Codes, and guidance in the generation of winds and pressure fields in Lake Michigan; David Mark and Alan Cialone (CHL) for their contributions to grid development of ADCIRC and WAM, respectively. Lastly, Dr. Chris Massey (CHL) for the development, testing, and implementation of new ice routines used in the WAM and ADCIRC simulations.

Unit Conversion Factors

A sponsor requirement for this study was the use of English Customary units of measurement. Most measurements and calculations were done in SI units and then converted to English Customary. The following table can be used to convert back to SI units.

Multiply	By	To Obtain
Feet	0.3048	meters
cubic feet	0.02831685	cubic meters
pounds (force)	4.448222	newtons
square feet	0.09290304	square meters

1 Wind and Pressure Field Generation

1.1 Introduction

The development of a wind, wave and water level climate is a necessary step to define the storm event population that will be used to estimate the potential for coastal flooding in Lake Michigan. The approach being taken is to simulate wave and storm surge conditions associated the major storm events via computer modeling. Wave conditions and water level conditions are dictated by meteorological events. These events can vary from large-scale synoptic-scale events, meso-scale systems like frontal boundaries to micro-scale systems synonymous with the development of thunderstorm cells. If the meteorology of these events can be accurately quantified, the associated impact of the surge and waves on a coastal reach also can be quantified.

Weather Prediction Centers have routinely generated long-term meteorological fields including surface winds and pressure fields (NCEP/NCAR Re-Analysis Program, Kalnay et al 1996). Despite their consistency and accuracy, complete definition of the meteorological conditions in the Great Lakes is limited by the temporal (6-hr) and spatial resolution (about 2-deg in longitude and latitude) adopted in these analyses. Considering the geographical extent of the Great Lakes, covering about 9-deg in latitude and 17-deg in longitude, there would be at most 45 active grid points defining all meteorological events. This normally would yield the large-scale synoptic events, but would misrepresent any frontal passages or major storms. Even if the spatial resolution were on the order of 10s of kilometers, temporal resolutions on the order of one hour or less are required so that rapid moving meteorological events are captured as they pass from west to east or north to south over the lakes. There was a study by Lin and Resio (2000) to recreate surface winds from NCEP/NCAR database at moored buoy locations in the Great Lakes. There was some success, however only the broad, large-scale features were replicated. The motivation for this work was that all measurement platforms in the Great Lakes are removed in the early fall season and re-deployed during the late spring because of lake icing. The implication of gage removal is that many of the large-scale storm events impacting the Great Lakes shoreline occur during those times and prior to fast-ice development along the coast. The need for data at these buoy locations was critical to the development of temporally varying wind fields.

Alternate formulations for generating wind fields for the Great Lakes have been focused on transforming land-based meteorological station information and projecting the information over the water body (e.g. Resio and Vincent, 1976). This assumes that the geostrophic winds above the Great Lakes are not different from the winds over adjacent land stations, i.e., the driving mechanism for lower level winds in each case is the same. The fundamental differences between the lower level winds must then be primarily a function of the boundary characteristics. This means that, if the transformation between geostrophic winds to overland winds and geostrophic winds to over-lake winds were both known, a relationship between land winds and lake winds could be defined. This pioneering effort by Resio and Vincent (1976, 1976a) provided the basis for further development of techniques used to construct temporal and spatially varying winds in the Great Lakes. Schwab (1989) used a Barnes (1964, 1973) technique that is based on an exponential spatial weighting function with a decay rate that can be adjusted based on iteration and separation distance. Schwab (1978) and Schwab et al. (1984, 1998) modified this approached and developed what is called the Natural Neighbor Method (NNM). This method of wind field generation has been used successfully in the Lake Michigan Operational Forecast System (LMOFS) for water levels as shown in (Kelly et al. 2007). This approach is based on land- and water-based (from NOAA NDBC buoys) meteorological information to produce time and space varying wind fields. Because of this success, it seemed appropriate to use the NNM to generate wind fields in this study. For any surge modeling efforts, the spatially varying pressure fields are also required. One pursuit of this work was to investigate the appropriateness of the NNM for scalar quantities.

One of the key elements to the development of long-term climatologic estimates for winds and atmospheric pressures is to maximize the use of high quality meteorological data while recognizing the fact that availability of data decreases as one goes back in time. For example, the number of land-based meteorological stations has increased from decade to decade, significantly in recent decades. The quality of data from earlier decades might also be an issue. Careful examination of this information is required. The quality of any wave or surge modeling is only as good as the quality of the input meteorological input. Data mining and evaluation must be performed to determine the number of sites, their relevance to wind conditions in Lake Michigan; accuracy levels in the measurement device; sensor elevation and time averaging interval reflected in the measurement;

and local constraints such as wind blocking because of up-wind buildings, terrain or vegetation.

Work was initiated under the assumption that the NNM would be used to construct all meteorological input to the storm surge and wave modeling. During the course of the work, results from a new NCEP Climate Forecast System Re-analysis (CFSR) (Saha et al. 2010) became available, on 0.5-deg longitude/latitude grid with global coverage, with meteorological variables (wind speed and direction, surface barometric pressure fields) provided at hourly time intervals. The latter data source was ultimately adopted for all storms contained within the re-analysis period (1979 to present). The NNM was adopted for storm events prior to 1979.

1.2 Mining wind data bases

There are a number of point source meteorological data available surrounding the Great Lakes. The longest data record available consists of land-based Global Surface Airways Hourly records available at NOAA's National Climate Data Center. The second longest data records are from NOAA's National Data Buoy Center (NDBC), where all Coastal-Marine Automated Network (CMAN) and buoy data reside. This database spans nearly 25-years; however, the buoys are generally recovered during the early fall and then re-deployed during the late spring. Shorter term meteorological stations have been deployed by NOAA's National Weather Service (NWS), the National Ocean Service (NOS) and locally by the Great Lakes Environmental Research Laboratory (GLERL). These locations despite their length of record are valuable data sources because of their geographical positions being close to the lakefront.

1.2.1 The Global Integrated Surface Hourly database: ISH

The Global Integrated Surface Hourly database resides at NOAA's National Climate Data Center. This database is the most complete archive of meteorological information. It has and continues to be used by GLERL in their nowcast wave and circulation efforts in the Great Lakes. One of the provisions to access this database is to have a priori knowledge of the land-based stations. The station identification number consists of both a US Air Force station number and a NCDC Weather Bureau Army Navy Number (WBAN). These numerical identifiers are used as the naming convention for specific station files provided in the database. The problem is to determine the appropriate stations specific to Lake Michigan. For each

station, there is a defined name, longitude/latitude pair that can be used to identify those stations residing in the area surrounding Lake Michigan. For the U.S. stations the state names and an International Civil Aviation Organization (ICAO) designator code are provided. One last data set vital to the proper selection of land-stations is from the GLERL forecast system (<http://coastwatch.glerl.noaa.gov/marobs/>). This site contains the GLERL station database file, listing all Airways stations used during the posted forecast.

A final list of the ISH Airways stations is provided in Table1-1. There are multiple listings for the same station name. In general, if there are multiple listings, either the location or the elevation of that particular station has changed; or in years less than roughly 1970, the designated station was originally designated with the WBAN number. The cross-referenced GLERL station database file provides a similar list of the ISH stations, and identifies the year these locations changed.

The entry point for the ISH database is from NOAA's National Climate Data Center (<http://www.ncdc.noaa.gov/oa/climate/climatedata.html>)¹. Software, and documentation are also available from the following (<http://www1.ncdc.noaa.gov/pub/data/ish/>).

The Global and U.S. Integrated Surface Hourly Database is accessed via File Transfer Protocol (FTP). It is an anonymous entry point using a local FTP application. The database is structured by year and all reference files are identified by either the USAF Station Number or the WBAN number. Generally, the more recent information uses the USAF Numbers. An automated system was developed; however, it failed routinely because of the latency in accessing the yearly and individual station information. It was found that starting in 2009 and proceeding back in time was the most effective way to download all of the files. Although there is a provision to download ASCII data, it is limited to small data sets and could not be used. However, this procedure was used to spot-check the final decoding procedures that are described below.

All files are coded requiring a converter routine to transform the original information to readable formats. NCDC provides documentation and software to accomplish this task (<http://www1.ncdc.noaa.gov/pub/data/ish/>). This software (FORTRAN routine) was modified to recover the necessary

¹ Also check the Climate Data Online (CDO)

Table 1-1. List of airways stations (2009).

USAF	WBAN	LOCATION NAME	ICAO	GEOGRAPHICAL LOC.		ELEV (m)
				LATITUDE	LONGITUDE	
727436	4863	ANTRIM CO ARPT	KACB	44.989	-85.185	189.9
727436	99999	ANTRIM CO ARPT	KACB	44.983	-85.200	190.0
726355	94871	BENTON HARBOR/ROSS	KBEH	42.129	-86.422	196.0
726355	99999	BENTON HARBOR/ROSS	KBEH	42.133	-86.433	196.0
725394	4839	HOLLAND/TULIP CITY	KBIV	42.746	-86.097	209.7
725394	99999	HOLLAND/TULIP CITY	KBIV	42.750	-86.100	210.0
726505	4845	KENOSHA RGNL	KENW	42.595	-87.938	226.5
726505	99999	KENOSHA RGNL	KENW	42.583	-87.917	226.0
726394	4874	NEWBERRY LUCE CO.	KERY	46.311	-85.451	264.9
726394	99999	NEWBERRY LUCE CO.	KERY	46.317	-85.450	265.0
726480	94853	ESCANABA (AWOS)	KESC	45.723	-87.094	185.6
726480	99999	ESCANABA (AWOS)	KESC	45.750	-87.033	187.0
726413	4875	WEST BEND MUNI	KETB	43.422	-88.118	270.4
726413	99999	WEST BEND MUNI	KETB	43.417	-88.133	270.0
726450	14898	GREEN BAY/A.-STRAUB	KGRB	44.513	-88.120	214.0
999999	14898	GREEN BAY A.-STRAUB	KGRB	44.513	-88.120	214.0
725337	4807	GARY CHICAGO	KGYY	41.616	-87.401	180.4
725337	99999	GARY CHICAGO	KGYY	41.617	-87.400	180.0
725408	4881	MANISTIQUE	KISQ	45.974	-86.167	208.8
725408	99999	MANISTIQUE	KISQ	45.967	-86.183	209.0
726364	4883	LUDINGTON/MASON	KLDM	43.963	-86.401	196.6
726364	99999	LUDINGTON/MASON	KLDM	43.967	-86.400	197.0
726385	94894	MANISTEE (AWOS)	KMBL	44.272	-86.234	189.3
726385	99999	MANISTEE (AWOS)	KMBL	44.267	-86.250	189.0
727435	54820	MACKINACK ISLAND	KMCD	45.865	-84.637	225.6
727435	99999	MACKINACK ISLAND	KMCD	45.867	-84.633	300.0
725340	14819	CHICAGO/MIDWAY	KMDW	41.786	-87.752	188.4
725340	99999	CHICAGO/MIDWAY	KMDW	41.783	-87.750	190.0
999999	14819	CHICAGO MIDWAY AP	KMDW	41.786	-87.752	188.4
726400	14839	MILWAUKEE/GEN. MITC	KMKE	42.947	-87.897	211.2
999999	14839	MILWAUKEE NB SIDE PO	KMKE	42.947	-87.897	211.2
726360	14840	MUSKEGON	KMKG	43.171	-86.237	192.9
999999	14840	MUSKEGON COUNTY ARPT	KMKG	43.171	-86.237	192.9
726487	94986	MENOMINEE (AWOS)	KMNM	45.126	-87.634	190.5

USAF	WBAN	LOCATION NAME	ICAO	GEOGRAPHICAL LOC.		ELEV (m)
				LATITUDE	LONGITUDE	
726487	99999	MENOMINEE (AWOS)	KMNM	45.133	-87.633	191.0
726455	94897	MANITOWAC MUNI AWOS	KMTW	44.129	-87.668	198.4
726455	99999	MANITOWAC MUNI AWOS	KMTW	44.133	-87.683	198.0
726405	94869	MILWAUKEE/TIMMERMAN	KMWC	43.110	-88.034	227.1
726405	99999	MILWAUKEE/TIMMERMAN	KMWC	43.117	-88.033	227.0
999999	94869	MILWAUKEE TIMMERMAN	KMWC	43.110	-88.034	227.1
725300	94846	CHICAGO/O'HARE ARPT	KORD	41.986	-87.914	205.4
999999	94846	CHICAGO OHARE INTL	KORD	41.986	-87.914	205.4
727347	14841	PELLSTON RGNL ARPT	KPLN	45.571	-84.796	217.9
999999	14841	PELLSTON EMMET CNTY	KPLN	45.571	-84.796	217.9
725339	99999	CHIGAGO-WAUKEE ARPT	KPWK	42.117	-87.900	197.0
744665	4838	CHICAGO/PALWAUKEE	KPWK	42.121	-87.905	197.2
744665	99999	CHICAGO/PALWAUKEE	KPWK	42.117	-87.900	197.0
726424	94818	RACINE	KRAC	42.761	-87.814	205.4
726424	99999	RACINE	KRAC	42.767	-87.817	205.0
726284	94836	SAWYER INTL	KSAW	46.354	-87.384	372.2
726284	99999	SAWYER INTL	KSAW	46.350	-87.383	372.0
726425	4841	SHEBOYGAN	KSBM	43.769	-87.851	228.3
726425	99999	SHEBOYGAN	KSBM	43.783	-87.850	228.0
725350	14848	SOUTH BEND/ST.JOSEP	KSBN	41.707	-86.333	235.6
999999	14848	SOUTH BEND ST.JOSEP	KSBN	41.707	-86.333	235.6
722186	4892	BEAVER ISLAND AIR	KSJX	45.689	-85.551	203.9
722186	99999	BEAVER ISLAND AIR	KSJX	45.700	-85.567	204.0
726458	4824	STURGEON BAY	KSUE	44.844	-87.417	220.7
726458	99999	STURGEON BAY	KSUE	44.850	-87.417	221.0
726387	14850	CHERRY CAPITAL	KTVC	44.741	-85.583	192.0
999999	14850	CHERRY CAPITAL	KTVC	44.741	-85.583	192.0
726409	4897	WAUKESHA	KUES	43.041	-88.234	277.7
726409	99999	WAUKESHA	KUES	43.033	-88.233	284.0
725347	14880	CHICAGO/WAUKEGAN	KUGN	42.422	-87.868	221.6
725347	99999	CHICAGO/WAUKEGAN	KUGN	42.417	-87.867	222.0
725327	4846	PORTER CO MUNI	KVPZ	41.453	-87.006	234.7
725327	99999	PORTER CO MUNI	KVPZ	41.450	-87.000	241.0

information for Lake Michigan, and used to test the data based on quality control flags and guidance provided in the documentation. Final verification of the results produced by this routine was performed by directly accessing the ISH ASCII database for a series of stations and time periods.

The NCDC ISH database is not as complete as suggested by summary information provided. For example, meteorological information for Milwaukee (USAF/WBAN: 726400/14839) was said to start in 1929; however, the earliest record was in the late 1940s. Despite the archive data suggesting hourly information, there are data gaps ranging from a few hours to weeks. Also, the older data generally are available at 3-hour intervals, or longer. No data archive is completely error free. Some of the errors uncovered during the processing included incorrect longitude/latitude location of the station. Some files were corrupted. Whether the download corrupted the original file or it occurred during the *un-zipping* process, the input file became contaminated. This is relatively easy to spot; the output file contains only the header record and one line of re-formatted data. This problem can be corrected by deleting the top line from the input file and re-running the conversion software, until the output file is approximately the same size as other station files.

The conversion of the coded ISH files is not computationally demanding; however, the procedure of making sure all of the original station data are processed correctly can become time consuming. However, given the number of years to process (approximately 50 or 60), this step does not become a daunting task. Checking of the station data is vital. Note that NNM is an interpolation routine which is strongly dependent on the position of each station, so care is required to assure the station data are accurate. The entire data set can also become quite large, on the order of 30 Gb once it is expanded and processed. A summary plot of the number of active stations for each year from 1950 through 2009 is provided in Figure 1-1. There is a significant increase in the number of active stations over the last 60 years.

1.2.2 Additional meteorological stations (NDBC/NOS/NWS/GLERL)

There are other meteorological stations in operation in or around Lake Michigan. These include NOAA's NDBC buoys, CMAN stations, as well as NOAA's NOS and NWS stations, and regionally deployed stations such as those deployed by GLERL. The best and most up to date record of available station information can be obtained from (<http://coastwatch.glerl.noaa.gov/marobs/>).

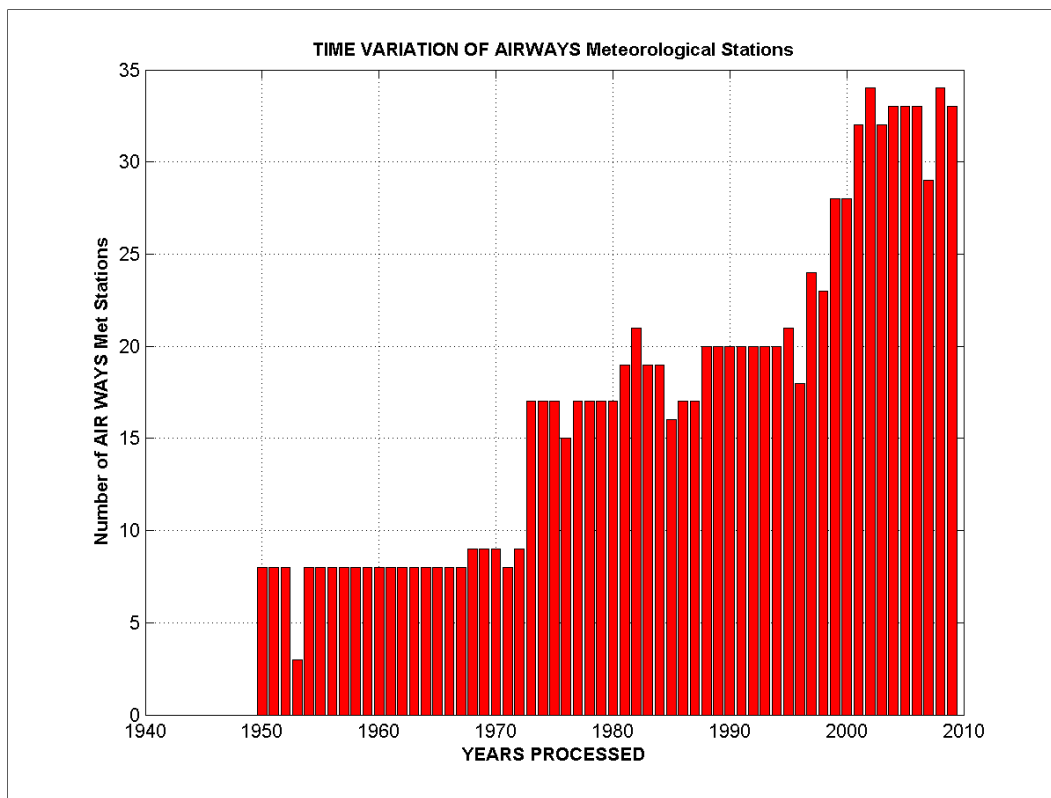


Figure 1-1. Time variation of active airways stations found in the NCDC ISH data archive.

Archive information for these data sets is available from various sites. NOAA's National Oceanographic Data Center (NODC) has all of the NDBC data (<http://www.ndbc.noaa.gov/BUOY/buoy.html>), including the buoy and CMAN station data, summary information for buoy locations by year and other valuable meta-data. These data have been quality controlled for data integrity, and the location is the official NOAA archiving center for all oceanography/meteorological information. Note that all Great Lakes (including Lake St. Clair) data buoys are re-deployed on a yearly basis; hence, the location of that station will change. These location changes can affect the generation of the NNM wind fields, as well as cause temporal phase shifts between model-to-measurement comparisons. The NOS, NWS and GLERL stations have their own unique archives. Access to those data can be performed via the NDBC Data Portal (e.g. for Lake Michigan, <http://www.ndbc.noaa.gov/maps/WestGL.shtml>). Ship observation data are available; however, they were not accessed or used in this study.

Software was built to reformat these additional meteorological station data into the identical form generated for the ISH data, to create one unique data format for all meteorological stations covering the period from 1950 through 2009. These stations are summarized in Table 1-2. Note that

Table 1-2. Additional meteorological station information.

STATION	OPERATED	LOCATION		ELEVATIONS (m)		TIME PERIOD	
		LONGITIDE	LATITUDE	STATION	ANEM	START	END
BHRI3	NWS	-87.1469	41.6467	180.4	10.1	2006	Present
CMTI2	NOS	-87.5383	41.730	179.4	9.1	2004	Present
CHII2	GLERL	-87.500	42.000	176.0	25.9	2005	Present
WHRI2	NWS	-87.8133	42.3606	179.8	9.0	2009	Present
KNSW3	NWS	-87.8086	42.5889	176.0	19.5	2005	Present
MLWW3	GLERL	-87.8789	43.0456	176.0	12.2	2005	Present
PWAW3	NWS	-87.8678	43.3875	178.0	10.0	2006	Present
KWNW3	NOS	-87.4958	44.4650	Unkn	Unkn	2006	Present
AGMW3	NWS	-87.4331	44.6081	178.9	9.1	2005	Present
GBLW3	NWS	-87.9017	44.6550	176.0	25.0	2005	Present
MNMM4	NOS	-87.5900	45.0958	176.0	6.62	2006	Present
CBRW3	NWS	-87.3597	45.1983	179.8	10.0	2008	Present
SYWW3	NWS	-87.1208	45.2022	178.9	3.0	2005	Present
NPDW3	NWS	-86.9778	45.2903	178.3	10.0	2005	Present
FPTM4	NWS	-86.6594	45.6189	184.4	10.1	2006	Present
PNLM4	NOS	-85.8711	45.9700	178.9	10.2	2006	Present
NABM4	NWS	-85.6097	46.0869	178.3	10.1	2006	Present
MACM4	NOS	-84.7194	45.7778	178.5	10.4	2009	Present
GTLM4	NWS	-85.5169	45.2106	176.2	16.0	2006	Present
GTBM4	GLOS/UoM*	-85.6058	44.7667	176.0	8.5	2007	2007
45020	GLOS/UoM	-85.6044	44.7889	176.0	2.4	2009	2009
45021	GLOS/UoM	-85.4931	45.0481	176.0	3.2	2009	2009
BSBM4	NWS	-86.5139	44.0547	184.4	10.0	2006	Present
LDTM4	NOS	-86.4417	43.9467	179.4	Unkn	2004	2009
MKGM4	GLERL	-86.3389	43.2278	179.1	24.4	2005	Present
SVNM4	GLERL	-86.2889	42.4014	176.0	16.8	2005	Present
SJOM4	NWS	-86.4942	42.0989	182.3	10.0	2007	Present
MCYI3	GLERL	-86.9125	41.7286	176.0	21.3	2005	Present
SGNW3	NDBC	-87.6835	43.7500	176.0	19.0	1985	Present
45007	NDBC	Variable	Variable	Variable	Variable	1981	Present
45002	NDBC	Variable	Variable	Variable	Variable	1979	Present

*GLOS/UoM: Great Lakes Observing System/ University of Michigan

NDBC buoy data location and elevation information varies over each successive deployment. Also, two of the NOS station locations do not provide information for the station and anemometer elevations. These locations are assumed to be located at the shoreline and anemometer elevation was assumed to be 10 m.

1.2.3 Data mining summary

The final outcomes of the data mining were: 1) all point source measurements were obtained; 2) the meta-data (generally the location, location and anemometer elevations) were compiled; and 3) all stations were formatted to one unique form and archived locally on a yearly basis. These were vital steps in the procedure, as was assuring that all data sets are properly checked for consistency and quality.

1.3 Natural Neighbor Method (NNM): Wind and pressure fields

1.3.1 MET-EDIT: Building of meteorological station information

In generating wind and pressure fields for a particular storm simulation, there are two additional steps required. Because of the changing ISH and additional meteorological station information, these steps cannot be automated and user input is required. The first step is to take the existing individual station files and construct one file containing all station information for each time record. Software was written (*INPUT2METEDIT.f*) which serves two purposes: 1) to isolate all software provided by NOAA/GLERL minimizing the need for modifications to their routines, and 2) to serve as an intermediate step to evaluate the input meteorological conditions prior to the generation of the wind fields. This piece of “wrapper” software (wrapped around the GLERL software) also fills data gaps with identifiable flags, and has the option to temporally smooth the meteorological parameters. The latter option was added as a result of initial testing of storm simulations where water level calculations in Green Bay were somewhat sensitive to oscillations and high-frequency fluctuations in the wind.

The *INPUT2METEDIT.f* software requires three basic input files and a set of point-source station files. The first input file contains the starting and ending date of the simulation, the interval for each output, and the number of points used in the temporal averaging. The second file contains a list of stations to be processed, and also defines the physical location, station type, and anemometer elevations for the stations. The third input file (obtained from NOAA/GLERL) contains daily average water temperature data. Lastly, there is a set of individual station files, point source meteorological input files, consistent with the file list provided earlier.

Four output files are generated by the software. The first is a reformatted list of station information, also containing flags for octant wind direction

transformation. Certain meteorological stations are located at the land/water interface. For winds blowing from land to water, the over-land to over-water transformation is applied; for winds blowing from the water to land, no transformation is performed. The NOAA/GLERL site provides this information for all stations and is used for this procedure. The second output file generated by the *INPUT2METEDIT.f* contains all land meteorological stations (sorted by date and by station), and the meteorological parameters (air temperature, dew point, wind direction, wind speed, maximum gust, cloud cover, solar radiation, barometric pressure) formatted consistently with the input requirements for the next developed software routine called *metedit.f*. The fourth output file contains the daily mean water temperatures specific to the simulation period identified above. The final file built will become the general input file for the *metedit.f* routine. Saving these intermediate output files provides the means to check the input conditions. For example, Figure 1-2 displays the station locations for a particular evaluation storm (referred to here as Storm-6W) where all available meteorological station information was used. Figure 1-3 shows a plot of the original wind speed and direction (black symbols), compared to the smoothed (1:1:1) output. Although only wind speed and direction data are provided, all meteorological parameters (air temperature, barometric pressure) are smoothed using the same technique.

The next step in the generation of the NNM wind and pressure fields is a pre-processing routine called *metedit.f*. This FORTRAN routine takes the existing individual station files consisting of point source meteorological parameters, transforms the winds from over-land to over-water (i.e., marine exposure), equivalent neutral stable 10-m winds. *Metedit.f* (developed by Dr. D. Schwab, NOAA/GLERL and provided to USACE) has been used for the past two decades as the pre-processing routine for the NNM. The code checks for reasonable limits for all input values (criteria on the wind magnitude, surface barometric pressure, air temperature). All parameters are additionally checked against lake-wide averages at each time-step. The general input file for *Metedit.f* defines all of the input files and the naming convention for all output files (see Figure 1-4). Note that the model domain is defined in a spherical coordinate system for the Lake Michigan work. One output file will be built during the processing of the point-source meteorological station information. That particular file is the designated input file properly formatted to be read by the NNM.

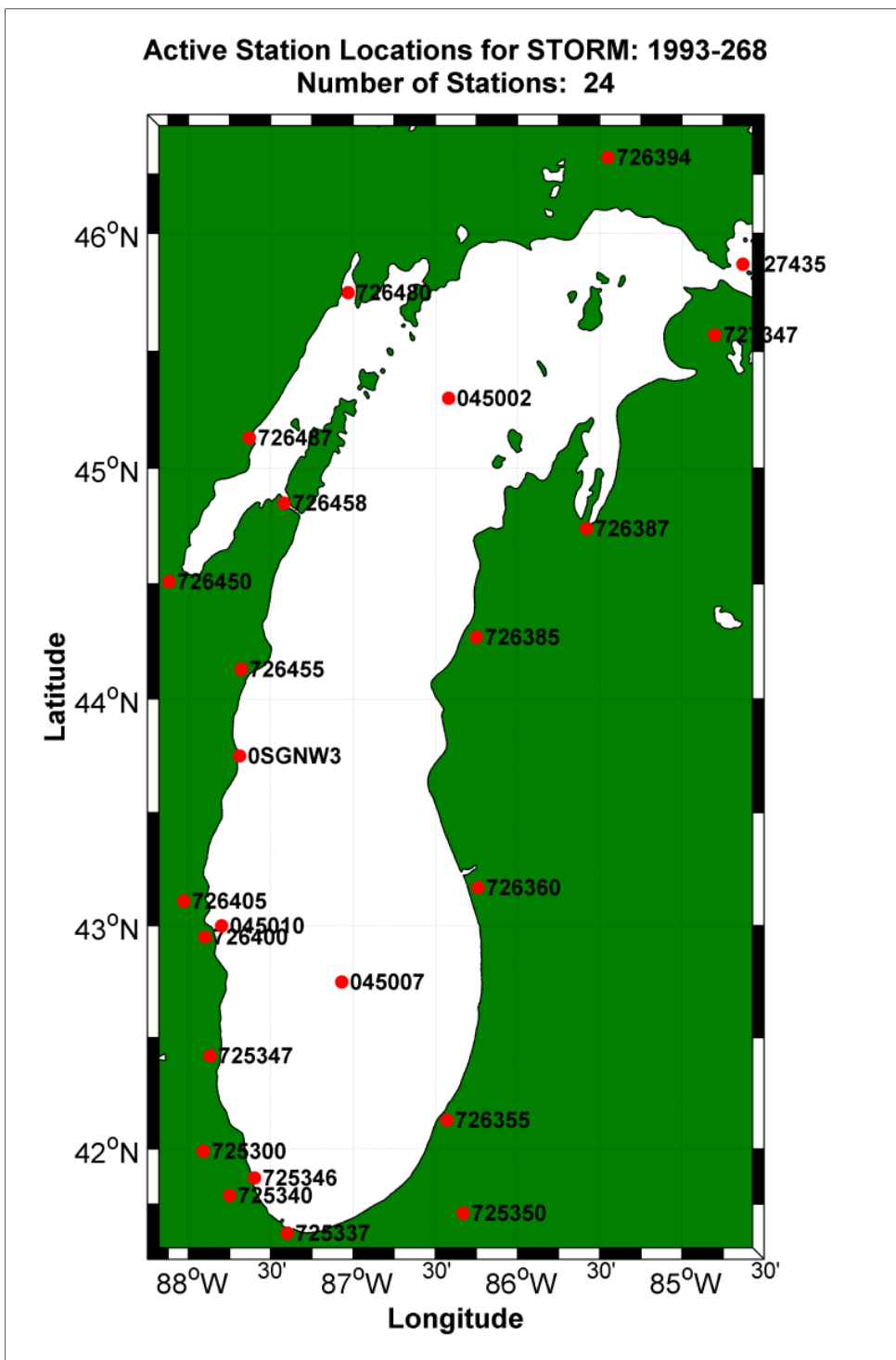


Figure 1-2. Available meteorological station locations accessed and preprocessed for Storm 6W.

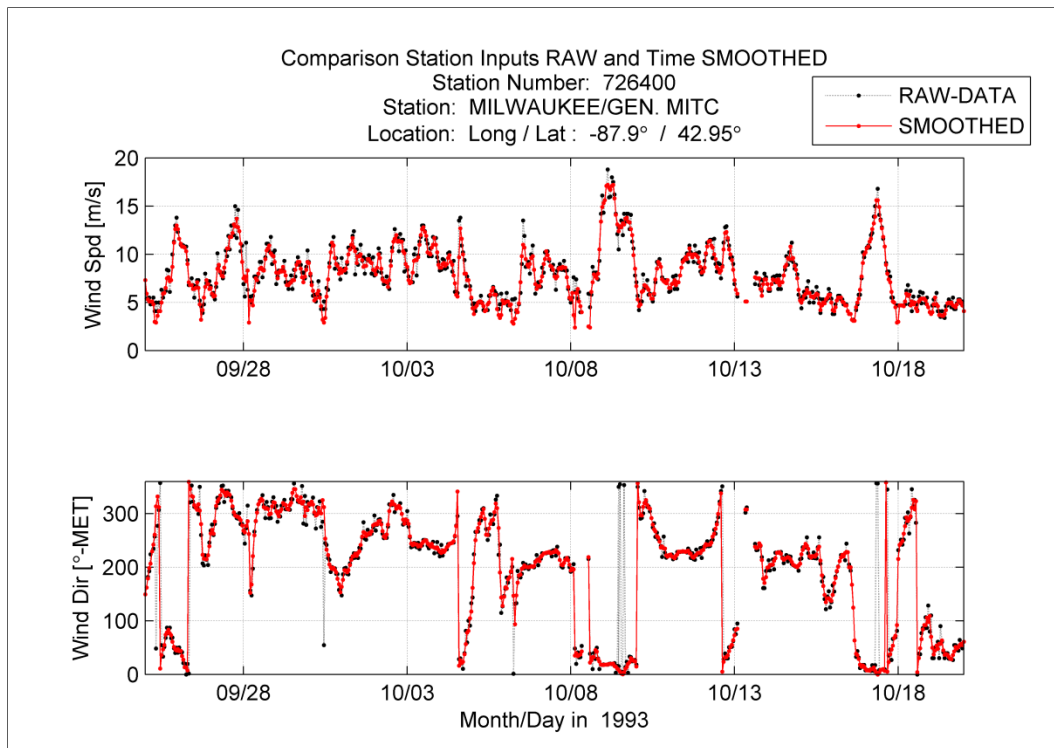


Figure 1-3. Comparison of input wind speed, direction and temporally smoothed (1:1:1) for Storm 6W at Milwaukee, WI.

	BLANK LINE (used for model grid)
STNLOC-1993-268.dat	INPUT FILE
METOBS-1993-268.dat	INPUT FILE
MICHTEMP1993-268.OUT	INPUT FILE
MICHTEMP1993-268	OUTPUT FILE
1993 268 0	YEAR JULIAN-DAY HOUR [START TIME]
1	WIND INTERVAL (HRS)
601	NUMBER OF DATES TO PROCESS

Figure 1-4. Example of general input file for *Metedit.f*.

Again, the output file generated by *Metedit.f* is checked and evaluated for consistency, assuring quality of input prior to the final step of generation of the wind and pressure fields by the NNM required for the subsequent wave and surge modeling efforts. An example of the results from this processing step is provided in Figure 1-5, where the original un-smoothed input winds are compared to the output derived from *Metedit.f*. The increase in wind speed is a result of the transformation to marine exposure winds. Also notice the slight clockwise rotation of the wind direction as it is transformed to an over-water exposure. Lastly, note that the barometric pressure is not affected. Note that all simulations used the 1:1:1 smoothing routine on the initial land-station data prior to transforming the winds from over-land to over-water winds.

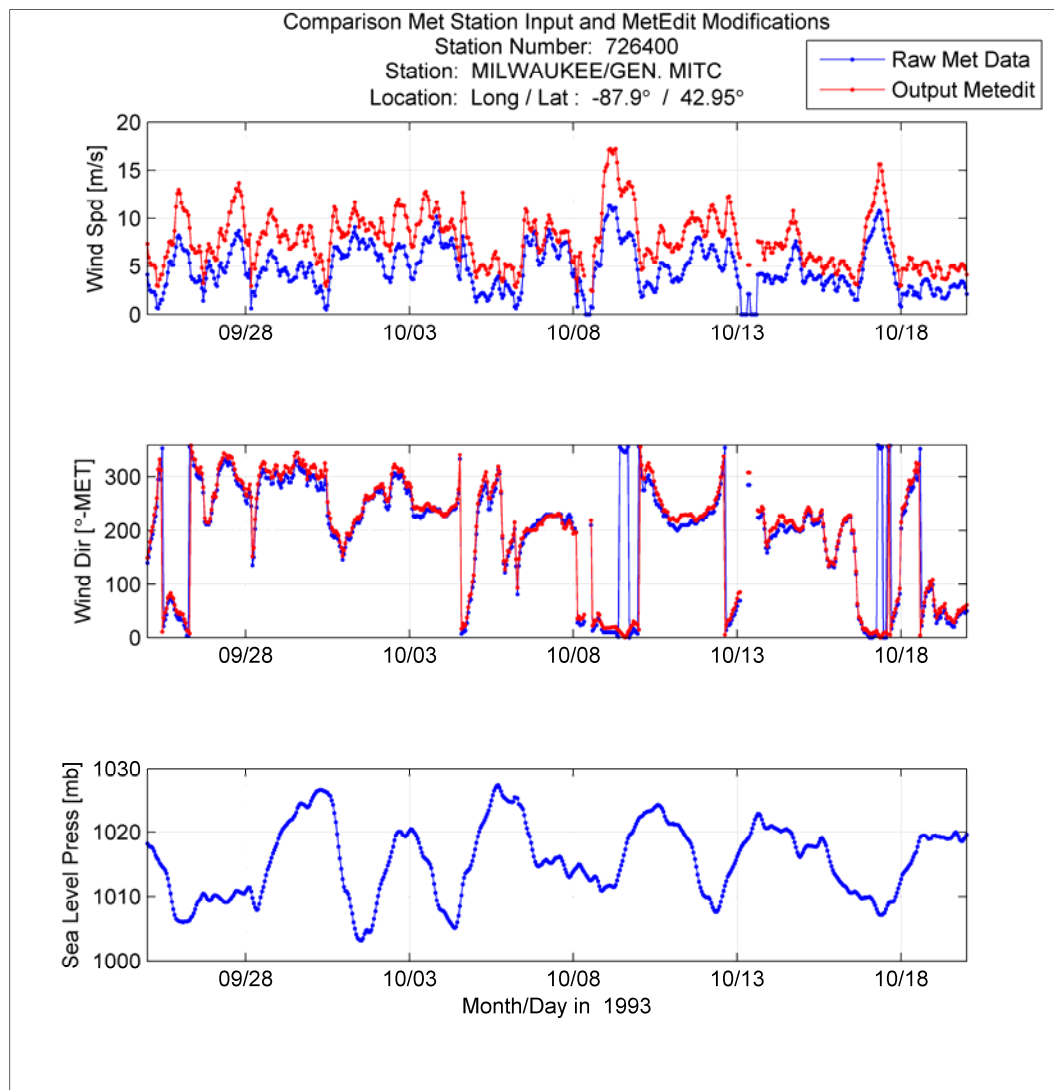


Figure 1-5. Comparison of input wind speed, direction and barometric pressure and output from *Metedit.f* for Storm 6W.

One very obvious difference using *Metedit.f* is that all dates are *Julian* convention whereas all input meteorological data and modeling efforts (wave, and surge) use *Gregorian* dates. Rather than modify the GLERL software, provisions were made to convert Gregorian dates to Julian dates in the pre-processing codes, and ultimately converting the final wind and pressure fields derived from the NNM back to Gregorian dates. All of the customized software used has been written in standard FORTRAN, and run on a 32-bit PC. Computational overhead for the meteorological data processing is not large; processing required on the order of an hour to complete the two intermediate steps. Note that de-coding of the ISH Airways wind data can be performed once for all years and archived locally. For individual storm simulations, it becomes a matter of selecting the year from the ISH

and, if necessary, the alternate meteorological station data base, copying those files and then using *INPUT2METEDIT.f* to access and sub-sample the appropriate time period.

1.3.2 Application of Natural Neighbor Method: Building of model-ready wind and pressure fields

As previously mentioned, there are a number of methods that could be used to develop temporal and spatially varying wind and pressure fields to force the hydrodynamic models used in this study. The Natural Neighbor Method (NNM) developed by NOAA's GLERL has been shown to provide accurate estimates of the varying meteorological events that affect the waves, and circulation in Lake Michigan. NNM is a very sophisticated geometrically based technique that provides a more realistic representation of two-dimensional wind fields compared to alternate formulations, such as the Nearest-Neighbor method (Beletsky and Schwab 2001). The following are excerpts from Beletsky et al. 2003).

“The NNM approach is based on the Delaunay triangulation of the meteorological stations. The “natural neighbor” of a particular point on a regular grid (defined in this case on a fixed longitude/latitude spherical coordinate system with the resolution of X and Y at a constant interval of 0.02-deg) are determined by performing a Delaunay triangulation on a new set of points which includes the grid point as well as the observation point. The “natural neighbors” of the grid point are then the observation points which lie in the Voronoi cells surrounding the cell which contains the grid point. Hence, the defined meteorological variables (wind speed, direction, and barometric pressure) from the fixed stations are weighted by the area of overlap between the new Voronoi cell corresponding to the grid point and the original Voronoi cell corresponding to the fixed station location. The weighted values are summed and divided by the sum of the weights to determine the value at the resulting grid point.”

The benefit of using this method is that not every meteorological station contains information on an hourly basis, or intermittently. The interpolation is entirely local, or every point is only influenced by its “natural neighbor,” whereas other interpolation methods extrapolate the information across the entire grid domain (e.g. Hubertz, et al., 1991).

The NNM software was provided to the USACE for the generation of the wind fields for Lake Michigan. Subsequent modification of the source code

was performed to include the generation of the barometric pressure fields. This modification followed the procedures used for other scalar meteorological parameters such as air temperature. The NNM consists of a series of modules written in FORTRAN and “C”. The latter algorithms were originally obtained directly from Braun and Sambridge (1995), and the algorithms used follow the work of Lasserre (1983). Computational load running NNM is not demanding; however, the platform must have FORTRAN and “C” compilers.

The bulk of the FORTRAN routines were developed at GLERL by Dr. David Schwab for the specific purpose of integrating this method into their operational forecasting system. The original code was built for a regular fixed Cartesian coordinate system; however, it has been adapted for irregular grids such as a fixed longitude/latitude spherical grid. Input to this software includes a general file containing a list of files to be read, the naming convention for the output files, the start date, the time interval for gridded fields, and the number of fields to process. The unstructured version of NNM requires the actual model domain containing the longitude/latitude pairs for each grid point. The NNM converts to a Cartesian coordinate system. The NNM performs the interpolation on scalar quantities so the winds (vector parameter) are split into U (x-directed) and V (y-directed) scalar variables. In addition to the winds, air temperature, dew point and cloud cover fields are generated. The addition of barometric pressure field generation was added for this project, and followed the general logic provided for the other variables. The output consists of one binary, network Common Data Form (netCDF) file for each of the parameters. The netCDF files were then converted to ASCII formats consistent with the input criteria used in the wave and surge modeling efforts.

Testing and evaluation of the NNM wind and pressure fields are made indirectly based on the results generated by the wave and surge models. Direct examination, testing and evaluation of the wind fields were performed to assure the reasonableness of the interpolation and continuity between wind field intervals. An example of a NNM wind field is shown in Figure 1-6, where wind speeds are color contoured (isotachs, or lines of constant wind speed) and wind direction is indicated by the small vectors. Wind data are sub-sampled every eighth grid point for the graphical display shown in the figure. This figure shows a snap-shot of the wind field at a time that corresponds to the peak of a strong wind event where the wave height observed at an NDBC buoy (45002) attained a peak height of 5.2 m.

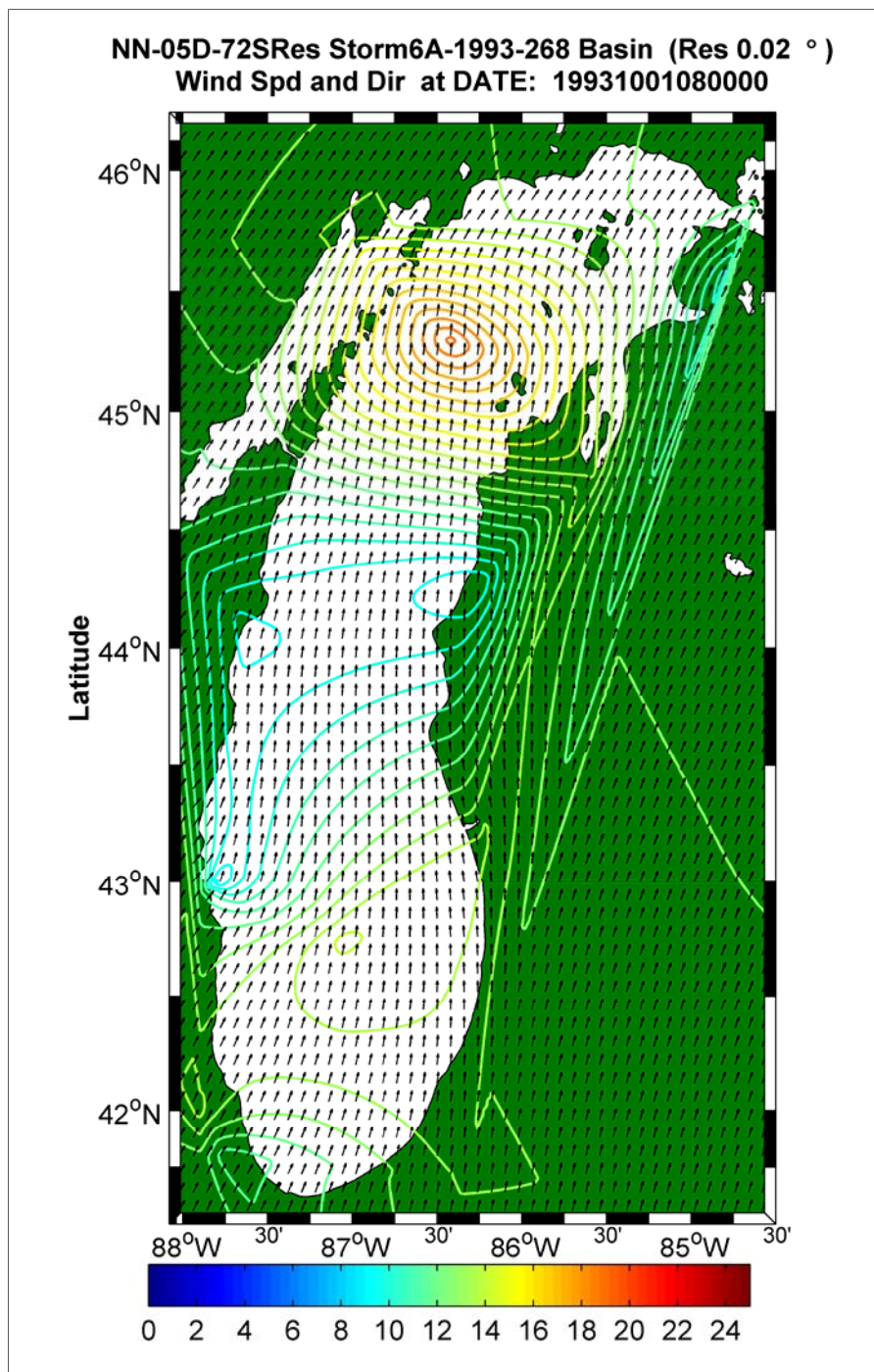


Figure 1-6. Snapshot of wind speed isotac color contour (m/sec) and wind directions (arrows) using the NNM for Storm 6W.

There are two concentrated lobes of high wind speeds; one in the northern portion of Lake Michigan and one of smaller intensity in the southern region. A possible artifact associated with application of the NNM are the north-northeast to south-southwest color contours emanating from Mackinaw Island, a meteorological site used in this procedure. A hypothesis

for this artifact was that the bounding box used in the generation of the Lake Michigan wind fields was positioned too close to the target domain. The NNM uses “pseudo-stations” at the four corners of the target domain to insure complete coverage. Those corners use the closest point source location. The only corner that appears to be affected is the northeast, where Mackinaw Island and potentially Pellston Regional Airport reside.

One alternative would be to expand the target domain in all directions, and add additional meteorological sites in hopes of decreasing the apparent impact of the two northeasterly locations. A sensitivity test was performed to examine the influence of including additional stations in the analysis. The four sites added include: Sault Ste Marie (727340), Alpena (726390), Saginaw (726379), and Detroit (725370), and they are displayed in Figure 1-7.

The resulting NNM revised wind snapshot is shown in Figure 1-8. The obvious change by increasing the NNM target domain is the removal of the north-northeasterly to south-southwesterly isotacs emanating from Mackinaw Island. This is replaced by a localized low region. However, over Lake Michigan proper, there are minor if any appreciable changes that arise by expanding the number of wind stations.

1.3.3 NNM summary

The NNM provides a means to generate spatially and temporally varying wind and barometric pressure fields to be used in wave and surge modeling efforts for Lake Michigan. There are a number procedural steps required to complete this effort. These steps must be performed with great care, checking and validating the information for accuracy and quality. The entire method is dependent on point-source measurements, their accuracy, location and continuity in observations over time. Input data errors at any one location, or locations, could potentially contaminate the final set of fields over a significant portion of the domain. Wave heights and surge estimates scale to the wind speed squared or cubed, depending on the drag law utilized. Thus, an error in the wind speeds of 10 percent will result in the potential errors in wave height and surge as much as 20 to 30 percent. The ultimate test of the quality in these fields will be based on the performance of the wave and surge modeling efforts. In light of the elongated shape of Lake Michigan and Green Bay, errors in wind direction can also produce significant errors in calculated waves and water levels, which are sensitive to wind fetch.

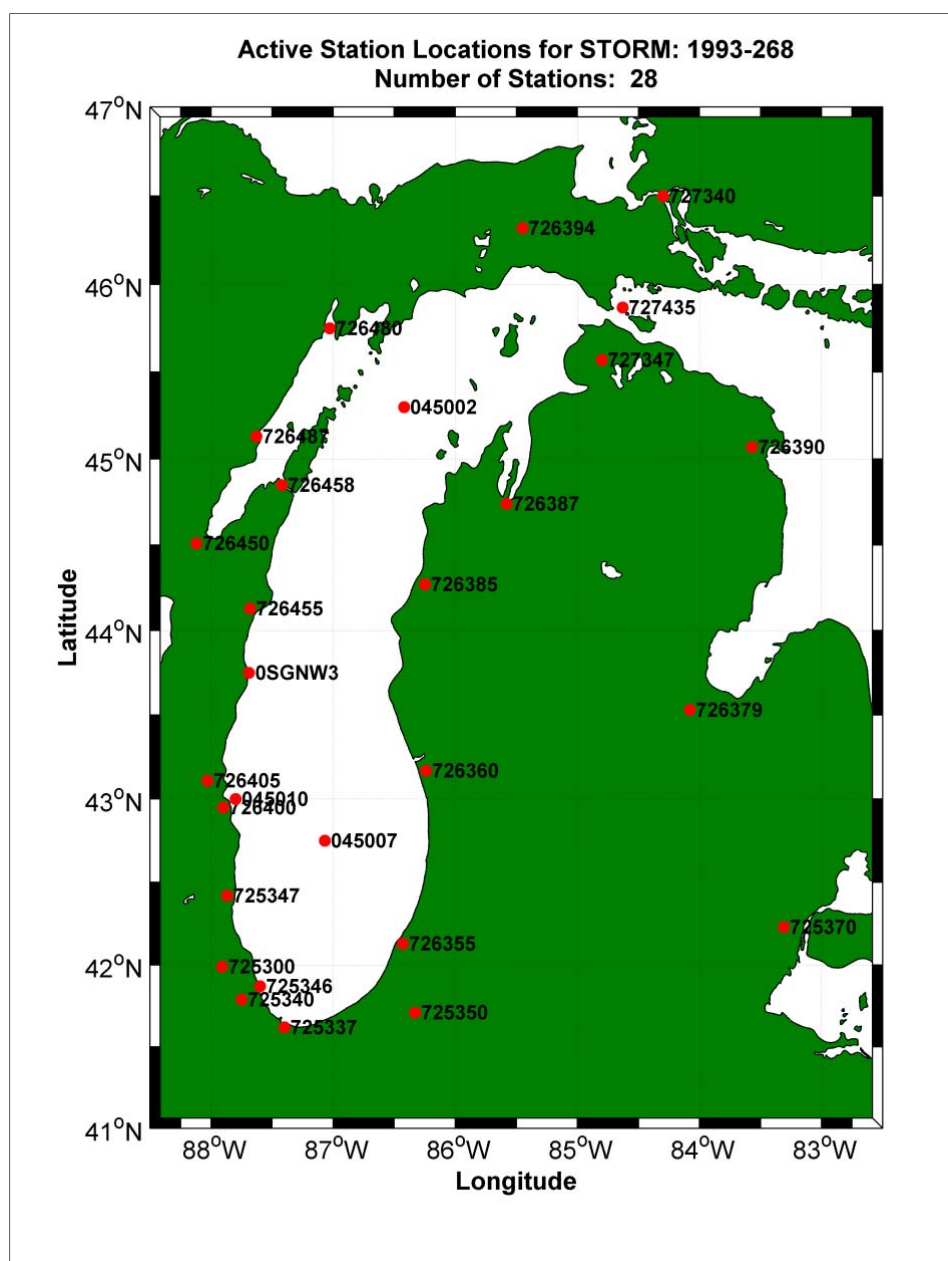


Figure 1-7. Increase NNM target domain and added four new meteorological sites for Storm 6W.

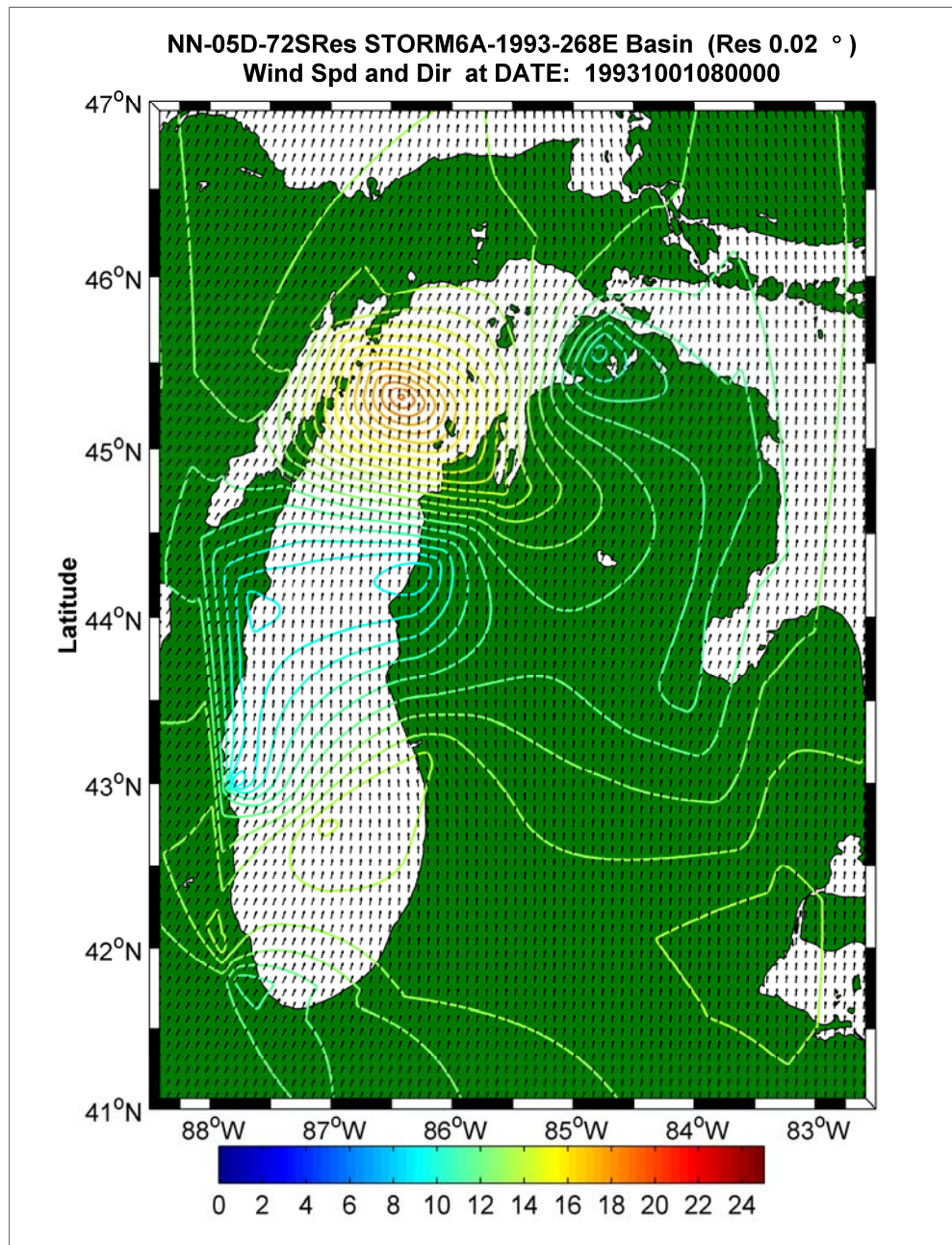


Figure 1-8. Snapshot of extended grid domain wind speed isotac color contour (m/sec) and wind directions (arrows) using the NNM for Storm 6W.

1.4 NCEP Climate Forecast System Re-analysis (CFSR): Wind and pressure fields

Very recently, a new set of high-resolution meteorological products have been produced by NOAA. The NCEP Climate Forecast System Re-analysis (CFSR, Saha et al. 2010) archive is based on a re-analysis program of all meteorological products generated by NOAA's National Center for Environmental Predictions (<http://dss.ucar.edu/pub/cfsr.htm>). This 31-year archive (1979 to

2009) provides wind fields on a Gaussian grid with resolution of approximately 38 km, and barometric fields on a 0.5-deg global geographical resolution, at one-hour intervals.

This archive only became available in early 2010, and was not originally considered as a source to be used for the Lake Michigan studies. This additional wind and pressure archive was examined as a potential alternative to the NNM generated fields. The initial effort to examine use of the CFSR products focused on seven storms selected for validation of wave and water level modeling for Lake Michigan. The archive is structured by year with available field products documented from the following website, (<http://dss.ucar.edu/md/datasets/ds093.1/detailed.html>). The high resolution winds at 10-m elevation provided on a Gaussian grid (e.g. wnd10m.gdas.YYYYMM.grb2) and the barometric pressure fields, (e.g. prmsl.gdas.YYYYMM.grb2) were identified as fields of interest. The CFSR archive (<http://nomads.ncdc.noaa.gov/data/cfsr/>) was accessed and appropriate wind and pressure files were downloaded. These files were generated in a Grid In Binary (GRIB) format, where software is provided (<http://www.cpc.noaa.gov/products/wesley/wgrib2/>) to translate from their original form to netCDF, and ultimately to an ASCII format. The winds and pressure fields were then interpolated from the Gaussian grid, to a spherical grid with a set resolution of 0.02 deg in both longitude and latitude.

The time required for downloading and processing these fields is fairly significant (based on the seven storms simulated, or 13-months of files). In light of project schedule considerations and level of effort to download and process the data, this work was contracted to Oceanweather, Inc. Rather than sub-sample for only the Lake Michigan domain, winds and pressure fields were generated for all Great Lakes including Lake St. Clair to support flood risk map updates for all the lakes.

A fuller evaluation of the CFSR wind and pressure fields will be provided later; however, some initial insights to the differences and similarities between the CFSR and NNM winds are provided below. The focus for these evaluations is based on the wind field specification because they are used both in the wave and surge modeling effort while the pressure fields contribute only to the surge modeling.

One of the attributes of the NNM wind field estimation is that the spatial coherence in the wind fields is dictated by the observed winds at point-

source meteorological stations which are operational and by the fact that few exist over open water. As shown in Figures 1-6 and 1-8 the NNM wind field produces one major storm peak in the northern portion of Lake Michigan and a minor peak of lower intensity in the southern domain. The isotacs in the zone of low winds in the center of the lake are oriented easterly/westerly. This feature is a result of the land stations along the eastern and western coast of the lake having similar winds. This is also evident in the wind speed and direction time plot provided in Figure 1-9. The NNM has no information between these stations (in the middle of Lake Michigan) to suggest differently. One of the hypotheses offered is that NNM does not retain spatial coherency down the central axis of Lake Michigan. This becomes important when the winds measured in the north (45002) and south (45007) are nearly identical in direction (see Figure 1-10 for example) and show only a slight wind speed difference of about 3 m/sec or less between the northern and southern locations at the first three storm peaks. This suggests the magnitude of the wind is nearly uniform along the central north/south axis of Lake Michigan. As indicated earlier, the NNM places a local minimum in wind speed in the central portion (around 45-deg N latitude).

A CFSR wind snapshot consistent in time with the NNM result is provided in Figure 1-11 (original and extended versions are seen in Figures 1-6 and 1-8). The location and magnitude of the maximum lobe in the north compared to the NNM are nearly identical, indicating that the CFSR wind fields do assimilate measured data (e.g. from 45002). The CFSR secondary maximum wind zone in the south has wind speeds of about 5 m/sec greater, and located further north compared to the NNM winds. The CFSR wind field aligns the isotacs to the outline of Lake Michigan and it retains a spatial coherency along the central axis of the lake. CFSR winds de-emphasize the central minima observed in the NNM result, and they subjectively remove most local-scale features. The CFSR winds display large spatial gradients along the Lake Michigan coastline that could suggest smearing of the winds at the land/water boundary.

What is interesting to note is that the wind directions from both the NNM and CFSR winds throughout the entire domain are very similar. Only in the southern portion of Lake Michigan do the CFSR winds display a more northerly flow.

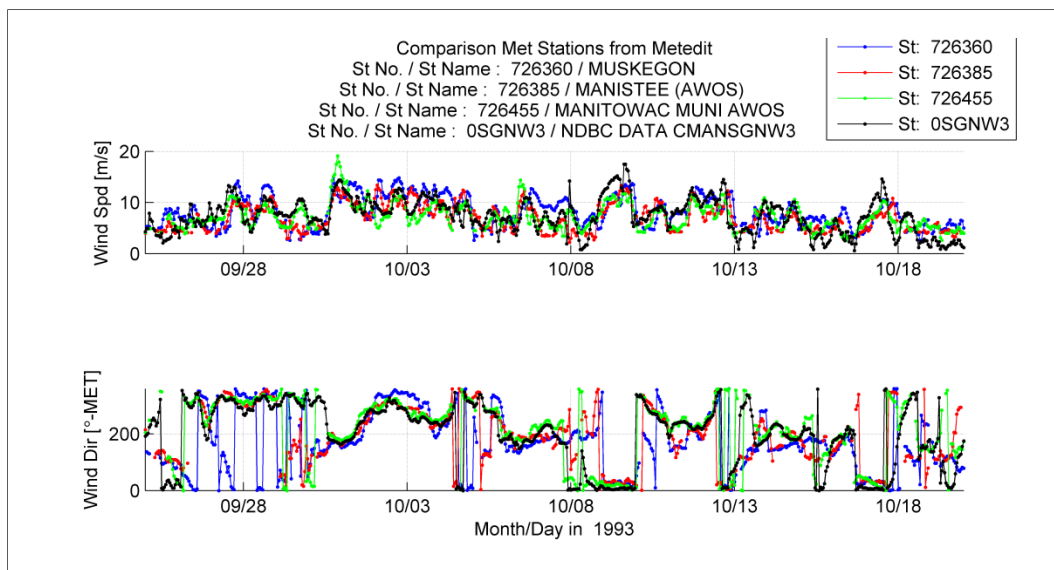


Figure 1-9. Comparison of easterly and westerly meteorological stations for Storm 6W.

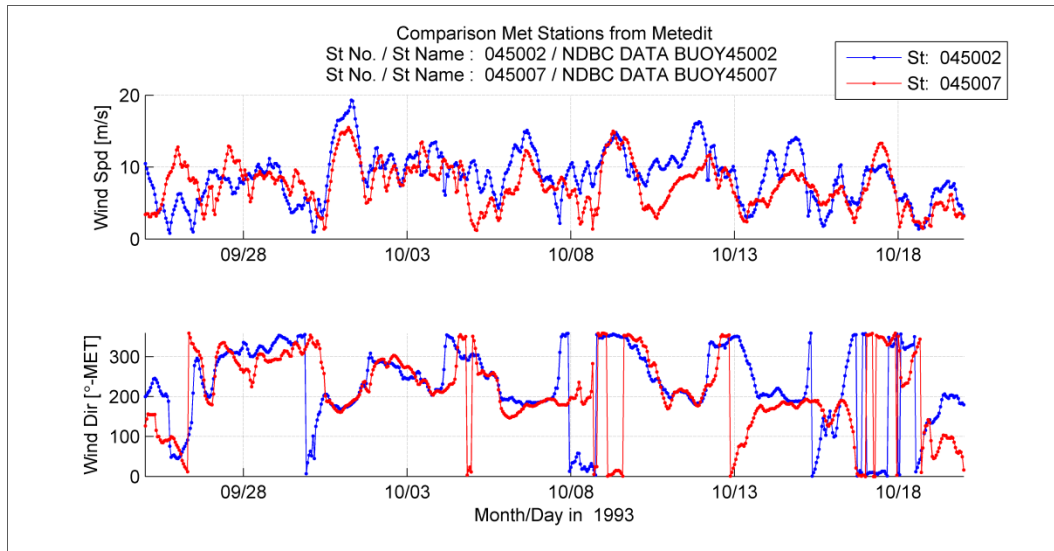


Figure 1-10. Comparison of NDBC Buoy 45002 and 45007 wind speed and direction during Storm 6W.

CFSR product summary

It seems evident that there are positive attributes contained in the CFSR wind fields¹. The spatial coherency found along the central axis of Lake Michigan, as suggested by data from the two NDBC buoys, seems to appear in the wind fields; and it appears to be missing in the NNM wind field. Because of a lack of point-source measurements along that central axis of the lake, there is no way to completely validate this assumption that the

¹ It is assumed the pressure fields from the NNM and CFSR will show similar trends.

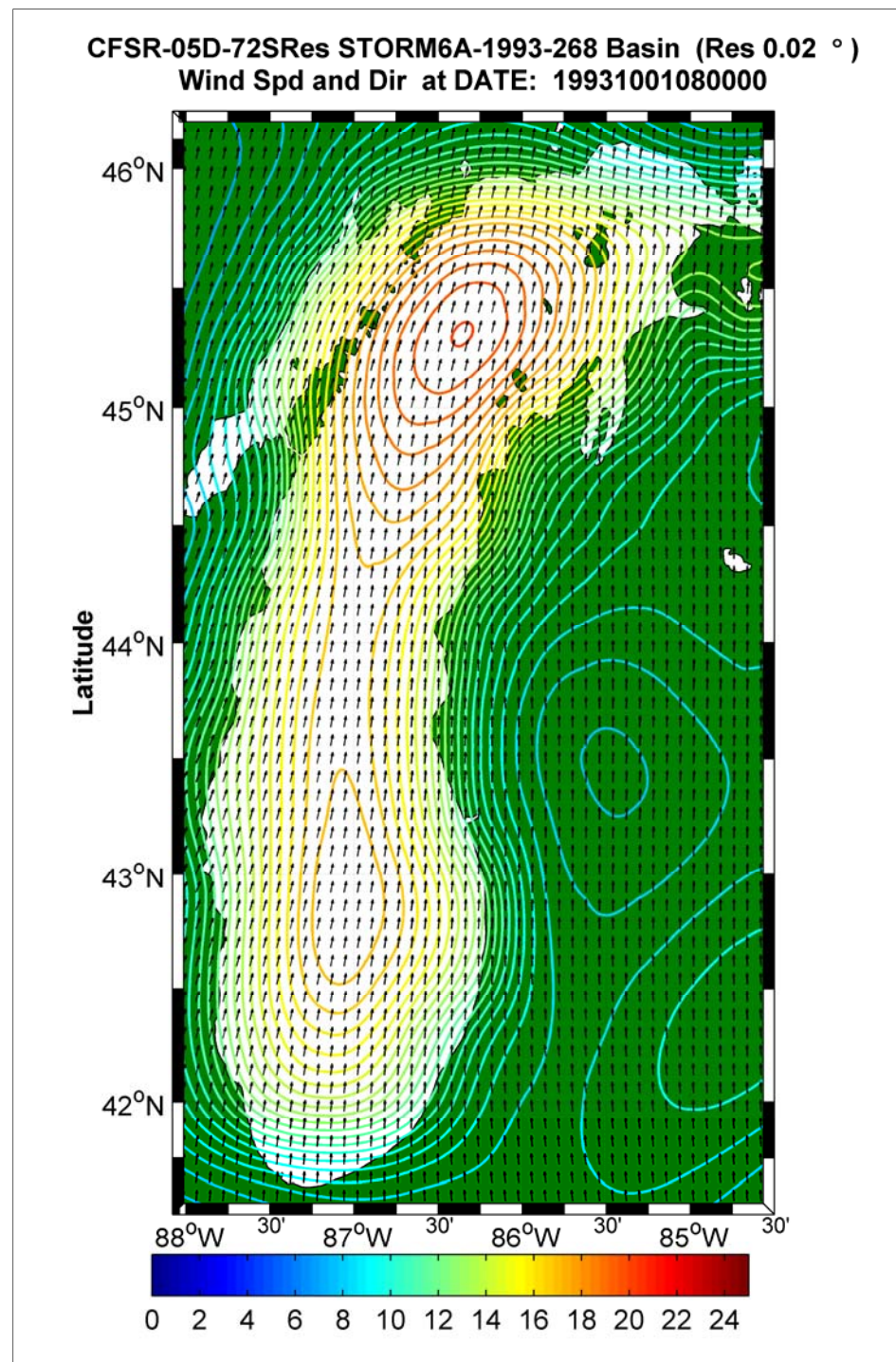


Figure 1-11. Snapshot of wind speed isotac color contour (m/sec) and wind directions (arrows) using the CFSR for Storm 6W.

CFSR winds have better spatial coherence for this event, except via comparison of wave model results. There is some concern with the strong spatial gradients in CFSR winds along portions of the land/water boundary of Lake Michigan, i.e., if in fact this is an artifact of the land/water interface

treatment in the original CFSR modeling effort. Lastly, the length of record for the CFSR wind and pressure field archive is 31 years, and there is the necessity of using NNM for storm conditions prior to 1979 and mixing the two approaches for extremes to maximize the record length to 50 years.

The quality of the CFSR versus NNM winds are examined more closely later in the wave and water level modeling sections of the report, where more extreme events are simulated using both sources of meteorological input. The wave model validation work led to a decision to adopt the CFSR winds/pressures for the period 1979 to 2009.

A decision to adopt CFSR wind and pressure fields in no way suggests that the NNM's performance is deficient, because the use of this method is important for storm simulations not covered in the CFSR archive. Also, conclusions drawn from Lake Michigan evaluations of the two sources for meteorological input might not in-fact be the same for all other Great Lakes regions. Work done for each lake should evaluate both sources of wind and pressure field input.

2 Ice Field Generation

2.1 Introduction

During each year the Great Lakes become ice covered, some completely, some partially. In general, the formation of ice develops from the shoreline (fast ice) lake-ward. This will present a natural impediment for storm generated waves to reach the shoreline under certain conditions and at certain locations. If ice coverage were not considered, the quality of the long-term wave and surge climatology might suffer, with potential for introducing biases into the flooding analysis. Neglecting ice cover could overstate the frequency and severity of storms that produce energetic wave and surge conditions at the shoreline. A decision was made to include treatment of ice coverage in the modeling.

Assel (2005) has been producing digital weekly ice atlases for the Great Lakes. Synoptic ice chart observations for the Great Lakes began in 1960. A synoptic ice chart usually covers only a portion of one or more of the Great Lakes. Synoptic ice charts for a 20-winter base period (1960 to 1979) were digitized (Assel 1983), and a multi-winter statistical analysis of ice concentration patterns over nine half-month periods (Dec. 16-31 to April 16-30) was published as a National Oceanic and Atmospheric Administration (NOAA) Great Lakes Ice Atlas (Assel 1983) 20 years ago. Composite ice charts, a blend of observations from different data sources (ships, shore, aircraft, and satellite) that cover the entire area of the Great Lakes for a given date, and which may contain some estimated ice cover data, were produced starting in the 1970's. A 30-winter (1973-2002) set of composite ice charts was digitized, and a multi-winter statistical analysis of the climatology of the ice cover concentration was completed.

As is the desire to generate a consistent accurate set of long-term wind and pressure fields for climatologic storm studies, application of a consistent data set is also needed for ice coverage. Unfortunately the data archives are inconsistent, where the observation period varies from daily (and generally interpolated, 1973-2002), to weekly, to bi-weekly. Historically, these products were based on mean monthly distributions of ice. More recently, the digital maps have been constructed based on mean weekly analysis techniques. One approach for treating ice cover is desirable and was developed and implemented. In general, digital ice information is in

the form of a longitude, latitude and ice concentration level. The concentration level is estimated from either photographs or based on the return pulse from satellite based remote sensing methods.

This concentration level needs to be pre-selected for implementation in the present numerical wave modeling approach. The wave model implementation treats ice as a land-water mask that is delineated based on a choice of the ice concentration that represents open water. As the ice cover increases, the open water points in the wave model domain at these locations are set to land. In the spring, as the ice-edge disappears, those locations are then set back to water points in the wave model calculations.

Application of ice in the surge model applies the spatially variable ice field to the target grid. The model internally adjusts the momentum flux from the air to the water surface via the drag coefficient, which is dependent upon the ice field concentration. This adjustment to the drag coefficient is at a maximum for an ice concentration level of 50 percent and decreases (according to a parabolic curve) to the original drag formulation for concentrations of 0 and 100 percent. Details are provided later in the water level modeling section.

Application of ice fields in the modeling efforts and selection of an appropriate concentration level becomes relatively important. Unfortunately, for the Great Lakes, all wave measurement buoys are generally removed so that the ability to examine model validation results as a function of ice concentration level are limited. Two shallow water nearshore wave gages were deployed in southern Lake Michigan outside of Chicago and Burns Harbors. These gages were actively recording in winter months during the ice periods; however the wave estimates were based on pressure sensors and then transformed to make an estimate of the water free surface. Questions arise regarding what is specifically measured, and the overall accuracy levels of those measurements when the free surface is iced over.

The past Wave Information Study for the Great Lakes (Hubertz et al. 1991; Reinhard et al. 1991, 1991a; Driver et al. 1991, 1992) used a concentration level of 50 percent. More recent studies in the western Alaska waters (Jensen et al. 2002, and Jensen 2009) suggested a concentration level of 70 percent was more appropriate for defining the land-water mask, validated to a limited amount of wave data; and that approach is adopted for the Lake Michigan study. Implementation of ice fields in surge modeling

has been validated along the western Alaska coast (Chapman et al. 2009) and that approach is adopted for the Lake Michigan study.

2.2 Composition of ice fields

There are three primary ice cover data bases available, which are identified in Table 2-1. Each database has its own unique characteristics that can potentially complicate the generation of one consistent data set. Note there is overlap in time between two of the data bases. For development of ice cover input to the wave and water level model simulations, the Digital Ice Atlas (Assel 2003) is the primary source. For storms prior to 1973, the ice concentration database (Assel 1983) is used. The ice thickness database listed in the table was not used in this study.

Table 2-1. Ice atlas database archives.

ARCHIVE NAME	LOCATION	TIME PERIOD		DESCRIPTION			DOCUMENTATION
		SRT	END	NX	NY	ΔT	
Ice Conc. Data Base	http://nsidc.org/data/g00804.html	1960	1979	77	117	Var.	Individual Lakes Source Codes Long/Lat Table
Digital Ice Atlas	http://www.glerl.noaa.gov/data/ice/atlas/	1973	2002	516	510	Daily	All Lakes Long/Lat Table
N/A	Obtained directly from NOAA/GLERL	2003	2009	516 1020 1024	510 1031 1024	Var.	All Lakes Lambert Conformal Conical
Ice Thickness	http://nsidc.org/data/g00803.html	1966	1979	99 Individual Station Sites		Var.	All Lakes Source Codes Long/Lat Table

All databases originated from NOAA/GLERL and they were originally defined in a Cartesian, Lambert Conformal-Conical coordinate system. All of the modeling efforts performed in this study used a fixed longitude/latitude spherical coordinate system. Transforming the ice locations from the original coordinate system to the model domains was accomplished given the mapping tables as identified in the 1960-1979 and 1973-2002 data bases. The documentation provided for these two data sets (1960-1979 and 1973-2002) contain all of the information required to process the individual files. The latter database is more complete. It contains both graphical and digital products of the ice cover for the 30-year period.

2.2.1 Ice Concentration Data Base, 1960 to 1979

For the 1960-1979 Ice Concentration Database, the digital ice concentration of each lake and digital climatologic information are provided. No images were generated for each ice coverage map. Access of this archive was made directly from the National Snow and Ice Data Center (<http://nsidc.org/data/g00804.html>), where the data and documentation are provided. The files are available for one-half month periods, December through April, containing concentration levels at 10-percent ice concentration intervals on a 5- by 5-km grid. The individual files also contain the geographical location (longitude, latitude pairs) that can be used directly to interpolate to the modeling domains. As part of the archive, there are FORTRAN routines to access the data set.

2.2.2 Digital Ice Atlas, 1973 to 2002

The Digital Ice Atlas archive for 1973 to 2002 (Assel 2005) is composed from information provided by two ice centers, the NOAA's National Ice Center (NIC) and the Canadian Ice Service (CIS). The yearly archive is based on the winter season. For example, the 1989 files contain ice information from the first ice appearance during the winter season, starting on 1 December 1988. The numbering convention of the files starts at day 100 and progresses until the last ice day occurs. The daily ice concentration data are identified by either "nic" (National Ice Center) or "cis" (Canadian Ice Service) depending on the source. There are flags associated with each data set. They are designated by a 0, 1 or 2, where 0 indicates no ice, 1 indicates an interpolated data set and 2 indicates observed data. Any file prior to the first date indicated with a 2 (observed data) that is identified with a 0 in the data file flag can be assumed to be ice free. The grid resolution is 2.8 by 2.8 km covering all of the Great Lakes. Land locations are appropriately flagged, and the concentration levels are provided in one-percent intervals for each water point. An example is provided in Figure 2-1. This example was randomly selected from the Assel (2005) data base, and was used for testing of the algorithm summarized below. The ice estimates were derived from the Canadian Ice Service and are based on an interpolation between two observed data sets.

A FORTRAN routine was built to read either the 1960-1979 or the 1973-2002 ice fields. This routine reads the longitude, latitude grid information file, the ice field(s) and the model grid. There is no header record defining the ice files; the name of a file contains the date (YEAR, ICE DAY), data flag

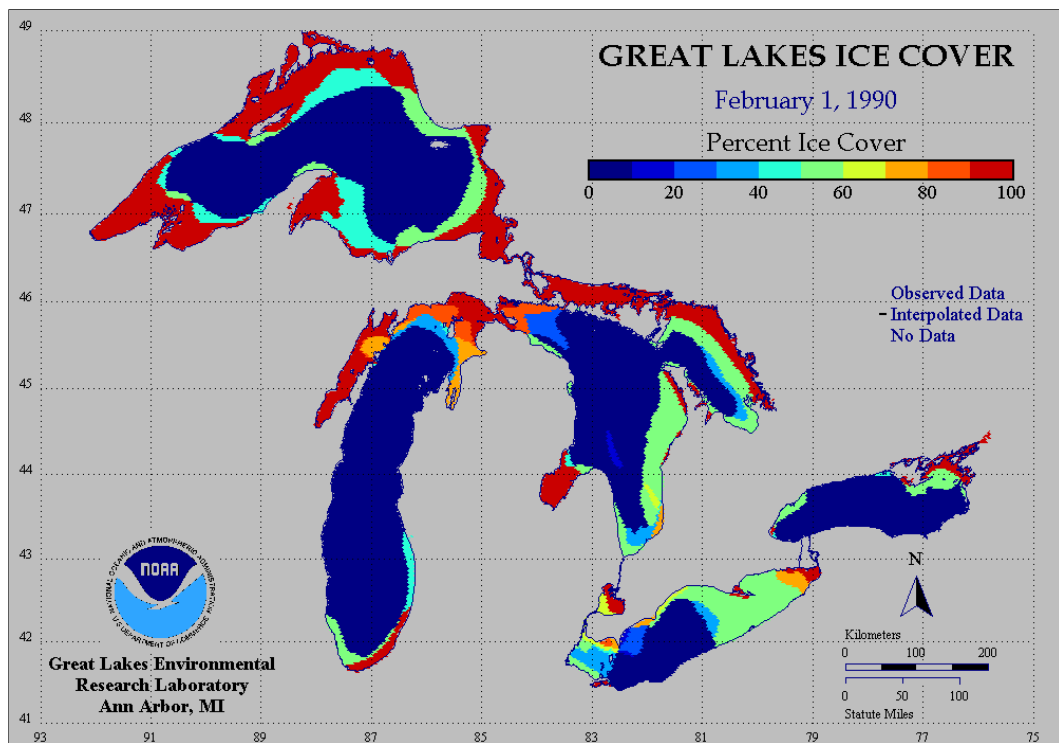


Figure 2-1. Example of ice coverage graphic for 1 February 1990. Accompanying data file (901631.dat).

and either cis or nic identifiers. Because each file contains ice information for all Great Lakes (including Lake St. Clair), the ice file is sub sampled, extracting only (for this study) the Lake Michigan domain. The grid resolution of the ice data and the model domain differ, so the concentration information is bi-linearly interpolated onto the higher resolution model grid. Lastly, the wave model land-sea grid information is applied setting all conditions to zero on “land”. One output file is generated containing the longitude, latitude and concentration level for each of the model grid points. An example of the output interpolated ice map is provided in Figure 2-2. The results are derived from the input ice coverage map file presented graphically in Figure 2-1. Overall, the interpolation routine results are very similar to the original graphic. The domains for different concentration percentages are very similar in size and location, verifying consistency between the interpolated fields and the originally archived ice cover data.

2.2.3 Recent digital ice data, 2003 to 2009

The newer ice data archive, 2003 to 2009, was obtained directly from the staff at NOAA’s GLERL. Despite indications that these fields are available up to the present at the National Ice and Snow and Ice Data Center

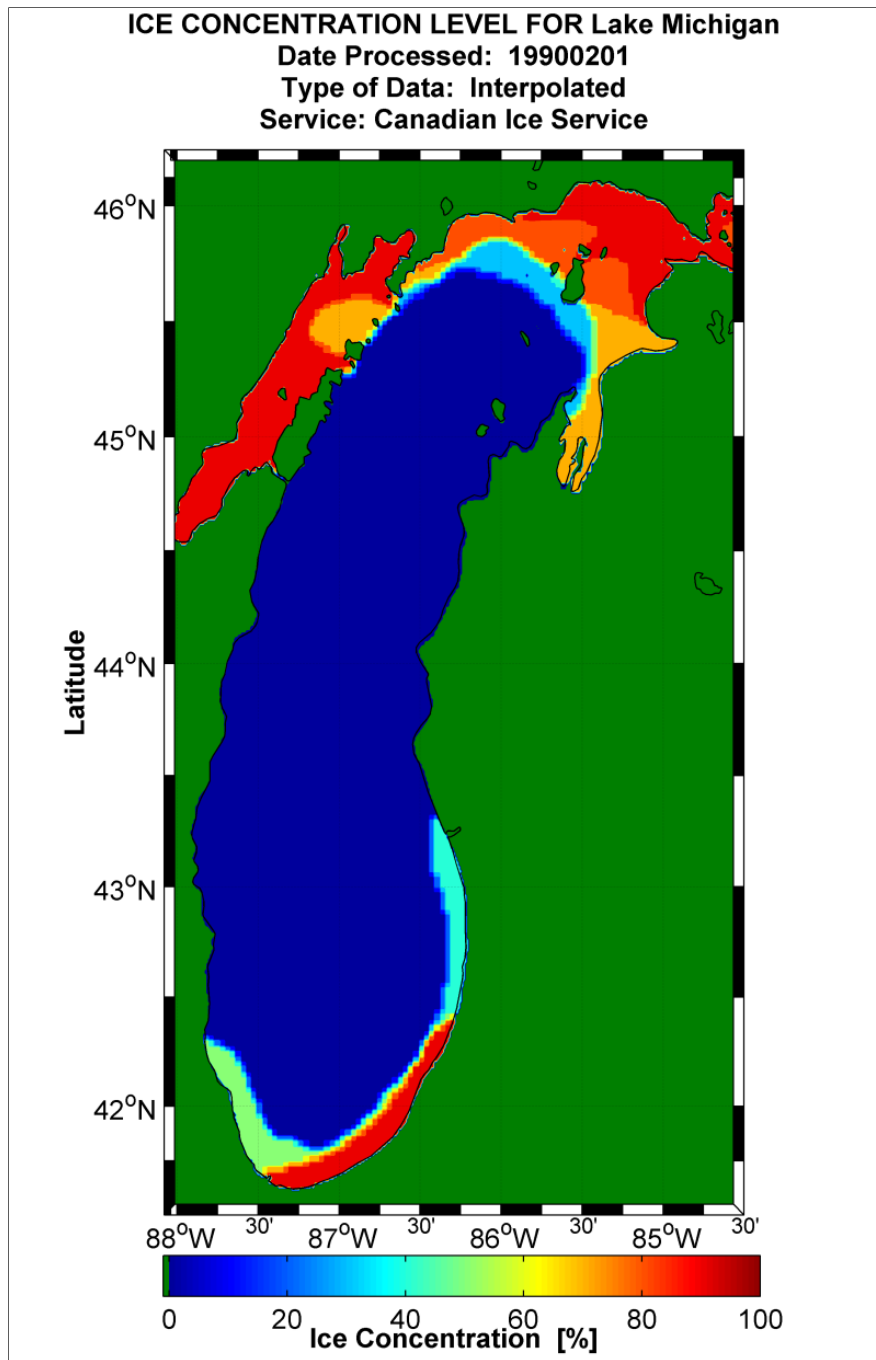


Figure 2-2. Interpolated ice field output for 1 February 1990.

(<http://www.glerl.noaa.gov/data/pgs/ice.html>), they did not exist at that site. These data have not been synthesized, compiled and documented to the extent of the other two ice coverage archives. The intra-annual grid resolution in these recent data can change from about 2.5 km to 1.25 km depending on the year, which can become problematic in the processing to get to a consistent ice cover data set. Lastly, these data are only available in the

original Lambert Conformal-Conical coordinate system, and they lacked two important pieces of information (reference longitude and latitude) to transform the ice cover data onto a fixed longitude latitude grid. An interactive Matlab® routine was built to manually identify registration points in the original Lambert Conformal-Conical grid and map to points in a fixed longitude/latitude spherical coordinate system. This was performed using a minimum of four locations for reference and the quality of the mapping was assessed graphically. At the completion of the process, all water locations were displayed with a high resolution shoreline and the resulting ice cover maps were assessed for quality. This was an iterative process, and quality can become somewhat arbitrary. However, the potential errors in the ice fields applied to either a wave or surge model are relatively small compared to errors in the wind estimates.

2.2.4 Addendum to the ice field evaluation

During the production of the extreme storm events, it was discovered that the 2003 through 2009 ice field archive became available at the National Ice Center (http://www.natice.noaa.gov/products/great_lakes.html). These fields were in various grid resolutions and one was identical to that of the Assel (2005) archive. Only those fields in 2008 through 2009 were of a different grid resolution where a unique transfer function from the Lambert Conformal-Conical grid to spherical coordinate system was determined and source codes modified.

Also during the production runs, additional time paired observation to model results were available and provided valuable information regarding the a priori concentration level threshold of 70-percent used in the WAM simulations to identify ice coverage. This information is summarized in Chapter 6, Lake Michigan Extreme Storm Production.

3 Wave Modeling

3.1 Previous Great Lakes wave hindcasts

Over the past three decades the USACE has performed various wind/wave hindcasts in the Great Lakes as part of the Wave Information Studies (WIS). The initial study by Resio and Vincent (1976) used a technique to derive wind fields from land-based meteorological stations, accounting for differences in the sampling duration, elevation of the anemometer; surface roughness between the land and water; and the air-water stability effects. They also made an assumption that geostrophic winds above the Great Lakes were not significantly different from the land-based measurement sites. Wind fields were subsequently developed using a component-wise weighted sum. The wave model used would be classified as a 2nd generation model solving the energy balance equation incorporating the atmospheric, nonlinear wave-wave interaction, white-capping, and wave-bottom source/sink terms parametrically. In general, the method used by Resio and Vincent (1976a) was limited by available computational resources and by limitations in both meteorological input and wave measurements for verification/validation.

Since that time, various updates of the hindcasts for the Great Lakes have been performed. Hubertz et al (1991) used an increased number of land based meteorological stations (including stations along the Canadian coast), interpolating those point source measurements, converting to a constant sampling duration and reference elevation, compensating for the air-water stability and roughness lengths (i.e. land to water), and ultimately using a weighted inverse distance interpolation routine with an r^{-3} spatial weight function to derive wind fields. The wave model used in this study was an updated version of DWAVE, as summarized in Resio (1981). These studies ran on similarly resolved wave model grid grids (10-statute miles) to compare hindcast wave results to the previous Resio and Vincent results.

The newer WIS Great Lakes updates included ice coverage (Assel 1983) where a 50-percent concentration level or greater was used to set the open water to land. The updated hindcasts also had the luxury of an increased number of point-source wave measurements to perform verification. The updated 32-year hindcast (time periods varied from lake to lake) was documented in a series of WIS Reports (Hubertz et al. 1991; Reinhard et

al. 1991, 1991a; Driver et al. 1991, 1992). Some of the deficiencies of the Great Lakes WIS hindcast were that they considered deep water wave transformation only, with the exception of Lake Erie, and information was saved at locations roughly 10-statute miles (about 16-km) from the shoreline. Many of the connecting bays such as Green Bay and Traverse Bay off of Lake Michigan were not resolved because of the coarse wave model grid resolution that was employed to render the long-term wave hindcast computationally feasible. Several years later Lake Michigan was updated for the 1980-1990 time period using a refined wave model grid, and implementation of a two step Barnes technique (Schwab 1989) for the construction of the wind fields.

In 2003 under direct funding from the USACE Buffalo District, Baird and Associates (2003) were contracted to perform an update for the WIS hindcast in Lake Ontario (40-yr duration, 1961-2000). This study used a consistent land based meteorological data set and the NNM which was new at the time, a 2nd generation wave model similar to the Resio (1981) version, considered ice coverage, and was implemented on a wave model grid having resolution of 3 km. The results from this hindcast study indicated that the NNM was the best method available to generate a consistent set of wind fields to drive a wave model in the Great Lakes. Adjustment of the resulting wind fields was found to be necessary based on wave buoy data and a quantile-quantile analysis of measured and calculated wave conditions. Hindcast wave heights replicated measurements reasonably well for two long-term buoy data sets, however the calculated peak spectral wave period results were positively biased.

These past studies have provided the USACE and others with valuable information for the past two decades or more. However with the advent of more sophisticated 3rd generation (3-G) wave modeling technologies including WAM (Komen et al. 1994), WAVEWATCH III (Tolman and Chalikov 1994), and SWAN (Ris, R.C. 1997) there is an opportunity to improve upon past work. These types of models are presently used at most all of the world's Weather Prediction Centers.

3.2 Wave modeling approach

To rectify some of the short-comings in previous hindcasts, new high-resolution wave model grids were generated from GLERL digital bathymetry database sets for Lake Michigan. The resolution of these bathymetry data sets is three arc seconds (about 90 m). A sensitivity study was

performed to determine the optimal wave model grid resolution and optimal directional resolution, defined by considering the computational requirements versus the value-added of the higher resolution wave modeling. Sensitivity to the two different wind and atmospheric pressure input sources, NNM and CFSR, were also examined.

Validation of the wave model results is critical to the success of this project. At the present time there are two operational NOAA/NDBC buoys in Lake Michigan. The starting date of these data sets varies from 1979 to 1981. Two other buoys were deployed for limited time periods, one just offshore of Milwaukee, WI and the second offshore of South Haven, MI. All four locations were utilized to validate the wave modeling of severe storm events done in this study. Unfortunately these assets are removed each year in the late fall and re-deployed in early spring to minimize damage due to icing of Lake Michigan. Hence, any storm simulation from late October through April will generally have either no data or a limited amount of data for validation.

In addition to these measurements, there were two pressure gages deployed seaward of Chicago and Burns Harbors by the USACE for limited periods of time. NOAA/GLERL has been involved in field programs with other organizations measuring wind-generated waves. A wave buoy and a coastal wave gage have been in operation by Dr. Guy Meadows (University of Michigan) in Traverse Bay for the past two to three years.

3.3 WAM wave model

The specification of the wave modeling approach is as critical to an extreme storm study as the external forcing functions namely the winds and ice coverage. Selection of the wave model approach must meet these requirements:

- Quantification of the temporal and spatial variation of the two-dimensional wave spectra.
- Complete source term specification of the atmospheric input, nonlinear wave-wave interaction, wave dissipation in the form of white-capping.
- Shallow water mechanisms, refraction, shoaling, wave-bottom effects and depth-induced wave breaking.
- Time and spatial varying specification of wind and ice fields.

As previously discussed, there are a number of wave modeling technologies that could be selected for the Lake Michigan study. Because of general improvements made in 3-G wave models over the past two decades, recent successes in wave modeling of extreme storm events done using WAM in support of USACE Gulf of Mexico projects and in FEMA flood risk map updates (Bunya, et al. 2010) in the Gulf, implementation of temporal and spatial ice maps in the WAM model (Jensen et al. 2002) and successful application of this model to simulate rapidly moving severe storm systems along the coast of Alaska and the Bering and Chukchi Seas, in light of extensive favorable comparisons between wave model results and measurements in these project applications, and in light of documented evidence of WAM's performance in Lake Michigan (Lui et al. 2002), WAM Cycle 4.5.1C was selected for this work. A brief summary of the theoretical description of the model is provided below.

3.3.1 WAM Cycle 4.5.1C description

WAM is classified as a third generation wave model, where the most important modification to previous spectral wave models is that:

There are no a priori assumptions governing the shape of the spectrum in frequency or direction.

The number of degrees of freedom between the source terms is consistent with the directional wave spectrum. The source/sink mechanisms are solved in the discrete frequency and direction space for which the wave model spectrum is defined.

This model solves the action balance equation for the time rate change of directional wave spectra over a fixed grid.

$$\frac{DN(\vec{x}, t, f, \theta)}{Dt} = \sum_i S_i \quad (3-1)$$

where $N(\vec{x}, t, f, \theta)$ is the wave action and equal to $E(\vec{x}, t, f, \theta)/\omega$ where E is the directional wave energy spectrum in frequency (f) and direction (θ), and ω is the radial frequency. S_i represents the source sink mechanisms:

$$\sum_i S_i = S_{in} + S_{nl} + S_{nl} + S_{ds} + S_{w-b} + S_b \quad (3-2)$$

and S_{in} is the atmospheric source term, S_{nl} is the nonlinear wave-wave interaction, S_{ds} is the high frequency dissipation, S_{w-b} is the sink mechanism for bottom effects and S_b is the sink mechanism for depth limited wave breaking.

The solution to the temporal and spatial variation of the wave climate is performed in two parts. The first is to solve for the spatial change in action density, i.e., the second term on the right hand side of the equation below:

$$\frac{DN(\vec{x},t,f,\theta)}{Dt} = \left\{ \frac{\partial}{\partial t} + \vec{c}_g \cdot \frac{\partial}{\partial \vec{x}} \right\} N(\vec{x},t,f,\theta) \quad (3-3)$$

where \vec{c}_g is the group speed of the wave component defined at each frequency and is functionally related to the water depth based on the linear dispersion:

$$\omega^2 = g\kappa\tanh(\kappa h) \quad (3-4)$$

and ω is the radial frequency ($\omega=2\pi f$), h is the water depth and κ is the wave number ($\kappa=2\pi/L$, where L is the wavelength defined at frequency f , and dependent on the water depth). This is the propagation step.

Once the spectra are updated from propagation over the fixed grid, the source term integration, $\partial N / \partial t$ is computed. The computational burden on this second step is generally an order of magnitude greater compared to the propagation step, and also to second-generation wave-modeling technologies. The source term integration involves the computation of the source terms in discrete frequency and direction space; whereas, second generation models generally use bulk parameterizations of these mechanisms, reducing computational requirements often at the expense in the accurate specification of the resulting directional wave spectra.

Implementation of ice coverage effects occurs after the source term integration. This is performed using a land-water mask, thus zeroing out the energy at any location defined as ice (or “land”). When the ice points return to open water points, wind wave growth commences from a zero-sea state. If the surrounding area has remained as open water the energy quickly spills into this newly created open water domain. There may be some slight phasing errors in this approach dictated by relaxation times of the physical process; however, there is insufficient data to suggest and validate better alternatives.

One difference between the current WAM version and older versions can be classified as cosmetic, where Cycle 4.5.1C is written in Fortran 90 whereas its predecessor version is written in Fortran 77. There were only minor differences between the versions of WAM used in the Alaska wave hind-casting projects compared to that version used in this current study. These modifications corrected small deficiencies, such as a time and spatially dependent limiter (Tolman, 2002), and implementation of more robust numerical stability requirements dictated by the water depth and geographical location. In addition, recent work in the simulation of hurricane-generated wave conditions suggested spatial growth rates were over-estimated using the older version of WAM (Jensen et al. 2006). To limit wave growth for winds in excess of 36-m/sec, the drag coefficient was capped at this value. Comparisons have indicated that these modifications incorporated in the newer version of WAM produce differences of less than five percent in wave results.

3.3.2 Model domain

Lake Michigan can be described as a very diverse model domain (see Figure 3-1). In it there are very deep water regions (from a waves perspective), bordered by steep slopes with no appreciable shelf characteristics. Only in the southwestern corner of Lake Michigan does a shelf with slowly varying slope exist. Green Bay contains slowly varying bottom topographic features and water depths of 20 m or less, generally. Grand Traverse Bay is dominated by deep water and steep slopes. In the context of wave modeling, deep water will dominate the growth, propagation and source/sink specification. However, in the near coastal area, shallow-water will control all wave related processes.

3.3.3 Bathymetry and grid resolution

The WAM wave model bathymetry grid was derived from the NOAA/NESDIS “Bathymetry of Lake Michigan,” (<http://www.ngdc.noaa.gov/mgg/greatlakes/michigan.html>). The original bathymetry data were at a 3-arc-second resolution. The WAM bathymetric grid was derived via bi-linear interpolation of the final surge model unstructured grid system to the fixed longitude/latitude spherical grid system WAM uses, to ensure consistency between wave and surge model grids. An initial wave model grid (see Table 3-1) was set with a resolution of 0.01 deg (36 sec, or approximately 1,111 m). This grid provided extremely good representations of the offshore islands, strong bathymetric gradients, and the coastline.

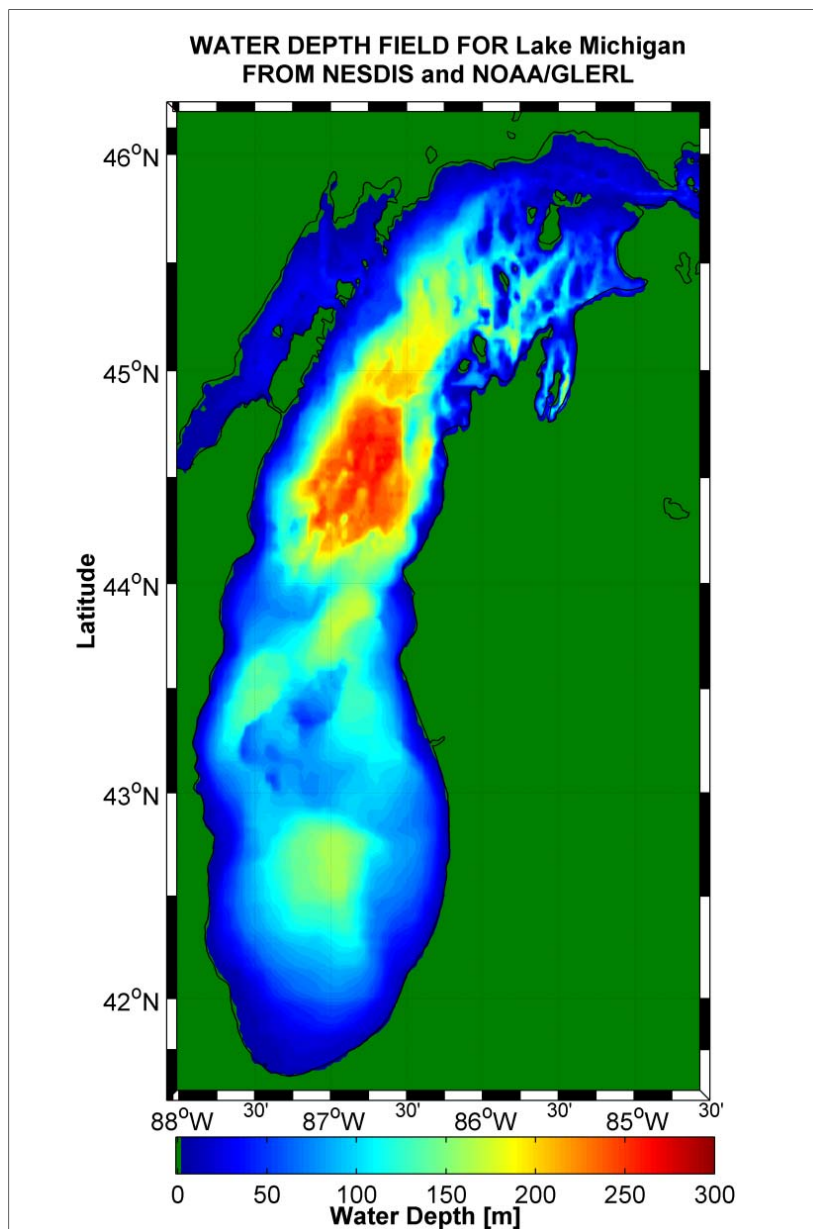


Figure 3-1. Domain and bathymetry for the Lake Michigan WAM model.

Table 3-1. Grid and model characteristics.

Grid Name	Geographical Bounds				Res (deg)	Model Resolutions		Time-Steps (sec)		
	Longitude		Latitude			freq(0)	$\Delta\theta$ (deg)	Δ_{PROP}	Δ_{SOURCE}	
	West	East	North	South						
Version 1	-88.08	-84.50	46.24	41.50	0.01	0.06116	15	40	300	
Version 1D	-88.08	-84.50	46.24	41.50	0.01	0.06116	5	40	300	
Version 2	-88.08	-84.50	46.24	41.50	0.02	0.06116	15	120	300	
Version 2D	-88.08	-84.50	46.24	41.50	0.02	0.06116	5	60	300	

3.3.4 Frequency resolution

All wave models separate the frequency domain into two distinct regions, the discrete region, and the parametric region. The discrete region considers the energy contained in each frequency band in the propagation and source/sink term calculations. The parametric region is defined as the entire energy contained in the spectrum from the last frequency band to some finite limit in frequency space, i.e. the remaining energy outside the discrete frequency range. This approach is used to minimize computational loads and decrease memory requirements. In general, the parametric region accounts for the initial energy formed during wind-wave growth, based on scaling of the winds to the waves, with the assumption that wave direction is fixed to be the direction of the local winds.

Lake Michigan can be considered nearly an enclosed body of water. The waves generated in this domain are for the most part short-period waves compared to that of, for example, the Atlantic Ocean. Hence, the active frequency domain needs to be adjusted for these conditions. Based on the nearly 30-yr records of NOAA's two NDBC buoys, the frequency range was set for WAM. The discrete frequency bands are defined as:

$$f(n+1) = 1.1 * f(n) \dots \text{where } n = 1, NFRE \quad (3-5)$$

The starting frequency band is set at 0.06116 Hz which corresponds to the longest wave period considered, 16.5 sec ($T = 1/f$). Setting the starting frequency band to this low value will assure there is a reasonable lower limit for frequency downshifting during an extreme storm event. That discrete frequency range limit also needs to be consistent with the required range in WAM to assure the Discrete Interaction Approximation (nonlinear wave-wave interaction source) is properly defined. Lastly, to minimize the approximations for initial wind-wave growth, the number of discrete frequency bands (NFRE) is set to 28, and the last frequency is set equal to 0.8018 Hz or a wave period of approximately 1.2 sec. Neither WAM nor any other discrete spectral wave model was developed to accurately estimate wind-generated wave conditions down to 1.2 sec. However, the relaxation time for initial wind-wave growth is relatively short (on the order of minutes) and the amount of energy contained in these higher frequency bands will be, at their maximum, an order of magnitude less than that contained at the spectral peak. Selection of this high frequency limit reduces the approximations made in the parametric region of the estimated

spectrum, minimizing most sources of error, and does not increase computational loads inordinately.

3.3.5 Directional resolution

Table 3-1 identifies two different directional resolutions (5 deg and 15 deg) and two different grid mesh resolutions (0.01 deg and 0.02 deg) that were considered in the wave modeling. Tests were conducted to determine the optimal combination that provided consistent results, balanced by the computational load for storm simulations. The wave model grid resolutions and the starting frequency and direction resolution were determined from buoy data and evaluated using results from initial wind-wave growth tests.

3.4 Initial wind-wave growth tests: Constant winds

Prior to any storm simulations, testing was performed with WAM to assure the model remained stable, to tune the propagation time-step, and to determine the most optimal settings of grid and directional resolutions and the frequency domain. Simple growth tests using uniform winds set to 20 m/sec for eight different directions were performed. The simulations were made for a 24-hr duration. The directions adopted in these tests were the eight primary compass directions (North, Northeast, East, Southeast, South, Southwest, West and Northwest). Not only did these tests determine the optimal settings, but they also provided a basis for determining the relaxation timing for the source term specification, and more importantly how long it took for fully developed wave conditions (Pierson and Moskowitz 1964) to be attained.

From the initial testing it was determined there were very limited differences between the 0.02- and 0.01-deg grid resolution results. At most these differences were on the order of 1- to 5-percent for the maximum wave height conditions that were calculated (approximately 6 m to 6.5 m). Selecting the 0.02-deg grid reduced the computational load by a factor of eight. Based on this test result a decision was made to run all subsequent WAM simulations on the 0.02-deg grid. The results for these growth rate tests are provided in Table 3-2.

WAM oscillates slightly during the growth sequence. This is not entirely unexpected, especially during the initial sequences. Despite attempts to start the domain at near zero conditions, there is always a small energy field observed at the first time-step (presetting the wave field for the first

Table 3-2. Growth tests for constant winds of 20 m/sec.

Direction Test	Maximum Wave Height Snapshot (m)			Max Wave Height (m)
	06	12	24	
North	6.65	6.54	6.58	6.59
Northeast	5.46	5.95	5.97	5.97
East	5.11	5.11	5.11	5.25
Southeast	5.58	5.52	5.48	5.61
South	5.72	6.62	6.62	6.62
Southwest	5.47	5.83	5.83	5.86
West	5.06	5.08	5.08	5.29
Northwest	5.50	5.37	5.36	5.52

time-step). This energy propagates through the domain, eventually dissipating. The East and West constant wind tests reached their wave energy saturation levels very quickly. This occurs roughly 3-hr after the simulation starts. For most other directions saturated conditions were reached within 6-hr and within 12 hr for the Northeast and Southwest wind conditions. Once saturation is reached, as shown in Table 3-2, wave conditions remain relatively constant (at the maximum wave height) for the duration of the 24-hour simulation.

There were appreciable differences between the two sets of directional resolution results. These differences grew as the simulation progressed, and amounted to approximately a 20-percent difference in the significant wave height field in certain areas of the domain. Regions in a down-wave direction from offshore islands, and capes (especially along the eastern Lake Michigan shoreline) were most affected. One example is shown in Figure 3-2, where simple differences between the 5-deg and 15-deg directional resolution WAM simulations are plotted. Red contours indicate regions where 5-deg results are larger than 15-deg results. Blue contours indicate regions where 15-deg results are larger than 5-deg results. The snap-shot shown in the figure is taken at the 24th hour of the simulation. Based on these results, and others from the constant wind tests, a 5-deg directional resolution was selected and used in all subsequent wave model simulations.

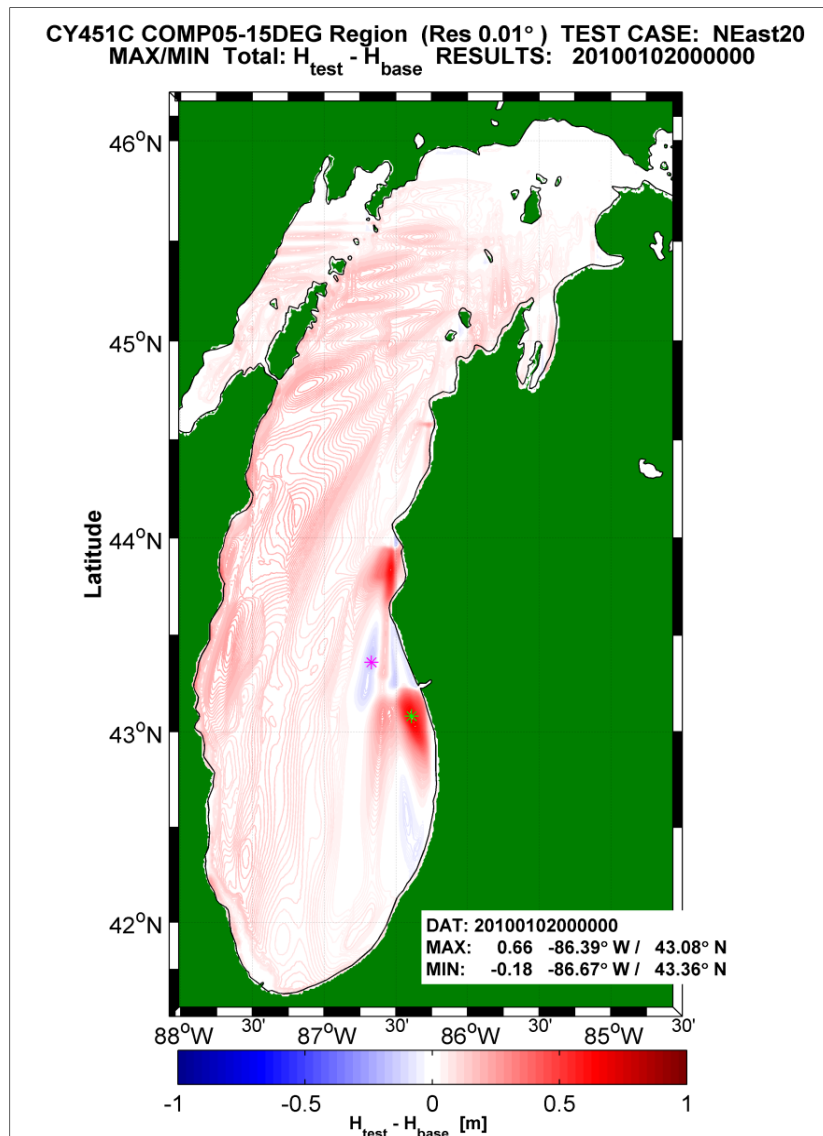


Figure 3-2. Difference between 5-deg and 15-deg directional resolutions for the Northeasterly wind wave growth test.

3.5 Point-source wave measurements for model validation

To assure a level of quality in any model result, validation is required. Valuable long-term non-directional and directional wave measurements have been made at two established locations in Lake Michigan. NDBC buoys 45002 and 45007 have been in operation for nearly 30-years (see Table 3-3). Those buoys are pulled out of the water generally in the late fall season, and re-deployed in the early spring. In addition to these buoys, two other short-term NDBC deployments were made in Lake Michigan. There are two buoy locations (45007 and 45010) that estimate the directional properties of the wave climate. The Great Lakes Observing System Program (GLOS) deployed

Table 3-3. Available wave measurements.

Buoy	Location		Water Depth (m)	Data Availability		Description
	Longitude	Latitude		Start Date	End Date	
45002	-86.411*	45.344*	181.0*	19800506	Present	Directional 2008-Present
45007	-87.027*	42.674*	160.0*	19810715	Present	Directional 1992-Present
45010	-87.833"	43.000*	18.0*	19930626	19951113	Directional
45011	-86.275	43.025	17.1	19970813	19971124	Nondirectional
45020	-85.6044	44.7889	NaN	2009052900	2009121300	Directional
45021	-85.4931	45.0481	NaN	2009041900	2009103100	Directional
45022	-85.0878	45.4031	NaN	2009072300	Present	Directional
Chicago IL001	-87.570	41.920	10.0	19911001	20040101	Nondirectional
Burns IN1	-87.182	41.647	13.0	20010501	20050801	Nondirectional

*Station information from 2009. Both buoys change location on a yearly basis

three directional buoys during the open water season of 2009. Two shallow water wave gages were deployed by the USACE seaward of Chicago and Burns Harbors. The wave gages at Burns and Chicago Harbor were deployed during the winter months. Figure 3-3 displays the locations of the point source wave measurements¹.

All NDBC buoy data were recovered from NOAA's National Oceanographic Data Center (<http://www.nodc.noaa.gov/BUOY/buoy.html>), in various standard archive formats. The original data, the frequency spectra and directional estimators ($a_1, a_2, r_1, r_2, C_{11}$) comparable to the 5-fourier coefficients, were decoded and synthesized. These estimators are used to define the directional distribution and directional wave spectrum using the Maximum Likelihood Method. This assures consistency between integrated wave parameter analyses. Downloading integral wave parameter data directly from the NDBC site will restrict any analysis to the definitions used by NDBC. In addition, it has been found that the NDBC and NODC data sets differ. Because the NODC site is the OFFICIAL NOAA archive center, those data are the correct set for any use in model validation.

Despite missing, on an annual basis, about five of the twelve months each year, the archive database contains valuable information; not only to

¹ Yearly wave height time plots for the NDBC and other wave measurements are provided in Appendix 7-1A.

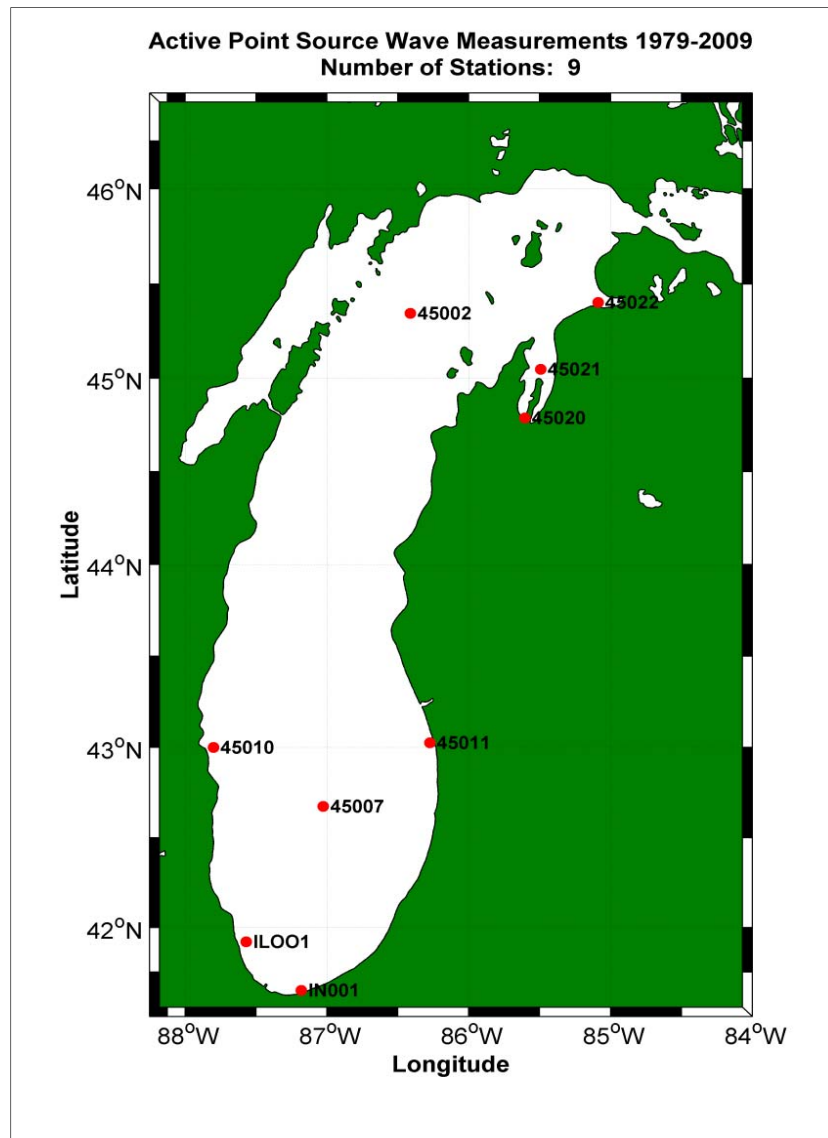


Figure 3-3. Active point-source wave measurement sites in Lake Michigan.

evaluate WAM model performance for a given storm simulation, but also as previously noted, to provide information for frequency domain specification and to promote enhanced understanding of what severe storms can produce in terms of wave conditions. Tables 3-4 through 3-7 provide information regarding the top events found in the NDBC station 45002, 45007, 45010 and 45011 data records, respectively. Note that the short deployment cycles for buoys 45010 (three open water seasons) and 45011 (only one open water season) will not adequately define any long-term climatologic information. However, these data provide additional valuable spatial coverage for evaluating model predictive skill and are complimentary to the longer-running buoys at 45002 and 45007, which have been deployed routinely for nearly 30 years.

Table 3-4. NDBC 45002 extreme wave conditions list.

RANK	STORM DURATION		PEAK CONDITIONS OF STORM			
	START	END	DATE	H _{mo}	T _p	θ _{MEAN}
1	1991110202	1991110317	1991220307	5.9	10.81	NaN
2	1991012220	1991012312	1991012304	5.6	10.29	NaN
3	1995101716	1995101805	1995101720	5.3	9.60	NaN
4	1993093021	1993100117	1993100111	5.2	9.29	NaN
5	2001102817	2001102908	2001102900	5.0	9.11	NaN
6	2001102508	2001102612	2001102521	4.8	9.53	NaN
7	1989012119	1989012210	1989012202	4.8	9.72	NaN
8	1988102720	1988102815	1988102723	4.8	9.05	NaN
9	1995111002	1995111017	1995111010	4.6	9.36	NaN
10	1994102720	1994102909	1994102820	4.6	8.60	NaN
11	1990120312	1990120408	1990120322	4.6	8.11	NaN
12	2008101917	2008102004	2008101923	4.5	8.84	198.5
13	2002110719	2002110807	2002110723	4.5	8.48	NaN
14	1991110519	1991110610	1991110602	4.5	9.45	NaN
15	1990112014	1990120107	1990113021	4.5	8.95	NaN
16	1984112211	1984112304	1984112217	4.5	8.31	NaN
17	1983112403	1983112501	1983112407	4.5	8.63	NaN
18	1983041421	1983041509	1983041504	4.5	9.27	NaN
19	2001101017	2001101108	2001101102	4.4	8.37	NaN
20	1985100810	1985100900	1985100817	4.4	8.85	NaN
21	1984101916	1984102009	1984101921	4.4	8.65	NaN
22	2006101301	2006101323	2006101315	4.3	8.97	NaN
23	1993102019	1993102900	1993102819	4.3	9.08	NaN
24	1998101804	1998101819	1998101809	4.2	9.01	NaN
25	1993102811	1993102817	1993102815	4.2	8.50	NaN
26	1991120700	1991120709	1991120704	4.2	8.75	NaN
27	2004111002	2004111014	2004111009	4.1	8.97	NaN
28	2002040712	2002040804	2002040715	4.1	7.73	NaN
29	1995110601	1995110702	1995110619	4.1	8.84	NaN
30	1994100718	1994100805	1994100801	4.1	8.11	NaN
31	1989111610	1989111622	1989111617	4.1	7.16	NaN
32	1988103116	1988110102	1988103120	4.1	8.34	NaN
33	1986103112	1986110200	1986103118	4.1	8.68	NaN
34	1983112023	1983112121	1983112113	4.1	8.28	NaN
35	1983102719	1983102804	1983102800	4.1	8.14	NaN
EVENTS: H _{mo} > 2.63-m MEAN : 0.75-m VARIANCE: 0.47-m			NOTE: NaN (No Directional Wave Data)			

Table 3-5. NDBC 45007 extreme wave conditions list.

RANK	STORM DURATION		PEAK CONDITIONS OF STORM			
	START	END	DATE	H _{mo}	T _p	θ _{MEAN}
1	1998111010	1998111119	1998111104	6.2	9.39	213.2
2	1989092302	1989092319	1989092306	5.6	9.79	NaN
3	2005112307	2005112510	2005112413	5.3	10.22	354.3
4	1983111013	1983111202	1983111119	5.3	9.66	NaN
5	2001092401	2001092601	2001092403	5.2	9.61	359.2
6	2000040808	2000040821	2000040809	5.2	9.72	352.6
7	1995111105	1995111111	1995111111	5.2	9.58	1.7
8	1992032709	1992032721	1992032709	5.1	9.59	356.8
9	1992032705	1992032707	1992032707	5.1	8.82	350.4
10	1995111115	1995111117	1995111115	5.0	9.92	355.6
11	1982040313	1982040402	1982040316	4.9	8.47	NaN
12	2005042504	2005042422	2005042307	4.8	8.98	352.4
13	1999102210	1999102408	1999102317	4.8	9.77	0.4
14	1987100212	1987100312	1987100300	4.8	9.64	NaN
15	1984043011	1984043021	1984043013	4.8	8.41	NaN
16	1981112000	1981112111	1981112009	4.8	9.07	NaN
17	2003111307	2003111317	2003111307	4.7	8.79	316.9
18	1982040404	1982040420	1982040406	4.7	8.01	NaN
19	2003111223	2003111305	2003111303	4.6	7.69	272.2
20	2000040806	2000040806	2000040806	4.6	8.98	353.3
21	2001102505	2001102711	2001102521	4.5	8.04	238.5
22	1997040620	1997040715	1997040700	4.5	7.96	220.8
23	1981100119	1981100220	1981100208	4.5	8.91	NaN
24	2006040314	2006040321	2006040315	4.4	7.94	331.1
25	2004040402	2004040413	2004040405	4.4	9.14	354.9
26	1988090501	1988090516	1988090506	4.4	9.65	NaN
27	2007110520	2007110704	2007110618	4.3	8.63	344.7
28	2000042108	2000042122	2000042113	4.3	8.92	351.1
29	1997050108	1997050118	1997050110	4.3	8.85	337.6
30	2005111605	2005111705	2005111607	4.2	8.24	222.2
31	2005092903	2005092915	2005092906	4.2	8.20	345.9
32	2002032112	2002032201	2002032115	4.2	8.90	352.2
33	2006051113	2006051209	2006051123	4.1	10.02	352.6
34	2002113012	2002113009	2002113015	4.1	8.29	339.6
35	2001041712	2001041800	2001041715	4.1	8.62	1.8
EVENTS: H _{mo} > 2.47-m MEAN : 0.68-m VARIANCE: 0.45-m			NOTE: NaN (No Directional Wave Data)			

Table 3-6. NDBC 45010 extreme wave conditions list.

RANK	STORM DURATION		PEAK CONDITIONS OF STORM			
	START	END	DATE	H _{mo}	T _P	θ _{MEAN}
1	1995090713	1995090813	1995090718	3.8	8.67	22.8
2	1993100900	1993101003	1993100911	3.4	8.90	19.5
3	1995111103	1995111209	1995111110	3.3	8.35	24.4
4	1994080421	1994080516	1994080504	2.8	8.04	21.4
5	1995110918	1995111009	1995110921	2.5	7.10	144.7
6	1994052614	1994052701	1994052616	2.5	7.06	18.3
7	1994060802	1994060811	1994060805	2.4	5.98	23.6
8	1994110601	1994110619	1994110607	2.2	5.89	27.6
9	1993110518	1993110616	1993110522	2.2	8.32	17.1
10	1993103018	1993110102	1993103023	2.2	6.82	15.7
11	1995100513	1995100618	1995100517	2.1	6.19	76.6
12	1993101706	1993101720	1993101712	2.1	6.18	9.7
13	1994110102	1994110122	1994110103	2.0	5.30	29.6
14	1994100112	1994100208	1994100115	1.9	6.28	29.9
15	1993093022	1993100105	1993100102	1.9	6.15	147.8
16	1993092007	1993092100	1993092017	1.9	6.82	103.9
17	1993082105	1993082111	1993082105	1.9	6.62	23.5
18	1995091708	1995091800	1995091711	1.8	6.22	18.0
19	1994080904	1994080916	1994080908	1.8	6.62	23.3
20	1993063013	1993063018	1993063013	1.8	6.11	123.6
21	1995092017	1995092105	1995092100	1.7	6.41	17.4
22	1995091004	1995091008	1995091006	1.7	5.94	36.0
23	1995082507	1995082516	1995082510	1.7	5.37	85.3
24	1994110915	1994111000	1994110917	1.7	5.58	45.3
25	1994092610	1994092614	1994092612	1.7	7.25	10.5
26	1994062407	1994062420	1994062413	1.7	4.95	26.4
27	1995102400	1995102401	1995102401	1.6	5.91	147.8
28	1995101716	1995101719	1995101717	1.6	5.96	148.7
29	1995092114	1995092118	1995092115	1.6	5.89	14.1
30	1995082412	1995082415	1995082413	1.6	5.62	34.8
31	1995050907	1995050911	1995050909	1.6	6.29	110.6
32	1994071313	1994071315	1994071313	1.6	5.62	8.9
33	1993063011	1993063011	1993063011	1.6	4.84	123.3
34	1995102322	1995102322	1995102322	1.5	5.55	145.4
35	1995092108	1995092112	1995092111	1.5	5.58	12.1
EVENTS: H _{mo} > 1.35-m						
MEAN : 0.47-m						
VARIANCE: 0.22-m						

Table 3-7. NDBC 45011 extreme wave conditions list.

RANK	STORM DURATION		PEAK CONDITIONS OF STORM			
	START	END	DATE	H _{mo}	T _P	θ _{MEAN}
1	1997092003	1997093013	19997093007	3.20	7.54	NaN
2	1997111712	1997111712	1997111712	2.50	7.01	NaN
3	1997092917	1997092917	1997092917	2.50	7.18	NaN
EVENTS: H _{mo} > 2.47-m MEAN : 0.68-m VARIANCE: 0.45-m			NOTE: NaN (No Directional Wave Data) NOTE2: ONE OPEN WATER SEASON			

It is not surprising to see little or no correlation between the top 10 storm producing wave events at the northern (45002) and the southern (45007) locations. Generally speaking, winds from the south will produce the highest wave conditions at the northern locations and winds from the north will produce the highest wave conditions at the south locations. The top events for 45002 occur primarily in the September to January period (most often in October and November). At buoy 45007 the largest events occur in the September to May period, with a larger percentage of the largest events occurring in the springtime. Interestingly, the top wave producing event at 45007 (6.2-m significant wave height) was actually a very small localized meteorological system that started along the southern end of Lake Michigan and had very strong south-southwesterly sustained winds in excess of 20 m/sec. A few of the other higher-energy wave events at this location also were generated by winds blowing from the southwest.

Most of the extreme events at buoy 45007 were created by strong winds blowing from the north. The top event at 45002 (5.9-m significant wave height) was produced by south-southwesterly sustained winds of 10-15 m/sec for nearly 24 hours. Peak wave periods associated with extreme wave conditions at buoys 45002 and 45007, in which wave heights exceed 4 m, are generally in the 8 to 10 sec range.

3.6 Storm event simulations

A series of extreme storm events were selected for model validation based on analysis of water level and wave data at selected sites around Lake Michigan. Storms that produced unusually high water levels at one or more sites around the periphery of Lake Michigan were selected, as were storms that produced high wave conditions. The selected storms are listed in Table 3-8. Locations shown in the table indicate NOAA water level gage sites where the event produced a maximum water level which ranked

Table 3-8. List of extreme events, locations and times.

RUN	DATE	LOCATION	Start Date	End Date	WAVES (m) / RANK			
					45002	45007	45010	45011
1	1990 12 03	Green Bay Milwaukee Holland	1990112700	1990120600	4.6	N/A	N/A	N/A
2	1989 09 23	Calumet	1989091500	1989093000	3.0	5.1	N/A	N/A
3	1992 11 02	Kewaunee Sturgeon Ludington Port Inland	1992102200 1992102800	1985110700	3.2 Peaks	4.0	N/A	N/A
4	1985 03 04	Milwaukee Kewaunee Sturgeon Ludington Port Inland	1985022200	1985031500	N/A	N/A	N/A	N/A
5	2009 12 09	Green Bay Holland	2009113000	2009121000	N/A	N/A	N/A	N/A
6W	1993	Wave Event	1993092500	1993102000	5.2 (4)	4.0 (38)	3.4 (2)	N/A
7	1998 05 31	Calumet	19980521	19980602	3.0	3.0	N/A	N/A

among the top 20 events at that site. Also noted in Table 3-8 are the availability of measured wave conditions, the measured maximum significant wave heights for the event, and the starting and ending time for each event simulation.

It is important to note that only the wind-generated surface gravity wave evaluation is documented in this section of the report. This evaluation also will cover the evaluation of winds because of strong dependency of winds and waves. Simulation of water levels for these events is discussed later.

Originally the storm simulations were to use the NNM wind and pressure fields. Preliminary evaluations revealed that NNM forcing generally resulted in underestimates of the storm peak wave conditions. An alternative source of wind and pressure fields became available midway during the study, the NCEP/CFSR product. The CFSR wind and pressure fields for the seven storms were acquired, processed and modeling was repeated. Results using both the NNM and CFSR wind and pressure fields will be presented throughout this section.

3.6.1 December 1990 storm

The first storm studied was the 3-4 December 1990 event that produced the largest recorded water level in the lake, at the Green Bay gage site which is located at the southern tip of Green Bay. This storm system tracked from southwest to northeast and the storm center passed directly over the southern tip of Lake Michigan. Wind and pressure fields were generated with the NNM using data from 20 land stations surrounding Lake Michigan. The input land station data were temporally smoothed (1:1:1) as part of the preprocessing prior to the generation of the fields. As shown in Figure 3-4 the northwestern corner of the Lake Michigan does not include any meteorological station information. This could potential influence the quality of the NNM field estimates in this region. Despite NDBC 45002 still being active during this period, the wind speed and direction data were not available. There were two primary peak storm wave conditions during this simulation. The largest recorded wave height was 4.6 m late on 3 December 1990 at Buoy 45002. There was no ice coverage in Lake Michigan (based on Assel 2005).

One of the quality assessment metrics used for this study was to generate maximum wind speed and wave height envelopes. This graphical product is generated by interrogating the variable wind speed or wave height at each grid location, through time, and saving the maximum value for the storm simulation at each grid cell. The maximum wind speed envelope results for Storm 1 using NNM and the CFSR are shown in Figures 3-5 and 3-6, respectively, followed by the maximum wave height envelopes in Figures 3-7 and 3-8. Note that the color contouring/scaling is slightly different between the NNM and the CFSR results.

There are significant differences between the NNM and CFSR maximum wind speed envelopes. The most dramatic difference is that the NNM establishes a maximum lobe of wind speeds (~20 m/sec and greater) in the southern portion of the lake. There is a clearly defined positive gradient in those wind speeds from south to north (high speed to low speed) shown clearly by the color contours. There is a small lobe of 17 m/sec winds west of the Mackinaw Straits in the northern portion of the Lake. In Green Bay, the winds appear to be relatively constant at around 16 to 17 m/sec, and varying spatially (increasing slightly from north to south).

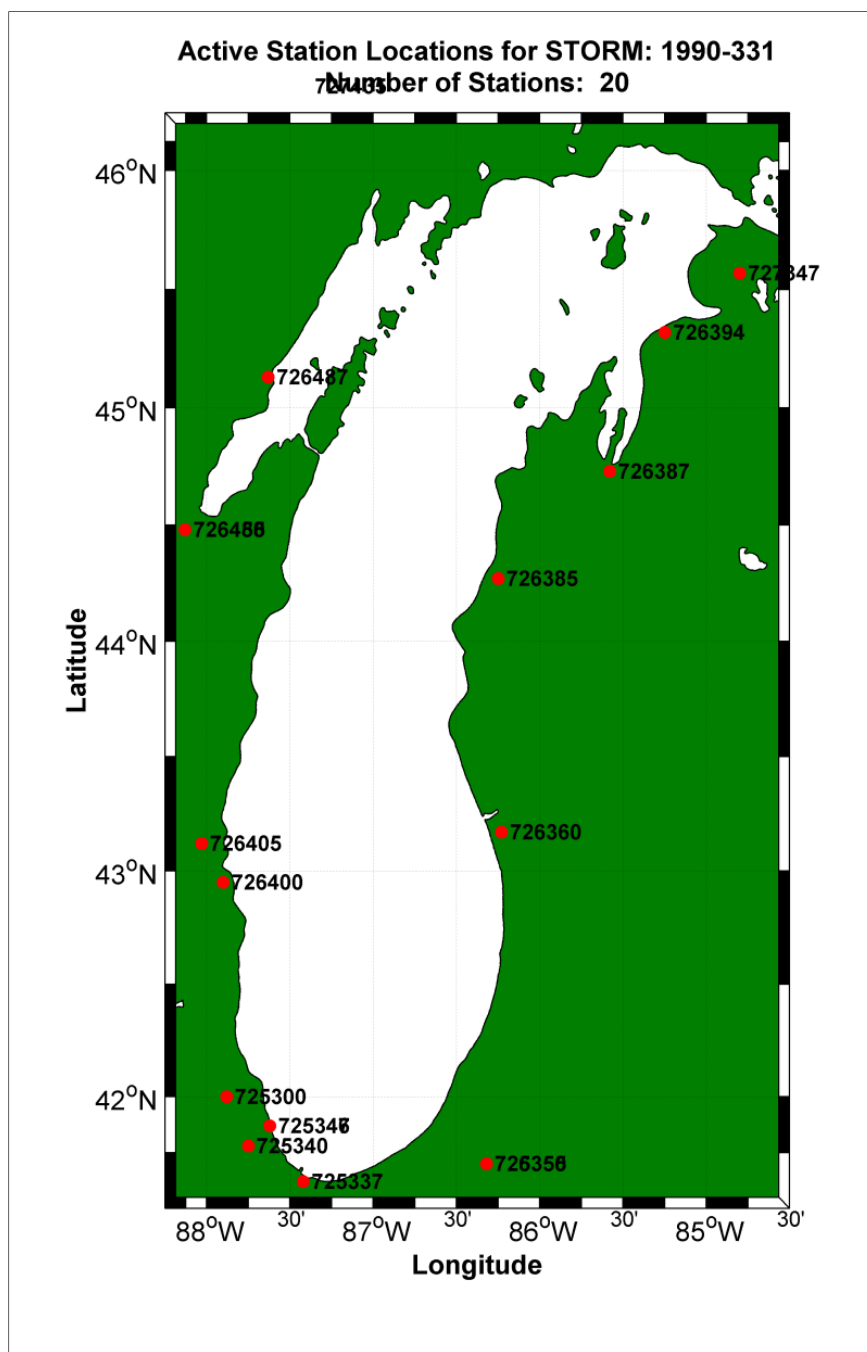


Figure 3-4. Available meteorological station locations accessed and preprocessed for the December 1990 storm.

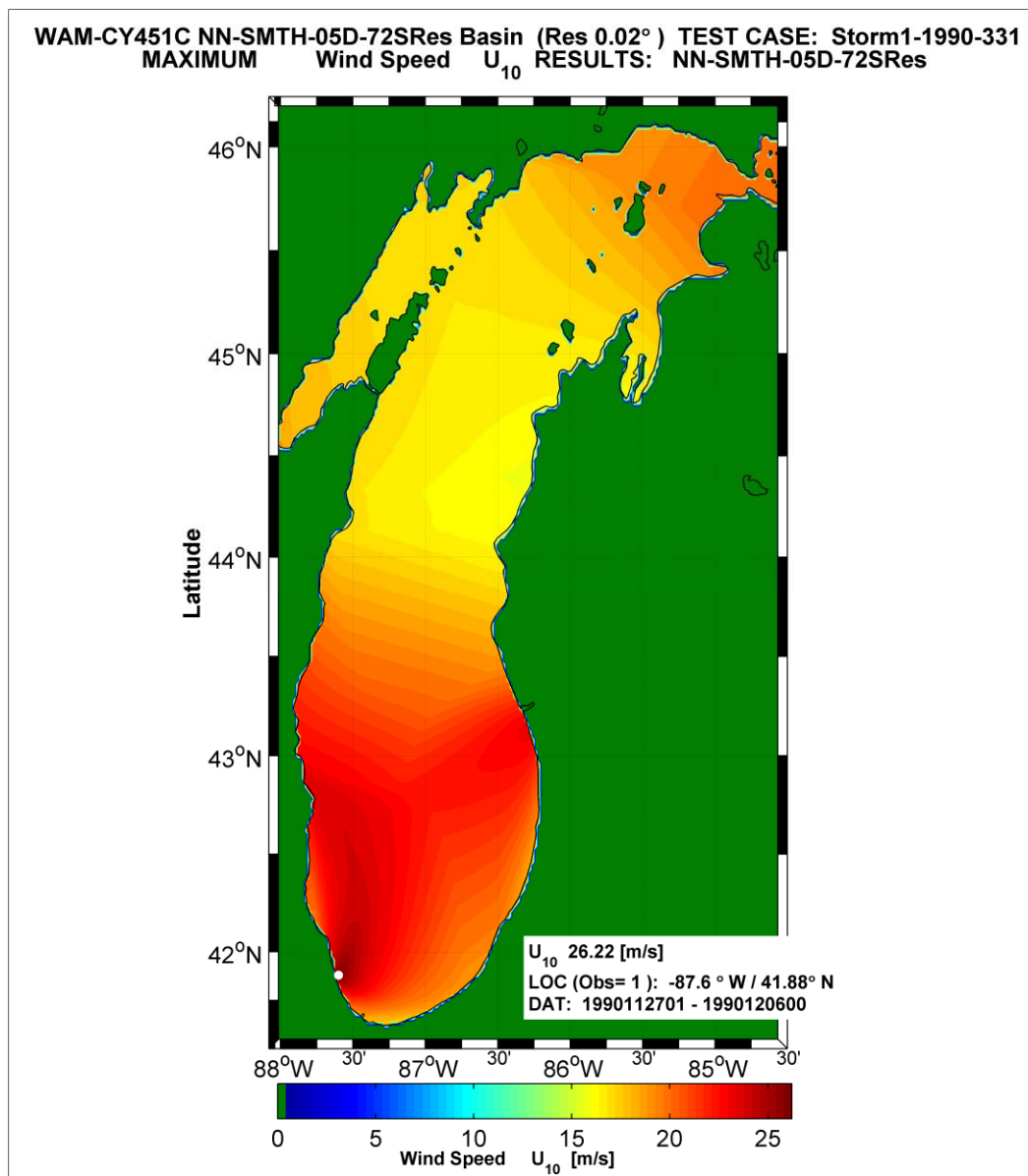


Figure 3-5. Maximum wind speed envelope for the December 1990 storm derived from the NNM wind field generation routine.

The CFSR maximum wind speed envelope shows nearly the entire Lake Michigan domain with wind speeds greater than 19 m/sec. The zone of highest wind speeds for the CFSR indicates speeds of 20 to 25 m/sec in the area where the NNM indicates speeds of 15 to 17 m/sec. The relative magnitude of the maximum winds in central Lake Michigan and in Green Bay appears to be on the order of 5 m/sec greater for CFSR than for the NNM.

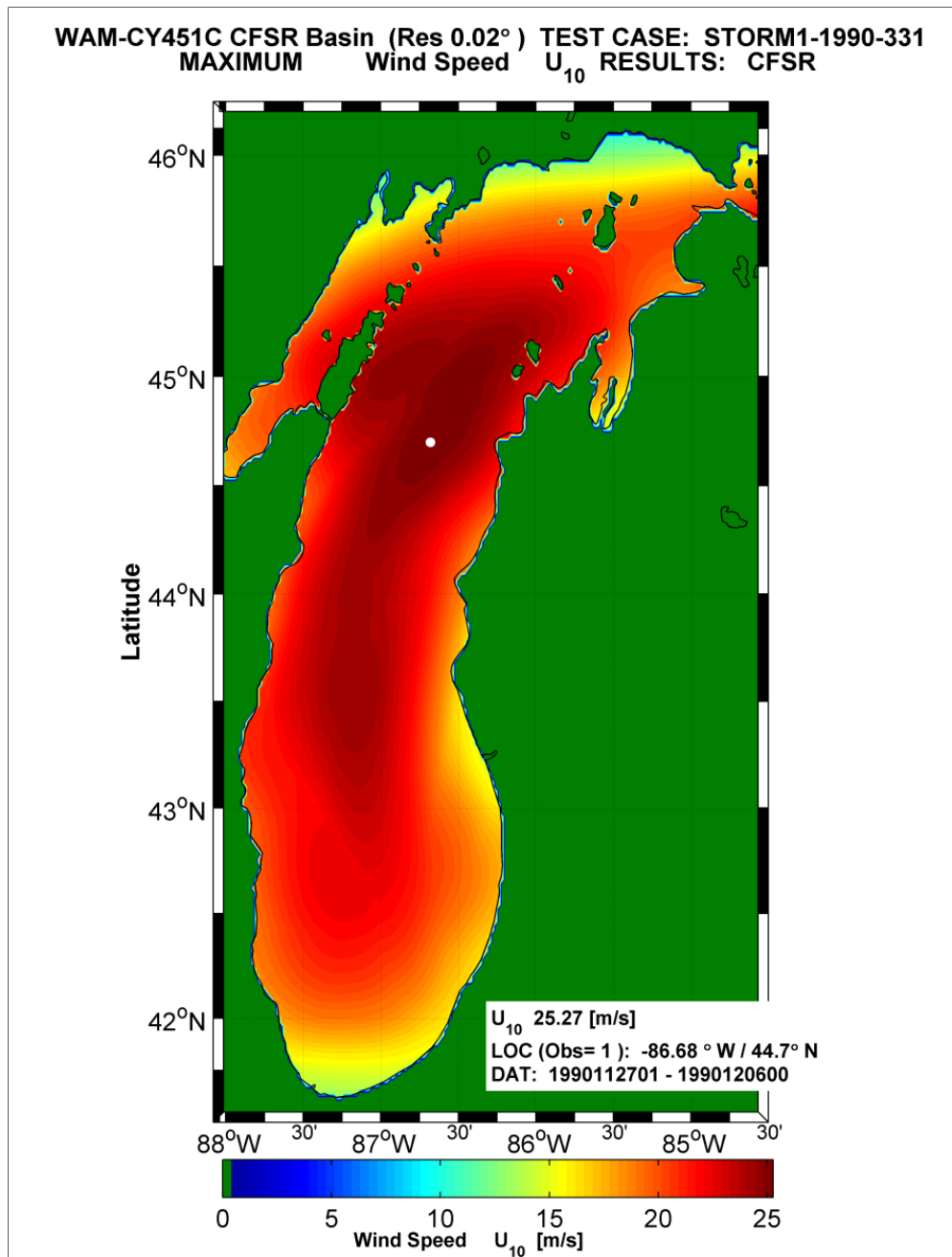


Figure 3-6. Maximum wind speed envelope for the December 1990 storm derived from the CFSR wind field.

The significant wave height scales to the square of the wind speed, so differences between the NNM and CFSR forced WAM simulations should also be quite evident for this storm. Note that the scaling of the maximum wave height envelopes (Figures 3-7 and 3-8) differs. The analysis of these graphics focuses on the overall distributions and gradients in the wave fields.

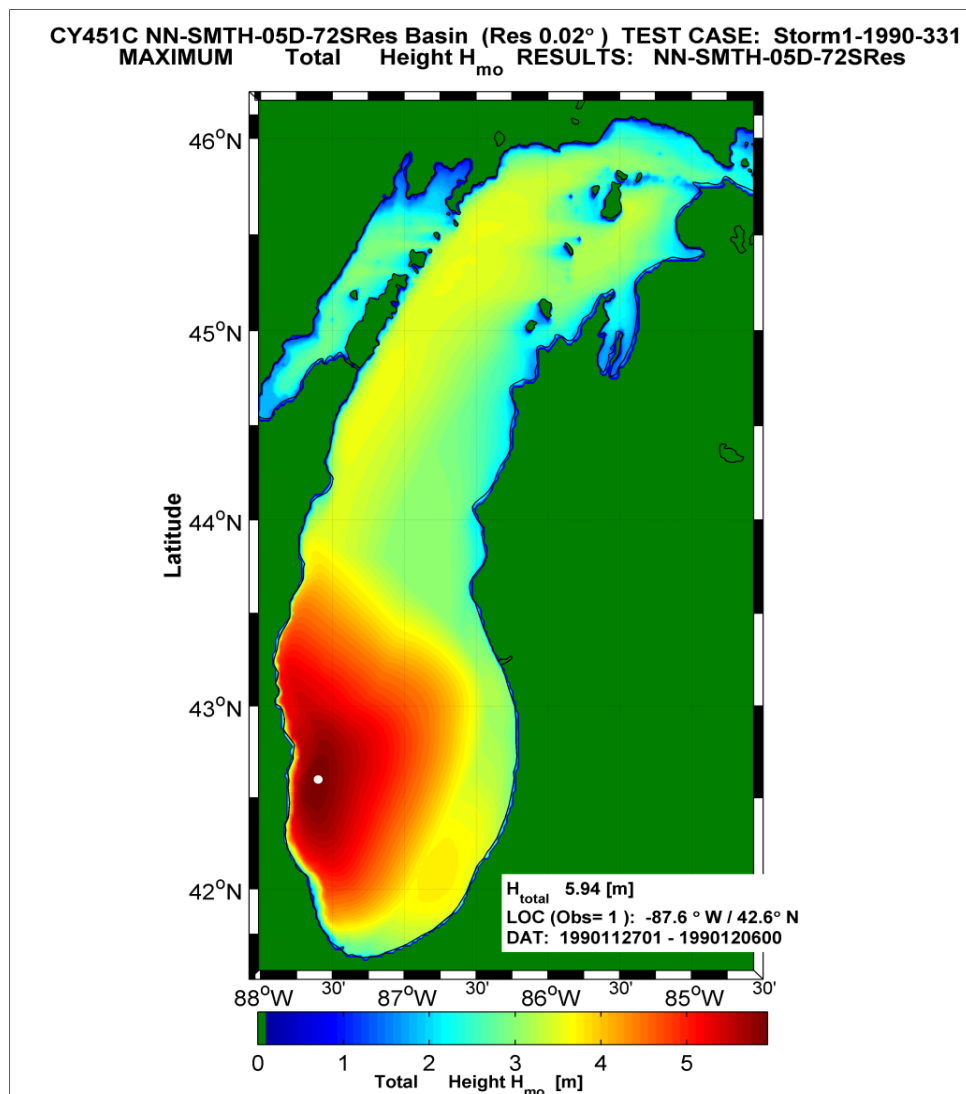


Figure 3-7. Maximum significant wave height envelope for the December 1990 storm derived from the NNM wind field generation routine.

Analysis of the NNM maximum significant wave height envelope (Figure 3-7) displays a concentrated lobe of high sea-states in the southwest corner of Lake Michigan. That lobe is indicative of a local-scale wind event seemingly to migrate from southwest to northeast. It also emulates the maximum wind speed envelope in terms of areal extent. The western coastline of Lake Michigan shows a band of 3.5-m wave heights, suggesting a concentration of winds (or jet streak) focused in half of the central portion of the lake. In the proximity of buoy 45002 (-86.4-deg / 45.3-deg) in the northern part of the lake, the maximum significant wave height value attained is about 3.5 m. The maximum wave height calculated anywhere in the lake is 5.9 m at the southwestern end. In Green Bay there is evidence of a gentle wave height gradient from the mouth (~2.5 to 3 m) down to about 2 m at the southern end of the bay.

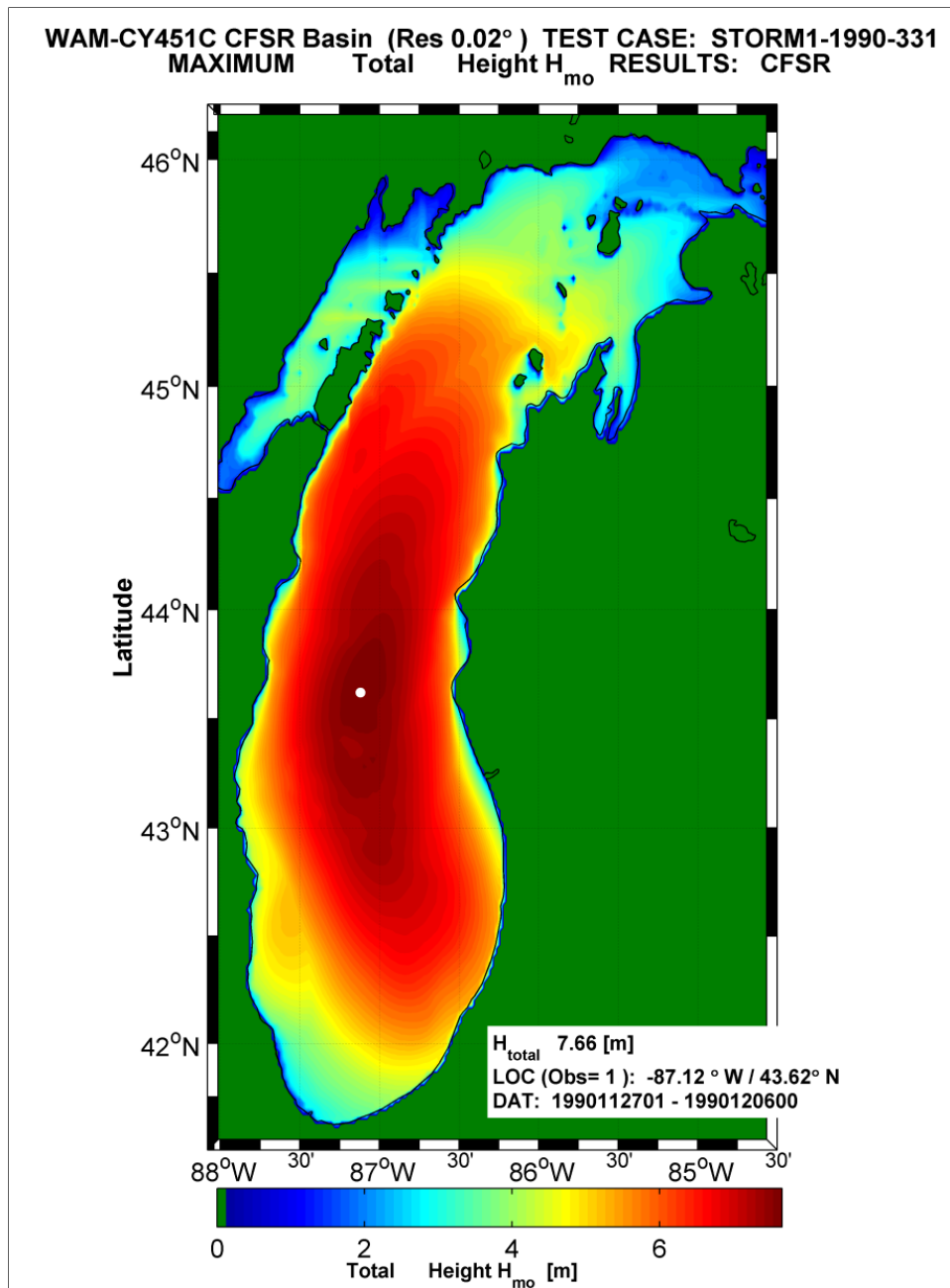


Figure 3-8. Maximum significant wave height envelope for the December 1990 storm derived from the CFSR wind field.

The maximum wave height envelope derived from the CFSR forced WAM simulation (Figure 3-8) looks very similar in structure to the winds (Figure 3-6). The distribution follows the lake's coastline, has a very symmetric structure along the central axis of Lake Michigan, and fills the lake with maximum wave heights exceeding 5.5 m. This is characteristic of a larger meso-scale low pressure system moving southwest to northeast and the maximum wave height values are derived from the left hand side of a

storm system that tracks in this direction. One other observation noted from Figure 3-8 is the small lobe around 42.5-deg along the western Lake Michigan coastline. This location is very similar to that found in the NNM results, and of a similar magnitude. There are dramatic differences in wave heights along the entire eastern and central western shorelines of the lake. The wave heights in Green Bay appear to be on the order of that generated for the NNM, or around 2 to 3.5 m, and slowly varying from the north to south.

It was fortunate to have one buoy operational (45002) for the December 1990 storm simulation to provide quantitative information with which to assess the two sources of wind/pressure forcing. A time plot for the simulation is shown in Figure 3-9 at the buoy location. The results are derived from the both NNM (temporal smoothed input meteorological conditions) and the CFSR forced WAM runs. All other input conditions for these simulations remained constant for the two separate runs. The six-panel plot displays the significant wave height, parabolic fit of the peak wave period, the inverse first moment of the mean wave period, the vector mean wave direction, wind speed (adjusted to 10-m equivalent neutral stable value), and the wind direction. Definitions and formulations for these parameters are provided below. All directions are in a meteorological coordinate system where 0-deg indicates winds/waves from the north; 90-deg is for winds from the east. During the peak of the event, strong winds out of the east shift slowly to strong winds out of the northeast.

$$H_{mo} = 4^* \left[\iint_0^{2\pi} F(f, \theta) df d\theta \right]^{1/2}$$

$$T_{peak} = f_{peak}^{-1}, \text{ where } f_{peak} = \text{parabolic fit to } \frac{dE(f)}{df} = 0,$$

$$\text{where } E(f) = \int_0^{2\pi} f(f, \theta) d\theta$$

$$T_{mean} = f_{mean}^{-1}, \text{ where } f_{mean} = \left[\frac{\int_0^{2\pi} \int_0^\infty f^{-1} F(f, \theta) df d\theta}{\int_0^{2\pi} \int_0^\infty F(f, \theta) df d\theta} \right]^{-1}$$

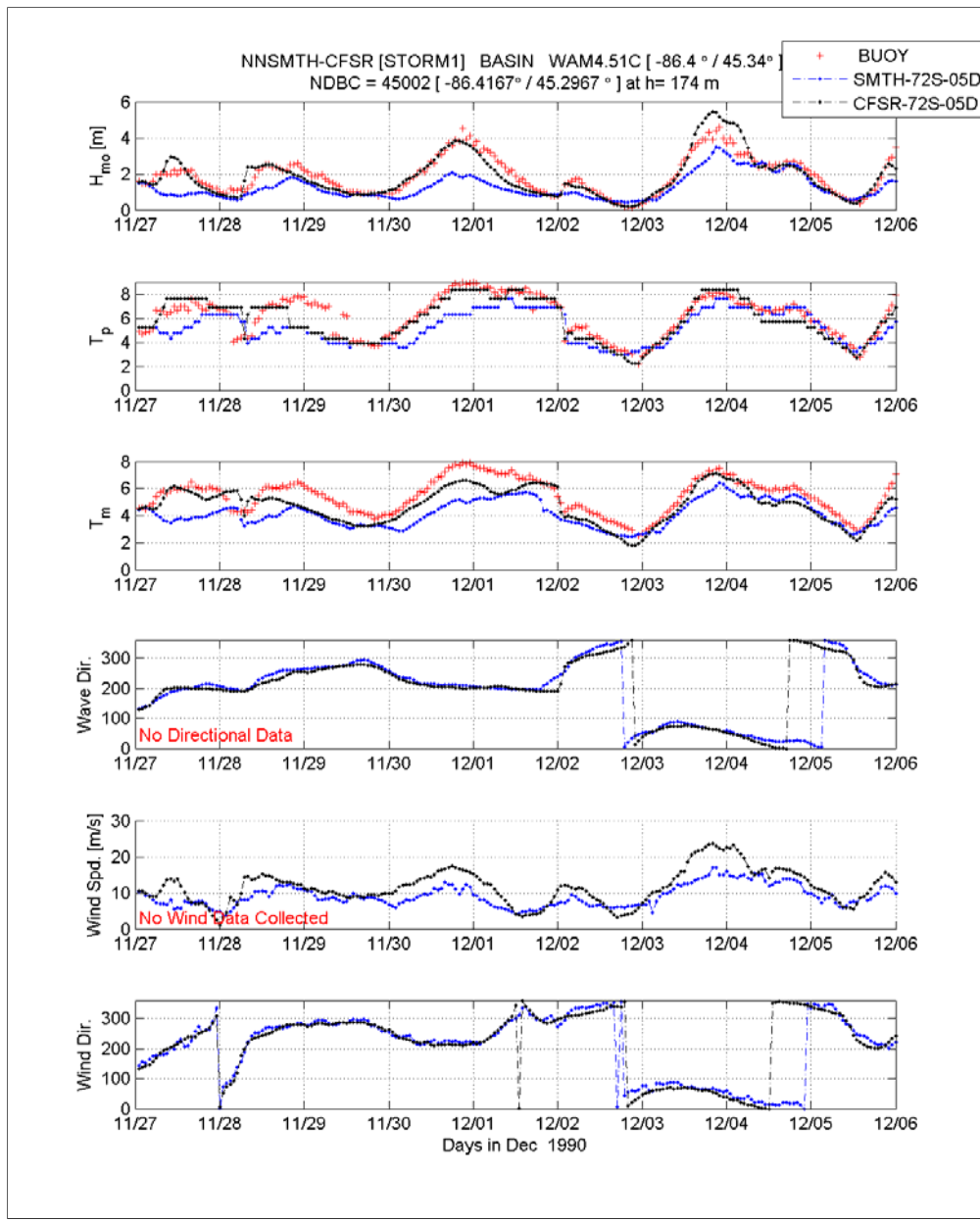


Figure 3-9. Time plots of significant wave height, peak and mean wave period, vector mean wave direction, wind speed and direction at NDBC 45002 for the December 1990 storm.

$$\theta_{\text{mean}} = \tan^{-1} \left[\frac{\int_0^{2\pi} \int_0^{\infty} \sin \theta F(f, \theta) df d\theta}{\int_0^{2\pi} \int_0^{\infty} \cos \theta F(f, \theta) df d\theta} \right]$$

All simulations are initiated with simple fetch laws using the initial wind information contained at each grid point; hence comparisons at the far left portion of each time plot might show differences attributed to this start-up effect.

The patterns of variation in significant wave height with time for each of two simulations (NNM, blue line and CFSR, black line) follow the measurements (red symbols) qualitatively. This means that the growth and decay cycles of WAM are performing well given the forcing function derived from the spatial and temporal evolution of the wind fields. However, there is a distinct negative bias in the NNM significant wave height results, for the main event and for several prior less energetic events, especially at the storm peaks, and by as much as 2 m during the main 3-4 December event. The two time periods of time when the major deviations occur are when the wind speeds are increasing, with near constant or slowly varying directions. The first storm peak (around 31 November to 1 December) contain winds that are at 200-deg (winds from the south-southwest), at speeds from 8 to 12 m/sec (NNM estimates) and roughly parallel to the central long axis of Lake Michigan. Using the NNM winds, wave heights grow, however they do not attain the H_{mo} levels measured at the buoy. This observation combined with a consistent negative bias in the T_p and T_m results suggest NNM wind speeds are too low. These same tendencies for NNM forcing also occur for the 3-4 December 1990 storm peak. For this event the WAM results follow the buoy data during the very early growth stage but then diverge significantly toward lower H_{mo} conditions at the peak. The T_p and T_m results from the NNM at the major storm peak agree with the measurements much better than in the previous storm peak case, but are still slightly biased low. The NNM wind speeds during this event peak were around 15 m/sec, and the directions are rotating clockwise from easterly to northeasterly directions.

At this point of the study, the first storm simulation, the biased results obtained using NNM and WAM were, in the context of how the wind fields were constructed, not adequate for making overarching conclusions. Preferentially increasing the wind speeds could reduce the negative biases in the WAM results. However, the persistence of the negative biases in other subsequent simulations, the apparent lack of spatial coherency in winds within the Lake Michigan domain at times and resultant treatment of what could be considered as a meso-scale event as a local-scale (a result of using point-source measurements) suggested an alternative to the NNM was worth examining. Thus, when the CFSR wind and pressure fields became available, they were examined as an alternate source for meteorological forcing input.

The CFSR generated WAM results follow the buoy data quite well. Growth, decay and estimates of H_{mo} , T_p , and T_m at all storm peaks (five events)

including the 3-4 December period are reasonably well simulated. The simulation using the CFSR forcing produced improved agreement with measurements, compared to the NNM forcing. There is an over-estimation at the major storm peak on 3-4 December of about 0.75 m, (~17 percent). The T_p model results match the measured data better than those using NNM forcing, with exception of a 12-hour period starting on 28 November 1200 UTC. The T_m results show a tendency to be lower than the buoy data, but are a better match than those using the NNM forcing. Lastly, there is a general trend for CFSR to match the NNM wind directions for this particular storm simulation, at this location. However, there are significant differences in wind speeds; the tendency is for the CFSR to be greater at every storm peak compared to NNM, by as much as 5 m/sec. This difference is the reason why the CFSR forced wave heights track much better with the measurements.

This storm was selected because of the extreme water levels experienced at the southern end of Green Bay. An output location at the southern end of Green Bay was chosen from the WAM domain to assess differences between the NNM and CFSR wind forcing in this shallower bay for this same event where there were significant differences in Lake Michigan proper. There are no wave measurements in Green Bay, hence no firm conclusions can be drawn from this comparison other than they either differ or are similar. The results are presented in Figure 3-10, which contains the six-panel plot of H_{mo} , T_p , T_m , θ_{mean} , the wind speed (U_{10}) and the wind direction (θ_{wind}). What is interesting to see is that despite major differences found in Lake Michigan (at the location of NDBC 45002 and in the maximum wind speed envelopes), the wave estimates from the two simulations are similar in Green Bay. In fact, unlike Lake Michigan proper, the NNM-forced wave heights are generally higher because the wind speeds are greater compared to the CFSR winds. The NNM-forced decay of the wave conditions after the peak event of 3-4 December is slower to dissipate than with CFSR forcing. The event produces high wave conditions (and high water levels) at southern Green Bay because the wind direction is nearly parallel to the long axis of the narrow bay.

3.6.2 September 1989 storm

The 23 September 1989 storm produced high water levels at Calumet. For this simulation, unlike the previous December 1990 storm, both NDBC buoys (45002, Northern and 45007 Southern) and the C-MAN station at Sheboygan, WI were operational. Wind fields were generated from 23

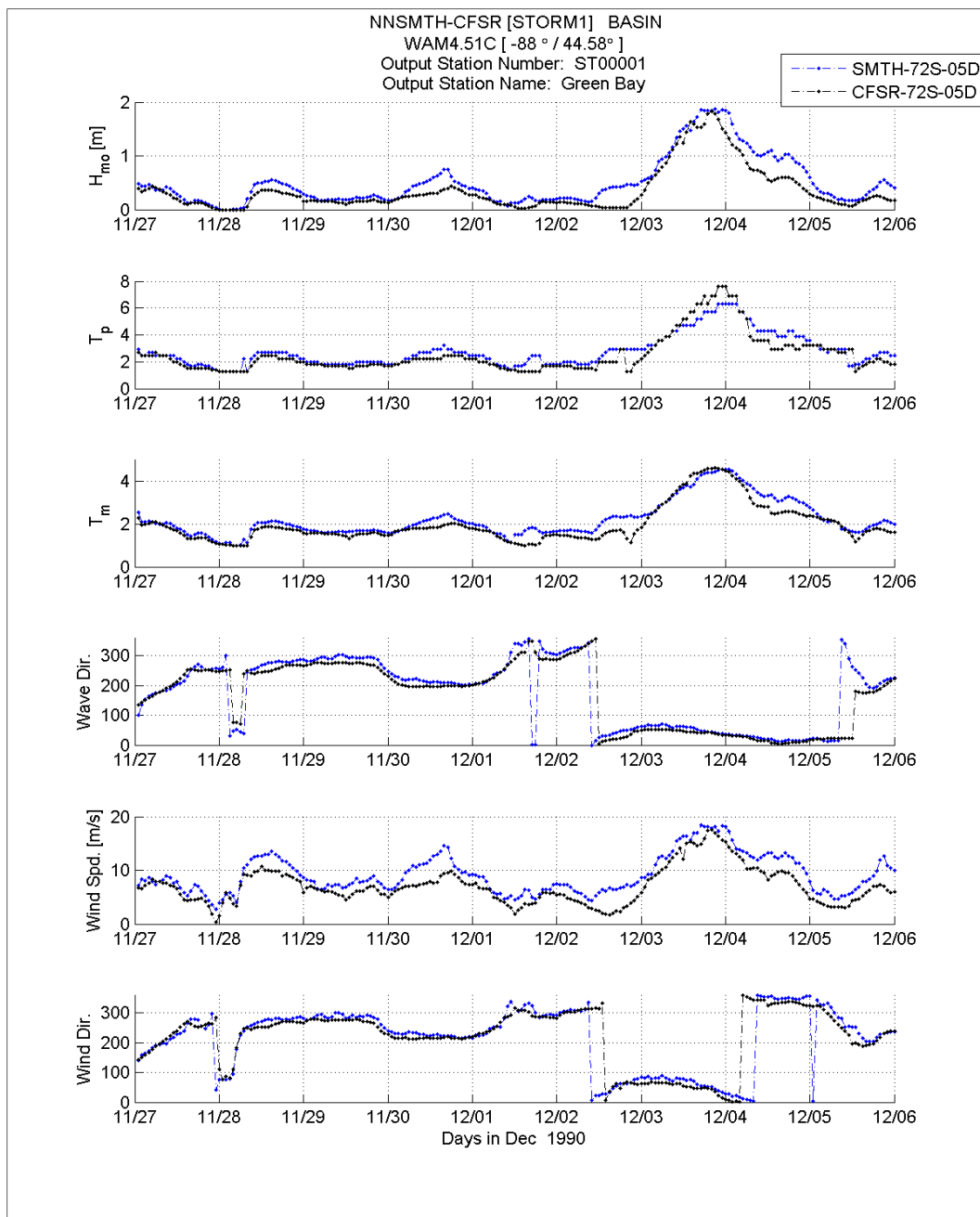


Figure 3-10. Time plots of significant wave height, peak and mean wave period, vector mean wave direction wind speed and direction at a WAM save location in lower Green Bay for the December 1990 storm.

point-source stations. The locations of these operational stations are shown in Figure 3-11. There are slightly more stations covering the western Lake Michigan coast, especially in the southwestern corner. Also, there are additional stations (compared to the December 1990 storm) in the northwestern corner which should improve the quality of the wind and pressure fields derived from the NNM.

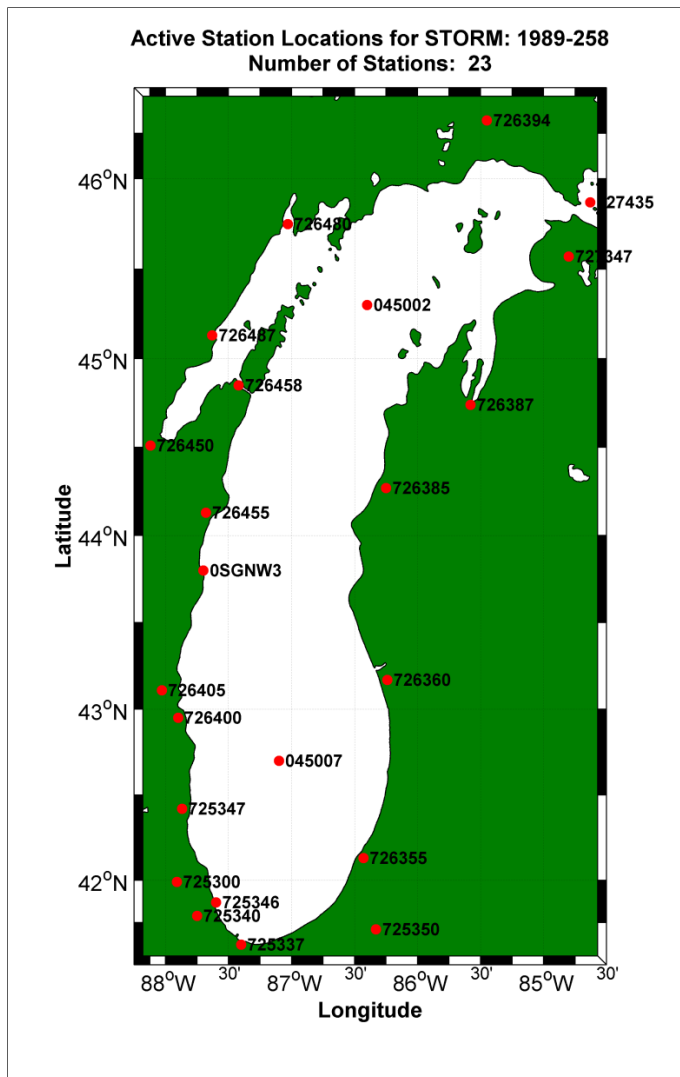


Figure 3-11. Available meteorological station locations accessed and preprocessed for the September 1989 storm.

The maximum wind speed envelope graphic for the input NNM simulation is shown in Figure 3-12. There are two areas containing wind speeds approaching 18 to 20 m/sec, the first in the north, and the second one starting near Chicago, IL and ending at about Muskegon, MI and including the southern buoy 45007. Again, there is evidence of a signature of localized reduced spatial coherency in the wind field in the central Lake Michigan domain where wind speeds are less than in the northern and southern parts of the lake. This pattern is different from the pattern seen in Figure 3-13, the maximum wind speed envelope derived from the CFSR wind fields. In Lake Michigan proper, the maximum wind speed envelope for this storm looks similar to that for the December 1990 storm (Figure 3-6). The zones of peak magnitudes differ, however the overall structures appear very consistent.

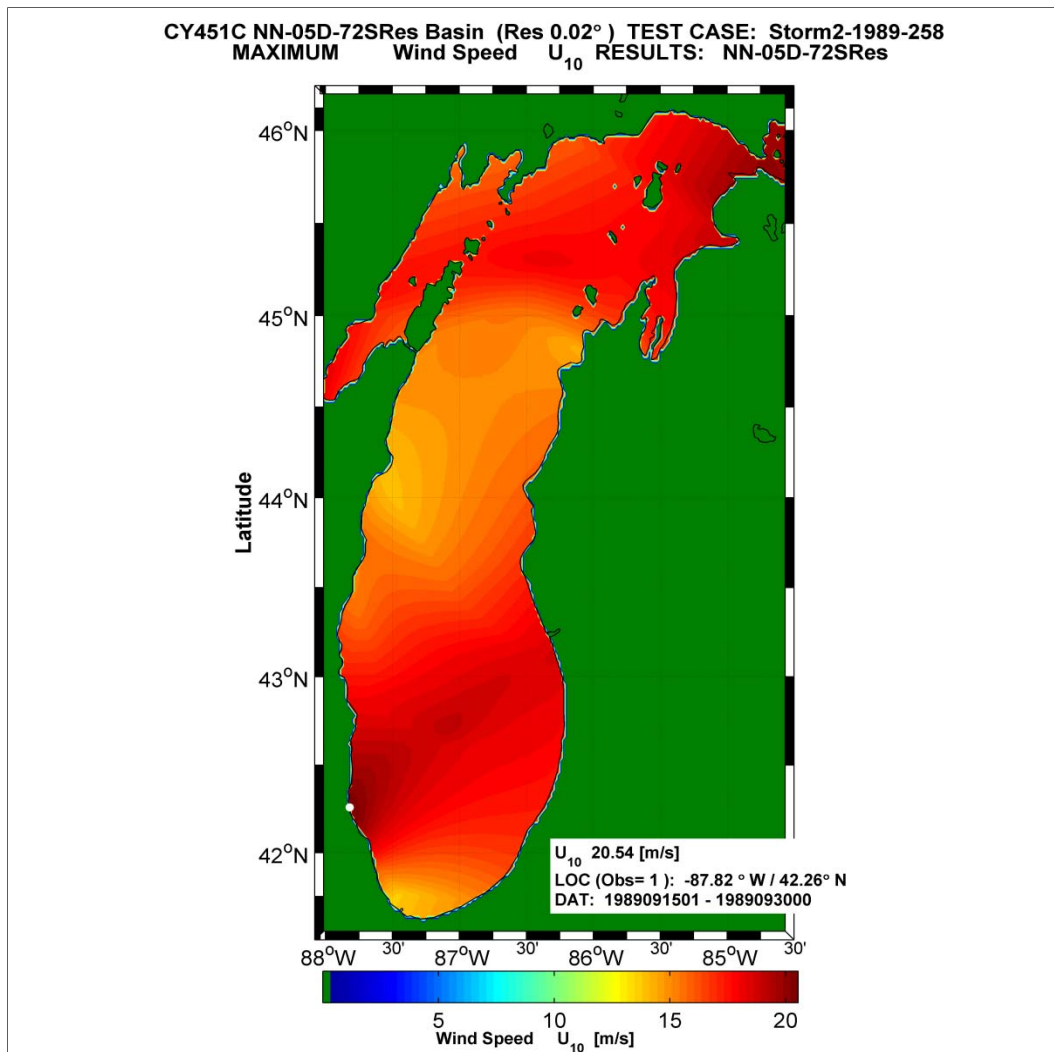


Figure 3-12. Maximum wind speed envelope for the September 1989 storm derived from the NNM wind field generation routine.

There are differences between the NNM and CFSR maximum wind speed envelopes. NNM suggests a larger region of stronger wind speeds in the north. The CFSR southern maximum lobe is well defined elongated in a north/south orientation, and exhibits strong east/west gradients toward both coastlines. In the middle of Lake Michigan, CFSR peak wind speeds are greater than NNM peak wind speeds.

The differences in the maximum wind envelopes provide general information for the entire Lake Michigan domain regarding the two methods. The validation of WAM forced by NNM and CFSR wind fields at two wave measurement sites in the lake locations (45002 and 45007) can offer quantitative results and insights. Figures 3-14 and 3-15 are time plots of the wave and wind comparisons for NDBC 45002 and 45007, respectively. In

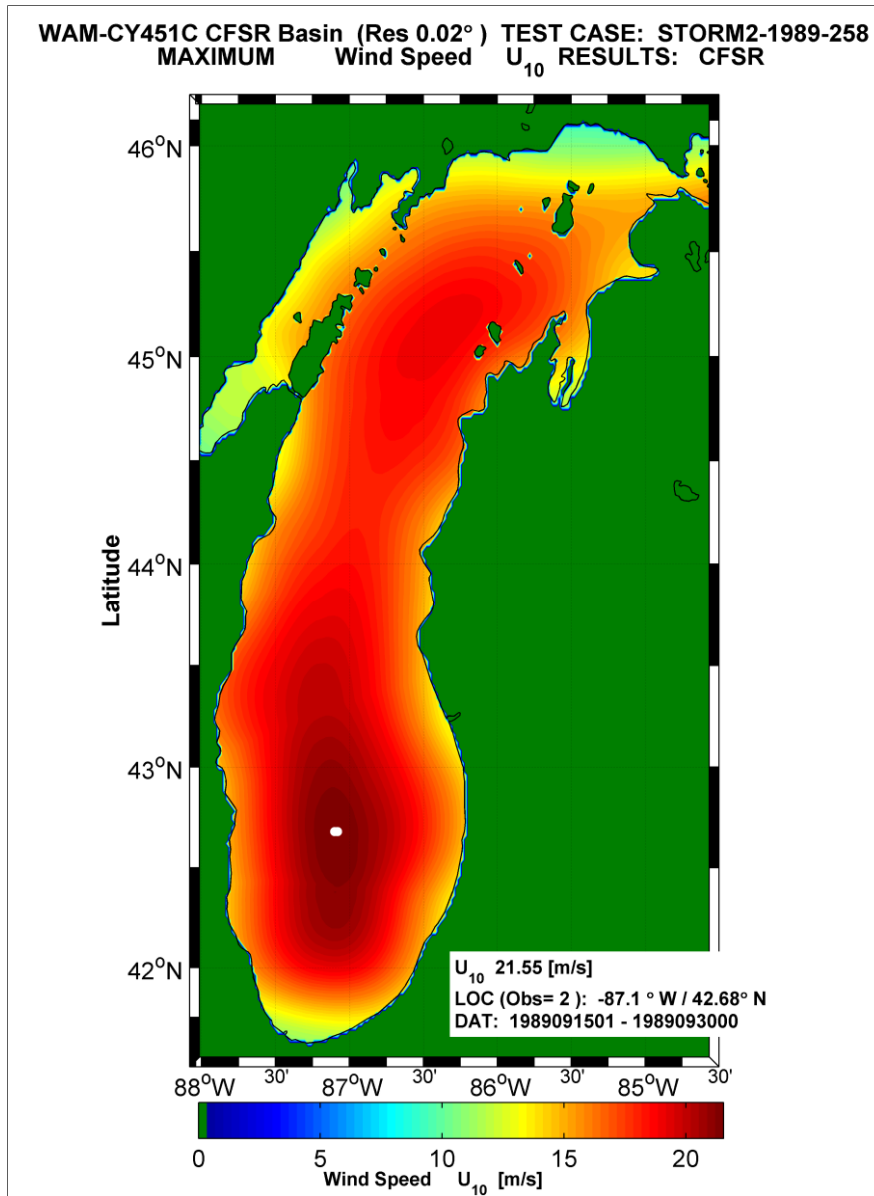


Figure 3-13. Maximum wind speed envelope for the September 1989 storm derived from the CFSR wind fields.

general, the WAM wave parameter estimates compare well to the measurements for the entire Storm 2 simulation period. NNM forced wave height results are biased low in height and period for the last two events in the simulated period. However, they capture the rapid growth sequence, the effects of the 180-deg wind directional shift (a 3-m change in wave height in two-hours) for the first (and highest) storm peak around 23 September. This is for winds peaking near 20 m/sec and from northerly directions. For the second two events (25 September and 28-29 September), the wind magnitudes are 15 m/sec and from the south and southwest. The WAM

estimates forced by NNM diverge from the measurements and are biased low in H_{mo} , T_p and T_m . For the lower wave activity from 17 through 22 September, the NNM forced wave estimates show only biases in the two wave period results and not in height, despite southerly directed winds.

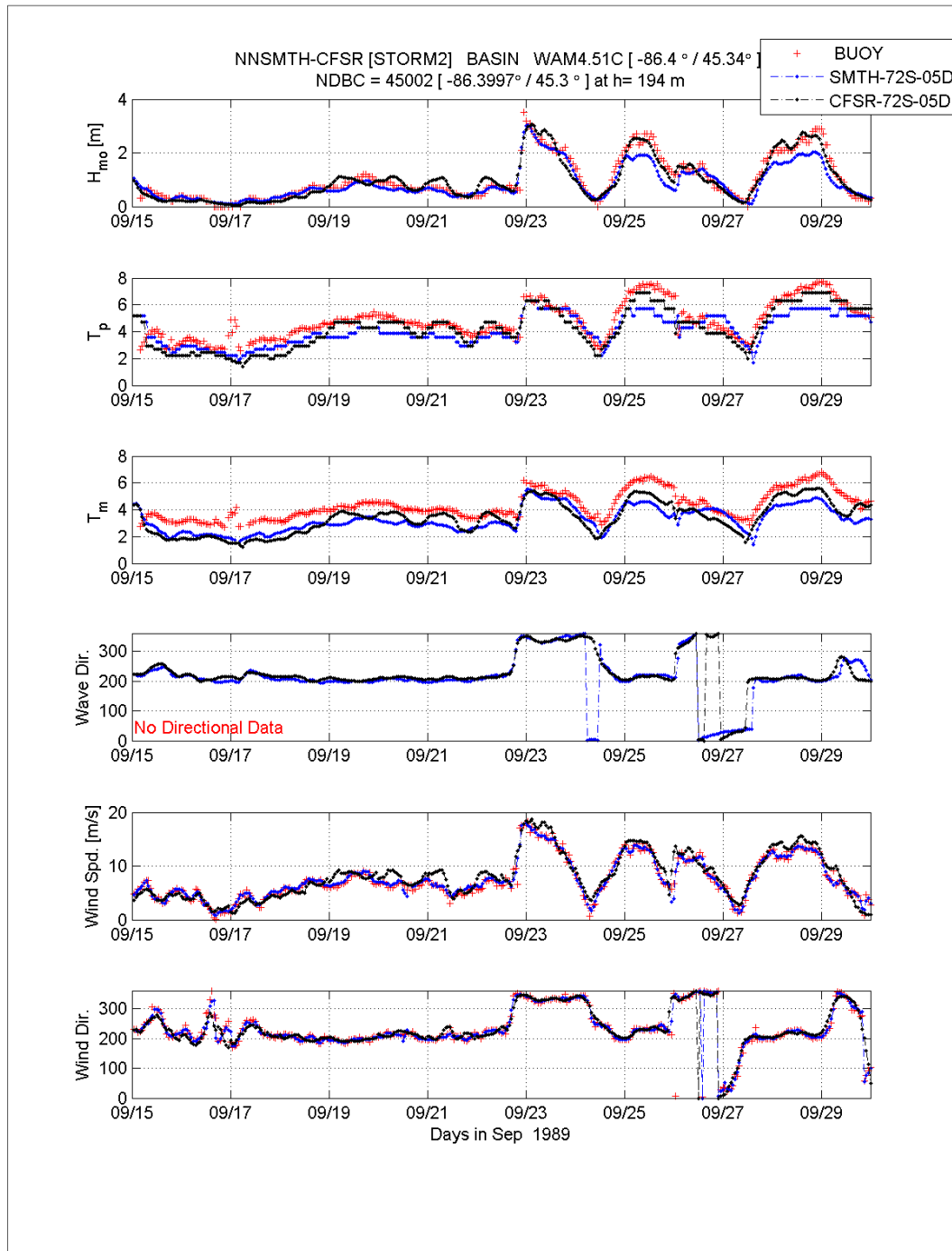


Figure 3-14. Time plots of significant wave height, peak and mean wave period, vector mean wave direction, wind speed and direction at NDBC 45002 for the September 1989 storm.

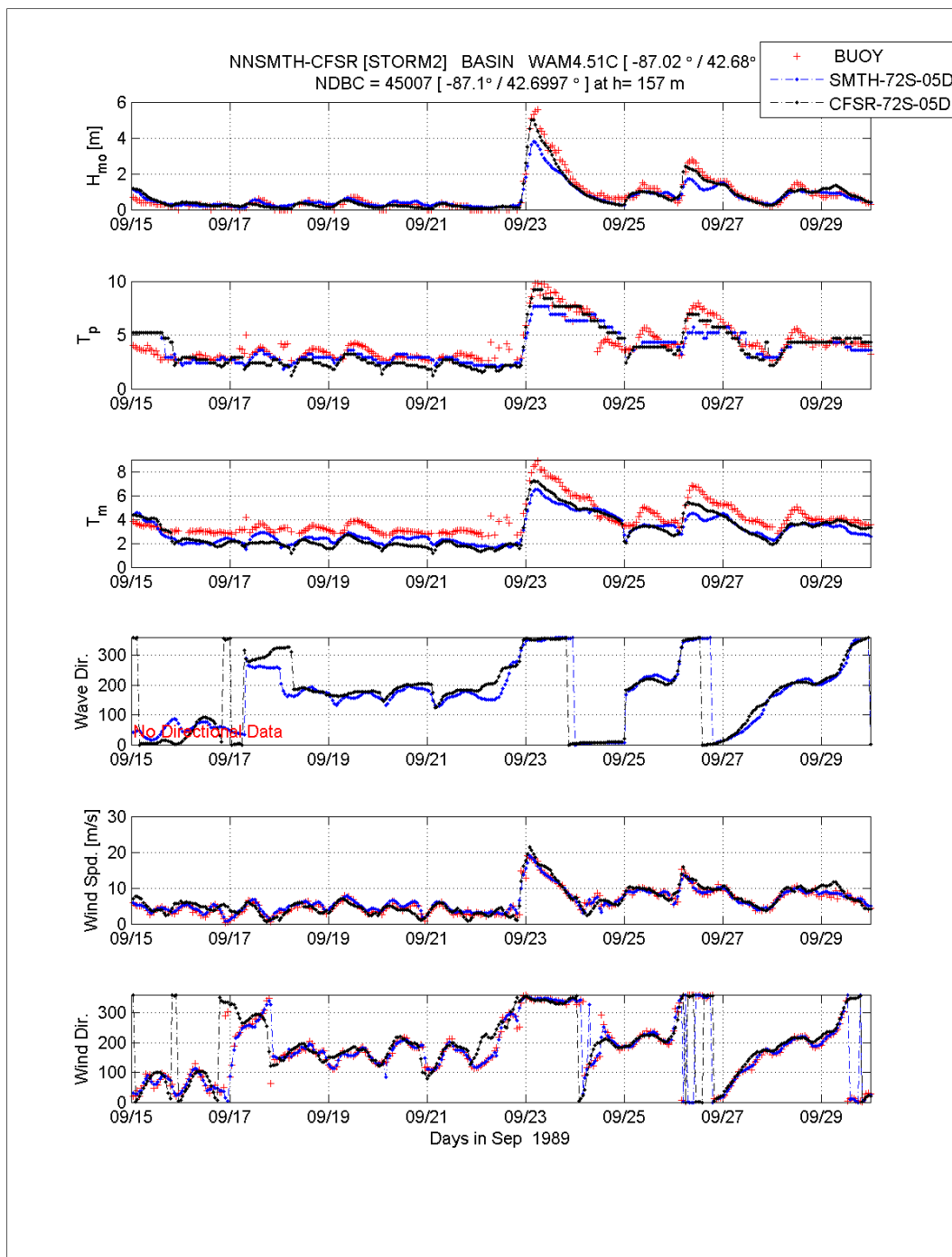


Figure 3-15. Time plots of significant wave height, peak and mean wave period, vector mean wave direction wind speed and direction at NDBC 45007 for the September 1989 storm.

The CFSR wind forcing of WAM compares more favorably to measurements at the three storm peaks, both in terms of wave height and peak period. The T_p , and more so for the T_m results, are biased low throughout the simulation; and the persistent bias for southerly winds is a concern. However, these biases are not as large as in the case of the NNM results. Lastly, NNM

uses the buoy winds as input to generate the spatially and temporally varying wind fields, so it is not surprising to see the blue line (NNM results) overlay the wind measurements. Even though the NNM winds match the wind measurements at the buoy locations better than the CFSR winds, the NNM-forced wave conditions are biased low and are lower than the CFSR-forced wave conditions. This result suggests that the CFSR winds represent the spatial coherence in wind field structure throughout the lake better than the NNM winds. What is comforting to see is CFSR estimates of the wind speed and direction at this location compare very well to the measurements. An initial concern regarding the temporal and spatial variability in the CFSR wind fields was that accuracy in winds might be diminished because of the model's resolution and inherent behaviors of 3-D atmospheric models. However, based on this simulation, CFSR does reflect the geophysical variability in the wind fields much like that of the NNM method, which is based on point source measurements.

The second validation point NDBC 45007 is located much closer to Calumet, IL. The maximum wind speed envelopes from NNM and CFSR showed very different distributions and wind speed gradients in the southern end of Lake Michigan. The time plot for these comparisons (Figure 3-15), clearly show the intense growth sequence of the major storm event around 23 September produced by strong northerly winds. The measured change in significant wave height was approximately 3 m in a two-hour interval. The minor events following this storm produced peak wave conditions of about 2 m, approximately the same level seen at the northern buoy. The four directional shifts (in wind and wave directions) of nearly 180-deg were not as abrupt, and more slowly varying over time, are reasonably well simulated with the modeling. Qualitatively, the NNM (blue line) results followed the wave measurements; however, the NNM forced significant wave heights underestimated peak wave heights by close to 2 m. For the two subsequent less-energetic events this bias persisted, although by lesser amounts. The modeled peak and mean periods continue to be biased low for nearly the entire simulation.

The CFSR (black line) performs much better, only missing the maximum peak wave height by 0.5 m, and approximately by the same or lesser amount for the remaining minor storm peaks. The CFSR-forced results for T_p (up to 10 sec) and T_m again more accurately match the measurements than do the NNM results; however, persistent low biases are reflected in the T_m values forced with CFSR. The CFSR wind speed and direction

estimates generally track with the measurements. There are cases where temporal phasing differences are evident, and the directional shifts do not emulate the data. However, these differences mostly occurred when the wind speeds were relatively low, less than 5 m/sec.

Lastly a time plot of the wave estimates for a location just offshore of the Calumet, IL site is provided in Figure 3-16. This plot only shows the relative differences in wave and wind conditions because of the absence of measurements at this site. The H_{mo} , T_p and T_m results for NNM and CFSR are very similar for the two events. CFSR wave heights tend to track lower than the NNM results for the low-energy period from 17 through 23 September. The CFSR wave decay cycle just after the major storm event on 23 September and also the storm around 26 September occurs faster than for the case of NNM forcing. There is a phase difference in the peak wave period results. For the low energy period, the mean wave directions show dramatic differences, as much as 90 deg and similar phasing differences found in the T_p results. These differences can be attributed to differences in the local wind estimates. For this time period CFSR winds track below the NNM wind speed trace, by about 2 to 3 m/sec, with exception of the rapid growth sequence of the 23 September storm. The CFSR wind directions also do not show the temporal variability that is reflected in the NNM results. Given all of these differences, CFSR and NNM produce nearly identical results at all of the storm peaks, the most important consideration in this study.

3.6.3 November 1992 storm

The storm that occurred on 2 November 1992 was the fourth largest water level event occurring at the Kewaunee, WI site and it produced extreme water levels at a number of other locations around the lake. There was no ice field data during this time period similar to that of the previous two storm simulations. Twenty three meteorological stations were used to construct the NNM wind and pressure fields. Of the 23 sites used, two were the seasonally deployed NDBC wave buoys. For this storm, the southern buoy (45007) had been upgraded to estimate directional wave parameters.

The analysis of the differences between NNM and CFSR wind fields is again examined using the maximum wind speed envelopes. Figure 3-17 displays the NNM maximum wind field. As in the previous simulations, this maximum wind speed envelope is strongly identified with the input land-station data; considerable spatial variability within the lake is evident. Local conditions dominate, with little spatial coherency along the central axis of Lake Michigan.

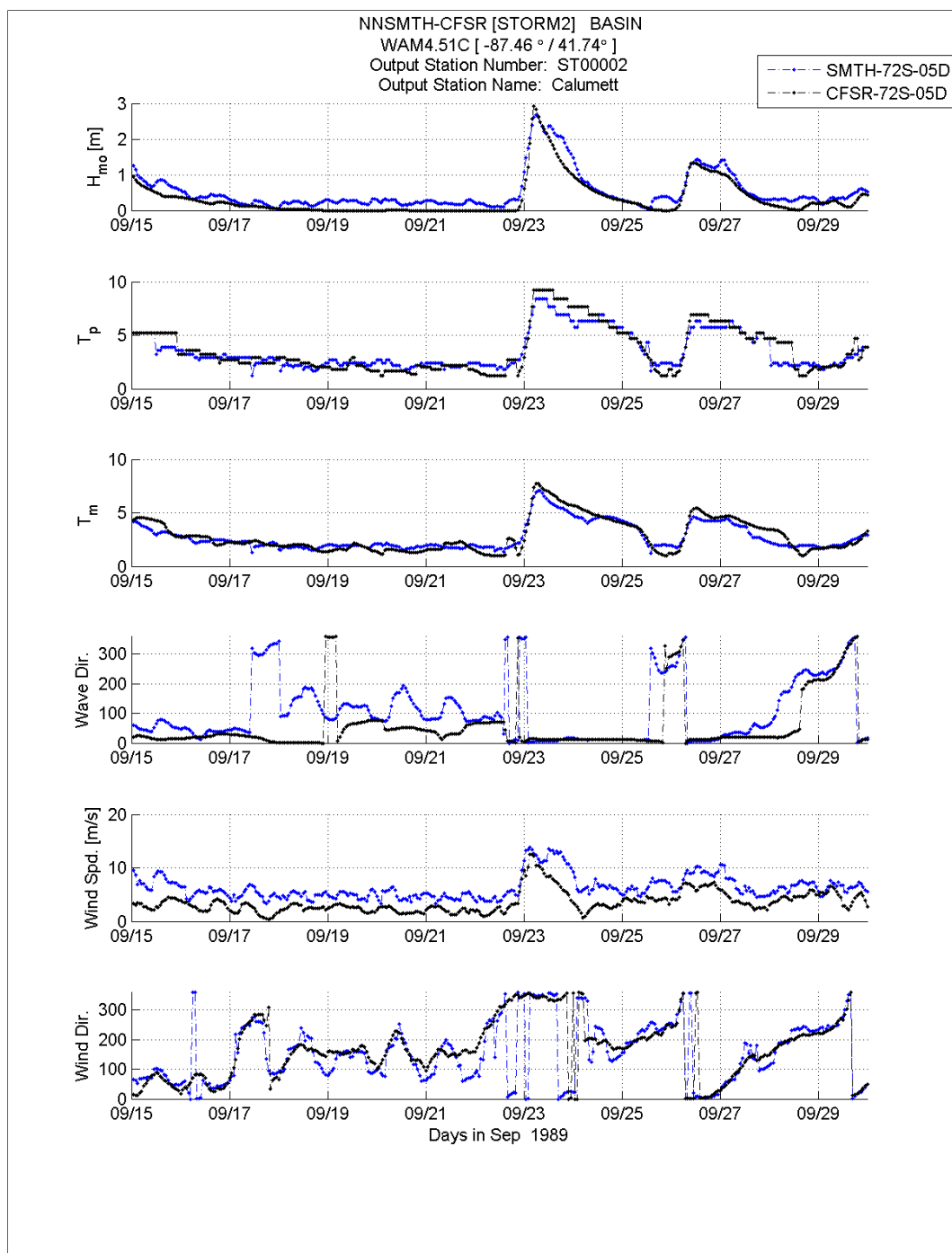


Figure 3-16. Time plots of significant wave height, peak and mean wave period, vector mean wave direction wind speed and direction at a WAM save location offshore from Calumet, IL for the September 1989 storm.

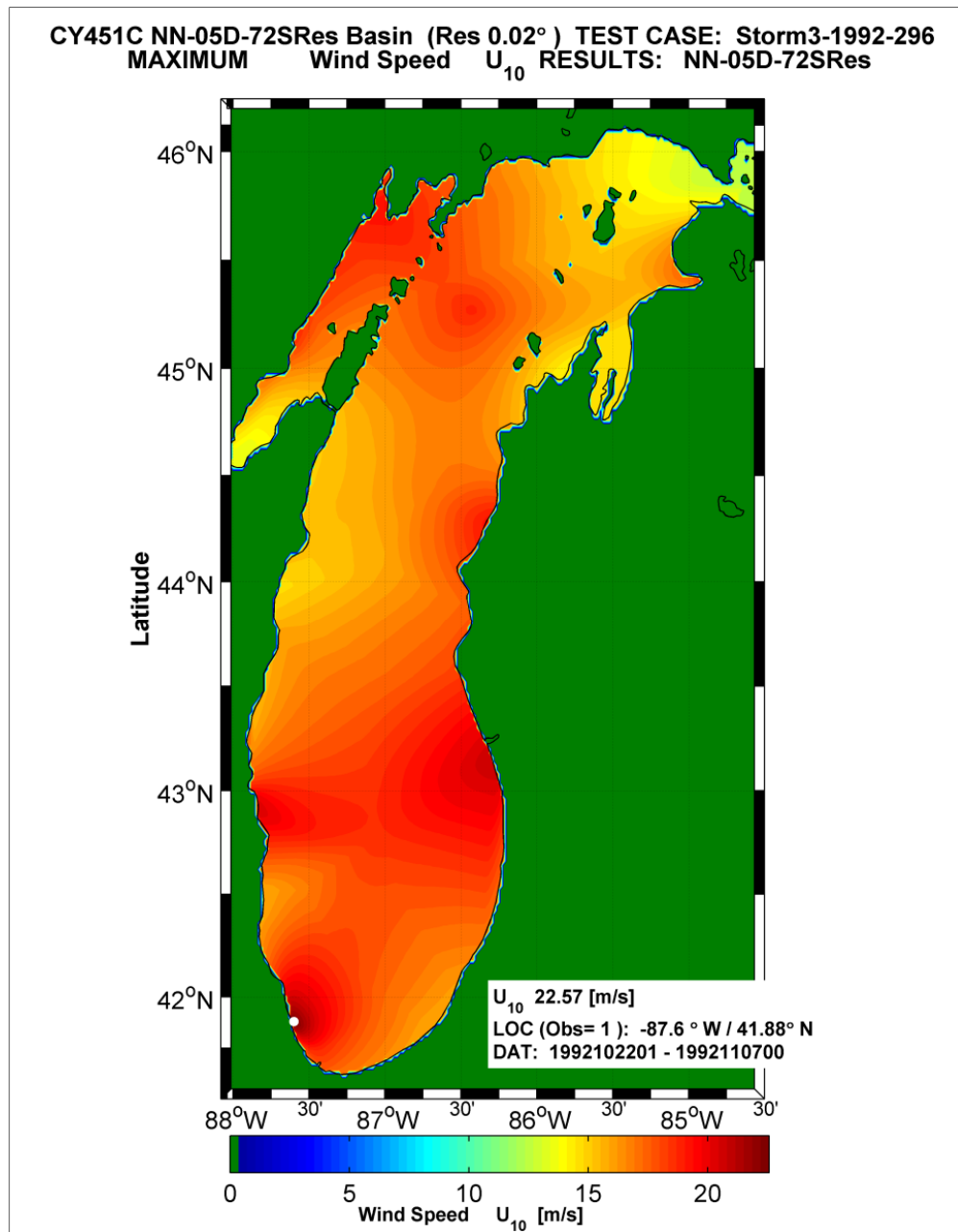


Figure 3-17. Maximum wind speed envelope for the November 1992 storm derived from the NNM wind field generation routine.

The CFSR maximum wind speed envelope (Figure 3-18) shows significantly more spatial coherence and significant differences in upper Lake Michigan compared to the NNM winds. There is one principle maximum lobe (nearly 25 m/sec) in northern Lake Michigan. Wind speeds in this region are much higher than the NNM winds. There also are areas along the eastern and western Lake Michigan coastlines that have lower wind speeds compared to those in the central region of the lake.

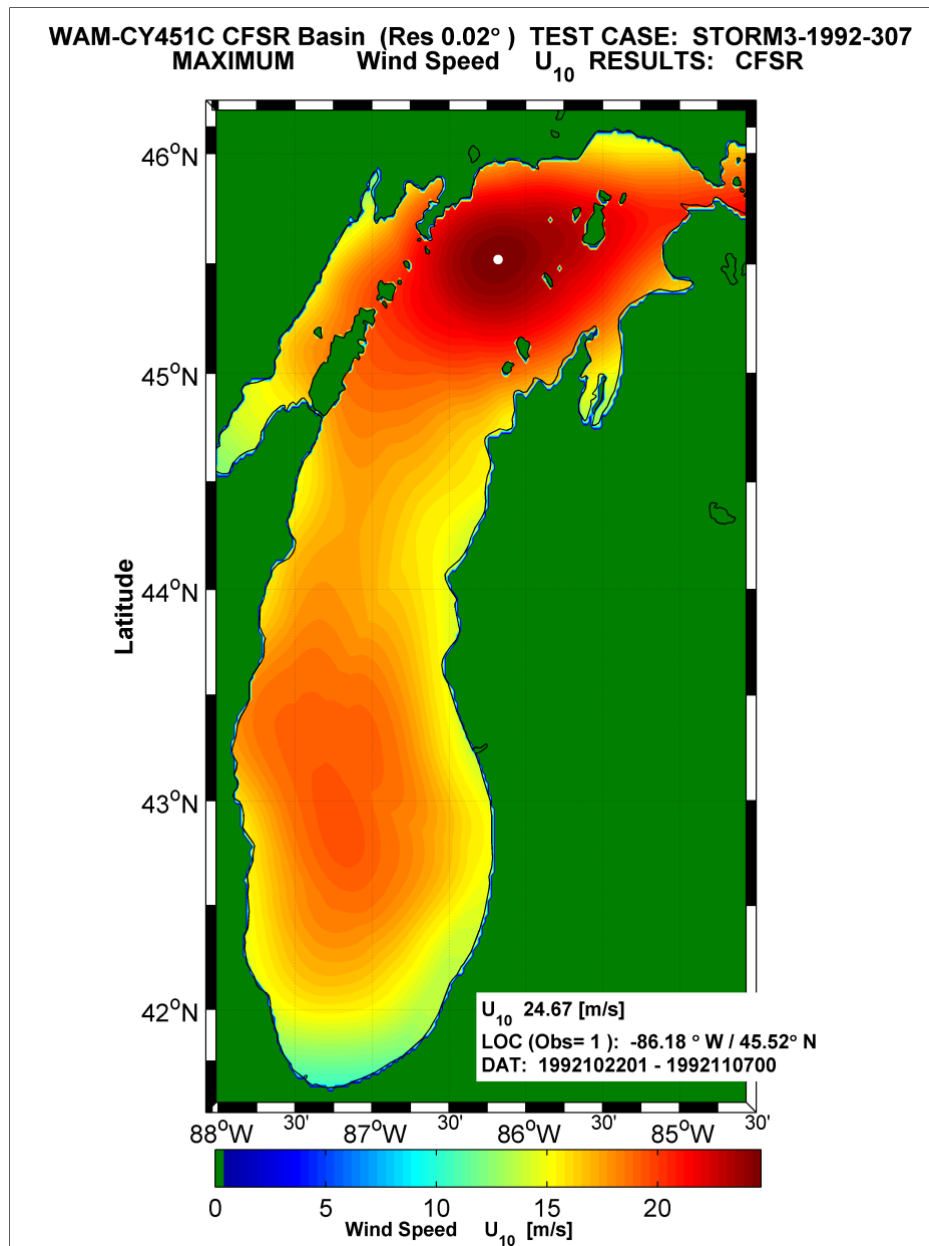


Figure 3-18. Maximum wind speed envelope for the November 1992 storm derived from the CFSR wind fields.

Validation of the WAM results relies on the two NDBC wave measurement sites (45002, and 45007). Figure 3-19, a comparison of model results and measurements at buoy 45002, illustrates how complex the wave environment can be in Lake Michigan. Over the 16-day simulation period there were numerous rapid wind directional shifts. During one of these directional shifts the winds varied from near calm conditions to a maximum of 20 m/sec on 2 November. The 2 November storm is an easterly wind condition; the secondary storm peak (4 November) is a south-southwesterly

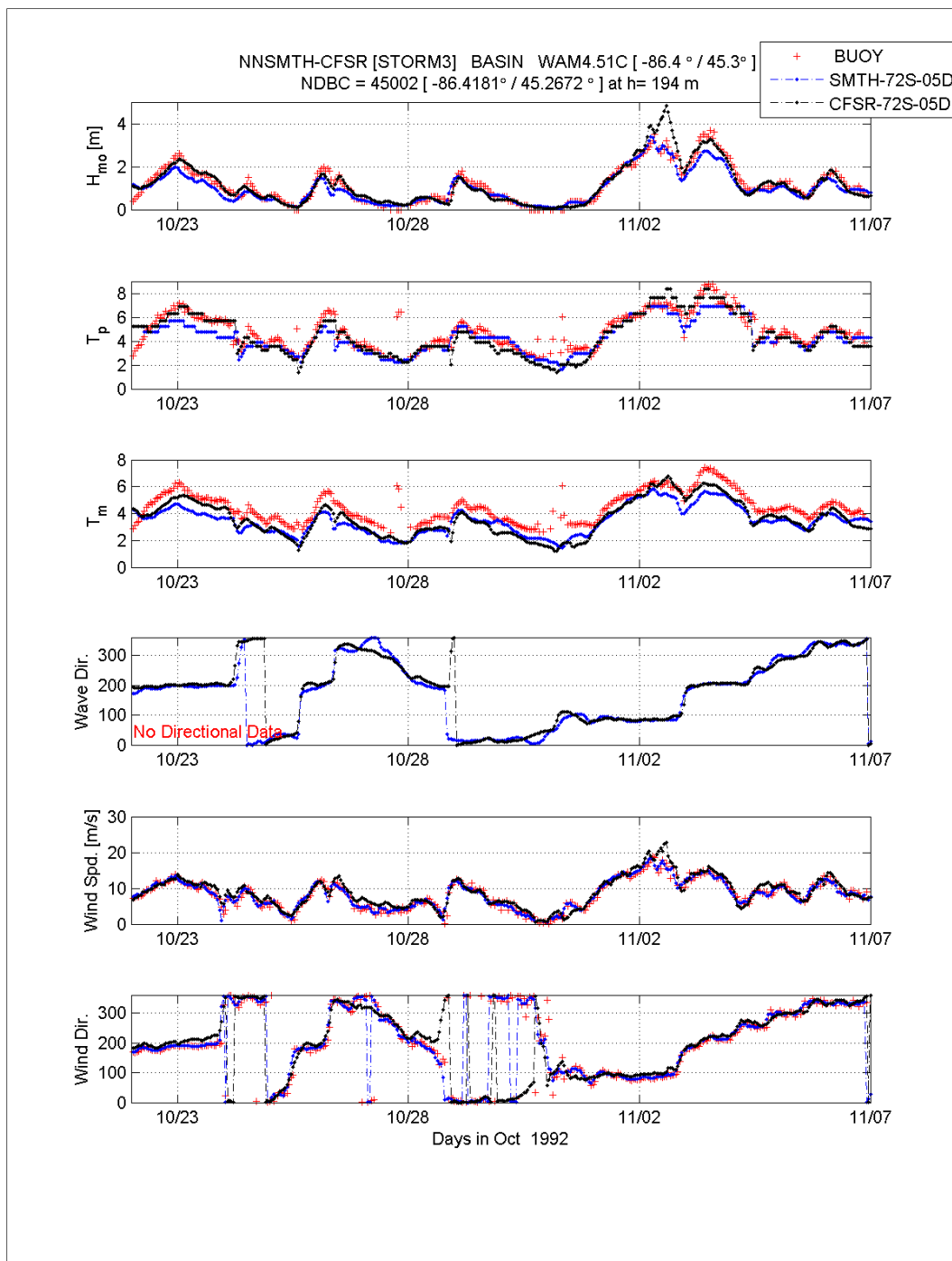


Figure 3-19. Time plots of significant wave height, peak and mean wave period, vector mean wave direction wind speed and direction at NDBC 45002 for the November 1992 storm.

wind forcing event. The WAM wave results consistently trend with the measured data. The NNM forced WAM results capture the significant wave height at the 2 November storm peak very well, but underestimate the secondary peak by about 1 m one day later. The lower peak storm conditions found throughout this simulation are well replicated using NNM wind

forcing. The T_p and T_m results do track slightly below the measurements. The NNM wind forcing results better replicate the measurements than in the previous two storm simulations.

The CFSR forced WAM significant wave height results follow the trends and measurements very well, with exception of the main 2 November storm. The model wave height results, rather than dissipate in the decay cycle like the measurements, increase to about 4.5 m about 1.5 m higher than the recorded data. The increase in wave height mimics the increase in wind speed CFSR estimates compared to measurements. This increase is about 5 m/sec and would scale to the errors found in the wave height estimates. As in the previous two storm simulations, the WAM peak and mean wave period results are slightly negatively biased compared to the measurements; however, not as much as in the case of the NNM wave periods.

The southern NDBC buoy 45007 was upgraded to include directional wave estimates when deployed in 1992. These data become very valuable for validation of the wave model and also the wind field specification. The results for 45007 are presented in Figure 3-20. The signature of the 2 November storm is captured at this location at nearly the identical time, and H_{mo} , as found in the data from 45002. Even the secondary storm peaks arriving one, two and then four days later are simulated well. All of Lake Michigan responded nearly uniformly over this five day period of time, with multiple directional shifts in the winds. It is apparent from a meteorological standpoint, there are meso-scale events passing through Lake Michigan with super-imposed sub-scale local events, a complex environment to model. The WAM results forced by NNM and CFSR winds do very well in capturing the storm peaks especially the 2 November event. Most of this success is attributed to the quality of the wind fields. In general, the H_{mo} results of WAM forced by NNM appear to slightly better replicate the measurements than results using the CFSR winds. The NNM wave height results exhibit a slight phase shift relative to the measurements, which is evident during the decay cycle. The mean wave period results again are biased slightly low; however, peak periods match the measurements well. The model results tend to respond slightly slower than the measurements during directional shifts, but the differences do not appear to be more than 10 deg.

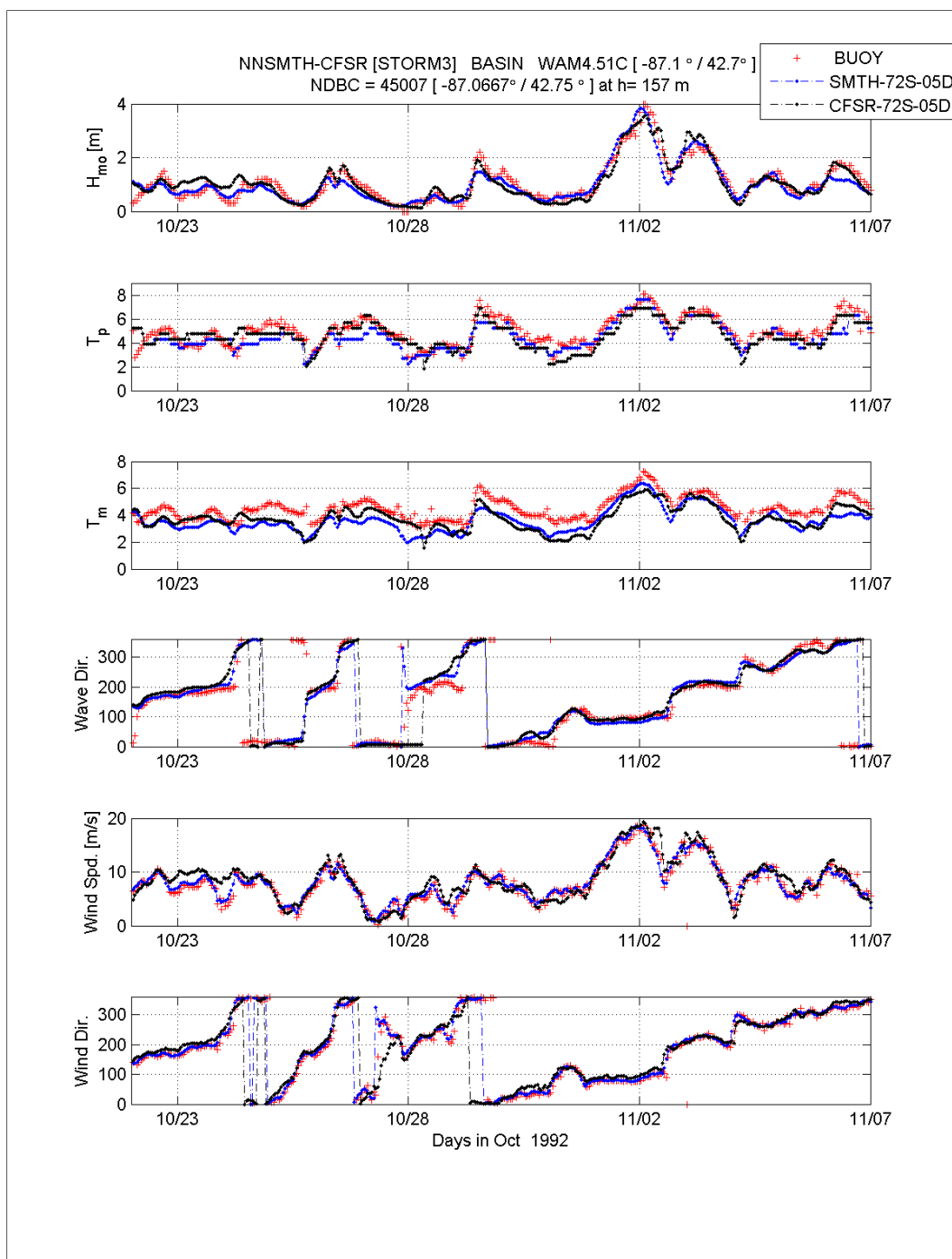


Figure 3-20. Time plots of significant wave height, peak and mean wave period, vector mean wave direction wind speed and direction at NDBC 45007 for the November 1992 storm.

The WAM significant wave height results forced by the CFSR winds track the measurements, with exception of the growth and storm peak estimates for the 2 November event, and slightly over-estimating the secondary event on 3 November. Agreement between CFSR-forced wave period and

wave direction results and measured values are comparable to the quality of results achieved using the NNM forcing.

This storm was selected as a Kewaunee, WI extreme water level event. The WAM results for a location just offshore of the harbor are shown in Figure 3-21. This graphic provides insights to the differences found in the wave estimates forced by NNM and CFSR at the western periphery of the lake. The estimates of the wave height, periods, and directions for each of these simulations are generally similar. There are slight differences on the order of 0.25 to 0.5 m in height; the wave periods and mean vector wave directions are nearly identical. Differences in the H_{mo} results are a result of differences in the wind speed. What is interesting to note though, the observed maximum significant wave height for the 2 November event was on the order of 4 m, and at Kewaunee the maximum is nearly 3 m, suggesting the easterly event does retain wave energy as it propagates to the coast.

3.6.4 March 1985 storm

The 3-5 March 1985 storm event was selected based on the water level extreme measured at Kewaunee (7)¹, Ludington (3), Milwaukee (4), Sturgeon Bay (18) and Port Inland (14). Meteorologically speaking, this event affected most of the central and northern water level stations. The event was characterized by strong winds from the east that shifted abruptly to strong winds from the west. Ice was present during this event along the periphery of the lake in certain locations, and the estimates of ice cover came from the Ice Atlas Archive (Assel 2005). Unfortunately there were no wave measurements available to validate either the WAM results or the two wind fields. The only conclusions that can be drawn from the analysis presented below are that results differ.

The WAM simulation was started on 22 February 1985 and ended on 15 March 1985. The NNM used 16 land-based stations, and all were Airport Airways sites. The distribution of these stations is shown in Figure 3-22. Note that the Green Bay location is absent from the list of stations and, as previously mentioned, no buoy data existed hence the winds in the central portion of Lake Michigan are constructed using only land-station information. The distribution of the land-stations is weighted to the west side of the lake, and also to the south. This will have an impact on the generation of the NNM wind and pressure fields.

¹ Note the number indicates the rank of the water level event over the data recovered for each station.

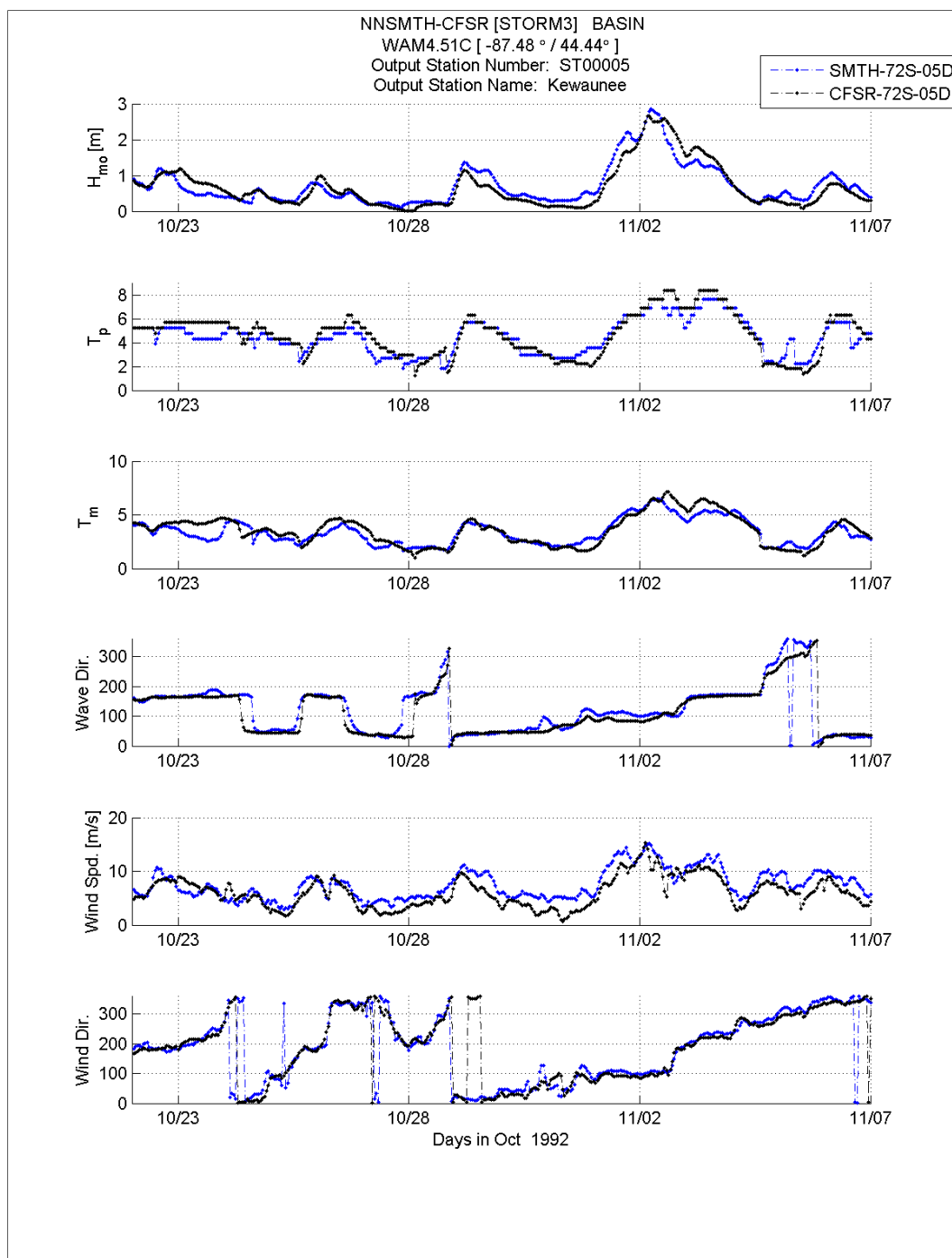


Figure 3-21. Time plots of significant wave height, peak and mean wave period, vector mean wave direction wind speed and direction at a WAM save location offshore of Kewaunee, WI for the November 1992 storm.

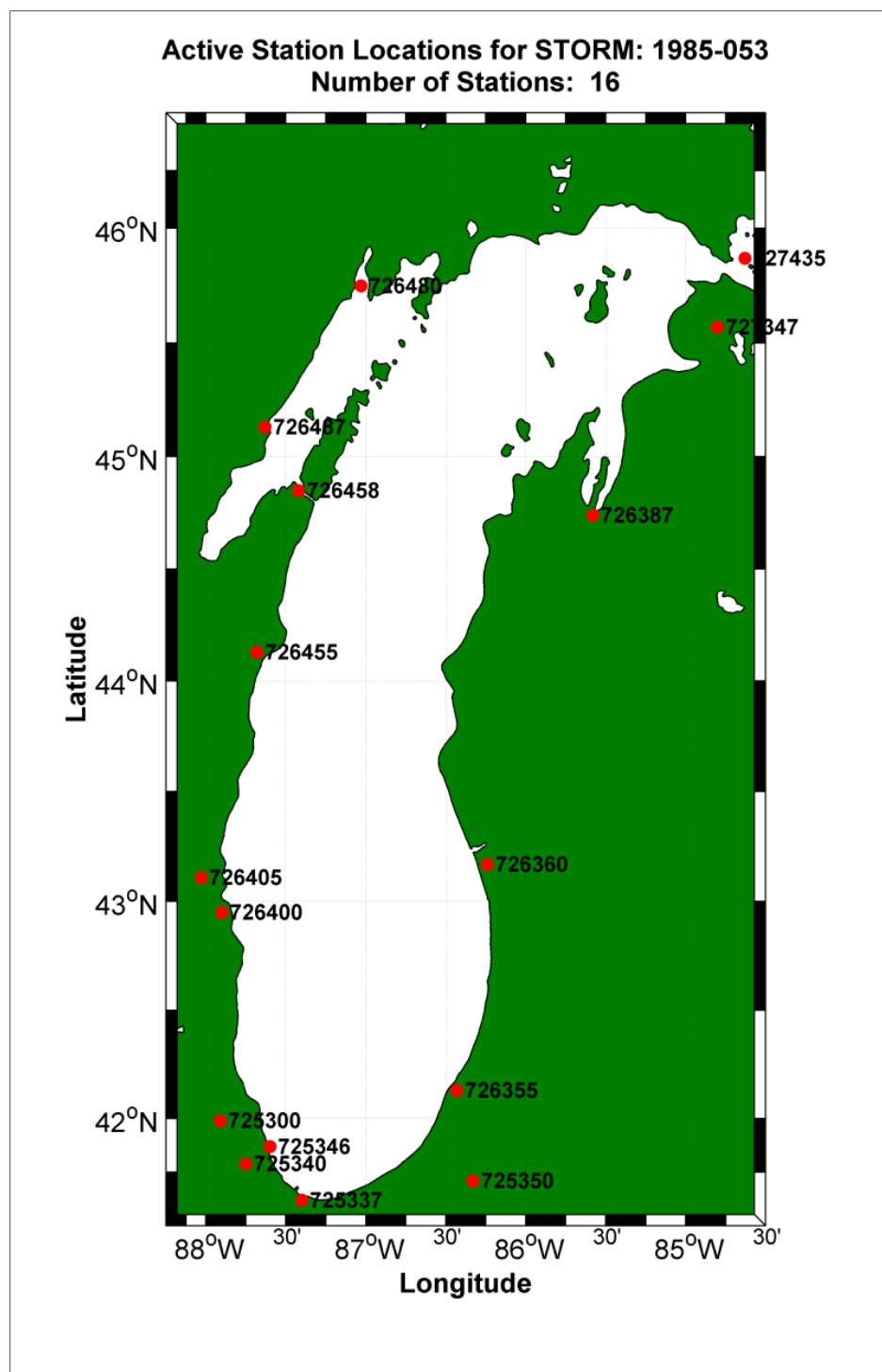


Figure 3-22. Available meteorological station locations accessed and preprocessed for the March 1985 storm.

The maximum wind speed envelope for this simulation is shown in Figure 3-23. It is not surprising to see the entire domain of Lake Michigan is comprised by wind speeds in excess of 15 m/sec, because nearly all of the water level stations on the east and west sides of the lake recorded extreme water level events. The persistent east/west contour orientation from Milwaukee, WI east to Muskegon, MI is the result of the stations recording very similar peak wind speeds as indicated in Figure 3-24. There are only slight temporal phase differences (about 2 hours) for the peak wind speeds of 20 m/sec, for easterly directions. One other observation from this time plot is the occurrence of two storm peaks, the first peak with winds of 20 m/sec out of the east, followed by a sudden drop in wind speed and a equally sudden shift in wind direction to winds of 20 m/sec out of the west. This wind cycle would influence water levels and wind conditions on both sides of Lake Michigan.

The CFSR maximum wind speed envelope (Figure 3-25), is significantly different from the NNM result. The absolute maximum wind speed is slightly higher (25 m/sec versus 22 m/sec), and the location of that maximum is located in the northern region of Lake Michigan. The wind speed falls off rapidly in a southerly direction to about 12 m/sec.

During the simulation the ice fields were accessed and processed. For all local coastal stations along much of the Lake Michigan shoreline the ice concentration level was not less than 80 percent. Based on previous Arctic work (Jensen et al. 2002), these locations would be set to land, resulting in no waves for that period of time. However, the simulation was originally run with no ice coverage to determine the net impact.

As noted previously, there are two ice data sources (Canadian Ice Service, and National Ice Center), and three different flags identifying daily ice field information, no data, interpolated data and observed data (Assel 2005). For the winter ice season, four observed data sets near the time of the event were available (16 February 1985, 23 February 1985, 2 March 1985 and 9 March 1985). All other daily ice fields were interpolated from these four data sets. Displayed in Figures 3-26 through 3-29 are the ice fields for observed data from 16 February 1985 through 9 March 1985. The amount of coverage varies from one set to the next, where the eastern sections of Lake Michigan are apparently ice free then become covered, and along the northern shoreline the region is ice covered and then becomes ice free. The estimation of ice coverage and concentration levels is not exact, so these estimates have to be treated as approximations. The net effect on the wave

simulations (assuming a 70-percent concentration level to set the WAM water point to land) for the noted water level stations are as follows:

- Milwaukee, WI Ice covered for all of the storm
- Kewaunee, WI Ice covered for all of the storm
- Ludington, MI Ice free until 9 March
- Sturgeon Bay, WI Ice covered for all of the storm
- Port Inland, MI Ice covered until 2 March then ice free

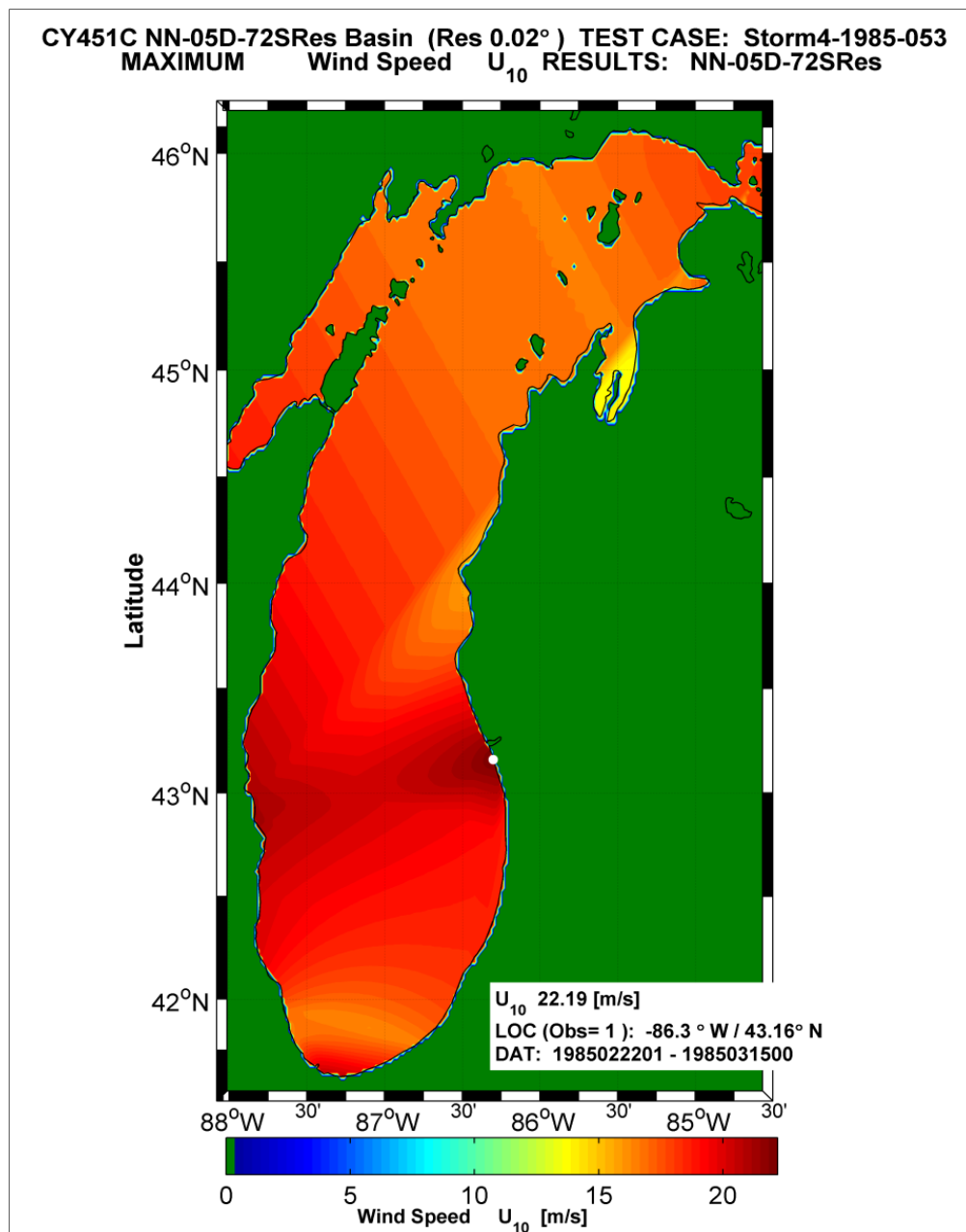


Figure 3-23. Maximum wind speed envelope for the March 1985 storm derived from the NNM wind field generation routine.

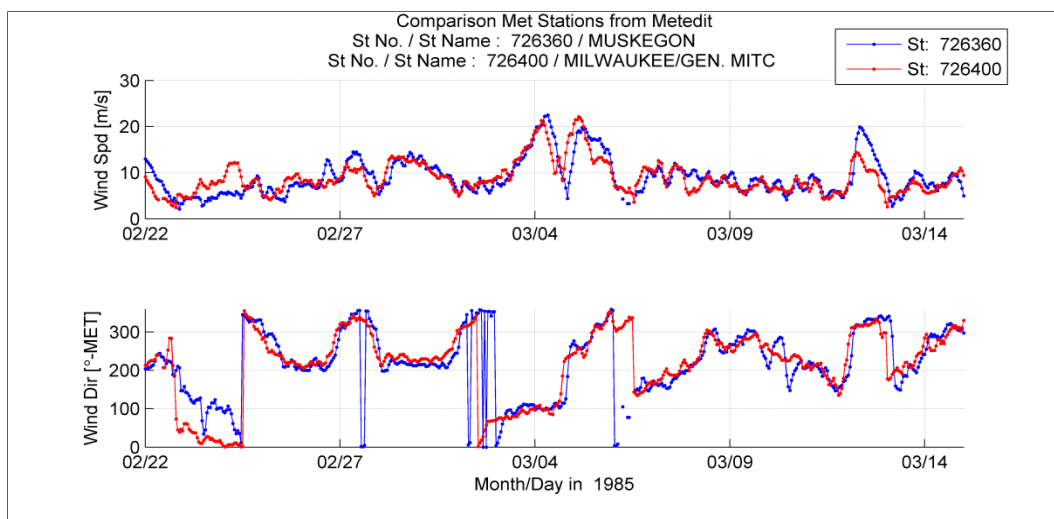


Figure 3-24. Time plot of winds at Muskegon (726360) and Milwaukee (726400) Airways Stations for the March 1985 storm.

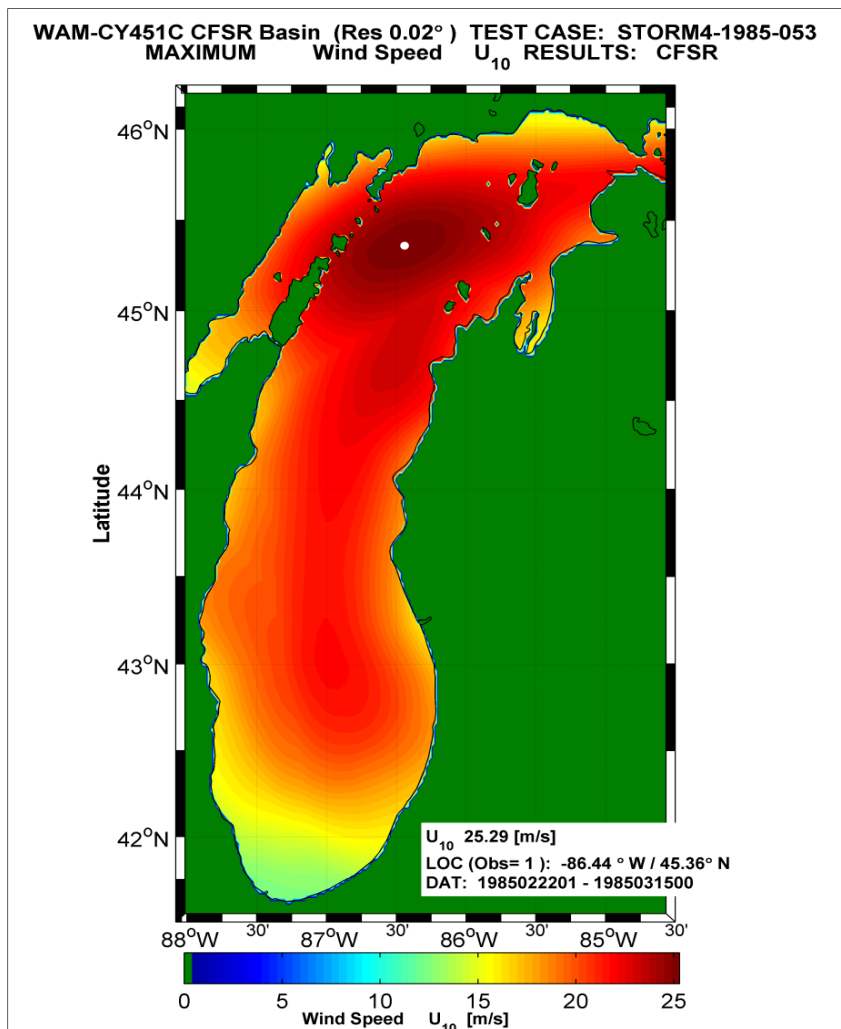


Figure 3-25. Maximum wind speed envelope for the March 1985 storm derived from the CFSR wind field generation routine.

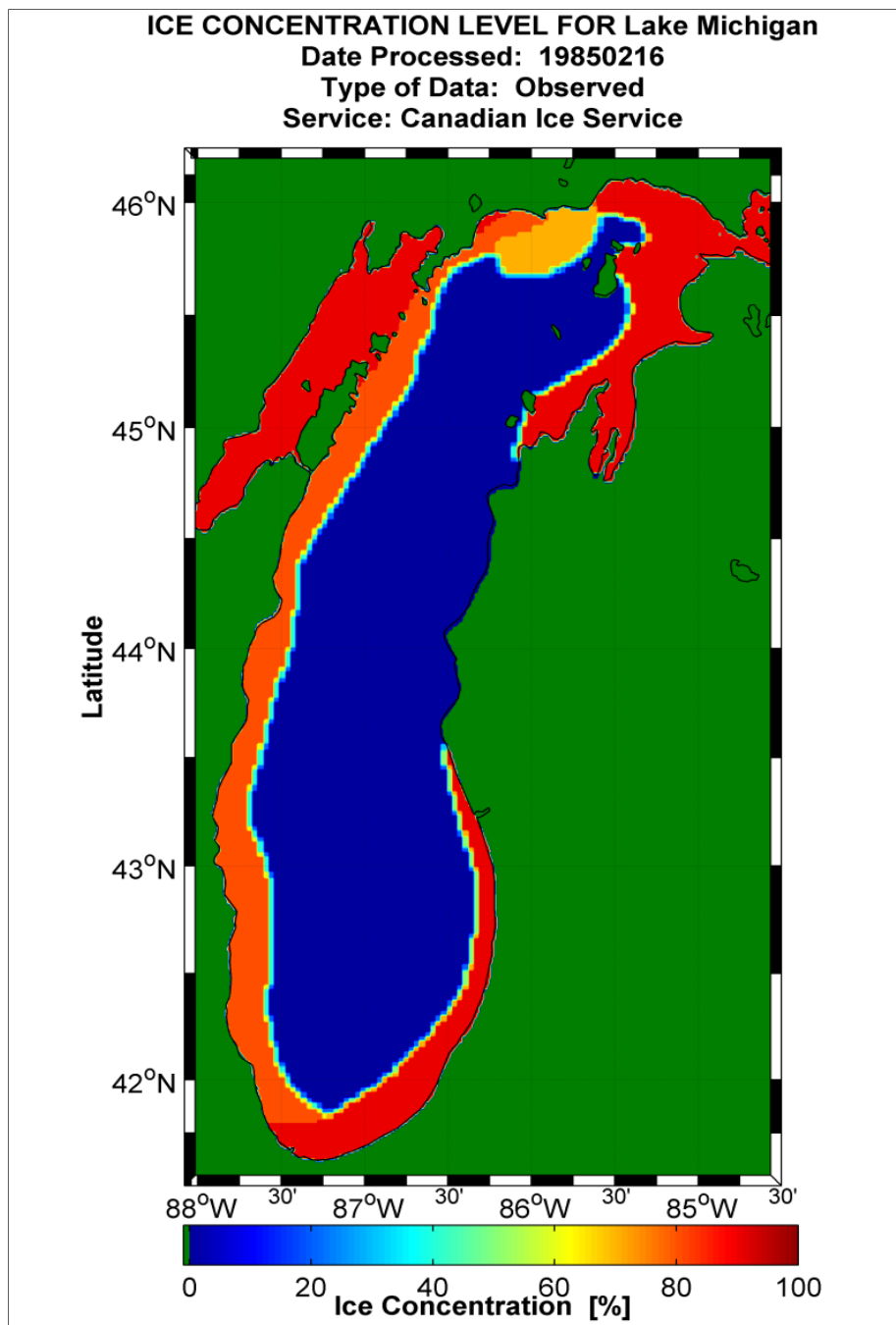


Figure 3-26. Ice concentration level for 16 February 1985 (Assel 2005).

The March 1985 storm was originally run without ice fields as input. A time plot of the WAM results for a site just offshore of the Ludington, MI water level site is shown in Figure 3-30. As stated earlier, this location at the start of the simulation was ice free. Based on the Assel (2005) ice field archive, Ludington, MI was iced over on 9 March 1985. In general, the wave estimates displayed in Figure 3-30 would be zero from 9 March 1985 to the end of the simulation.

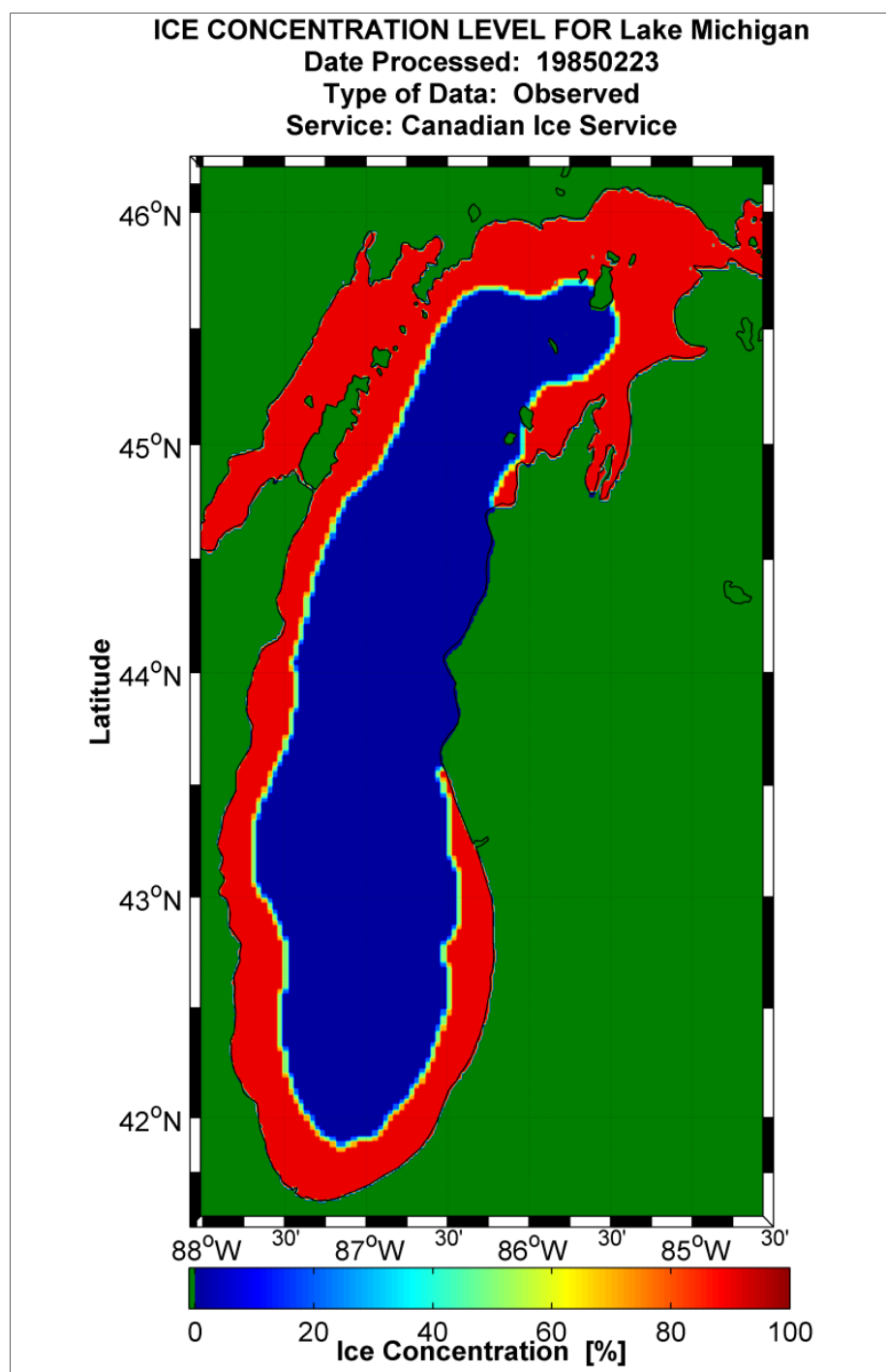


Figure 3-27. Ice concentration level for 23 February 1985 (Assel 2005).

3.6.5 December 2009 storm

This storm event, which occurred on 9 December 2009, was selected based on the extreme water levels measured at both Green Bay, WI, and Holland, MI, the second and tenth highest events on record at those two sites,

respectively. The two NDBC buoys had been retrieved for the winter in mid-November; therefore validation of the WAM results could not be performed using these data. There was a newly found data set at Buoy 45020 a directional wave buoy in Grand Traverse Bay where it remained in the water through this storm simulation. However this data set was not processed at the time of this report.

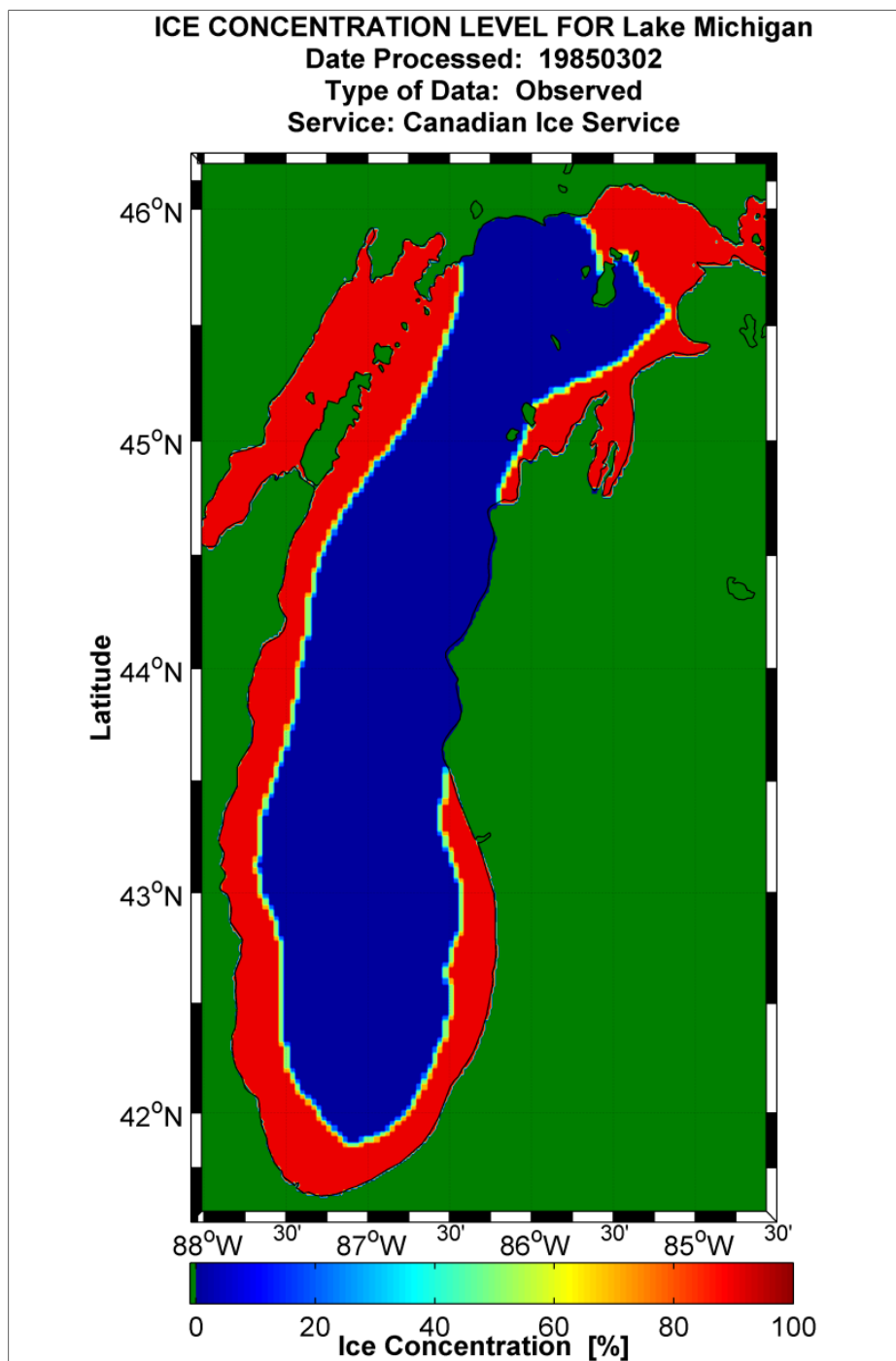


Figure 3-28. Ice concentration level for 2 March 1985 (Assel 2005).

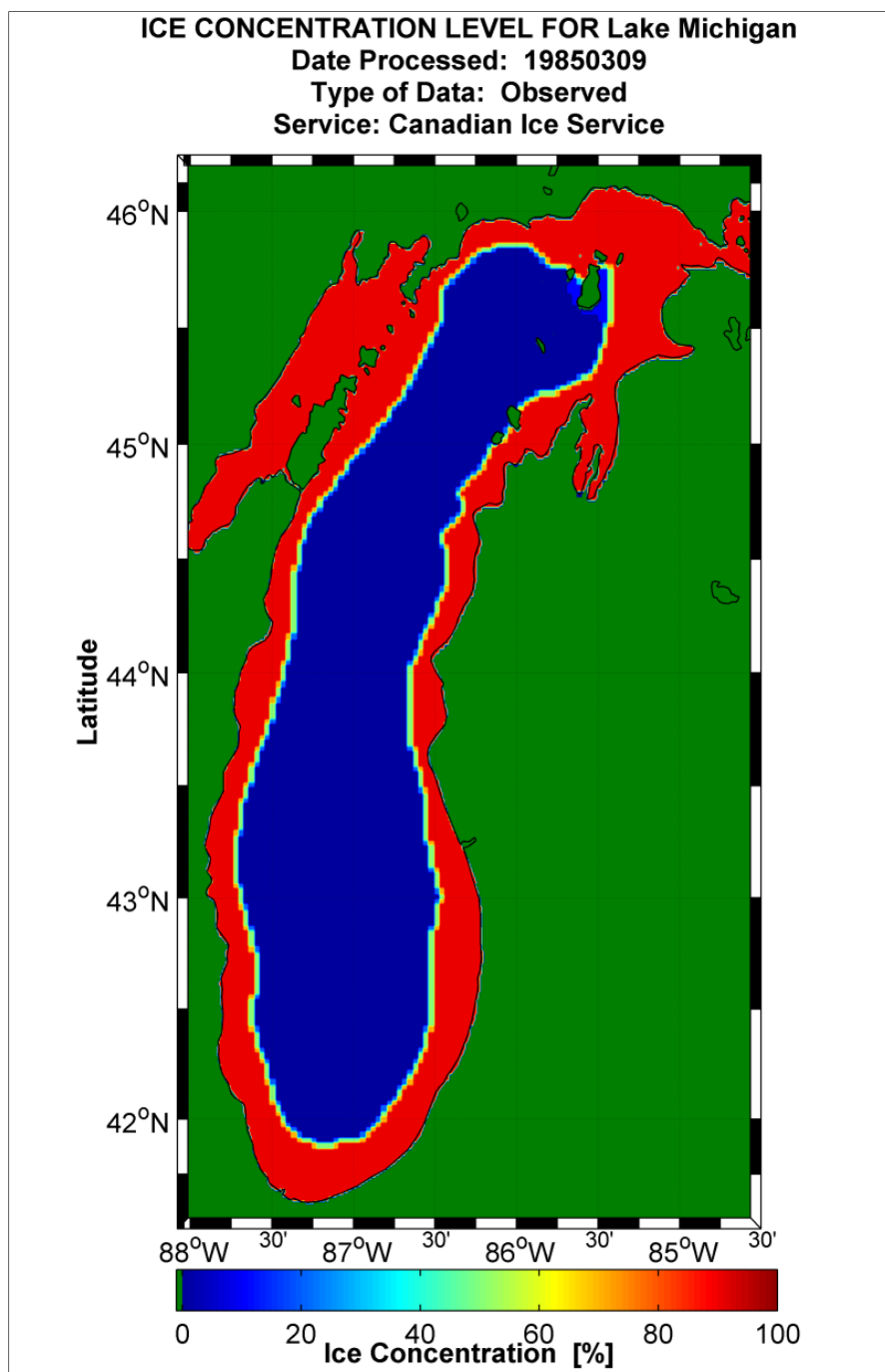


Figure 3-29. Ice concentration level for 9 March 1985 (Assel 2005).

The simulation for this storm was initiated on 30 November 2009 and ran through 10 December 2009. Information regarding ice coverage was limited to two graphic products (7 and 14 December 2009) which were obtained online from the North American Ice Service. The digital information was ultimately obtained from NOAA/GLERL and is presently being analyzed. The NNM used a total of 58 land-based meteorological sites. The location

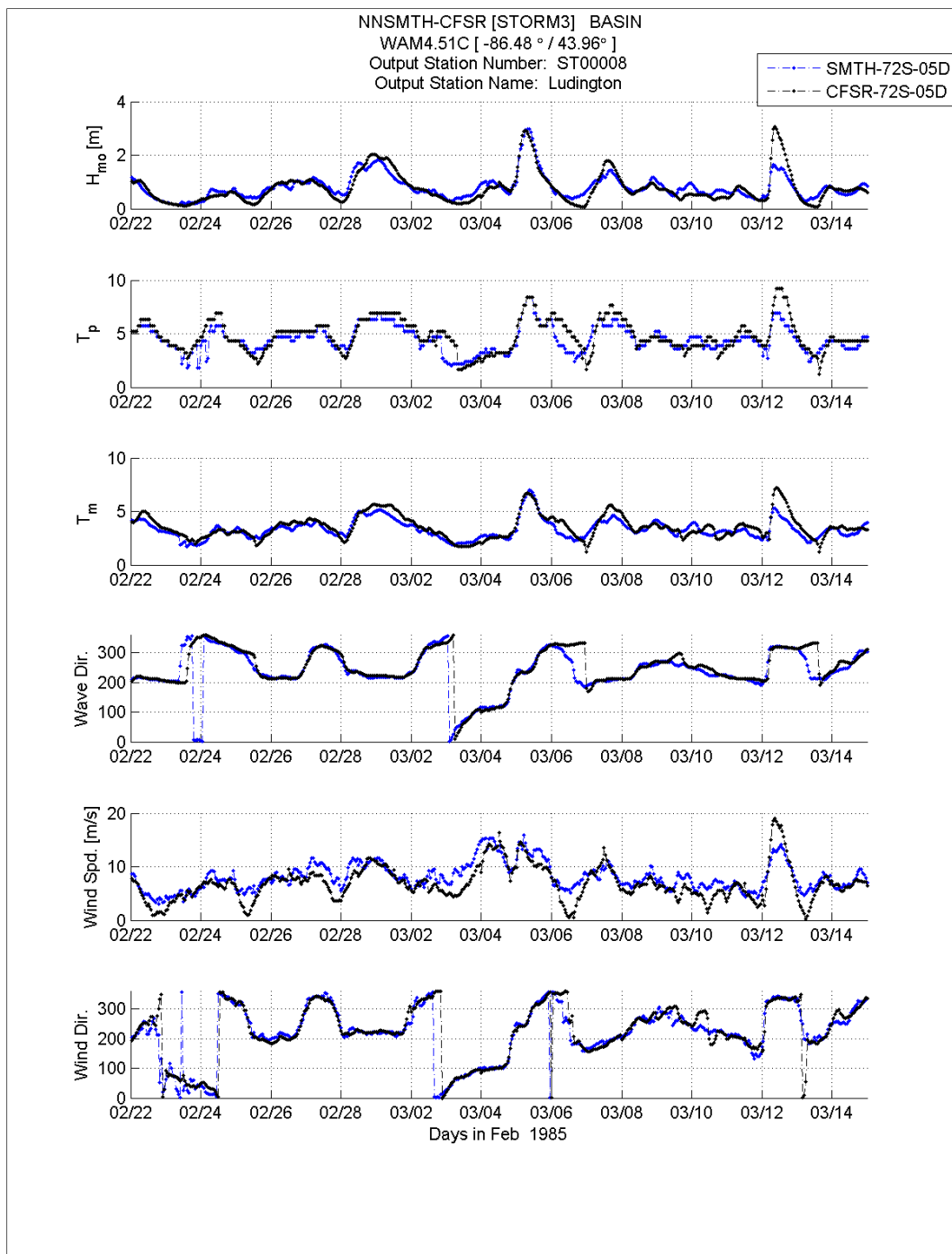


Figure 3-30. Time plots of significant wave height, peak and mean wave period, vector mean wave direction wind speed and direction at a WAM save location offshore of Ludington, MI for the March 1985 storm.

and coverage for those sites is provided in Figure 3-31. There is a significant amount of redundancy of station data especially along the western Lake Michigan coastline. However, many of the individual stations were subject to data drops over time, or acquired only limited data for the storm dura-

tion. For example, the Green Bay, WI site (726450), wind data was only available at 3-hr intervals. This compared to the previous storm simulations where the data interval was generally 1-hour. Also, based on the individual wind speed and direction traces, the duration of high winds (e.g. 20 m/sec) varies from 6 to as much as 12 hours depending on the geographical location.

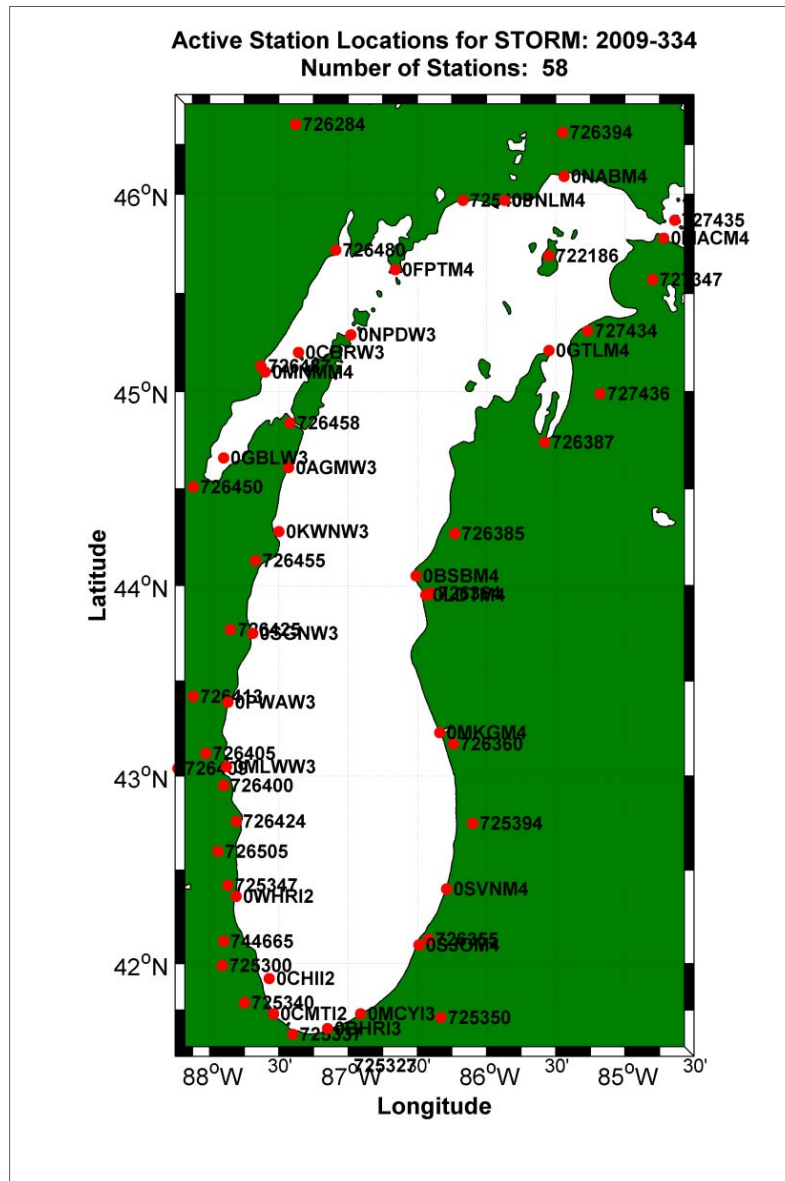


Figure 3-31. Available meteorological station locations accessed and preprocessed for the December 2009 storm.

The NNM maximum wind speed envelope for this storm is displayed in Figure 3-32. Despite the number of land-based stations surrounding Lake Michigan, these winds are constructed without any measurements from the

buoys in the middle of the lake. The NNM again reflects the pockets of point-source data. The NOAA/NWS station GLTM4 at the northern end of the Grand Traverse Bay Peninsula recorded a wind speed of 20 m/sec. After transforming to over-water and compensating for stability effects, the original wind speed increased by nearly 30 percent. The Beaver Island Station (722186) and Charlevoix (727434) original data were in the range of 10 to 15 m/sec. On the western side the NOAA/NWS station NPDW3 at Northport Pier station recorded winds of about 17.5 m/sec just before the data stopped. This major lobe of relatively high winds is to be expected. Inside of Green Bay, the NOS Station MNMM4 along with the NWS Chambers Island (CBRW3) recorded 17.5 m/sec peak winds, while the Menominee (726487) peaked at over 20 m/sec, all providing input to NNM generating 20 m/sec wind maximum lobes. In the southeastern portion of Lake Michigan a similar situation exists, where multiple land station data sets are in a range of 18 to over 20 m/sec before any transformation to over-water wind estimates are performed. Lastly, much of Lake Michigan is comprised of maximum wind speeds of 14 to 17 m/sec.

The CFSR maximum wind speed envelope (Figure 3-33) shows a much different trend in the fields. Note the change in the color scale. There are three distinct lobes of high wind speeds, of nearly 20 m/sec. The lobe in the northern region of the lake is in a similar position as the high-wind region in the NNM result. Winds throughout the rest of the central and lower parts of the lake are much higher in wind speed than the NNM winds. There is no high wind peak in the southeastern corner of Lake Michigan as indicated in the NNM wind maximum envelope.

What occurred was a very intense low pressure system moving from southwest to northwest with an accompanying occluded front¹. The storm system moved from about Chicago to just east of the Mackinaw Straits in about 9 hours. Based on the track and surface weather charts the resultant CFSR maximum wind speed envelope appears to be consistent. The wind field shown in Figure 3-33 looks very similar in structure and features as fields shown in previous storm scenarios.

As previously indicated, there were only two ice fields available for this storm simulation, 7 and 14 December 2009. The 7 December ice analysis showed the entire Lake Michigan domain to be ice free. On 14 December,

¹ Cold front overtaking a warm front as part of the latter stages of cyclogenesis.

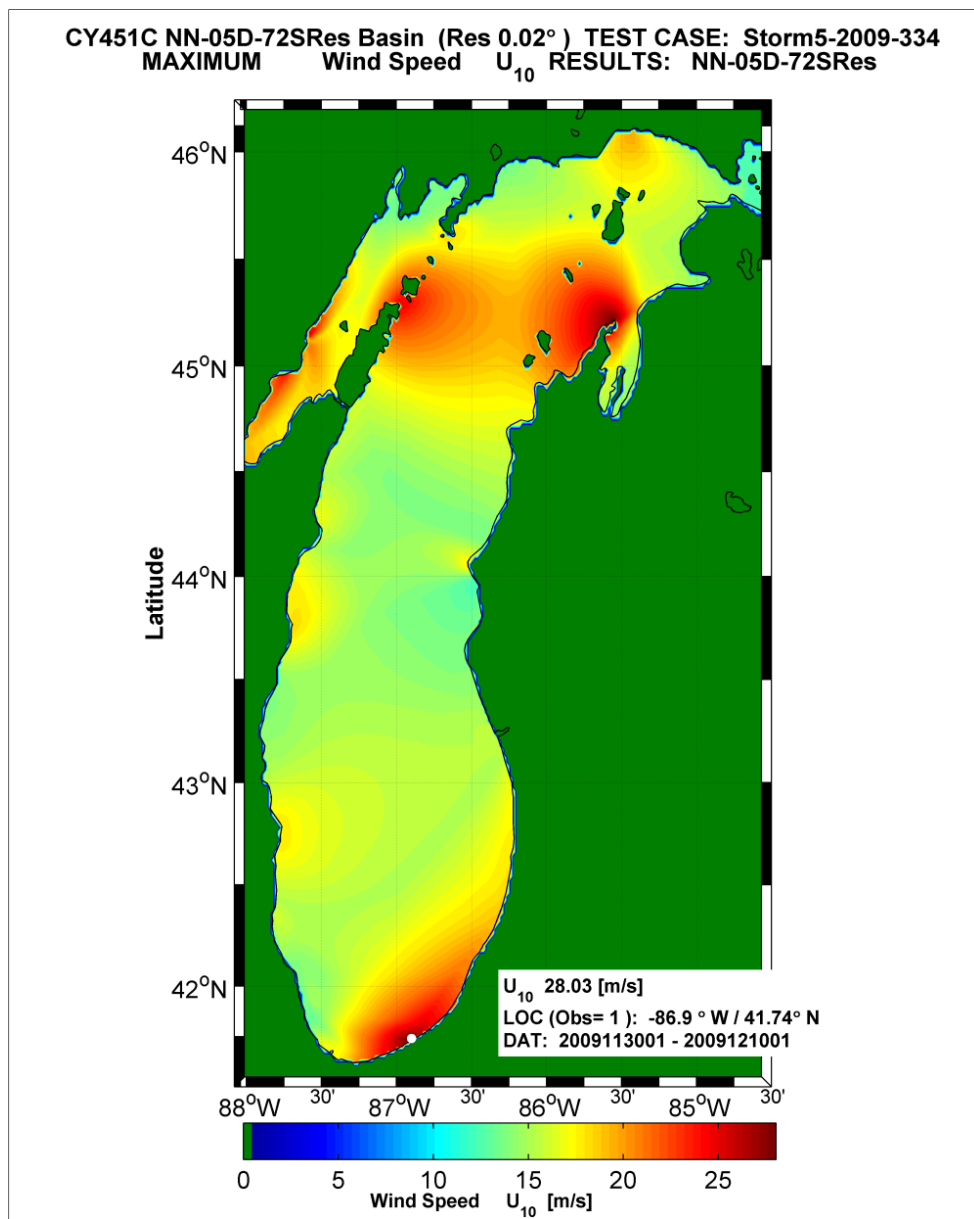


Figure 3-32. Maximum wind speed envelope for the December 2009 storm derived from the NNM wind field generation routine.

the conditions changed, and the extreme southern and northern portions of Green Bay contained estimates of ice concentration exceeding 90 percent (see Figure 3-34). About one quarter of the south end of the bay contained concentration levels of 70 to 80 percent; and the remainder of the bay had estimates of 10 percent concentration or less.

The water level peak at Green Bay occurred on 9 December 2009. It is unknown when ice began to form in Green Bay during the time 7 until 14 December; therefore the model simulations assumed no ice coverage.

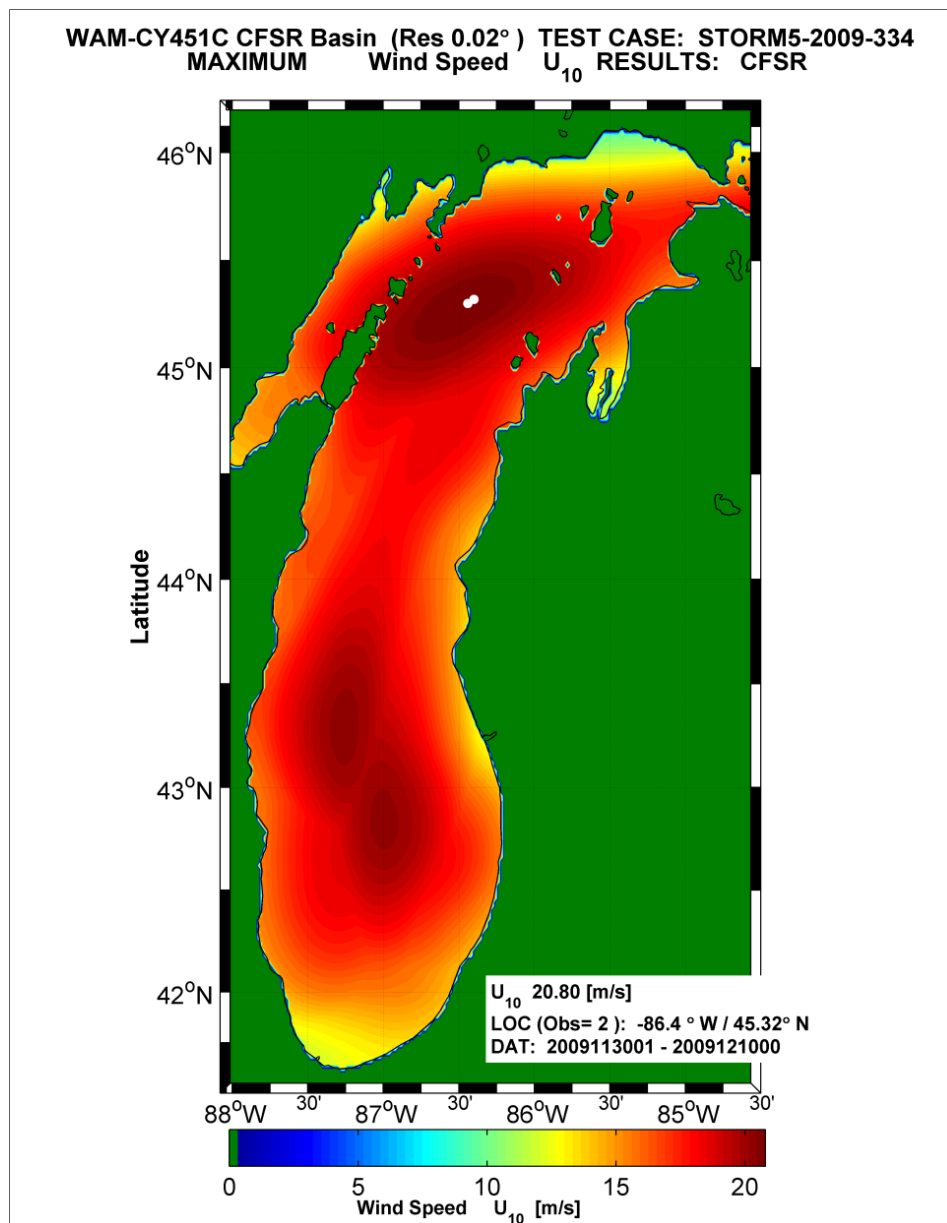


Figure 3-33. Maximum wind speed envelope for the December 2009 storm derived from the CFSR wind field generation routine.

Unfortunately no validation of the wave model results could be performed due to lack of data. Only differences between NNM and CFSR wind forcing can be assessed. Two sites in the WAM grid are compared to evaluate those differences. The first is offshore of the Green Bay gage location (identical site used in previous storm simulations) where results are shown in Figure 3-35. For this simulation there are identifiable differences between the NNM and CFSR results. All wave parameter differences between the two simulations can be explained by differences in the wind estimates. The NNM wind speeds are greater by about 5 to 7.5 m/sec than the CFSR

estimates. And despite the 1:1:1 temporal smoothing used in the NNM the wind speed trace is quite noisy. There are more available land based meteorological stations for the construction of the wind fields for this case compared to the previous simulations (Figure 3-36). Secondly, there are clear definable differences in the wind magnitudes near the storm peak. Two stations located at Menominee, WI (MNMM4 located closer to the water, and 726487) shown by the green and black lines display major differences. The Menominee Airways station is phase shifted by nearly

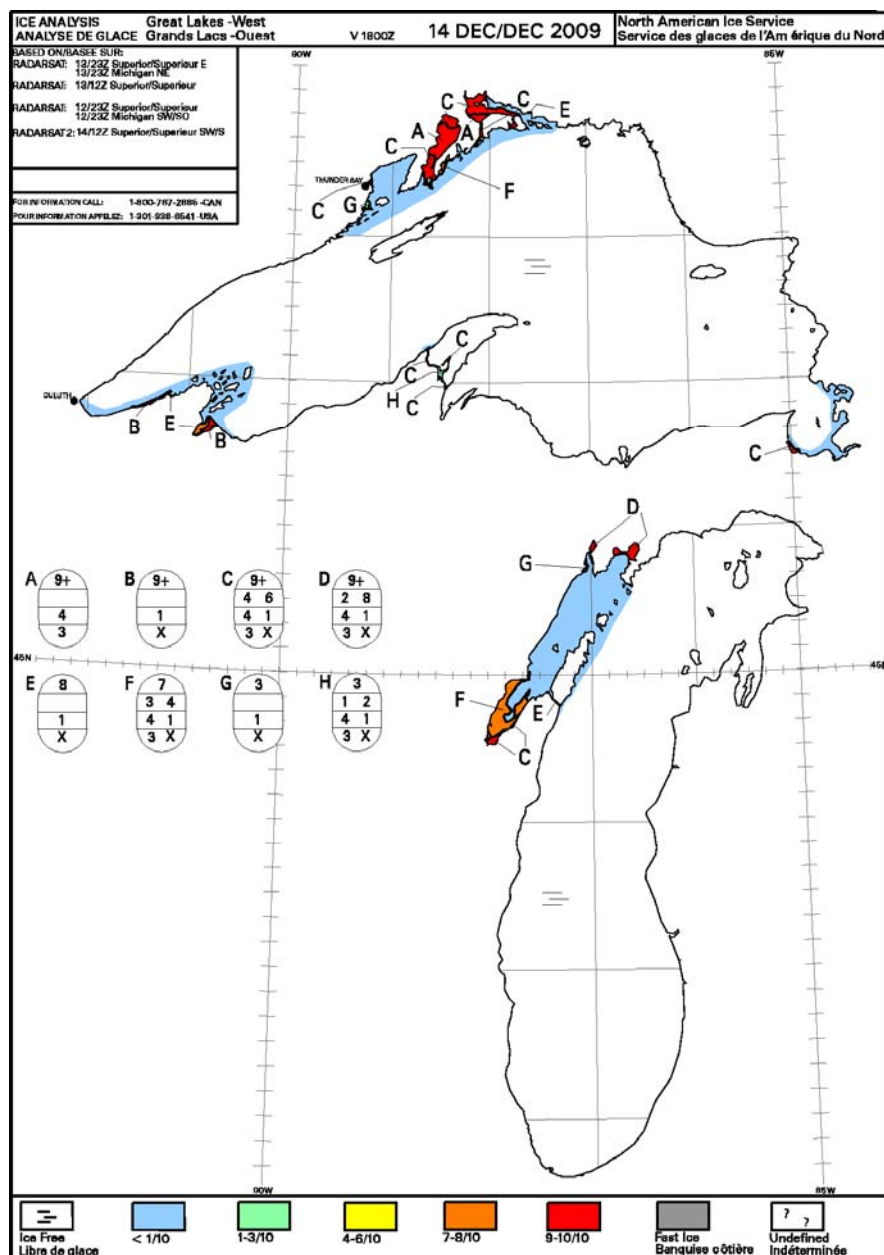


Figure 3-34. Ice concentration estimates for 14 December 2009, from the Canadian Ice Service.

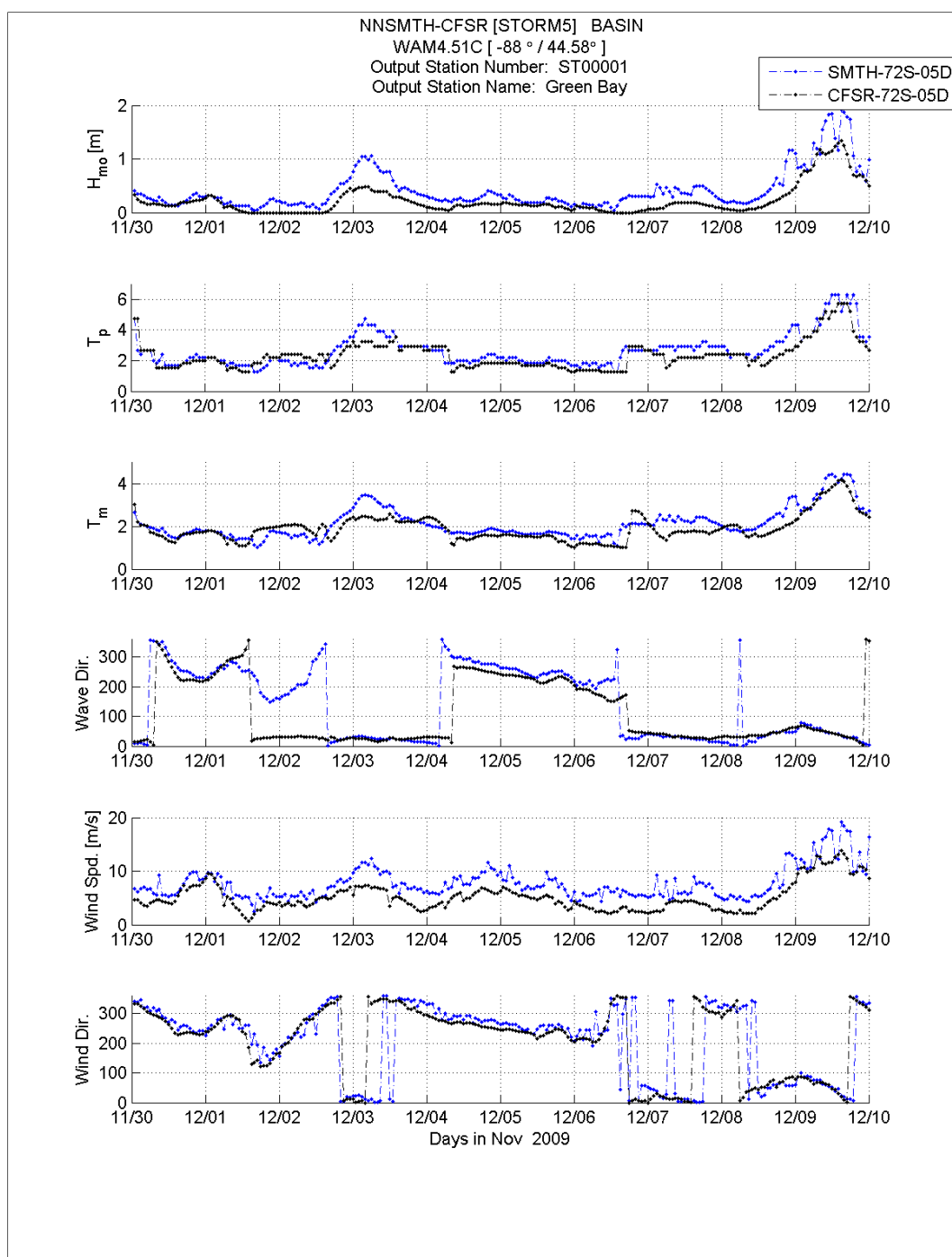


Figure 3-35. Time plots of significant wave height, peak and mean wave period, vector mean wave direction wind speed and direction at a WAM save location offshore of Green Bay, WI, for the December 2009 storm.

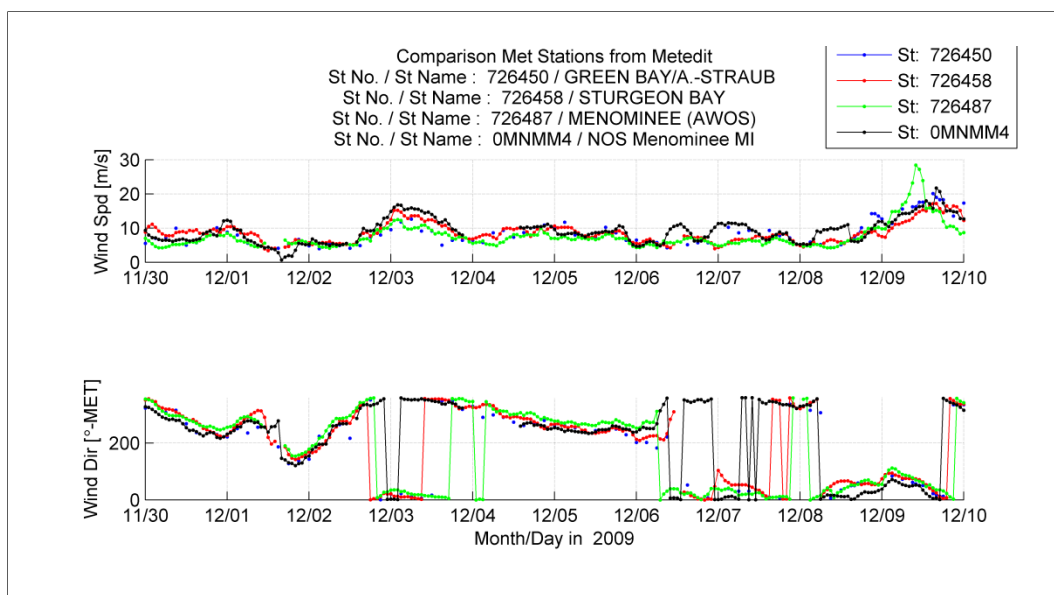


Figure 3-36. Time plot of wind speed and direction from four meteorological stations in the mid- and southern portions of Green Bay, used in the NNM wind field generation for the December 2009 storm.

7-hours, and measures peak winds near 30 m/sec. At the second Menominee station (MNMM4), the wind speeds and phasing are consistent to the other two sites. This does raise questions regarding the implementation of the NNM. All land-station data with co-located operational stations require additional evaluation and perhaps selectively removing inconsistent data sets, as in the case of the Airways station 726487. This could actually remove a very local wind event that would have an impact on the local estimates of the waves and water levels. Without water level and wave data in the area, this procedure could remove an extreme event. Retaining data that appears to be inconsistent with surrounding meteorological stations as shown in Figure 3-36 could potentially introduce errors in the wind speeds and affect the wave and water level estimates. Additional testing by selectively removing land-stations like past hindcast studies (e.g. Hubertz, et al. 1991; and Resio and Vincent 1976a) may be required especially in light of requiring use of NNM when the CFSR wind and pressure fields are not available (e.g. pre-1979).

As indicated all of the differences between the integral wave parameters based on the two simulations are wind speed related. This example demonstrates that generalizations regarding CFSR tending to provide higher H_{mo} , T_p and T_m results cannot be made universally. For this case, the NNM-forced wave heights trend higher, by as much as 0.75 m at the storm peak

on 9 December 1200UTC, and show more temporal oscillations compared to the slowly varying conditions defined from the CFSR wind forcing.

Also included in this evaluation are the wave model results from a location offshore of Holland, MI (see Figure 3-37). This storm event is the 10th highest water level event over the record period at Holland. The wind speed traces show relatively similar trends. Again the CFSR wind speeds are lower than the NNM winds at this location. Also there seems to be a persistent 6-hr oscillation in the CFSR wind speed, of unknown origin. One possibility is that some of the Airway meteorological stations in more recent time (derived from the ISH data archive) only recorded at 6-hr intervals. Using data assimilation procedures and a lower temporal resolution on these measurements could produce these results. Also during the peak wave event at Holland the wind directions shifts dramatically, with an accompanying decrease then increase in intensity suggesting a low pressure center moving through this location. The winds shift from easterly to southwesterly, and the wave heights rapidly grow from 0.5 m to about 2.5 m.

3.6.6 October 1993 storm

The 1 October 1993, was added to the list of validation events in light of the occurrence of extreme storm generated wind waves observed in Lake Michigan and availability of wave data from three buoys. As noted in the previous section on Point-Source Wave Measurements during this time period, one additional NDBC buoy was deployed just offshore of Milwaukee, WI (See Figure 3-3). During this event, waves measured at 45002 (NDBC-North Lake Michigan) recorded the fourth largest condition in its 30-year record; while at 45007 (NDBC-South Lake Michigan) the event was the 38th largest condition in the record. The simulation period contained the second largest wave height measured at 45010; however the data record was only 3 years long.

The NNM winds were constructed from 24 land based stations surrounding the lake, including the three buoy sites, and one NDBC CMAN location. During this simulation there were eleven shifts in the wind direction of at least 90 deg. The largest storms peaks were caused by southerly and northerly winds that were observed at all three buoy sites. These wind directions have been shown to be problematic for the NNM in other events, by not retaining spatial coherency along the central axis of Lake Michigan. Because these conditions frequently occurred during the 22-day simulation, simulation of this storm provides more insights to this issue. Rather than

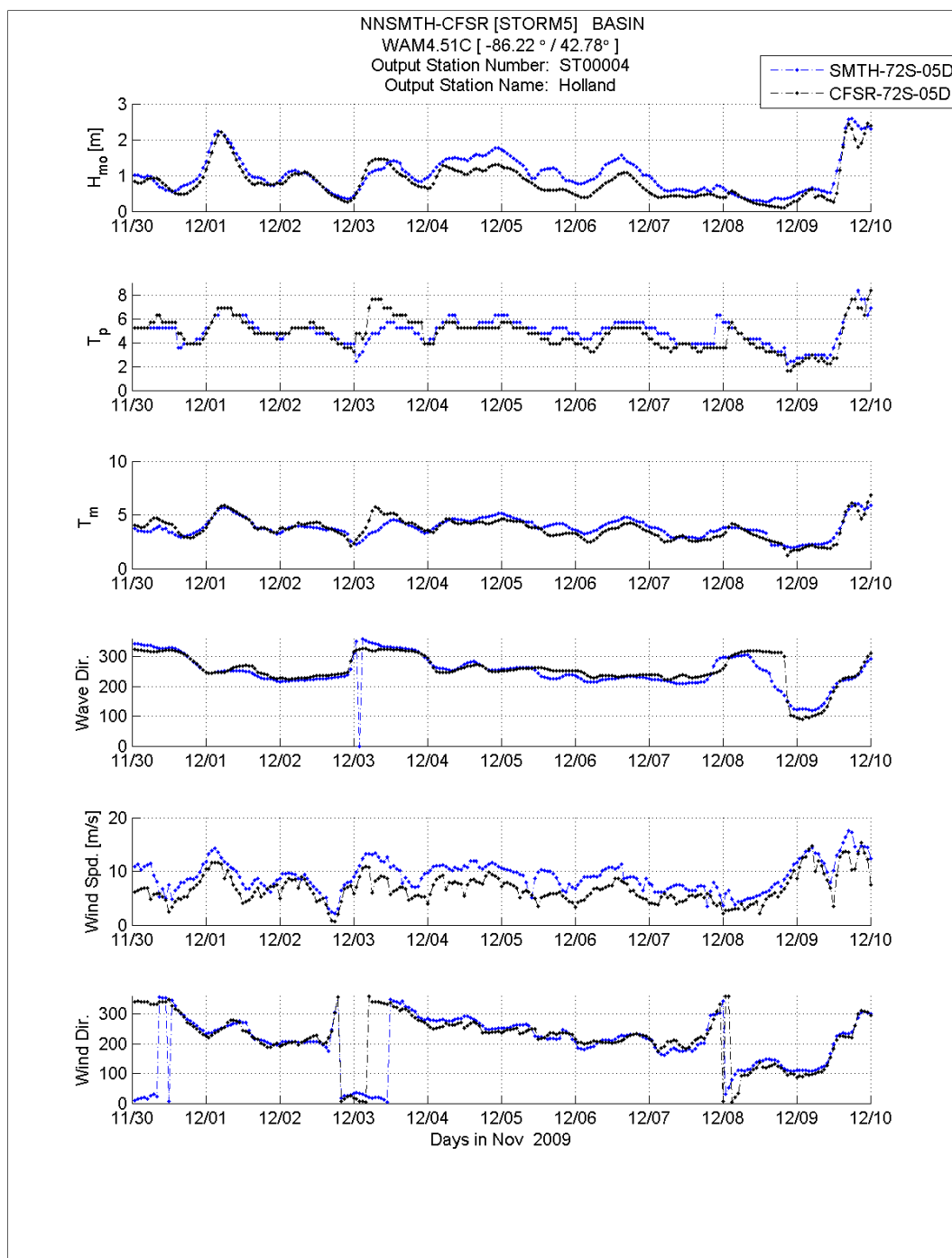


Figure 3-37. Time plots of significant wave height, peak and mean wave period, vector mean wave direction wind speed and direction at a WAM save location offshore of Holland, MI, for the December 2009 storm.

focus on the differences between the NNM and CFSR wind speeds using the maximum envelope method, it is sufficient to say that similar differences found in previous storm simulations occurred in for this case too. The CFSR maximum wind speed envelope contains one primary lobe of high winds in

the northern portion of Lake Michigan (overall maximum of 20 m/sec), a secondary lobe around 43-deg N latitude, and the remainder of the lake contained maximum wind speeds in excess of 15 m/sec. The NNM maximum wind speed envelope consists of multiple lobes radiating outward from many of the land based meteorological stations. The absolute maximum wind speed of about 21 m/sec is located just offshore of Chicago. The remainder of the lake was filled with maximum winds of about 15 m/sec.

Time plots for the validation study are provided in Figures 3-38 through 3-40 for NDBC stations 45002, 45007 and 45010, respectively. The first event on 1 October is a south-southwesterly wind, topping out at nearly 20 m/sec at 45002, (Figure 3-38).

This storm produced similar trends at the northern buoy (45007, Figure 3-39), and at Milwaukee (45010, Figure 3-40); however the magnitude of the winds at these two buoys peaked at about 18 and 13 m/sec, respectively. Wind traces derived from NNM and CFSR closely followed the measurements. Because the NNM uses all buoy data it is not surprising to see good agreement. However, the CFSR showed very similar trends during the initial growth in the storm, but in the decay diverged slightly. The WAM wave height results closely followed the trends of the measurements at 45002. The NNM simulation appears to be lower around the peak and through the decay of the 1 October event, whereas the CFSR nearly matches the storm peak, and well replicates the decay.

These trends persist for the entire duration of the simulation, where CFSR derived wave estimates fall closer to the peaks and NNM results are biased low by at most 0.25 m. The peak spectral wave period results for the CFSR run are in close agreement with the measurements at 45002, whereas NNM is slightly lower. As in all previous test cases, the mean wave period model results tend to be lower than the measurements.

At the northern buoy 45007, (Figure 3-39), the winds from the CFSR fields show some phase shifts relative to measured winds for the first storm, and a tendency to be biased slightly higher than the observations from about 2 October through 8 October. This tends to bias the wave estimates at 45007 during the first storm, and subsequent minor events during the same period. However, for the second major storm on 9 October (a northerly wind), CFSR nearly matches the growth, peak and decay cycles, whereas the NNM wave model simulation clips the peak. This is most

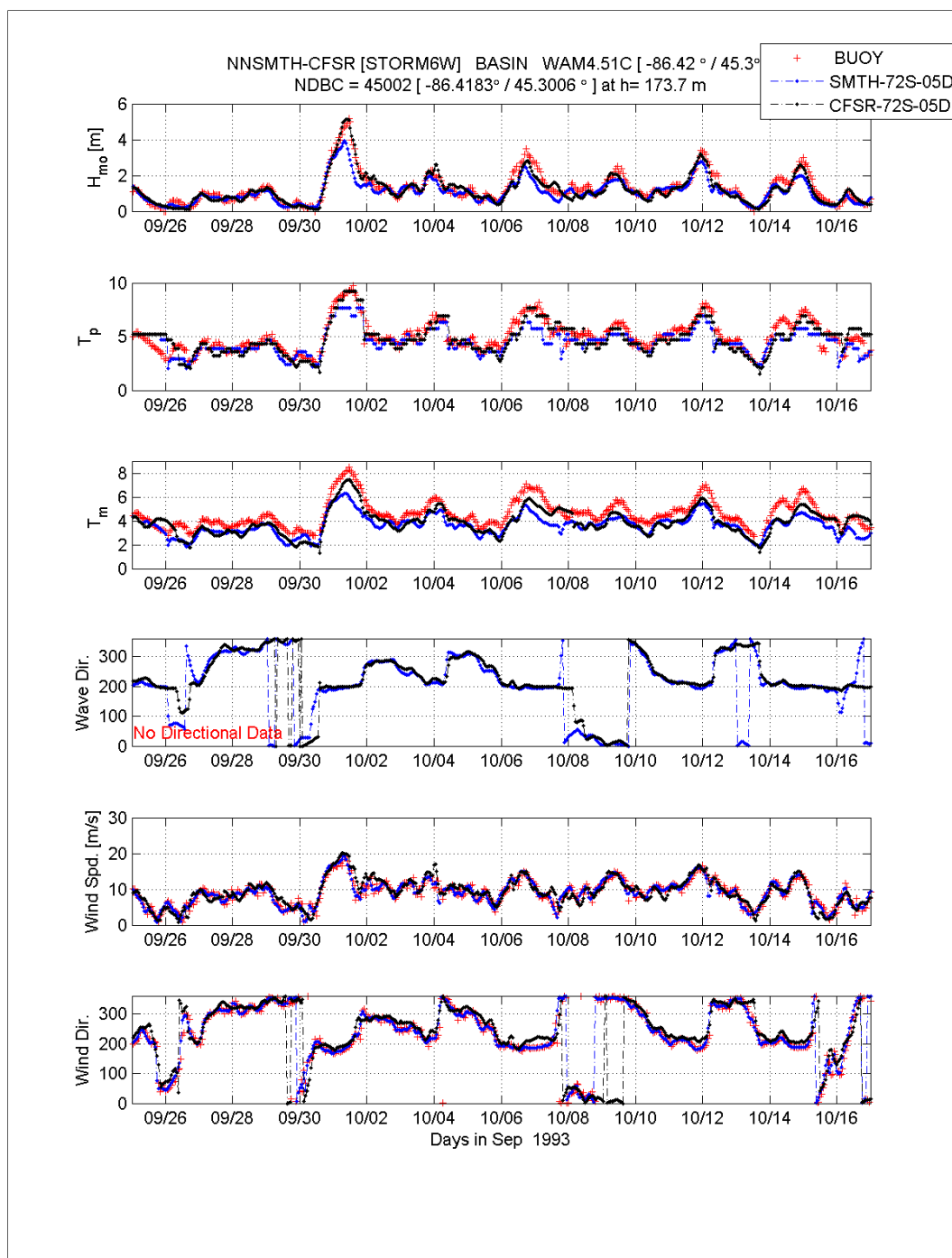


Figure 3-38. Time plots of significant wave height, peak and mean wave period, vector mean wave direction wind speed and direction at NDBC 45002 for the October 1993 storm.

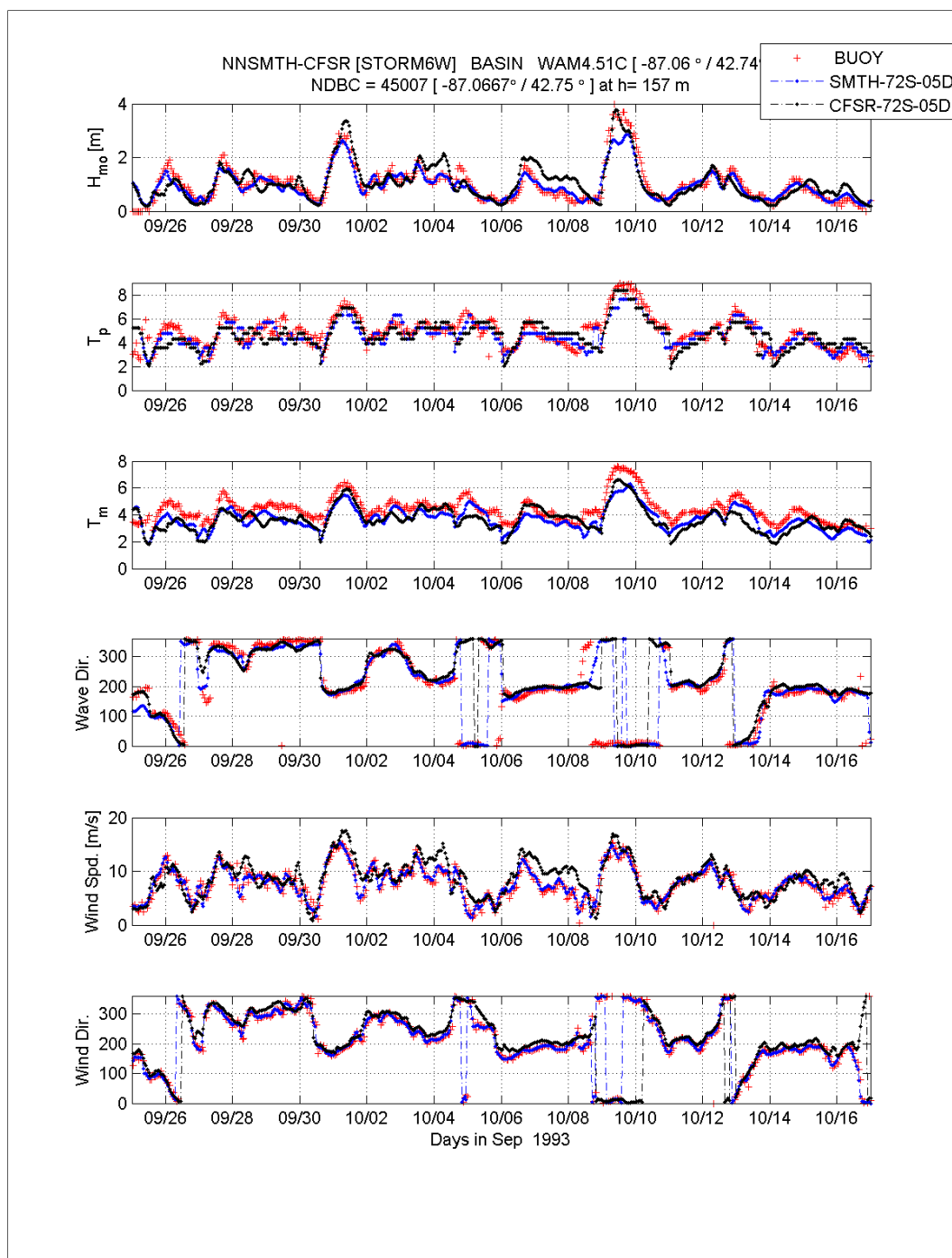


Figure 3-39. Time plots of significant wave height, peak and mean wave period, vector mean wave direction wind speed and direction at NDBC 45007 for the October 1993 storm.

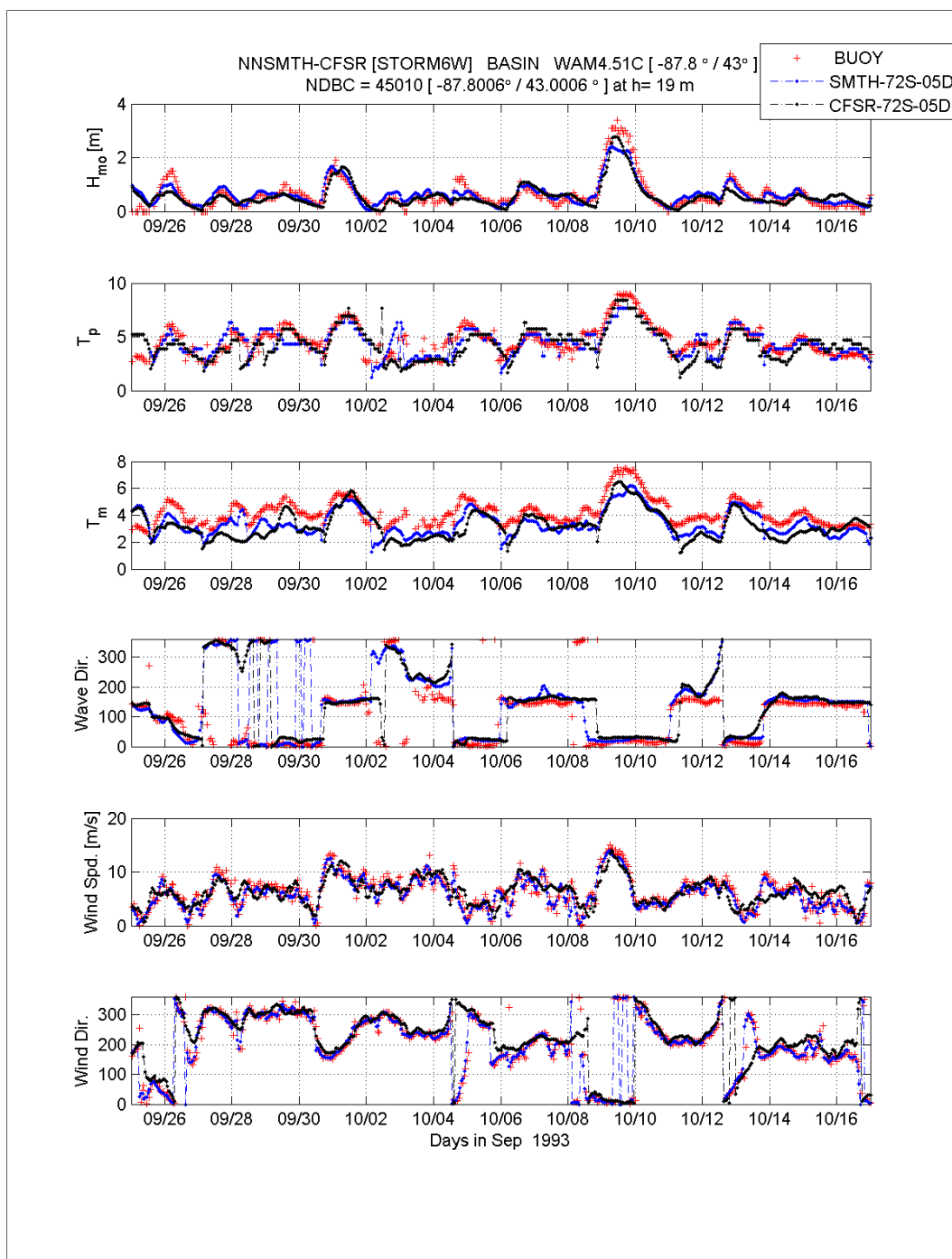


Figure 3-40. Time plots of significant wave height, peak and mean wave period, vector mean wave direction wind speed and direction at NDBC 45010 for the October 1993 storm.

likely due to the loss in spatial coherence in the NNM winds. The peak and mean wave period results are similar to those found at the northern buoy, where both simulations nearly replicate the peak spectral wave period, and tend to be lower for the mean wave period. The vector mean wave directions derived from NNM and CFSR simulations match the measurements for

the entire simulation period, which is good skill considering the frequent shifts in wind and wave directions.

The primary reason for selecting this event is having one added point source wave measurement site for comparison. This location (see Figure 3-3) is just offshore of Milwaukee, WI in a water depth of 19 m. It is also in the region where there have been discernible differences in the maximum wave height envelopes from previous tests. The time plot (Figure 3-4o) illustrates some of the similarities and also differences between observed predictive skill at the north and south buoy sites. The first storm (1 October) is well replicated using the NNM winds whereas the CFSR forced wave model run shows some phase differences, and slightly under-estimates the peak of the storm by about 0.25 m. For the second storm peak on 9 October, both results fall below the measurements. The CFSR results better approximate the temporal structure of the storm, whereas the NNM derived wave estimates clip the storm's peak conditions by about 0.75 m.

The peak and mean spectral wave period model results emulate the under-estimation found in the other two locations. The vector mean wave direction for both wind forcing WAM runs show larger differences especially during the directional shifts. The errors in the CFSR wave estimates seem to be correlated to differences found in the wind estimates, not only in magnitude but also the directions. CFSR does not show the geophysical variability over time as well as the NNM winds; however, note that the buoy winds are used in the construction of the NNM fields.

3.6.7 May 1998 storm

The 31 May 1998 event was the only event that did not occur in the fall or winter months. This May 1998 water level event at Calumet was the fourth largest in the water level data base, and only consisted of one extremely elevated observation, derived from hourly data records. There was a rapidly moving low pressure center that propagated across the northern portion of Lake Michigan along a line from the southern end of Green Bay to Grand Traverse Bay. The two mid-lake NDBC buoys were deployed during the simulation, and will be used for validation. Twenty-six meteorological stations were used in the construction of the NNM wind fields. One can note that for the maximum wind speed envelope, the CFSR winds generate a lobe of wind speeds in the northern area of Lake Michigan, with an overall maximum speed of 18 m/sec. There is a secondary lobe covering the mid lake domain extending from 42- to 44-deg N latitude with magnitudes of

about 12 m/sec. The NNM results show a similar northerly maximum wind speed lobe with its overall maximum of 15 m/sec. There is also a secondary southerly lobe with a magnitude around 12 m/sec.

What is interesting to see are the vast differences between meteorological station wind speed (note speeds have not been adjusted from overland to overwater, stability, or elevation) and direction, a near uniform time variation in the sea-level pressure (Figure 3-41). Based on the magnitude in the winds only reaching above 10 m/sec at the northern NDBC buoy (45002), the actual driving mechanism producing this event at Calumet water-level station is strongly correlated to the pressure drop of around 23 mb, over the entire lake.

For the WAM simulation, NNM and CFSR wind fields were used as forcing and compared to the existing two NDBC sites, 45002, and 45007.

Figure 3-42 displays the integral wave parameters, wind speed and direction results. Wind speeds do not exceed 10 m/sec at this site until the storm system moves well east of Lake Michigan and a high pressure center enters and the wind directions become southerlies.

Under the wind conditions observed at the northern buoy, it also is not surprising that the significant wave heights rarely exceed 2 m with T_p values of 6 sec consistent with the measured wave magnitudes. The NNM forced WAM simulation performs quite well for the simulation until the winds shift to a southerly direction on 2 June, and then the modeled H_{mo} values are generally biased low. The CFSR results also follow the measurements, with exception of a positive bias in the wave heights at the first storm peak around 28 May 1200UTC, but matching the primary wave event of 2 June, two days after the peak water level event at Calumet. It appears that the peak water level event on 31 May was caused by a more local-scale event, fast-moving frontal passage, or induced by atmospheric pressure changes and not winds; and not a major wave producing event.

In earlier storm simulations there was a general consistency between the observations from the two buoys. Results for the southerly buoy, 45007, are shown in Figure 3-43. In comparison to all other storm simulations, the wave climate could be considered as benign. There are a few storm peaks defined in the buoy data and rarely are they greater than 1 m in wave height. The peak and mean wave period measurements can be described as wind-generated *chop*; however the increase in those values just before 31 May is a

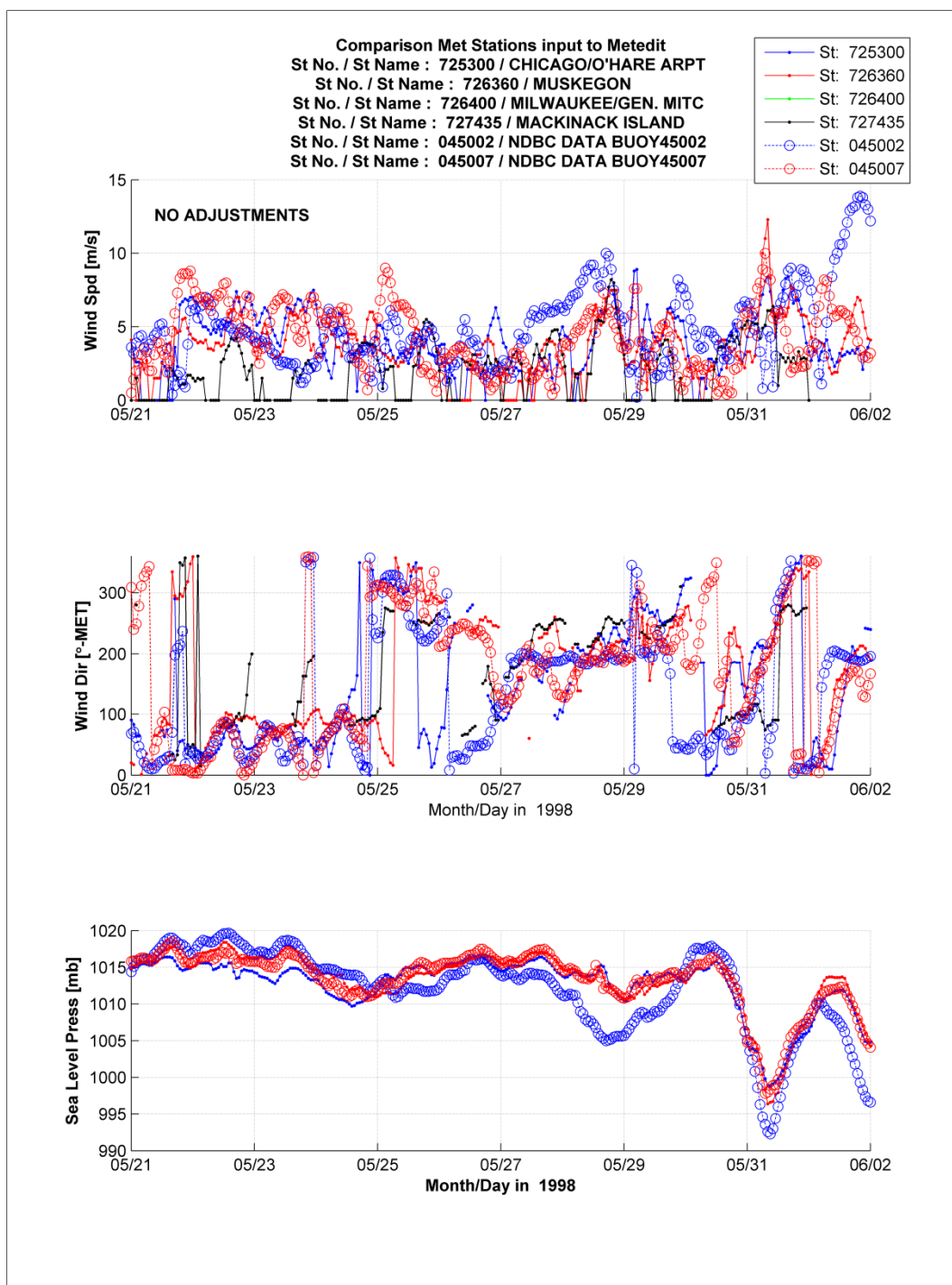


Figure 3-41. Time plots of raw non-adjusted wind speed, wind direction and sea-level pressure at six selected point-source measurement sites surrounding Lake Michigan for the May 1998 storm.

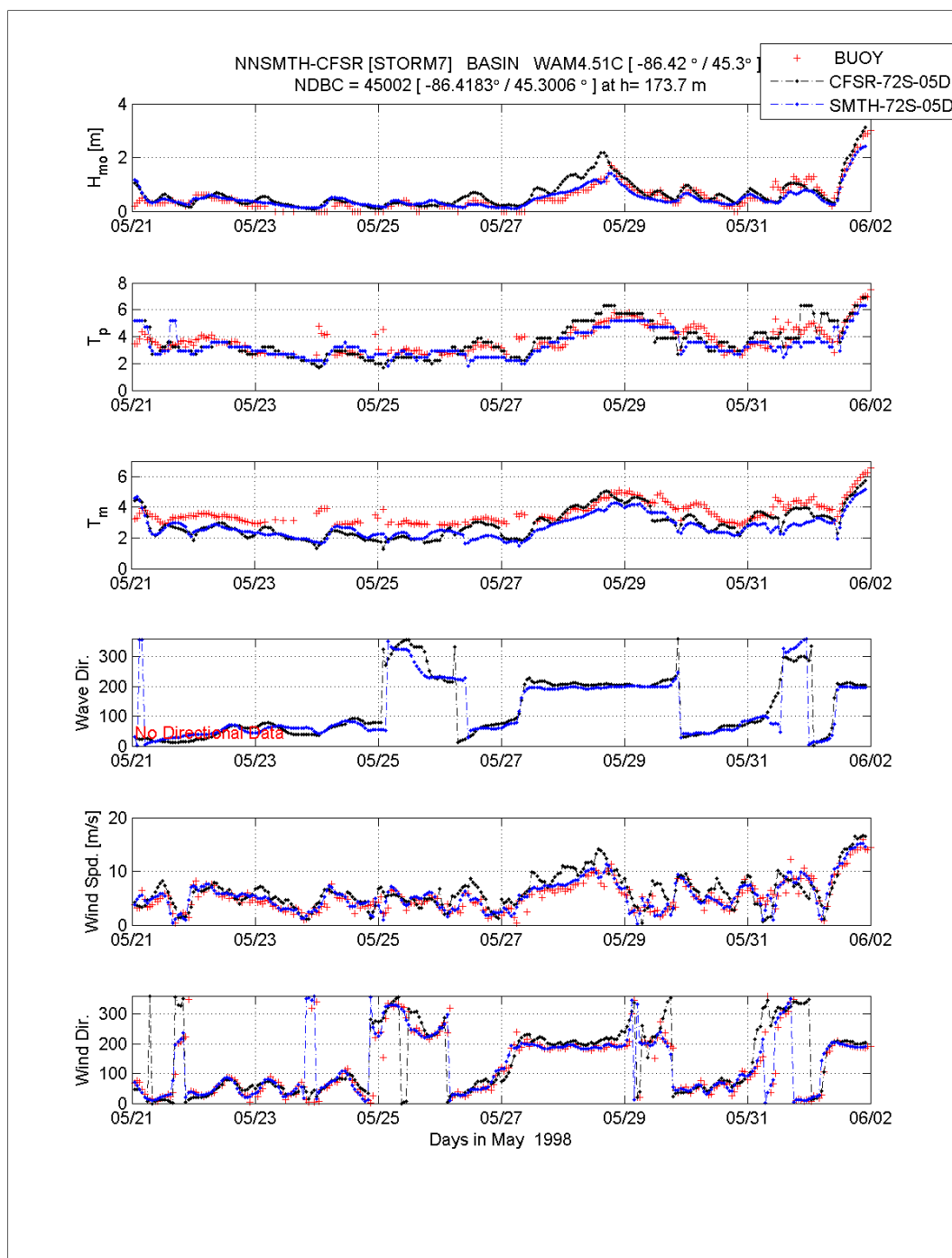


Figure 3-42. Time plots of significant wave height, peak and mean wave period, vector mean wave direction wind speed and direction at NDBC 45002 for the May 1998 storm.

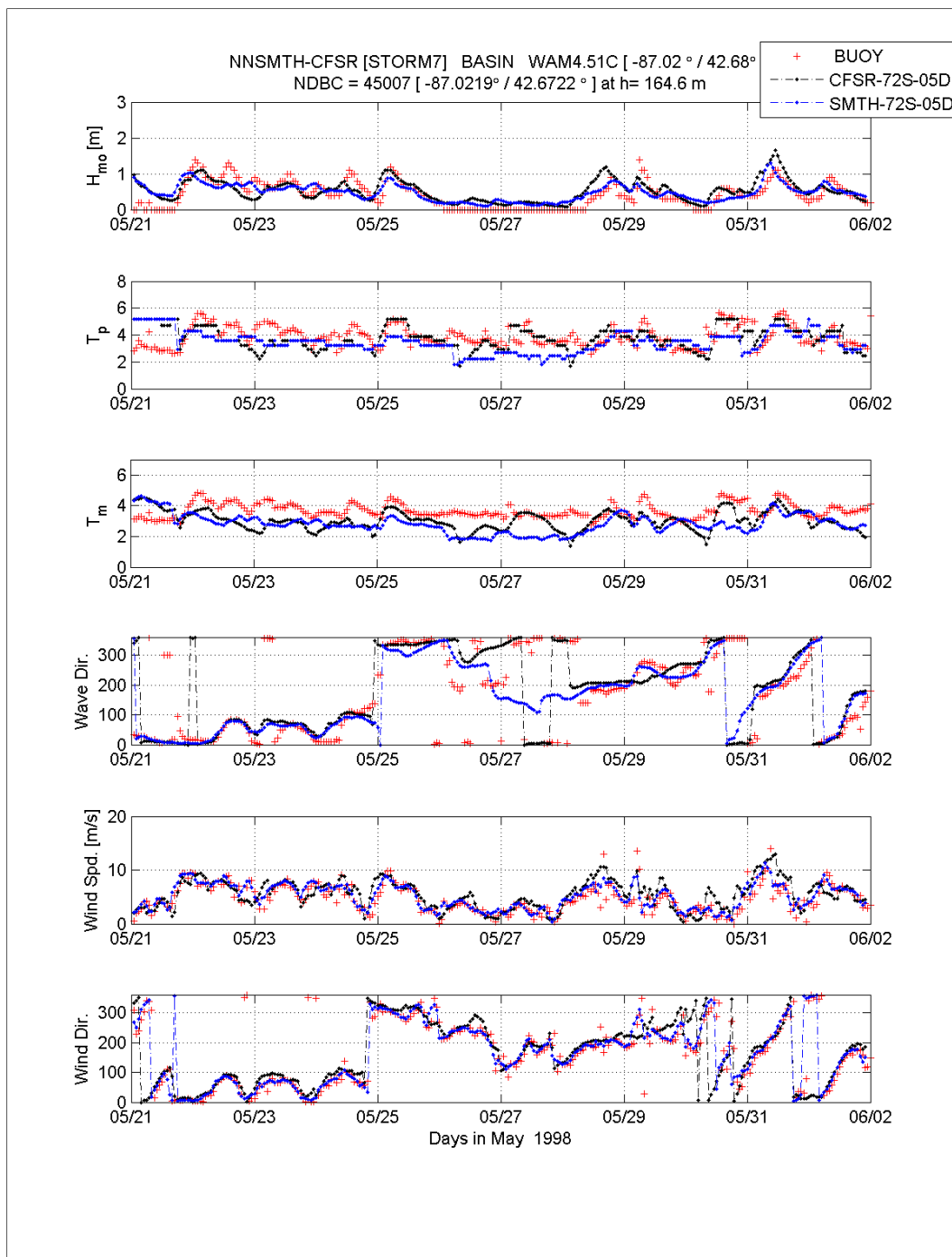


Figure 3-43. Time plots of significant wave height, peak and mean wave period, vector mean wave direction wind speed and direction at NDBC 45007 for the May 1998 storm.

good indication of the storm activity in the north, allowing the faster moving swell waves to arrive at this location. The model results for the two simulations follow the trends evident in the buoy data. There are a few times where WAM results underestimate the storm peaks (22nd, 24th, and 29th 1200 UTC), however the errors can be attributed to wind errors. The H_{mo}

over-estimation around 1 June again can be attributed to the over-estimation in the winds. Both wave period estimates derived from the model runs tend to be biased low, with exception of the storm peak of 1 June.

Lastly, the WAM results for a location offshore of the Calumet station are shown in Figure 3-44. As previously indicated, in the central portion of Lake Michigan, the wave climate could be considered as benign. This is also true for the Calumet location at the south end of the lake. The H_{mo} estimates do not exceed 1 m and are accompanied by very short wave periods. However, the NNM and CFSR wind fields generate two distinctly different wave conditions. The NNM forced results show more local temporal changes in the wave conditions. As the wind speed changes (generally below 10 m/sec at the maximum) so do the wave estimates.

The NNM tends to produce larger significant wave heights, local storm peaks that are 0.25 to 0.5 m higher than the CFSR results. This again can be attributed to the differences in the local wind fields, where NNM is developed by the local meteorological conditions.

3.6.8 Examination of negative bias in modeled wave periods

Thus far, the WAM results have been compared to point source measurements for the seven selected storms using NNM and CFSR forcing. In general, the model emulates the growth, peak and decay cycles of storm wave conditions found in these data records. CFSR forcing tends to perform better for northerly and southerly lake-wide wind events capturing the peak conditions better than the NNM. The NNM may describe very locally generated wind-seas more appropriately.

There was one glaring deficiency found in all the wave simulations, whether forced by NNM or CFSR, and that was the low bias in the peak and mean wave period results. The following analysis described below will rectify the problems. This analysis will focus on the October 1993 storm using the CFSR results. The conclusions drawn can be applied to the NNM results and to all storm simulations.

Evident in many of the comparisons, there is a persistent bias in the peak and mean wave period results, despite capturing not only the significant wave height variation in time, but also the mean vector wave direction measured at the buoys (45007 and 45010, Figures 3-39 and 3-40 respectively). An analysis was performed to determine where and why those

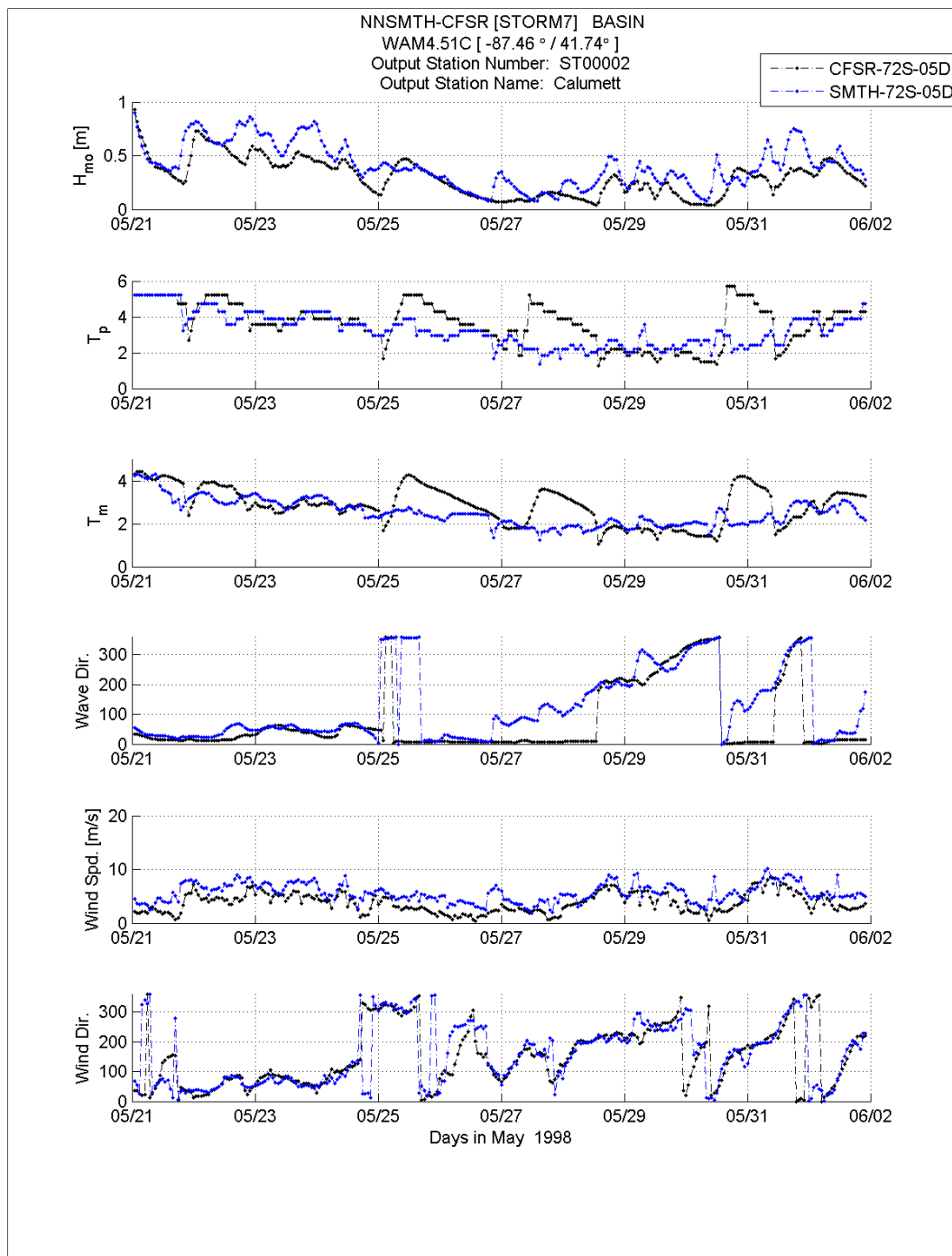


Figure 3-44. Time plots of significant wave height, peak and mean wave period, vector mean wave direction wind speed and direction at a WAM save location off shore of Calumet, IL, for the May 1998 storm.

differences occur. Definitions for the spectral peak wave period and the mean wave period are provided below. For the peak wave period, rather than be dependent on the discrete frequency bands for the wave buoy and the WAM results, a parabolic fit to the spectrum is applied where the peak

wave frequency is computed using information obtained at the peak frequency and frequency bands on either side. The weighting is determined by the relative energy contained at those bounded frequency bands. This produces a pseudo-continuous result rather than relying on the differences between frequency bands and range. The frequency bands for the NDBC data are 0.04-Hz to 0.40-Hz at a frequency resolution of 0.01-Hz. The WAM results follow $f(n+1) = 1.1 \cdot f(n)$, where $f(0) = 0.0612$ Hz and $f(\text{NFRE}) = 0.80$ Hz, where NFRE is the total number of frequency bands, or 28. A portion of the error can be attributed to differences in frequency ranges; however, the relative amount of energy contained in the WAM spectra are nearly an order of magnitude lower than at the peak frequency. The mean wave period is defined again as:

$$T_{\text{mean}} = f_{\text{mean}}^{-1}, \text{ where } f_{\text{mean}} = \left[\frac{\int_0^{2\pi} \int_0^{\infty} f^{-1} F(f, \theta) df d\theta}{\int_0^{2\pi} \int_0^{\infty} F(f, \theta) df d\theta} \right]^{-1}$$

This definition weights the energy contained in the lower frequency bands over the higher frequency bands. Time paired measured and model spectra are evaluated. Because the discrete frequency bands differ as well as the frequency range, both spectra are non-dimensionalized by the peak frequency and interpolated (cubic-spline fit) to one common independent variable.

The spectra are compared for each time-paired observation for the duration of the simulation. Comparison plots for NDBC 45002, 45007 and 45010 and the WAM forced with CFSR winds are shown in Figures 3-45 through 3-47.

The large differences (green lines) for individual comparisons are generally attributed to phase errors of 1-hour intervals used in this evaluation. The mean difference at the $f/f_m \geq 1$ in all cases is positive indicating WAM results tend to under-estimate the energy level at the spectral peak and the rear face of the spectrum. For both deepwater centrally located NDBC sites (Figure 3-45 and 3-46) WAM tends to over-estimate the energy level just below the spectral peak frequency on the forward face. Overall, the biases in the WAM results (mean difference) are relatively small and can be the cause of the slight under-estimation in the mean wave period. At 45010 (Figure 3-47), a slightly different situation exists, WAM generally under-estimates the energy levels slightly below and above the spectral peak, indicated as a

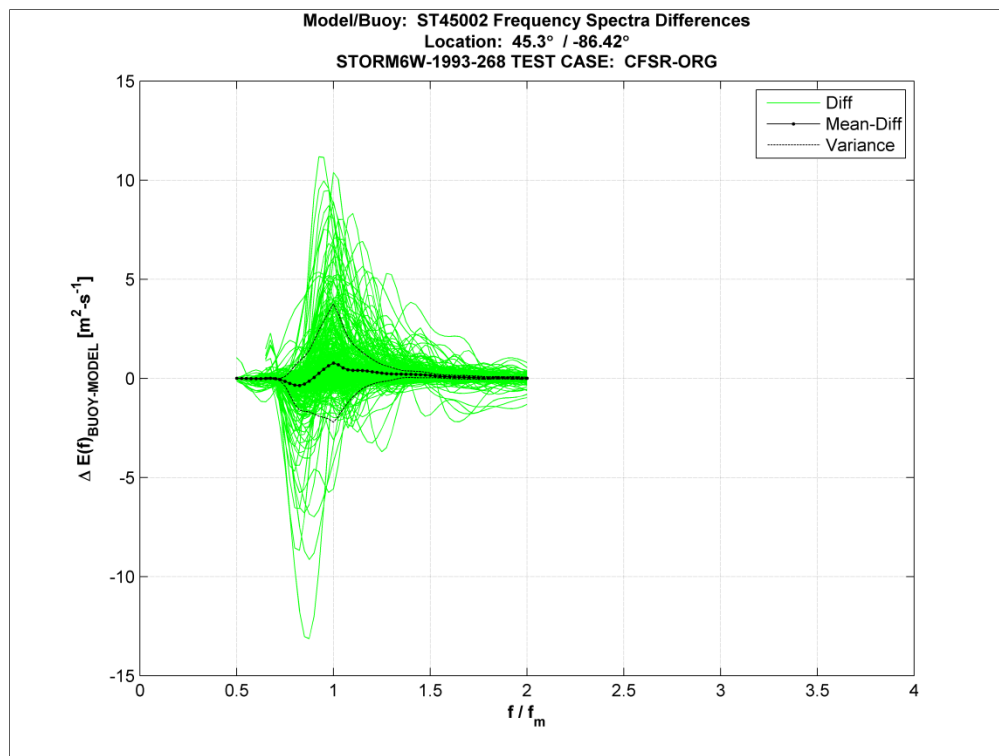


Figure 3-45. Time paired comparison differences in the frequency spectra (Buoy minus Model) at NDBC 45002 for the October 1993 storm.

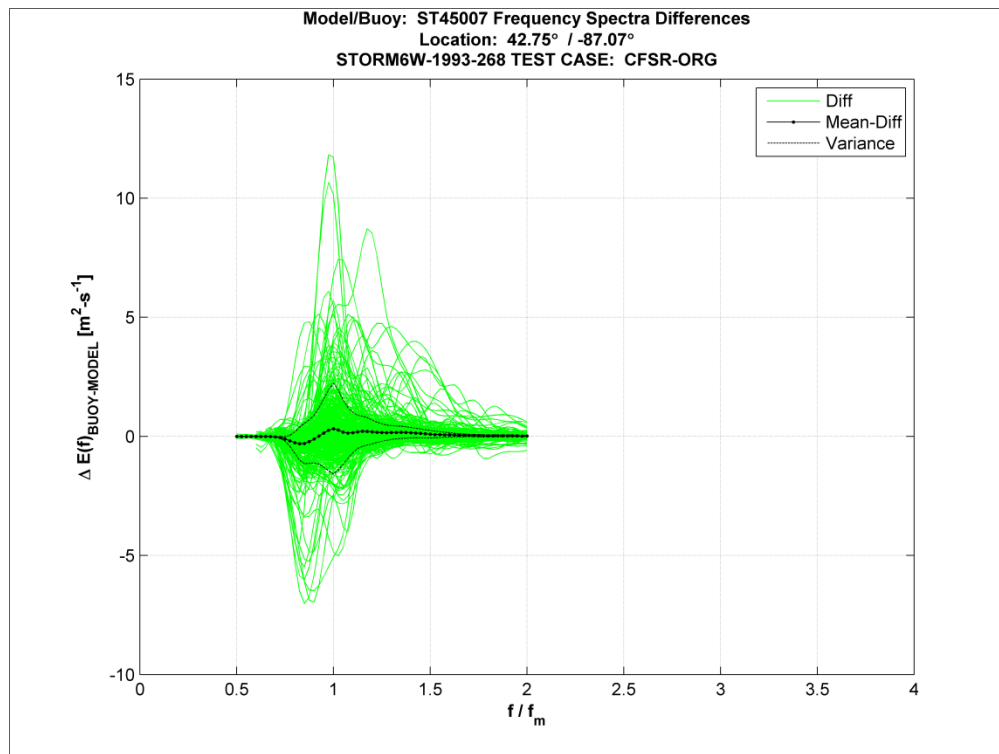


Figure 3-46. Time paired comparison differences in the frequency spectra (Buoy minus Model) at NDBC 45007 for the October 1993 storm.

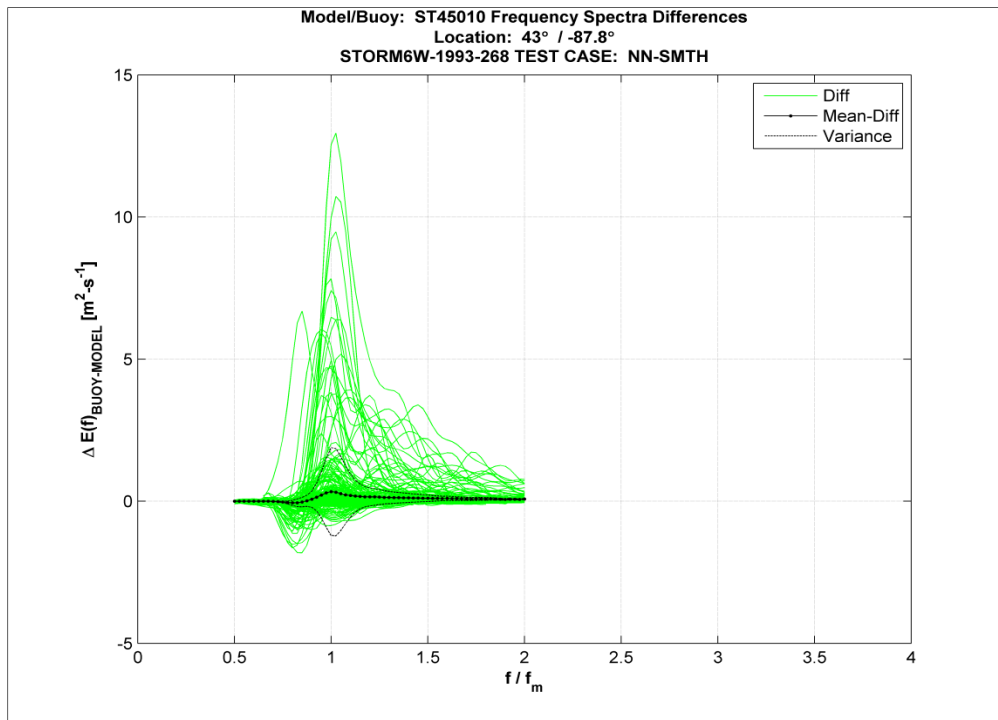


Figure 3-47. Time paired comparison differences in the frequency spectra (Buoy minus Model) at NDBC 45010 for the October 1993 storm.

positive bias. Although for individual cases, WAM has a definite positive bias, and is not offset proportionately when computing the mean wave period results. The magnitude of the bias at and slightly about the spectral peak tends to drive the WAM mean wave period lower than values computed from the observations.

3.6.9 Statistical comparison of model results and measurements

Examining model predictive skill for the complete set of storm simulations is an important aspect of the validation of the WAM results. The procedure used is to combine each NDBC buoy data set for all storms, and time-pair the WAM results to each of the individual buoy records. Scatter plots, and statistical analyses can then be performed using only those WAM results occurring when measurements exist. This insures proper evaluation of the model estimates where there is a 1-to-1 correlation between the measurements and model data records. For the seven storms simulated there were 1615 time-paired observations at the northern NDBC buoy 45002, 1341 time-paired observations at the southern NDBC buoy 45007, and 468 (data only available for the October 1993 storm) time-paired observations at NDBC Milwaukee 45010 site. For all scatter plots, the buoy data are the independent parameter, and the model results are the dependent, (x and y

axis, respectively). Results for the wave height comparisons are provided, however statistical analyses are performed on the remaining wave parameters, T_p and T_m . Figures 3-48 through 3-50 show the distribution of the model results versus the measurements for NDBC 45002, 45007 and 45010, respectively. The CFSR (blue symbol) and NNM (red symbol) forced model-generated wave height estimates are plotted together. It is rather difficult to identify the NNM results, however, the trend for these estimates do fall below the 45-deg (green line) of perfect agreement for the northern NDBC buoy 45002 (Figure 3-48). This confirms the results found in the time plots for the individual storm simulations, where NNM tends to be biased low. The WAM results, using CFSR winds, show a uniform distribution above and below the perfect fit line, up to about 3 m. The large differences found above that 3 m threshold are more indicative of phase differences between the modeled maxima and what was observed.

At the southern NDBC location 45007 (Figure 3-49), the NNM and CFSR results are in better agreement with the measurements, and also to one another. The distributions seem to be balanced above and below the line of perfect fit; however there is a strong indication that for larger observed wave heights, the NNM method will generate about a 1-m negative bias in wave heights. For the similar set, CFSR also indicates a negative bias for approximately one half of the observations. These differences again are most likely temporal phase shifts between the model and measurements.

The final scatter plot illustrates the time-paired comparisons at 45010 for only the October 1993 storm (Figure 3-50). One point of note is that the NODC derived data for all NDBC buoys show a lower limit of 0.2 m in their data records. The WAM results go below that threshold. The main data cloud of NNM results appear to be more in balance above and below the line of perfect fit for wave estimates below about 1.5 m compared to a more negative bias of the CFSR forced WAM significant wave heights. Above the 1.5-m threshold, both of the WAM simulations, for NNM and CFSR) are biased low by about 0.5 m. These data points are from the northerly event on 9 October 1993. One potential reason for the biases to occur are, the modeled winds at the buoy are slightly under-estimated by about 2.5 m/sec, which in and of itself would only increase the H_{mo} values by approximately 0.2 m. Greater errors over the entire fetch would tend to produce greater errors in calculated wave heights. It is important to exercise caution when trying to render conclusions based on results for a single storm event. A larger sample spanning multiple storms would yield a data set upon which more defensible conclusions can be drawn.

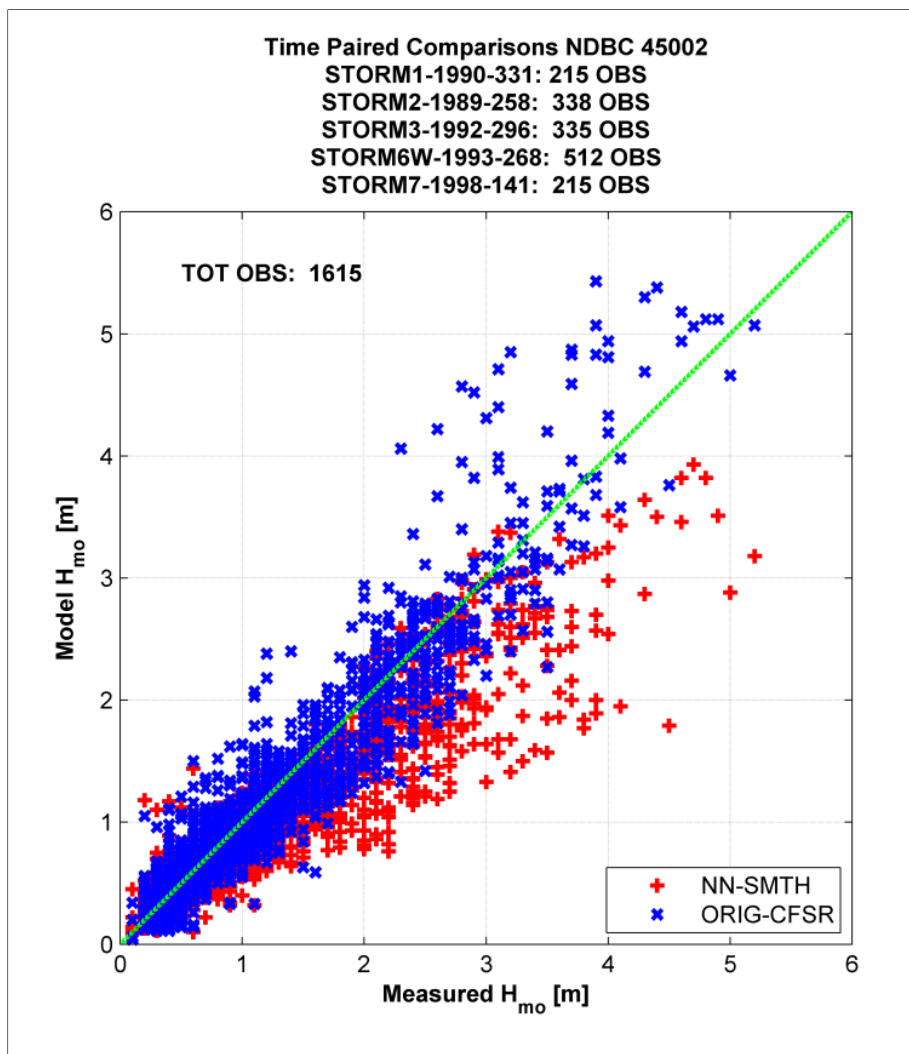


Figure 3-48. Time-paired scatter plot of at NDBC 45002 and WAM wave height results using NNM and CFSR forced winds for all storm simulations.

Statistical analyses were performed for the three buoy sites covering the individual storm simulations, and for all observations. The following skill metrics were examined: bias, root mean square error, Scatter Index, regression analysis, providing the slope and intercept, and correlation for the significant wave height (H_{mo}), peak wave (T_p) and mean wave periods (T_m). The results for the WAM estimates forced by the NNM and CFSR wind fields are found in Tables 3-9 through 3-11 for significant wave height, peak wave period and mean wave period, at the three buoys, respectively.

The remaining analysis focuses on the accuracy of storm peaks in the modeled estimates. This evaluation will provide insights to the accuracy in the modeling technology capturing extreme events. In this case the extreme event is classified as the largest significant wave height occurring during a

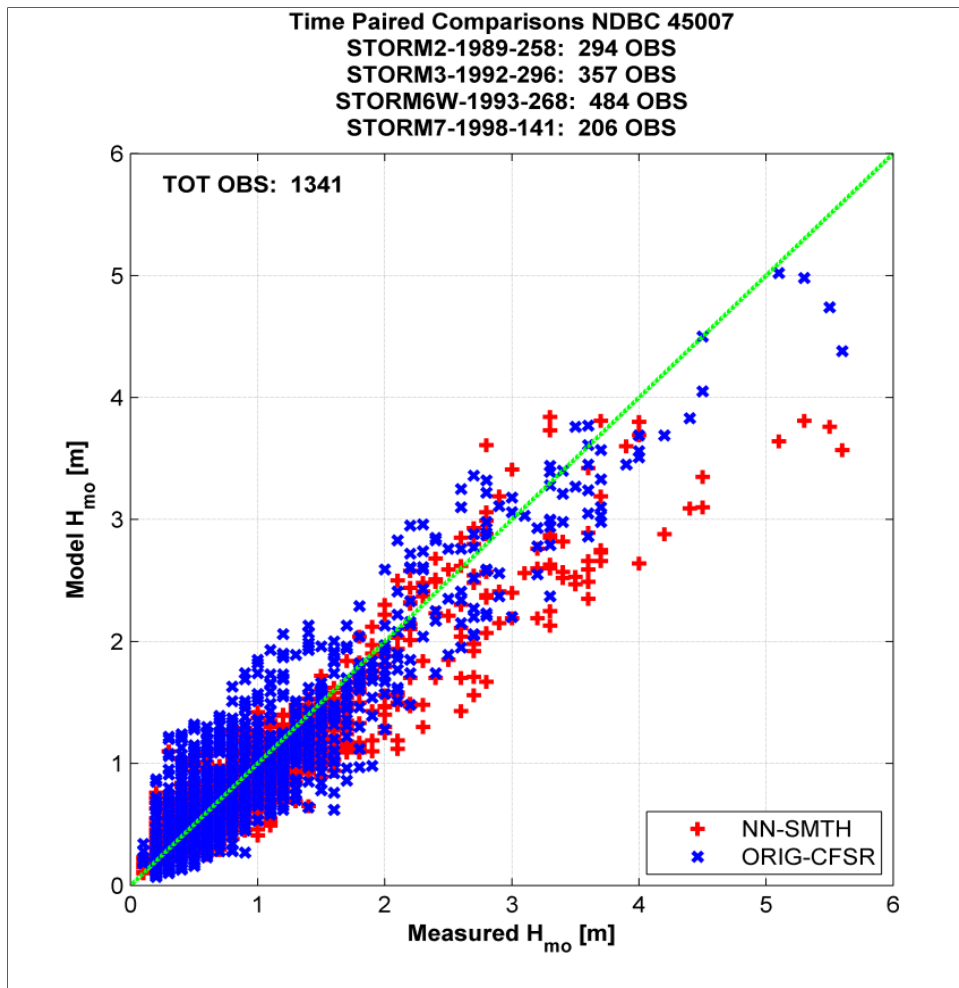


Figure 3-49. Time-paired scatter plot of at NDBC 45007 and WAM wave height results using NNM and CFSR forced winds for all storm simulations.

time window above some given threshold value. That threshold was computed from the combined time-paired observations for all storm simulations. For this case that threshold was the mean plus two times the variance of the measured wave measurements. The analysis was only performed for the two NDBC stations 45002 and 45007. The data set size for 45010 was considered too small for this analysis and was omitted.

Figures 3-51 (45002) and 3-52 (45007) are three panel plots; the top plot displays the time-series for the buoy measurement (in red) and the designated threshold that was used in the storm selection. The bottom panels plot the measured data versus the model estimates for the peak wave conditions. The left-hand plot is the results obtained from the NNM winds and the right panel is the results from the CFSR winds. For this analysis, the phase differences are removed; all WAM results in the storm's time interval are interrogated to find the maximum wave height in that interval.

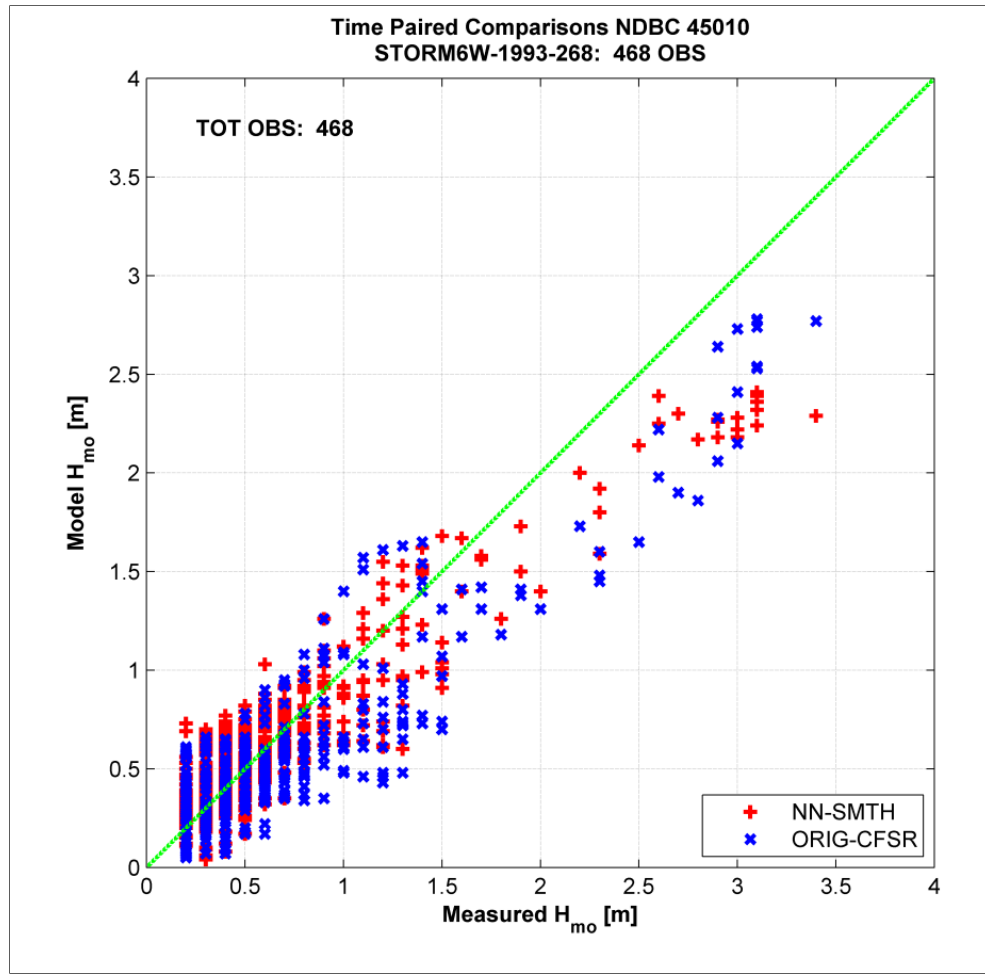


Figure 3-50. Time-paired scatter plot of at NDBC 45007 and WAM wave height results using NNM and CFSR forced winds for ONLY the October 1993 storm

Table 3-9. Statistics for seven Lake Michigan test storms H_{mo} (m).

Table 3-9 Statistics for Seven Lake Michigan Test Storms H_{mo} (m)																				
Storm Name	Location	NDBC	Mean	Mean Model		Bias		RMSE		Scat Index		Slope		Intercept		Slope		Corr		No. Obs
				NN	CFSR	NN	CFSR	NN	CFSR	NN	CSFR	NN	CFSR	NN	CFSR	NN	CFSR	NN	CFSR	
Storm1 199012	Green Bay	45002	1.90	1.27	1.87	-0.62	-0.03	0.57	0.43	30	23	0.57	1.07	0.19	-0.16	0.67	1.02	0.85	0.93	215
		45007	N/A																	
Storm2 198909	Calumet	45002	1.05	0.89	1.02	-0.16	-0.03	0.28	0.24	26	23	0.75	0.94	0.10	0.03	0.83	0.98	0.95	0.95	338
		45007	0.91	0.77	0.83	-0.14	-0.07	0.37	0.25	41	28	0.65	0.87	0.18	0.04	0.76	0.91	0.97	0.97	294
Storm3 199210	Keweenaw	45002	1.28	1.11	1.29	-0.16	0.01	0.27	0.32	21	25	0.82	1.07	0.06	-0.08	0.87	1.05	0.95	0.94	335
		45007	1.10	1.02	1.08	-0.07	-0.01	0.25	0.28	23	25	0.92	0.92	0.01	0.07	0.95	0.99	0.94	0.93	357
Storm4 198502	Milwaukee	45002	N/A																	
		45007	N/A																	
Storm5 200912	Green Bay	45002	N/A																	
		45007	N/A																	
Storm6 199309	Wave Event	45002	1.31	1.10	1.24	-0.21	-0.08	0.35	0.28	27	21	0.70	0.93	0.18	0.02	0.82	0.95	0.93	0.95	512
		45007	1.05	0.96	1.06	-0.08	0.02	0.24	0.36	23	35	0.74	0.84	0.19	0.19	0.88	1.00	0.95	0.86	484
Storm7 199806	Calumet	45010	0.68	0.67	0.59	-0.01	-0.08	0.24	0.27	35	39	0.71	0.70	0.19	0.12	0.91	0.84	0.93	0.84	468
		45002	0.61	0.58	0.75	-0.03	0.14	0.21	0.27	35	44	0.77	1.01	0.11	0.13	0.92	1.20	0.89	0.87	215
ALL		45007	0.59	0.57	0.64	-0.03	0.04	0.24	0.27	41	46	0.39	0.48	0.34	0.35	0.91	1.05	0.56	0.52	206
		45002	1.23	1.01	1.22	-0.22	-0.01	0.38	0.31	31	25	0.69	0.97	0.16	0.02	0.80	1.00	0.92	0.94	1615
		45007	0.96	0.87	0.95	-0.09	-0.01	0.28	0.31	29	32	0.76	0.87	0.15	0.12	0.87	0.98	0.94	0.91	1341

Table 3-10. Statistics for seven Lake Michigan test storms T_p .

Storm Name	Location	NDBC	Mean	Mean Mod		Bias		RMSE		Scat Index		Slope		Intercept		Slope		Corr		No. Obs	
				NN	CFSR	NN	CFSR	NN	CFSR	NN	CFSR	NN	CFSR	NN	CFSR	NN	CFSR	NN	CFSR		
Storm1 199012	Green Bay	45002	6.14	5.25	5.89	-0.89	-0.25	0.57	0.86	16	14	0.64	0.89	1.33	0.44	0.85	0.96	0.80	0.87	215	
		45007	N/A																		
Storm2 198909	Calumet	45002	4.88	4.18	4.35	-0.70	-0.53	0.76	0.63	16	13	0.67	0.97	0.93	-0.40	0.85	0.91	0.82	0.90	338	
		45007	4.43	4.12	4.15	-0.31	-0.28	0.95	0.88	21	20	0.67	0.92	1.13	0.07	0.91	0.95	0.84	0.88	294	
Storm3 199210	Kewaunee	45002	4.98	4.54	4.75	-0.45	-0.23	0.67	0.66	13	13	0.76	1.03	0.76	-0.38	0.91	0.97	0.88	0.91	335	
		45007	4.99	4.52	4.65	-0.47	-0.34	0.63	0.67	13	13	0.68	0.69	0.63	0.70	0.81	0.83	0.84	0.83	357	
Storm4 198502	Milwaukee	45002	N/A																		
		45007	N/A																		
Storm5 200912	Green Bay	45002	N/A																		
		45007	N/A																		
Storm6 199309	Wave Event	45002	5.10	4.59	4.86	-0.51	-0.24	0.74	0.74	15	14	0.67	0.87	1.18	0.45	0.79	0.85	0.89	0.88	512	
		45007	4.93	4.63	4.65	-0.30	-0.28	0.70	0.80	14	16	0.70	0.71	1.19	1.16	0.93	0.94	0.84	0.79	484	
Storm7 199806	Calumet	45002	4.76	4.61	4.38	-0.15	-0.38	0.83	0.99	17	21	0.69	0.74	1.34	0.84	0.96	0.93	0.80	0.75	468	
		45007	3.93	3.64	4.03	-0.29	0.10	0.68	0.74	17	19	0.73	0.93	0.76	0.37	0.93	1.04	0.75	0.77	215	
ALL		45002	4.03	3.63	3.87	-0.40	-0.16	0.81	0.79	20	20	0.20	2.84	0.47	1.98	0.89	0.96	0.29	0.48	206	
		45007	5.01	4.46	4.76	-0.56	-0.25	0.79	0.74	16	15	0.69	0.92	0.98	0.14	0.88	0.96	0.85	0.88	1615	
			45007	4.70	4.34	4.42	-0.36	-0.28	0.76	0.79	16	17	0.70	0.80	1.06	0.66	0.92	0.94	0.83	0.83	1341

Table 3-11. Statistics for seven Lake Michigan test storms T_{mean} .

Storm Name	Location	NDBC	Mean	Mean Mod		Bias		RMSE		Scat Index		Slope		Intercept		Slope		Corr		No. Obs	
				NN	CFSR	NN	CFSR	NN	CFSR	NN	CFSR	NN	CFSR	NN	CFSR	NN	CFSR	NN	CFSR		
Storm1 199012	Green Bay	45002	6.12	4.63	5.27	-1.49	-0.86	0.97	0.77	16	13	0.54	0.76	1.31	0.64	0.75	0.86	0.83	0.89	215	
		45007	N/A																		
Storm2 198909	Calumet	45002	4.87	3.66	3.84	-1.21	-1.03	0.75	0.58	15	12	0.60	0.85	0.71	-0.31	0.75	0.80	0.83	0.90	338	
		45007	4.42	3.63	3.63	-0.79	-0.79	0.90	0.79	30	28	0.59	0.77	2.03	0.23	0.80	0.83	0.80	0.89	294	
Storm3 199210	Kewaunee	45002	4.97	4.05	4.24	-0.92	-0.73	0.64	0.57	13	11	0.66	0.88	0.77	-0.15	0.81	0.86	0.90	0.91	335	
		45007	N/A																		
Storm4 198502	Milwaukee	45002	N/A																		
		45007	N/A																		
Storm5 200912	Green Bay	45002	N/A																		
		45007	N/A																		
Storm6 199309	Wave Event	45002	5.09	4.08	4.35	-1.01	-0.74	0.73	0.67	14	13	0.58	0.73	1.12	0.62	0.79	0.85	0.89	0.88	512	
		45007	4.92	4.09	4.07	-0.83	-0.85	0.66	0.81	13	17	0.61	0.59	1.07	1.17	0.82	0.82	0.87	0.77	484	
Storm7 199806	Calumet	45002	4.75	3.88	3.70	-0.87	-1.05	0.74	0.88	16	18	0.61	0.64	0.98	0.66	0.81	0.78	0.85	0.77	468	
		45007	3.92	3.24	3.55	-0.68	-0.37	0.58	0.56	15	15	0.65	0.81	0.70	0.39	0.83	0.91	0.80	0.80	215	
ALL		45002	4.03	2.28	3.46	-0.75	-0.56	0.81	0.70	20	17	0.13	0.36	2.76	2.03	0.81	0.86	0.23	0.49	206	
		45007	5.00	3.95	4.24	-1.06	-0.77	0.77	0.66	15	13	0.61	0.80	0.91	0.24	0.78	0.85	0.87	0.89	1615	
			45007	4.69	3.84	3.89	-0.84	-0.79	0.74	0.76	16	16	0.61	0.67	0.99	0.75	0.81	0.83	0.84	0.83	1341

There are about 14 storm peaks defined from the NDBC 45002 data set. They range from about 3 m to a maximum of slightly over 5 m. The storm durations are quite short, and generally are indicative of fast moving systems, or even frontal passages. What is found from the evaluation of the NNM and CFSR forced WAM estimates is that NNM results show a negative bias in estimating the storm peak conditions. These results are not surprising based on the previous time and scatter plot results. These differences range from nearly zero to as much as 2 m, where the larger errors are derived from southerly storm conditions. The CFSR results compare more favorably to the measurements. There are positive biases in the range of 1 to 1.25 m, the extreme event based peak H_{mo} values are better replicated.

The peak to peak analysis was also performed for NDBC 45007 and results are shown in Figure 3-52. Note 45007 was pulled for the season during the first storm simulation; therefore, there is no direct correlation between observation number defined for NDBC 45007 and that presented in Figure 3-51 (45002). Figure 3-52 again provides the time plot of the measurements, threshold, and identification of the maximum peak wave

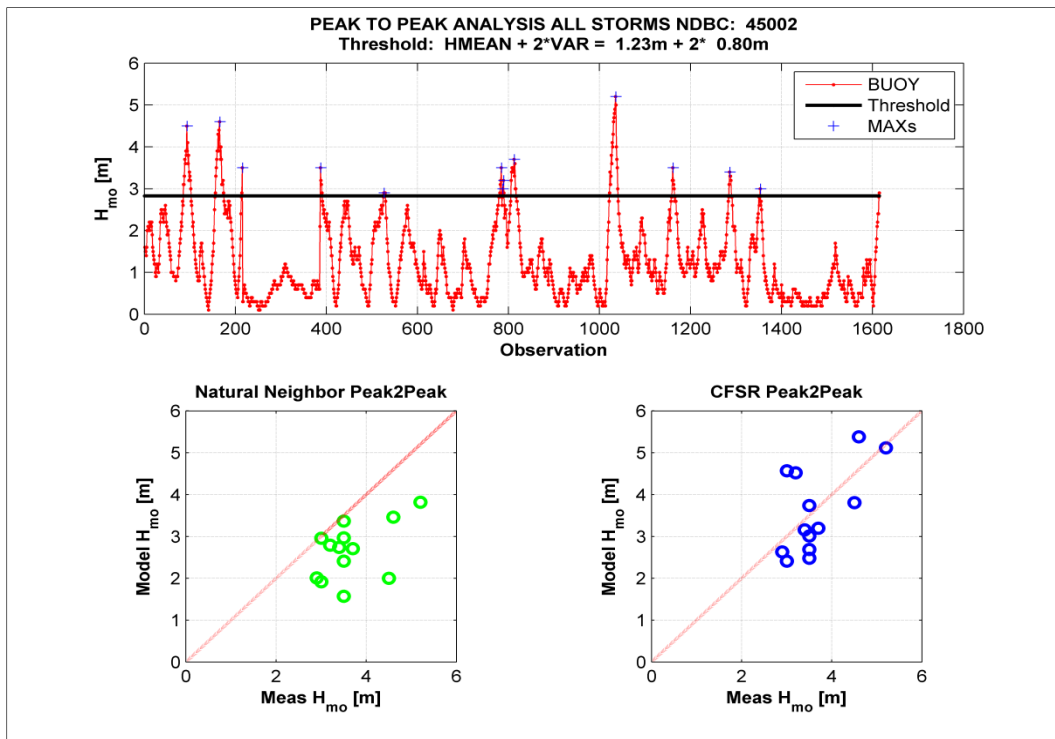


Figure 3-51. Peak to peak analysis of all seven storm simulations at NDBC 45002. Top panel contains the cumulative time series of buoy data, with defined threshold, and peak conditions. Bottom two panels are scatter plots of NNM results (left) and CFSR (right) WAM estimates.

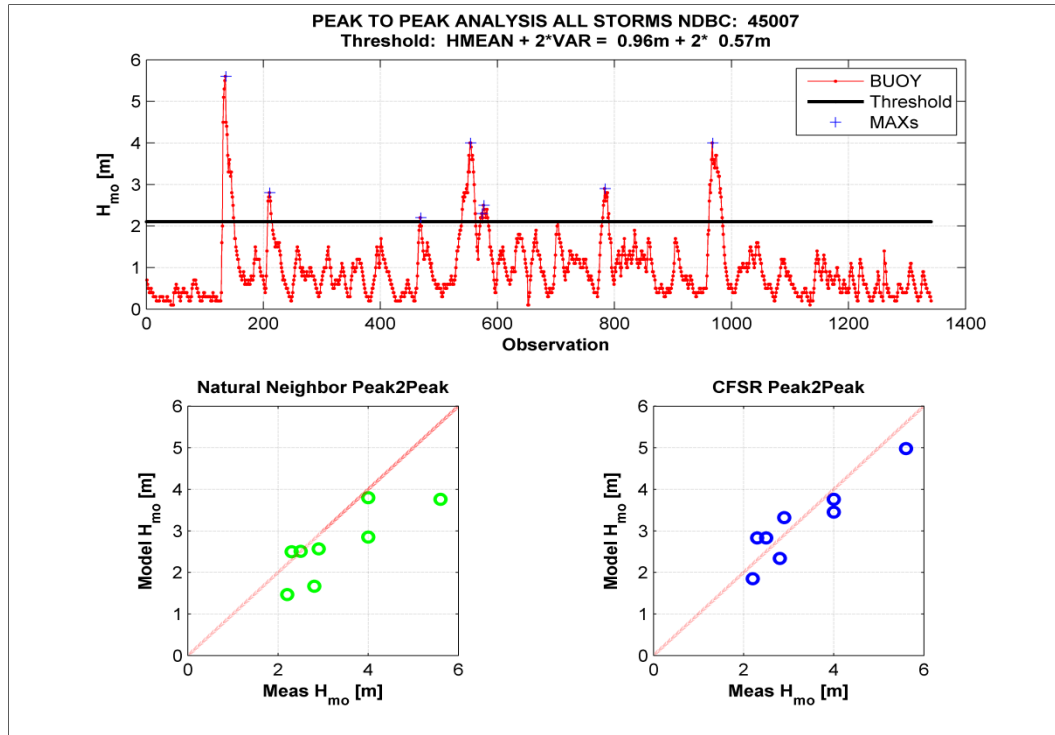


Figure 3-52. Peak to peak analysis of all seven storm simulations at NDBC 45007. The top panel contains the cumulative time series of buoy data, with defined threshold, and peak conditions. The bottom two panels are scatter plots of NNM results (left) and CFSR (right) WAM estimates.

height event defined by the storm. There are only eight defined peaks for this location compared to the fourteen found at 45002. The maximum of about 5.5 m wave height occurred for a northerly wind situation. The NNM and CFSR results again are plotted in the lower panels. At NDBC 45007, the NNM does reasonably well in comparison of the peak events; however, they also possess an error of nearly 2 m for the second storm peak significant wave height. For the remaining seven events biases of 1 m or less are the general trend, but much better than at 45002. The CFSR results nearly fall along the line of perfect fit for the peak to peak evaluation at 45007. There does not appear to be a consistent positive or negative bias in the results, with errors generally less than 0.5 m.

3.7 Summary of observations and recommendations

The following summarize *OBSERVATIONS*, defined here as findings that occurred during the processing of winds, ice and/or wave modeling tasks. The *OBSERVATIONS* can be further pursued in the future and have modest bearing on the outcome of the study. The *RECOMMENDATIONS* should be specifically pursued to assure overall success of the study.

3.7.1 Observations: Winds

- There is a general inconsistency in the ISH (Airways) data base. Manual checking of each file may be required.
- The *NNM* wind and pressure fields are generally weighted toward highly local events.
- The *NNM* wind fields develop strong east/west alignment of wind speed contours in the lake.
- The *NNM* wind fields weight station information at the outermost boundaries which might produce unrealistic isotac representations.
- The CFSR wind and pressure fields exhibit large gradients in speed and pressure at land/water boundary which might not be accurate.
- The CFSR wind and pressure fields in the December 2009 storm simulation display 6-hour temporal oscillations.
- The CFSR wind and pressure fields exhibit a general spatial coherency along the central axis of Lake Michigan that seemed to be missing in the NNM results for some of the severe events with northerly and southerly winds.
- The NNM wind field specification could be trained by the CFSR wind fields, including control points along the central axis of the lake to

better represent the spatial coherency that seems to be missing for some of the severe events that were modeled.

- With testing, control points based on buoy observations could be synthesized into the NNM to generate better representations of southerly and northerly wind events.
- CFSR winds exhibit strong gradients at the land/sea boundary, which might adversely impact accuracy near the shoreline. Accuracy along the coast could be examined based on recently available wind measurements (2000-2009 time frame) for data from a large number of land station winds.

3.7.2 Observations: Ice fields

- The ice data bases consist of three identification flags, NO DATA, INTERPOLATED DATA and OBSERVED DATA.
- The ice data bases generally start on 1 December each year.
- There is an inconsistency in grid resolutions between the three ice field data bases (1960-1979), (1973-2002), and (2003-2009).
- The frequency of ice field information is not consistent between ice field data bases.
- There are no graphic products for the 1960-1979 ice field data base.
- The mapping from Lambert Conformal Conical Cartesian coordinate system to a spherical coordinate system is an approximation.

3.7.3 Observations: Wave measurements

- There are differences in the wave data archived by NOAA/NDBC and the NOAA/NODC.
- The NOAA/NODC is the official NOAA archiving center.
- The wave measurements posted on the NOAA/NDBC site contain specific wave parameter definitions that may be inconsistent with a model definition.

3.7.4 Observations: Wave model and modeling effort

- There are a number of different 3rd Generation Discrete Spectral Wave Models available to estimate the time and spatial change of directional wave spectra.
- The majority of errors manifested from a wave model can be attributed to errors in the wind estimation.

- Grid and model resolution (frequency and direction) selection can play an important role in the quality of the wave estimates.
- This evaluation of extreme events was based on about 3500 time paired observations, and approximately 8 to 14 peak storm conditions.

3.7.5 Recommendations: Winds

- The NNM produces quality wind fields however the method fails to replicate strong southerly and northerly wind events. For Lake Michigan use CFSR winds where available to define event-scale winds.
- Pursuit of the entire CFSR wind and pressure fields for the Great Lakes domain for evaluation as an alternate method to the NNM.
- NNM should be used when CFSR winds are not available

3.7.6 Recommendations: Ice fields

- Use only the OBSERVATIONAL DATA records to estimate the net impact of ice on the wave and water level estimates.
- Run the simulations with no ice cover, and at various concentration percentages (e.g. 25, 50, 75) to assess proper concentration to define the land-water ice cover mask in the wave modeling.

3.7.7 Recommendations: Wave measurements

- For all NOAA/NDBC buoy measurements, all data should be derived from the NOAA/NODC archive.
- For all NOAA/NDBC buoy measurement usage, knowledge of changes in positions, hull, sensor, super-structure, mooring configurations, and analysis packages needs to be documented.
- For all wave measurements used in validation other than NOAA/NDBC, wave parameters must adhere to a standard set of definitions, and documented. In addition, the meta-data defined above should also be known.

3.7.8 Recommendations: Wave model and modeling effort

- WAM should be the modeling technology used for estimating wave conditions in the Great Lakes.
- Proper preliminary investigations must be preformed to examine optimal setting all of the model's frequency (preferably based on long-term wave measurements) and direction resolutions.

- The grid used by WAM should be consistent with the surge model, coastline, (e.g. 0.0 water depth).
- The grid resolution should be determined for each lake to be simulated. Islands and highly variable coastlines must be considered.
- Extensive testing and evaluation must be performed. This includes graphic products, time, scatter, Quartile-Quartile plots, and statistical testing.
- The most important evaluation is Peak-to-Peak comparisons between model and measurements for the defined extreme storm events.
- Additional testing and evaluation of the importance of ice coverage may be necessary.
- More testing and evaluation should be performed, and based on the extreme wave events, and for as many point-source measurement sites as possible.

4 Water Level Modeling

4.1 Introduction

This chapter describes the process to develop and apply the ADCIRC storm surge simulation model (Luettich et al. 1992) for estimating storm event-driven water levels for the Lake Michigan, a system that is characterized by irregular coastlines and the presence of multiple islands and irregularly shaped embayments and harbors along the coast. Initially, the Lake Michigan model mesh development was for the entire lake complex as a single system, including connectivity between Lake Michigan and Green Bay. Modeling one system enabled more accurate treatment of the complex hydrodynamic interactions that occur between the two main water bodies in response to meteorological forcing, thereby eliminating the need to specify approximate boundary conditions at open-water boundaries that might otherwise be needed to model the two water bodies separately. However, as this chapter will show, further expansion of the mesh to include the connection between Lake Michigan and Lake Huron, Georgian Bay, and North Bay was found to be necessary in the model validation process to best capture the complex hydrodynamic interactions in response to meteorological forcing. Therefore, this chapter will cover the grid development and progression from Lake Michigan and Green Bay, to Lake Michigan/Green Bay and Lake Huron, Georgian Bay, and North Bay, then finally to include the harbors around Lake Michigan.

4.2 The ADCIRC model

4.2.1 Model description

The ADCIRC model has been extensively applied to simulate extreme levels of storm surge which are forced by winds, pressures, and waves; most recently in support of FEMA flood risk map updates in the northern Gulf of Mexico region and in support of USACE projects in Louisiana and Mississippi (see Bunya et al 2010). A detailed description for the general application of ADCIRC is available at <http://www.adcirc.org>. The specific application of the model to this system is described in this chapter. In addition, a procedure to account for the effects of ice cover in the simulation of water levels has been integrated into the ADCIRC model applied, and that formulation is also presented. This storm surge model, with ice cover capability, has been applied by Chapman et al. (2005) to the western coast of Alaska. ADCIRC

employs an unstructured mesh that is particularly well suited to resolving and representing the complex and irregular bay, island, and shoreline features of Lake Michigan and Green Bay.

4.2.2 Storm surge modeling approach

The modeling approach for Lake Michigan consisted of the following steps: developing the bathymetric dataset and model grid mesh for the system; assembling input files for atmospheric forcing (wind and pressure fields) from both the NNM and CFSR input sources and surface ice fields; testing the initial model setup; validating the model for a number of historical extreme storm events; and assessing model sensitivity to bottom friction, presence of ice, and wind speed. The model validation effort consisted of simulating the following severe storm events: December 1990, December 2009, May 1998, October 1993, November 1992, September 1989 and March 1985.

4.2.3 Treatment of ice cover – method for specifying the coefficient of drag

The ADCIRC model ordinarily uses the wind drag coefficient formulation of Garratt (1977) in the calculation of surface wind stresses. It is a widely-applied formulation and has been found to work well for storm surge applications. An additional physical process that has been examined in ice-covered regions such as the Great Lakes is the influence of sea ice as aerodynamic roughness elements. Banke and Smith (1973), Macklin (1983) and Pease et al. (1983) found that measurements of wind drag coefficients over first year sea ice typically yielded values that were significantly larger and varied less with wind speed than that predicted for open water. More recent work (Birnbaum and Lupkes (2002) and Garbrecht et al. (2002)) has formalized the effect of form drag on the specification of wind drag coefficients within marginal ice zones. From their work, Chapman et. al. (2005 and 2009) utilized an empirical fit to the range of field data for the air-ice-water wind drag coefficient, C_{DF} , and suggested:

$$C_{DF} = [0.125 + 0.5 / C (1.0 - /C)] \cdot 10^{-3} \quad (4-1)$$

in which IC is the ice concentration varying from 0.0 to 1.0 for open water and complete ice cover conditions, respectively. Inspection of the air-ice-water-wind drag coefficient formula shows that a maximum value of 0.0025 occurs with 50-percent ice coverage. This value is very close to the Macklin (1983) measurement of 0.0028 for first year ice. Furthermore, it is seen that

the value of the drag coefficient is symmetrical at about 50-percent ice coverage suggesting that the drag coefficient needed to represent 75-percent ice coverage is close to that of 25-percent ice coverage. An alternative linear fit dependence on ice concentration has been applied by Danard et al. (1989). These notions regarding variation of wind drag coefficient with ice cover have been supported by a number of Chukchi and Beaufort Sea storm surge simulations (Henry and Heaps 1976; Kowalik 1984; and Schafer 1966) in which, wind drag coefficients greater than or equal to 0.0025 where utilized.

The method adopted for this study considers the increased wind drag due to the presence of ice as developed by Chapman et al. (2005). The method requires reading ice field concentration files into ADCIRC and calculating the wind drag coefficient values (variable over the model domain) from Equation 4-1. If ice cover is present, and the increased drag coefficient exceeds the value calculated using the standard Garratt (1997) formulation, the standard Garratt drag coefficient is replaced with the increased value associated with ice cover.

4.2.4 Initial grid mesh development

The NOAA Electronic Navigation Charts (ENC), together with NOAA-published 3- and 9-arc-sec data files from NOAA's National Environmental Satellite Data and Information Service Lake Michigan digital bathymetry database were used to develop the ADCIRC grid bathymetry. These data were processed and merged with ArcView to a consistent IGLD 1985 vertical water level datum. In addition, the NOAA's IGLD 1985 zero-depth coastline file was incorporated into the data set. ADCIRC grid development also included acquiring geo-rectified photography and images to aid in establishing the shorelines.

The model mesh was developed with the Surface-water Modeling System (SMS). SMS and user documentation is commercially available at <http://www.aquaveo.com/sms>. SMS contains linkages with the Environmental Science and Research Institute's ArcView and ArcEditor software for displaying GIS layers and shape files. The U.S. National Ocean Service has published and released its navigational charts in electronic form. GIS layers composing these NOS Electronic Nautical Charts (ENC) were input to the SMS, as were the other data sources.

A SMS “feature map” file that allows grid generation and modification was built as an initial step. Figure 4-1 displays the feature map. It is composed of numerous arcs, and SMS joins intersecting arcs to form polygons. The SMS will generate sub-grids of each polygon, using the vertices that lie along the arc and a paving algorithm. Sub-grids are then merged forming a cursory ADCIRC grid.

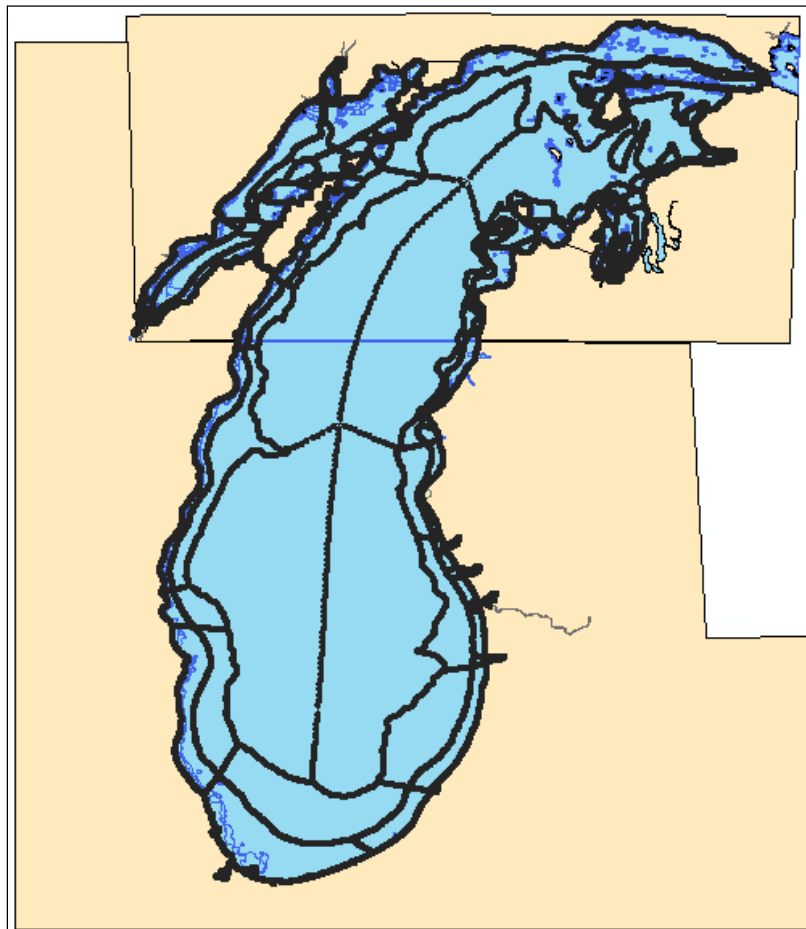


Figure 4-1. Feature map adopted for ADCIRC grid mesh generation.

After generating the initial grid, the builder performs the meticulous and time consuming task of refining the grid, which includes smoothing skewed element shapes so that each is roughly an equilateral triangle, optimizing agreement between the grid and the shoreline and coastal features, such as breakwaters and jetties. Arc spacing between vertices varies from 30 m, specified for the shoreline of southern Green Bay, including the lower Fox River from its confluence with Green Bay to DuPere Dam. For the initial mesh, only a few of the larger harbors such as Chicago, Calumet, Milwaukee, Green Bay and Ludington were highly

resolved. Additional grid refinement was performed for improving grid resolution along the Brown County, Wisconsin shoreline and other locales where fine grid resolution is desired. Grid resolution was on the order of 3000 m in the central region of Lake Michigan. A 500-m grid resolution was adopted along most of the coastline. Using SMS, the bathymetric database, or XYZ file, was imported and interpolated onto the grid mesh.

The initial ADCIRC mesh of Lake Michigan proper and Green Bay is shown in Figure 4-2. Figures 4-3 through 4-6 show the grid at several locations where measurement sites are located. Grid development assumptions included: overland flooding or wetting and drying was not addressed along the lake periphery under the assumption that local flooding will be addressed in work to develop flood risk maps, which resulted in specification of vertical walls and no-flow boundary conditions at the shoreline; the effect of Lake Huron was neglected by defining a no-flow boundary condition at the Straits of Mackinac. The unstructured grid mesh contains a total of 383,688 elements and 196,870 nodes.

4.3 Validation for Lake Michigan/Green Bay only storm simulations

4.3.1 December 1990 storm

Initial model validation was conducted for the December 1990 storm event, which produced the highest storm surge evident in the record for Green Bay. Model simulations applied atmospheric forcing from both the NNM and the CFSR product that were described previously. Figure 4-7 shows a comparison between measured (denoted as “NOS”) and computed water surface elevation (WSE), or storm surge, at Green Bay for both model simulations. In this figure and others that show water level comparisons, an amount of approximately 176 m or 578 feet was subtracted from the observed water surface elevations, which are referenced to the IGLD85 vertical datum. The exact amount subtracted was adjusted so that the mean of smaller scale water level oscillations that occurred several days prior to the main wind event was approximately zero. Selecting the point in time at which to define a zero surge level for the purposes of comparing model results to observations is subjective.

In the time period leading up to the primary wind-driven surge event, both the NNM and CFSR winds qualitatively reproduce the observed trends and patterns in water level variability, including the discrete oscillations that are evident in the observations, but with some vertical offset. In the day

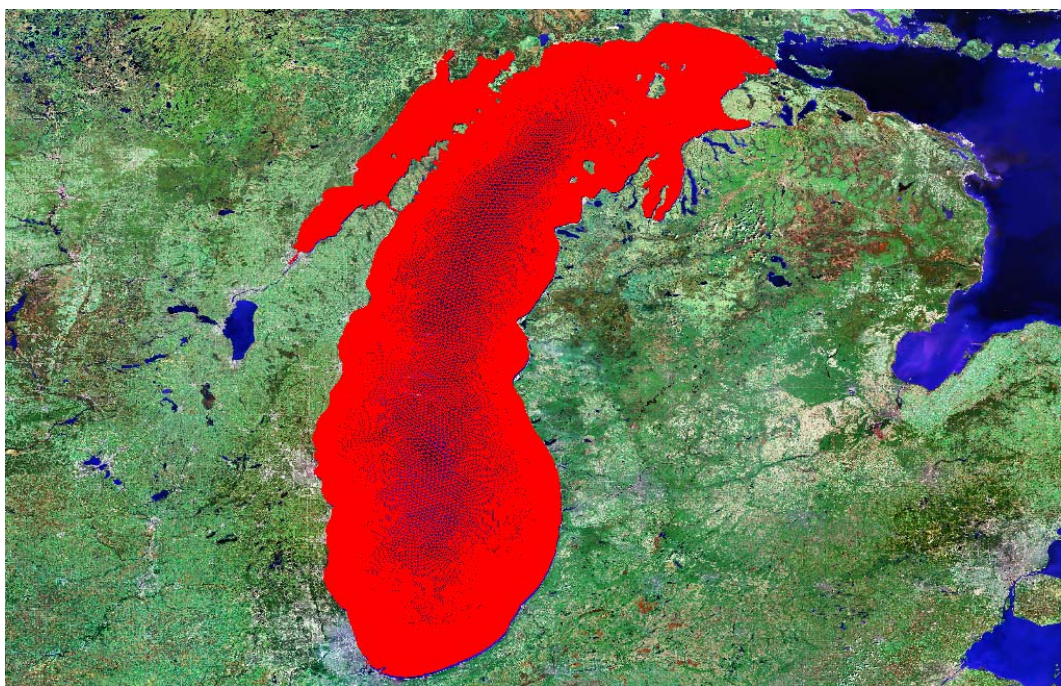


Figure 4-2. ADCIRC grid of Lake Michigan and Green Bay.

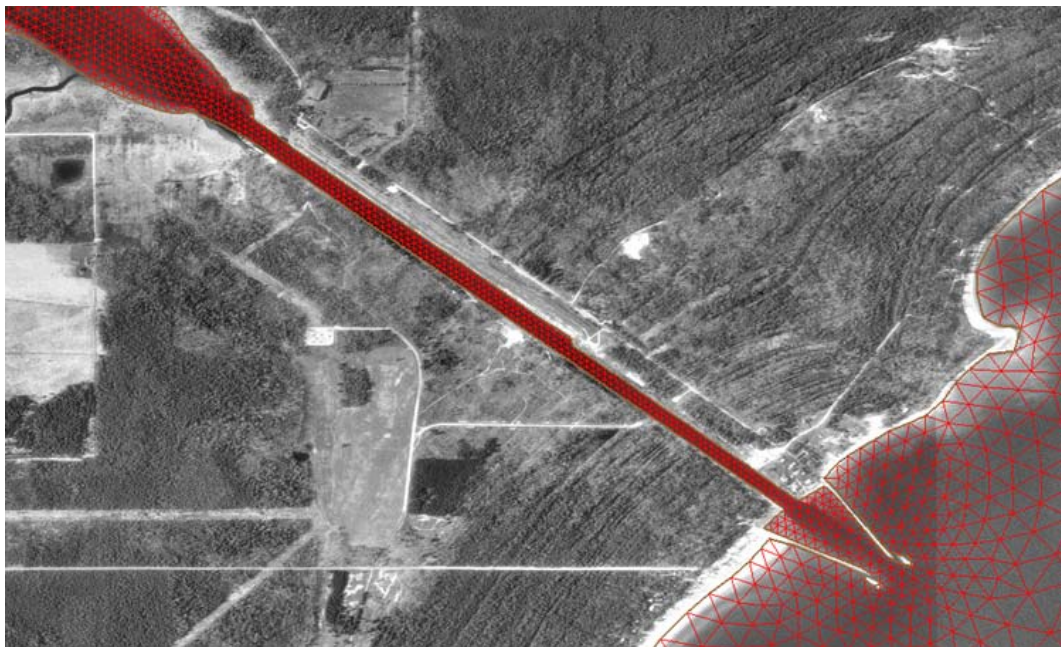


Figure 4-3. Refined grid in the vicinity of Sturgeon Bay Canal.

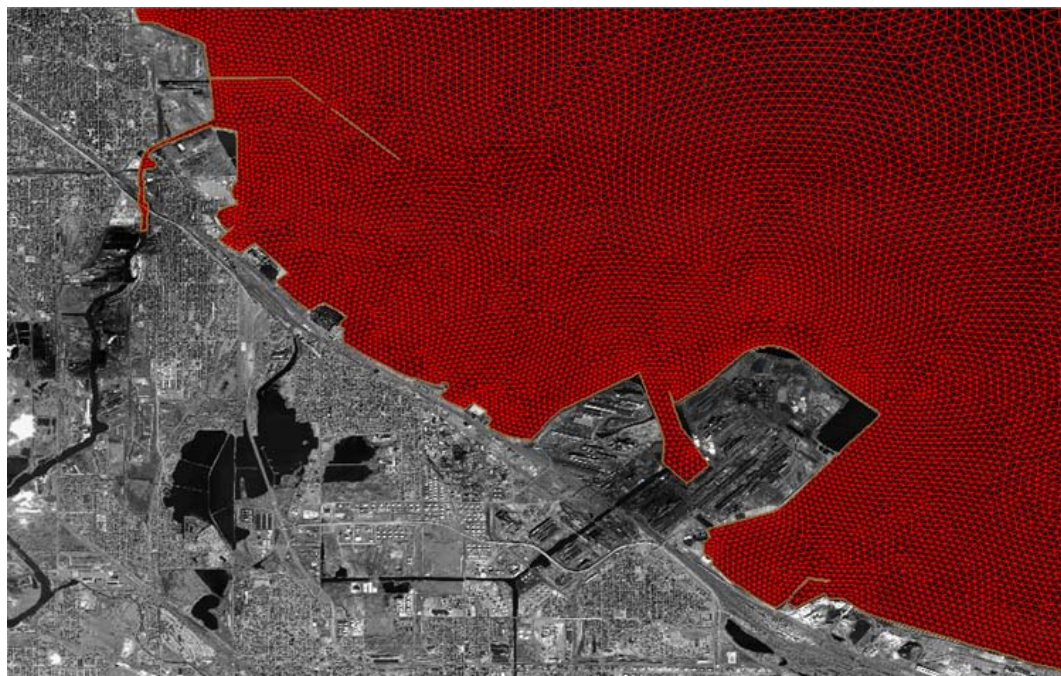


Figure 4-4. Refined grid in the vicinity of Calumet Harbor.

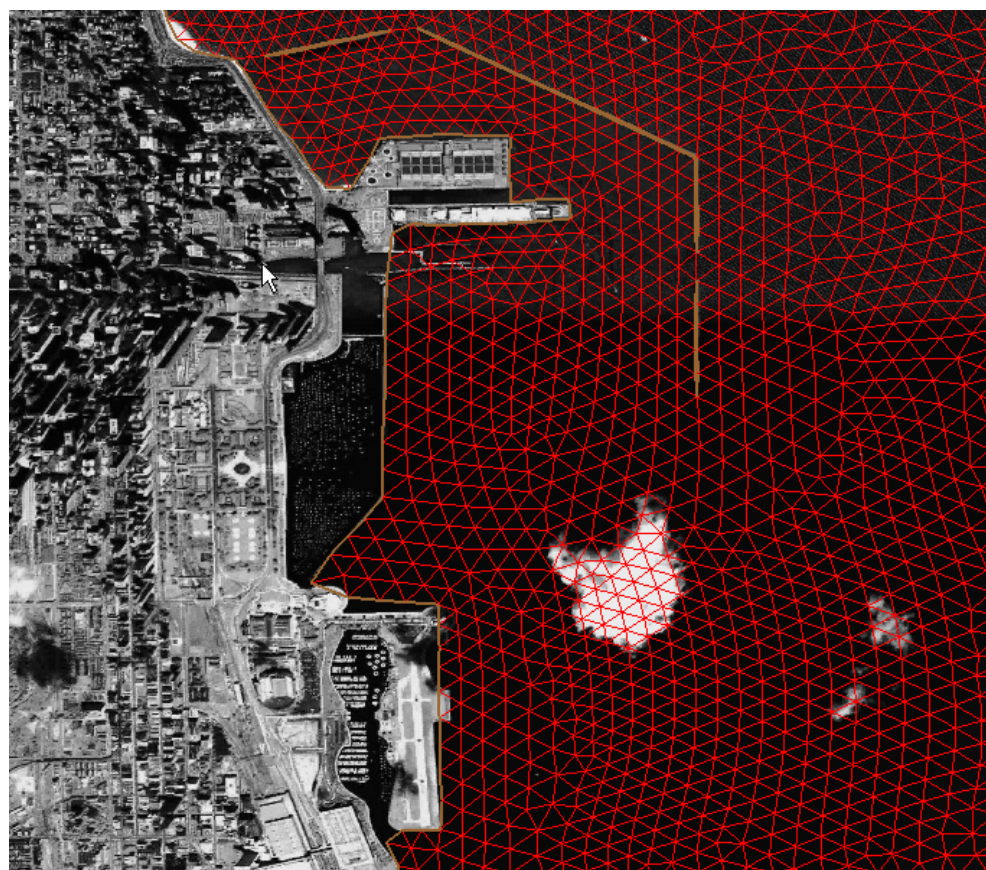


Figure 4-5. Refined grid in the vicinity of Chicago Harbor.

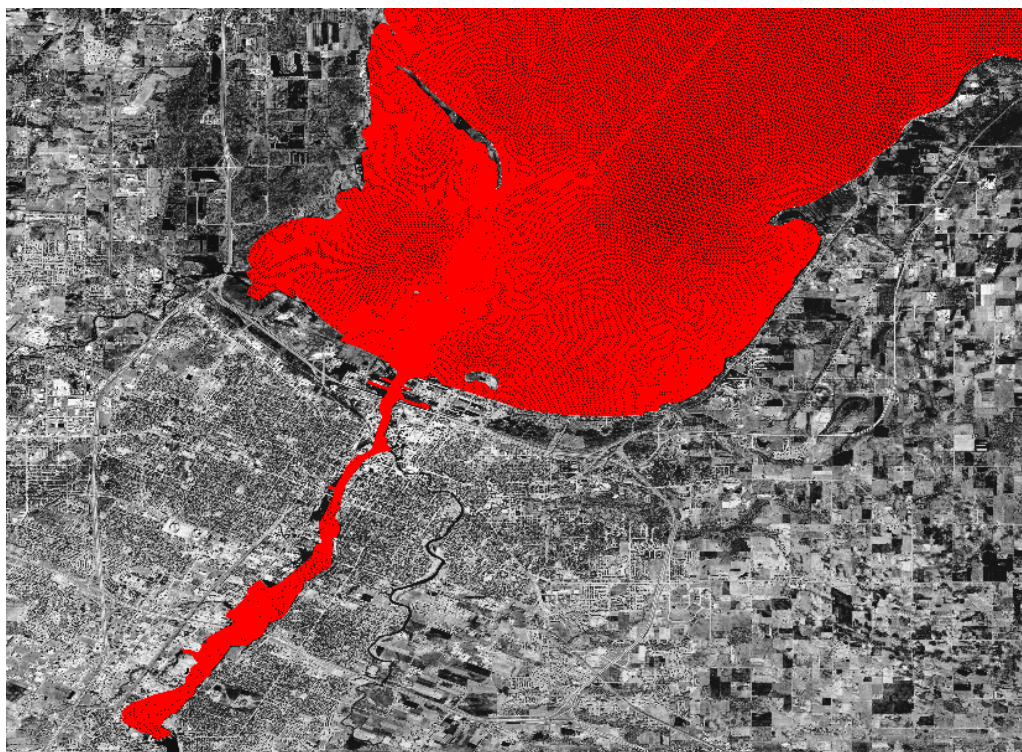


Figure 4-6. Refined grid in the vicinity of Green Bay.

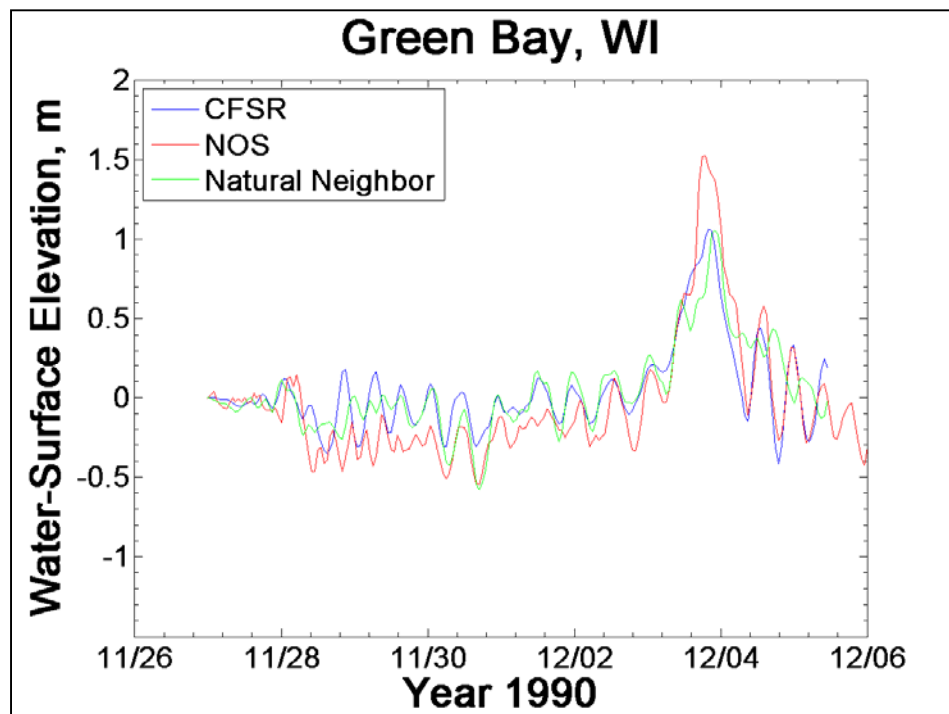


Figure 4-7. Comparison of observed and model-generated water levels at Green Bay, WI, December 1990 event.

preceding the large surge event, both sets of wind forcing produce a similar oscillation response, albeit somewhat muted relative to the observed water surface fluctuations. Water level oscillations that occur within the bay just prior to the main wind forcing can contribute to both the timing and magnitude of peak surge created by the event.

The overall shape and duration of the surge hydrograph associated with the main surge event is reasonably well simulated with both wind sources. However, the magnitude of peak storm surge is underestimated by approximately 0.4 m (1.3 ft) for both. The observed peak is approximately 1.5 m (5 ft); computed peaks are approximately 1.1 m (3.5 ft). The seiche-induced oscillations that are observed after the main surge peak are not well simulated with the NNM winds; however, the CFSR winds result in a good prediction of these features. Overall, the primary water level features comprising the main event are simulated better with the CFSR winds.

In general, considering all of the extreme events that were simulated, and considering both wave and storm surge modeling results, the CFSR winds yielded a better match with observed waves and water levels. Overall, the CFSR winds tended to better represent the spatial and temporal coherence in storm wind fields. Therefore, the CFSR winds were adopted as the preferred source for wind input, when they are available. Comparisons shown throughout the rest of this chapter reflect model results using the CFSR winds only.

The December 1990 event also produced the largest surge peak evident in the measured water level record for Holland, MI. A comparison of measured and calculated water surface elevations for this location is shown in Figure 4-8. For several days prior to the event, the calculated water level trends are qualitatively similar to the observed changes; water level changes are small in magnitude with a few minor higher-frequency oscillations. The shape and duration of the main wind-driven surge event are qualitatively reproduced by the model and wind input; the calculated and observed hydrograph shape and primary water level features are very similar. However, the calculated surge levels, including peak surge, are less than observed values, as was the case in Green Bay, by similar amounts. The observed peak surge is approximately 0.7 m (2.2 ft), which is approximately 0.3 m (0.9 ft) greater than the calculated peak value of 0.4 m (1.3 ft).

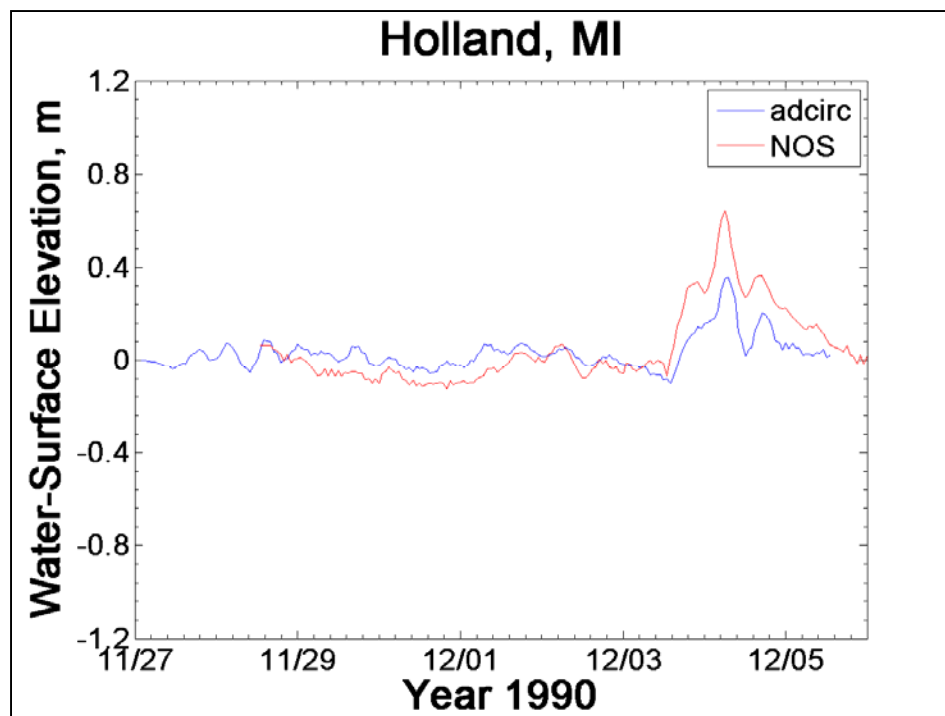


Figure 4-8. Comparison of observed and model-generated water levels at Holland, MI, December 1990 event.

The same event produced a slightly smaller but noticeable water level increase at Calumet Harbor, IL. Measured and calculated water levels for this location are compared in Figure 4-9. For several days prior to the surge event, the trends and features of water level change are reproduced well by the model, both qualitatively and quantitatively. The shape, duration and phasing of the water level features associated with the main wind-driven surge event, and seiche-induced features reflected in the event, are qualitatively predicted by the model. There is a strong coherence between hydrograph features in the model results and measurements. However, calculated surges including peak surge are less than observed surges, by amounts ranging from 0.1 to 0.3 m, less than one foot.

The December 1990 event produced the 7th highest ranked water level at Milwaukee, WI. A comparison of water surface elevations for Milwaukee is shown in Figure 4-10. The same types of similarities and differences seen at other gage sites are seen at Milwaukee: high coherence between measured and simulated hydrograph features, but with calculated water levels consistently less than measured water levels in amounts varying from 0.2 to 0.4 m around the peak of the main surge event.

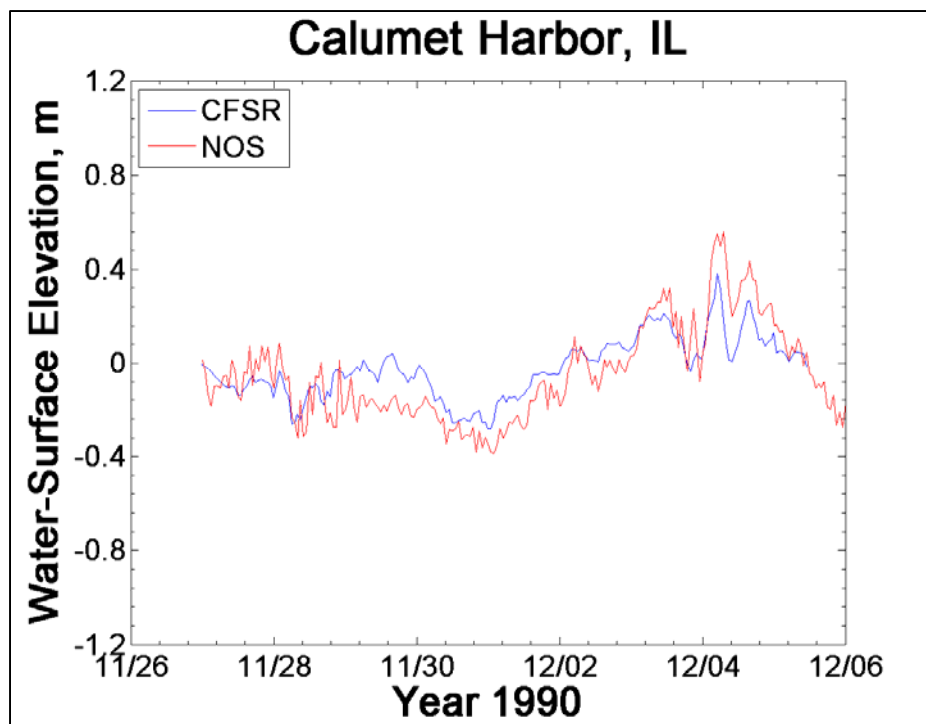


Figure 4-9. Comparison of observed and model-generated water levels at Calumet Harbor, IL, December 1990 event.

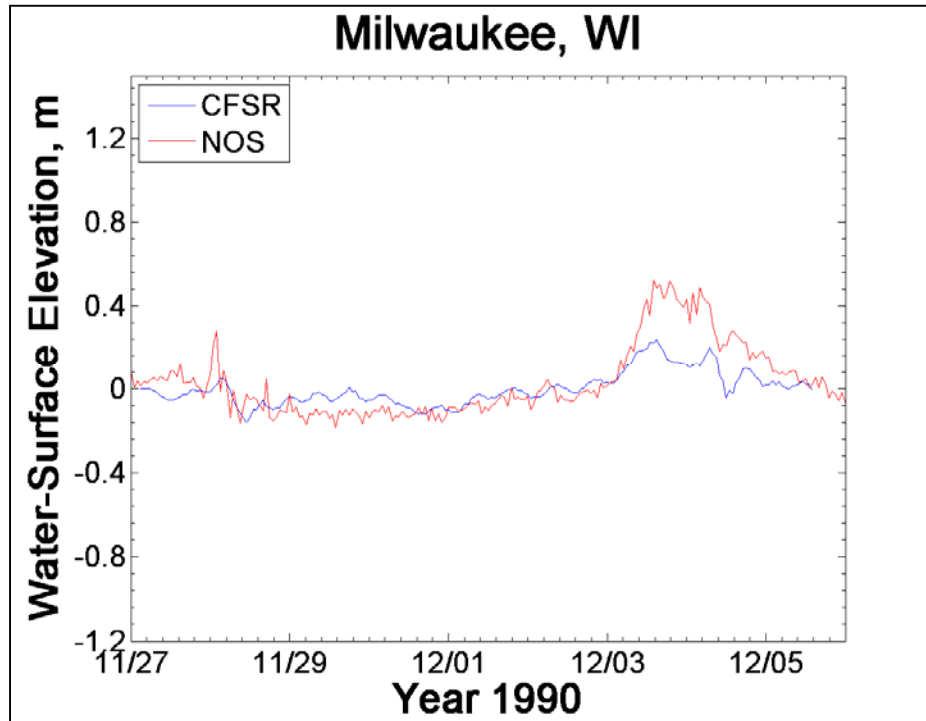


Figure 4-10. Comparison of observed and model-generated water levels at Milwaukee, WI December 1990 event

For this event, the modeled significant wave heights were greater than the measured wave heights, suggesting that the CFSR winds are greater than the actual winds. If the winds are overestimated in the CFSR product, then the reasons for the low bias in water levels is due to another factor as described later in this chapter.

4.3.2 December 2009 storm

The 9-10 December 2009 event was a significant surge event at Green Bay, WI (2nd ranked), Menominee, MI and Holland, MI (10th ranked). Water level comparisons at Green Bay are shown in Figure 4-11. It is evident that in the two to three days prior to the event, trends in water level changes are reasonably well simulated by the model. Seiche-induced oscillations that occur immediately before this event are qualitatively but not quantitatively simulated. Seiche in this highly complex lake and bay system can be introduced by moving high and low pressure centers and fast-moving weather fronts and squall lines which are not resolved well, spatially or temporally, by either of the methods adopted here for defining input winds and pressures. The features of the primary surge event are reasonably well represented by the model, both in shape and duration.

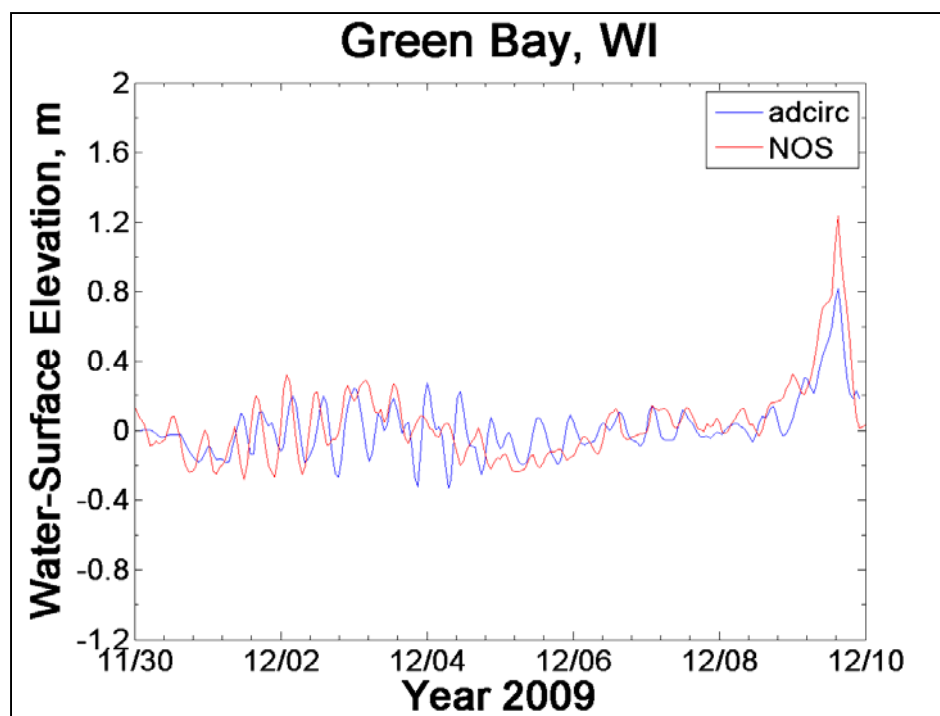


Figure 4-11. Comparison of simulated and observed water surface elevations at Green Bay, WI, December 2009 event.

Calculated surges throughout the main surge event, and peak surge, are less than observed values. Observed peak surge is approximately 1.2 m (4.0 ft), whereas calculated peak surge is 0.8 m (2.6 ft). The magnitude of difference between observed and computed peaks is similar to that for the 1990 event, 0.2 to 0.4 m.

Figure 4-12 shows results for Calumet Harbor. Considering the apparent vertical offset between measurements and calculations for the adopted choice of zero elevation, the calculated trends and patterns and even some of the low-amplitude seiche are reasonably well represented by the model, prior to the event. Calculated peak surge is similar to but slightly less than the observed peak, differing by amount of approximately 0.1 to 0.2 m.

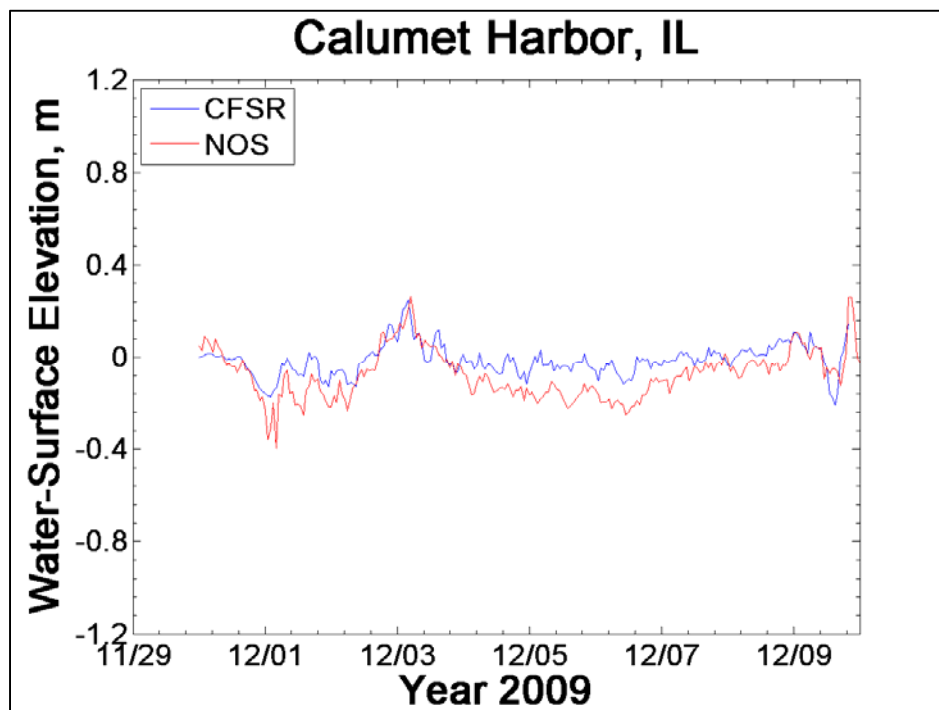


Figure 4-12. Comparison of simulated and observed water surface elevations at Calumet Harbor, IL, December 2009 event.

Figure 4-13 shows results for Menominee. Differences between calculated and observed water levels for the first event are similar to those for Green Bay. In the several days preceding the main surge event, calculated trends and patterns and even some of the low-amplitude seiche are well represented by the modeling. Calculated peak surge for the event is reasonably well simulated by the model, slightly less than the observed peak. The calculated duration of the surge event is less than observed.

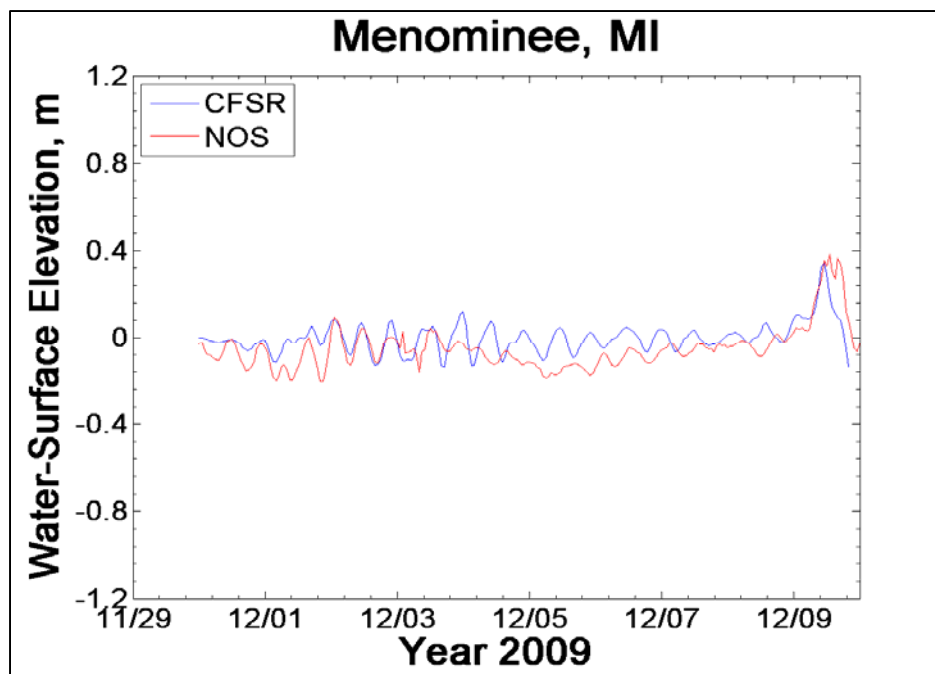


Figure 4-13. Comparison of simulated and observed water surface elevations at Menominee, MI, December 2009 event.

Results for Holland are shown in Figure 4-14. The days leading up to the event are simulated well by the modeling. It appears as though the calculated surge levels are less than observed levels by several tenths of a meter.

Calculated peak water levels for the Dec 2009 storm event show the same general tendency to be biased low as was seen for the December 1990 event.

4.3.3 May 1998 storm

The May 1998 event was selected to examine the capability of simulating a fast-moving, short duration frontal passage event. This event produced an anomalously high water level at Calumet Harbor, the fifth ranked event in the observed record. Comparisons of measured and calculated water level for this event are shown for Calumet Harbor (Figure 4-15) and for Green Bay (Figure 4-16). The rapid speed with which this weather system moves through the region is reflected in the rapid fluctuations evident in the water level record at Calumet. Simulation results indicate that the model is unable to accurately represent, even qualitatively, water level changes associated with this event. This is due to the inability of the wind and pressure fields to accurately represent the event meteorology. Only with much higher spatial and temporal resolution of the atmospheric input would this event be able to be simulated better. This deficiency reflects an overall inability to model rapidly moving frontal systems.

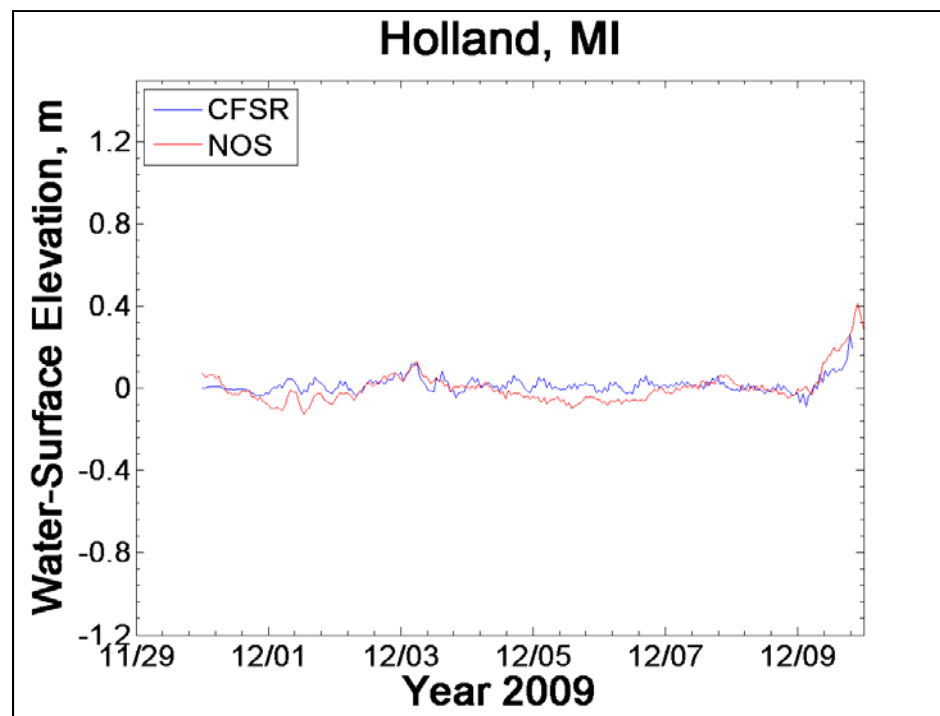


Figure 4-14. Comparison of simulated and observed water surface elevations at Holland, MI December 2009 event.

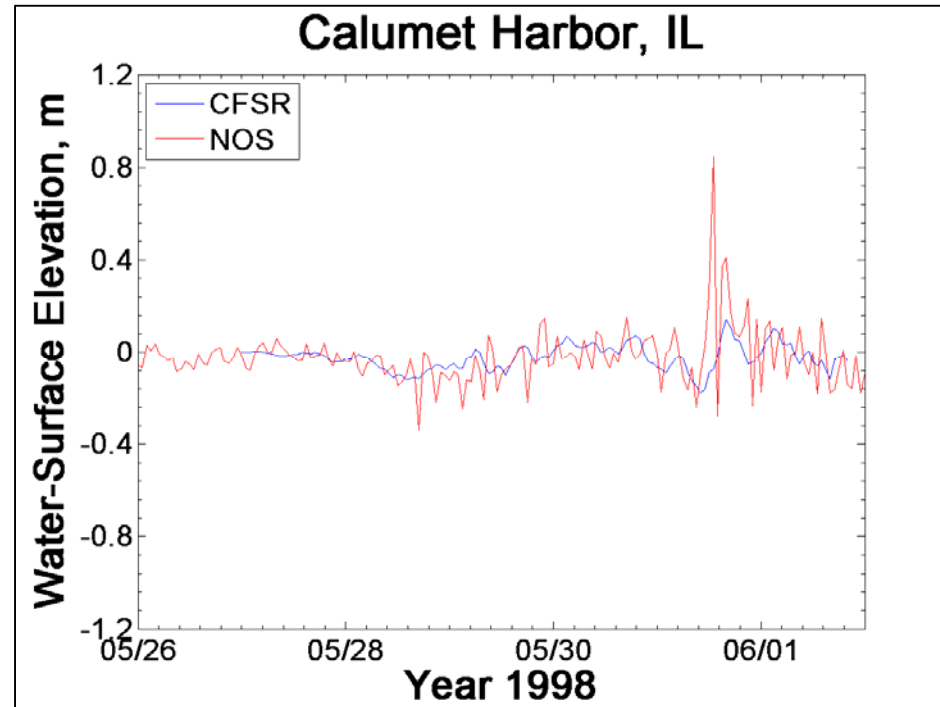


Figure 4-15. Comparison of simulated and observed water surface elevations at Calumet Harbor, IL May 1998 event

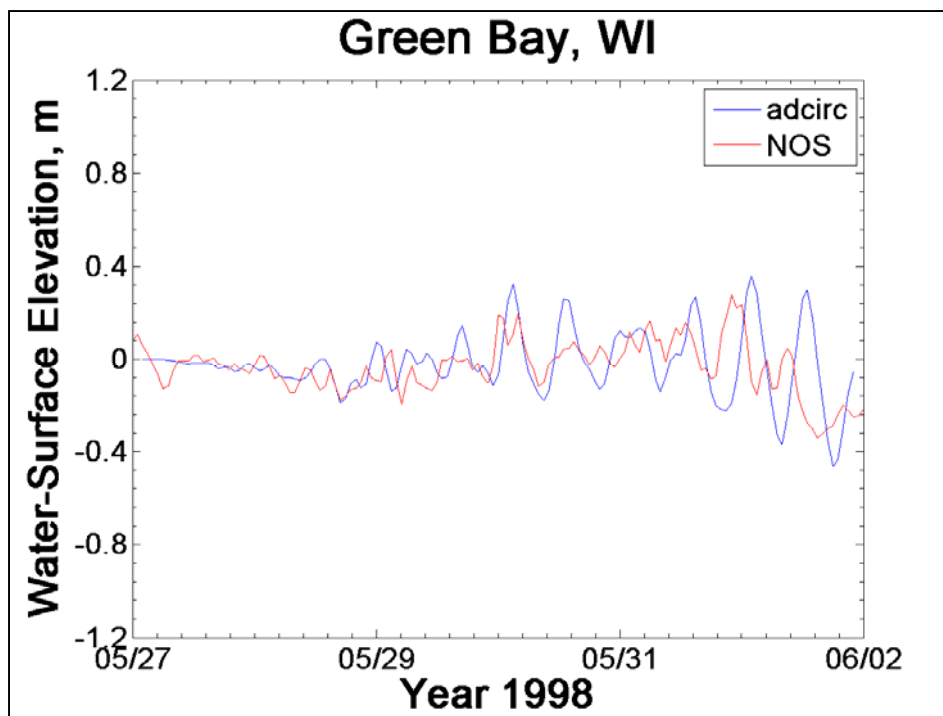


Figure 4-16. Comparison of simulated and observed water surface elevations at Green Bay, WI May 1998 event.

4.3.4 October 1993 storm

The 9 October 1993 event was selected as an extreme event from a wave perspective not a water level perspective. Storm surge produced by this event was not among the top 20 observed maxima for any of the water level measurement sites. This event illustrates the fact that events which produce the highest wave conditions do not necessarily produce the highest water level conditions. Comparisons between observed and calculated water levels for this event are shown for Calumet Harbor (Figure 4-17) and Green Bay (Figure 4-18). Qualitatively, the hydrograph shape is simulated well at Calumet Harbor, including the days leading up to and following the event; the main features of the surge event are represented by the model. Quantitatively, predictive skill is good, overall; however, calculated surges for the primary surge peak are slightly less than observed surges, by amounts of approximately 0.2 m.

At Green Bay, the October 1993 event produced relatively small surge values. The overall mean water level and the peak level are similar for the model and measurements, but the duration of observed elevated water levels are not captured by the model. The model calculates seiche-induced water level fluctuations whereas the measurements show only minor oscillations. The

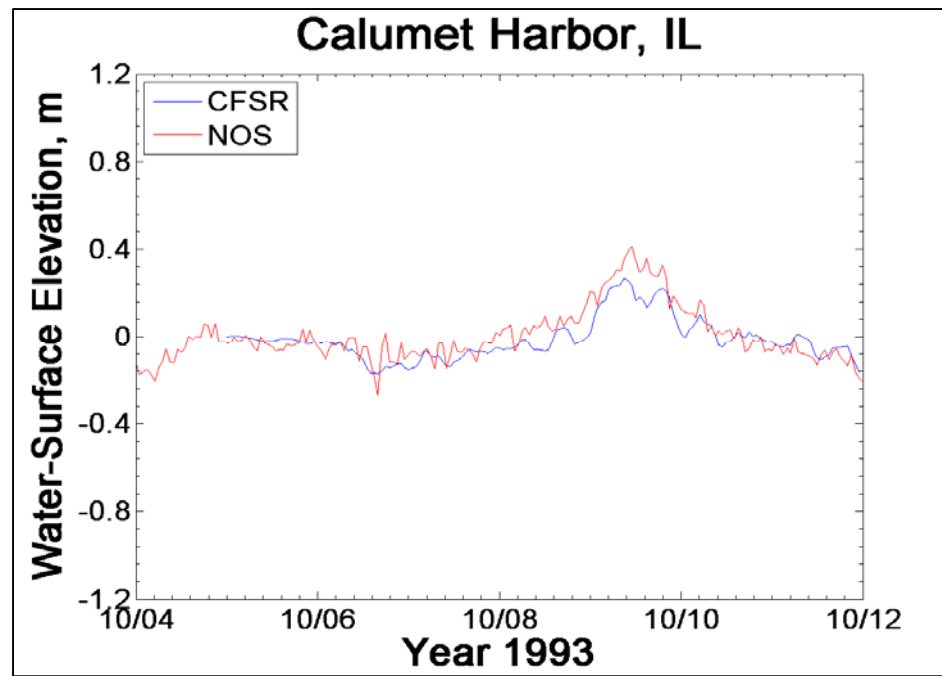


Figure 4-17. Comparison of simulated and observed water surface elevations at Calumet Harbor, IL October 1993 event.

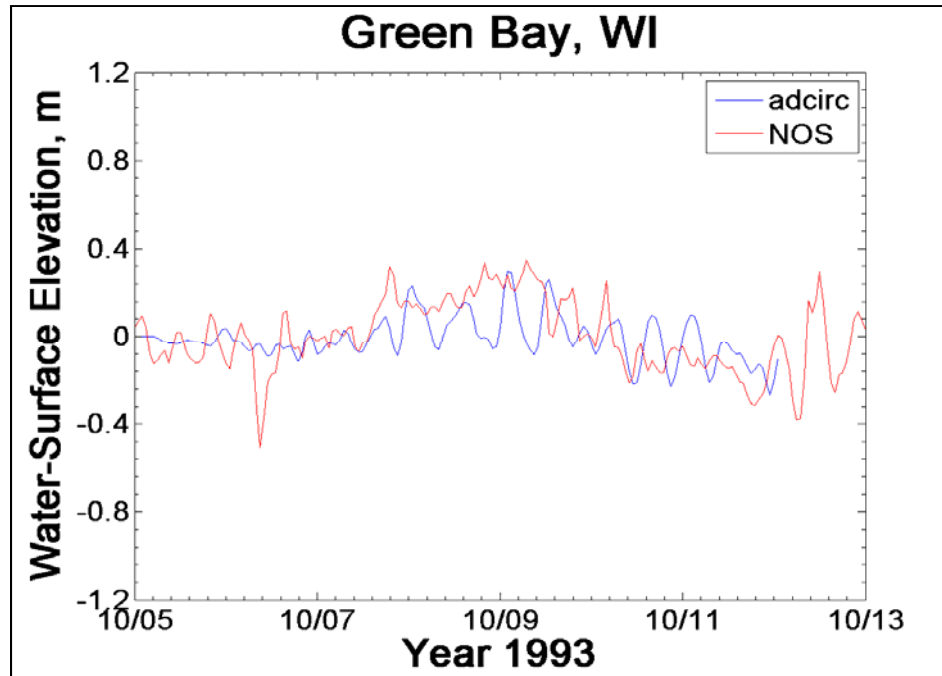


Figure 4-18. Comparison of simulated and observed water surface elevations at Green Bay, WI October 1993 event.

observed peak surge is similar to the modeled peak surge, but the observed hydrograph shape is not well represented in the modeling. The mean of the model calculations around the time of peak observed water level are 0.2 to 0.3 m less than the observed water levels.

4.3.5 November 1992 storm

The November 1992 event was a severe water level event at a number of locations around Lake Michigan. The storm was the 4th, 8th and 12th ranked in terms of water level events at Kewaunee, Ludington, and Sturgeon Bay gage sites, respectively. Comparisons of observed and calculated water levels for Kewaunee (Figure 4-19), Ludington (Figure 4-20) and Sturgeon Bay (Figure 4-21) are similar. Each set of observations shows a single surge event that spans approximately two days, reaching a peak surge level of 0.4 m, with no significant water level fluctuations in the days prior to or after the event. There is no significant seiche at any of these three mid-lake gage sites. The surge hydrograph shape is similar at Kewaunee/Sturgeon Bay (west side) and at Ludington (east side), which are on opposite sides of the lake. The calculated water level at Ludington shows a slight drawdown in the calculated water level followed by an immediate slight rise which occurs midway through the event. The observed water level at Ludington shows a slight increase in water level initially, followed by a more rapid increase leading to the peak water level.

Figure 4-22 shows the water level comparison for Calumet. This event was not a major surge-producing event at Calumet. Again, prior to and after the surge event, the model results match the observations. During the surge event, the decreasing water surface elevation clearly seen in the model results is also evident as a general trend in the observations. If one examines the differences between predicted and calculated water levels, the residual as a function of time would look similar to the observed water levels at the other gage sites, with a peak value of 0.3 to 0.4 m.

These results suggest that either the lake levels in the entire lower portion of the Lake Michigan were increasing for this event, perhaps due to a low pressure system over the lake drawing in water from areas with higher atmospheric pressure, or perhaps waves were creating wave setup of similar magnitude around the periphery of the lake. If the winds were biased low, which would create low biases in calculated rising water levels at Calumet, then as the wind shifted to produce a decrease in water level, the model should simulate a stronger rate of water level decrease than measurements suggest, which is not the case (see Figure 4-22). While there is a decrease in water levels on 3 November third, the rate of decrease is similar to or less than the rate of decrease predicted by the model.

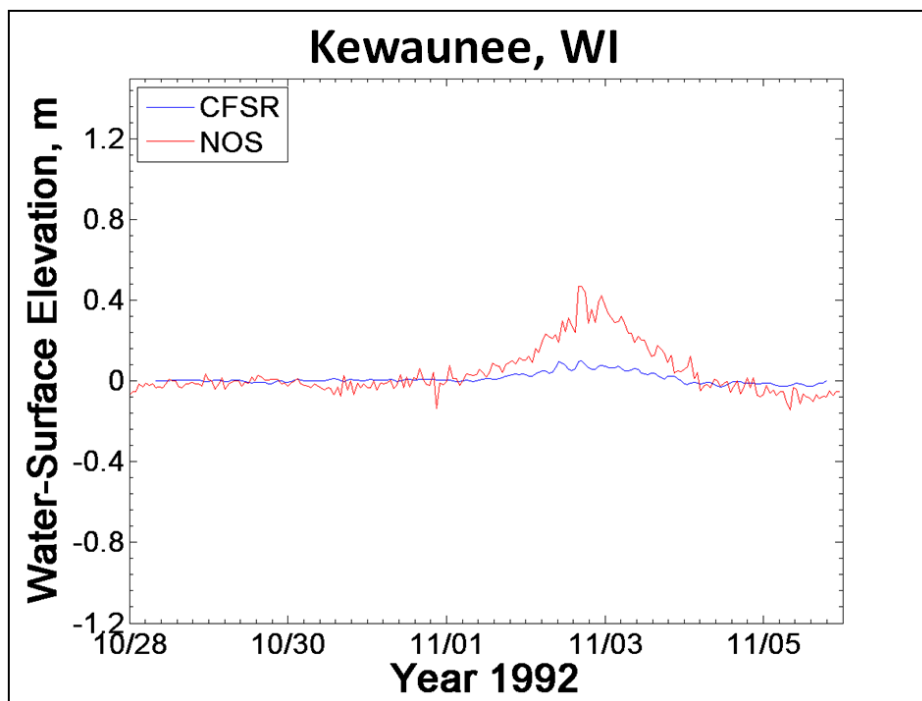


Figure 4-19. Comparison of simulated and observed water surface elevations at Kewaunee, WI November 1992 event.

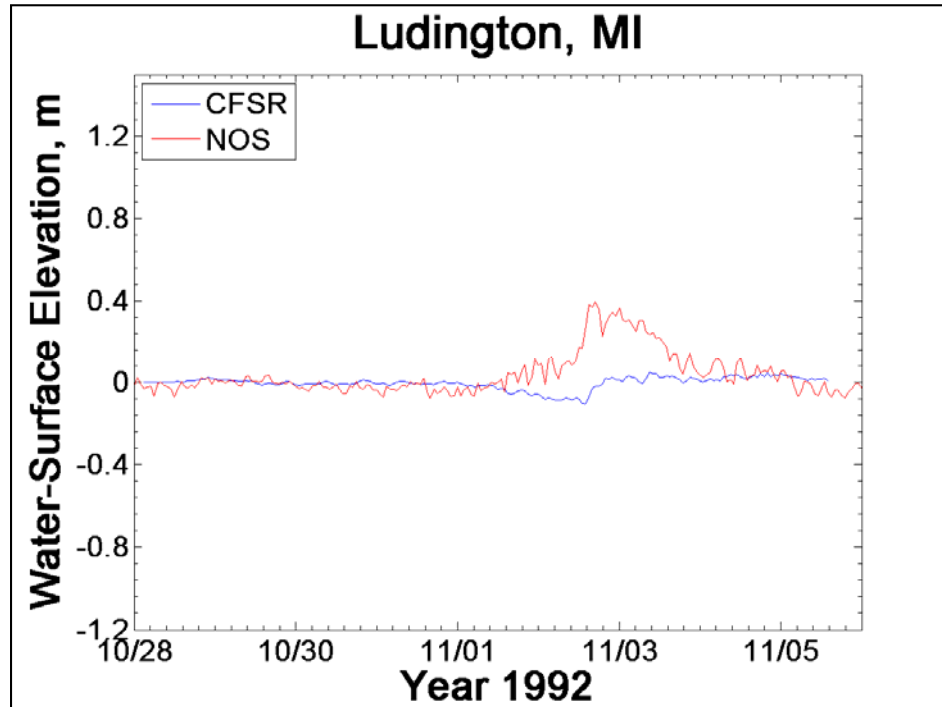


Figure 4-20. Comparison of simulated and observed water surface elevations at Ludington, MI November 1992 event.

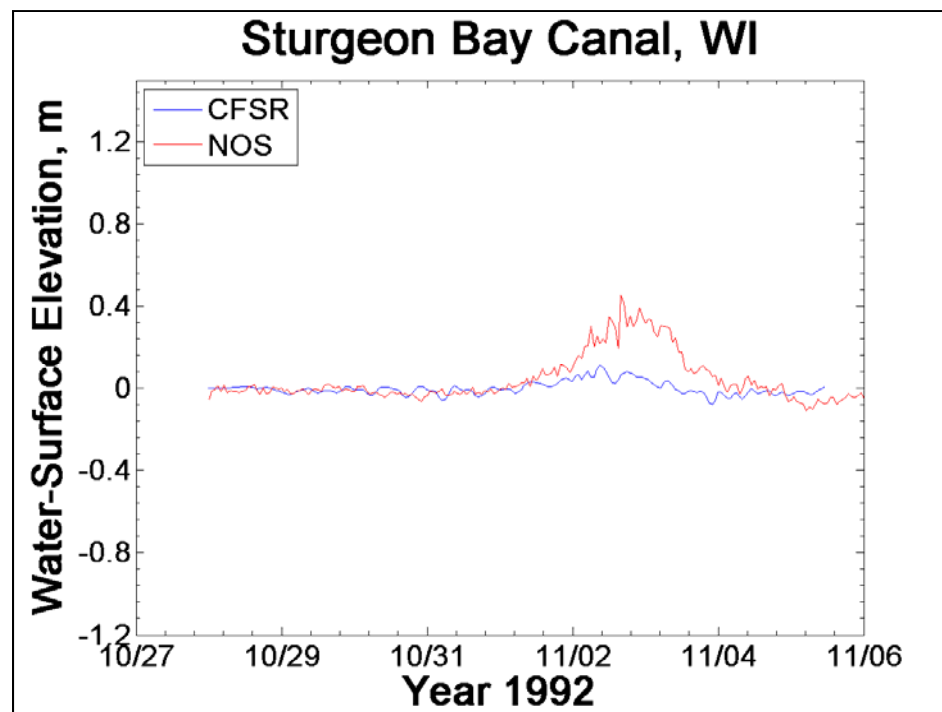


Figure 4-21. Comparison of simulated and observed water surface elevations at Sturgeon Bay Canal, WI November 1992 event.

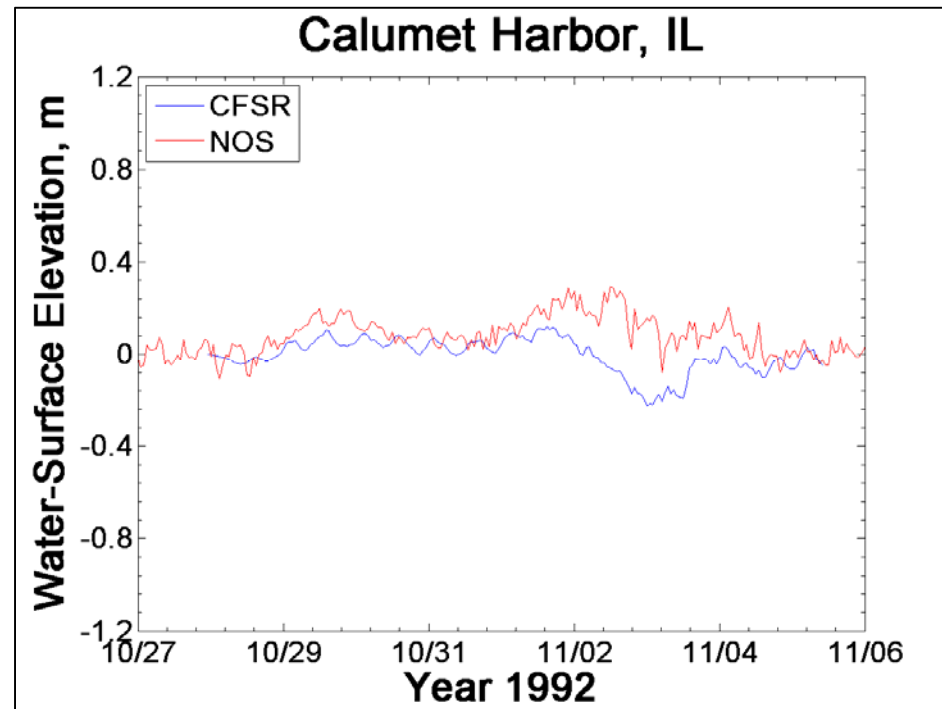


Figure 4-22. Comparison of simulated and observed water surface elevations at Calumet Harbor, IL November 1992 event.

Figure 4-23 shows results for Green Bay. Qualitatively, the calculated hydrograph for the main surge event is very similar to the observed hydrograph, although the details of the numerous low-amplitude oscillations prior to the main surge event are not simulated as well as the main event surge. Calculated peak surge is approximately 0.2 m less than the observed peak surge. Calculated surge appears to occur earlier than the observed surge, as evidenced by phase differences for each of the three oscillations that comprise the main surge peak.

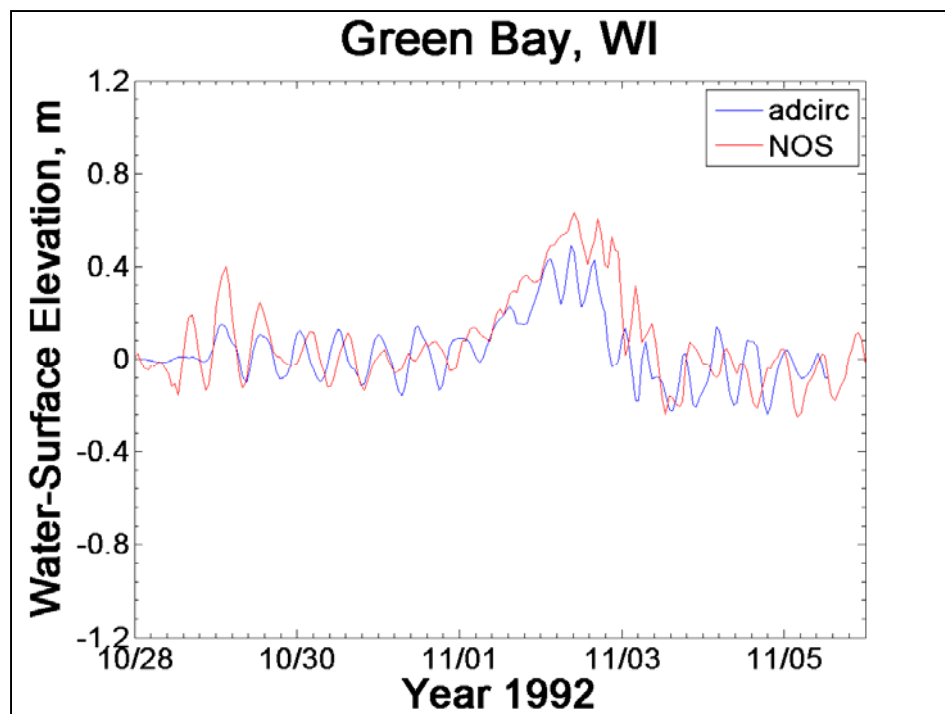


Figure 4-23. Comparison of simulated and observed water surface elevations at Green Bay, WI November 1992 event.

At all gage sites, the calculated peak surges were biased low compared to observed peak surges, a result seen for the previous storms examined. Wave modeling for this storm showed a significant overestimate of significant wave heights at the location of buoy 45002 and good agreement at the other, buoy 45007, compared to measured values. CFSR winds were higher at buoy 45002 by 5 m/sec but matched measured winds at buoy 45007 well. A low bias in computed water levels for this event is not consistent with those wave model results or comparisons between CFSR and measured winds, again. The low bias in simulated water levels again suggests the possibility of a low pressure system over the lake drawing in water from areas with higher atmospheric pressure which were not included in the initial model domain.

4.3.6 September 1989 storm

The September 1989 event was the 3rd ranked surge event at Calumet Harbor. The event is a very short-duration surge event, not unlike the short duration of the rapidly moving May 1998 event. Qualitatively, the simulated hydrograph at Calumet Harbor (Figure 4-24) is similar to the measured hydrograph, both the water level trend prior to, during the surge event, and water level trend following the surge peak. The duration of the event is represented well in the simulation. The calculated peak surge (approximately 0.4 m) is about 0.4 m less than the observed peak surge of approximately 0.8 m. The calculated time of peak surge slightly lags behind the observed time of peak surge.

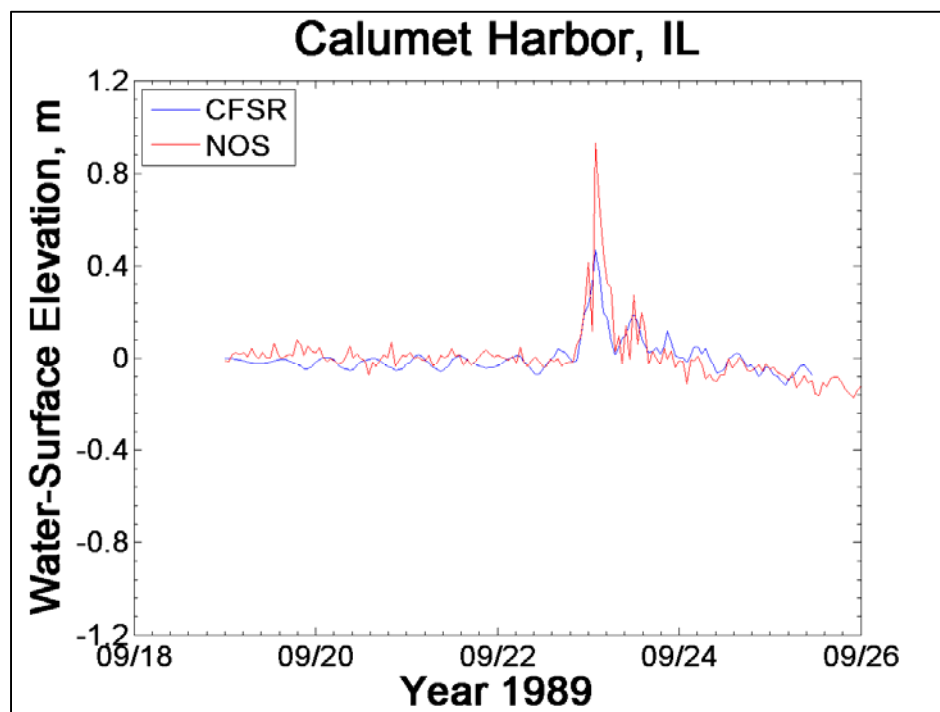


Figure 4-24. Comparison of simulated and observed water surface elevations at Calumet Harbor, WI September 1989 event.

Results for Green Bay are shown in Figure 4-25. Low-amplitude, higher-frequency oscillations leading up the main event are not simulated accurately. The leading larger-scale water level oscillation making up the event is qualitatively simulated. However the calculated surge peak for this oscillation is about 0.3 m less than the observed peak.

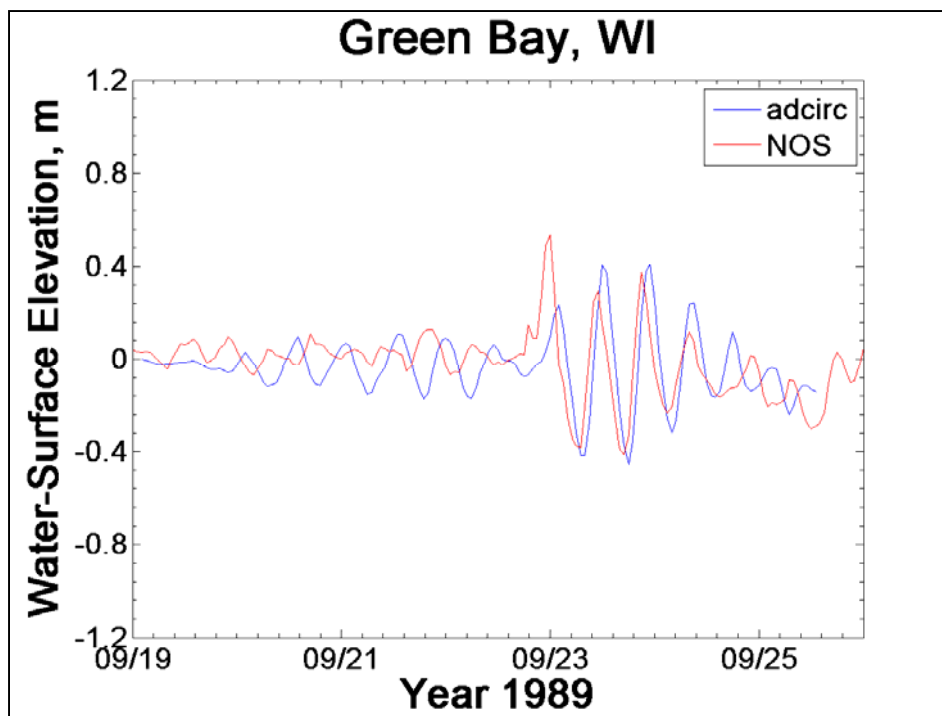


Figure 4-25. Comparison of simulated and observed water surface elevations at Green Bay, WI September 1989 event.

The subsequent three seiche-induced water surface oscillations within the bay are reasonably well simulated. For the water surface oscillations comprising the main event, there is an overall slight phase lag in the modeled results, compared to the measurements. This is indicated at both gages sites suggesting a slight error in phasing of the event as represented in the input wind and pressure data.

4.3.7 March 1985 storm

The 4-5 March 1985 event was the 3rd ranked water level event at Ludington, MI, 7th ranked event at Kewaunee, WI, 4th ranked event at Milwaukee, WI, 14th ranked event at Port Inland, MI, and 17th ranked event at Sturgeon Bay Canal, WI. This event was characterized by persistent strong winds from the east followed by a rapid directional shift and persistent strong winds from the southwest and west.

Comparisons of observed and calculated water levels for Ludington (Figure 4-26) and Kewaunee (Figure 4-27) are similar despite being on opposite sides of the lake. Like the November 1992 storm event, each set of observations shows a single surge event that spans approximately two days, reaching a peak surge level of 0.3 to 0.4 m, with no significant water

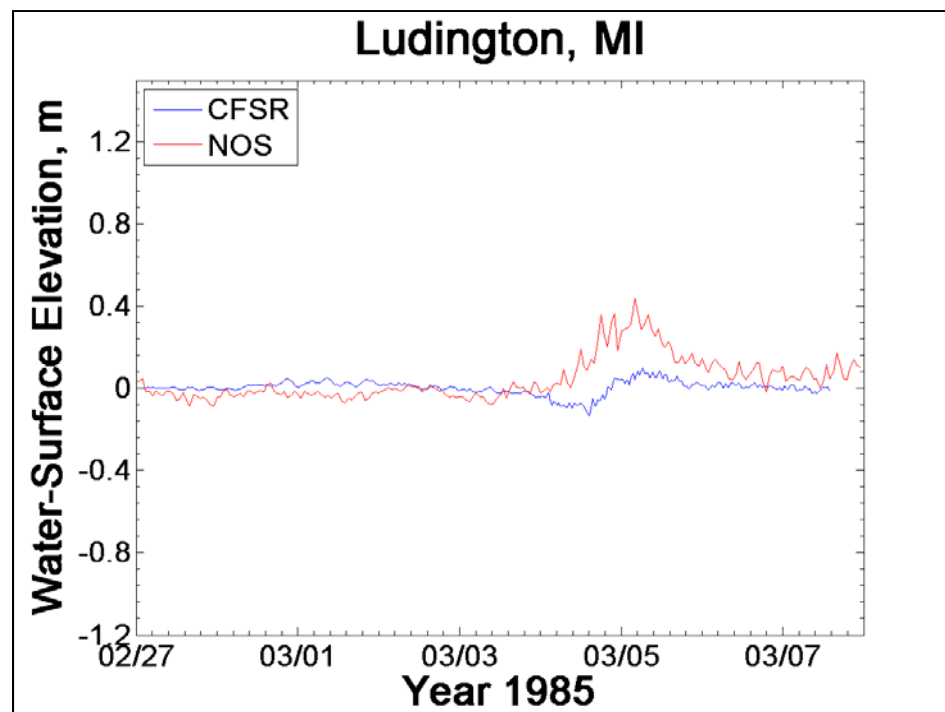


Figure 4-26. Comparison of simulated and observed water surface elevations at Ludington, MI March 1985 event.

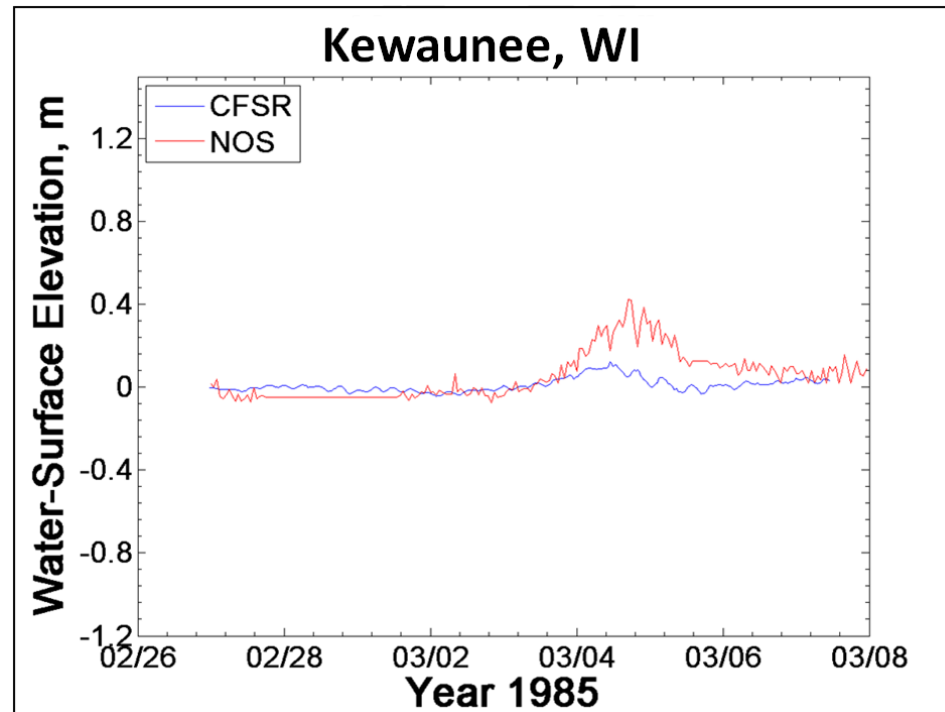


Figure 4-27. Comparison of simulated and observed water surface elevations at Kewaunee, WI March 1985 event.

level fluctuations in the days prior to or after the event. The calculated water level at Ludington shows a slight drawdown in the calculated water level followed by an immediate slight rise which occurs midway through the event. Since Ludington is on the east side that pattern of wind-driven water level changes is consistent with the wind pattern for this event. However, the observed water level at Ludington shows a slight increase initially, followed by a more rapid increase leading to the peak water level. At Kewaunee, on the west side of the lake, calculated water levels show the opposite pattern of changes, an initial slight rise and then a fall. This pattern is also consistent with easterly winds that shift to westerly winds. Measured water levels at Kewaunee show a much greater rise toward the peak than a decline.

Figure 4-28 shows the water level comparison for Port Inland at the northern end of Lake Michigan. Prior to and after the surge event, the model results match the observations. During the surge event, the decreasing water surface elevation clearly seen in the model results is also evident as a general trend in the observations. Calculated peak surge is biased low through the event, about 0.3 m less near the peak of the event. If one examines the differences between predicted and calculated water levels, the residual as a function of time would look similar to the observed water levels at Kewaunee and Ludington, with a peak value of approximately 0.3 m.

Figure 4-29 shows the water level comparison for Calumet. Accounting for the apparent vertical offset, in the few days prior to and after the surge event, the model results match the observations quite well. The features of the observed surge hydrograph are qualitatively simulated by the model. During the surge event, the decreasing water surface elevation clearly seen in the model results is also evident in the observations. As with the other gage sites, the calculated water levels are biased low compared to measured water levels. If one examines the differences between predicted and calculated water levels, the residual as a function of time would look similar to the observed water levels at the other gage sites, with a peak value of approximately 0.3 m. The low bias in simulated water levels again suggests the possibility of a low pressure system over the lake drawing in water from areas with higher atmospheric pressure which were not included in the initial model domain.

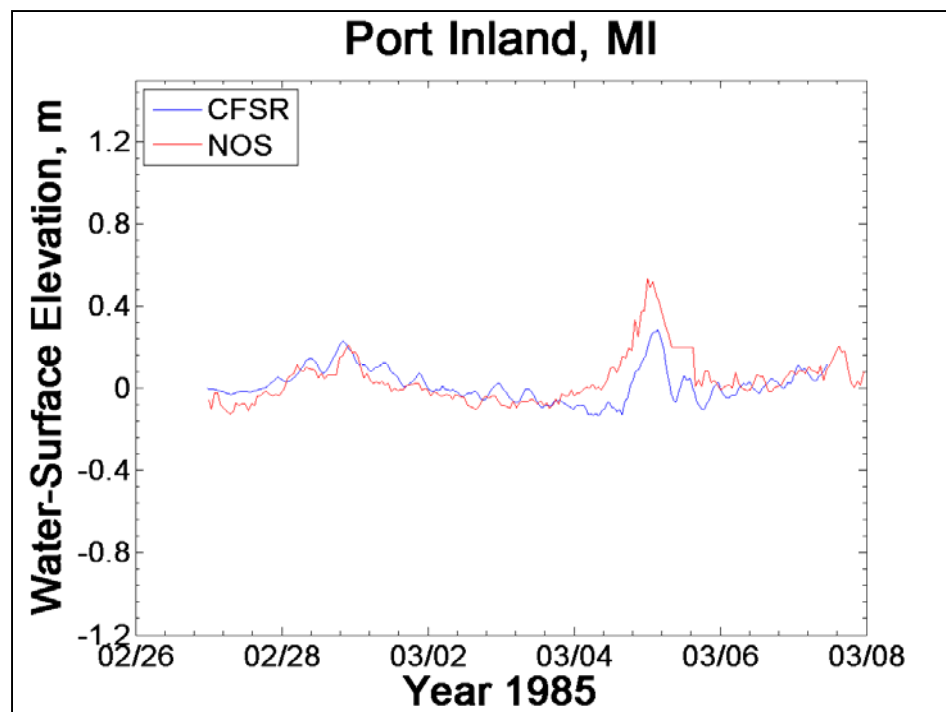


Figure 4-28. Comparison of simulated and observed water surface elevations at Port Inland, MI March 1985 event.

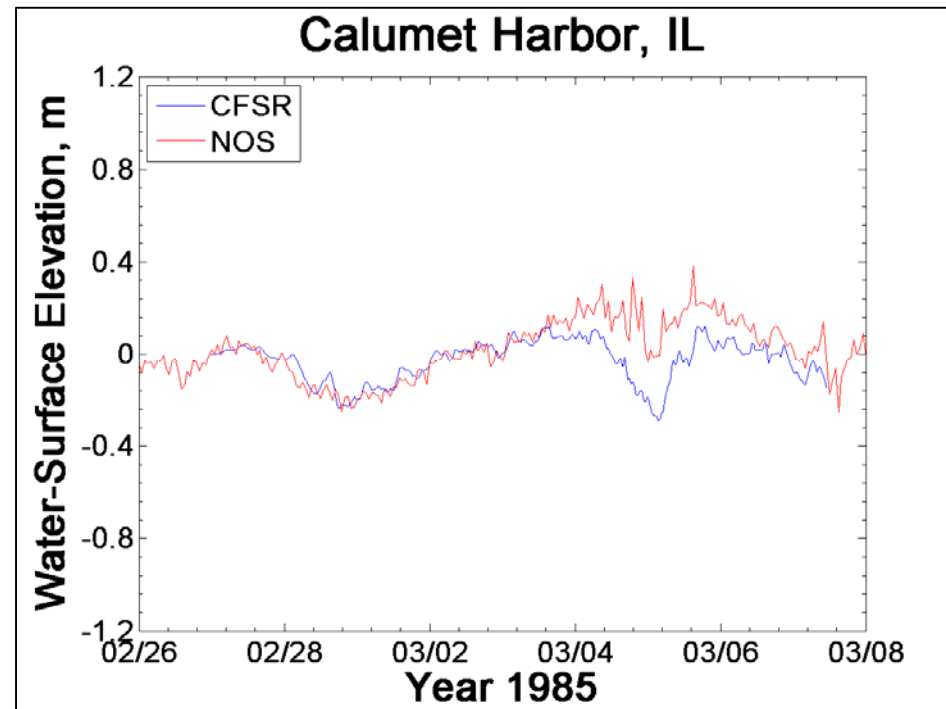


Figure 4-29. Comparison of simulated and observed water surface elevations at Calumet Harbor, IL March 1985 event.

4.4 Systematic low bias in simulated water levels

For several of the extreme storm events, gages on opposite sides of Lake Michigan showed roughly the same bell-shaped rising and falling storm surge hydrograph. Some of those same hydrographs showed evidence of expected wind-driven water level behavior, but with another process dictating the shape of the hydrograph. The similarity between the mid-lake gage sites (Kewaunee and Ludington) that are less influenced by wind and deviations between calculated and observed hydrographs at the north (Port Inland) and south (Calumet) ends of the lake, and at Green Bay, which respond more to the wind, suggested a filling action within Lake Michigan.

For those events when low atmospheric pressure is situated over Lake Michigan and high pressure is situated over Lake Huron, water will tend to be driven from areas of high pressure to low pressure through the Mackinac Straits that connect the two lakes. To provide a fast response to such forcing, the Mackinac Straits must rapidly convey a significant amount of water back and forth between Lake Huron and Michigan to produce water levels changes of 0.3 to 0.5 m, the magnitude of the bias in calculated water levels that was often evident.

The sensitivity of water levels to application of CFSR pressure field forcing within Lake Michigan proper during these simulations was relatively small. Unlike hurricanes and other low pressure systems that are typically modeled to evaluate extreme water levels in open coastal regions, where central pressures within the storm center and ambient pressures at the storm periphery can differ by as much as 80 to 100 mb, the storms simulated here exhibited a broad weakly varying spatial distribution of atmospheric pressure within Lake Michigan proper. Figure 4-30 shows the spatial distribution of the minimum modeled atmospheric pressure for the December 2009 storm. The figure shows that there is approximately a 0.1 m spatial elevation difference associated with atmospheric pressure forcing over the entire length of Lake Michigan (1 mb decrease in atmospheric pressure results in approximately a 1 cm increase in water level). However, as seen in Figure 4-31, the temporal distribution of atmospheric pressure from the available meteorological stations (Chicago, Milwaukee, Mackinaw and Muskegon) compared with CFSR pressures at the same location, shows a pressure difference of nearly 50 mb during the event. A 50 mb pressure deficit is equivalent to a 0.5 m increase in static water level.

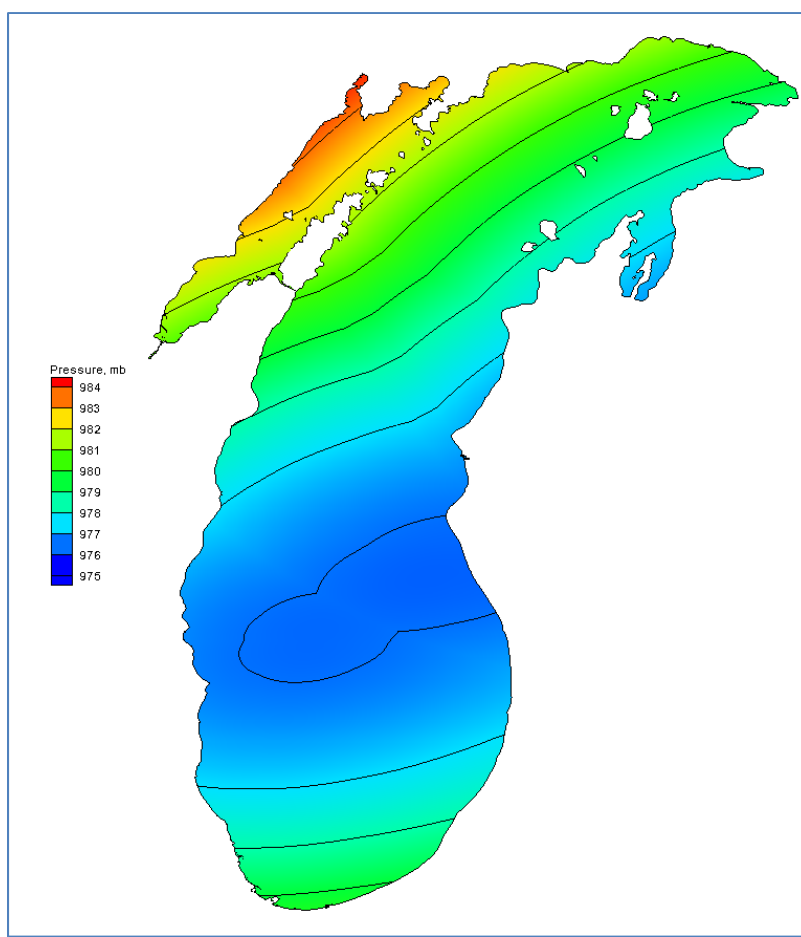


Figure 4-30. December 2009 storm event, minimum modeled pressure.

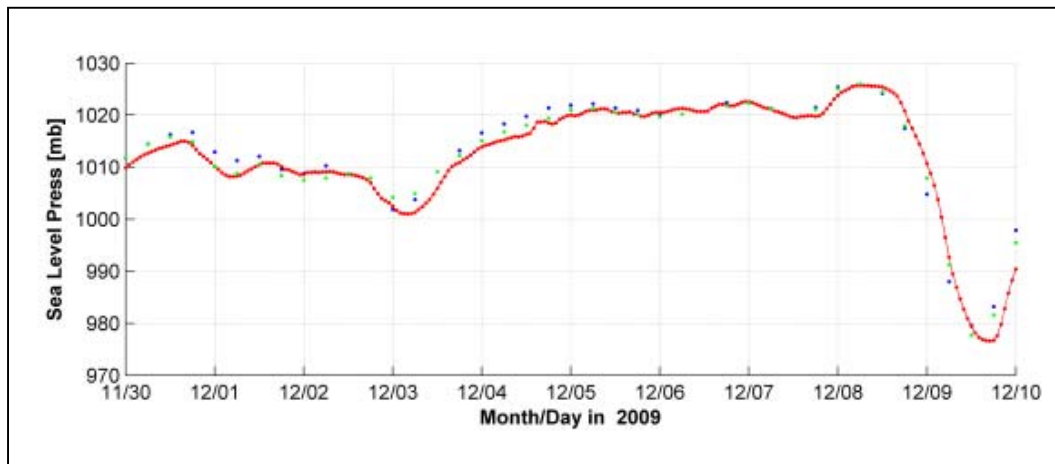


Figure 4-31. December 2009 storm event, observed (symbols) and modeled CFSR atmospheric pressure at Chicago, Milwaukee, Mackinaw and Muskegon.

An examination of the minimum pressure data and the temporal pressure variation revealed a 30 mb pressure deficit at Green Bay and Calumet and a 20 mb deficit at Menominee. Accounting for these inverted barometer

corrections in the simulated peak water levels at these stations would improve the predictions and is the likely source of some or most of the negative bias in calculated peak water levels. Including Lake Huron in the model domain to allow water to be driven from areas of high pressure to low pressure through the Mackinac Straits that connect the two lakes is the better solution, as will be described later in this chapter.

Figure 4-32 presents the minimum modeled pressures in meters of water for the March 1985 storm. The figure shows that for this event there is a negligible variation in minimum pressure within the lake, less than 5 cm of an equivalent inverted barometer effect. However, as seen in Figure 4-33, the temporal distribution of atmospheric pressure shows a pressure deficit of nearly 30 to 40 mb during the event which is consistent with the 0.3 m to 0.4 m under prediction of peak water levels seen in earlier results.

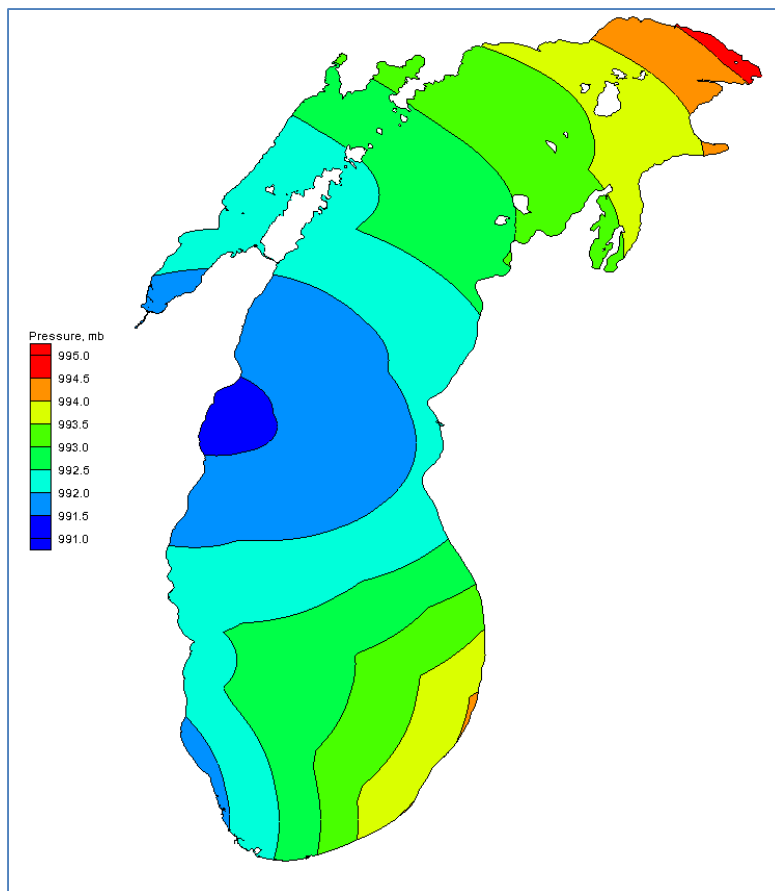


Figure 4-32. March 1985 storm event, minimum modeled pressure.

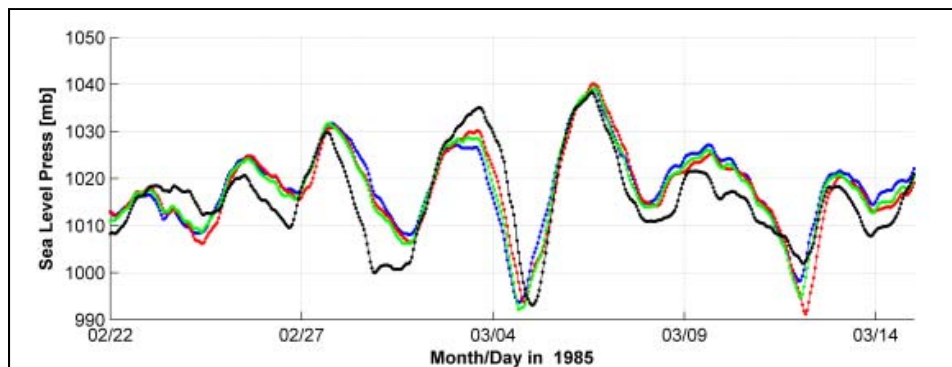


Figure 4-33. March 1985 Storm, observed atmospheric pressure throughout Lake Michigan.

This lack of proper pressure forcing response is due to modeling Lake Michigan as an independent water body. The work of Schertzer et. al. 2008 showed that volume exchange between Lake Michigan and Lake Huron takes place on a seasonal scale and that flows through the connecting straits can be significant at event scales. Comparisons of model results and measured water level data suggest this exchange is an important factor during several-day duration storm events in Lake Michigan, producing water level changes of 0.5 m, and that the two lakes respond relatively rapidly and efficiently to the pressure differential that exists between them. Persistent high pressure over Lake Huron with concurrent persistent low pressure over Lake Michigan can explain significant water level increases in Lake Michigan that are different from patterns of change induced by the wind speed and direction patterns. This appears to be the case where 0.4 m of the water level increase at both Ludington and Kewaunee occurred during the 1992 and 1985 easterly/westerly wind events in addition to the water level changes induced by the wind (see Figures 4-19 and 4-20, and 4-26 and 4-27). As confirmation, for the March 1985 storm, water levels at a mid-lake gage site in Lake Huron were examined. While Lake Michigan water levels were rising by amounts of up to 0.4 m, Lake Huron was falling by similar amounts.

In summary, during the passage of low pressure systems, the spatial variation in pressure over Lake Michigan and Lake Huron causes a relatively rapid response through the Mackinaw Straits. The pressure differential that exists between Lake Michigan and Lake Huron requires the low pressure lake to draw water from the high pressure lake through the Mackinaw Straits to fill the void caused by the low pressure system. For this reason, the Lake Michigan model domain was expanded to include Lake Huron, Georgian Bay, and North Channel.

4.5 Model sensitivity testing

4.5.1 Sensitivity to wind speed

To examine the effect that a bias in wind speed might have on calculated water levels, the December 2009 event was simulated with an increase of 12-percent in wind speed applied to the CFSR winds throughout the model domain for the entire storm duration. Figures 4-34 through 4-36 compare simulated and observed water-surface elevations at Green Bay, Calumet Harbor and Menominee, respectively. For Green Bay and Calumet Harbor, the increase in wind speed improves agreement between calculated and observed peak surge levels. At Menominee the increase in wind speed leads to an overestimate of the storm surge. At Green Bay the increase in wind speed increased peak surge levels by several tenths of a meter.

4.5.2 Sensitivity to bottom friction

The sensitivity of the ADCIRC simulations to bottom friction was also investigated. For the previous simulations shown, the Manning's n was 0.02, which is the recommended value to be used for Lake Michigan. Figure 4-37 compares simulated storm surge levels generated with a reasonably low bottom roughness (Manning's $n = 0.01$) and a high bottom roughness ($n = 0.04$); the December 1990 event was simulated in this sensitivity test. Results show that the large range of Manning's n produces reasonably small changes in the peak water-surface elevation even for the shallower Green Bay region, which would be most sensitive to the value of Manning's n . Effects are greater for the low amplitude oscillations than for the main wind-driven surge event. In the deeper regions (Lake Michigan), it is expected that the variability of water-surface elevation should less sensitive to the value of bottom friction coefficient.

4.5.3 Sensitivity to presence of ice cover

A sensitivity test was conducted to examine the effect of the presence of ice on simulated water levels. Figure 4-38 compares simulated water-surface elevations, during the December 1990 event at Green Bay, with and without free-floating ice coverage of 50-percent (50-50 mixture of ice and water) applied to the entire lake. A 50-percent ice concentration produces the maximum surface shear stress, using the drag coefficient formulation discussed previously. This example illustrates the maximum influence ice cover can have on calculated water levels, and the relative role of surface stress changes associated with ice compared to water level changes induced by other factors. In general, peak surge values with ice coverage can be increased by several tenths of a meter.

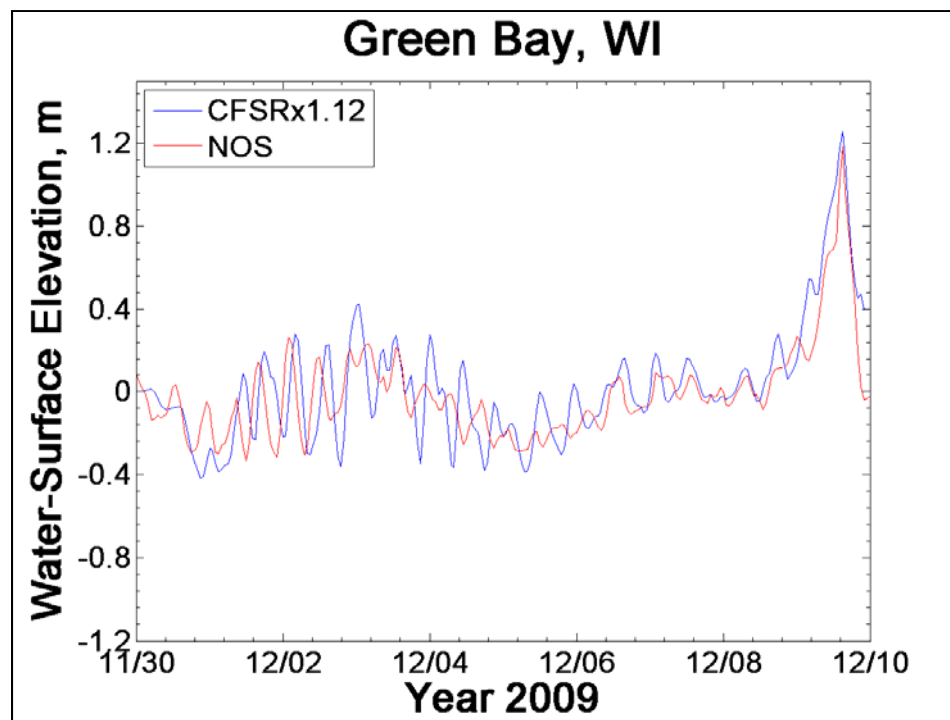


Figure 4-34. A comparison of simulated and observed water-surface elevation at the Green Bay, WI December 2009 event, with a 12-percent increase in wind speed.

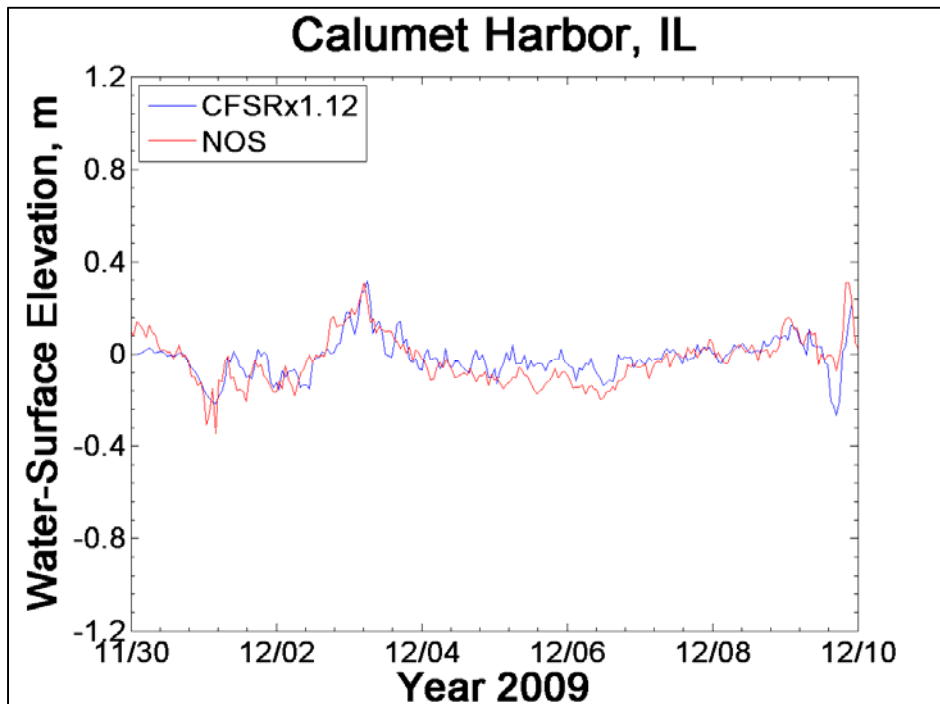


Figure 4-35. Comparison of simulated and observed water-surface elevations at the Calumet Harbor, IL December 2009 event, with a 12-percent increase in wind speed.

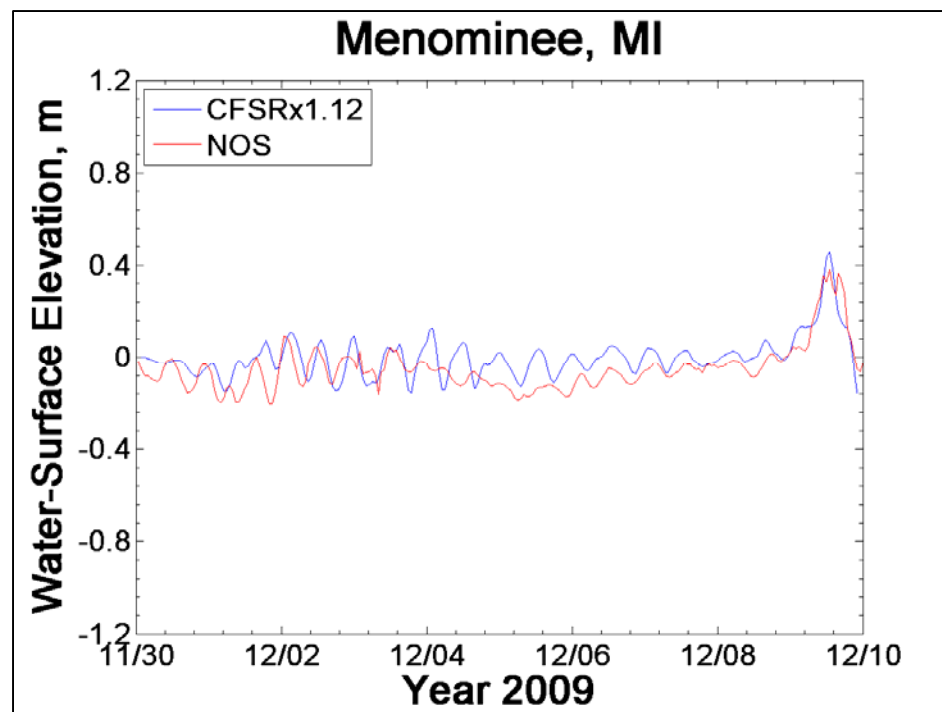


Figure 4-36. Comparison of simulated and observed water-surface elevations at the Menominee, MI, December 2009 event, with a 12-percent increase in wind speed.

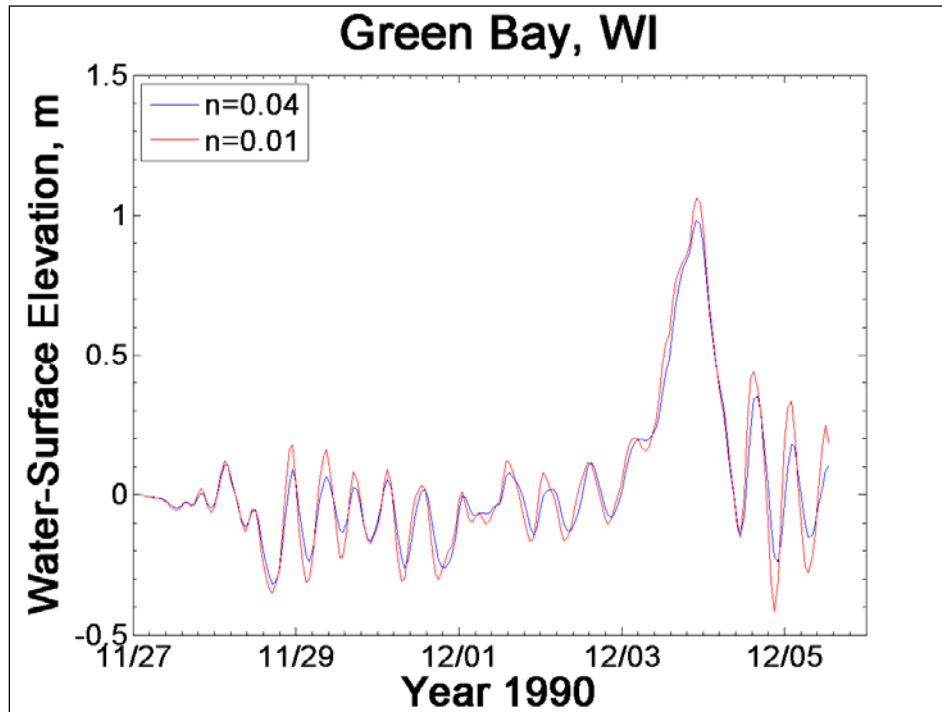


Figure 4-37. Comparison of Manning's n.

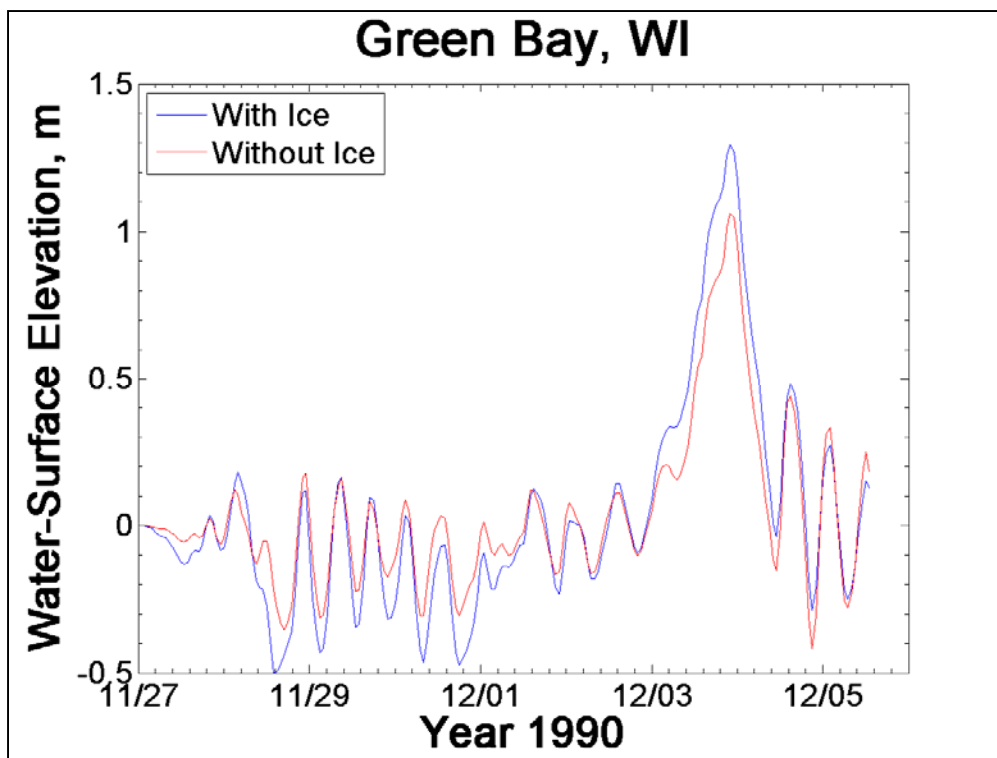


Figure 4-38. Comparison of with- and without-ice conditions.

4.6 ADCIRC mesh expansions

This section describes two levels of expansion that were made to the ADCIRC mesh. The first expansion of the ADCIRC mesh was to extend the domain from Lake Michigan alone to Lake Michigan and Lake Huron. As described in the previous sections, the ADCIRC validation with Lake Michigan alone indicated an under-prediction of water levels from low pressure events. These storms require a large volume of water to “fill the void” created by the low pressure system. By numerically opening the connection to Lake Huron and including the water bodies of Lake Huron, Georgian Bay, and North Channel, the observed response in Lake Michigan was modeled more accurately. A description of changes to the ADCIRC mesh to expand to the two lake system will be described in this section.

The second level of expansion of the ADCIRC mesh was to include 48 harbors around Lake Michigan so that FEMA would have water levels time series in the harbors for computing wave run-up. A description of procedures undertaken to add the harbors to the ADCIRC mesh will also be described in this section.

4.7 Expansion of the ADCIRC mesh to Lake Michigan-Lake Huron

Oscillatory water level fluctuations within the Great Lakes induced by wind and atmospheric pressure gradients over the region have been well studied by numerous researchers (As-Salek and Schwab 2004). Their findings suggest that water level fluctuations in Lake Michigan contain oscillatory modes that are unique to that Lake itself, but also contain oscillation modes that are shared with Lake Huron via the Straits of Mackinac connection. Quantifying the added contribution to the water levels within Lake Michigan caused by the inverted barometer effect during the passage of a storm, where higher atmospheric pressure resides over Lake Huron than over Lake Michigan, would determine whether Lake Michigan can be modeled as a sole entity, or whether the model must also include Lake Huron for generating reasonable storm surge.

The original numerical modeling application described in the previous sections involved simulating storm water levels for a 197000-node ADCIRC model domain covering Lake Michigan, Green Bay, and the lower reaches of several major rivers, such as the Chicago River with a closed boundary at the Straits of Mackinac. However, Lake Michigan and Lake Huron are hydraulically connected through the Mackinac Straits. When a low pressure storm event of finite dimensions passes over Lake Michigan and a high pressure system is occurring over Lake Huron, the pressure differential, often referred to as the inverted barometer effect, is sufficient to drive substantial flow through the Straits from Lake Huron into Lake Michigan. Water level does not adjust immediately to a change of pressure, but responds to the average change over a considerable area, thus requiring a large volume (Lake Huron) to make up for the deficit in water volume in Lake Michigan where the low pressure event exists.

A series of tests with model domain expansions to include Lake Huron proper, Georgian Bay, and North Channel were conducted to determine the significance of various water bodies to water levels in Lake Michigan. The grid expansion procedure to include these regions was similar to the development for Lake Michigan. Electronic navigation charts from NOAA were used to extract coastline information as well as soundings. A feature map of the expansion region was developed and the SMS tools described in Chapter 4 were used to generate a mesh for Lake Huron and the surrounding bays. Hand refinement to improve the mesh quality and elemental connectivity was accomplished and finally the combining or stitching of the two lakes into one larger mesh completed the mesh

development. The mesh expansion increased the model computational nodes and elements by approximately 68 percent.

Comparison of model-generated water levels showed that the Lake Michigan grid combined with Green Bay, Lake Huron proper, Georgian Bay, and North Channel had the best agreement with water levels measured at the 10 National Ocean Service-maintained stations throughout Lake Michigan (Figure 4-39). Without the inclusion of the Lake Huron water body/volume in the Lake Michigan domain resulted in an under-prediction of water level by as much as 0.5 m as will be demonstrated with the following re-validation storm events.

December 1990 storm

The first example of the model re-validation is to demonstrate the improvement in simulated water levels when the domain is expanded from Lake Michigan-Only to Lake Michigan and Lake Huron. In this example, the harbors are not included in the mesh or the simulation to simply demonstrate the overall improvement in water level prediction with the inclusion of the Lake Huron. (In actuality, the harbors have little effect on simulated water levels as will be demonstrated in the final validation process.)

The December 1990 storm-of-record for Green Bay, shown previously for Lake Michigan-Only, under-predicted water levels by as much as 0.4 m. Figure 4-40 through 4-43 show the same comparisons of Lake Michigan-Only and Lake Michigan-Lake Huron modeled water to measure water levels at Green Bay, Holland, Calumet Harbor, Milwaukee that were shown previously for Lake Michigan-Only. The inclusion of the Lake Huron, Georgian Bay, and North Channel water bodies in the simulations provides sufficient flow volume to increase water levels by as much as 0.4-0.5 m. The December 1990 (Storm 099) results were for the storm of record for Green Bay and model results for the two-lake system compare well for all locations. The water level time series show a marked improvement on the models ability to simulate storm surge for Lake Michigan with the inclusion of Lake Huron in the model domain.

Most of the storm-induced water level change reflected in measurements made at NOAA NOS stations can be explained by considering surface wind stress, atmospheric pressure gradient forcing and seiching. Where the wind fetch is long and water depths are shallow, wind stress is the dominant contributor. However, where the fetch is short and/or water is deep, the

inverted barometer effect can be equal to or greater than the contribution from wind stress. Modeling the entire lake complex as a single system, including connectivity between Lake Michigan and Lake Huron, enables more accurate treatment of the complex hydrodynamic interactions that occur between the two main water bodies in response to meteorological forcing, including the inverted barometer effect, thereby eliminating the need to specify approximate boundary conditions at open-water boundaries that might otherwise be needed to model the two water bodies separately.

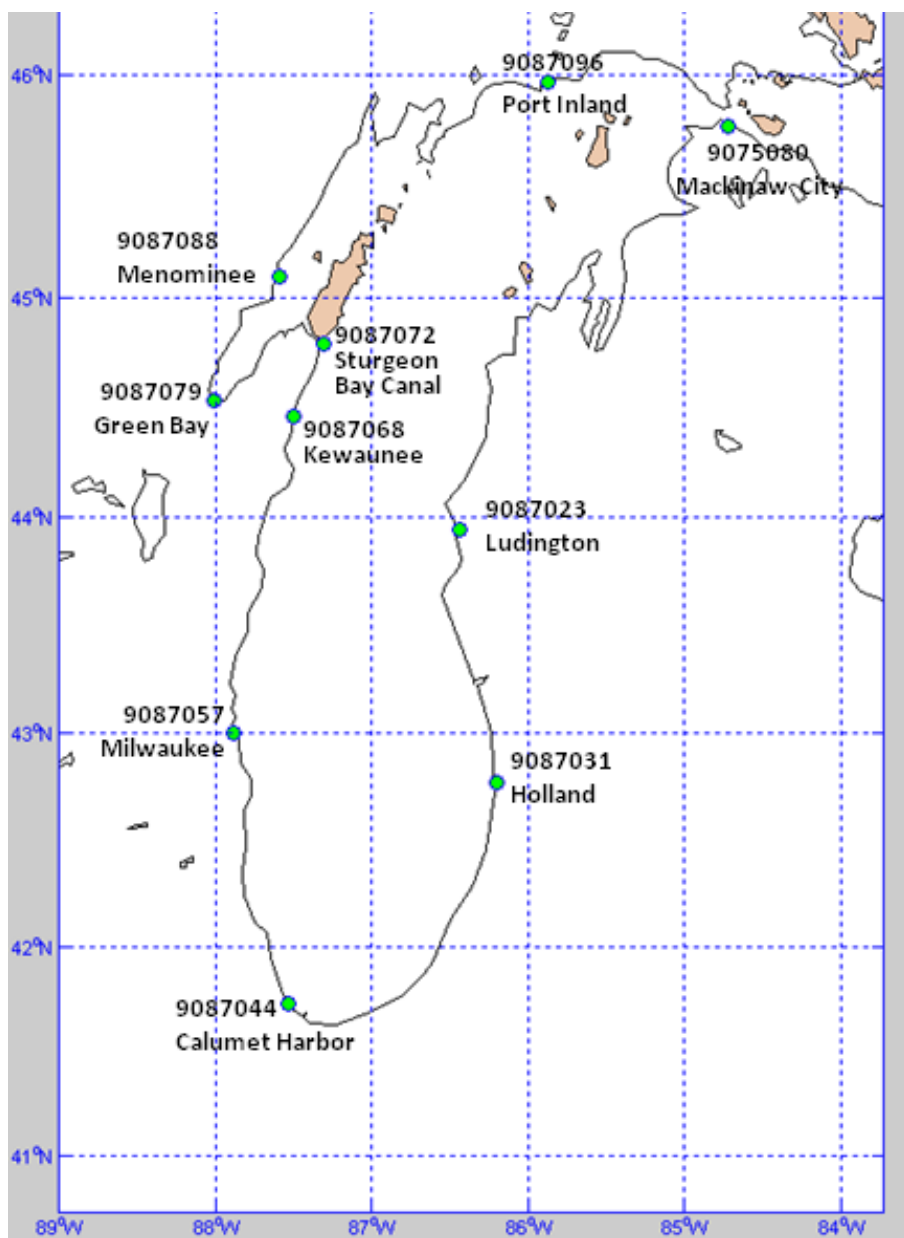


Figure 4-39. NOAA water level stations.

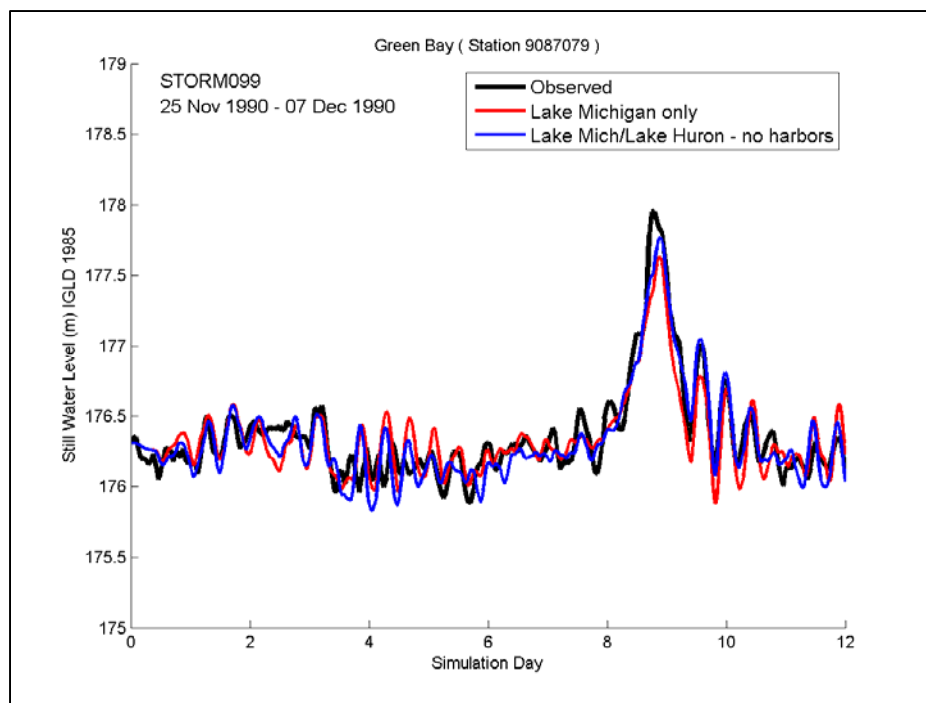


Figure 4-40. Dec 1990 Green Bay modeled and observed water level time series.

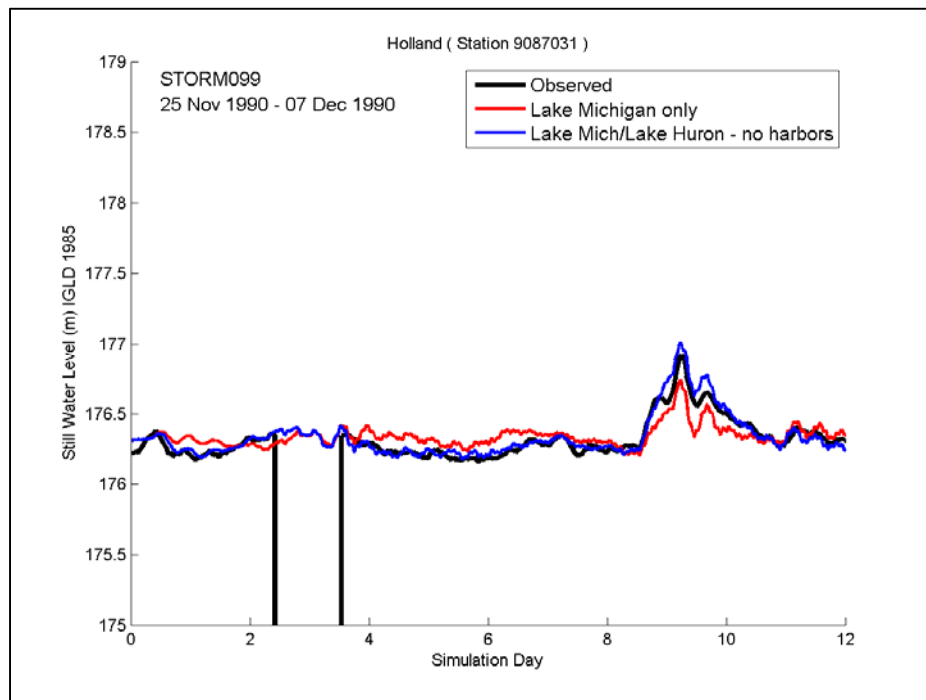


Figure 4-41. Dec 1990 Holland modeled and observed water level time series.

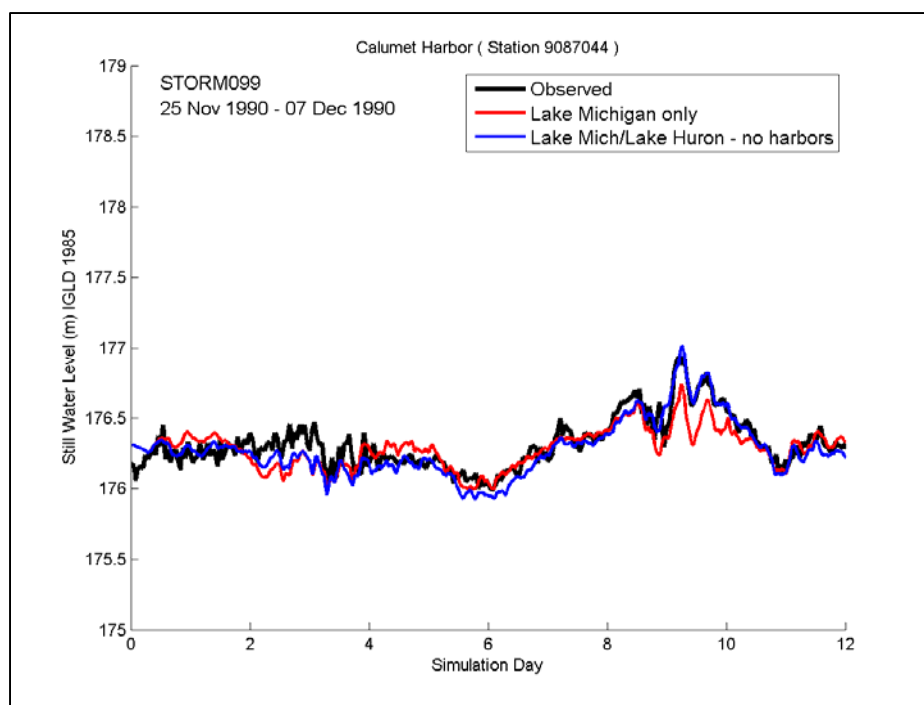


Figure 4-42. Dec 1990 Calumet Harbor modeled and observed water level time series.

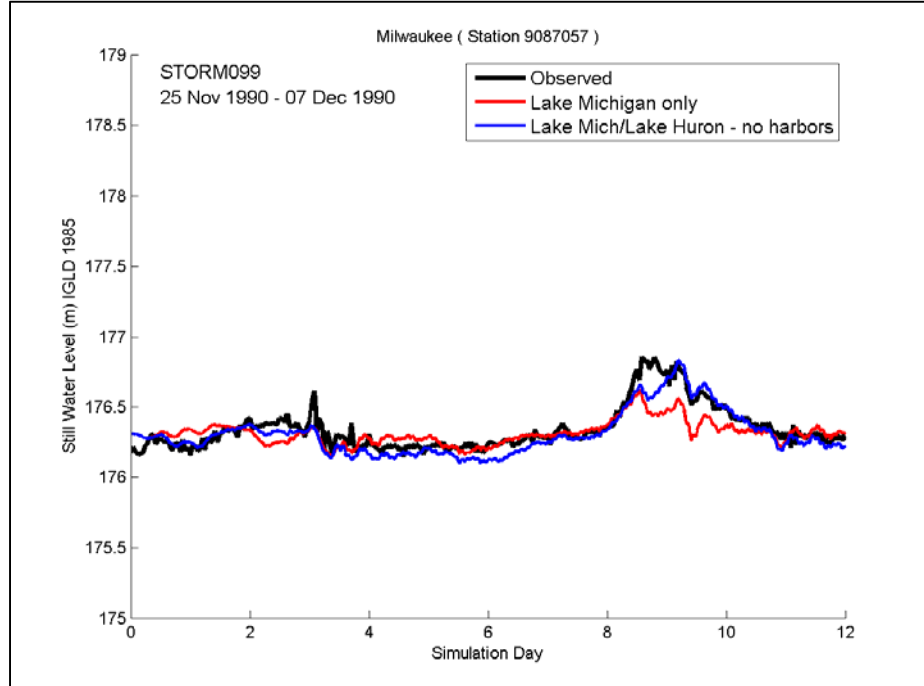


Figure 4-43. Dec 1990 Milwaukee modeled and observed water level time series.

All remaining validation storms shown previously for Lake Michigan-Only were repeated for the expanded Lake Michigan-Lake Huron domain and show similar improvements in predicted water level. These storms were

also simulated in the final validation process with the inclusion of Lake Michigan harbors and will, therefore, only be shown in the following section for the final validation.

4.8 Expansion of the ADCIRC grid to Lake Michigan harbors

Using geo-referenced satellite imagery, the task of resolving the harbors and rivers around Lake Michigan and Green Bay in the Lake Michigan domain by constructing meshes for the selected harbors and entrances was undertaken. The process began with the rectified satellite imagery used to define the land/water boundaries of the rivers/harbors, then redistributing computational points along those boundaries, generating a rough estimate of the harbor mesh, refining the mesh, performing a series of mesh quality assessments, then interpolating LIDAR and other bathymetric data sources to the computation mesh nodes. Meshes were generated for 48 harbor sites which were then incorporated or “stitched” into the Lake Michigan-Lake Huron grid. Figure 4-44 shows an outline of the Lake Michigan-Lake Huron ADCIRC grid with the harbors added. As an example of the detailed resolution of each harbor, Figure 4-45 shows the Betsie Lake mesh incorporated into the ADCIRC mesh. The figure shows the original model (non-existent) representation of this region in the ADCIRC mesh, Lake Betsie with idealized bathymetry for initial testing, and Lake Betsie with actual bathymetry from LIDAR and Electronic Navigation Charts and that was incorporated into the ADCIRC model.

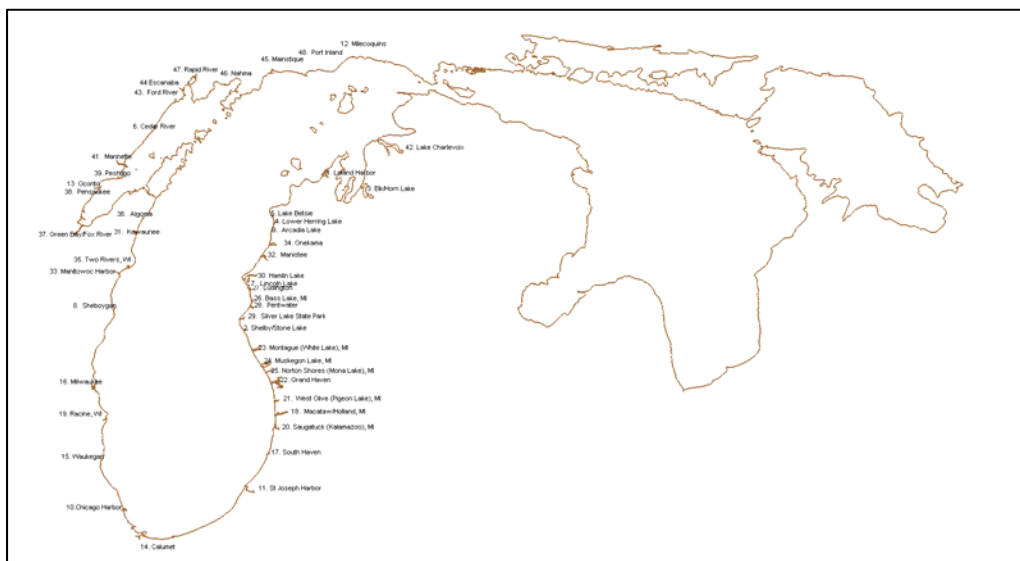


Figure 4-44. ADCIRC mesh boundary with 48 harbors.

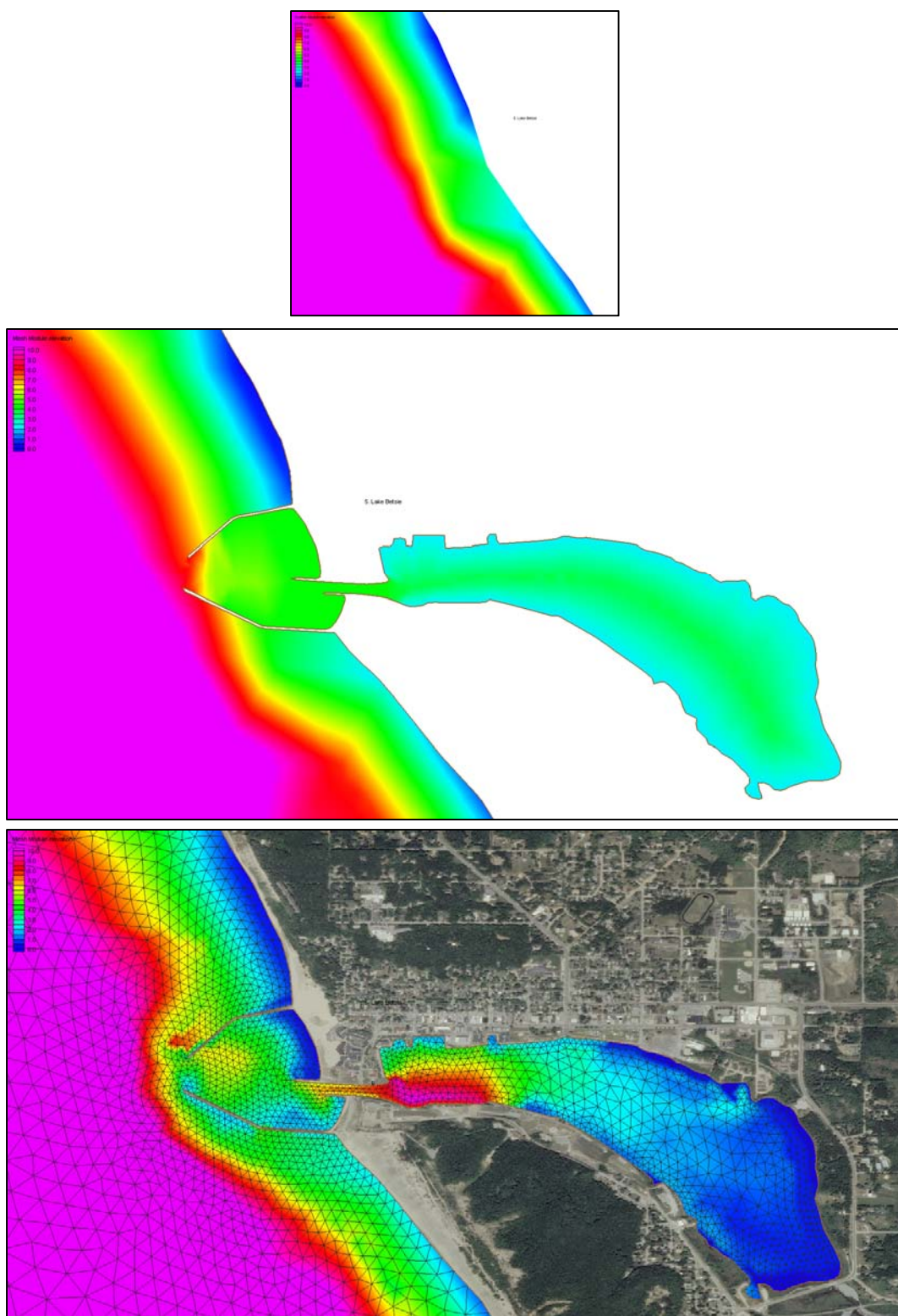


Figure 4-45. Original ADCIRC mesh in the vicinity of Lake Betsie (top panel), Lake Betsie shoreline and idealized bathymetry added to ADICRC mesh (middle panel); and Lake Betsie bathymetry and refined mesh (bottom panel).

The original ADCIRC mesh of Lake Michigan only that was described in Chapter 4 had approximately 385000 elements and 197000 nodes. With the expansion to Lake Michigan-Lake Huron the mesh contained approximately 646000 elements and 333000 nodes. The final mesh of Lake Michigan and Lake Huron with the addition of the 48 harbors contained approximately 778000 elements and 409000 nodes. Simulation run times on the High Performance Computing Center (HPCC) Cray XTE for the final expanded grid with harbors were on the order of 10 hrs per storm using 544 processors.

With the inclusion of the 48 harbors into the Lake Michigan-Lake Huron mesh, the ADCIRC validation process was repeated to determine if these small additions might have a significant impact on water levels in Lake Michigan at the 10 NOS gage locations. A comparison of the Lake Michigan-Lake Huron ADCIRC mesh (with 48 harbors) to the Lake Michigan-Lake Huron ADCIRC mesh without harbors for the 5 validation storms shows the inclusion of harbors into the model domain causes little change to the water level response at the 10 NOAA NOS sites. For example, Figures 4-46 through 4-49 show simulated and observed water level time series for the December 1990 storm. The simulated water levels are for all three ADCIRC mesh extents: Lake Michigan Only, Lake Michigan and Lake Huron, and the final mesh (Lake Michigan, Lake Huron, and the 48 harbors). The water levels with and without the harbors are nearly identical to each other and compare well with the measured water level data. The following section will show the final validation comparing observation and simulated water levels with the “Lake Michigan-Lake Huron with Harbors” mesh for some of the same storms shown in the Lake Michigan-Only validation.

4.9 Final validation: Lake Michigan-Lake Huron Mesh with harbors

The final “Lake Michigan-Lake Huron with Harbors” model validation effort consisted of simulating the storm events shown previously for Lake Michigan-Only and comparing simulated water levels for up to 10 NOAA NOS water level time series for those time periods. The December 1990 (Storm 099) results were already discussed for the two-lake and two-lake with harbors domains and will not be discussed in this section. Results for the December 2009, May 1998, November 1992, and March 1995 storms will be presented and discussed.

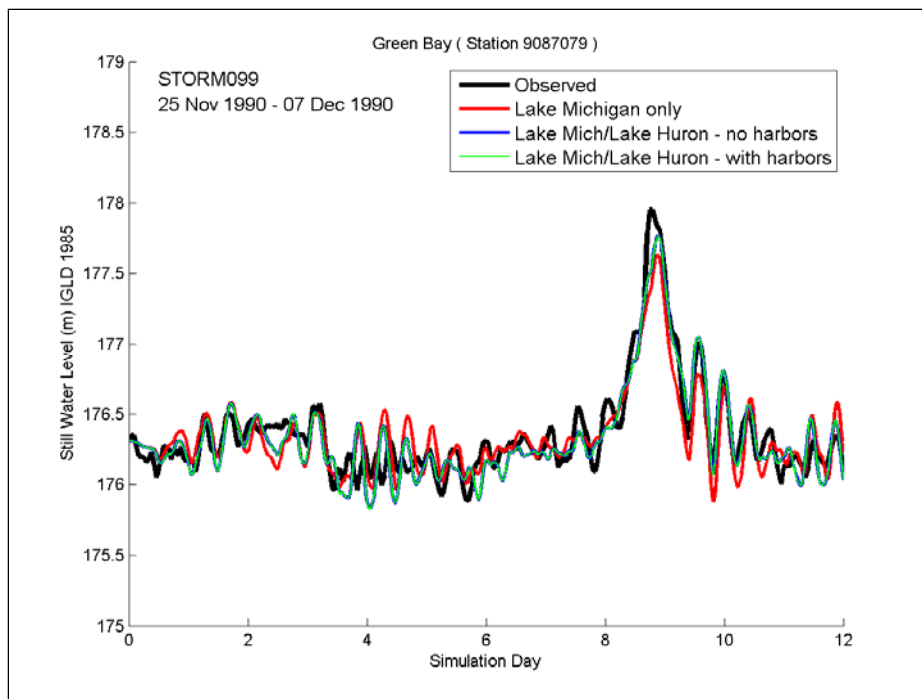


Figure 4-46. Dec 1990 Green Bay final modeled and observed water level time series.

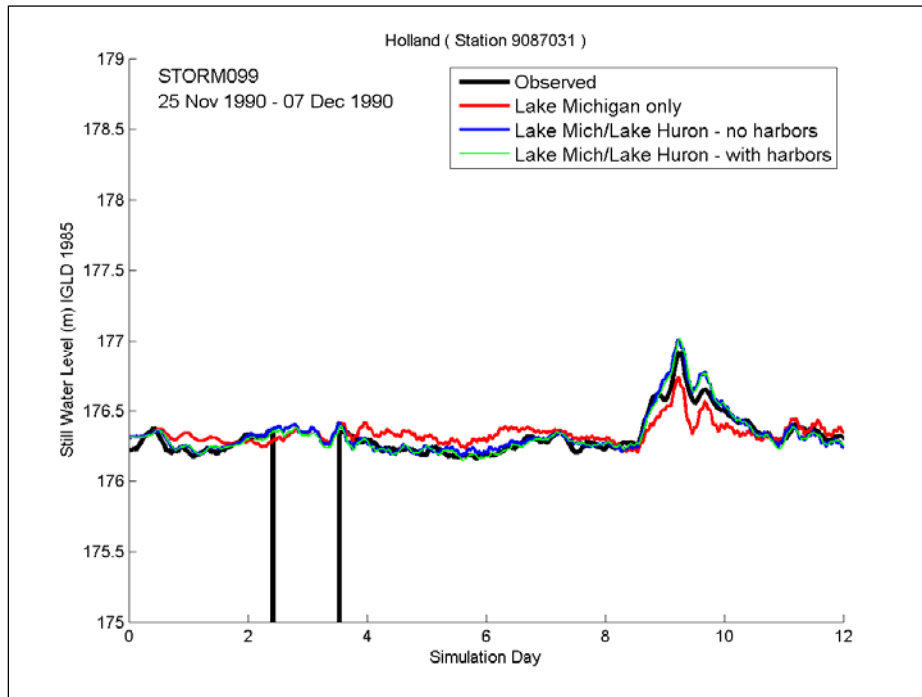


Figure 4-47. Dec 1990 Holland final modeled and observed water level time series.

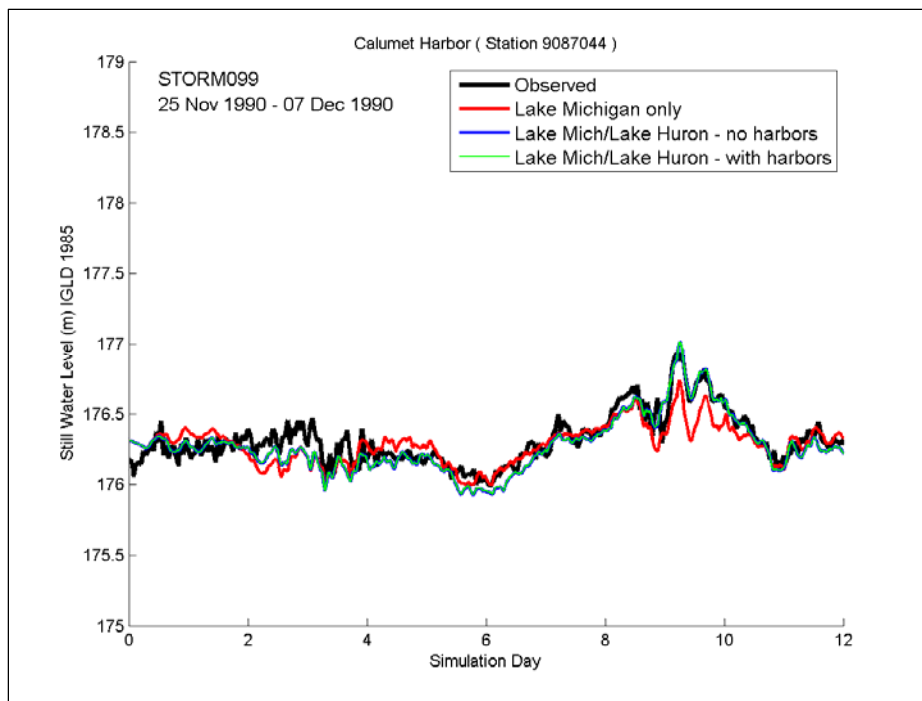


Figure 4-48. Dec 1990 Calumet Harbor final modeled and observed water level time series.

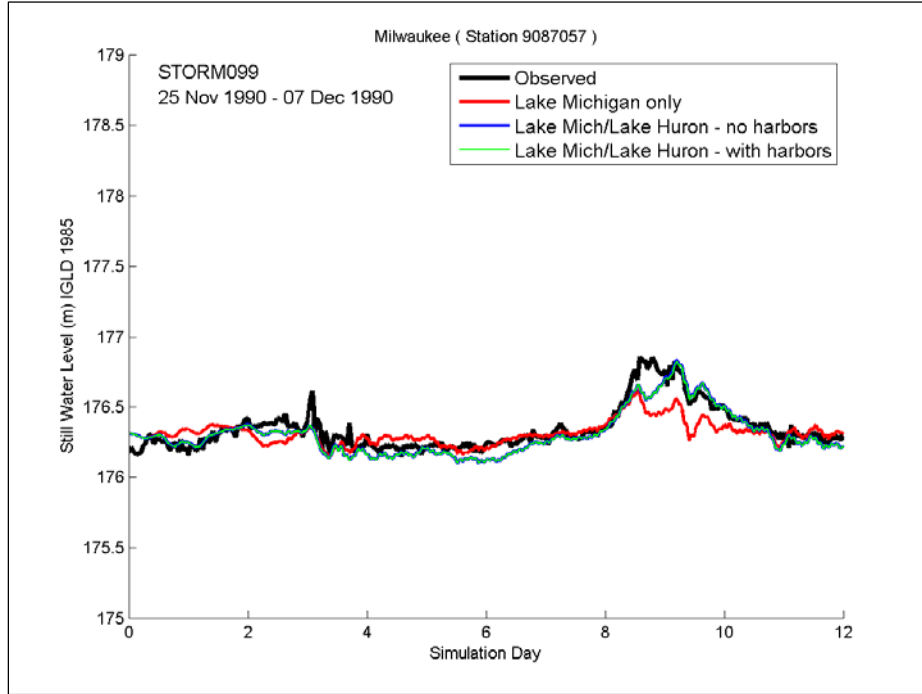


Figure 4-49. Dec 1990 Milwaukee final modeled and observed water level time series.

4.9.1 December 2009 storm

The 9-10 December 2009 event was a significant surge event at Green Bay, as well as Menominee and Holland. Water level comparisons at Green Bay show that trends are well simulated by the model, most notably improving the under-prediction of peak surge that was observed for the Lake Michigan-Only simulation (Figure 4-50). Calculated water levels throughout the event compare well with observed values, differing by no more than by 0.1 m. Features of the primary surge event are well represented by the model, both in shape and duration. The magnitude of difference between observed and computed peaks is similar to that for the 1990 event. As previously mentioned, seiche-induced oscillations that occur prior to this event are qualitatively but not quantitatively simulated. Seiche in this highly complex lake and bay system can be introduced by moving high and low pressure centers and fast-moving weather fronts and squall lines which are not resolved well, spatially or temporally, by the methods adopted for defining input winds and pressures described in Chapter one. Calumet Harbor trends and patterns as well as the low-amplitude seiche are well represented by the model throughout the event (Figure 4-51). Calculated peak surge slightly over-predicts the observed peak, differing by less than 0.1 m. Differences between calculated and observed water levels at Menominee are similar to those for Green Bay (Figure 4-52). At this location, calculated trends and patterns and some of the low-amplitude seiche are well represented by the modeling. Calculated peak surge for the event is reasonably well simulated by the model, but is slightly greater than the observed peak. Results for Holland show a marked improvement in trend and magnitude compared to the Lake Michigan-Only simulation of this storm event (Figure 4-53).

4.9.2 May 1998 storm

As previously mentioned, the May 1998 event was selected to examine the capability of simulating a fast-moving, short duration frontal passage event. Comparisons of measured and calculated water level for this event for Calumet Harbor (Figure 4-54) and Green Bay (Figure 4-55) show that including Lake Huron and the harbors into the model domain does not improve the model's skill in capturing this rapid event at Calumet. The rapid speed with which this weather system moves through the region is reflected in the rapid fluctuations evident in the water level record at Calumet. Simulation results indicate that the model is unable to accurately represent, even qualitatively, water level changes associated with this event.

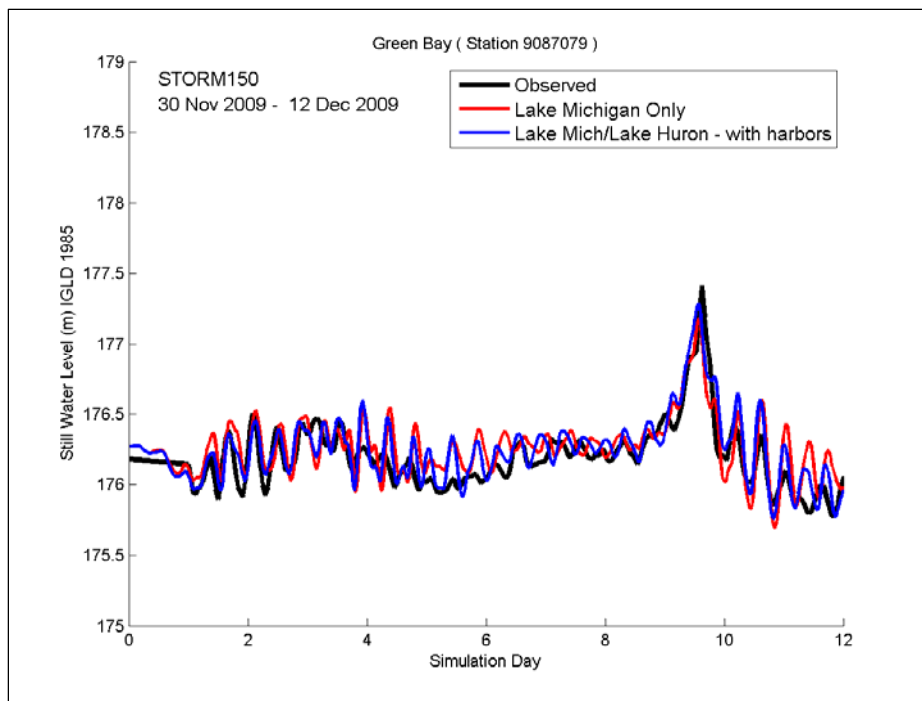


Figure 4-50. Dec 2009 Green Bay final modeled and observed water level time series.

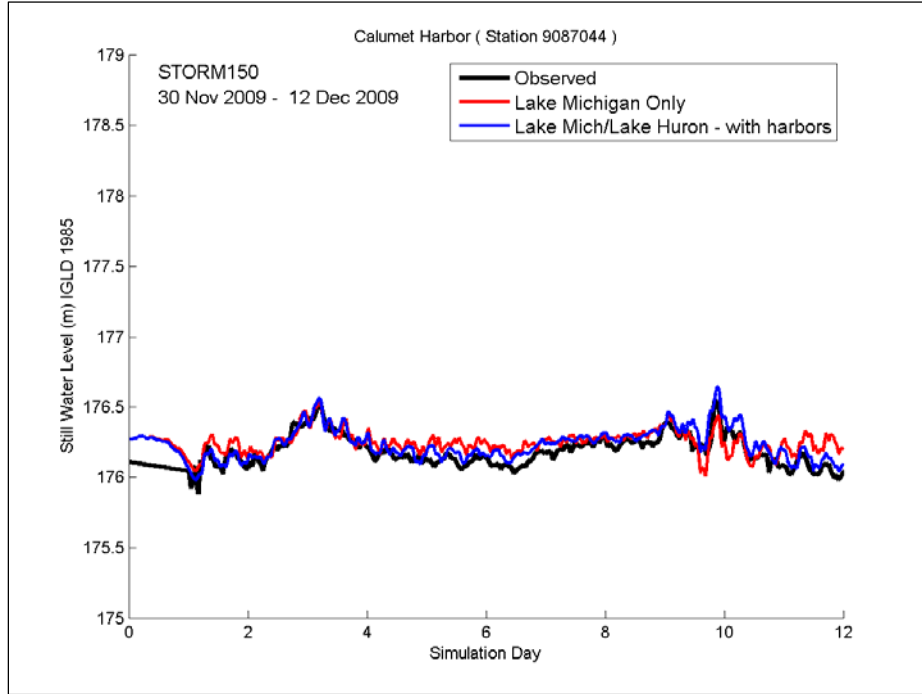


Figure 4-51. Dec 2009 Calumet final modeled and observed water level time series.

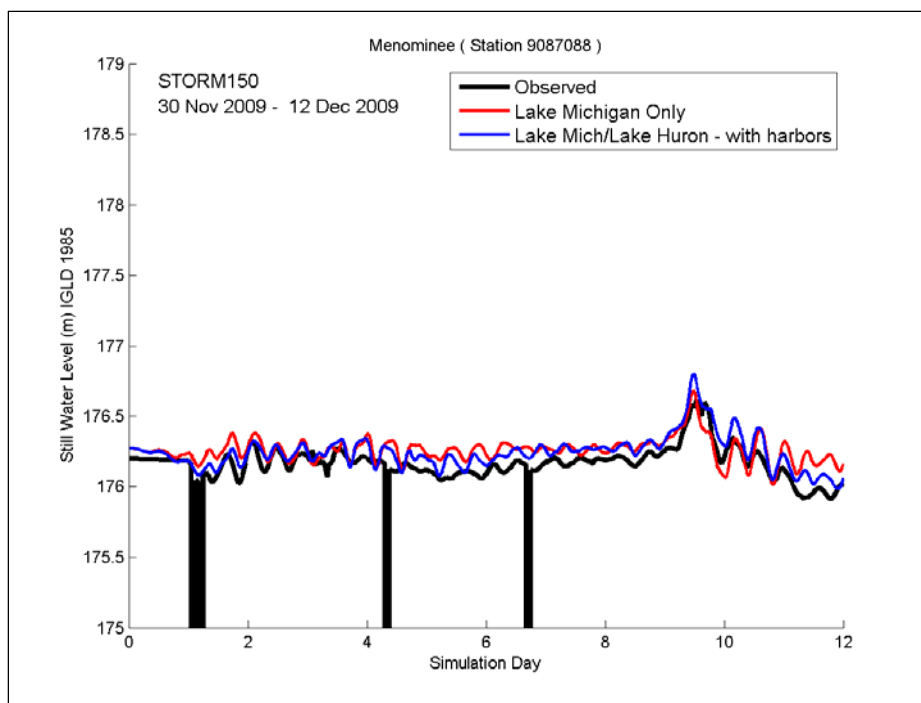


Figure 4-52. Dec 2009 Menominee final modeled and observed water level time series.

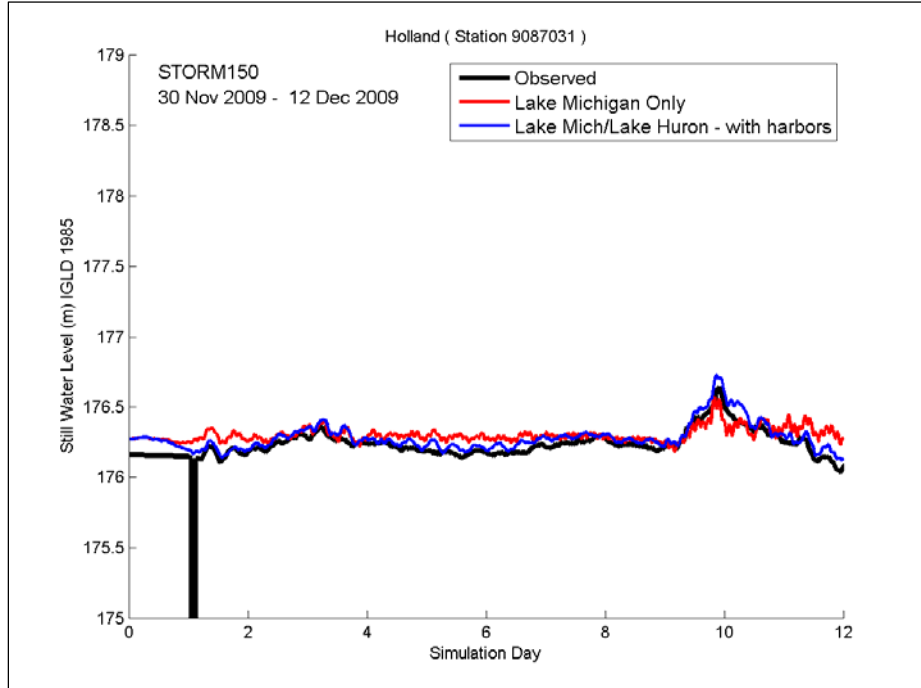


Figure 4-53. Dec 2009 Holland final modeled and observed water level time series.

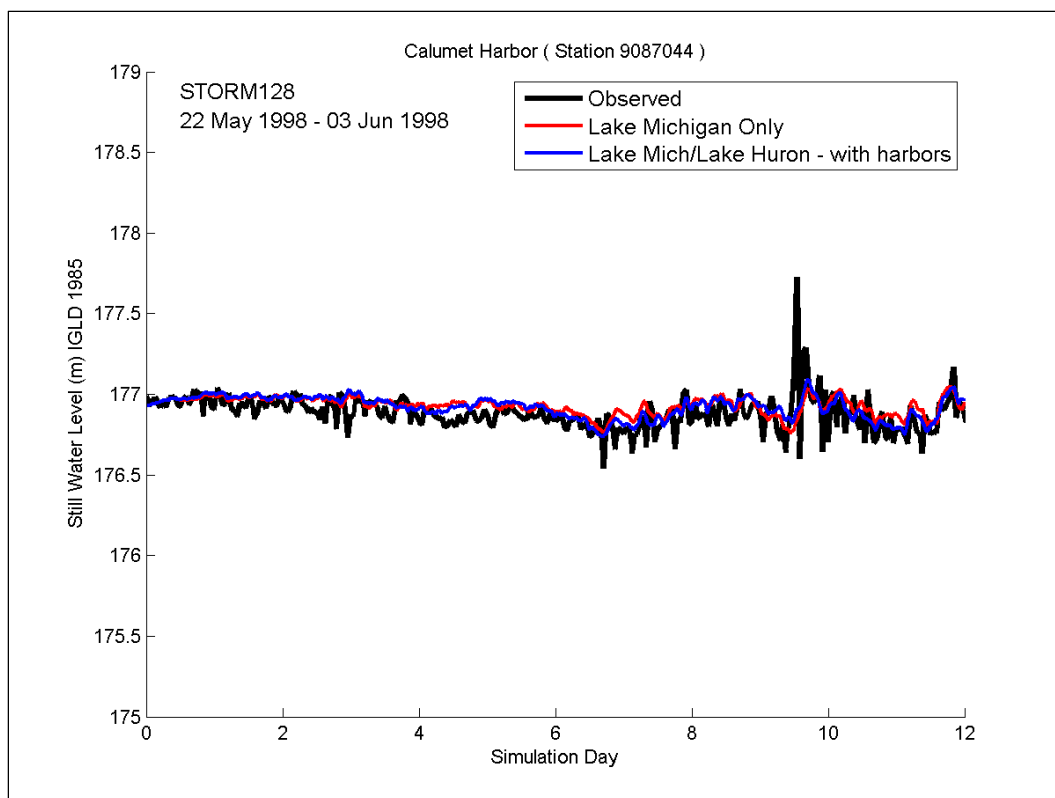


Figure 4-54. May 1998 Calumet final modeled and observed water level time series.

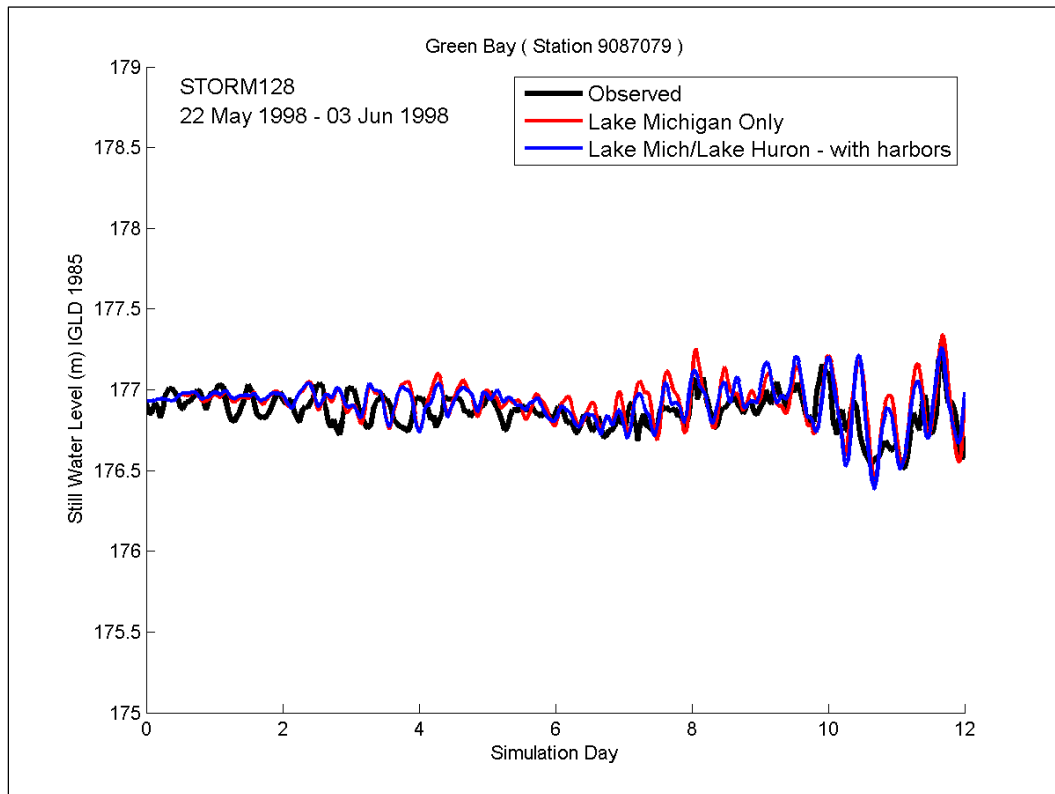


Figure 4-55. May 1998 Green Bay final modeled and observed water level time series.

This is due to the inability of the wind and pressure fields to accurately represent the event meteorology. Only with much higher spatial and temporal resolution of the atmospheric input would this event be able to be simulated better. Green Bay does not exhibit the high frequency oscillations observed at Calumet and the model performs fairly well at this location.

4.9.3 October 1993 storm

The early October 1993 event selected for the Lake Michigan validation was not repeated in the final validation, but a later October 1993 event was selected and is presented herein. This early October event was selected as an extreme event from a wave perspective not a water level perspective. Storm surge produced by this event was not among the top 20 observed maxima for any of the water level measurement sites. The early October event illustrates the fact that events which produce the highest wave conditions do not necessarily produce the highest water level conditions.

Comparisons between observed and calculated water levels for the late October event are shown for Calumet Harbor (Figure 4-56) and Green Bay (Figure 4-57). Qualitatively and quantitatively, the hydrograph shape is simulated well at Calumet Harbor, including the days leading up to and following the event. At Green Bay, the late October 1993 event produced more significant surge values than the early October event. The modeled peak water level under-predicts the measurements at this location, but the general trend and duration of observed elevated water levels are captured by the model.

4.9.4 November 1992 storm

As previously mentioned, the November 1992 event was a severe water level event at several locations around Lake Michigan. Comparisons of observed and calculated water levels for Kewaunee (Figure 4-58), Ludington (Figure 4-59) and Sturgeon Bay (Figure 4-60) show a marked improvement in model skill with the inclusion of Lake Huron and the harbors in the model domain. Each set of observations shows a single surge event that spans approximately two days, reaching a peak surge level of 0.4 m above the mean water level, with no significant water level fluctuations in the days prior to or after the event. There is no significant seiche at any of these three mid-lake gage sites. The surge hydrograph shape is similar at Kewaunee/Sturgeon Bay (west side of Lake Michigan) and at Ludington (east side of Lake Michigan). This event was not a major surge-producing event at

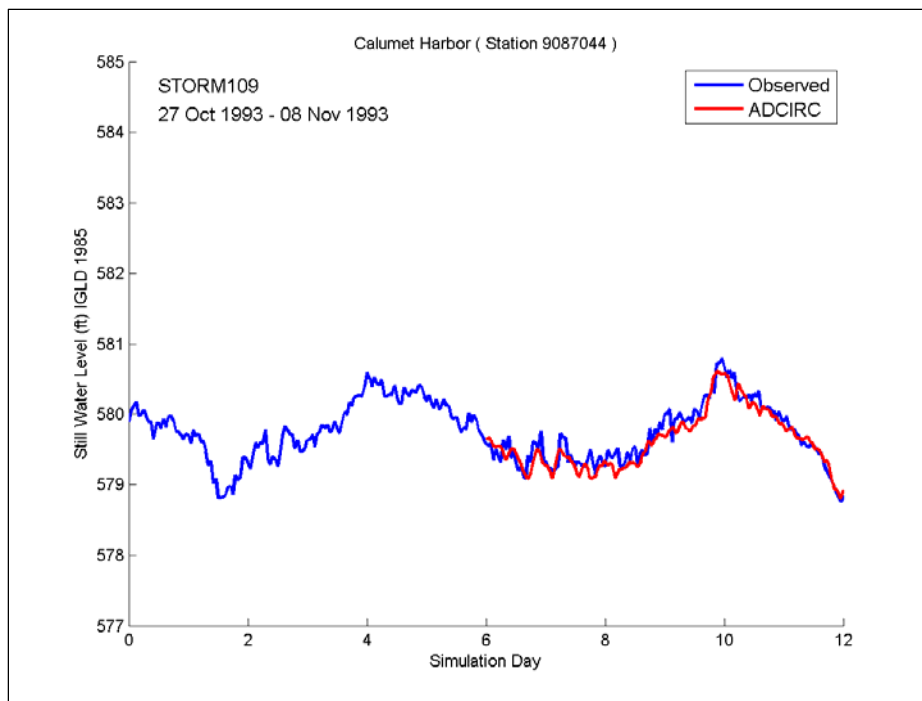


Figure 4-56. October 1993 Calumet final modeled and observed water level time series.

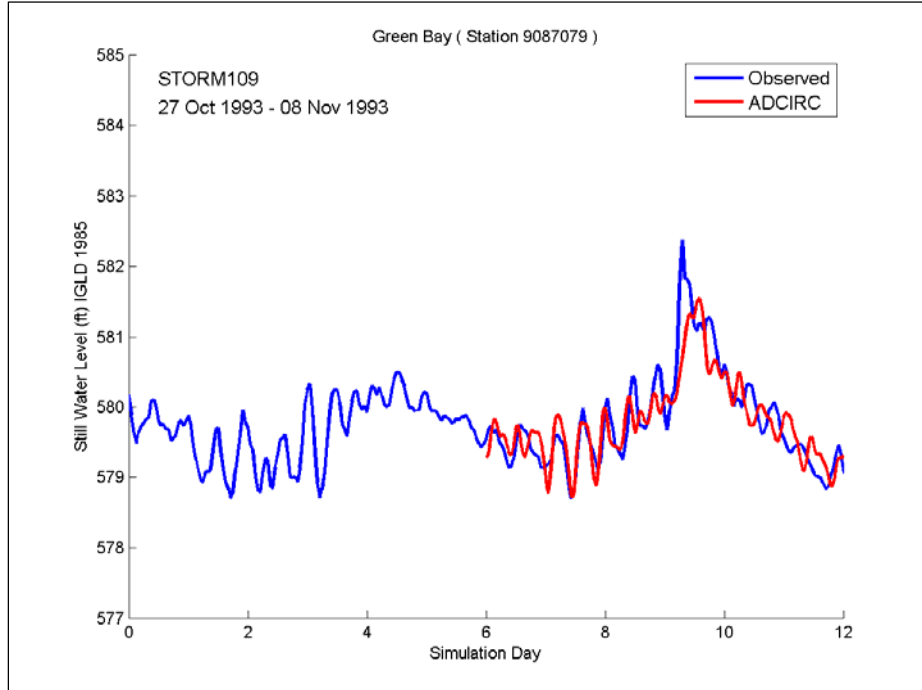


Figure 4-57. October 1993 Green Bay final modeled and observed water level time series.

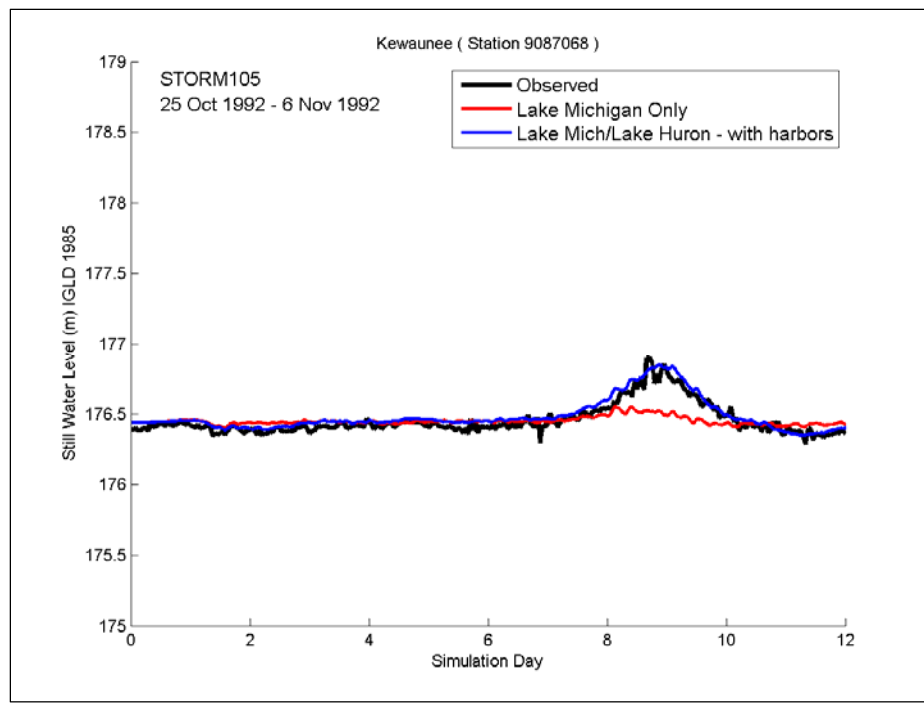


Figure 4-58. November 1992 Kewaunee final modeled and observed water level time series.

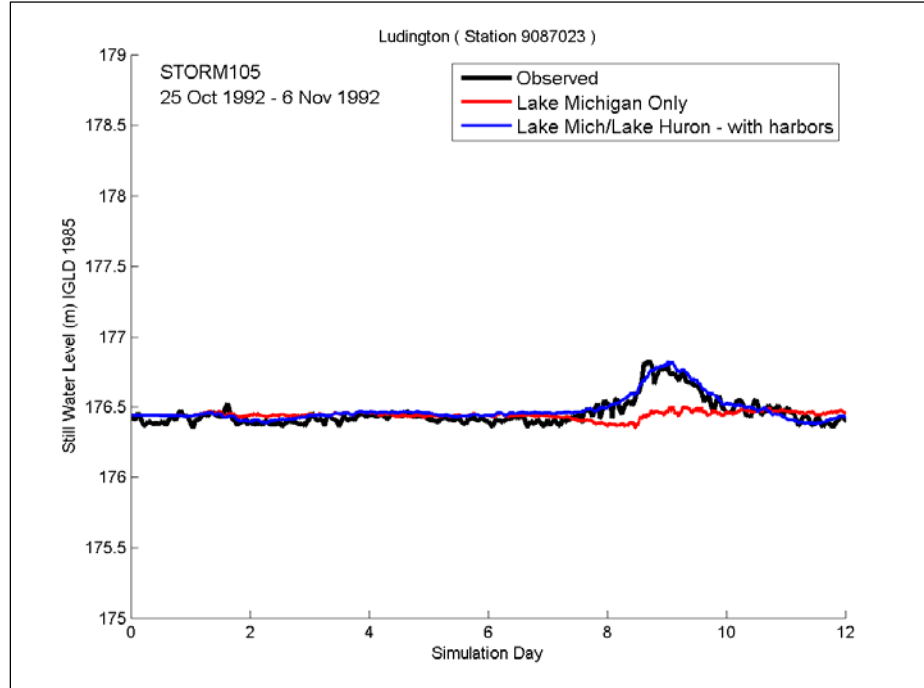


Figure 4-59. November 1992 Ludington final modeled and observed water level time series.

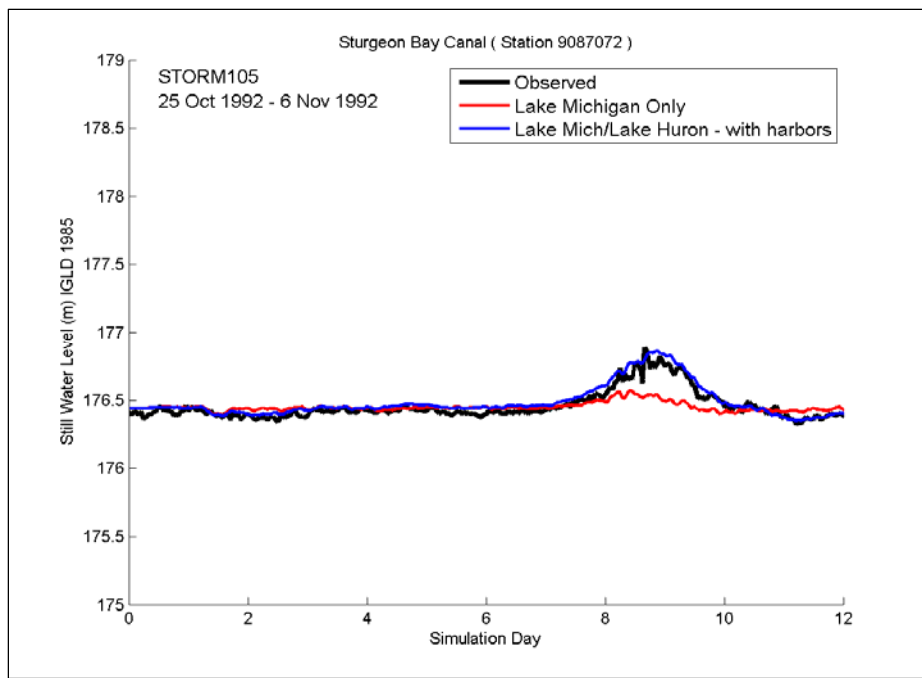


Figure 4-60. November 1992 Sturgeon Bay Canal final modeled and observed water level time series.

Calumet (Figure 4-61). Water level comparison for Calumet still capture the trend at very well and show marked improvement from the Lake Michigan-Only simulations. This event best depicts the impact of the inverted barometer effect on peak water levels, particularly at the mid-lake gages.

4.9.5 March 1985 storm

The 4-5 March 1985 event was characterized by persistent strong winds from the east followed by a rapid directional shift and persistent strong winds from the southwest and west. Comparisons of observed and calculated water levels for Ludington (Figure 4-62) and Kewaunee (Figure 4-63) are similar despite being on opposite sides of the lake. Such responses in the water level are indicative of the low pressure system dominating the surge response rather than the wind forcing. Like the November 1992 storm event, each set of observations shows a single surge event that spans approximately two days, reaching a peak surge level of 0.3 to 0.4 m, with no significant water level fluctuations in the days prior to or after the event. Figures 4-64 and 4-65 show the water level comparison for Port Inland at the northern end of Lake Michigan and Calumet on the southern end of Lake Michigan, respectively. As with the mid-lake comparison locations, the calculated water levels are biased low compared to measured water levels for Lake Michigan-Only and compare well with the inclusion of Lake Huron and the harbors in the model domain.

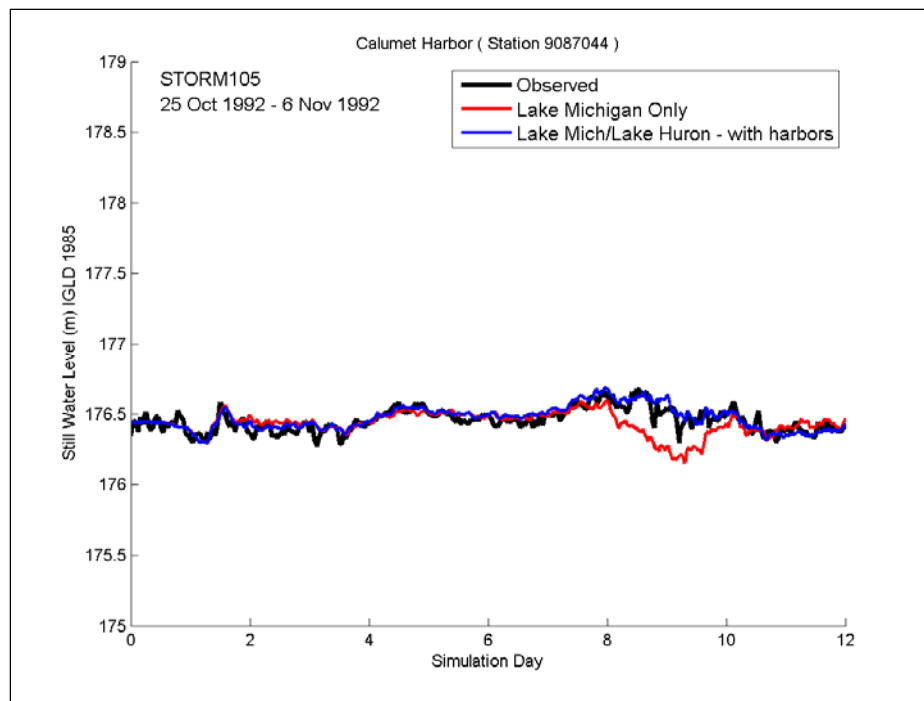


Figure 4-61. November 1992 Calumet Harbor final modeled and observed water level time series.

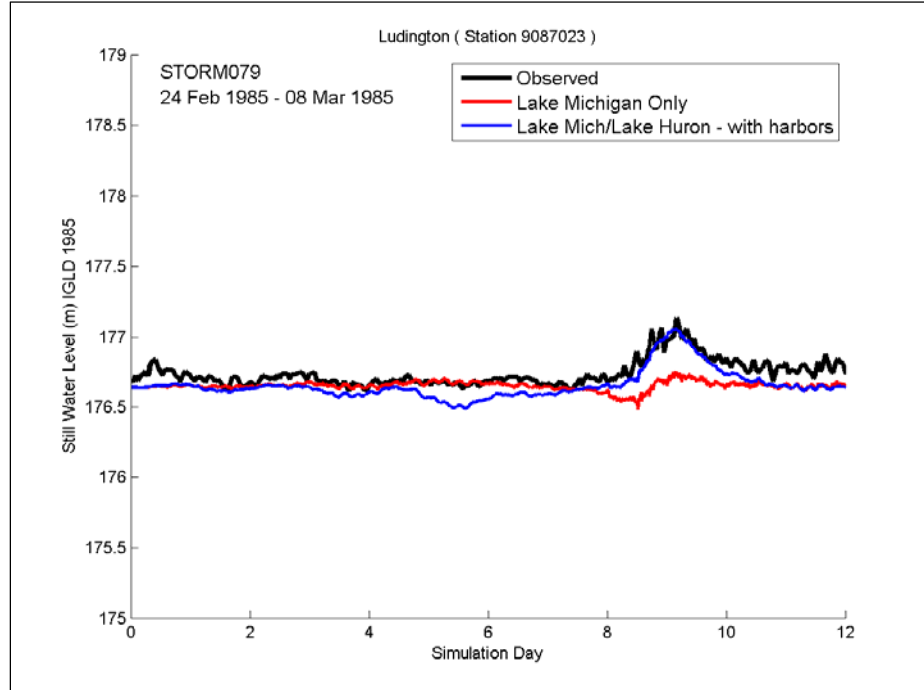


Figure 4-62. March 1985 Ludington final modeled and observed water level time series.

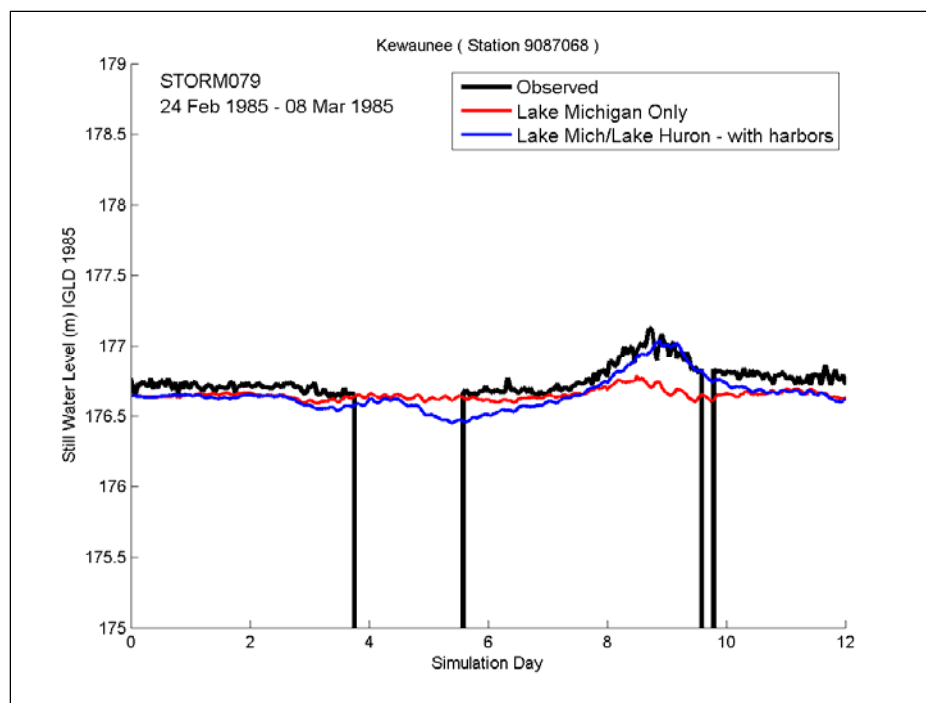


Figure 4-63. March 1985 Kewaunee final modeled and observed water level time series.

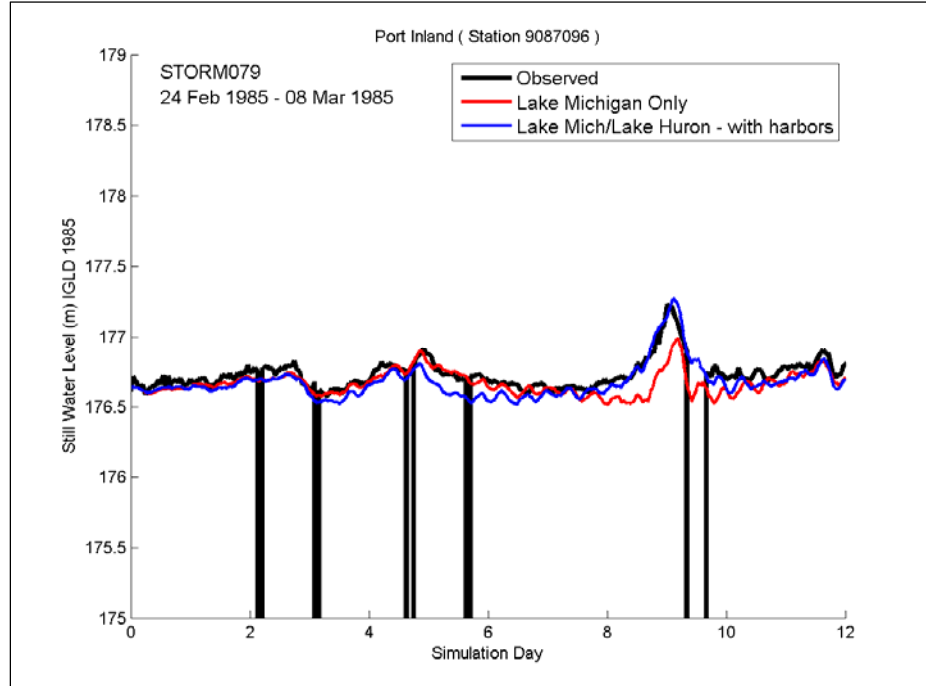


Figure 4-64. March 1985 Port Inland final modeled and observed water level time series.

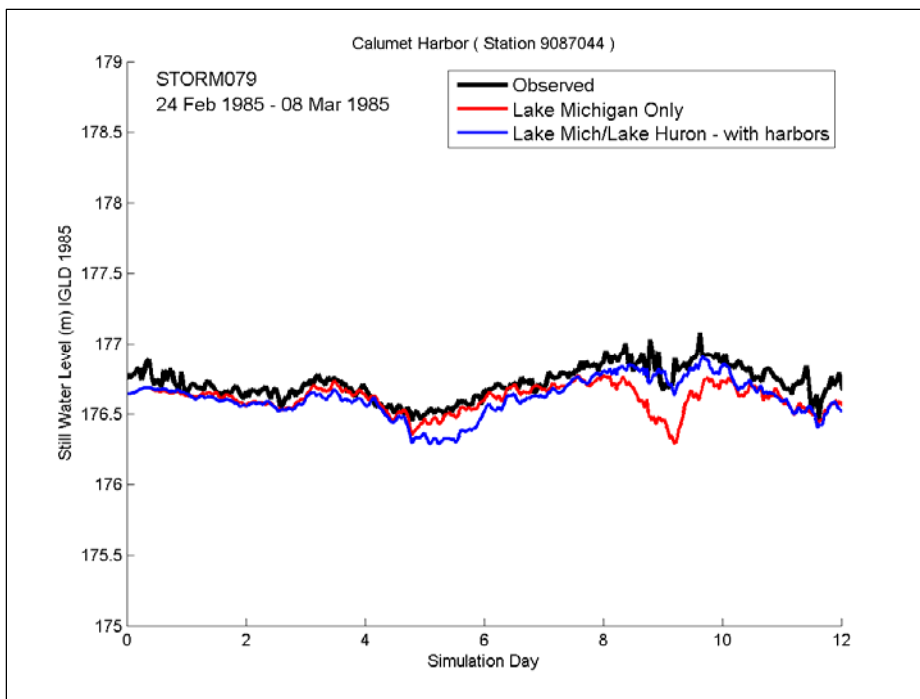


Figure 4-65. March 1985 Calumet Harbor final modeled and observed water level time series.

4.9.6 Statistical analysis

As demonstrated in this chapter, the water level time series show a marked improvement on the models ability to simulate storm surge for Lake Michigan with the inclusion of Lake Huron and the harbors in the model domain and the next step was to provide a numerical rating to quantify the models ability to reproduce measured water levels in Lake Michigan. The statistical analysis was performed on the 2-lake system with harbors and will be presented in the next section.

4.10 Summary of findings from Lake Michigan storm surge modeling

The construction of the wind, atmospheric pressure and ice fields is critical to reasonable prediction of storm surge. The frequency of the available data needed to develop these fields limits the ability to capture events that quickly traverse the lake. High frequency oscillations associated with these rapid events cannot be captured with the spatial and temporal resolution applied in the model simulations. In addition, the magnitude of the peak wind speeds and proper directional orientation near the coast should be carefully considered.

A methodology for including the presence of free-floating ice has been presented and applied to Lake Michigan. It has been validated in prior applications of the modeling approach in Alaska and has now been demonstrated and validated for Lake Michigan as well.

Given that the selection of the starting date for each event should represent an near initial undisturbed still water depth or elevation, care must be taken in selecting a starting date and duration so that the simulation is not unduly influenced by the initial zero water level assumption of ADCIRC. In cases where the primary storm event was preceded by smaller forcing events, sufficient lead time should be simulated so that the local seiche frequency is correct with respect to timing of the peak wind setup. In these simulations, the simulated event occurred on the 10th day of the simulation with two days following the main surge or wave event.

Examination of the cause for persistent low bias in calculated water levels indicated the need to consider the pressure differential effect on water levels in Lake Michigan. Because of this significant, persistent low bias in Lake Michigan surge levels, Lake Michigan and Lake Huron were modeled as one system connected through the Straits of Mackinac, as occurs in nature. This allows for the proper treatment of the event scale water exchange that occurs between the two water bodies through the Mackinac Straits, which is driven by atmospheric pressure differences between the two lakes. As expected, this greatly improved the accuracy of simulated water levels throughout Lake Michigan.

Radiation stress gradient output from WAM was generated for the December 1990 storm event, the water level event of record in Green Bay. Subsequent to converting these data to equivalent surface stress forcing, it was determined that contribution of the radiation stress gradient forcing to water level setup would be a factor of five to ten less than that of direct wind forcing. Therefore it was determined that two-way coupled wave and surge modeling was not necessary for this level of regional scale modeling. Coupling of wave transformation and storm surge modeling to include the wave radiation stress contributions to wave set up and runup should be considered at the detailed coastal mapping step and not in this regional modeling step. However, this is not a general observation that could be applied throughout the Great Lakes.

5 Nearshore Wave Modeling

5.1 Introduction

The purpose of applying nearshore wave transformation models is to describe quantitatively the change in wave parameters (wave height, period, direction, and spectral shape) of waves propagating from offshore to the shoreline. Offshore wave information obtained from wave gages or global- or regional-scale wave hindcasts and forecasts is transformed through the coastal region using these models.

STWAVE, a nearshore spectral wave model, was selected for the modeling effort in Lake Michigan. Three STWAVE grids (encompassing Chicago, IL, Kenosha, WI, and Green Bay, WI) were interpolated from the ADCIRC mesh with spectral boundary information provided by WAM. Sensitivity studies were performed to determine grid resolution and model parameters. In addition, ice coverage was implemented into STWAVE where water cells matching or exceeding a 70-percent ice concentration level were set to land.

One-way coupling between ADCIRC and STWAVE was facilitated with CSTORM-MS whereby a single instance of ADCIRC passed water elevations, wind fields, and ice coverage to multiple instances of STWAVE. More information about the coupling procedure is found in Chapter 6.

This chapter documents the theoretical description of STWAVE as well as grid development and simulation parameters for the Lake Michigan application.

5.2 STWAVE Version 6.0

5.2.1 Governing equations and description

STWAVE simulates nearshore wave transformation including depth-induced refraction and shoaling, current-induced refraction and shoaling, depth- and steepness-induced wave breaking, wind-wave growth, and wave-wave interaction and whitecapping.

Refraction and shoaling are implemented in STWAVE by applying the conservation of wave action along backward traced wave rays. Rays are traced in piecewise manner, from the previous grid column or row, and the

length of ray segment DR is calculated. Derivatives of depth normal to the wave orthogonal are estimated and substituted into Equation 5-1 to calculate the wave orthogonal direction at the previous column. The wave orthogonal direction for steady-state conditions is given by the following (Mei 1989; Jonsson 1990):

$$C_g \frac{D\alpha}{DR} = -\frac{Ck}{\sinh 2kd} \frac{Dd}{Dn} \quad (5-1)$$

where:

C_g = group celerity

α = wave orthogonal direction

R = coordinate in the direction of the wave ray

C = wave celerity

k = wave number

d = water depth

n = coordinate in direction of wave orthogonal.

The energy is calculated as a weighted average of energy between two adjacent grid points in the column and direction bins. The energy density is corrected by a factor that is the ratio of the 5-deg standard angle band width to the width of the back-traced band to account for the different angle increment in the back-traced ray.

The governing equation for steady-state conservation of spectral wave action along a wave ray is given by Jonsson (1990):

$$(C_g)_i \frac{\partial}{\partial x_i} \frac{CC_g \cos(\alpha) E(\omega, \alpha)}{\omega} = \sum \frac{S}{\omega} \quad (5-2)$$

where:

i = tensor notation for x- and y-coordinates

ω = wave radial frequency

E = wave energy density divided by the density of water and acceleration of gravity

S = energy source and sink terms.

Source and sink mechanisms include the flux of input energy due to wind (Resio, 1988), surf-zone breaking in the form of the Miche criterion (1951), energy distribution through wave-wave interactions (Resio and Perrie 1989), whitecapping (Resio 1987; Resio 1988), and energy losses due to bottom friction (Hasselmann et al. 1973; Padilla-Hernandez 2001; Holthuijsen 2007).

The assumptions made in STWAVE v6.0 as they apply to this study are the following:

- *Phase-averaged.* STWAVE is based on the assumption that relative phases of the spectral components are random, and phase information is not tracked.
- *Mild bottom slope and negligible wave reflection.* Waves reflected from the shoreline or from steep bottom features are neglected.
- *Steady-state waves, currents, and winds.* STWAVE is formulated as a steady-state model, which reduced computation time and is appropriate for wave conditions that vary more slowly than the time it takes for waves to transit the domain.
- *Linear refraction and shoaling.* STWAVE incorporates linear wave refraction, shoaling, and propagation, and does not represent wave asymmetry or other nonlinear wave features.

Readers are referred to STWAVE documentation (Massey et al. 2011; Smith 2007; Smith et al. 2001) for additional model features and technical details.

5.2.2 Grid geometry and bathymetry

STWAVE is formulated on a Cartesian grid and operates in a local coordinate system with the x-axis oriented in the cross-shore direction and the y-axis oriented alongshore, forming a right-handed coordinate system. The y-axis is aligned with the bottom contours so the offshore boundary is parallel with the shoreline. Angles are defined in a mathematical sense, measured counterclockwise from the x-axis.

Three STWAVE grids were interpolated from the ADCIRC mesh to UTM NAD 83 Zone 16 for this project. These grids, hereafter named for the city they include, are Chicago, Kenosha, and Green Bay. Figure 5-1 shows the location of the grids with respect to the ADCIRC mesh. The grids' offshore boundaries were extended into deepwater conditions (sufficiently offshore of wave breaking) and defined in locations of relatively straight and parallel

contours. The cell size of the grids was 200-m, which allowed fast execution times while still retaining high resolution and good representation of bottom features. Detailed bathymetry of the Chicago, Kenosha, and Green Bay grids is shown in Figures 5-2 to 5-4, respectively, with grid geometries presented in Table 5-1.

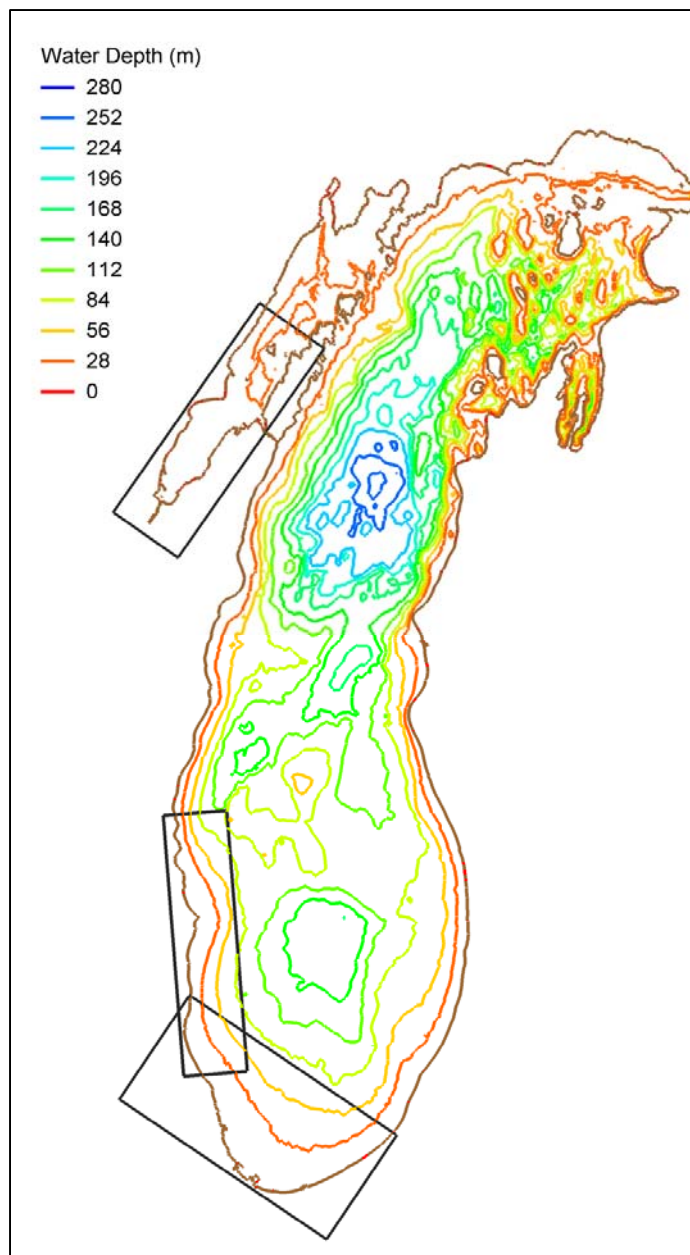


Figure 5-1. STWAVE grid locations.

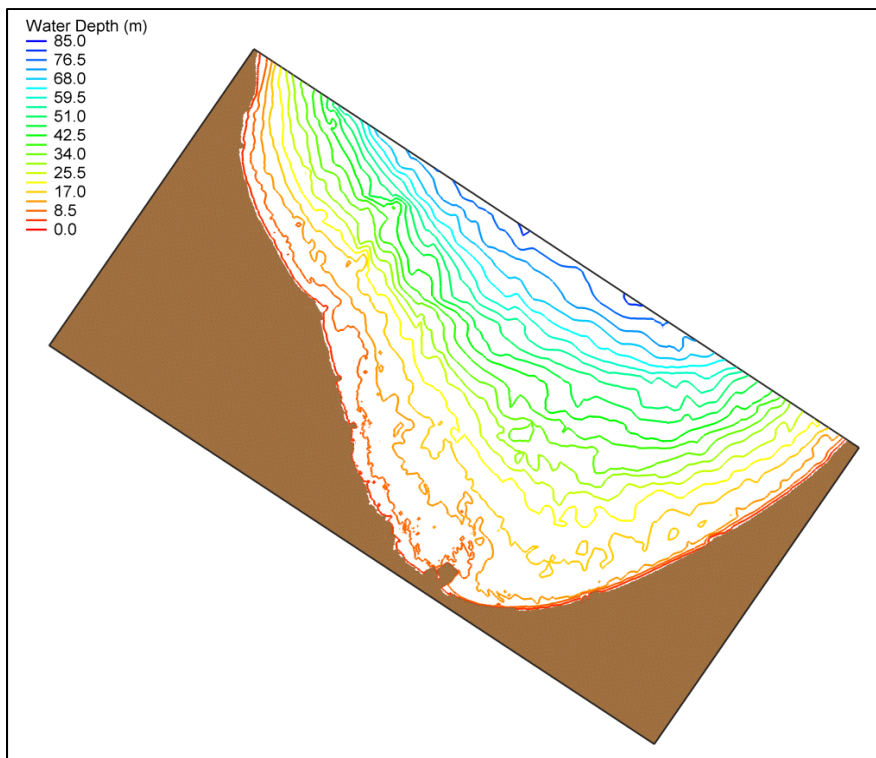


Figure 5-2. STWAVE Chicago grid bathymetry.

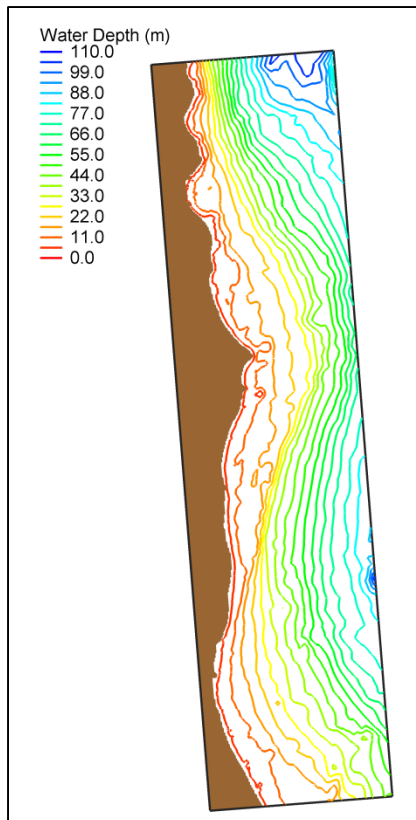


Figure 5-3. STWAVE Kenosha grid bathymetry.

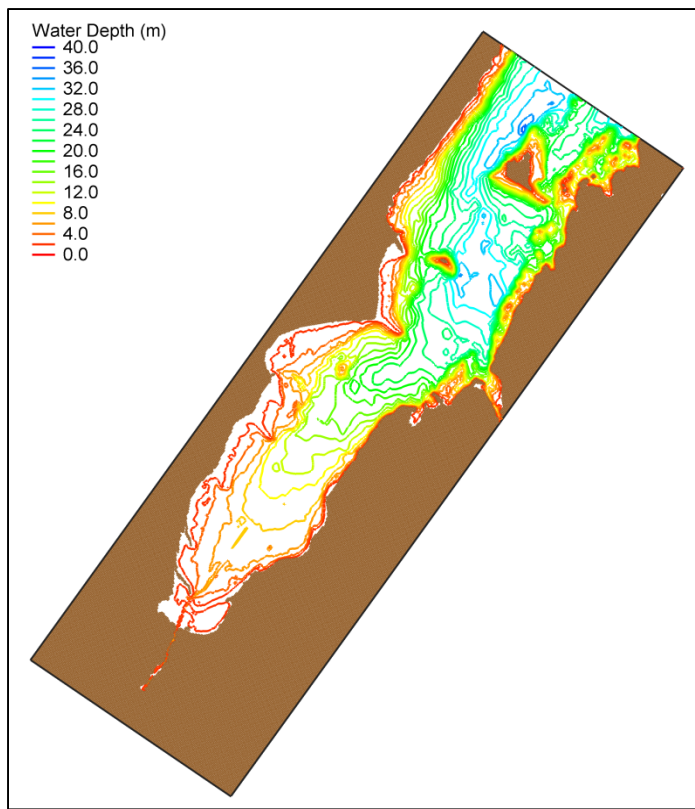


Figure 5-4. STWAVE Green Bay grid bathymetry.

Table 5-1. Grid geometry.

Grid	Grid Origin (x,y) (m)	Angle (deg)	Extent (m)		Number of cells	
			Cross-shore (I)	Alongshore (J)	Cross-shore (NI)	Alongshore (NJ)
Chicago	(433753.5, 4700297.6)	236.0	59000.0	117500.0	295	588
Kenosha	(451300.0, 4787100.0)	184.5	30000.0	122960.0	150	615
Green Bay	(466700.0, 5025500.0)	235.0	120000.0	37100.0	600	186

5.2.3 Boundary spectra

Spectral wave energy saved from WAM is transformed to STWAVE coordinates and applied as offshore boundary conditions for the STWAVE domains. The longitude/latitude of these boundary points is found in Table 5-2 with their location on the grids shown in Figures 5-5 to 5-7. Linear interpolation of the two-dimensional spectra was performed between these boundary points. Land boundaries were assigned zero spectra, and one-dimensional transformed spectra were set on the lateral boundaries of Kenosha. Boundary conditions were assigned for each STWAVE time-step or snap.

Table 5-2. Location of boundary points.

	Grid		
	Chicago	Kenosha	Green Bay
Longitude/Latitude of Boundary Points (deg)	(-87.70, 42.40) (-87.58, 42.34) (-87.46, 42.28) (-87.34, 42.22) (-87.22, 42.16) (-87.10, 42.10) (-86.98, 42.04) (-86.86, 41.98) (-86.74, 41.92)	(-87.60, 43.22) (-87.58, 43.06) (-87.56, 42.90) (-87.54, 42.72) (-87.52, 42.56) (-87.50, 42.36) (-87.48, 42.20)	(-87.38, 45.36) (-87.34, 45.34) (-87.30, 45.32) (-87.26, 45.30) (-87.22, 45.28) (-87.18, 45.26) (-87.14, 45.24)

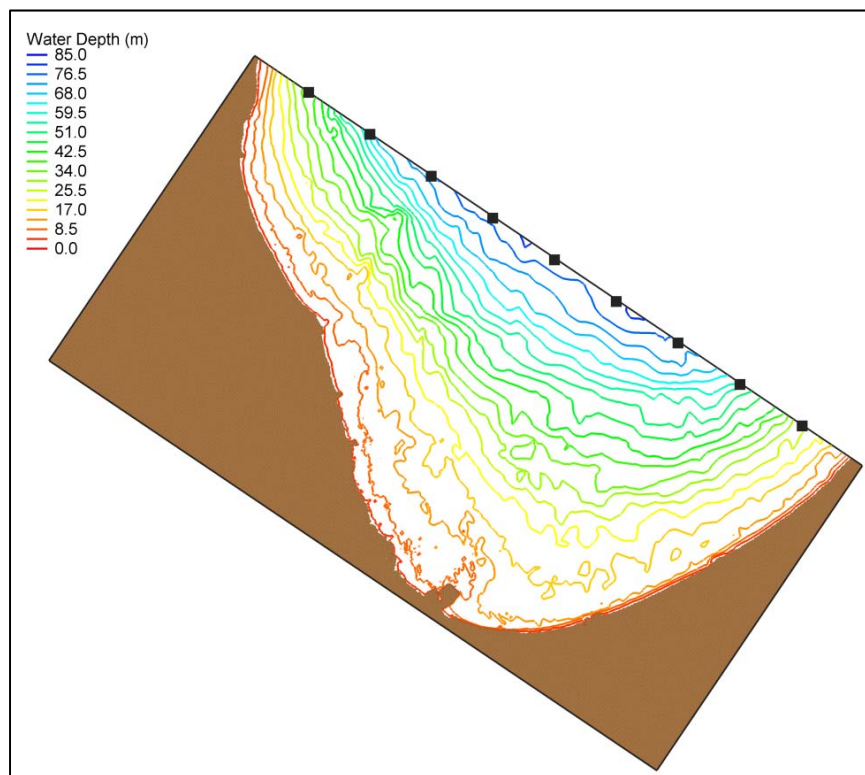


Figure 5-5. WAM spectra save points for Chicago.

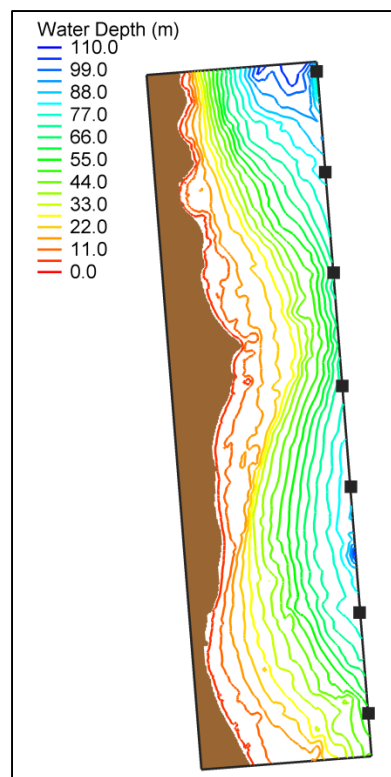


Figure 5-6. WAM spectra save points for Kenosha.

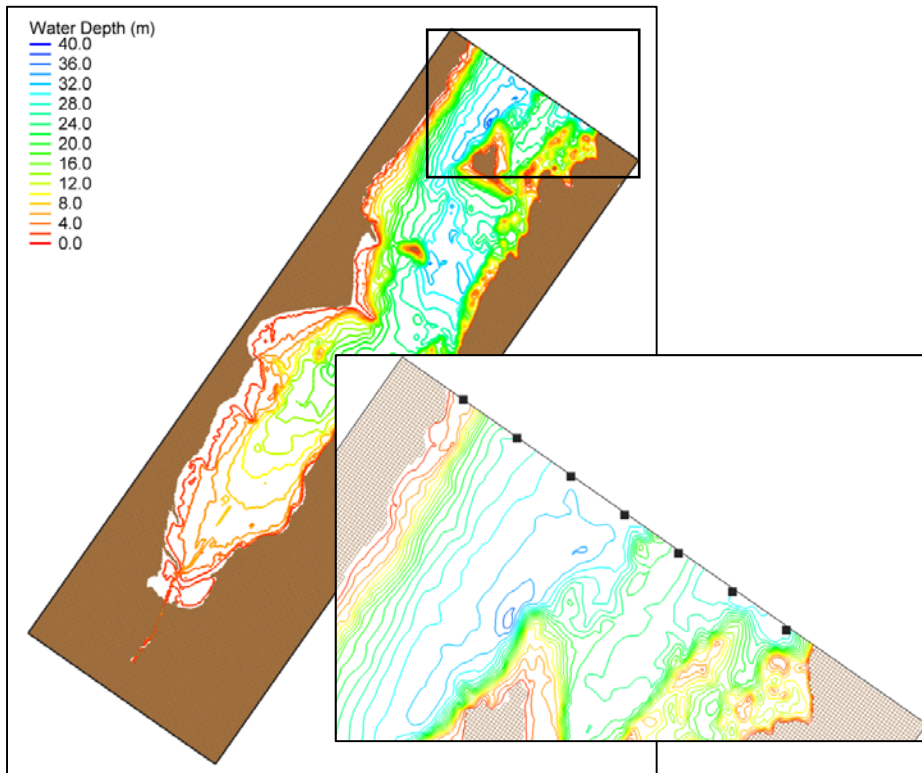


Figure 5-7. WAM spectra save points for Green Bay.

The number and values of the discrete frequency bands, as well as the starting and ending bands, were the same as those defined in WAM. The number and value of the frequency bands were defined as:

$$f(n+1) = 1.1 * f(n) \text{ where } n = 1, 28 \quad (5-3)$$

and the starting and ending starting bands were 0.0612 Hz ($T=16.3$ sec) and 0.8018 Hz ($T= 1.2$ sec), respectively. The angular resolution was set to 5-deg.

5.2.4 Save points

Zero-moment wave height (H_{mo}), mean wave period (T_m), mean wave direction (α_m), and 2-D spectra are exported at save points for every time-step. Save points were selected along the 10-m contour at an alongshore space of 1.5 km for Chicago and Kenosha. Save points were selected along the 2-m contour at an alongshore spacing of 500 m in southern Green Bay and other residential areas identified from Google Earth™. Remaining save points in Green Bay have an alongshore spacing of 1.5 km along the 5- or 10-m contour (in areas of steep slopes) to be well offshore of wave breaking. The number of save points for Chicago, Kenosha, and Green Bay was 132, 95, and 416, respectively, for a total of 644 points. Locations of the STWAVE save points for each grid is shown below in Figures 5-8 to 5-10.

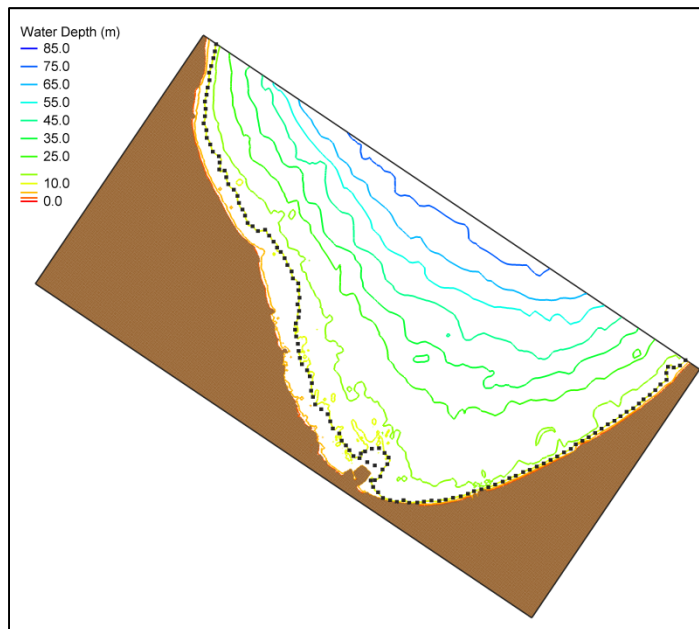


Figure 5-8. Save points for Chicago.

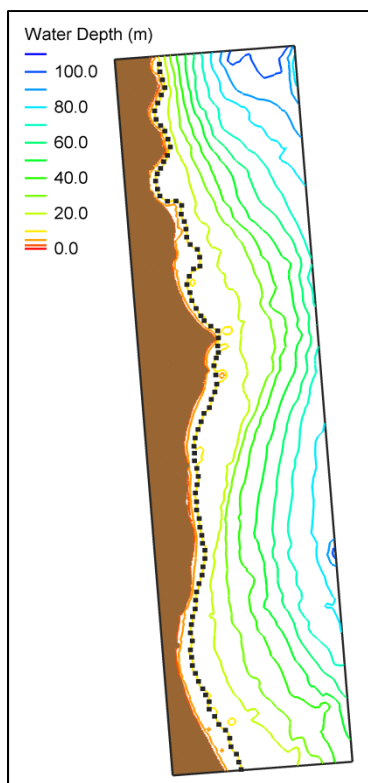


Figure 5-9. Save points for
Kenosha.

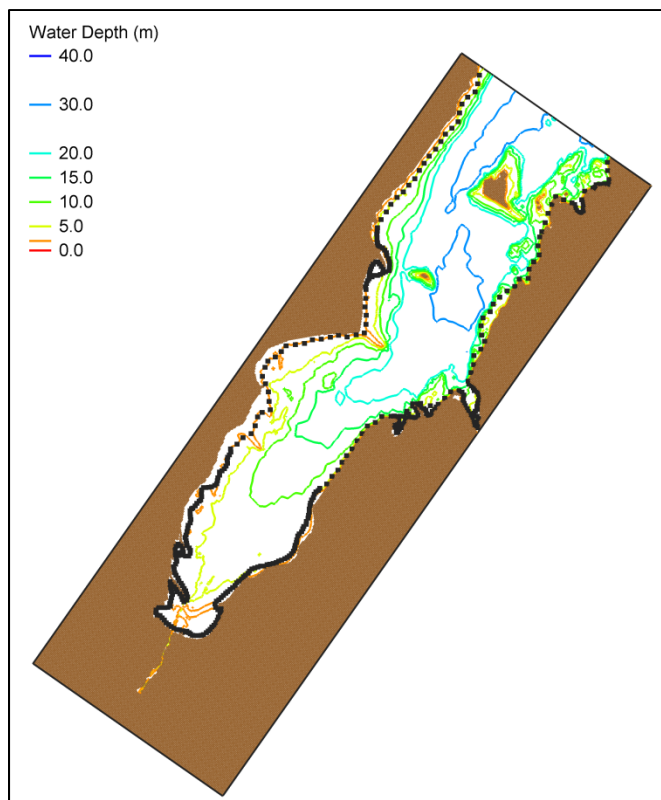


Figure 5-10. Save points for Green Bay.

5.2.5 Model parameters

Initial simulations using STWAVE's half-plane mode (which allows wave energy to propagate only from the offshore to the nearshore within a 180-deg arc) yielded erroneous results. Upon inspection, many of the storms with incorrect solutions had winds and wave spectra directed offshore for the majority of the event, which were neglected as a result of the half-plane definition. Based on these findings, STWAVE was switched to full-plane mode, allowing wave generation and transformation on the full 360-deg plane. These full-plane simulations produced much more reliable and stable solutions; thus, the full-plane capability was selected for this modeling effort.

The solution process for the full-plane version of STWAVE is an iterative process that requires user-defined convergence criteria to signal a suitable solution. Boundary spectra information is propagated from the boundary throughout the domain during the initial iterations. Once this stage converges, winds and surges are added to the forcing and this final stage iteratively executes until it also reaches a convergent state. The convergence criteria for both stages include the maximum number of iterations to perform (per time-step), the relative difference in average wave height between iterations, and the minimum percent of cells that must satisfy the stop criteria (i.e., have values less than the relative difference). Convergence parameters were selected based on a previous study by Massey et al. (2011) in which the sensitivity of the solution to the final convergence criteria was examined.

As full-plane requires considerably more memory requirements and run time than half-plane, STWAVE was setup with parallel in-space execution whereby the computational grid is broken into different partitions with each partition residing on a different computer processor. This allows for the modeling of larger domains with finer resolution as a full-plane grid can be separated in both the x- and y-direction. As energy can only cross one grid partition at a time during a single iteration, the maximum number of initial/final iterations was set to a value at least 15 higher than the largest grid partition while maintaining at least 25 cells in each partition. The convergence criteria and partitions for each grid are shown in Table 5-3.

Table 5-3. Full-plane and serial execution parameters.

Grid	Maximum Iterations		Relative Difference		Minimum Cell Percentage		Partitions		Number of cells per partition	
	Initial	Final	Initial	Final	Initial	Final	x	y	x	y
Chicago	40	40	0.1	0.05	100.0	99.8	11	22	27	27
Kenosha	40	40	0.1	0.05	100.0	99.8	6	24	25	26
Green Bay	40	40	0.1	0.05	100.0	99.8	22	7	27	27

5.2.6 CSTORM-MS coupler

CSTORM-MS is a physics-based modeling capability for simulating storm winds, waves, and water levels. The wave-circulation coupling is completed with one unstructured ADCIRC mesh and one or more structured STWAVE grids. One-way and two-way coupling is available in CSTORM-MS. One-way coupling passes information in one direction from one model to the other (i.e. ADCIRC → STWAVE or STWAVE → ADCIRC) while information is exchanged between both models during two-way coupling (ADCIRC ↔ STWAVE). The information shared between models is ADCIRC's surge and wind data and STWAVE's wave radiation stresses, which force wave-driven currents and water level changes. As part of this study, the information exchange was expanded to also allow ADCIRC to pass ice fields to STWAVE. One-way coupling (ADCIRC → STWAVE) was selected for application to Lake Michigan.

ADCIRC and STWAVE run sequentially during the coupling process. ADCIRC executes first and passes its surge, wind, and ice information (if applicable) to STWAVE at the end of the specified ADCIRC time increment. STWAVE then uses the surge, wind, and ice fields along with boundary forcing to compute the wave field. Control returns to ADCIRC when a suitable STWAVE solution is found, and the process is repeated.

All time values must be provided relative to ADCIRC to synchronize ADCIRC and STWAVE. Timing is performed via an external control file that specifies the ADCIRC starting and ending times in terms of the ADCIRC time-step, the starting and ending of all STWAVE simulations in terms of the ADCIRC time-step, and the number of ADCIRC time-steps that occur between STWAVE snaps.

ADCIRC is run for 12 days using a 0.5 sec time-step (for most of the storms), which corresponds to 1036800 sec or 2073600 time-steps. STWAVE starts

on Day 6 of the coupled simulation (518400 sec or 1036800 time-steps) and is run for six days (three days prior to the storm peak, the peak day, and two days following the storm peak). STWAVE is run every 30 minutes (1800 sec), which corresponds to 3600 time-steps. ADCIRC and STWAVE terminate on Day 12. The timing for this scenario in terms of ADCIRC time-steps is shown below in Table 5-4 and illustrated in Figure 5-11.

Table 5-4. Timing between ADCIRC and STWAVE in terms of ADCIRC time-steps.

ADIRC Start	ADCIRC End	Number of ADCIRC time-steps between STWAVE snaps	STWAVE Start	STWAVE End
0	2073600	3600	1036800	2073600

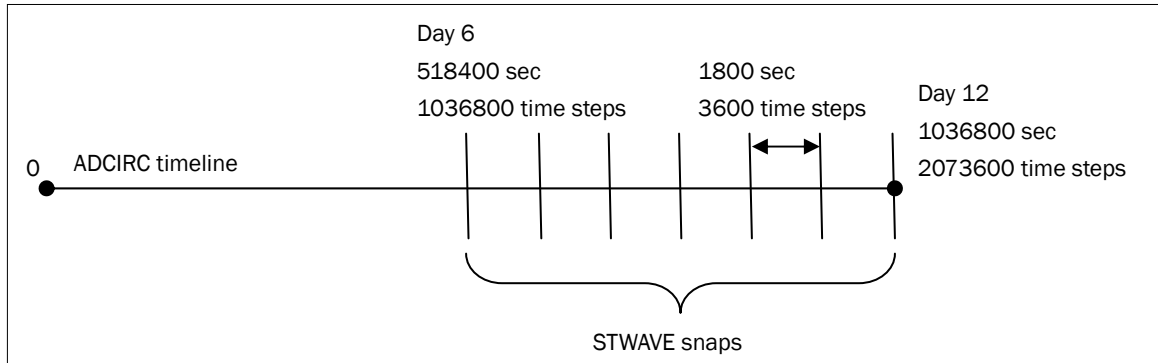


Figure 5-11. Diagram of timing between ADCIRC and STWAVE.

CSTORM-MS required 544 processors for each Lake Michigan storm simulation. One cpu is always reserved to serve as the controller, and one coupler (1 cpu/coupler) is required for each STWAVE grid. ADCIRC's efficiency is highest with 2000-4000 nodes per processor. The number of processors required by STWAVE is determined by multiplying the number of partitions in the x-direction by the number of partitions in the y-direction. The processors break down according to the following:

- Controller – 1 cpu
- ADCIRC – 157 cpu
- Couplers – 3 cpu (1 coupler/STWAVE)
- STWAVE Chicago – 242 (11 x 22)
- STWAVE Kenosha – 144 (6 x 24)
- STWAVE Green Bay – 154 (22 x 7)

ADCIRC and STWAVE share cpus so the number of processors in this case is dictated by STWAVE. All instances of STWAVE run simultaneously so

the total number of processors required by CSTORM-MS is the sum of the controller, the couplers, and the processors for each STWAVE grid (i.e, $1 + 3 + 242 + 144 + 154 = 544$).

All coupled simulations were run on the ERDC DSRC high performance Cray XE6 computer known as Garnet. Garnet contains 1,260 computer nodes (20,160 computer cores). Each compute node contains a 2.4-GHz AMD Opteron 64-bit quad-core processor and 32 GBytes of dedicated memory. The nodes are connected together using a Cray Gemini communications engine (<http://www.erdc.hpc.mil/>). The majority of the storm simulations finished within 8-9 hours.

6 Lake Michigan Storm Production

6.1 Introduction

The storm events were selected based on analysis of water level, wave and wind at ten long-term water level stations around Lake Michigan (Figure 6-1). The analysis and subsequent synthesis to define the top 150-events for simulations followed the procedure defined in Melby et al. (2012) and Nadal-Caraballo et al. (2012). The list was refined based on ice coverage for a given storm.

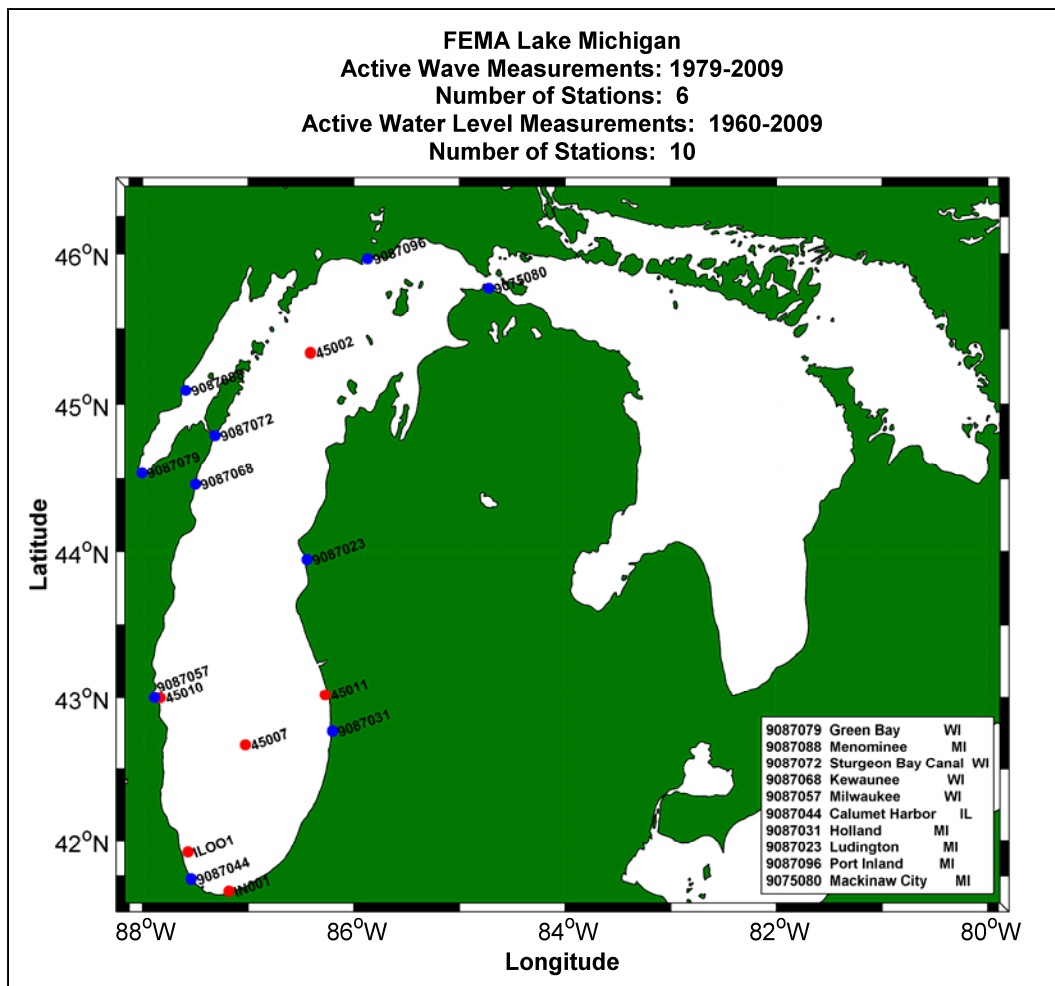


Figure 6-1. Location of wave measurement (red dots) and water level sites (blue dots).

The final list is presented in Table 6-1. The table lists the starting, ending and storm peak date, the water level site defined, the presence of ice in any part of Lake Michigan, and the rank of the storm event based on the water

Table 6-1. Extreme storm event list.

STORM No.	STORM DATES (YYYYMMDDHH)			ICE COVERAGE	STORM RANK	
	START DATE	STORM PEAK DATE	END DATE		SURGE	WAVE
ST0001	1960010600	1960011516	1960011800	NO DATA	5	19
ST0002	1960020100	1960021018	1960021300	NO DATA	29	1
ST0003	1960031300	1960032207	1960032500	ICE	2	10
ST0004	1960041000	1960041918	1960042200	NO DATA	15	8
ST0005	1961041100	1961042019	1961042300	ICE	6	8
ST0006	1961102500	1961110307	1961110600	OPEN	7	1
ST0007	1962010500	1962011409	1962011700	ICE	1	12
ST0008	1962041700	1962042622	1962042900	NO DATA	N/A	2
ST0009	1962051400	1962052321	1962052600	OPEN	28	10
ST0010	1963031200	1963032109	1963032400	ICE	7	16
ST0011	1963032600	1963040400	1963040700	ICE	7	7
ST0012	1964022000	1964022918	1964030300	ICE	1	30
ST0013	1964022500	1964030509	1964030800	ICE	18	17
ST0014	1964040500	1964041412	1964041700	ICE	N/A	4
ST0015	1964042700	1964050622	1964050900	OPEN	8	10
ST0016	1964092500	1964100404	1964100700	OPEN	40	25
ST0017	1965021600	1965022521	1965022800	ICE	N/A	9
ST0018	1965111800	1965112710	1965113000	OPEN	5	5
ST0019	1965121600	1965122515	1965122800	NO DATA	1	9
ST0020	1966032300	1966040102	1966040400	NO-DATA	4	N/A
ST0021	1966112000	1966112906	1966120200	OPEN	7	6
ST0022	1967010800	1967011706	1967012000	ICE	11	8
ST0023	1967011800	1967012703	1967013000	ICE	N/A	10
ST0024	1968012500	1968020303	1968020600	ICE	N/A	10
ST0025	1968032900	1968040722	1968041000	ICE	N/A	4
ST0026	1968120400	1968121318	1968121600	NO DATA	7	5
ST0027	1970012400	1970020216	1970020500	ICE	37	13
ST0028	1970020700	1970021622	1970021900	ICE	N/A	8
ST0029	1970032400	1970040212	1970040500	ICE	N/A	3
ST0030	1970100100	1970101004	1970101300	OPEN	N/A	28
ST0031	1970102500	1970110306	1970110600	OPEN	8	N/A
ST0032	1970111600	1970112522	1970112800	OPEN	N/A	28
ST0033	1970112500	1970120410	1970120700	NO-DATA	15	29
ST0034	1971011700	1971012615	1971012900	ICE	6	2

STORM No.	STORM DATES (YYYYMMDDHH)			ICE COVERAGE	STORM RANK	
	START DATE	STORM PEAK DATE	END DATE		SURGE	WAVE
ST0035	1971012700	1971020512	1971020800	ICE	13	17
ST0036	1971021800	1971022715	1971030200	ICE	28	3
ST0037	1971120600	1971121523	1971121800	NO-DATA	15	N/A
ST0038	1971122100	1971123020	1972010200	ICE	3	N/A
ST0039	1972011600	1972012510	1972012800	ICE	17	5
ST0040	1993092200	1993100109	1992100400	OPEN	17	12
ST0041	1972101400	1972102309	1972102600	OPEN	12	16
ST0042	1972122200	1972123100	1973010300	ICE	14	N/A
ST0043	1973040100	1973041000	1973041300	ICE	5	3
ST0044	1973100600	1973101519	1973101800	OPEN	5	N/A
ST0045	1973101900	1973102814	1973103100	OPEN	19	N/A
ST0046	1973120400	1973121321	1973121600	ICE	N/A	6
ST0047	1974032500	1974040322	1974040600	ICE	N/A	8
ST0048	1975010300	1975011200	1975011500	ICE	1	1
ST0049	1975021500	1975022409	1975022700	ICE	N/A	8
ST0050	1975110100	1975111018	1975111300	OPEN	2	21
ST0051	1975112100	1975113015	1975120300	OPEN	23	17
ST0052	1976011900	1976012810	1976013100	ICE	31	6
ST0053	1977110200	1977111112	1977111400	OPEN	N/A	19
ST0054	1977123100	1978010921	1978011200	ICE	N/A	9
ST0055	1978011800	1978012700	1978013000	ICE	N/A	2
ST0056	1978050400	1978051315	1978051600	ICE	50	27
ST0057	1978101600	1978102504	1978102800	OPEN	N/A	7
ST0058	1978121100	1978122020	1978122300	ICE	9	N/A
ST0059	1979040300	1979041208	1979041500	ICE	10	43
ST0060	1979102300	1979110121	1979110400	OPEN	37	19
ST0061	1979121600	1979122506	1979122800	ICE	20	2
ST0062	1980101400	1980102300	1980102600	OPEN	38	31
ST0063	1981050200	1981051107	1981051400	OPEN	N/A	8
ST0064	1981092200	1981100115	1981100400	OPEN	10	30
ST0065	1981122600	1982010419	1982010700	ICE	5	14
ST0066	1982011400	1982012321	1982012600	ICE	5	29
ST0067	1982032600	1982040406	1982040700	ICE	4	45
ST0068	1982101100	1982102015	1982102300	OPEN	16	N/A
ST0069	1983010600	1983011509	1983011800	ICE	25	43

STORM No.	STORM DATES (YYYYMMDDHH)			ICE COVERAGE	STORM RANK	
	START DATE	STORM PEAK DATE	END DATE		SURGE	WAVE
ST0070	1983012400	1983020221	1983020500	ICE	N/A	21
ST0071	1983032300	1983040100	1983040400	ICE	N/A	N/A
ST0072	1983040500	1983041416	1983041700	ICE	N/A	14
ST0073	1983042800	1983050722	1983051000	OPEN	18	3
ST0074	1983110200	1983111109	1983111400	OPEN	39	19
ST0075	1983111900	1983112822	1983120100	OPEN	11	N/A
ST0076	1984021900	1984022821	1984030200	ICE	41	4
ST0077	1984040700	1984041613	1984041900	ICE	N/A	14
ST0078	1985011600	1985012517	1985012800	ICE	36	N/A
ST0079	1985022400	1985030504	1985030800	ICE	3	N/A
ST0080	1985032200	1985033122	1985040300	ICE	17	N/A
ST0081	1985111100	1985112007	1985112300	OPEN	1	N/A
ST0082	1985112300	1985120215	1985120500	OPEN	2	35
ST0083	1987013000	1987020821	1987021100	ICE	9	4
ST0084	1987030100	1987031000	1987031300	ICE	1	21
ST0085	1987120600	1987121515	1987121800	ICE	2	7
ST0086	1988011100	1988012014	1988012300	ICE	35	10
ST0087	1988032800	1988040621	1988040900	ICE	40	17
ST0088	1988102200	1988103121	1988110300	OPEN	N/A	10
ST0089	1988110800	1988111703	1988112000	OPEN	4	2
ST0090	1989011300	1989012203	1989012500	ICE	N/A	2
ST0091	1997021300	1997022204	1997022500	ICE	50	15
ST0092	1989110700	1989111618	1989111900	OPEN	N/A	2
ST0093	19891112100	1989113000	1989120300	OPEN	18	44
ST0094	1989121700	1989122604	1989122900	ICE	8	11
ST0095	1990012000	1990012906	1990020100	ICE	12	30
ST0096	1990021800	1990022700	1990030200	ICE	15	5
ST0097	1990030700	1990031621	1990031900	ICE	N/A	39
ST0098	1990040100	1990041019	1990041300	ICE	N/A	8
ST0099	1990112500	1990120418	1990120700	OPEN	1	28
ST0100	1991011400	1991012306	1991012600	ICE	N/A	5
ST0101	1991022100	1991030219	1991030500	ICE	N/A	2
ST0102	1991102400	1991110209	1991110500	OPEN	13	14
ST0103	1992030100	1992031018	1992031300	ICE	14	23
ST0104	1992051400	1992052322	1992052600	ICE	N/A	2

STORM No.	STORM DATES (YYYYMMDDHH)			ICE COVERAGE	STORM RANK	
	START DATE	STORM PEAK DATE	END DATE		SURGE	WAVE
ST0105	1992102500	1992110315	1992110600	OPEN	4	27
ST0106	1992121600	1992122515	1992122800	ICE	N/A	4
ST0107	1993032300	1993040113	1993040400	ICE	13	2
ST0108	1993041100	1993042012	1993042300	ICE	4	37
ST0109	1993102700	1993110507	1993110800	OPEN	13	N/A
ST0110	1993111000	1993111918	1993112200	OPEN	N/A	2
ST0111	1994021400	1994022318	1994022600	ICE	N/A	8
ST0112	1994040800	1994041700	1994042000	ICE	N/A	14
ST0113	1994092200	1994100101	1994100400	OPEN	11	N/A
ST0114	1994110900	1994111821	1994112100	OPEN	N/A	14
ST0115	2004120400	2004121311	2004121600	ICE	N/A	17
ST0116	1994111900	1994112818	1994120100	OPEN	7	3
ST0117	1995040300	1995041204	1995041500	ICE	12	N/A
ST0118	1995110200	1995111115	1995111400	OPEN	22	39
ST0119	1995111900	1995112800	1995120100	OPEN	13	29
ST0120	1996012000	1996012922	1996020100	OPEN	21	36
ST0121	1996031100	1996032019	1996032300	ICE	26	6
ST0122	1996040600	1996041512	1996041800	ICE	6	N/A
ST0123	1996102200	1996103100	1996110300	OPEN	16	28
ST0124	1997032900	1997040706	1997041000	ICE	N/A	7
ST0125	1997042200	1997050101	1997050400	ICE	19	15
ST0126	1997123100	1998010905	1998011200	ICE	49	N/A
ST0127	1998022800	1998030916	1998031200	ICE	5	7
ST0128	1998052200	1998053113	1998060300	OPEN	4	N/A
ST0129	1998110200	1998111100	1998111400	OPEN	3	1
ST0130	1998122500	1999010300	1999010600	ICE	6	26
ST0131	1999020300	1999021207	1999021500	ICE	23	6
ST0132	2000041200	2000042104	2000042400	OPEN	9	2
ST0133	2001040300	2001041204	2001041500	ICE	16	N/A
ST0134	2001101700	2001102601	2001102900	OPEN	15	28
ST0135	2002020300	2002021203	2002021500	ICE	31	N/A
ST0136	2002021100	2002022022	2002022300	ICE	31	6
ST0137	2002030100	2002031007	2002031300	ICE	13	10
ST0138	2002043000	2002050916	2002051200	ICE	N/A	4
ST0139	2003102600	2003110420	2003110700	OPEN	28	N/A

STORM No.	STORM DATES (YYYYMMDDHH)			ICE COVERAGE	STORM RANK	
	START DATE	STORM PEAK DATE	END DATE		SURGE	WAVE
ST0140	2003111400	2003112322	2003112600	OPEN	13	N/A
ST0141	2005110700	2005111608	2005111900	OPEN	4	11
ST0142	2006050300	2006051200	2006051500	OPEN	50	N/A
ST0143	2006110700	2006111613	2006111900	OPEN	34	10
ST0144	2007022100	2007030203	2007030500	ICE	15	N/A
ST0145	2007040300	2007041202	2007041500	ICE	16	12
ST0146	2007111800	2007112715	2007113000	OPEN	29	4
ST0147	2007121400	2007122316	2007122600	ICE	6	N/A
ST0148	2008012100	2008013010	2008020200	ICE	N/A	3
ST0149	2009032800	2009040616	2009040900	ICE	N/A	1
ST0150	2009113000	2009120915	2009121200	ICE	2	1
				1960-1979 Archive		
				1973-2002 Assel		
				2003-2009 NESDIS		

level at the ten National Ocean Services sites, historical wave hindcasts (e.g. Hubertz et al. 1991), or a surrogate wave estimate derived from point source wind stations.

The length of storm simulation was limited to a 12-day period. The storm simulation was initiated 9-days prior to the storm peak, and was run 3-days after the storm peak. This allowed for proper initialization of the surge model, including Lake Huron (Figure 6-1), and phasing of local wind-wave specification for Lake Michigan.

6.2 Wind field production

Two methods were used to generate the wind and pressure fields for the Lake Michigan hydrodynamic modeling. From 1 January 1979 (1979010100) through 1 January 2010 the NOAA/NCEP, Climate Forecast System Re-analysis (CFSR, Saha et al. 2010) were used. Prior to 1 January 1979, all wind and pressure fields were generated using the Natural Neighbor Method (NNM, Schwab et al. 1984, 1998). Both methodologies are discussed in Chapter 1, and showed fairly consistent results in replicating wave measurements for approximately twenty storm events (Chapter 3). The primary reason for using both wind methodologies is that CFSR winds, despite

showing slightly better results compared to NNM, extend back in time to 1 January 1979. There were 59 storm events selected (Table 6-1) that exist from 1960 through December 1979 requiring winds and pressure fields. The only alternative is to generate these required fields from NNM. The basis of the wind and pressure field construction via NNM is active land-based meteorological stations. As shown in Figure 1-1 the number of stations decreases to about seven. The frequency in observations over time changes from hourly to a 3-hour interval at certain locations. The methodology based solely on point-source meteorological measurements tend to concentrate high winds in close proximity to these land based stations. Fortunately, the wave model is an excellent integrator, and focuses more on the larger scale events. Despite these factors, in all of the historical wave hindcasts (Resio and Vincent 1976, and Hubertz et al. 1991), the number of land-based stations used in their wind generation algorithms were set at six and seven, respectively. It is also worthy to note, wave measurements for evaluation purposes were not available until 1979.

6.3 Ice field analyses

The Great Lakes experiences time periods where shore-fast ice is developed. There is not only an intra-annual variation in ice coverage, but also decadal variations based on climate variation. The development is initiated in the late fall to early winter time periods. Daily ice concentration fields developed by Assel (2003) are the most reliable, consistent data archive covering 1973 through 2002 period of record. These fields were developed from visual observations (ship, shore, aircraft) and estimated from satellite measurements. An addition to this archive exists for the period of 1960 through 1979 and is found at <http://nsidc.org/data/g00804.html>. This archive was limited to half-month periods, and generally contained little concentration data. For storms to be simulated during this time period, the ice field closest in time was used throughout the storm simulation. The third archive (originally obtained directly from NOAA/GLERL), spans the period from 2003 through 2009. This archive, from the NOAA National Ice Center (http://www.natice.noaa.gov/products/great_lakes.html), contains bi-weekly estimates in the ice concentration field. There are multiple grid resolutions to select from, however, to remain consistent with other storm simulations, the 516 x 510 grids were used when available.

In general, the ice year covers the months of December through May of the following year. During this time period, the shore-fast ice grows from land to the open water, increasing in concentration level, where the open water is

replaced by ice acting as an impervious boundary between the land and the open water. In the spring thaw or ice breakup, this boundary can become detrimental to any shore structure. For example, if there is a major event where winds are blowing toward the coastline, wind-generated waves have the potential to fragment the ice sheet to the point where an elevated water level could transport the ice landward. In effect, ice sheets can cause significant structural damage to an existing shore-based building, increasing the flood potential where ice is effectively riding on top of the elevated water levels, causing more damage.

Originally, there was some concern in the Lake Michigan Study where an a priori selection of a concentration level was made. The selection of a unique threshold of 70-percent allows the water to remain open for a longer period of time, and during the spring thaw opens the water to be active wind-wave growth earlier. This is in comparison to selecting a threshold at a lower value. Noting that shore-fast ice builds from the land outward selecting a higher threshold will also allocate more open water during the simulation.

Implementation of the net effect of ice boundaries in the wave modeling technology was based on a simplified method of treating ice as land. The only a priori assumption was to determine the threshold of ice concentration level to apply this condition. From past studies in the Western Alaska domain (Jensen et al. 2002), it was found that treating the ice (pack and shore-fast) edge with a 70-percent ice concentration threshold provided consistency between the modeled wave estimates and available buoy data. Following this work, it was assumed that the process of shore-fast ice generation found in the Great Lakes was similar to that in the Western Alaska domain. Preliminary tests indicated the 70-percent threshold rule produced a consistency to a limited data set for buoy positions located in the middle of Lake Michigan (e.g. Figures 6-2 and 6-3). Figure 6-2 displays the maximum wave height color contour for February 1991, where the ice field is indicated by the grey color. All of the open water is assumed to be land, thus reducing the fetch length for active wind wave growth. This occurs for certain events for winds from 0- to 90-deg occurring numerous times during the entire month of February. A time plot of measurements to model results is provided in Figure 6-3. The six-panel plot shows excellent agreement of the model's significant wave height, peak and mean wave periods for a number of storm events, and only slightly over-estimates the largest event by about 0.5-m. This is one of many examples demonstrating the proper evaluation of selecting the ice concentration level, and its adequacy in the proper generation of wind-generated waves.

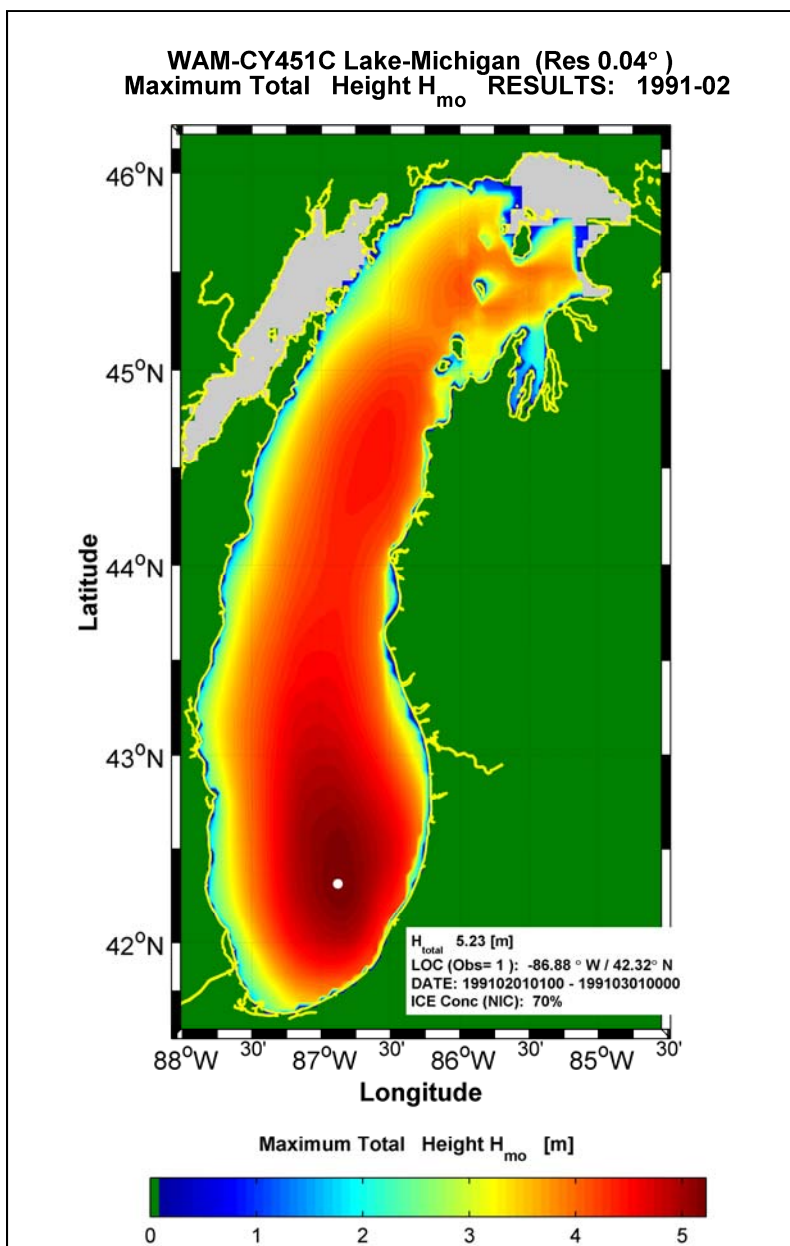


Figure 6-2. Maximum wave height color contour for February 1999, with ice coverage (grey shaded), selecting 70-percent concentration threshold.

Further evaluations were made with the wave model results for winter time periods for Lake Michigan. There were two coastal wave gages deployed in the southern Lake Michigan at offshore locations of Chicago and Burns Harbor (Figure 6-4). Both wave gages were deployed in about 10-m water depths, where Chicago Harbor gage was deployed from 1991 through 2003; and Burns Harbor with two deployments from 1987 through 1988 and 2001-2005. The usefulness of the data was that they were deployed during the winter months where shore-fast ice generation was taking place.

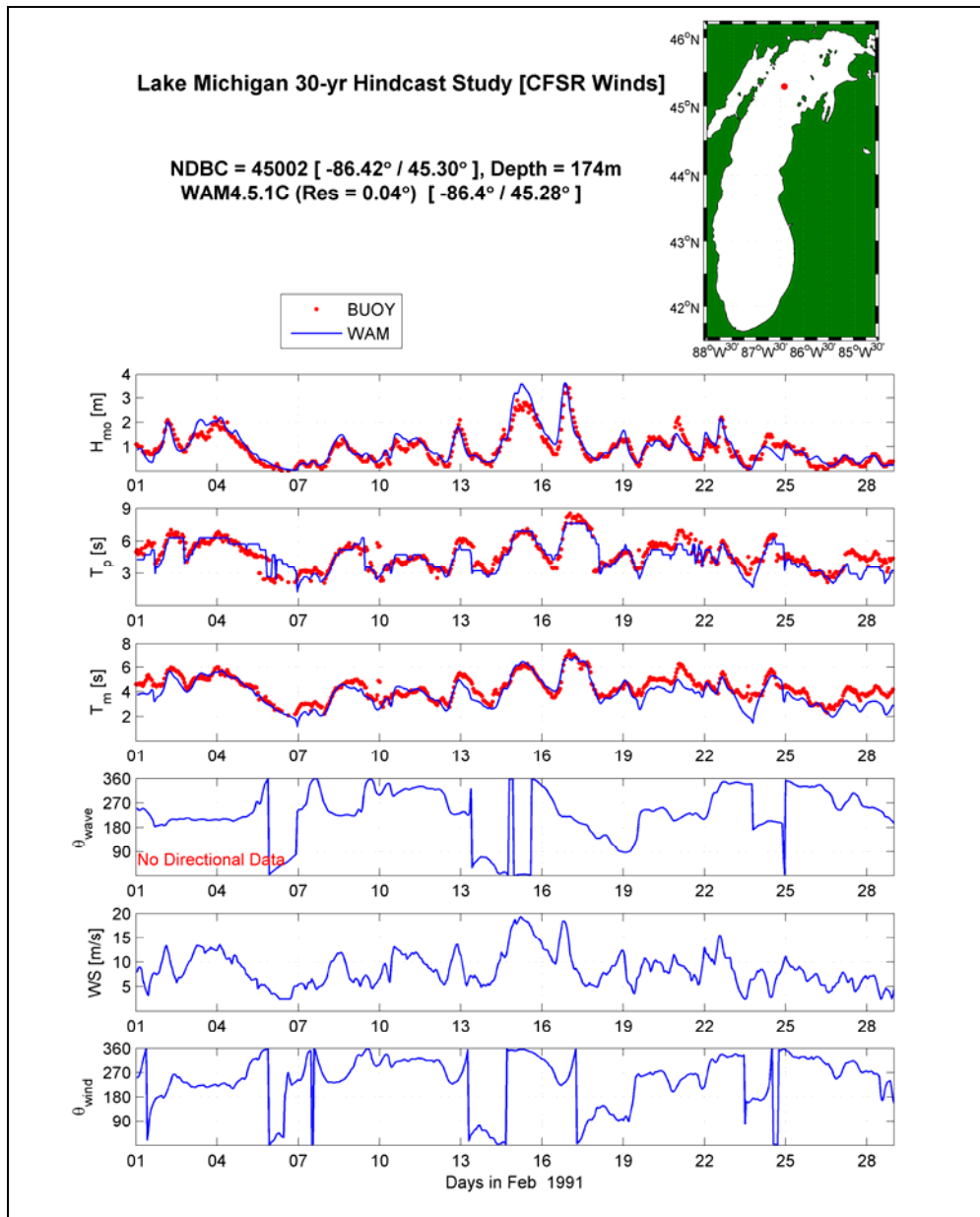


Figure 6-3. Wave height, peak, mean wave period, wind speed and direction time plot evaluation for WAMCY4.5.1C and NDBC Buoy 45002, February 1991.

Wave estimates derived from the Wave Information Study's (WIS) 31-year wave hindcast were used for this evaluation. The WIS methodology follows that of the FEMA Great Lakes Coastal Guidelines, the winds derived from the CFSR wind fields, the wave model WAMCY4.5.1C, and the bathymetry and grid defined from the FEMA Lake Michigan Storm Wave evaluation. One example in particular is a time plot of the wave estimates for March 2003 (Figure 6-5). During the first 12-days, the model estimates are zeroed out because of ice coverage. The Burns Harbor gage, however, shows signs of wave energy and fluctuate at a near diurnal interval. Measured wave

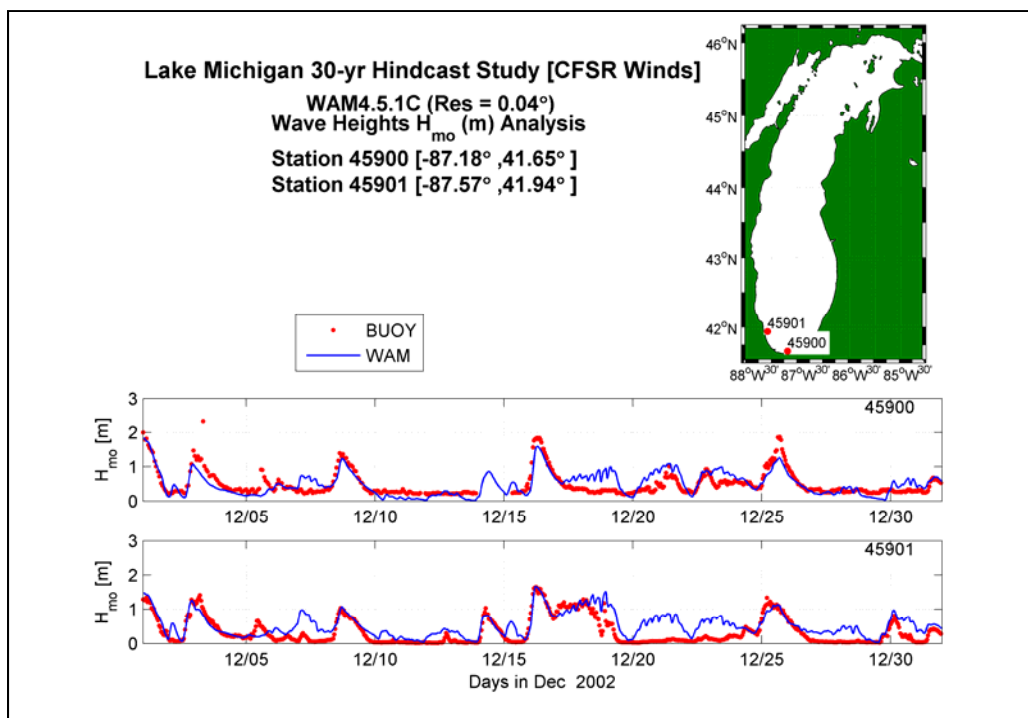


Figure 6-4. Wave height comparison at Burns Harbor (45900), and Chicago Harbor (45901) for December 2002 and WAMCY4.5.1C.

heights of roughly 0.25-m are evident, oscillating at about 0.1-m. After 10 March the gage indicates no wave energy. The cause of this oscillation is unknown, however, one could hypothesize that the diurnal pattern is a result of the daily heating and cooling of the water just below the ice sheet. Figure 6-6 displays the ice concentration estimates derived from the National Ice Center (http://www.natice.noaa.gov/products/great_lakes.html) where all ice data were obtained. The four-panel plot shows the time and spatial variation in the concentration level on 1, 5, 10 and 15 March. Focusing on the southern portion of Lake Michigan (Burns Harbor, see Figure 6-5 top panel) the concentration level is initially 70-percent on 1 March; splits on 5 March indicating 80 to 90-percent along the western side of southern Lake Michigan and 70-percent along the eastern side. On 10 March, the entire southern area of Lake Michigan is dominated by about 100-percent concentration coverage. On 15 March, a significant change in the concentration levels occurs, where the nearshore domain is occupied by concentration levels of about 40-percent. This demonstrates not only the spatial and temporal variability in ice concentration levels, but also the complexity of this process. One could assume that there is an ice sheet at the Burns Harbor site but it is nearly impossible to validate. However, this example does demonstrate that using one value for ice can provide adequate results.

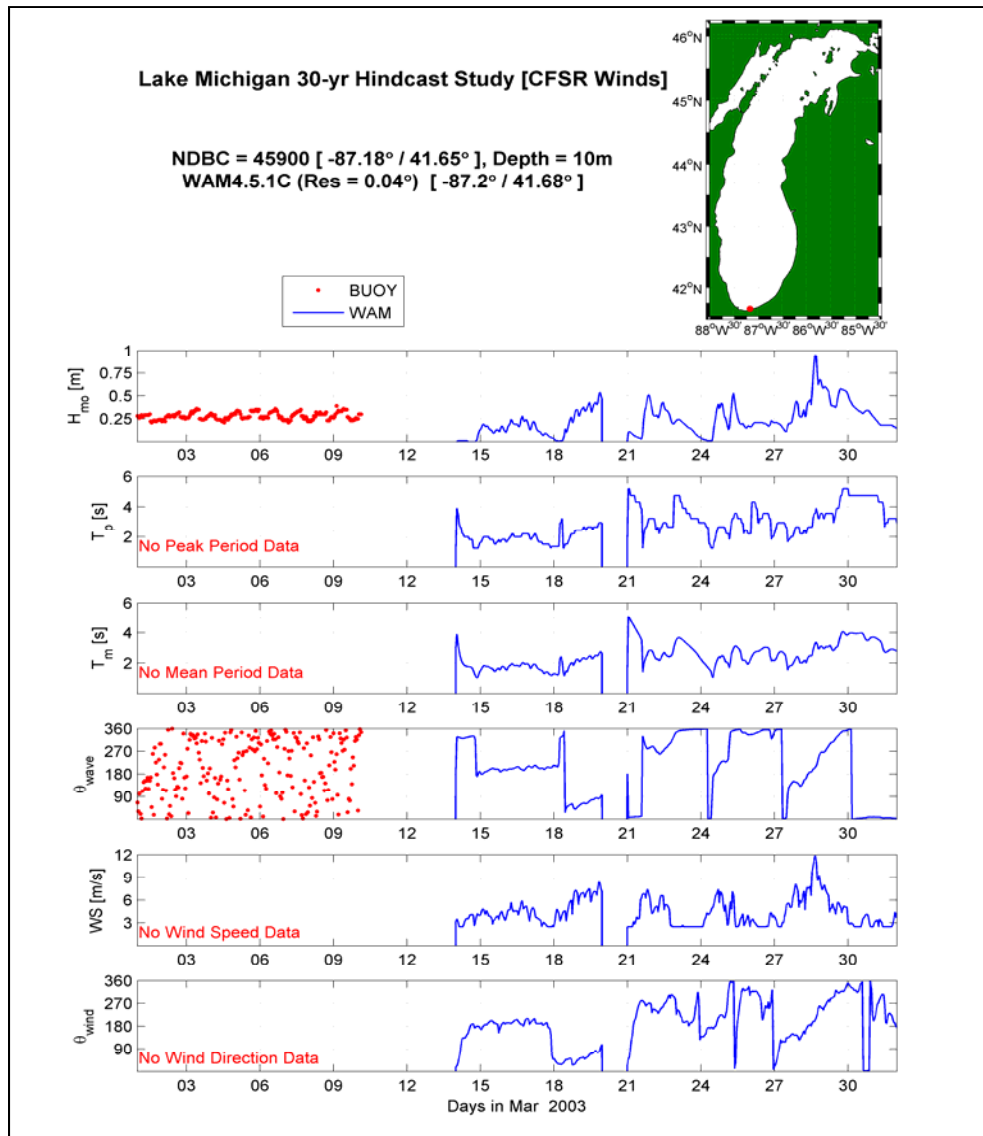


Figure 6-5. Wave height comparison at Burns Harbor (45900), and WAMCY451C for March 2003.

The Wave Information Study (<http://wis.usace.army.mil/hindcasts.shtml?dmn=lakesWIS>) estimates were used to increase the population size (by an order of magnitude, as will be shown in the evaluation section) for the evaluation for all time periods when Chicago and Burns Harbor wave gages were deployed. The results from this increased evaluation are provided in Figures 6-7 (Burns Harbor, ST 45900) and 6-8 (Chicago Harbor, ST 45901), where time-paired observations and model results are plotted. As shown in these figures, there are contours lining up with the ordinate, and abscissa suggesting the model results do not reflect ice coverage (red oval) while the measurements do; and where the measurements reflect no ice coverage (green oval) whereas the model does, respectively.

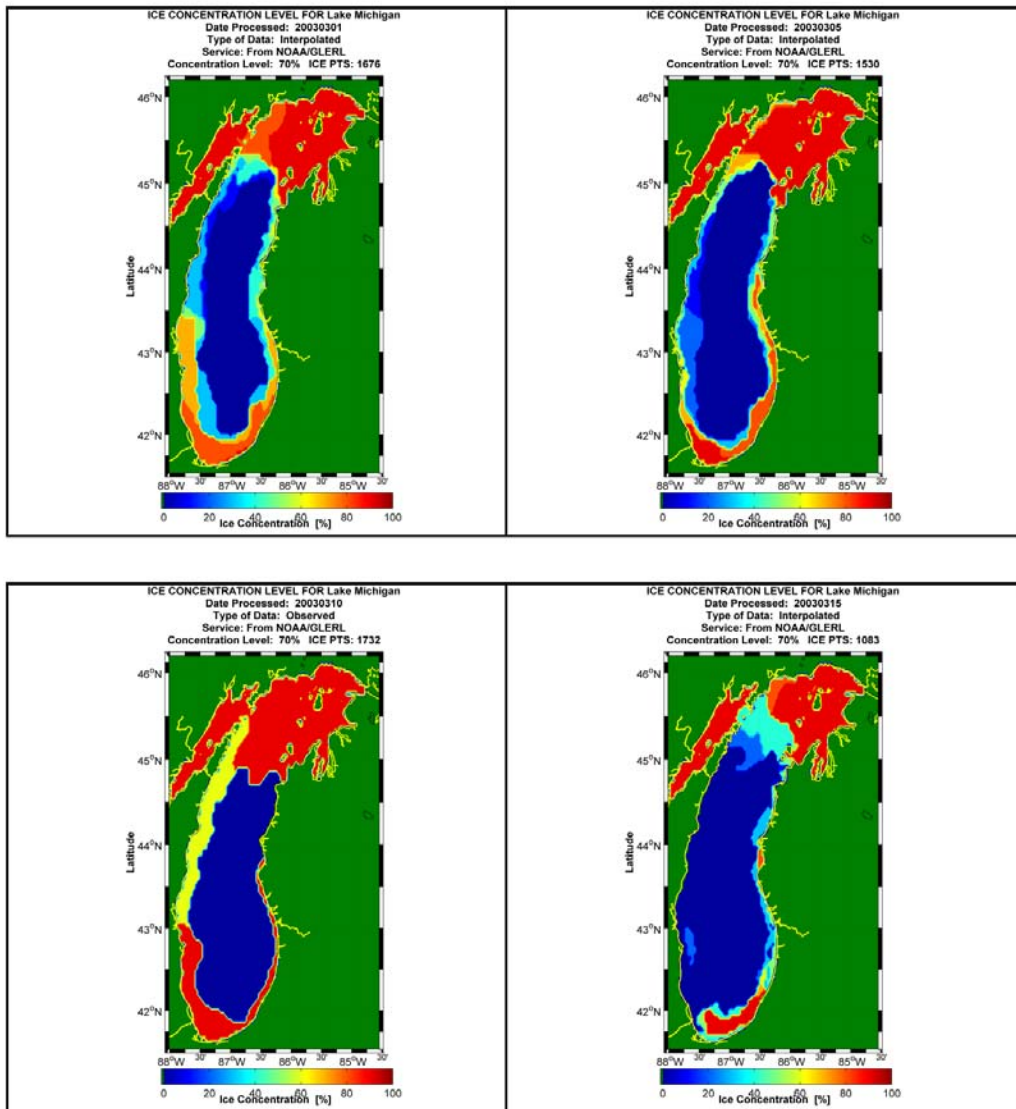


Figure 6-6. Ice concentration levels for 1 March (top left), 5 March (top right), 10 March (bottom left) and 15 March (bottom right) 2003, from http://www.natice.noaa.gov/products/great_lakes.html.

This net effect is not as evident at Chicago Harbor compared to the Burns Harbor data set; however, the bulk of time-paired model to measurements is skewed in the vertical direction, indicating a slight over-estimate in the model wave heights compared to the data. On average, the model performs well under iced conditions as well as in an open water situation.

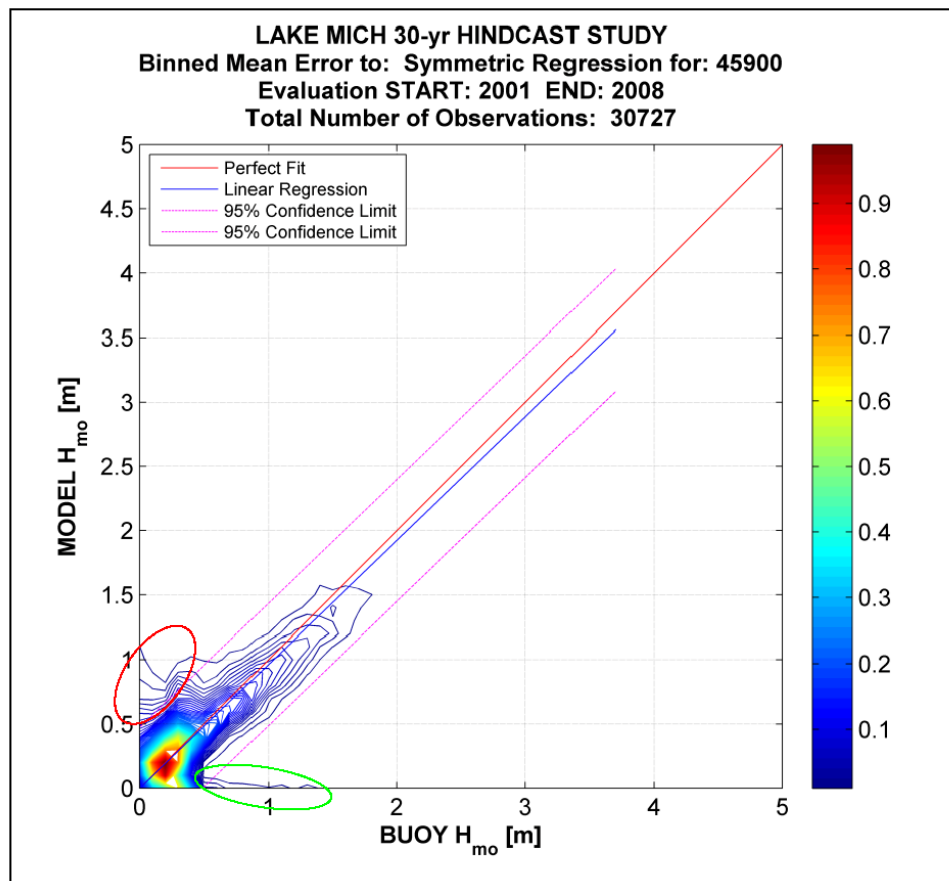


Figure 6-7. Wave height time paired comparison at Burns Harbor (45900) and WAMCY4.5.1C.

6.4 Ice field production

Original ice concentration fields were spatially interpolated to the existing WAM wave model grid (spherical grid with resolution of 0.02-deg in longitude and latitude). This was done for the Assel (2003) Ice Atlas (1973 through 2002). If the extreme storm event occurred post 2002, those ice fields were also temporally interpolated from observation ice concentration fields, and then spatially interpolated to the WAM grid. The historical storms (i.e. pre-1973) individual ice fields that fell within the storm sequence were interrogated. This single field was used for the entire storm simulation period. Table 6-1 is color coded indicating which of the three ice archives were used for that particular storm simulation. An entry of *NO DATA* indicates that no data existed for that particular event and that all water points were considered to be open water. *OPEN WATER* generally indicated that this storm event took place during a non-ice time period. The

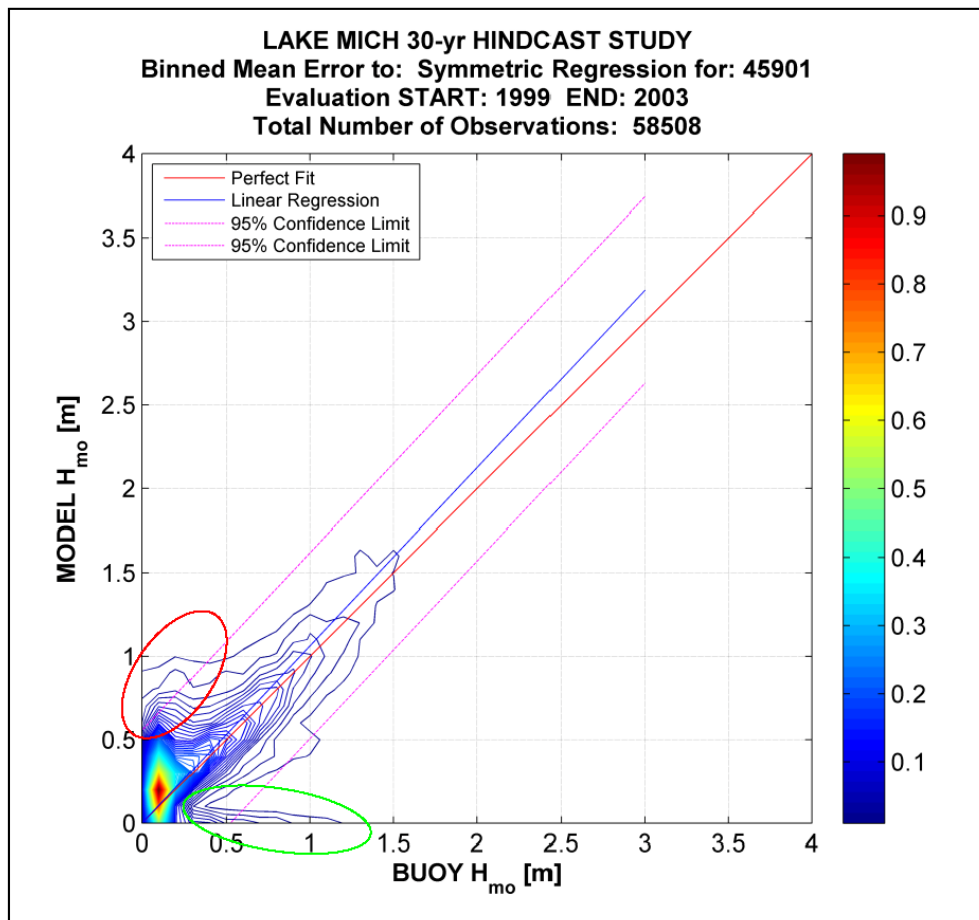


Figure 6-8. Wave height time paired comparison at Chicago Harbor (45901) and WAMCY4.5.1C.

actual WAM implementation¹ for temporally varying ice fields followed that of the wind field implementation. This version was tested and evaluated before the execution of the extreme storm events. There was little computation penalty incurred for these modifications, and the results were consistent with the graphical estimates of the ice fields provided by Assel (2003).

6.5 Offshore wave production

The original WAM grid (Chapter 3) was developed from a 3-arc second digital data base, where the water depths were scaled to the mean lower lake level. The lake level for each storm event was evaluated and the WAM water depth grid was re-generated. The assumption of vertical walls at the shoreline was made so that land would remain land, and water would remain water. However, all water depths were re-specified for each event.

¹ Dr. T.C. Massey modified the WAM code to implement temporally varying ice fields.

This required an additional step in the production to calculate all variables dependent on the water depth (wavelength, phase and group speeds, refraction and shoaling coefficients).

Each storm in the 150 extreme storm suite (see Table 6-1) is treated independent of any other in the list; hence, multiple storm events can be run simultaneously under one operational shell script. WAM requires two time-steps, propagation (CFL stability criteria), and source term integration. These were set to 30- and 300-sec, respectively. Twenty eight frequency bands were used starting at 0.06116, and based on the equation: $f(n+1) = 1.1 \cdot f(n)$, and seventy two direction bins starting at 7.5-deg.

The last step is to select the special output locations where two-dimensional (frequency, direction) wave spectra are to be saved. These were selected based on the proximity to the shoreline and consistency in the water depth of approximately 10-m. Three offshore islands were surrounded by output locations as well as all measurement sites. Boundary condition locations (input to STWAVE) were identified for the three sub-grid domains required in the study. The locations are displayed in Figures 6-9 through 6-11. The total number of special output locations was 662.

Once the input wind and ice fields have been processed, the production can be initiated. For all storm simulations, WAM Cycle 4.5.1C used all shallow water options, including shoaling, refraction, wave-bottom effects, and depth induced wave breaking. As part of this procedure the atmospheric input was adjusted so that the full dispersion relationship was applied and the nonlinear wave-wave interaction (Discrete Interaction Approximation) was modified based on the Herterich and Hasselmann (1980) scaling.

The automated system executes the following steps:

- Input the WAM water depth grid, adjust for lake level
- Output the time independent, depth and spatially dependent parameters
- Format the wind fields for WAM
- Generate the storm specific general input file (start date, end date, wind field name, and if appropriate ice field name)
- Run WAM
- Output the field information, spectral information (special output locations a priori defined)

- Output the 2-D spectra at the STWAVE boundary (three sets)
- Post-Process Phase I
- Generate the integral wave parameter file for each station at 30-minute intervals
- Generate flat ASCII files containing the field information for integral wave parameters (30-minute intervals).

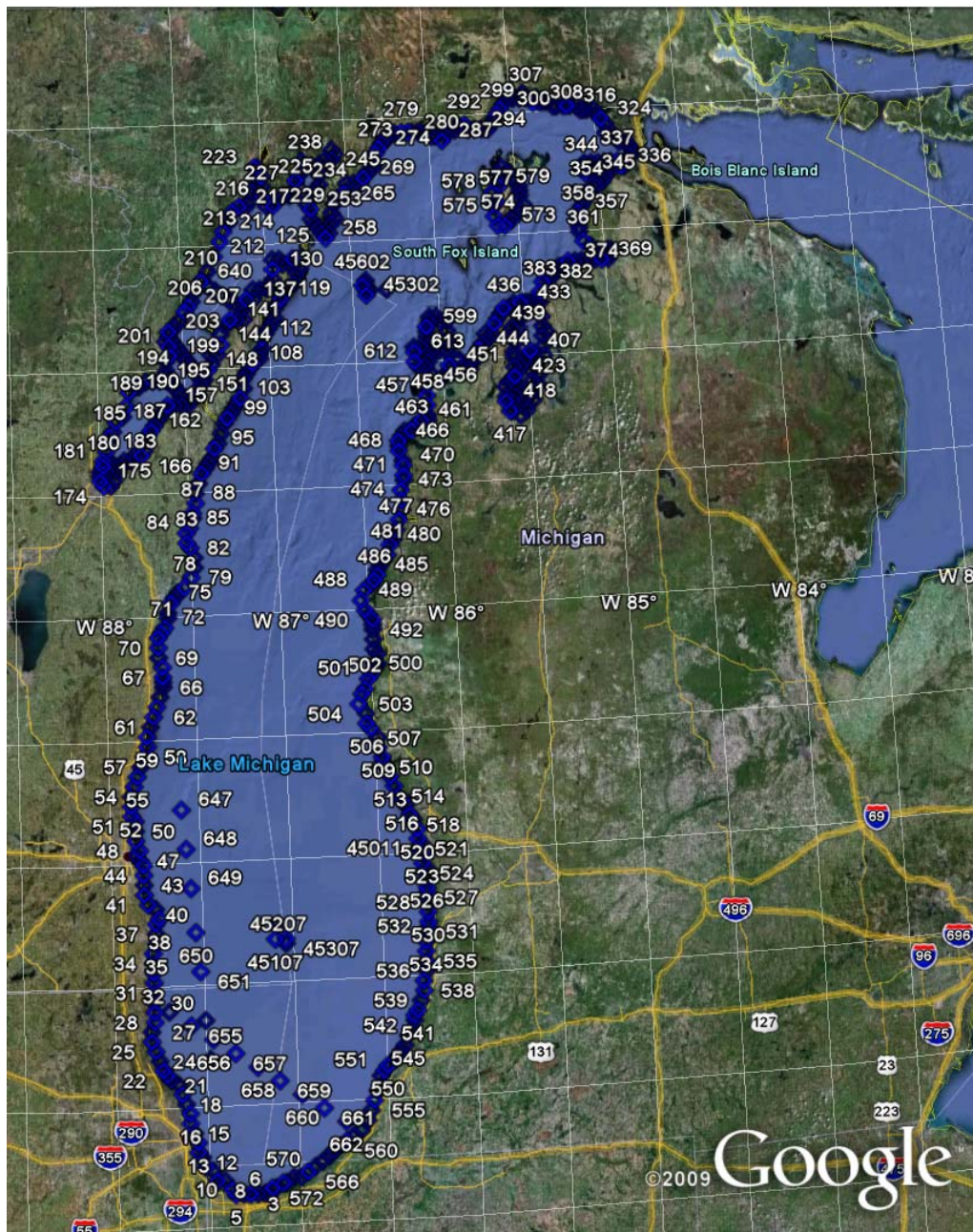


Figure 6-9. Special output locations for the WAM simulations.

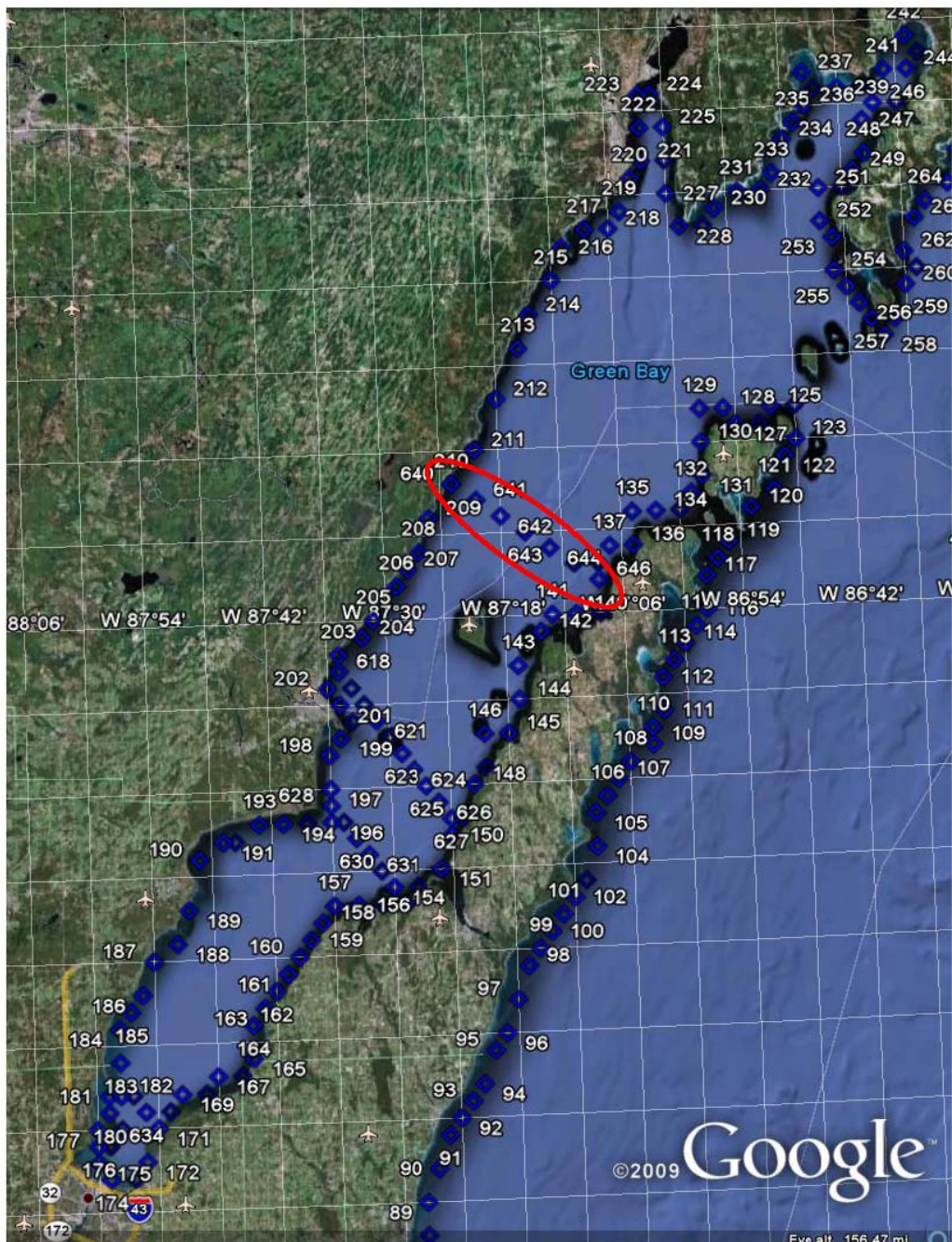


Figure 6-10. Zoom of the Green Bay area. The STWAVE boundary is identified by the red circle.

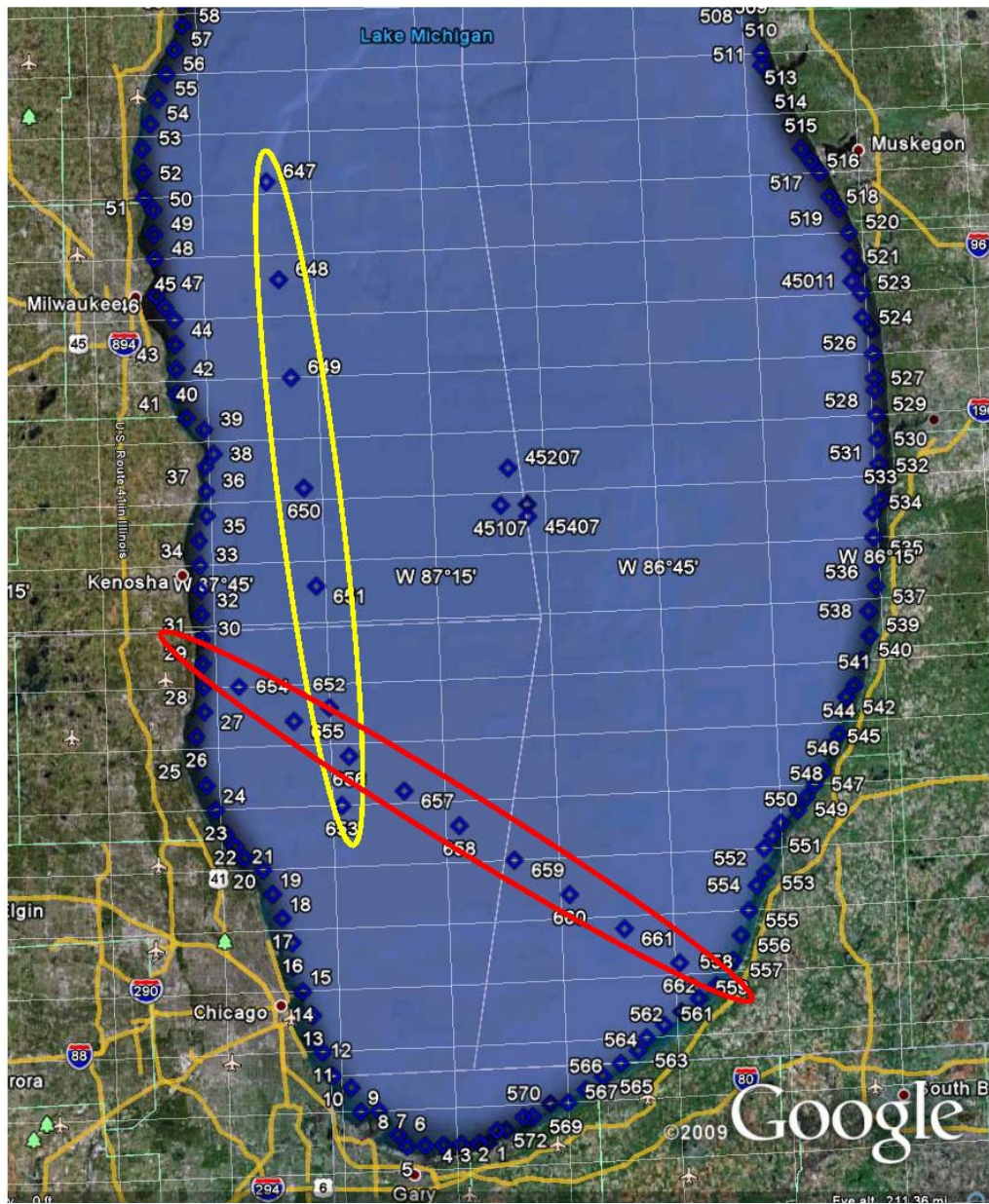


Figure 6-11. Zoom view of the southwestern domain of Lake Michigan, red and green ovals identify the two boundary input locations for STWAVE simulations.

- Generate 2-D spectral estimates for all special output locations including the locations set for STWAVE boundary condition information
- Post-Process Phase II (Quality Control/Quality Assurance, QA/QC)
- If appropriate evaluate the wave model results based on available wave measurements (a total of six locations). Generate time, scatter and Quartile-Quartile graphics; perform statistical tests and tabulate

- Generate Maximum and Mean wave parameter plots for the specified storm (wave height, peak and mean wave period, for the total, wind-sea and swell contribution), wind speed.
- Evaluate all results for consistency and accuracy, and when appropriate ice field specification.
- Archive
- Archive all output information to:
- Mass Storage Facility (ERDC HPC)
- External hard drive on resident PC
- Make all files available to the group
- ADCIRC / STWAVE production
- CSTORM-DB

6.5.1 Post-processing QA/QC

Upon completion of the WAM run (and post-processing of the original WAM output files) a series of graphical products are generated to assure consistency in the storm simulation; identification of the correctness in the ice implementation; and when applicable evaluate WAM results to point source wave measurements. For all extreme storm events occurring pre-1979 there were no wave measurements. In general, there were also no wave measurements in late fall to early spring (November through March) as the NDBC buoys were removed and not redeployed until the spring of the following year. Examples of the QA/QC graphical products are provided in Figures 6-12 through 6-15, displaying CFSR based wind forcing and NNM. The graphics color contour the maximum wind or wave height envelope that exists for a given storm simulation and the overall maxima (and location). The second graphic color contours the overall mean wind or wave height envelope for the storm. A total of 14 plots are generated for various wave parameters (height, parabolic fit wave period for the total, wind-sea, and swell contributions). These figures provide the means to locate any discontinuities in the wind or wave field; identify erroneous (generally elevated wind speeds or wave heights) estimates; and identify any misrepresentation of the ice field for a particular storm simulation.

As previously noted in Chapter 3 the trend in the wind fields derived from the CFSR was a retention of spatial coherency down the centerline of Lake Michigan (Figure 6-12), retaining the synoptic- to meso-scale meteorological conditions. This consistency is further illustrated in the resulting maximum wave height envelope (Figure 6-13). In contrast to this, the NNM, tends to place maxima in close proximity to the land-based meteorological

stations where the data are supplied (Figure 6-14). However, wave models tend to be excellent integrators and rely on the general structure of the wind fields to represent the wave field. This is true for the NNM forced simulations in Lake Michigan where the maximum wave height envelope (Figure 6-15) tends to follow the outline of the lake itself. In general the NNM forced WAM maximum wave height envelope fall closer to the coastline compared to the CFSR winds. Local injection of wind measurements at the land-sea boundary controls these features. This is best illustrated by a distinct shadow zone in the maximum wave height contour graphic for STO127 along the eastern coastline.

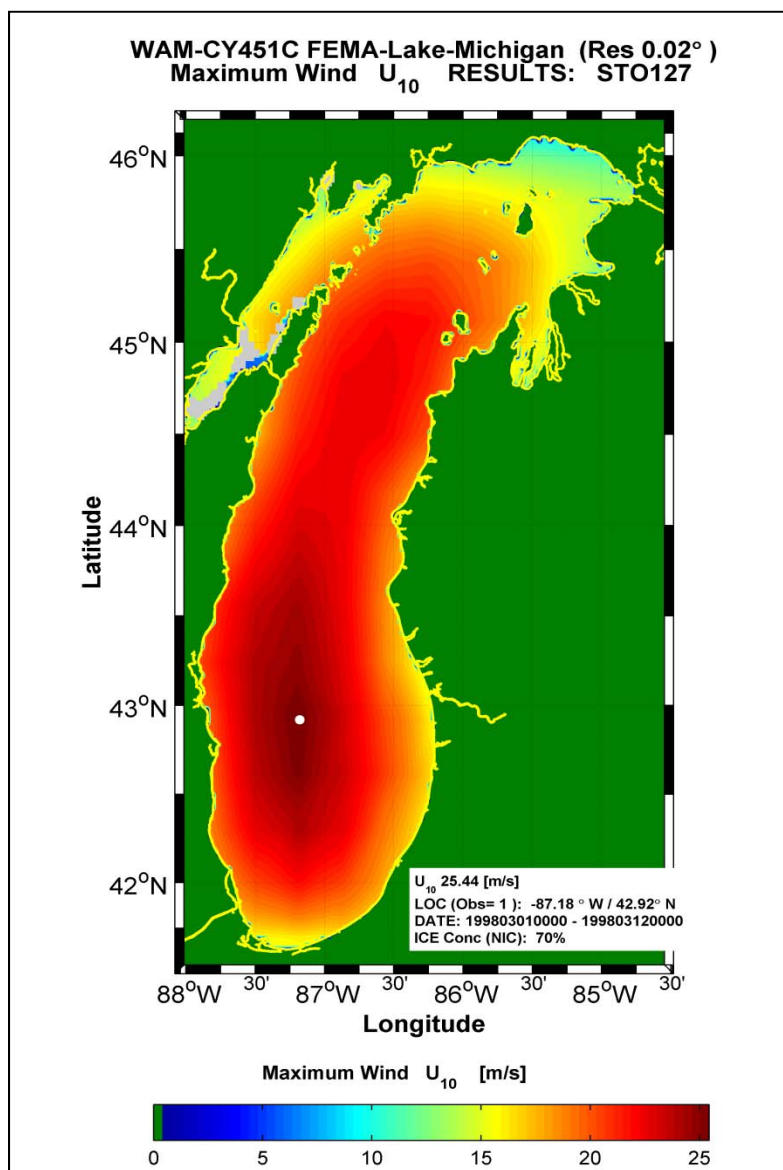


Figure 6-12. Maximum wind speed envelope for STO127 (1-12 March 1998). Note the grey area in lower Green Bay indicating ice cover for the entire storm simulation.

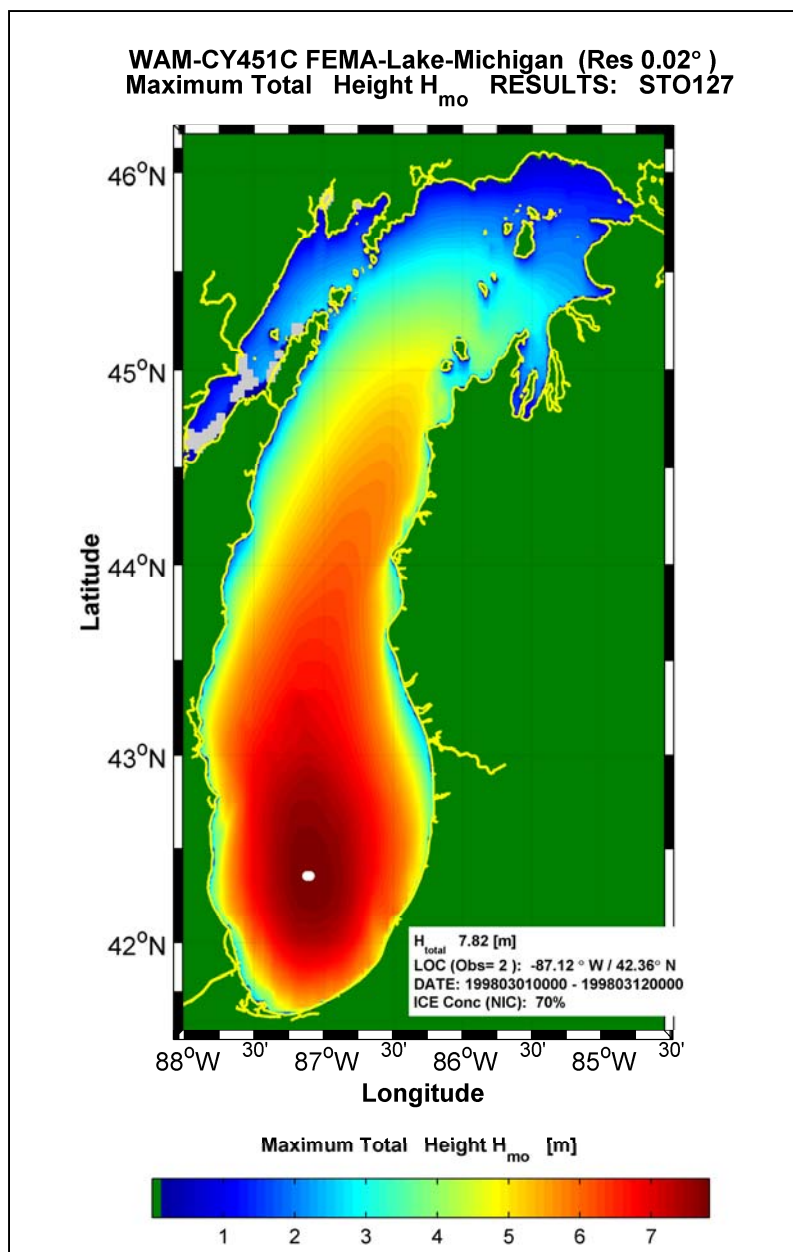


Figure 6-13. Maximum significant wave height envelope for STO127 (1–12 March 1998). Note the grey area in lower Green Bay indicating ice cover for the entire storm simulation.

The second phase of the QA/QC is to evaluate the performance of WAM. Archived point source wave measurements were initiated in the early 1980s (45002 in September 1979; 45007 in July 1980). Therefore, all NNM storm simulations did not contain direct model to measurement evaluations. While this is unfortunate, based on initial evaluations (Chapter 3), the performance of WAM using NNM clearly showed good results. At times the NNM forced wave simulations were better for

locations near the coast (e.g. NDBC 45010 and 45011). Meteorological events containing micro-scale features (thunderstorms, frontal passages) that dominated over synoptic-scale features were better represented in the NNM wind fields compared to that of the CFSR fields.

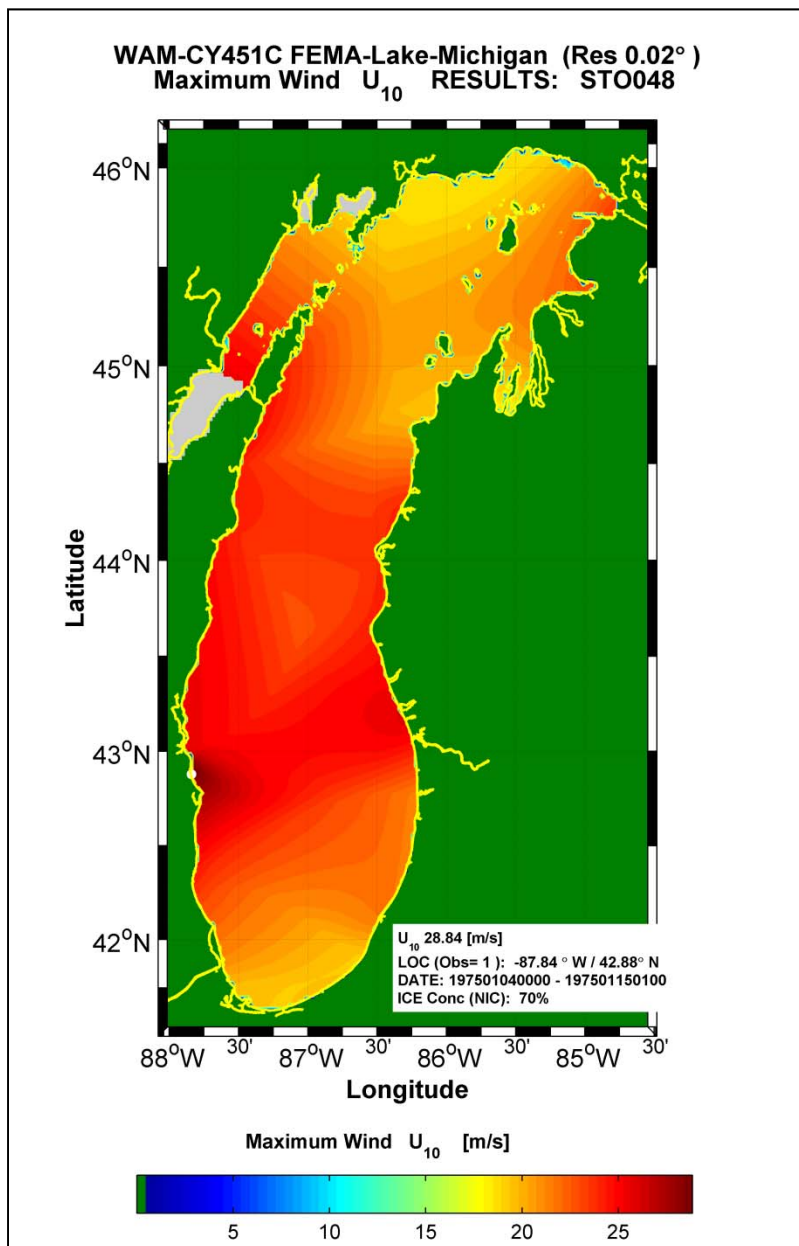


Figure 6-14. Maximum wind speed envelope for STO048 (1 – 15 January 1975). Note the grey area in lower Green Bay indicating ice cover for the entire storm simulation.

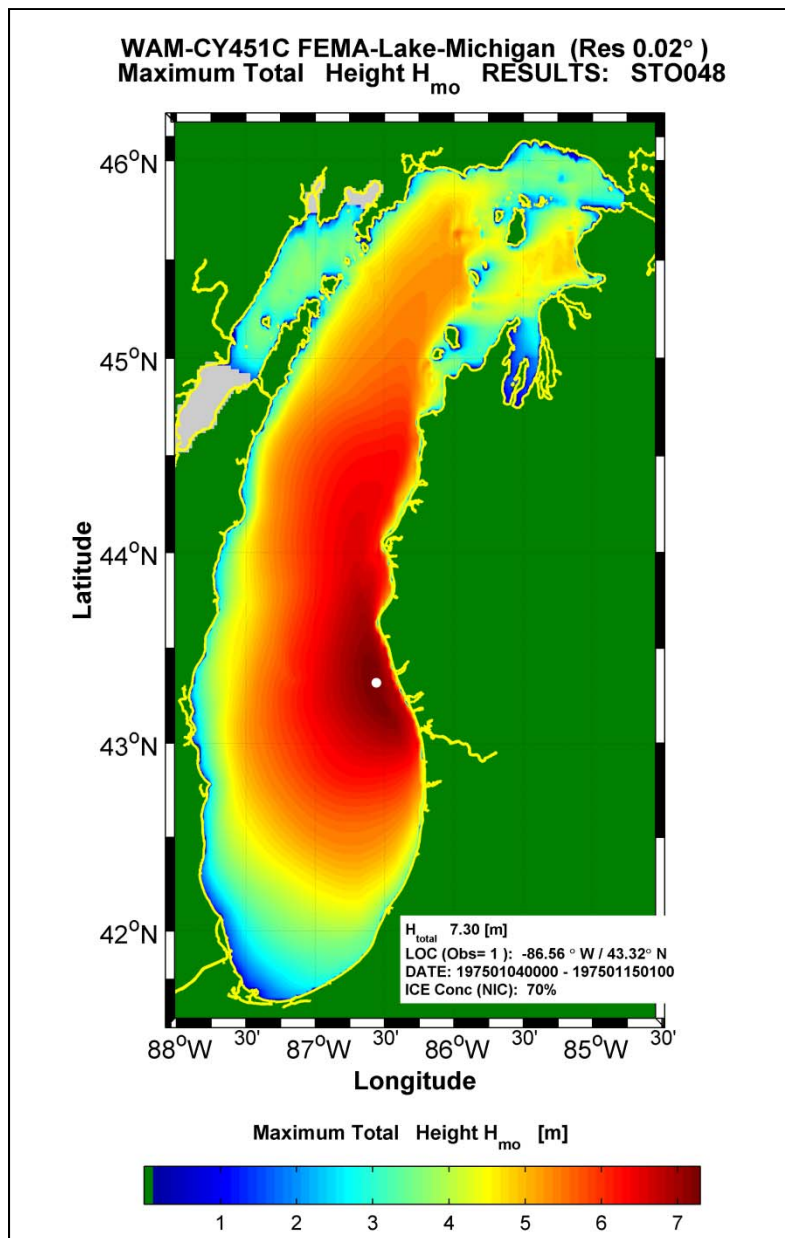


Figure 6-15. Maximum significant wave height envelope for STO048 (1 – 15 January 1975). Note the grey area in lower Green Bay indicating ice cover for the entire storm simulation.

When applicable, the WAM results were evaluated to existing point source measurements in the form of time, scatter, Quartile-Quartile graphical products. A battery of statistical tests was also conducted including:

- Bias
- Absolute Error
- Root Mean Square Error
- Scatter Index

- Skill Score
- Linear Regression
- Symmetric correlation
- Principle correlation
- Slope / intercept
- Systematic error analyses

Examples for STO118 are shown in Figures 6-16 through 6-19. The first is a time plot of model to measurement comparison at 45007 (Figure 6-16). The three panel figure shows the comparison of significant wave height, parabolic fit peak wave period, the mean wave period, the mean wave direction the wind speed and direction. For this example, the WAM results follow the measurements very well, capturing the growth sequences of the two primary events during the simulation. The peak storm wave height is well represented in the model results. The parabolic peak wave period model estimates again follow the buoy data, whereas there is an apparent negative bias in the mean wave period model results. This was originally identified (Chapter 3) as an inconsistency in the frequency range between the model and the measurements. The mean wave direction model estimates follow the buoy data through five directional shifts of 180-deg extremely well. These excellent results were primarily due to a consistency in the CFSR wind fields for STO118 replicating the meteorological scenarios quite well. The focus of the analysis is to assure that the model performs satisfactorily around the storm peaks, for growth and especially the peak conditions. For this example, the peak event occurred around 11 November and WAM captures it very well.

Scatter and Quartile-Quartile plots are presented in Figure 6-17 for the wave parameter evaluations. In addition, summary statistical information is presented in this figure. The graphical products are derived from time-pairing of model and wave measurements. There is no phase shift applied to either data set, and all wave measurements are used. Generally this evaluation uses a 1:1:1 temporal smoothing of the measurements to reduce the geophysical variability. It is a less restrictive approach, and tends to improve the model's performance metrics. However all Lake Michigan evaluations do not apply this smoothing routine. Its intent is to demonstrate the reliability in WAM for rapidly moving meteorological events passing through the Lake Michigan domain, and the ability to capture those events on the time scales they are generated. The results derived from the scatter and Q-Q plots emulate what occurs in the time plot. The distribution of the

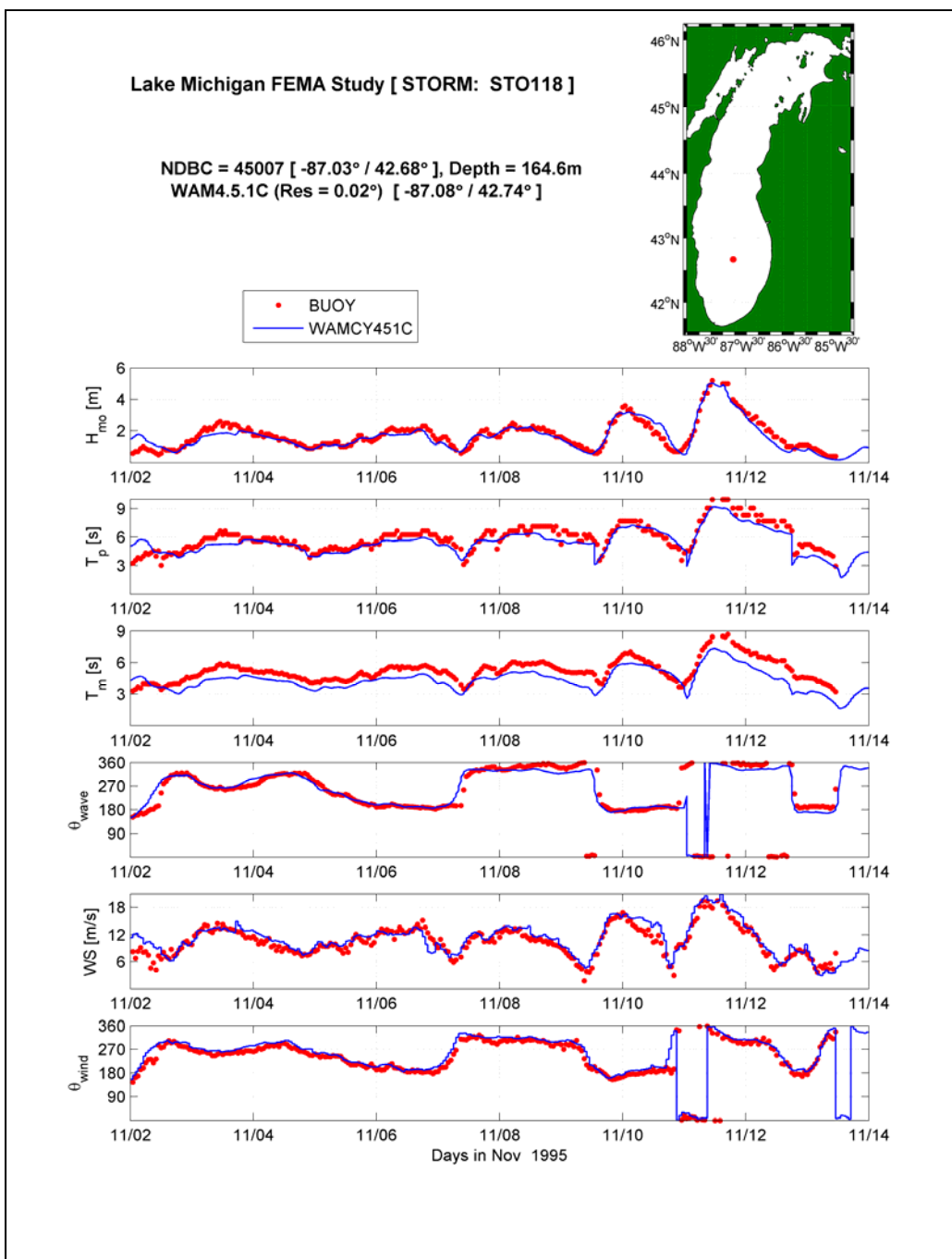


Figure 6-16. Time plot of WAM (blue line) versus measurements at 45007 for Storm 118 (2 - 14 November 1995). Top panel is the significant wave height, next is the parabolic fit peak wave period, mean wave period, vector mean wave direction, wind speed and direction.

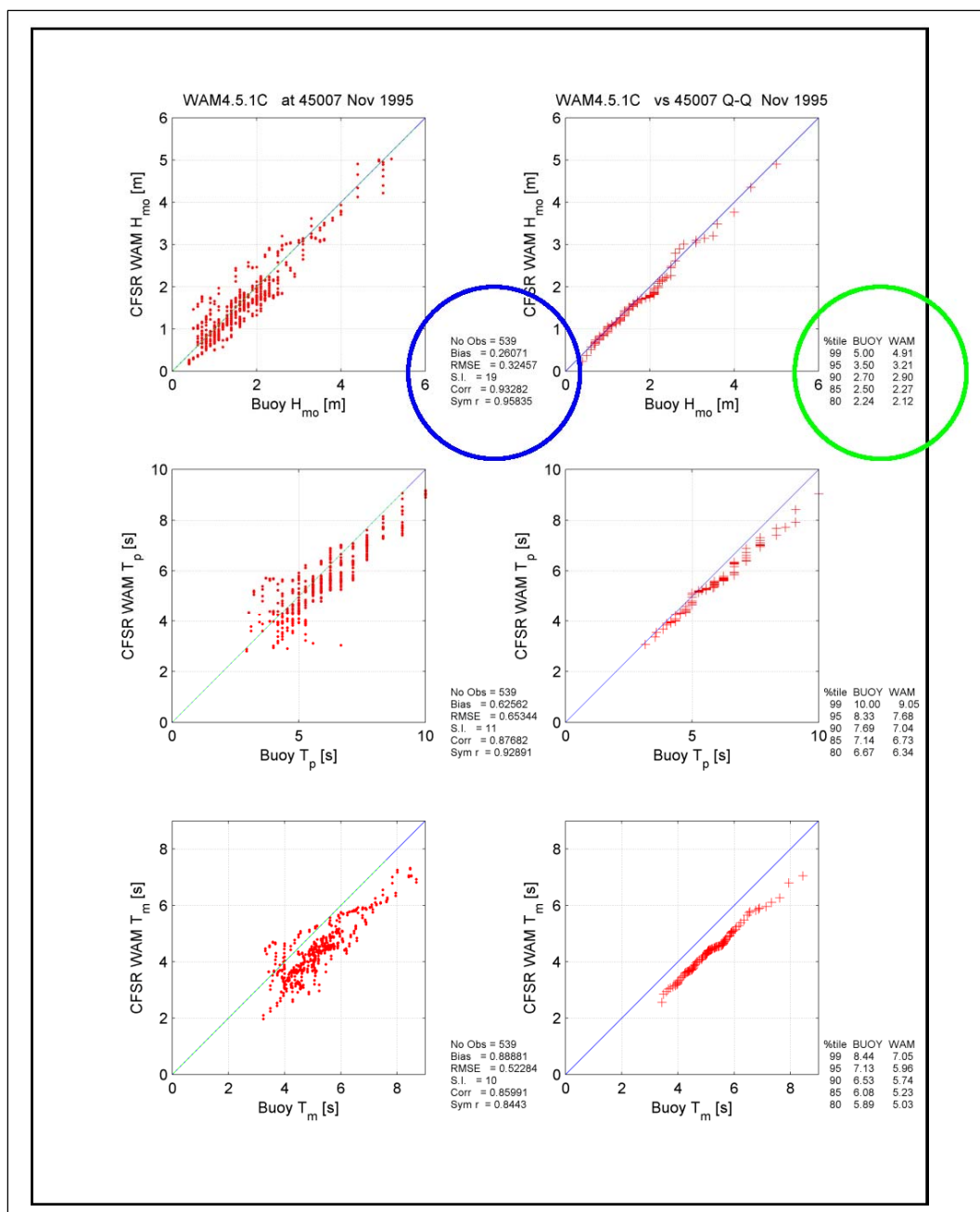


Figure 6-17. Scatter and Q-Q plots of WAM versus measurements at 45007 for Storm 118 (2 – 14 November 1995). Top two panels: significant wave height, followed by parabolic fit peak wave period and mean wave period. Statistical test results are given between the plots.

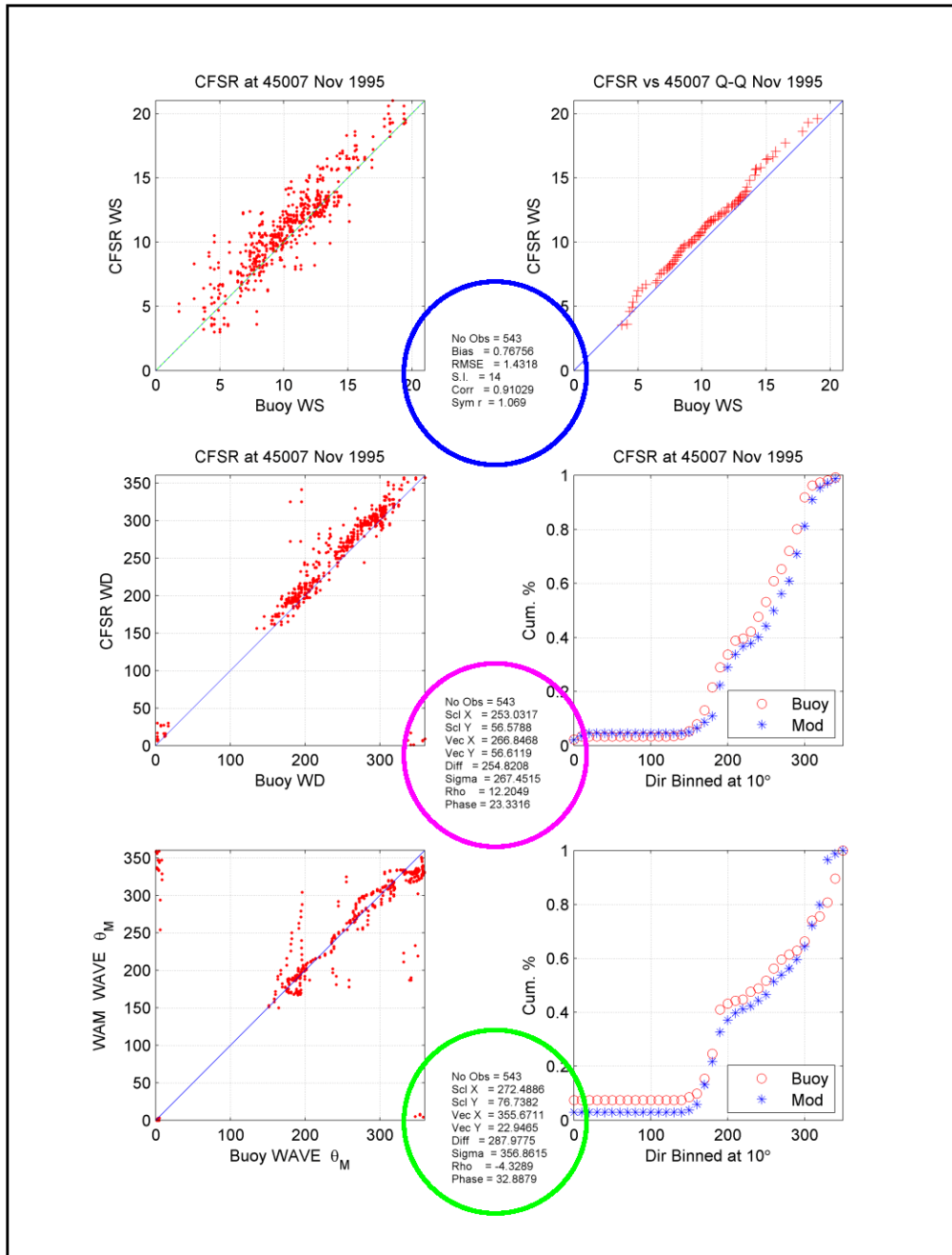


Figure 6-18. Scatter and Q-Q plots of WAM versus measurements at 45007 for Storm 118 (2 – 14 November 1995). Top two panels: wind speed, followed by wind and wave direction. Q-Q analyses are based on scalar values, hence a cumulative distribution replaces this test for the wind and wave directions. Statistical test results are given between the plots.

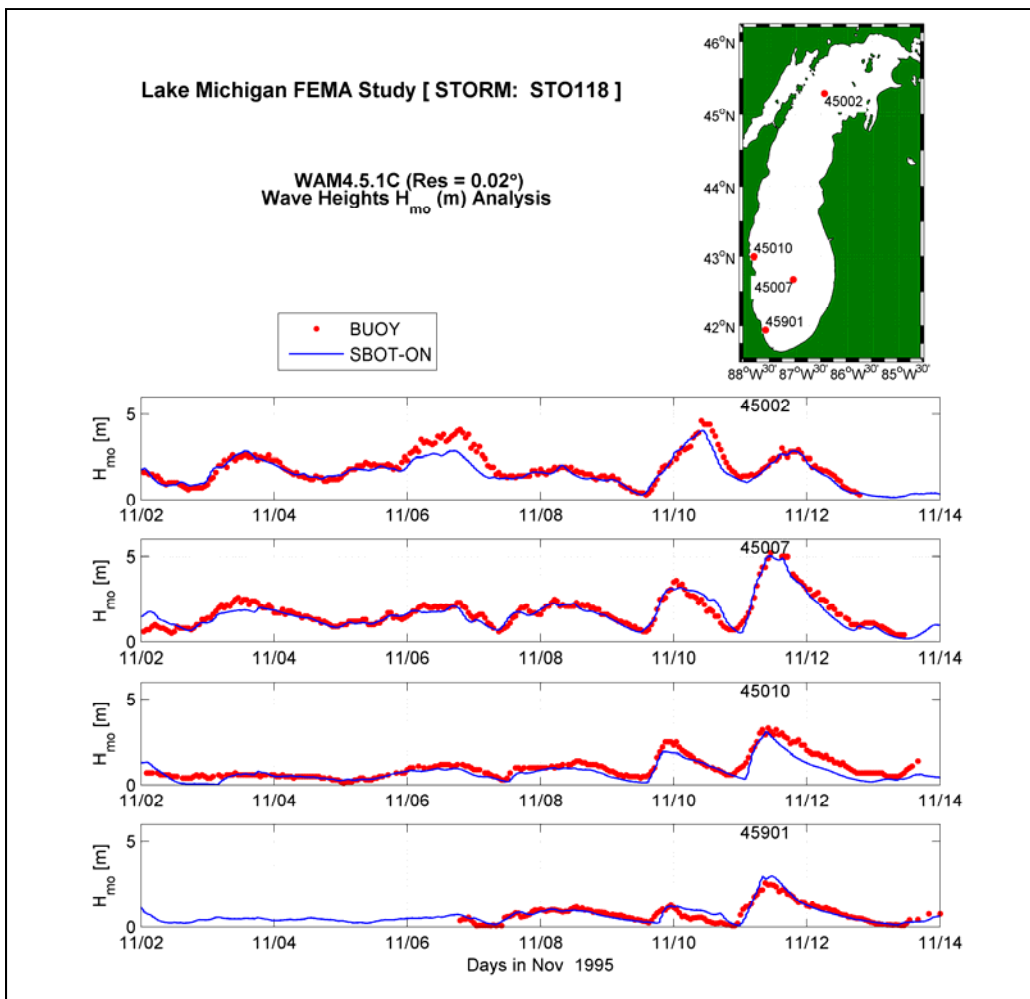


Figure 6-19. Compendium plot of significant wave height comparisons to all available measurement sites for Storm 118 (2 – 14 November 1995).

scatter in wave heights does not have a persistent bias, (0.26-m, blue circle), a RMSE of 0.32-m, a Scatter Index of 19 and a symmetric r (i.e. slope with zero intercept) of 0.958. On the right hand side of Figure 6-17 is the Q-Q plot. This plot shows the cumulative distribution of the parameter provided based on a pre-determined bin where both the model and measurements can be plotted in a consistent fashion. The key of the Q-Q graphic is to match the line of perfect fit, and also approximate the maximum condition (i.e. the highest value). A small portion of these results are shown in a table to the right of the graphic (green circle). For this example, the maximum wave height observed from the buoy data is 5-m, where the WAM results was 4.91-m or about 9-cm low at the storm peak. Similar information is provided for the parabolic fit of the peak wave period (middle panels), and the mean wave period comparisons.

The final graphic provides the wind evaluation (speed and direction) and whenever possible the vector mean wave direction, as shown in Figure 6-18. Similar information are provided (blue circle), however in terms of the directional comparisons, Q-Q analyses are based on scalar information (magenta circle). The conditional information again is to have the model to measurements follow the line of perfect fit as was the case for the wave parameters. A cumulative distribution of the wind and wave direction bins is generated to determine how favorably the model results compare to the measurements. In this case the results demonstrate that, given good winds (Figure 6-18), it is reasonable to assume the wave results will have comparable skill.

The final product (Figure 6-19) contains wave height comparisons at all active stations for a particular event. This compilation shows the consistency in the wave results for the same period, but multiple locations. The ability to compare favorably at many locations demonstrates the consistency in the wind field forcing and the modeling approach over the entire domain. For this example there is a slight bias in the storm event around 7 November at the northern most buoy location, however the other three sites do not indicate a bias. At the peak event of 11 November, it is apparent the wave climate is stronger in the southern portion of Lake Michigan compared to the north, and shows a clear phase difference between the two peaks. In the decay of this storm model results along the western side of Lake Michigan (45010) has a tendency to attenuate the wave energy at a slightly faster rate than that of the data.

6.5.2 Summary of Lake Michigan offshore wave model production

The approach taken simulates wave and storm surge conditions associated the major storm events via computer modeling. Wave conditions and water level conditions are dictated by meteorological events. These events can vary from large-scale synoptic-scale events, meso-scale systems like frontal boundaries to micro-scale systems synonymous with the development of thunderstorm cells. If the meteorology of these events can be accurately quantified, the associated impact of the surge and waves on a coastal reach also can be quantified.

Rather than present all time, scatter, Q-Q graphics, and statistic test results for each storm simulation, the WAM estimates are compared to a composite of all storm simulations containing wave measurements. Analyses are conducted for all storms, and summarized in terms of the

standard statistical evaluations used during the production. In addition, simplified peaks-over-threshold and return period estimates will be carried out for the ten water level sites shown in Figure 6-1.

6.5.2.1 *Wind speed and significant wave height maxima*

The maximum wind speed and wave height location for all 150 extreme storm events is presented in Figure 6-20. This analysis summarizes all storm simulations for the entire Lake Michigan domain to provide an overview of the wind and wave climate of the basin. During some events, portions of the lake were ice covered (generally the coastal regions, or shallow water areas, like Green Bay for example), hence for practical purposes, it is expected the maximum significant wave heights should reside in the central region of Lake Michigan. The wind maxima are more dependent on the track of the synoptic-scale systems passing the area and can occur anywhere in Lake Michigan; however, the methods to extract these events were dependent on water level data, or long-term land-based meteorological station information.

As found in the maximum wind and wave height envelope examples (Figures 6-12 through 6-15) there was a general trend in the NNM forced WAM simulation to place the maximum wave height lobes in a more coastal position compared to the CFSR forced simulation. This affect is clearly evident in the Figure 6-20. The wind maxima derived from the CFSR are, in general, located along the central north-south axis of Lake Michigan (red symbols), while the accompanying wave height maxima follow suit (blue symbols). In addition, there is an increased population of wave height maxima in the southern domain of the lake suggesting that many of the storms selected were northerlies. The NNM wind maxima clearly are dependent on land-based meteorological station inputs (magenta symbols). The locations for these peak wind speeds clearly are relatively uniformly spaced along the Lake Michigan coastline with exception to the mid-lake region, where as noted in Chapter 1, the isotacs in this area are generally in a west-to-easterly direction. This affect was primarily due to a consistency between western and eastern coastal meteorological stations measuring similar winds. It is also fairly apparent from Figure 6-20 that most of the earlier extreme storms were generated either by northerly or westerly events.

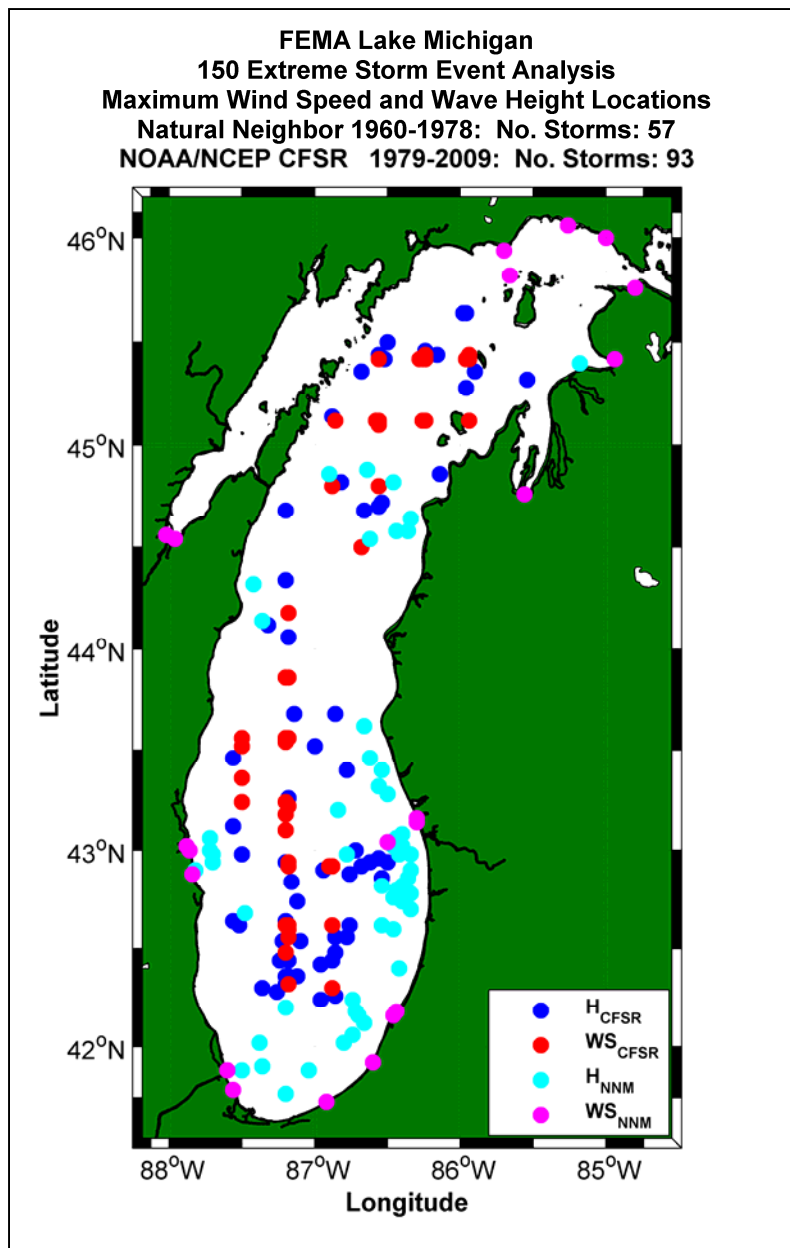


Figure 6-20. Overall maximum wind speed and significant wave height locations for the 150 extreme storm event population.

Figure 6-21 illustrates the results of this summary analysis. For the given population of wind events, it is clearly shown that the maximum wind speed falls between 15- to 30-m/sec with a mean value of 20.6 m/sec, and variance of 9.5-m/sec. These results fall within the range of the offshore NDBC buoy long-term wind records for their recorded annual maximum of about 16 m/sec at 45002 and 17 m/sec at 45007, (http://www.ndbc.noaa.gov/view_climplot.php?station=45002&meas=ws). The sampling of the major storm events based on Figure 6-21 is well supported by the limited data source. In addition, the

peak wave height event 11 November 1998 (1998111100) of 8.7-m was caused by a storm similar to an earlier storm (10 November 1975) that sank the Edmund Fitzgerald, Lombardy (2002).

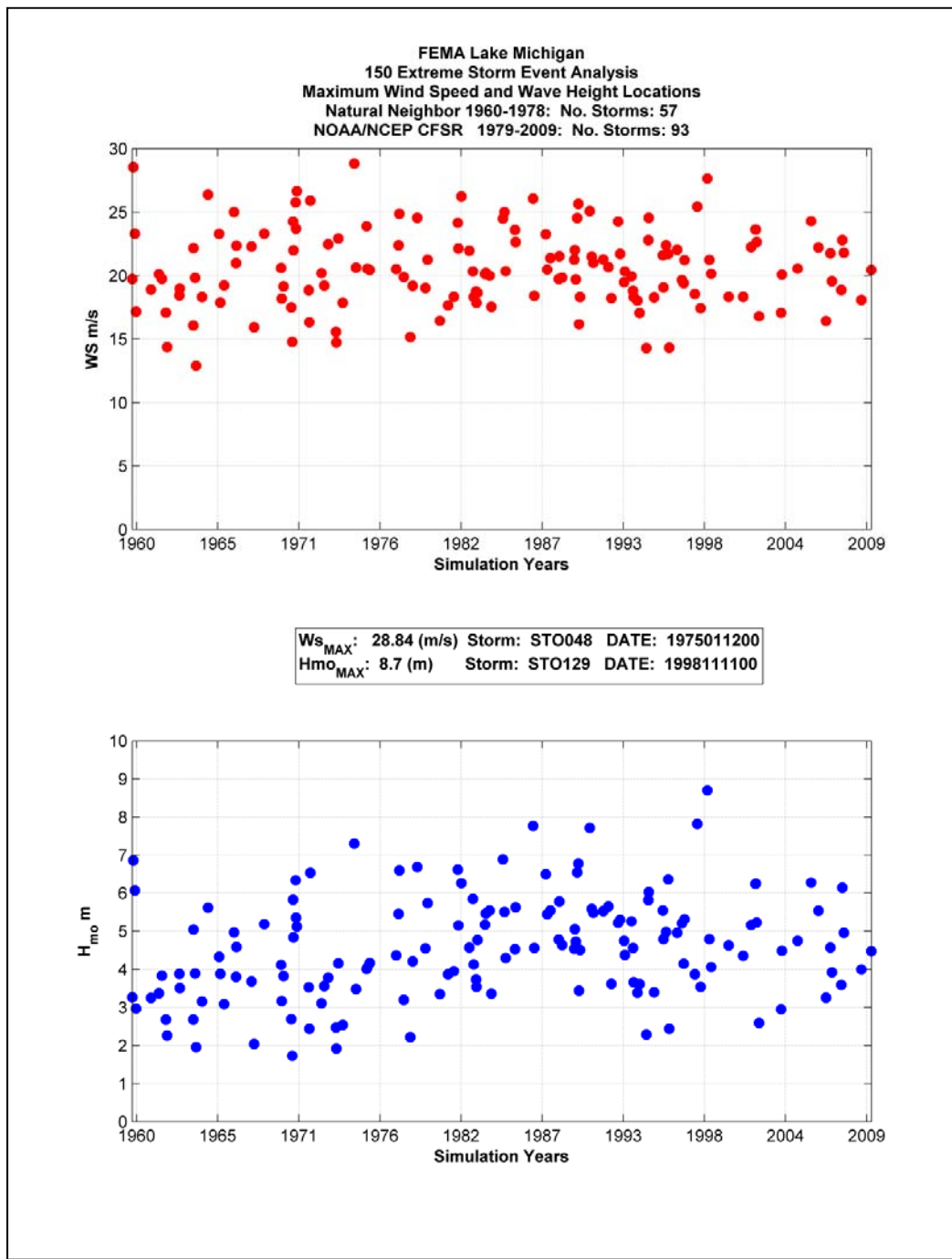


Figure 6-21. Magnitudes of the maximum wind speed (upper panel) and significant wave height (lower panel) for the 150 extreme storm events.

The wave height population is more scattered compared to the wind speed maxima. This in part is caused by the duration of the event, storm track, the relative amount of icing in the lake when the storm is present. However, the mean of all storm wave maximums is approximately 4.6-m with a variance of 1.8-m. Looking again to the two NDBC moored wave buoys, these results are consistent with the observations of about 4.5-m (45002) and 4.1-m (45007). Considering that these buoys are generally removed for the winter seasons, the results do appear to be consistent. One additional factor that must be considered is any distinct difference in the results from the two wind field forcing sources, and not caused by intra-annual climate variability. The mean wind speed maximum for the 57 storm events using NNM is 20.4-m/sec with a variance of 13.1-m/sec; the mean wind speed maximum for the 93 storm events using CFSR is 20.7-m/sec with a variance of 7.3-m/sec. Over the mean, the two are quite similar; however, there is a larger variation in the NNM winds which one would expect because the number of meteorological stations decrease over time and the variability between station information is more random than one would expect derived from an atmospheric model. In addition the CFSR population is nearly a factor of two larger than the NNM results, and can adversely affect the outcome if this analysis. The mean wave height maxima for the NNM is about 4.0-m (with a variance of 1.8-m) while the CFSR population is 4.9-m (and variance of 1.5-m). The cause of this is evident in Figure 6-21 where the number of maximum significant wave heights lower than 3-m is greater for the NNM population than CFSR. Given this, and the population size differences, wave height values skew lower for NNM, resulting in the 0.9-m difference. Based on the general results provided here, it does not seem as though the application of two different wind forcing methods has a large impact on the overall maximum wind speed and wave height results.

6.5.2.2 Point-source evaluation winds /waves

During the execution of the 150 extreme storm events the wind and wave model results were evaluated to point source measurements. Table 6-2 summarizes the number of point-source measurements available. The results of that analysis are summarized below. At most there were six wave measurement sites (see Figure 6-1), however not all were in operation during the same time period and in many cases were not deployed during an individual event. Summary graphics (scatter, bin-averaged, Quartile-Quartile plots) and results from a portion of the statistical analyses are presented. A peak-to-peak analysis was also performed on the model to

Table 6-2. Peak-to-peak analysis results.

Station No.	No. Storms / No. Peaks	No. Obs.	Threshold (m)	Regression Results	
				Slope	Intercept
45002	42 / 90	13060	2.61	0.880	0.107
45007	37 / 63	10892	2.81	0.850	0.112
45010	4 / 12	1201	1.62	0.686	0.074
45901 Chicago Harbor	32 / 69	8220	1.26	0.796	0.158
45900 Burns Harbor	8 / 20	2279	1.15	0.843	0.020

buoy data for: 45002, 45007, 45010, Burns Harbor (45900¹), and Chicago Harbor (45901). These sites provided the largest population of time paired model to observations. The NDBC 45011, and the Pentwater (45902) locations did not have either any data during any of the storm events, or the population size was extremely small to provide proper evaluations. Lastly, as previously noted, all evaluations are based on CFSR wind forcing. The NDBC buoys were initially deployed during the summer of 1979 (45002) or 1981 (45007). The nearshore wave gage (Burns and Chicago Harbor) data were confined to the early 2000's.

The procedure concatenated all time paired sets resulting from all extreme storm simulations, and then graphically presented the results. No averaging of the wind or wave measurements was made; only the time stamp on all data were set to the closest one-half hour to coincide with the model results. The graphics provide a general indication of the quality in the modeled wave results, and also the consistency in the wind estimates. One must note that not all 150 storm simulations were evaluated. Out of the 150 events, 90 were during the period of wave measurements. Of the 90 storms simulated the number of storms compared to each buoy is summarized as:

- NDBC 45002: 41 Storms
- NDBC 45007: 37 Storms
- NDBC 45010: 4 Storms
- Chicago Harbor: 32 Storms
- Burns Harbor: 8 Storms.

¹ Note that both Burns Harbor and Chicago Harbor sites were renamed to 45900 and 45901 for convenience in all comparisons.

This does not mean data exist for both the winds and waves. It only indicates there is a potential for evaluations as summarized in Figure 6-22. One of the impediments in this evaluation is that the Chicago and Burns Harbor wave gages had a pre-determined threshold of 0.2-m. If wave energy existed, the potential for flagging it as NO DATA was prevalent in the data archive. This would introduce some questions, especially during the winter months when ice was present.

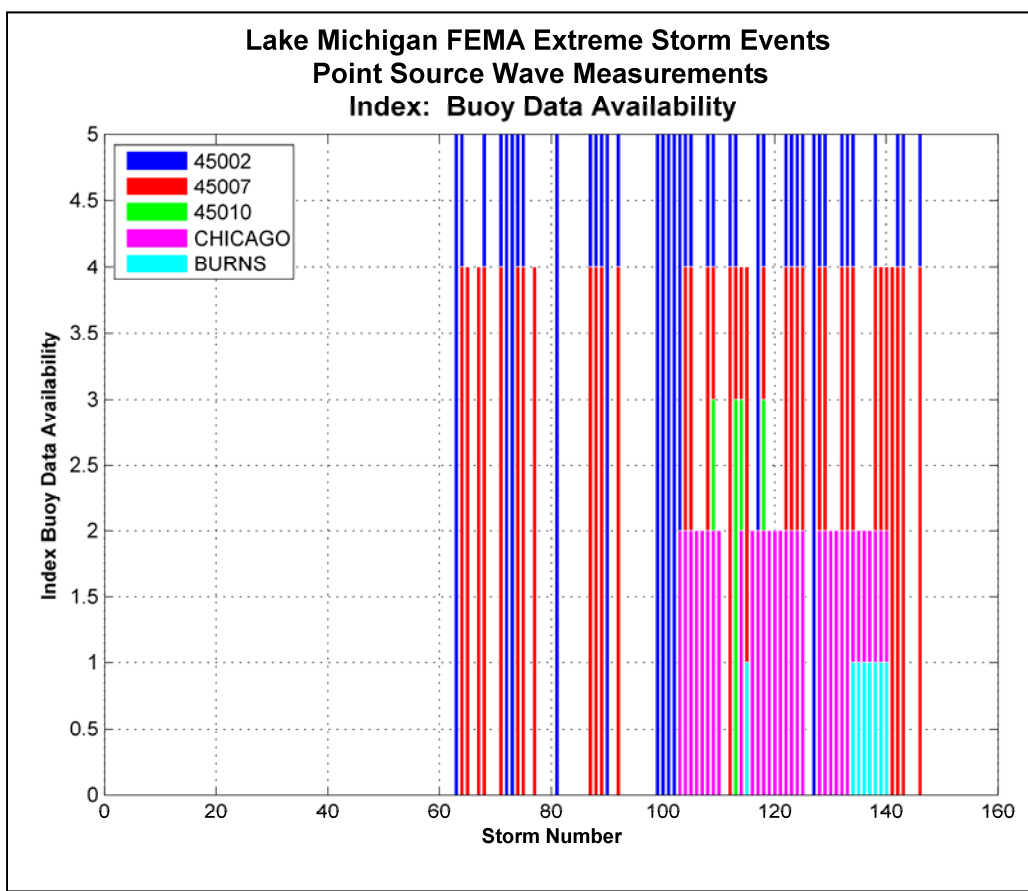


Figure 6-22. Measurement availability for the five buoy sites during the 150 extreme storm event simulation. Location of wave measurement sites found in Figure 6-1.

Results for NDBC 45002 versus WAM and CFSR (significant wave height, and wind speed, respectively) are presented in Figures 6-23 and 6-24. For the approximately 41 Storm simulations, WAM compares favorably to the wave measurements. The scatter rarely exceeds the 95-percent confidence limits. When it does, the wave heights are generally less than 2-m, far below the maximum wave conditions expected at the storm peak. Over the average, and based on the symmetric slope (i.e. setting the intercept to 0.0), the relative error is about 3.4-percent which is considered quite good. There is a slight positive bias in the lower wave height WAM results where the lobe of

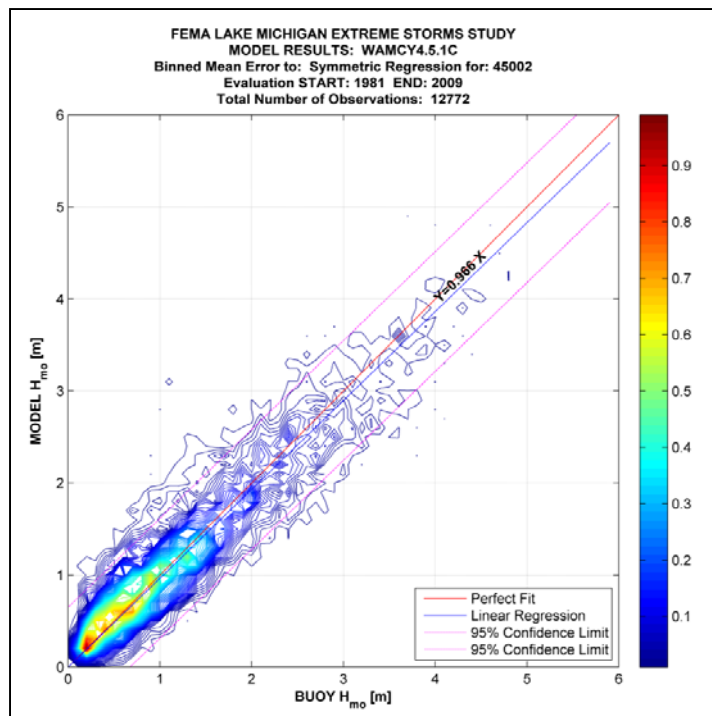


Figure 6-23. Color contour of time paired significant wave heights, buoy to WAM for NDBC 45002.

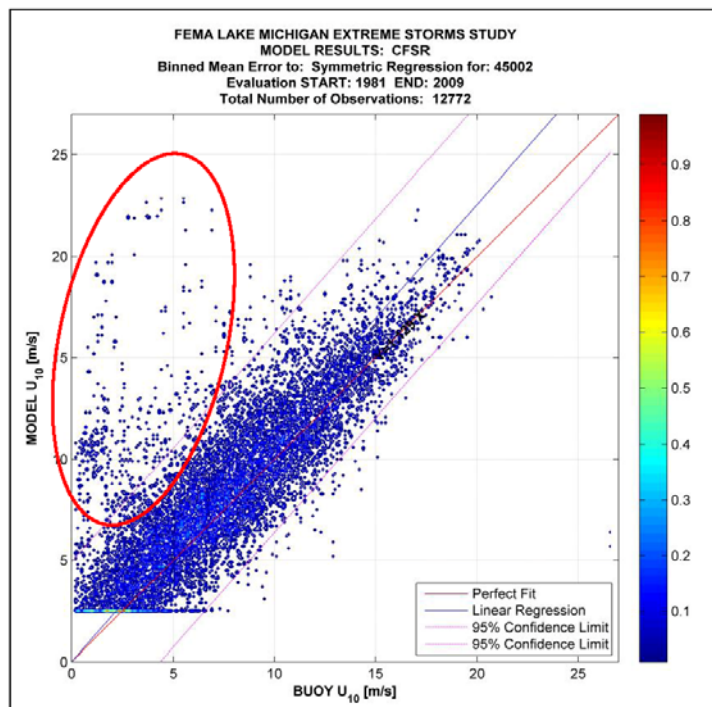


Figure 6-24. Color contour of time paired equivalent neutral stable 10-m wind speeds, buoy to CFSR for NDBC 45002.

higher percentages (e.g. red contour intervals) fall above the line of perfect fit. At the upper limit of the distribution, there does not appear to be the biases found in the lower intervals. The wind speed evaluation shows some similarities to the height distributions, but with a larger amount of scatter. One of the obvious features found in Figure 6-23 is a threshold of 2.5-m/sec, set on the CFSR wind estimates. Initial forensics analysis indicated under very low wind speeds the CFSR wind estimates were highly variable. By setting a threshold of 2.5-m/sec this reduced the noise level imposed in wind-wave growth. More importantly, this limit would have only a very slight increase in the wave energy at very low wave heights (as indicated by the positive bias at about 0.25-m in 6-23). It would have literally no impact at the extreme storm peak condition. There are situations where the CFSR winds are significantly positive biased (red oval area defined in 6-24). These results were all derived from one storm event STO141 where the CFSR winds were nearly a factor of two greater (12- to 20-m/sec) than the reported buoy measurements. There were no wave measurements at the time. However during this event the southern NDBC buoy was actively reporting winds in the range of the CFSR estimates with peak wave heights of 3.5- to 4.0-m. Thus, it seems clear the buoy data were in error during this time for some unknown reason. Lastly, over the average, the CFSR wind speeds are biased high by about 13-percent (symmetric regression), which is counter intuitive because the modeled significant wave heights show a negative bias. However, this evaluation is at one point in the middle of Lake Michigan, and roughly 5-percent of the winds used in this evaluation could conceivably be questioned (STO141), thus reducing the overall result.

The evaluation of the wind and wave results continues at the second long-term site NDBC 45007. The results are presented in Figures 6-25 and 6-26 for the significant wave height and wind speed, respectively. The significant wave height distribution generally emulates that found in the previous case. The scatter above and below the line of perfect fit is fairly well balanced, there is some over estimation in the wave heights below 2.0-m which affects the overall error negatively to 6.3-percent. The lobe of highest concentrated population is spread over roughly 1.0-m compared to 0.25-m in the case at 44002. From these time-paired data sets, it is evident the wave climate is slightly more elevated than at the northern station, suggesting a slight weighting of the extreme storm events toward northerly wind conditions. Another explanation is that, in Lake Michigan, wave heights are greater in the south than the north, which is essentially stating the same thing. One

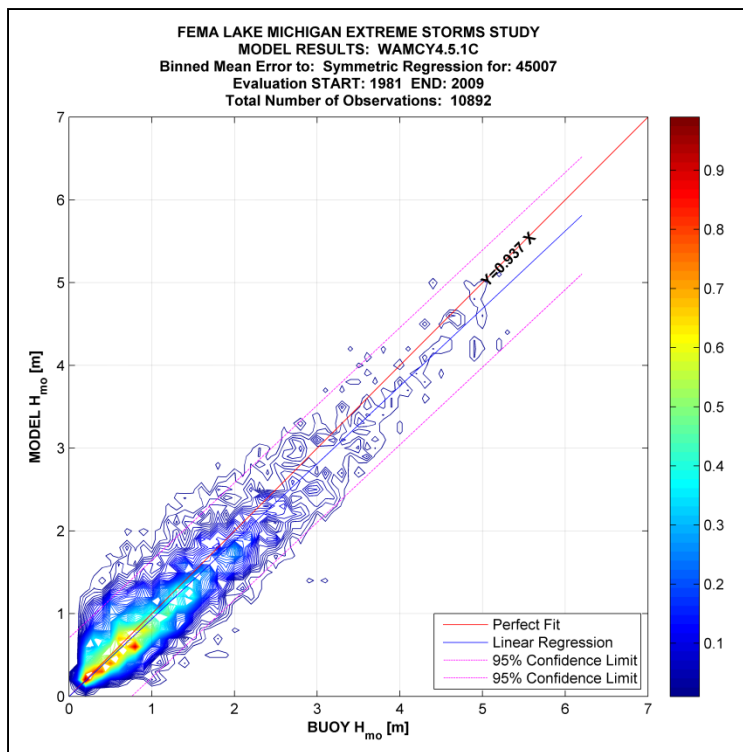


Figure 6-25. Color contour of time paired significant wave heights, buoy to WAM for NDBC 45007.

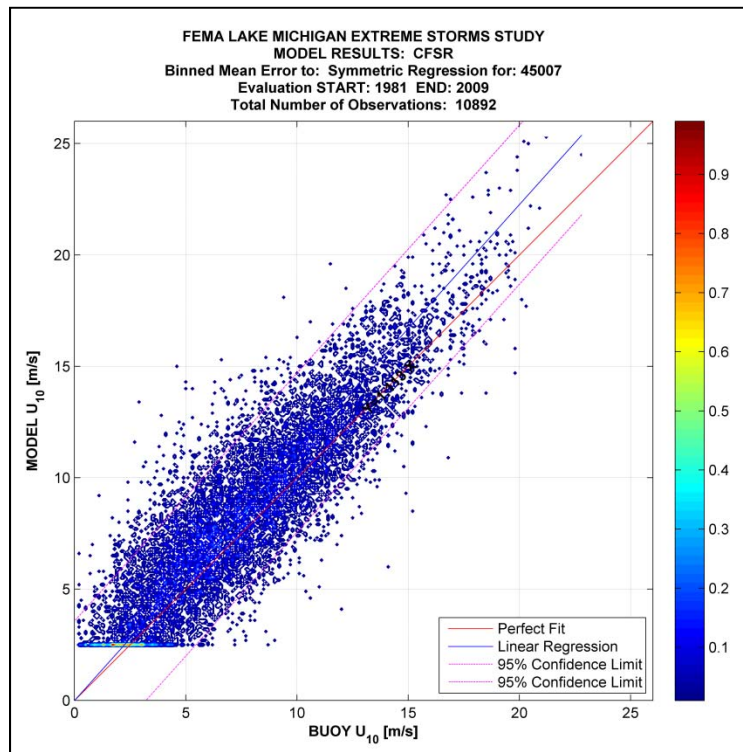


Figure 6-26. Color contour of time paired equivalent neutral stable 10-m wind speeds, buoy to CFSR for NDBC 45007.

must also realize the two comparison sites may not examine all of the identical storm simulations. The intra-annual variability of deployment cycles for the northern (45002) and southern (45007) differ as well as failure rates of the sensor packages.

The CFSR wind estimates compared to the buoy (45007) measurements show far more scatter (Figure 6-26) than the wave heights; however, the bulk of these time paired data sets remain, in general, within the 95-percent confidence limits. The threshold of 2.5-m/sec used on the CFSR estimates remains the same, while the overall error is biased positively at about 11-percent. Holding wind speed errors to about 10-percent is the general level most Weather Prediction Centers try to achieve. Considering that the CFSR wind fields were constructed in a hindcast mode rather than in an operational forecast, these errors seem to be somewhat elevated. The net impact on the wave heights remain low, but with a negative bias.

The remaining offshore NDBC measurement site is 45010, just offshore of Milwaukee, WI. The buoy when deployed was a 2.4-m foam discuss buoy a change from 45002 and 45007, based on a 3-m aluminum discus buoy. The anemometer elevation was 3.2-m above the free surface, compared to 5.0-m¹. Lastly, because of its location, this site could have potentially been in the land/sea interface susceptible to land effects such as the diurnal land/sea breeze oscillation. Local meteorological effects will play a role on changing the synoptic-scale events. Clearly the CFSR wind fields were derived from 0.5-deg resolution fields and interpolated to 0.02-deg; however, the land/water mask was not carried through this procedure. Hence, the land/water interface would be spread over a number of grid points, and linearly smoothed, compared to an abrupt interface common to the scales of the local conditions. This is an interesting research topic; there is sufficient data in the area (land based meteorological stations, Coastal Marine Automated Network at the land/water interface) along with the buoy data to evaluate this impact, however is beyond the scope of the study.

As found in Figures 6-27 (significant wave height color contour plot) and 6-28, the WAM results and CFSR are biased low. The relative population size reflects that 45010 was deployed during four storm events. Out of the four (one with limited data), two storms (STO109 and STO113) resulting in significant wave heights of about 2.5-m derived from two northerly events.

¹ Note that winds speeds were adjusted to an equivalent neutral stable 10-m wind based on a PBL model accounting for stability and anemometer elevation.

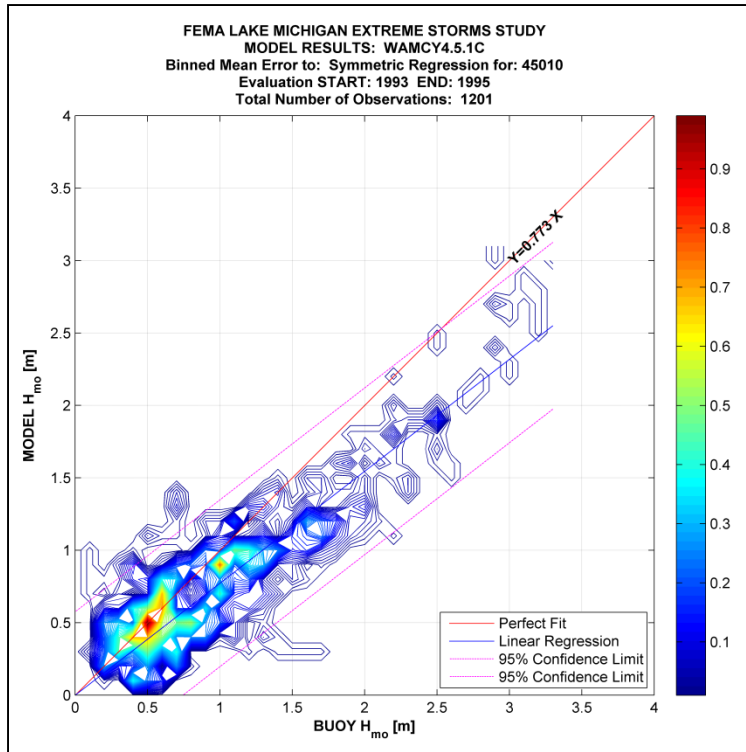


Figure 6-27. Color contour of time paired significant wave heights, buoy to WAM for NDBC 45010.

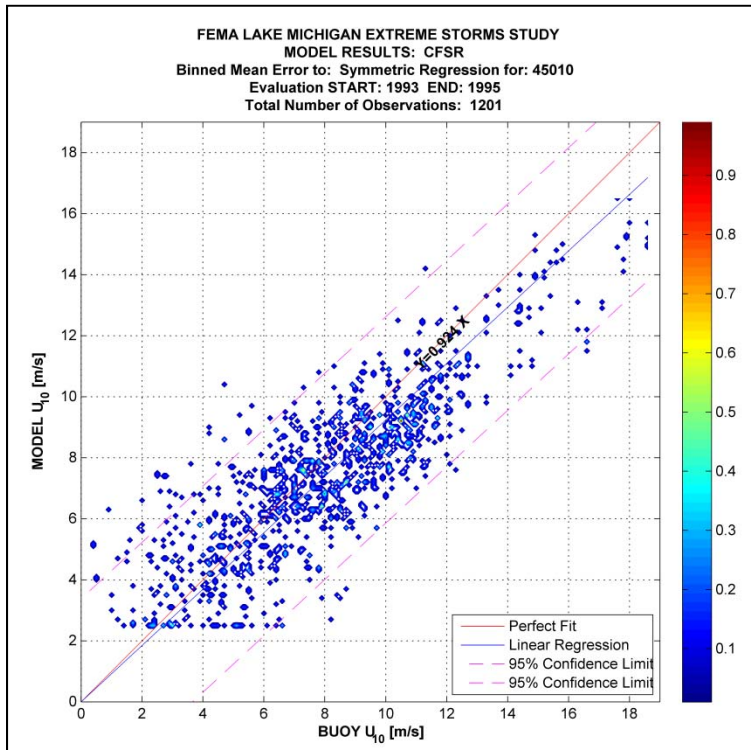


Figure 6-28. Color contour of time paired equivalent neutral stable 10-m wind speeds, buoy to CFSR for NDBC 45010.

Those events also contained local winds that were not captured by the CFSR wind field estimates allowing for this under-estimation in the wind speeds. The population lobe at about 2.5-m (relative to the measurements) found in Figure 6-27 is the result of the wind under-estimation (of roughly 4-m/sec). One storm (see Figure 6-19) the WAM results were considerably better, and at time slightly low during the extreme storm peak, while missing one event earlier on in the simulation.

The remaining time paired color scatter plots of significant wave heights for the two nearshore gage locations (Burns and Chicago Harbor) are displayed in Figures 6-29 and 6-30. As previously noted, the gages were deployed during the winter months. The time pairing methodology would remove both data sets when the model and measurements were flagged. However, if only one of the two data sets were flagged, both would be plotted. For no flagged gage data and finite wave model results, the color contours would be present along the ordinate; if the gage reported waves and the model flagged for ice, the contours would align with the abscissa. For the Burns Harbor comparison (Figure 6-29) there is a near uniform distribution along both the X and Y axes, suggesting both occurrences exist. A strong conclusion cannot be made because the gage data also removes any wave height less than 0.2-m, and is identified as NO DATA. There eventually would be some question as to what caused the flag; either a low wave condition caused by no energy in the region, or low wave energy caused by icing. In general, however the WAM estimates show good agreement throughout the measurement range, and yield about a 10-percent error over the mean. The final contour plot is derived from the time paired observations from Chicago Harbor (ST 45901, Figure 6-30). There is a strong tendency for WAM to over-estimate either low wave conditions or iced conditions compared to the measurements (red oval). However, these wave heights are relatively small and for the extreme storm event focus of the study are in general not relevant. In the upper range (significant wave heights in excess of 1.5-m) the WAM results are quite reasonable, and over the average, perform very well. One has to realize that this is an average error where the over-estimation in the lower range of wave heights is somewhat balanced by the under-estimation in the mid-range estimates.

The final evaluation analysis is based on the Quartile-Quartile (Q-Q) graphic. This analysis is based on recovering the cumulative distribution of two populations, and setting the discrete range of the population into identical sub-sets. This analysis is to be able to analyze a unique percentile,

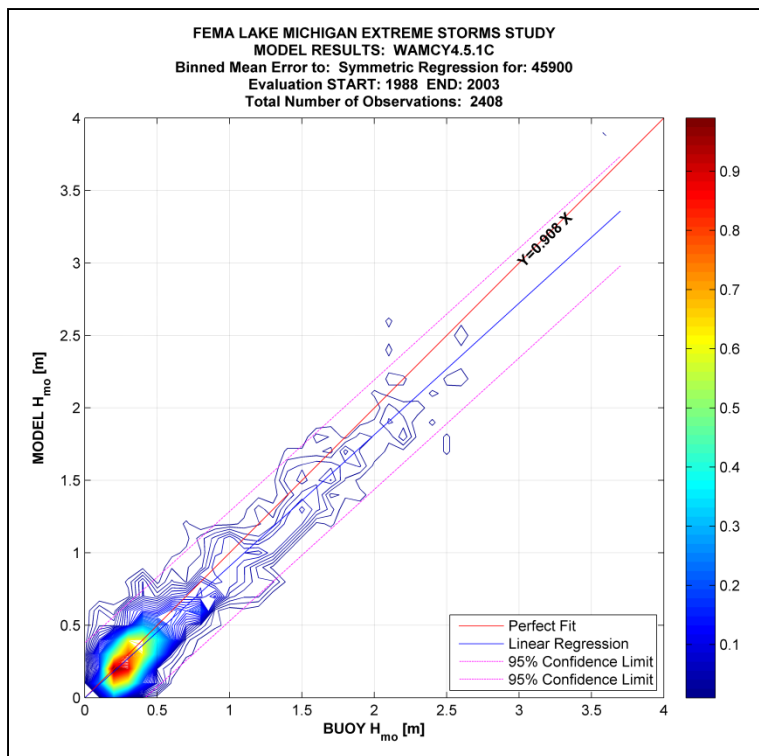


Figure 6-29. Color contour of time paired significant wave heights, buoy to WAM for Burns Harbor ST 45900.

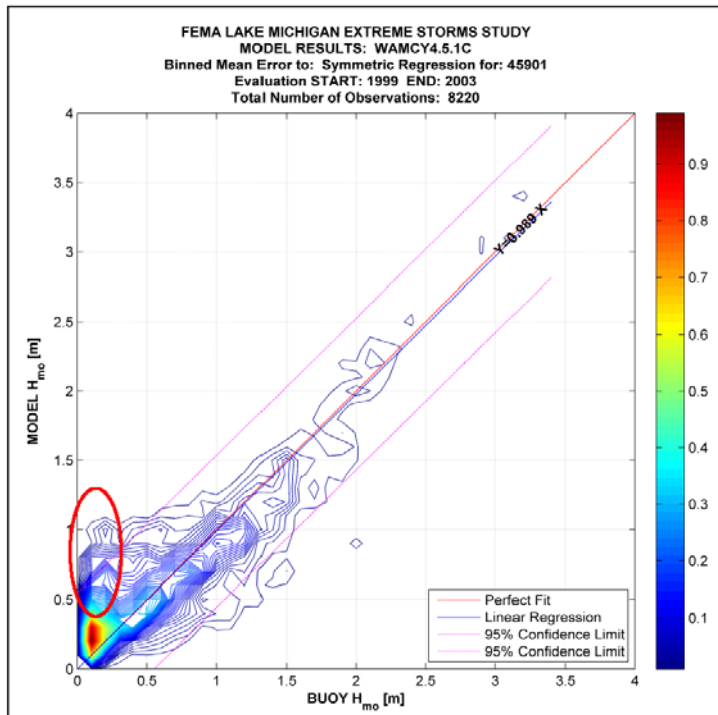


Figure 6-30. Color contour of time paired significant wave heights, buoy to WAM for Chicago Harbor ST 45901.

mainly in the higher ranges (e.g., 50th, 90th, 95th, 99th). The only assumption used in the procedure is that all sub-ranges for the two data sets are linearly interpolated to a unique set. Although the two data sets (model and measurements) are time paired, this method removes the time dependency from the procedure. A 0.1-percentage was used for the significant wave height resolution, to accommodate the 99.1- through 99.9-percentiles.

There will be two sets of symbols plotted in Figures 6-31 through 6-34 (45002, 45007, 45900, and 45901, respectively), significant wave heights for percentiles less than 99-percent, and remaining wave heights in the range of the top one-percent (identified by the green oval in Figure 6-31).

The general relationship between the models to follow the measurement cumulative distribution adequately is important, matching the upper percentiles for this project are paramount. Following the line of perfect fit (45-deg blue line) would suggest good agreement; above the line the WAM results over-estimate, and below the line WAM will under-estimate the measurements. The WAM results show over the entire time-paired distribution that it performed very well, then in the top one-percent showed a slight over-estimate (about 0.4-m) compared to the buoy data. One must note, the results are based on the time series and not on individual storm peak conditions (discussed latter in this section) and the top percentiles found in the following figures could be derived from one storm event depending on its relative intensity, duration compared to the other storm simulation results.

WAM evaluation for NBBC 45007 Q-Q analysis is shown in Figure 6-32. The results are generally consistent with the previous location, where WAM continues to compare favorably to the measurement cumulative distribution. For conditions greater than 99-percentile, WAM at this site tends to run slightly lower (0.25-m) compared to the buoy data. At low significant wave heights (less than 0.25-m) the WAM results tend to be slightly elevated (and similar to the results at 45002). The main cause of this is attributed to the lower limit threshold of 2.5-m/sec used during the CFSR wind field generation.

The nearshore wave gage sites are dependent on depth effects. Deployed in 10-m water depths shallow water mechanisms would control to a certain extent the results. These would include refraction, shoaling, wave-bottom energy loses, and depth induced wave breaking. However, given the general

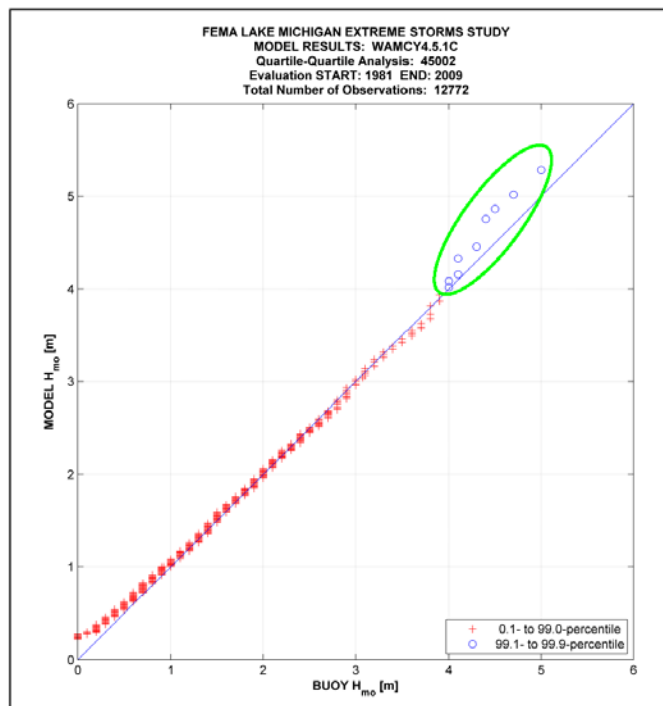


Figure 6-31. Quartile-Quartile graphic for WAM versus buoy data at NDBC 45002.

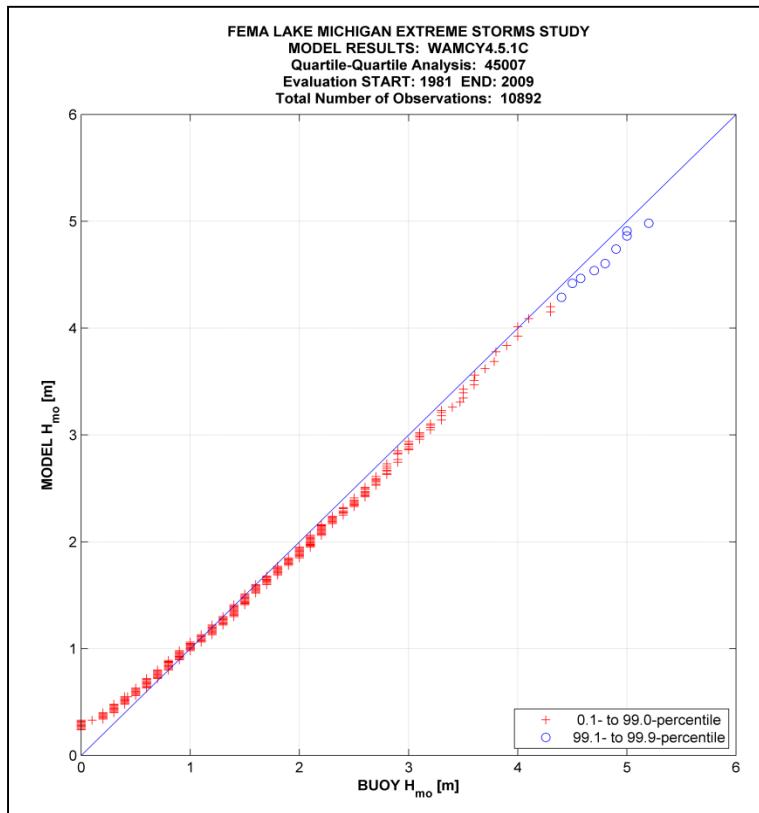


Figure 6-32. Quartile-Quartile graphic for WAM versus buoy data at NDBC 45002.

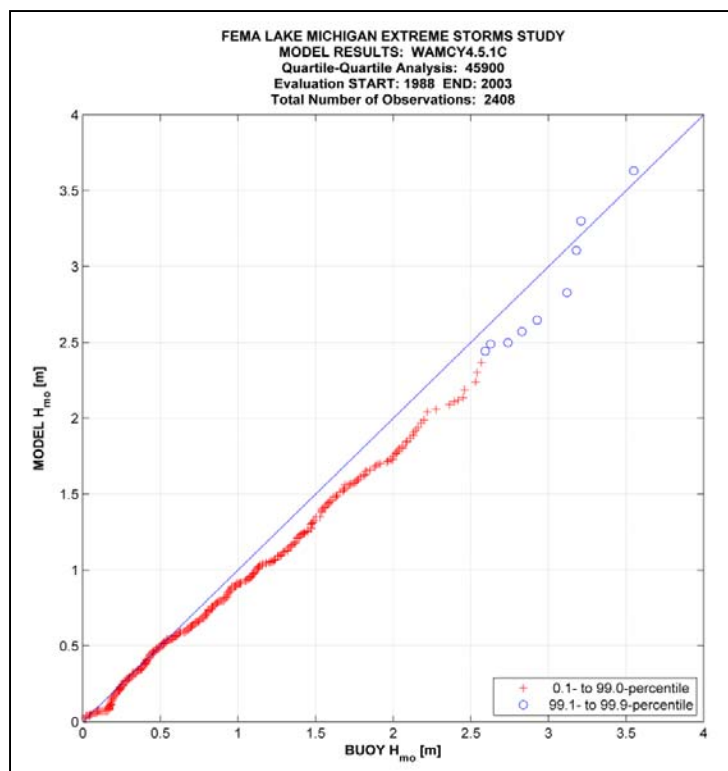


Figure 6-33. Quartile-Quartile graphic for WAM versus buoy data at Burns Harbor, 45900.

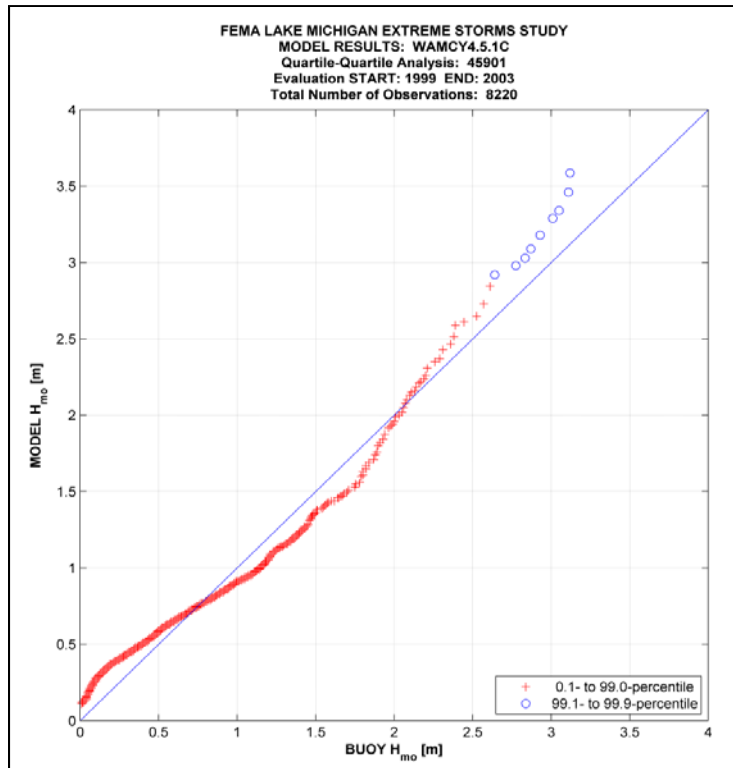


Figure 6-34. Quartile-Quartile graphic for WAM versus buoy data at Chicago Harbor, 45901.

characteristics of the wave climate for Lake Michigan, the controlling mechanism is wind-wave growth. The range of carrier frequencies remains high so that, even at a 10-m depth, the wave energy remains in a deepwater regime. Ice effects and/or low wave energy recorded would have a greater influence on the analysis of the WAM results.

Figure 6-33 displays the WAM versus buoy Q-Q analysis. It clearly shows WAM under-estimates the wave height distribution above about 0.6-m and continues this trend until about 3-m. For the top 0.2-percentiles, the WAM results improve. The differences shown in Figure 6-33 are relatively small, and at its maximum of about 0.5-m. However given the range in the distribution, these errors are large. This could be based on a limited data set, amplifying all errors because of the population size. If something is missing in the WAM simulations, the error should be constant, and is not. It does seem as though the mid-range of the distribution suggested some common difference and is magnified as the wave height increases. Unfortunately the spectra did not exist, hence a more compete evaluation of the reason why cannot be performed.

The investigation of the nearshore gage evaluation using the Q-Q procedure continues at Chicago Harbor. The deployment was in 10-m water depth. The shoreline would be more of a north-south orientation and somewhat sheltered from northerly wind-wave energy (Figure 6-1) compared to the Burns Harbor location. It is anticipated at the onset, the wave height distributions should be lower than at Burns Harbor.

Shown in Figure 6-34 the upper limit in the wave measurements is about 0.5-m lower, despite nearly matching the upper one-percent cumulative distribution of 2.6-m. The WAM results emulate the color scatter plot to some degree, over-estimating in the low wave height range, under-estimating in the mid-range (from missing one storm event STO139), then over-estimating at the last one-percent. The errors in the distribution are not that great, however as in the previous case, when scaled to the upper level in wave conditions being 0.5-m high out of 3-m is 16-percent. However, two main points can be gained from this exercise, 1) there does not appear to be a common deficiency in the WAM estimations for the shallow water gage sites, 2) a vast majority of the errors are caused by only one storm.

6.5.2.3 Peak-to-peak significant wave height analysis

Knowing the errors over the mean and cumulative distribution for the storm events containing wave measurements, the last test is to establish

the trends in the WAM results to accurately estimate the extreme storm wave heights. A peak-to-peak analysis is performed where a specified threshold is used (Table 6-2). These thresholds vary from site to site, and are based on the measurements rather than the model wave estimates. A storm is defined as the time duration from exceeding the threshold until it falls below the threshold. The peak wave height is the maximum condition contained in the time period in any given storm. The extreme storm event simulation may contain other minor events in the 12-day record, so there will not be a one-to-one correspondence between the number of storm simulations and the selected peak wave height condition. As in the other analyses, the peak-to-peak evaluation uses the same time paired (model to measurement) data set, where all storms are contained.

The five wave measurement sites are evaluated and graphically presented in Figures 6-34 through 6-38. The three panel plot illustrates the time series of the model and measurements (top panel), a scatter plot of the entire population (lower left panel), and a scatter plot of the peak events found in the analysis (lower right panel). A linear regression was generated for the storm peak evaluation as it was determined there was a very strong dependency on the selection of the peak storm events and the threshold, yielding a large population of values close to the threshold. This skews any analysis and could produce misleading results. Lastly, the time domain between measurement sites are unique and cannot be cross-correlated because of the deployment cycles of the gages.

The WAM results (Figure 6-35) generally follow the buoy (45002) trend, and capture the peak storm wave height, sometimes higher or lower. This is evident in the scatter plot of all model to measurement comparisons. It does appear the WAM results level off to about 5.2-m or there could be saturation occurring whereas the buoy data continue to about 6-m. It is unfortunate that the peak measured results (STO102) contained no wind measurements to directly compare the CFSR wind estimates. The modeled peak wind estimate was around 20-m/sec in a southwesterly direction for nearly 24-hours. This, however, is not always the case because WAM's estimates in significant wave height plot above the 45-deg line (red line) indicating an over-estimation. Investigating the peak-to-peak results (bottom right panel in Figure 6-34), emulates the scatter plot results. There is some bias in the model storm peaks compared to the measurements; however, the range seldom exceeds 0.25-m.

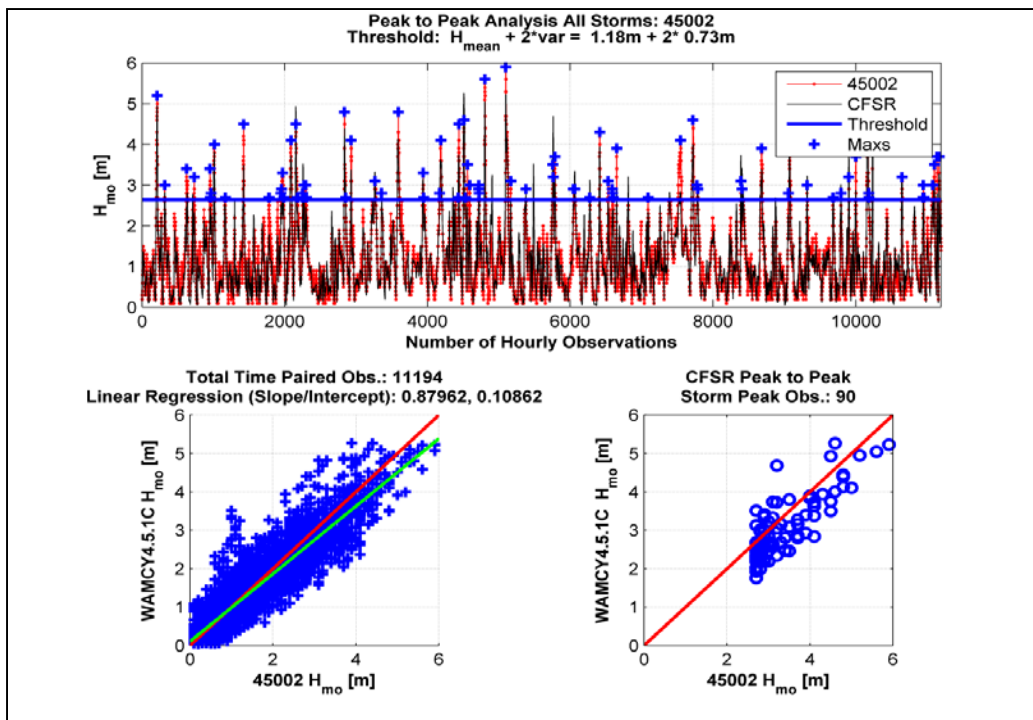


Figure 6-35. Peak-to-peak analysis, at NDBC 45002. Top panel compendium of all extreme storm events containing measurements with threshold defined; lower left panel scatter plot of WAM results and buoy data; lower right panel scatter plot of the storm peaks. Note forty-two extreme storm events contained measured data from 45002.

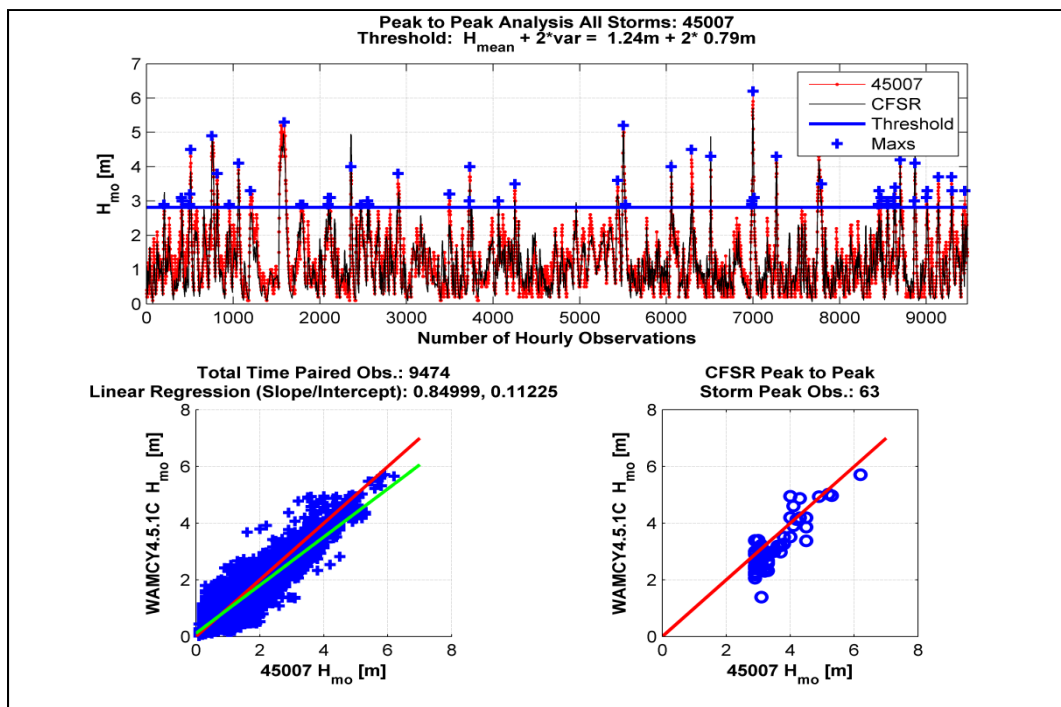


Figure 6-36. Peak-to-peak analysis, at NDBC 45007. Top panel compendium of all extreme storm events containing measurements with threshold defined; lower left panel scatter plot of WAM results and buoy data; lower right panel scatter plot of the storm peaks. Note thirty-seven extreme storm events contained measured data from 45007.

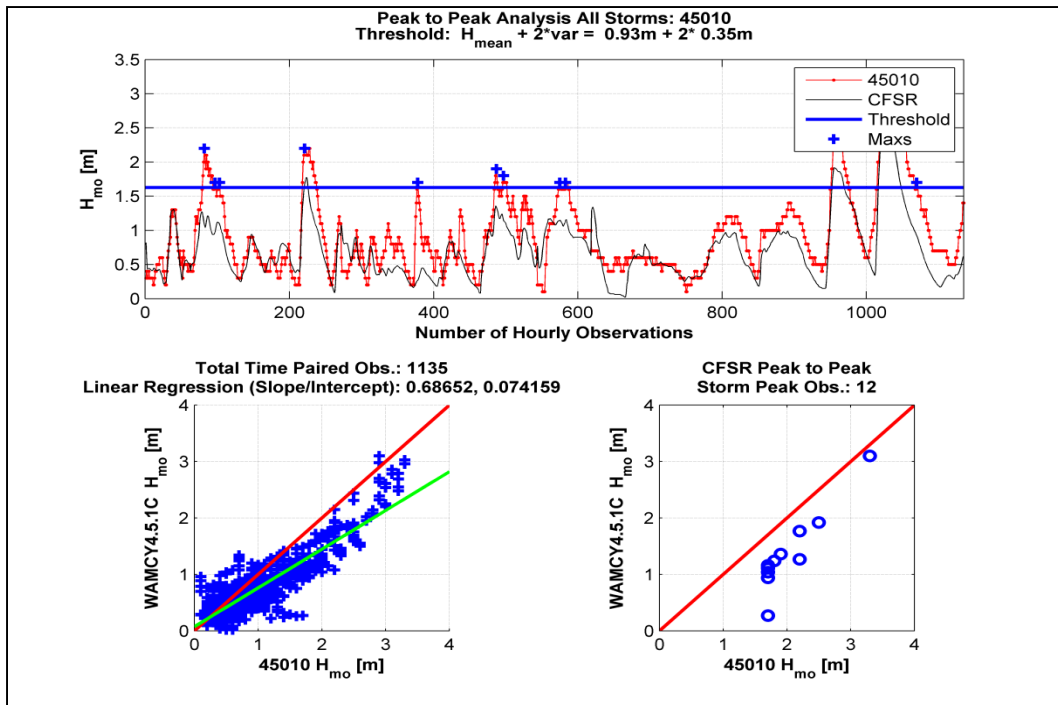


Figure 6-37. Peak-to-peak analysis, at NDBC 45010. Top panel compendium of all extreme storm events containing measurements with threshold defined; lower left panel scatter plot of WAM results and buoy data; lower right panel scatter plot of the storm peaks. Note four extreme storm events contained measured data from 45010.

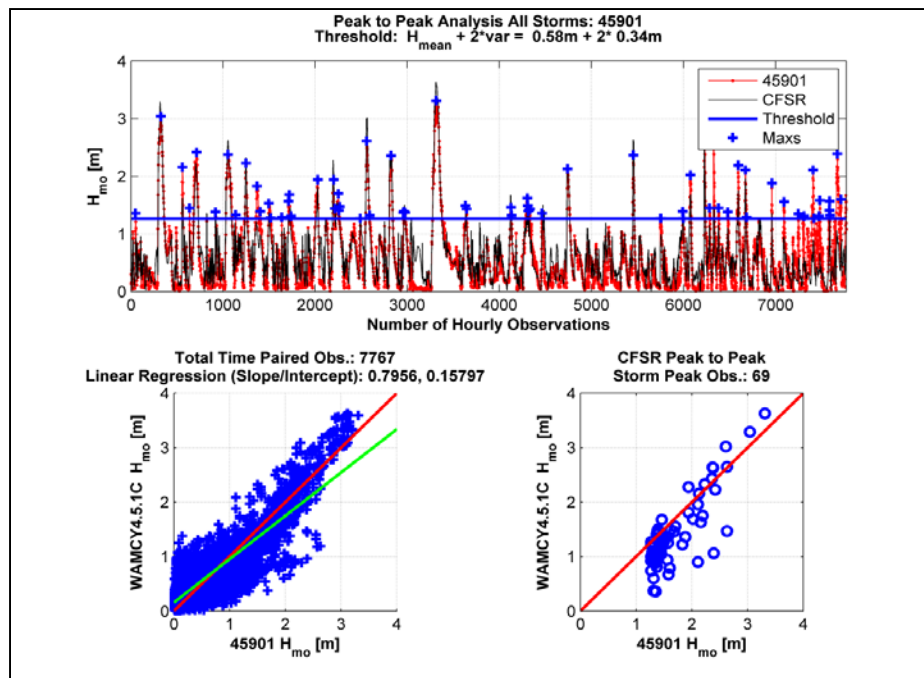


Figure 6-38. Peak-to-peak analysis, at Chicago Harbor (ST 45901). Top panel compendium of all extreme storm events containing measurements with threshold defined; lower left panel scatter plot of WAM results and buoy data; lower right panel scatter plot of the storm peaks. Note thirty-two extreme storm events contained measured data from Chicago Harbor gage.

The analysis continues at the southern NDBC buoy location, 45007 (Figure 6-36). The WAM results again compare favorably to the measurements over time, and it is clearly evident in the scatter plot (lower left panel), where the linear fit (green line) displays a negative bias. This is caused by the larger population of low wave conditions compared to that of the higher significant wave heights. This is obvious when the storm peak wave heights are compared (lower right panel of Figure 6-36) where the WAM results tend to show a very limited negative bias up to 6-m. These trends follow the previously described Q-Q analysis for the two deep water, centrally located buoy sites (e.g. Figures 6-31 and 6-32).

Despite limited data for NDBC 45010, it is instructive to analyze the WAM results at this nearshore location. Given that only four extreme storm events were selected during the three-year deployment of this buoy, the results of the WAM simulations (Figure 6-37) show a similar trend to that of the measurements; however, the model predictions are generally lower than the measurements. The only exception would be during the last storm simulation where the WAM results capture the measurement trace and also the peak condition of about 3-m. The scatter plot of the time-paired model to measurements (lower left panel of Figure 6-37) supports the general negative bias in the WAM results, and follows suit for the peak-to-peak storm wave heights where at most WAM tends to under estimate the buoy data by about 0.5-m. In one case (around hourly observation 400) the model completely misses the storm event altogether. This does not mean that WAM fails to estimate all local storm conditions. As previously discussed, the population size is somewhat limited; the location of the buoy may be near the land/water boundary affected by micro-scale meteorological events not captured in the CFSR wind fields. WAM does a credible job at estimating the time evolution of the storm event even though a very local-scale event may be missed.

The final two comparisons are composed of the nearshore gage sites at Chicago (ST 45901, Figure 6-38) and Burns Harbor (ST 45900, Figure 6-39). It is good to have these sites to evaluate WAM and, indirectly, the ice implementation. These gages were deployed during the winter months where in general the NDBC buoys were removed during the same period. Many of the extreme storm events occurred during the *Ice-Year* (December through the following May). As previously noted, it is difficult to determine whether low energy from the reported measurements were a result of ice or no storm event. However these data are derived from the extreme storm event analysis

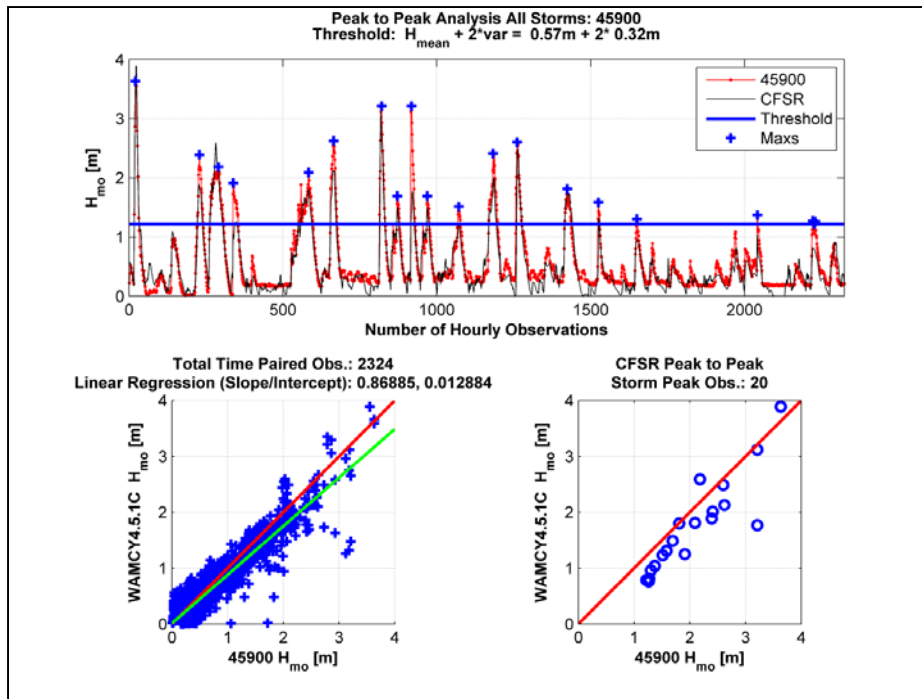


Figure 6-39. Peak-to-peak analysis, at Burns Harbor (ST 45900). Top panel compendium of all extreme storm events containing measurements with threshold defined; lower left panel scatter plot of WAM results and buoy data; lower right panel scatter plot of the storm peaks. Note eight extreme storm events contained measured data from Burns Harbor gage.

and should contain conditions for high wave energy. Figure 6-38 shows the WAM results compared to the Chicago Harbor (ST 45901) site. The time plot again demonstrates that WAM can emulate this nearshore site, capturing the trends (growth, peak and decay) of the selected storm events. The scatter plot does indicate (linear fit) a strong negative bias weighted more so because of the larger population of low wave heights. In general it does appear the ice implementation does well to replicate either iced (flagged for ice coverage), or for a low wave energy environment. Granted there are times when WAM indicates a larger wave climate when the data supports either low or no wave energy, however using the 70-percent concentration criteria does work successfully. For peak storm wave conditions (lower right panel), the WAM results show a very modest over estimation.

Similar results for the Burns Harbor (ST 45900) are presented in Figure 6-39. The time plot (upper panel), illustrates a smaller population of wave events compared to the Chicago Harbor site. The results show that WAM and the ice implementation emulate that found in the data. When the wave environment captured by the gage measurements is low, so are the modeled results. When storms appear, the model trends in a similar fashion

as the measurements, for the rapid growth, capturing the peak storm conditions, and ultimately decay. It is also quite interesting that the thresholds at both sites are similar despite the orientation of the shoreline and sheltering at Chicago Harbor, compared to the openness of northerly storm conditions at Burns Harbor. It is also evident there are similar misses of events at Burns Harbor (lower left panel where the WAM results are zero compared to 1.0- and about 1.75-m measured values), and the missed 3.25-m wave event (at about hour 900; STO136¹). This storm peak was not a selected extreme storm event. The storm was produced by a northerly wind event of 12-m/sec occurring at the beginning of the simulation. This underestimation was a result of the initialization of the Lake Michigan domain (cold starting) that would limit the far-field wave energy from propagating toward the southern coast of Lake Michigan. Despite the one or two events completely missed in the extreme storm record, the peak-to-peak estimates of the modeled results do compare well to the gage data.

6.5.2.4 Statistical evaluation of winds and waves

To complete the analysis of the CFSR wind field estimates and the WAM results, a battery of statistical tests were run on the time paired observations and model data sets. These tests include the Bias (always model – measurements), Root-Mean-Square-Error (RMSE), Scatter Index (ratio of standard deviation of difference to mean of measurements), Linear Regression (slope and intercept), Linear Regression (with a symmetric slope, or forcing the intercept to zero), and Correlation (based on the Linear Regression with symmetric slope). The tests are preformed on the wind speed, significant wave height, parabolic fit of the peak wave period (given the frequency spectra), and the mean wave period. The wind speed measurements were converted to an equivalent 10-m neutral stable wind (as defined in the CFSR wind fields). No smoothing of the measurements was performed, and only finite time paired observations to model results considered. Quite often there are gaps in the measurements, and these were removed from the analysis. In addition, if the modeled results were flagged at any time to indicate ice cover, these also were removed from the analysis. All five operational measurement sites (Figure 6-1) were used in this evaluation; however, there were no recorded meteorological measurements at the two nearshore sites, and frequency spectra were not available, so the mean wave

¹ This was verified based on the Wave Information Study 31-yr wave hindcast. The peak wave height on 11 February 2002 was captured by WAM.

period could not be generated. All of the statistical tests were performed for each storm simulation when measurements were available.

A wave model evaluation indirectly tests the reliability of the wind forcing as well as the mechanisms used in the simulations. Given good winds, the wave model should emulate the quality of the winds. Significant wave heights are scaled to the wind speed squared. Thus, errors embedded in the wind forcing fields will generate errors in the wave estimates. As shown in Table 6-3, the comparisons of the CFSR wind fields at three point source sites are very good. The biases are no more than +/- 1.5-m, and exhibit a positive bias at the two centrally located NDBC buoy sites. At 45010 (just offshore of Milwaukee, WI) there is a negative bias of 0.47-m/sec. This, as previously discussed, could be attributed to the lack of small-scale meteorological conditions located in the land/sea interface. The RMSE's are somewhat high at 1.7 – to 2.5 m/sec; however, this most likely is due to the threshold imparted on the original CFSR winds at the low end of the wind speed range. While the Scatter Index (SI, a measure of the general trends in the model estimates, and the reliability to estimate the mean) is unexpectedly high (a value of 20 or less is deemed good), this is likely primarily due to the population selected for extreme water level and wave events. The symmetric slope (i.e. linear regression defined with a zero intercept) is reasonable, suggesting a positive bias (at the offshore locations, 45002 and 45007), and error of 11- to 13-percent and correlations of 0.80 to 0.88. The nearshore buoy site, given a negative bias, also results in an average error of 8-percent. The CFSR winds, despite some error, perform well to the observations in Lake Michigan.

Table 6-3. Summary statistics for all storm simulations wind speed (m/sec).

STATION	Mean		Bias	RSME	Scat Indx	Slope	Intercept	Linear Reg.		No. Obs.
	Meas.	Model						Sym Slope	Corr.	
45002	7.47	8.68	1.21	2.50	34	0.80	2.72	1.13	0.80	10912
45007	7.55	8.53	0.98	1.82	24	0.83	0.15	1.11	0.88	10825
45010	8.00	7.53	-0.47	1.72	22	0.68	2.07	0.92	0.84	1121
45901	-	-	-	-	-	-	-	-	-	-
45900	-	-	-	-	-	-	-	-	-	-

The wave parameter evaluation (Tables 6-4 to 6-6) provides somewhat of a different result. If the significant wave height is scaled to the wind speed squared (linear for the parabolic fit wave period), the positive biases found in the wind analysis should also be evident in the wave parameters. This is

not the case for these simulations. Despite very low biases (-0.22- to 0.03-m) in height, and less than 1.0-sec for the parabolic fit and mean wave periods, both are biased negatively. One could argue that WAM requires additional wind speeds to grow proportionately to the wave heights. The mean wave period model estimate differences have been discussed (Chapter 3) and is based on the frequency range differences of the model and measurements. The RMSE are reasonable, less than 0.5-m for significant wave height and generally less than 1.0-sec for the wave period parameters. The Scatter Index results for the wave height are somewhat disappointing, but in general are similar to the wind speed error characteristics. The wave periods do much better. The Linear Regression (symmetric slope, with zero intercept) and correlation show that WAM approximates the wave field estimates well with the exception of station 45010 where the results are the poorest of the five locations. Even at the two nearshore gage sites, the results of WAM are surprisingly good. The grid resolution for all simulations is 0.02-deg or about 2.2-km and therefore many of the small scale variations in the bathymetry may not be adequately resolved. These features are better approximated in the STWAVE grid which has a 200-m resolution. In addition, these sites are subject to ice coverage, and it appears again from the statistical tests performed, that phase of the execution of the extreme storm events is evaluated providing good estimates.

Table 6-4. Summary statistics for all storm simulations significant wave height (m).

STATION	Mean		Bias	RSME	Scat Indx	Slope	Intercept	Linear Reg.		No. Obs.
	Meas.	Model						Sym Slope	Corr.	
45002	1.18	1.14	-0.03	0.33	28	0.88	0.11	0.97	0.92	11194
45007	1.15	1.11	-0.04	0.35	30	0.83	0.15	0.95	0.91	10130
45010	0.93	0.71	-0.22	0.29	32	0.69	0.07	0.77	0.87	1135
45901	0.68	0.59	-0.09	0.20	29	0.86	0.01	0.89	0.94	1760
45900	0.83	0.78	-0.05	0.28	34	0.86	0.07	0.96	0.88	5061

Table 6-5. Summary statistics for all storm simulations parabolic fit peak wave period (sec).

STATION	Mean		Bias	RSME	Scat Indx	Slope	Intercept	Linear Reg.		No. Obs.
	Meas.	Model						Sym Slope	Corr.	
45002	4.80	4.50	-0.29	0.90	19	0.80	0.65	0.94	0.81	11730
45007	5.00	4.70	-0.31	0.95	19	0.72	1.08	0.94	0.79	10130
45010	5.12	4.79	-0.33	1.00	19	0.77	0.85	0.94	0.79	1138
45901	5.36	4.71	-0.65	1.39	26	0.97	-0.51	0.92	0.70	1823
45900	5.68	5.25	-0.43	1.04	18	0.84	0.46	0.93	0.85	5137

Table 6-6. Summary statistics for all storm simulations mean wave period (sec).

STATION	Mean		Bias	RSME	Scat Indx	Slope	Intercept	Linear Reg.		No. Obs.
	Meas.	Model						Sym Slope	Corr.	
45002	4.34	3.62	-0.71	0.63	15	0.86	-0.09	0.85	0.84	11730
45007	4.46	3.75	-0.71	0.66	15	0.81	0.12	0.85	0.82	10130
45010	4.48	3.60	-0.88	0.66	15	0.82	-0.09	0.82	0.80	1138
45901	-	-	-	-	-	-	-	-	-	-
45900	-	-	-	-	-	-	-	-	-	-

6.6 Water level production

The ADCIRC mesh (Chapter 4) for Lake Michigan was developed from NOAA ENCs, 3- and 9-arc-sec data files from NOAA's National Environmental Satellite Data, and from the Information Service Lake Michigan digital bathymetry data base. These data were processed to a consistent IGLD 1985 vertical water level datum. In addition, the NOAA's IGLD 1985 zero-depth coastline file was incorporated into the data set. ADCIRC mesh development also included acquiring geo-rectified photography and images to aid in establishing the shorelines for the numerous harbors around Lake Michigan. In the validation process described in Chapter 4, the ADCIRC mesh was also expanded through the Mackinac Straits to include Lake Huron and the surrounding bays. This expansion was needed to account for the inverted barometer effect. That is, during the passage of low pressure systems, the spatial variation in pressure over Lake Michigan and Lake Huron causes flow through the Mackinaw Straits. The low pressure lake draws water from the high pressure lake through the Mackinaw Straits to fill the void caused by the low pressure system thus requiring the full two-lake system to properly account for storm water levels. As with the WAM model domain, the assumption of vertical walls at the shoreline was made and overland flow is to be computed based on wave and water level information provided by WAM, ADCIRC, and STWAVE within the main water bodies.

Each storm in the 150 extreme storm suite (see Table 6-1) is simulated independently. Based on the validation simulations, most production simulations applied a model time-step of 0.5 sec, but a few simulations required a smaller time-step. This smaller time-step requirement happened for storms that occurred at higher lake levels. With the higher lake levels, the propagation speed through the mesh is faster, thus requiring a smaller time-step to satisfy the Courant condition for model stability. Storms 041, 043, 045, 046, 079, 080, 081, 082, 083, 084, and 125 applied a 0.25-sec time-step. Another parameter that was set in the validation process was the

minimum water depth of 2.0 m. Water depths shallower than 2.0 m were set to 2.0 m in the initialization process. A few storms required the minimum depth to be increased for model stability. Storms 003, 006, 014, 017, 018, 036, 039, and 059 required a minimum depth of 2.5 m.

Another ADCIRC input requirement is the set of locations (save points) where model time series of water surface level and water velocity results are to be saved and applied as forcing for other model applications (Figure 6-40). These locations were selected based on their proximity to the shoreline in a water depth of approximately 2-3 m for Lake Michigan and 0.5 m for Green Bay. The alongshore spacing of the save points in Lake Michigan was approximately 3 km (Figure 6-41) and the alongshore spacing of save points in Green Bay was approximately 1.5 km (Figure 6-42). Save points were also placed around three offshore islands and at all 10 NOAA NOS water level measurement sites in Lake Michigan. The total number of save point locations was 916.

With the wind, wave, and ice fields processed, the ADCIRC (or CSTORM-MS) production was initiated. For all storm simulations, ADCIRC applied a two-dimensional, depth-integrated nonlinear bottom stress of 0.0015 and included finite amplitude and advective terms in the model computations. As previously mentioned, the model applications assumed vertical walls at the shoreline, therefore wetting and drying was turned off in the model applications.

The ADCIRC/CSTORM-MS applications included the following steps:

- Pre-processing of ADCIRC simulation forcing parameters:
- Input the ADCIRC mesh (fort.14) and the water level adjustment to the synoptic lake level (fort.13) for a specific storm event
- Generate the general input file (fort.15)
- Generate the storm specific control file (mf_config) including the start and end times for ADCIRC and STWAVE, ADCIRC and STWAVE grid names, and coordinate systems.
- Apply the storm-specific, time-dependent wind (fort.222) and pressure (fort.221) fields previously formatted for the WAM applications

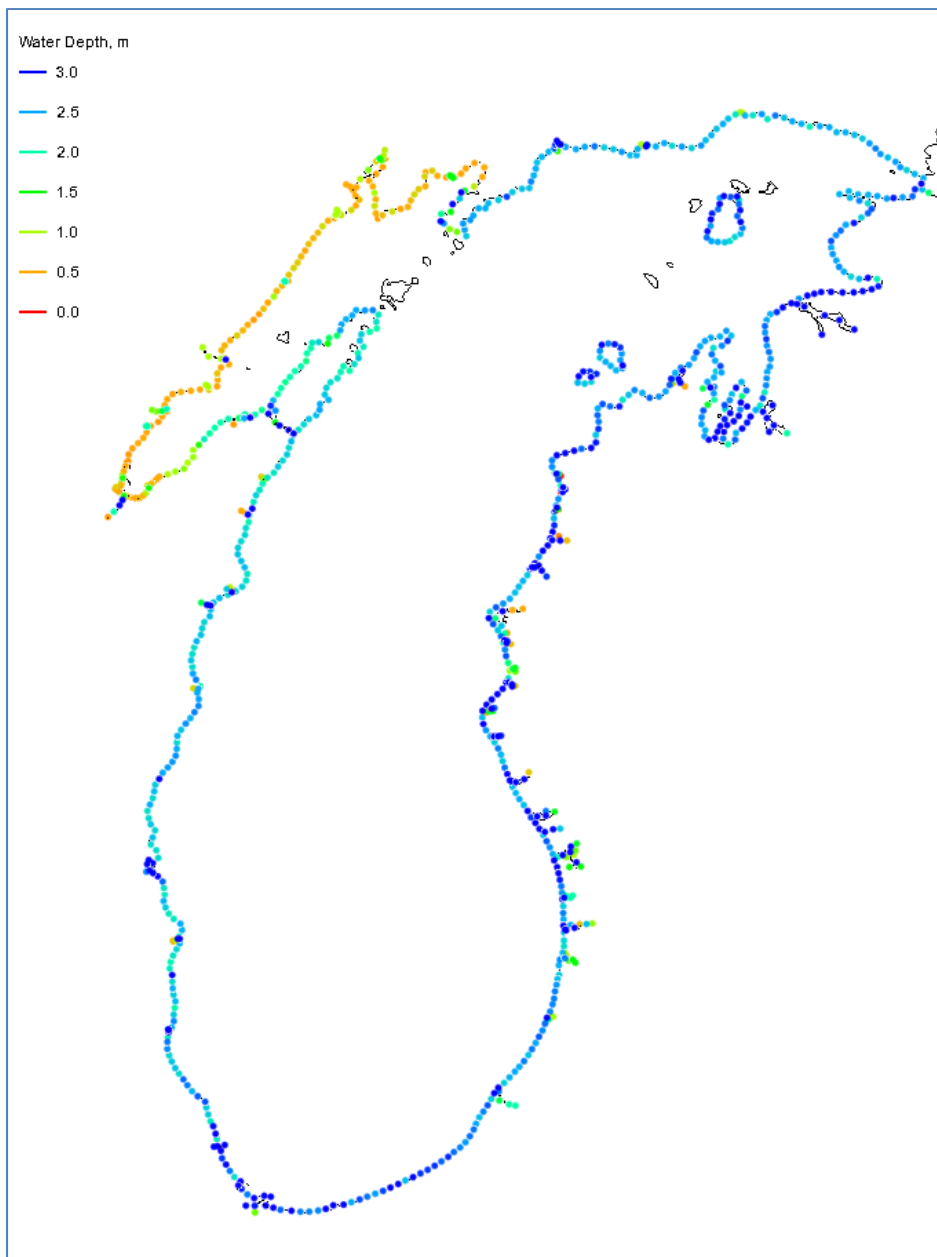


Figure 6-40. ADCIRC Save point locations for Lake Michigan and Green Bay. The color indicates the water depth at the save point location.

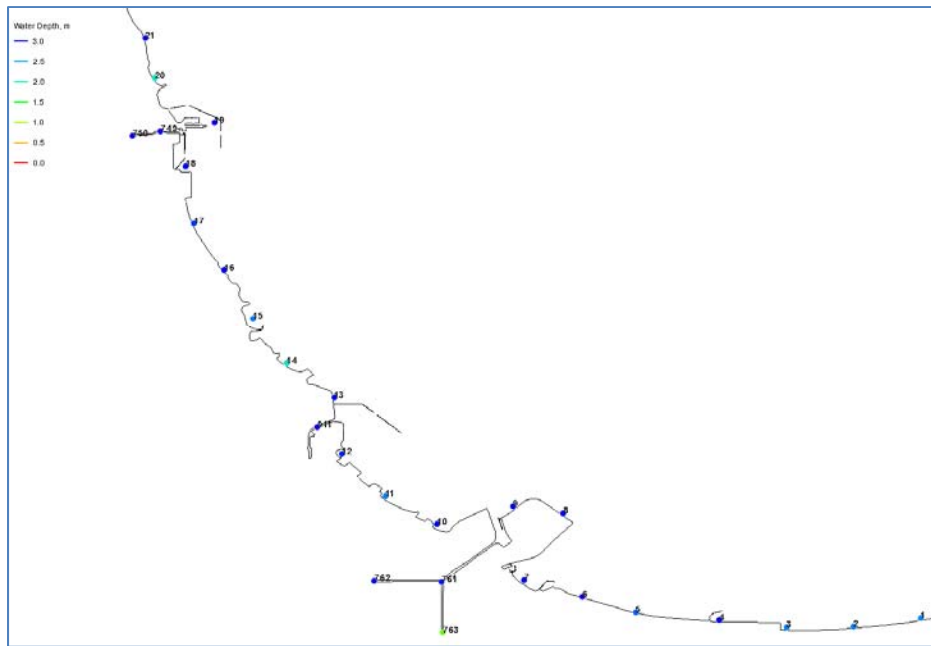


Figure 6-41. ADCIRC save point locations and numbers for lower Lake Michigan. The color indicates the water depth at the save point location.

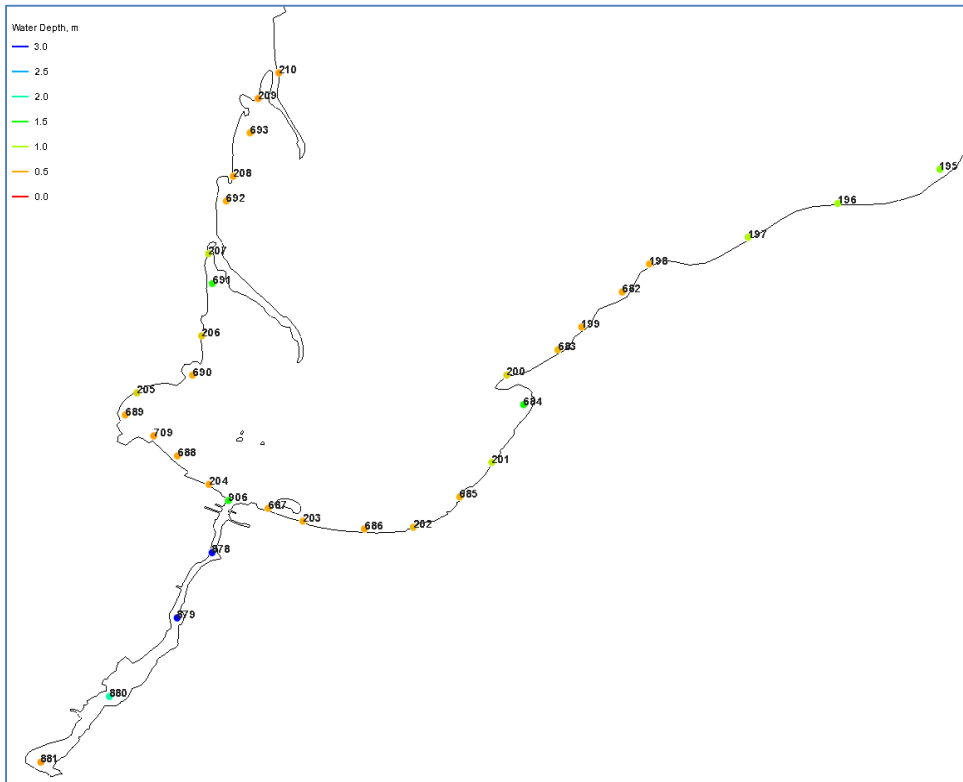


Figure 6-42. ADCIRC save point locations and numbers for lower Green Bay. The color indicates the water depth at the save point location.

- Apply the storm-specific, time-dependent ice fields (fort.225) previously formatted for the WAM applications
- Run ADCIRC (or CSTORM-MS)
- Output the time-dependent water level, water velocity, pressure, wind velocity, and ice distribution field files at all ADCIRC computational nodes
- Output the time-dependent water level, water velocity, pressure, wind velocity, and ice distribution time-series files at the 916 save point locations
- Post-Process Phase I
- Ensure simulation completion by checking output duration and values, log file messages, production of maximum envelopes of water level, water velocity, wind speed, and ice coverage, as well as the minimum pressure envelope
- Generate preliminary plots of water level time-series files at the several save point locations to ensure model completion.
- Post Process Phase II (Quality Control/Quality Assurance, QA/QC)
- From the time-dependent water level time-series files at the 916 save point locations, generate water level time-series plots for the locations corresponding to the 10 NOAA stations and compare to the measured water level time series for all 150 storm events
- Generate plots of the maximum wave envelope of water levels during the entire storm simulation for a subset of the storm events
- Generate animations of water level, wind speed, atmospheric pressure, and water velocity for a subset of the storm events
- Compute water level statistics (root-mean-square error and bias) for all storm events
- Archive
- Archive model results to:
 - Mass Storage Facility (ERDC HPC) (full set)
 - External hard drive on resident PC (subset)
 - Make all files available to the team
 - CSTORM-DB

6.6.1 Post-processing QA/QC

Upon completion of the ADCIRC simulations, a series of graphical and statistical products are generated to visually and numerically evaluate the model's skill in simulating the hydrodynamic response of the system to atmospheric forcing. Maximum water level envelopes provide an overall view of the extreme response of the water body to atmospheric forcing. The next level of evaluation of model performance is to examine the temporal variation of water level and compare it to measurements at several locations throughout Lake Michigan. Time series of water levels are saved for the latter six days of each model simulation and are compared to NOAA NOS water level gages for the same time period to determine if the temporal and spatial variation in water level is captured by the model. (The first six days were considered the model spin up time period and modeled time-series were not saved during that time period.) Lastly, the ADCIRC water level time series results are numerically evaluated and compared to measured NOAA water levels at 10 locations. The statistical comparisons tabulated for each storm and each location are the Bias and root-mean-square error. The statistical tests are performed on the time series of water levels for the final six days of the storm simulation.

6.6.2 Synopsis of Lake Michigan water level modeling

The post-processing comparisons described in the preceding section were done for all model simulations. Rather than present results from all storm simulations, ADCIRC estimates of water level are shown for a select set of storms and statistics are shown for all storms. For example, Figures 6-43 and 6-44 show the maximum surge envelopes for Storms 099 and 048, respectively. These figures provide an overall visual synopsis of the extreme response of the water body to atmospheric forcing. Storm 099 corresponds to December 1990 which produced the highest recorded water level at the NOS Station in Green Bay. The observed response is captured in the simulated surge envelope where water levels are nearly 178 m IGLD 1985 in Green Bay. By contrast, Storm 048 shows higher water levels in the northern portion of Lake Michigan. This storm was selected as the first ranked surge event at Port Inland. As shown in Figure 6-44 water levels are highest along the northern portions of Lake Michigan and Green Bay, including Port Inland for this storm event.

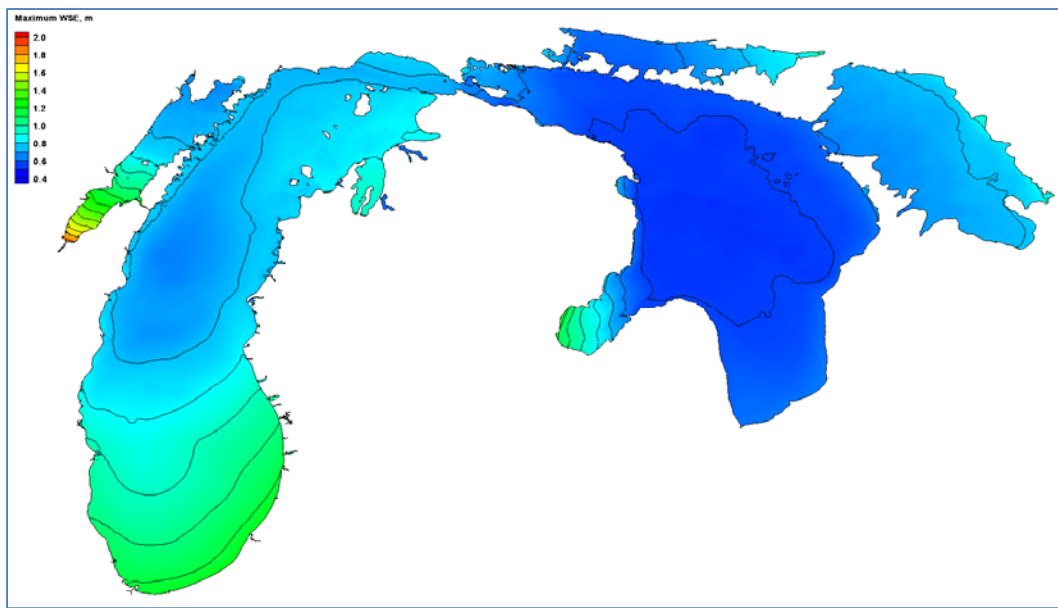


Figure 6-43. ADCIRC maximum water level envelope for Storm099 (December 1990) indicating highest water levels in Green Bay.

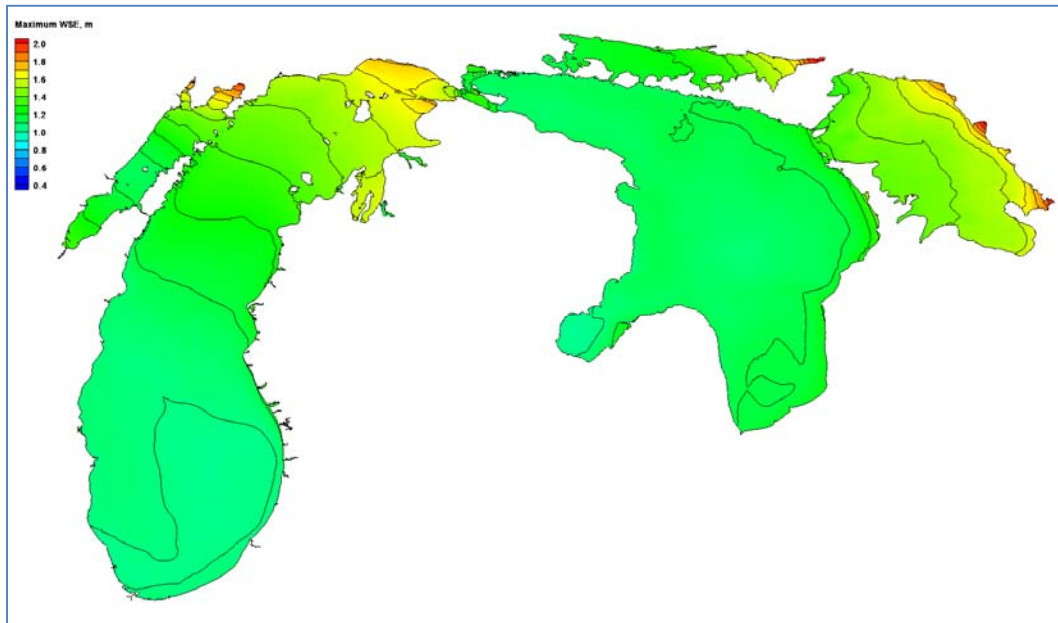


Figure 6-44. ADCIRC maximum water level envelope for Storm048 (January 1975) indicating highest water levels in northern Lake Michigan and Green Bay.

For a more detailed evaluation of model performance, the temporal variation of water level is compared to measurements at several locations throughout Lake Michigan. As previously noted, time series of water levels were saved at over 900 save point locations for the last 6 days of each model simulation, including the 10 NOAA NOS water level gage locations. ADCIRC water level time series were compared to NOAA NOS water level

gage time series for the same time period to determine if the temporal and spatial variation in water level is captured by the model.

Four storms were selected to show various aspects of the hydrodynamic response observed in nature and the ability or lack of ability to reproduce those responses by the model. Storm 099 was selected to give a complete examination of the storm previously discussed. This storm produced high surge in Green Bay and the southern portion of Lake Michigan, but the overall surge envelope shows smaller responses in other areas. The time series of water levels for this storm show a large variability in response from location to location (Figures 6-45 through 6-53). The time-series figures are arranged to begin at Ludington and then progress clockwise around the lake. Nine NOAA water level gages were operational during all or part of this storm event. The notable response at Green Bay is captured in magnitude, duration, as well as in the considerable post-storm seiching observed in the time series response (Figure 6-51). The gages in southern Lake Michigan (Milwaukee, Calumet, and Holland) have a fairly significant response that is also observed in the model simulation (Figures 6-46 through 6-48). The Milwaukee and Calumet gages respond sooner than the Holland gage as the storm system progresses from east to west. However, the peak response and post-peak response at Calumet and Holland are nearly identical. Moving northward, the responses at Ludington, Kewaunee, and Sturgeon Bay Canal show less effect from the storm event and have peak surges of less than 0.5 m (Figures 6-45, 6-49, and 6-50).

Ludington (on the east side of the lake) responds later than Kewaunee and Sturgeon Bay Canal (on the west). At the northern portion of Lake Michigan at Port Inland, the surge duration is significantly shorter and the surge magnitude is slightly less than at Sturgeon Bay Canal (Figure 6-52). Also, the time of the peak water level at Port Inland occurs more than 12 hrs after the time of peak water level at Green Bay. Mackinaw City, in Lake Huron, has the most muted response of all the NOAA gages and the model captures the trend at this location as well (Figure 6-53). For all locations in the lake, whether near the storm center or at a distance from the storm center, the model was able to capture the trend in surge response magnitude and duration. The ability to simulate the significant range of responses from Green Bay to Mackinaw City displays the skill of ADCIRC in simulating the storm surge hydrodynamics in Lake Michigan. Small scale oscillations that are finer than the temporal and spatial scales of the forcing conditions were not captured in the simulated responses.

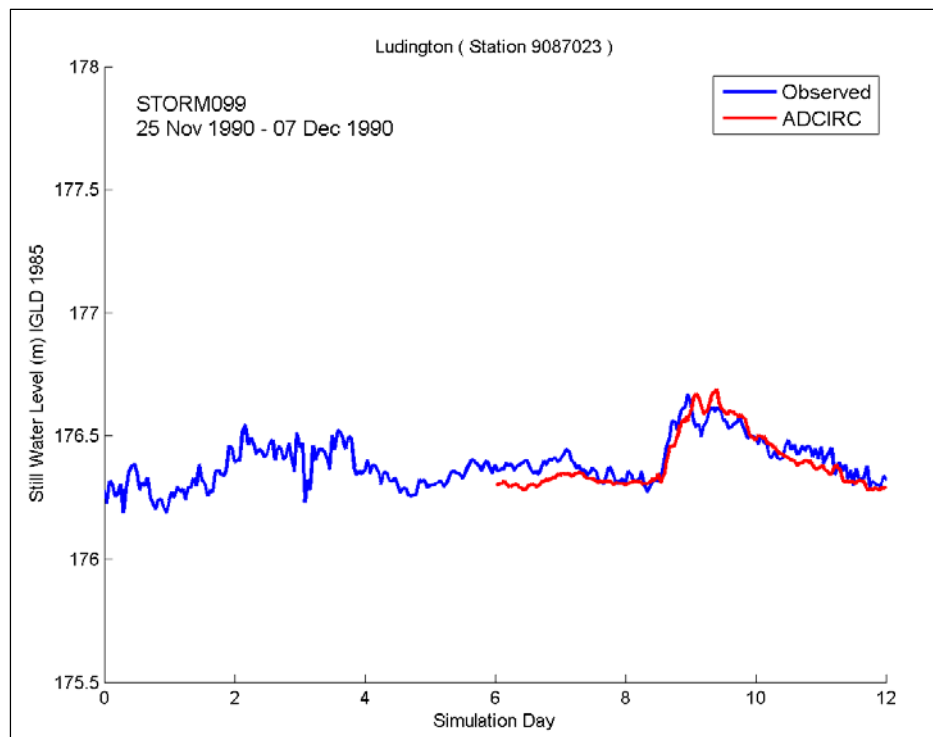


Figure 6-45. Time series of water levels for Storm099 (December 1990); Ludington.

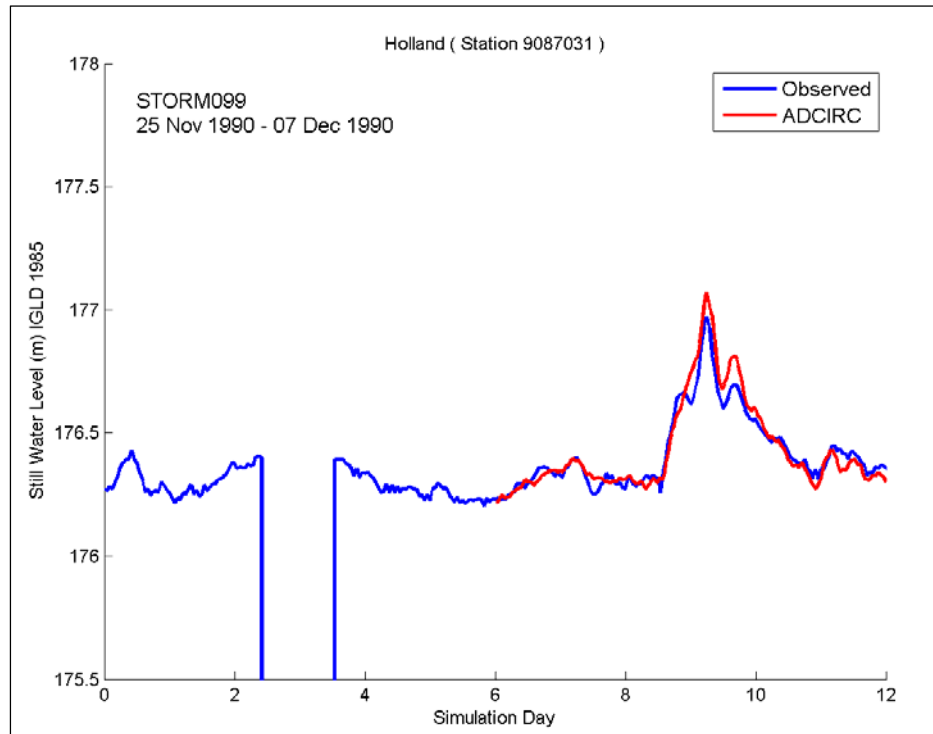


Figure 6-46. Time series of water levels for Storm099 (December 1990); Holland.

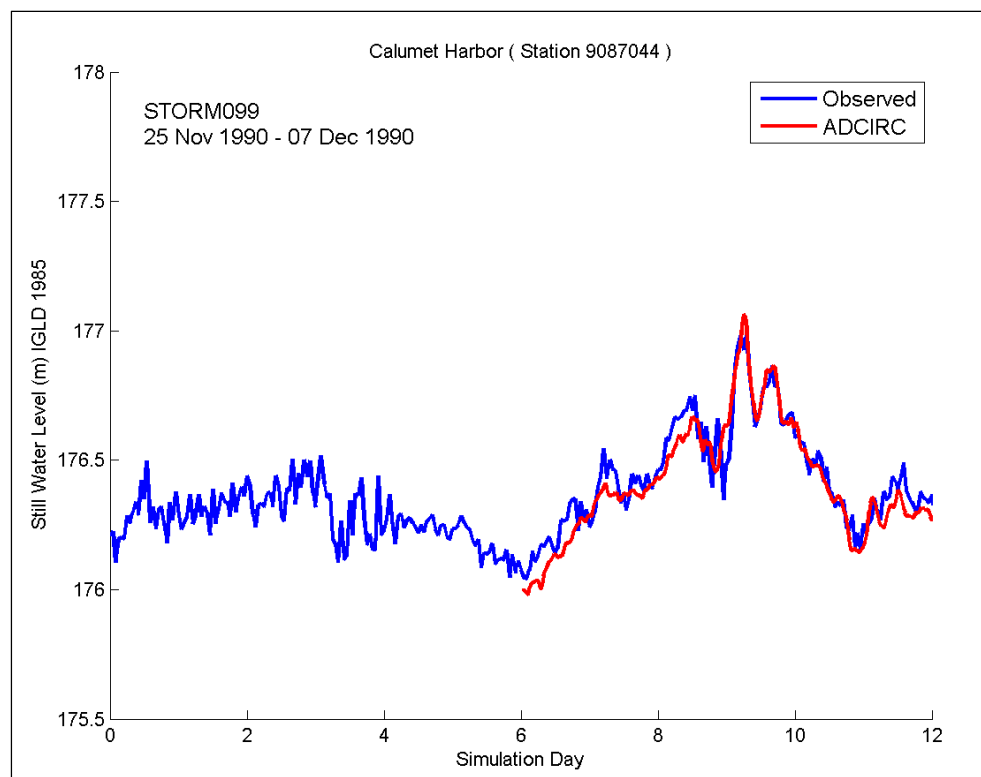


Figure 6-47. Time series of water levels for Storm099 (December 1990); Calumet.

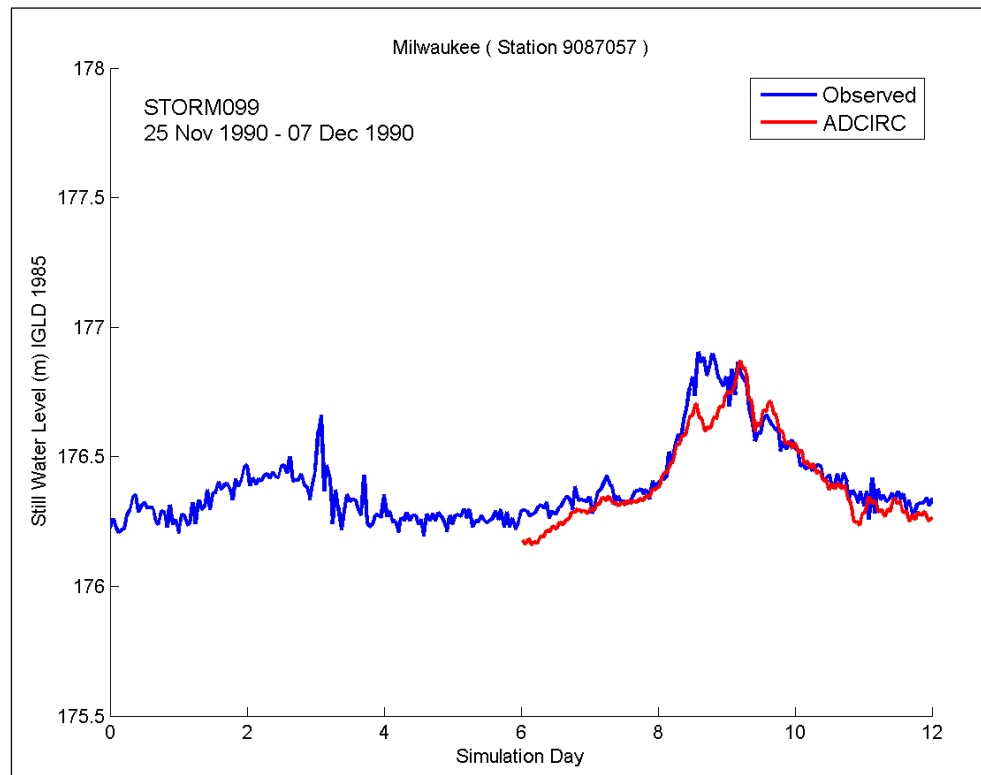


Figure 6-48. Time series of water levels for Storm099 (December 1990); Milwaukee.

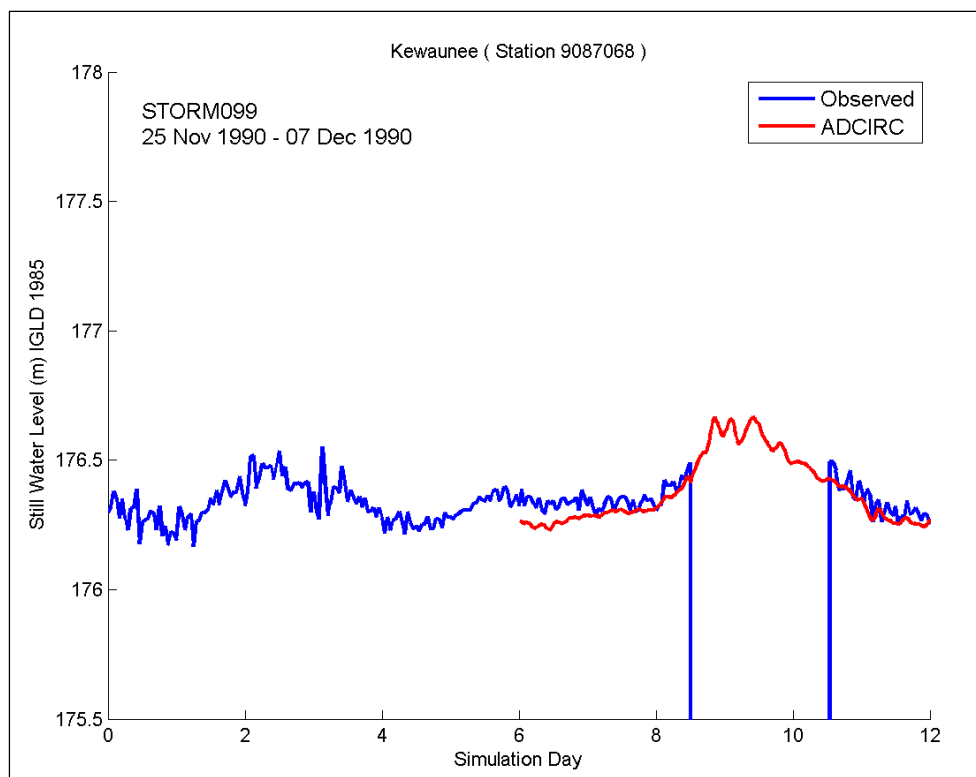


Figure 6-49. Time series of water levels for Storm099 (December 1990); Kewaunee.

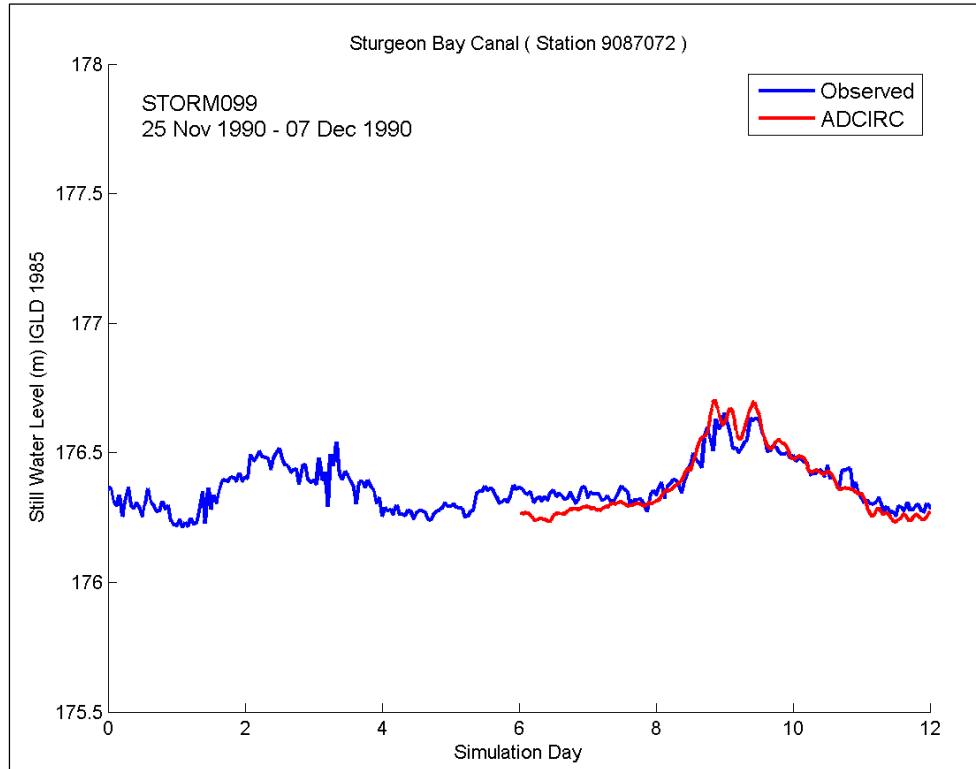


Figure 6-50. Time series of water levels for Storm099 (December 1990); Sturgeon Bay Canal.

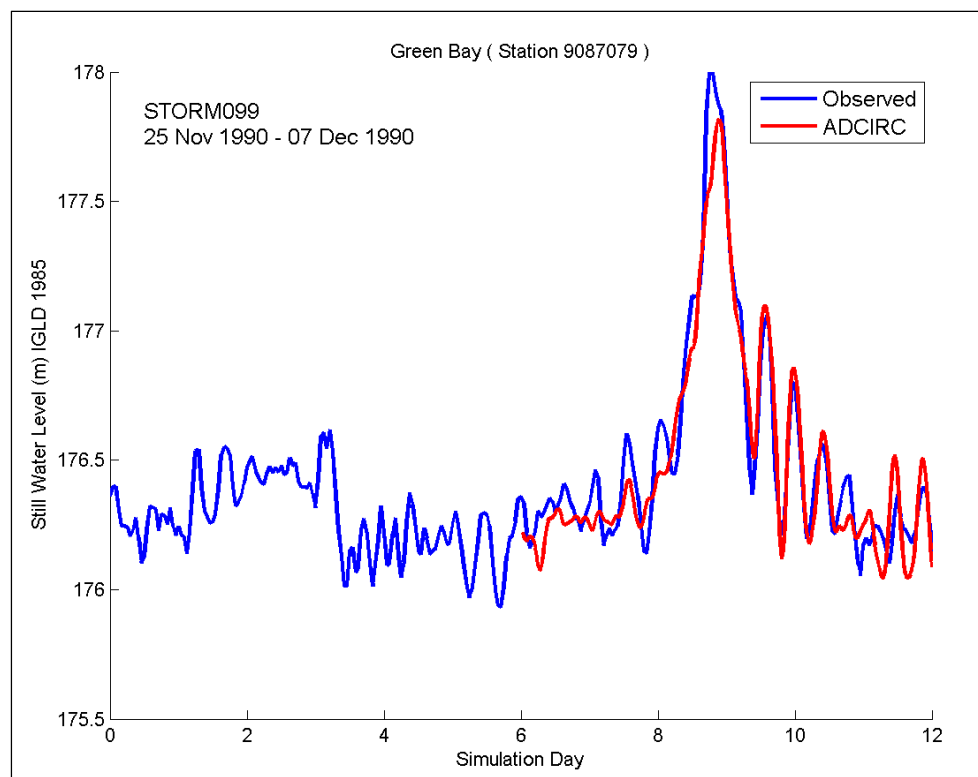


Figure 6-51. Time series of water levels for Storm099 (December 1990); Green Bay.

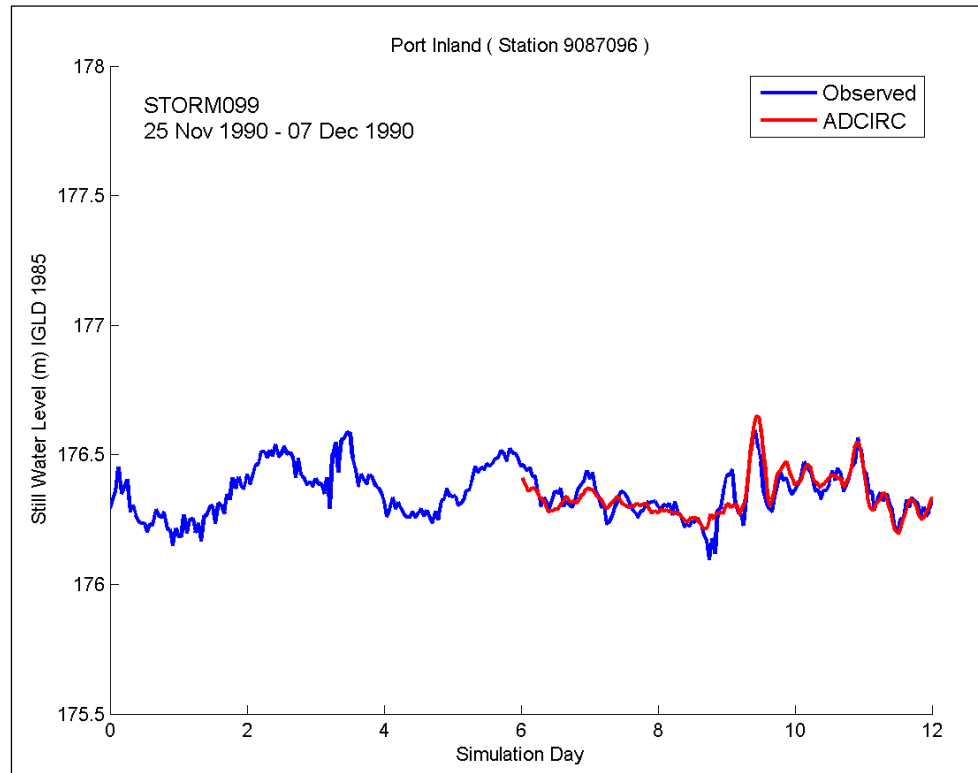


Figure 6-52. Time series of water levels for Storm099 (December 1990); Port Inland.

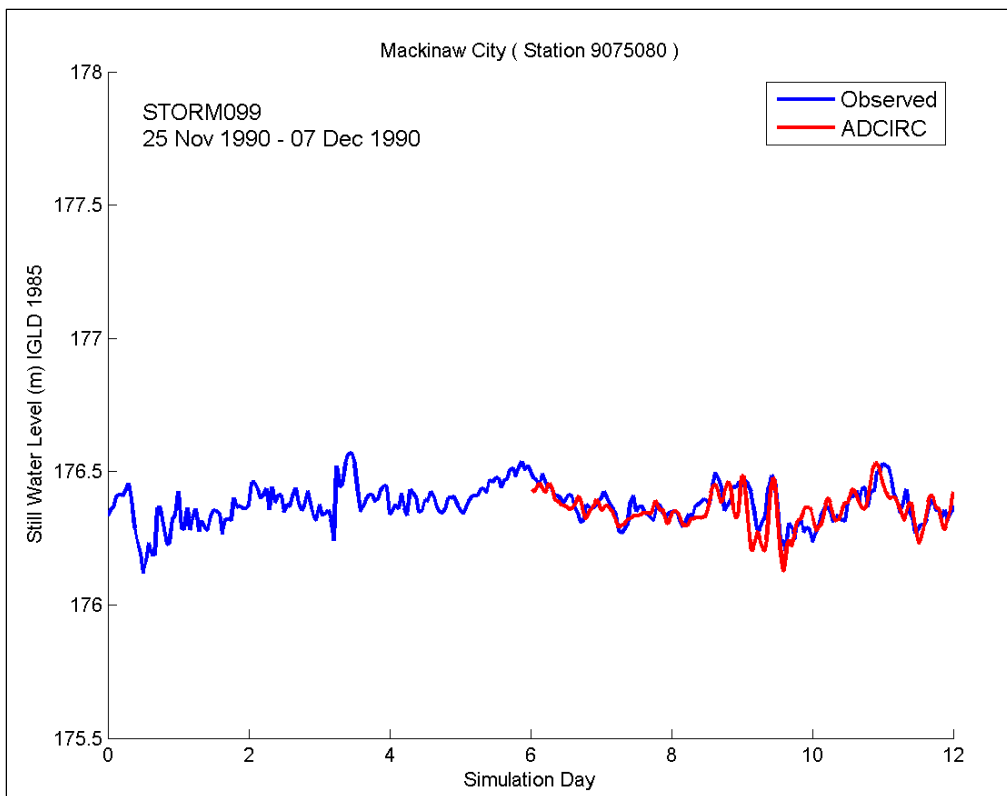


Figure 6-53. Time series of water levels for Storm099 (December 1990); Mackinaw City.

The second storm selected for discussion is Storm 048. This storm was selected because it produced the highest water levels at the northern end of Lake Michigan (at the Port Inland gage). The time series of water levels for this storm show a large variability in response from location to location (Figures 6-54 through 6-61). The time-series figures are arranged to begin at Ludington and then progress clockwise around the lake. Eight NOAA water level gages were operational during all or part of this storm event. Green Bay was not available, but simulated water levels at this location will be discussed. The simulated peak water level response at Port Inland is 0.3 m higher than any other gage location for this storm event, but the measurement device failed near the time of the peak of the storm (Figure 6-60). The measurement record three days prior to the gage failure shows that the modeled water levels were very close to the measured values. In addition, simulated water levels for the nearest gages at Mackinaw City (Figure 6-61) and Sturgeon Bay Canal (Figure 6-59) capture the trends observed in the measurements. Therefore, the simulated water level at Port Inland is assumed to be a reasonable estimate of the actual water level at this location for Storm 048.

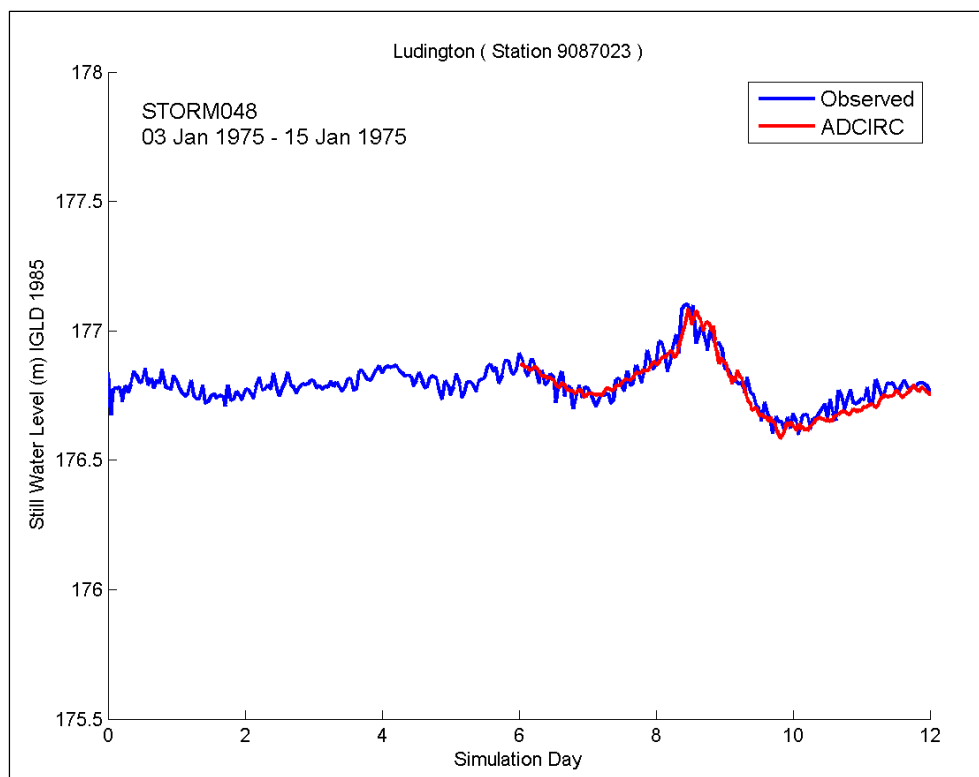


Figure 6-54. Time series of water levels for Storm048 (January 1975); Ludington.

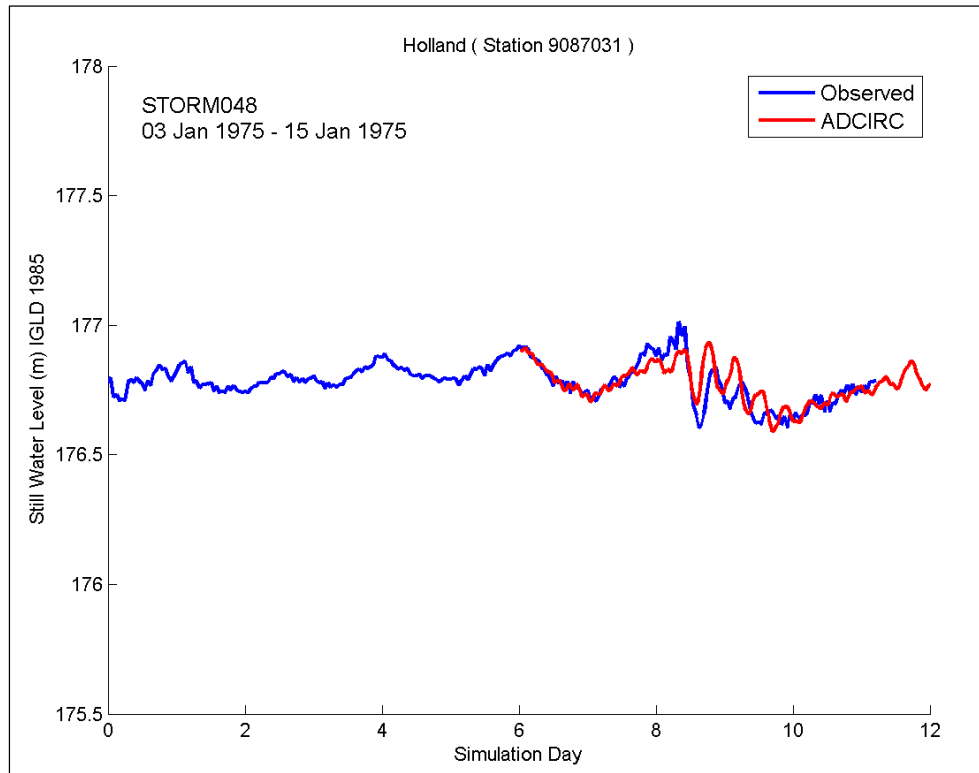


Figure 6-55. Time series of water levels for Storm048 (January 1975); Holland.

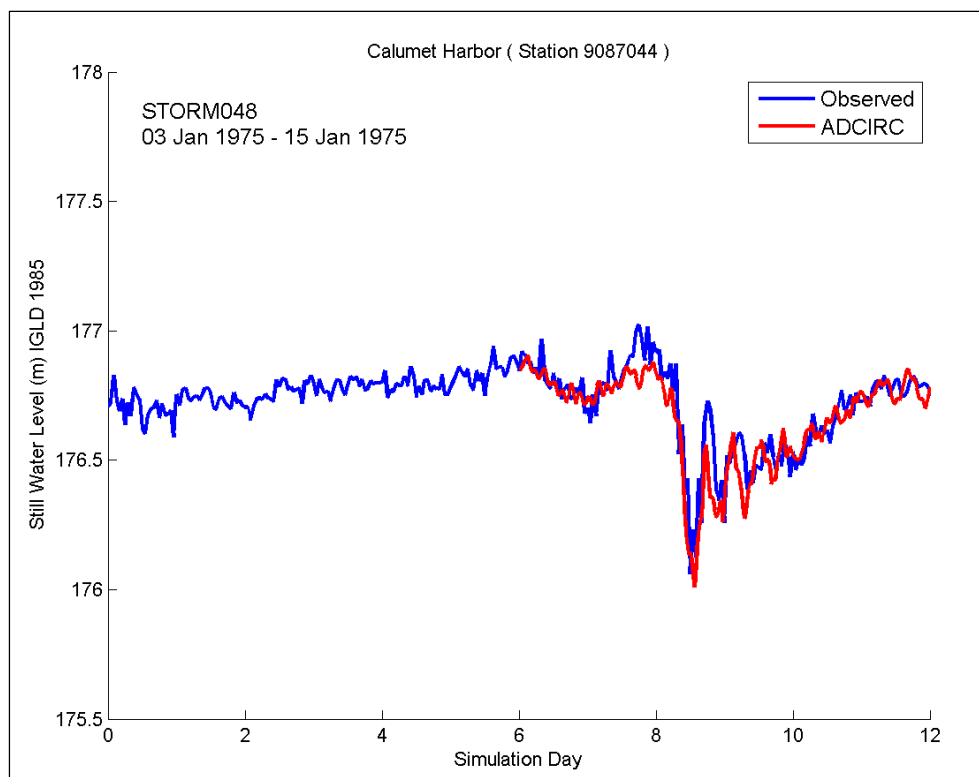


Figure 6-56. Time series of water levels for Storm048 (January 1975); Calumet Harbor.

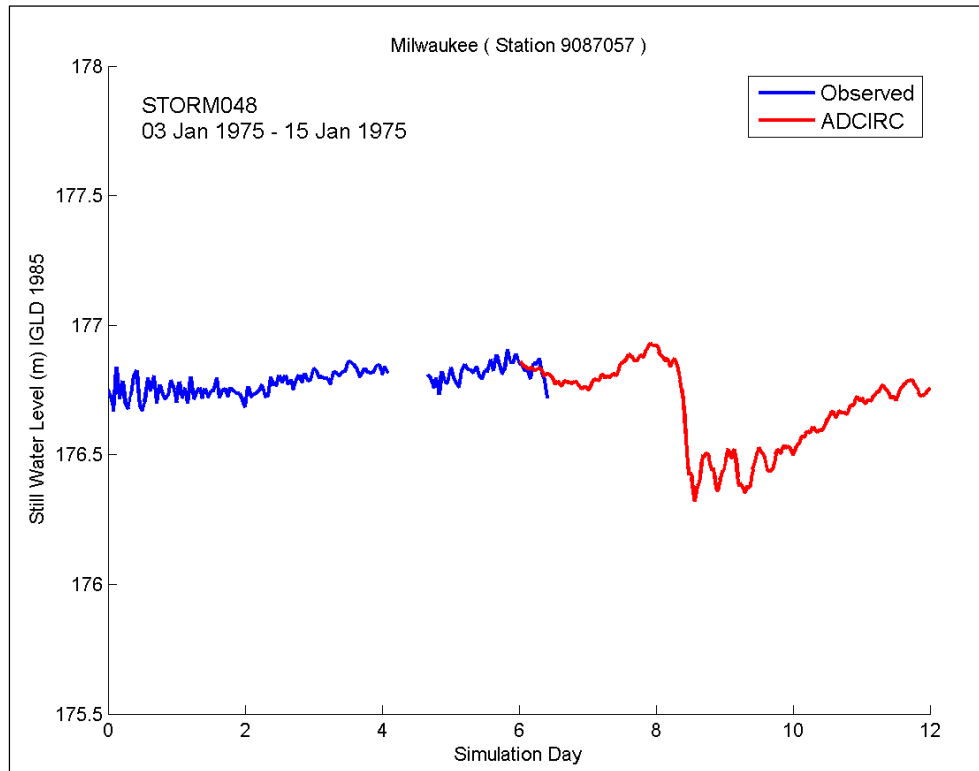


Figure 6-57. Time series of water levels for Storm048 (January 1975); Milwaukee.

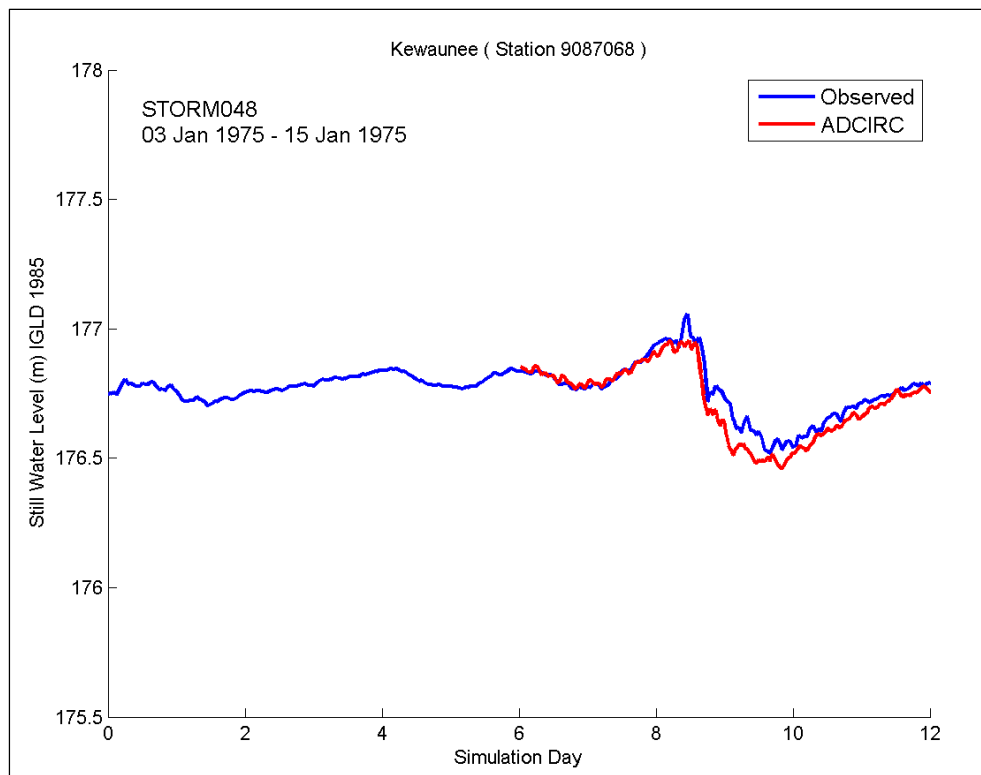


Figure 6-58. Time series of water levels for Storm048 (January 1975); Kewaunee.

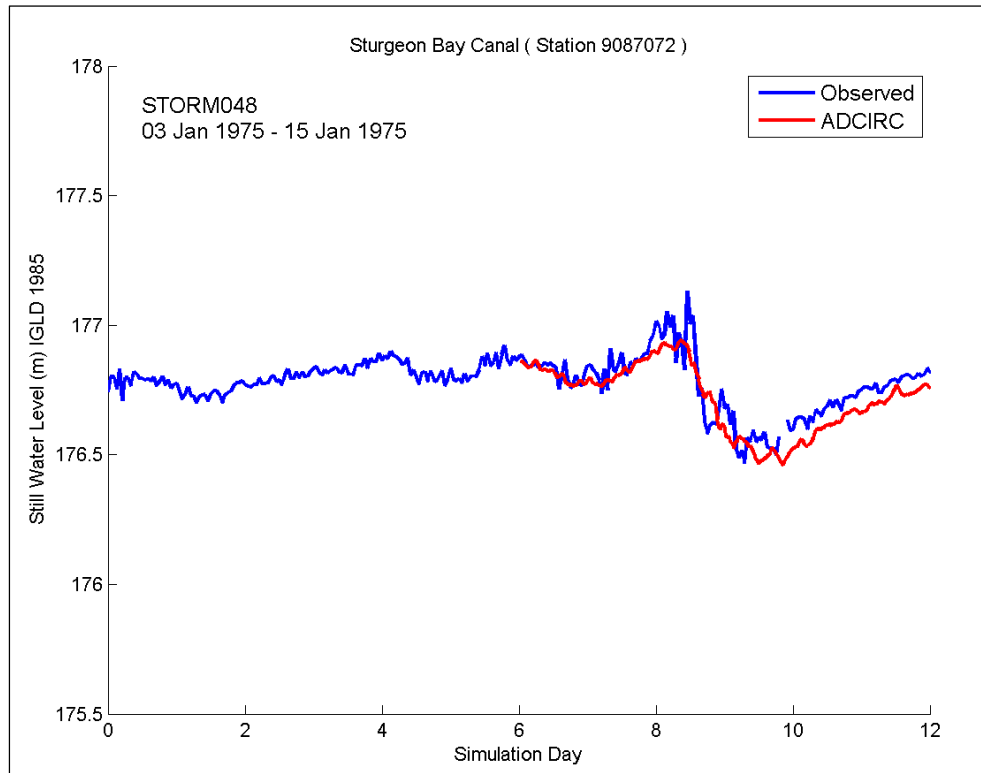


Figure 6-59. Time series of water levels for Storm048 (January 1975); Sturgeon Bay Canal.

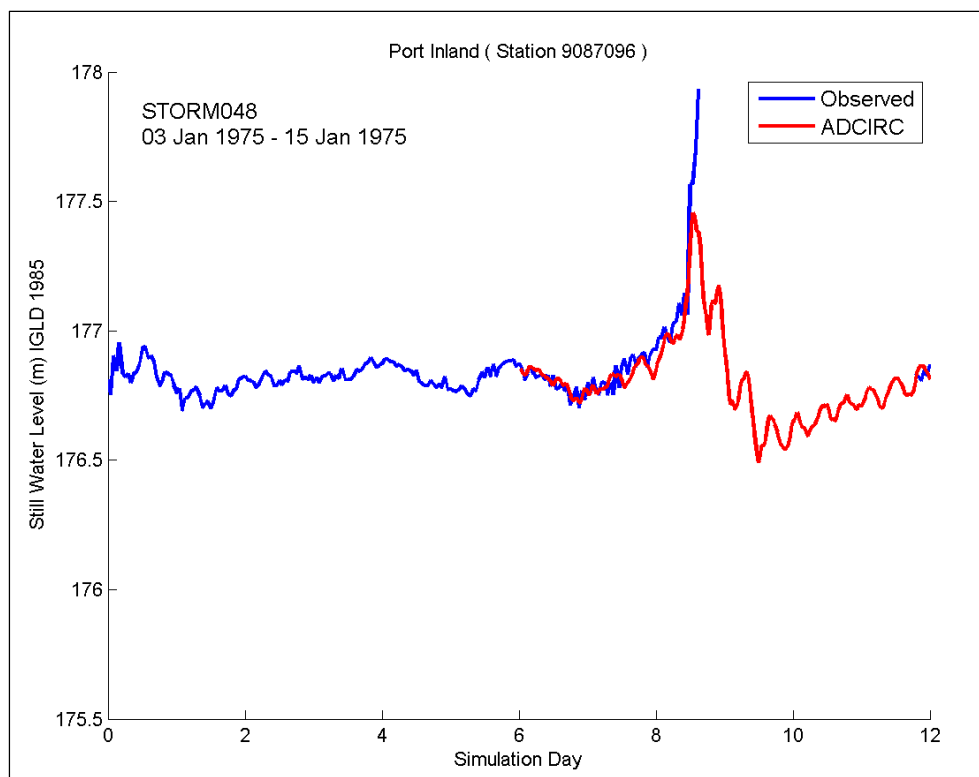


Figure 6-60. Time series of water levels for Storm048 (January 1975); Port Inland.

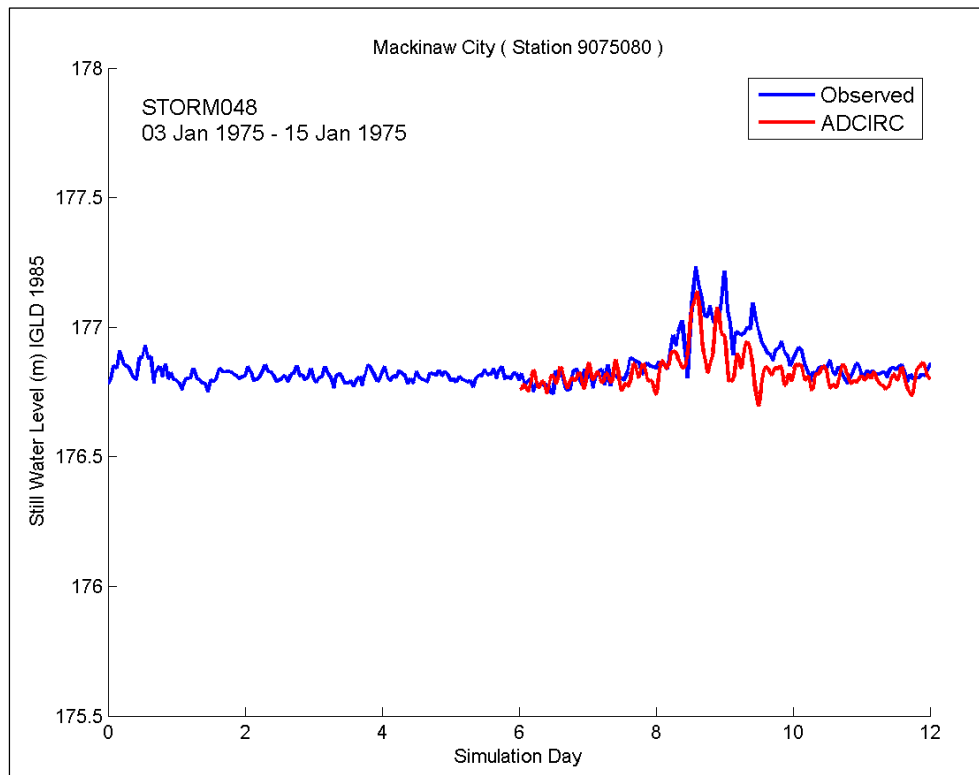


Figure 6-61. Time series of water levels for Storm048 (January 1975); Mackinaw City.

As mentioned, the simulated water level at Port Inland is the highest measured water level in Lake Michigan for this storm event; however, there is also a set down after the peak of the storm at this location. There is also significant set down in the south and southwest parts of Lake Michigan at Calumet Harbor (Figure 6-56) (0.8 m) and Kewaunee (Figure 6-58) (0.5 m) that occurs prior to the set down at Port Inland. In addition, the Green Bay and Milwaukee gages were not operational during part or all of this storm time period, but the simulated water levels indicate significant set down at these southern lake locations as well. An examination of wind and pressure fields for this storm indicates that wind direction is the main cause of this water level response. Storm 048 winds are from southwest to northeast, driving water away from Green Bay and Calumet and towards Port Inland. Low pressure tracks along the same path, contributing to the rise in water level at Port Inland. Other observations from this storm are that the simulated water levels at Ludington show that the model captures the trend in surge response extremely well; however, short period oscillations are not captured due to the spatial and temporal distribution of the atmospheric forcing conditions (Figure 6-54). The simulated surge response at Holland captures the general trend fairly well, but lacks some of the detailed oscillations observed in the measurements. For all locations in the lake, whether near the storm center or at a distance from the storm center, the model was able to capture the trend in surge response magnitude and duration. The ability to simulate set down at Calumet and set up and set down at Port Inland again displays the ability of ADCIRC to simulate storm surge hydrodynamics in Lake Michigan. Small scale oscillations that are finer than the temporal and spatial scales of the forcing conditions were not captured in the simulated responses.

The third storm selected for discussion is Storm 061. This storm was selected because its impact was greatest in southern Lake Michigan. Storm 061 produces the second largest waves recorded at Milwaukee and the 20th largest water levels recorded at Calumet Harbor. The time series of water levels for this storm show a large variability in response from location to location (Figures 6-62 through 6-70). The time-series figures are arranged to begin at Ludington and then progress clockwise around the lake. Nine NOAA water level gages were operational during all or part of this storm event. This storm passed over southern Lake Michigan with little impact observed at mid-lake and northern lake gages. (An examination of the wind and atmospheric pressure fields applied to the model for this storm event shows winds out of the north as the low pressure system passes from east to

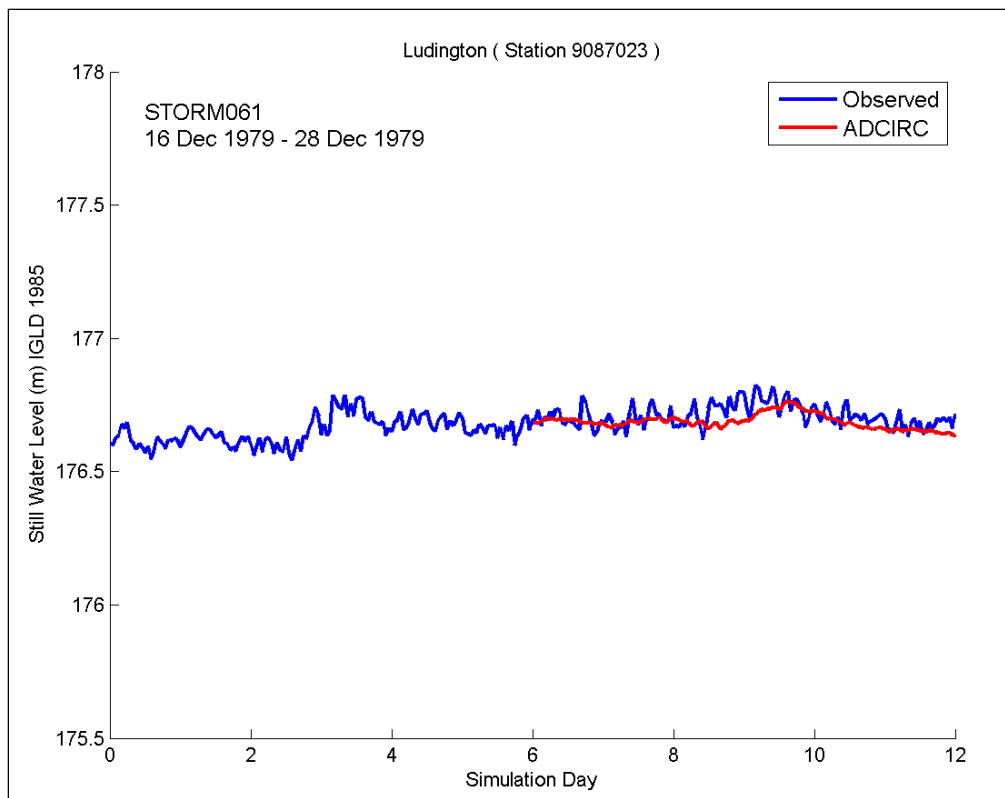


Figure 6-62. Time series of water levels for Storm061 (December 1979); Ludington.

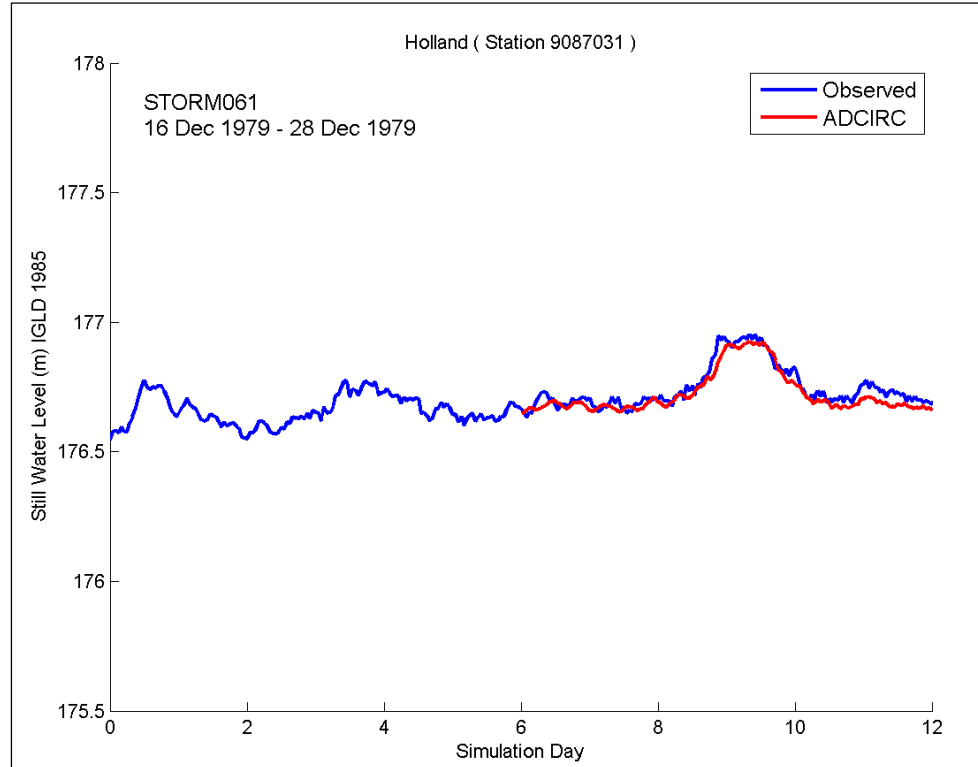


Figure 6-63. Time series of water levels for Storm061 (December 1979); Holland.

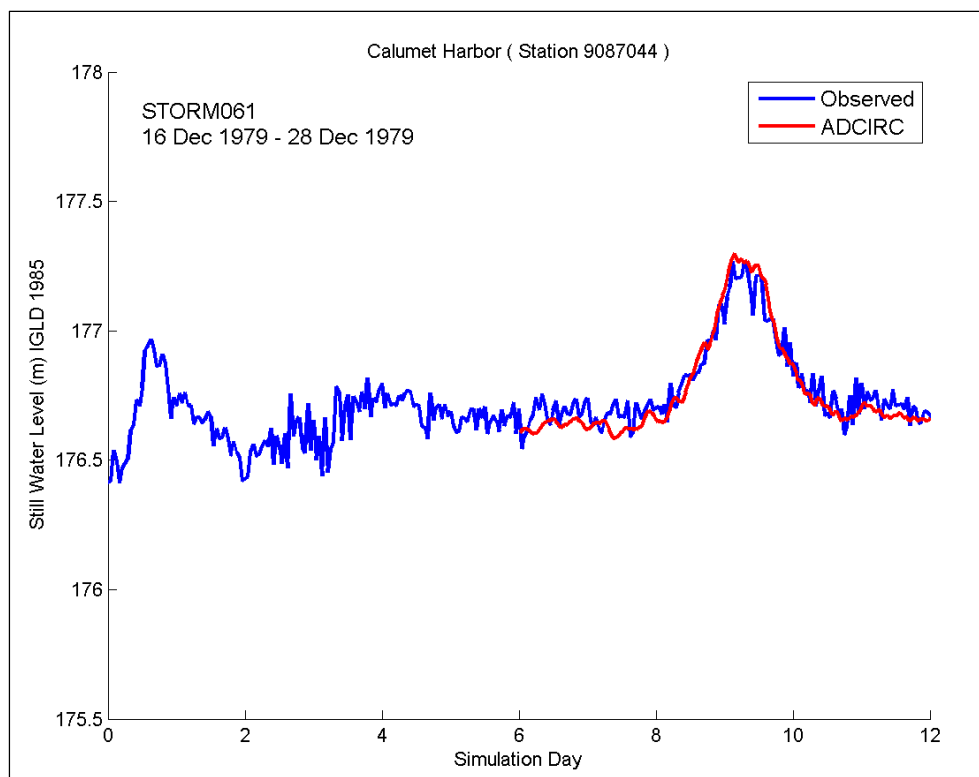


Figure 6-64. Time series of water levels for Storm061 (December 1979); Calumet Harbor.

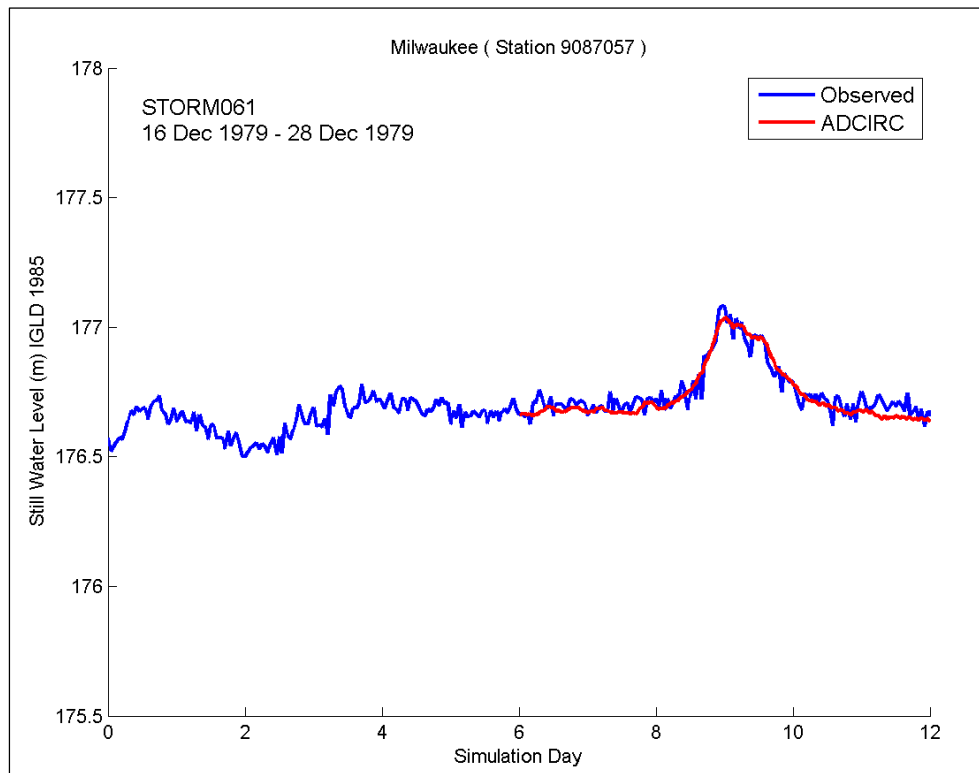


Figure 6-65. Time series of water levels for Storm061 (December 1979); Milwaukee.

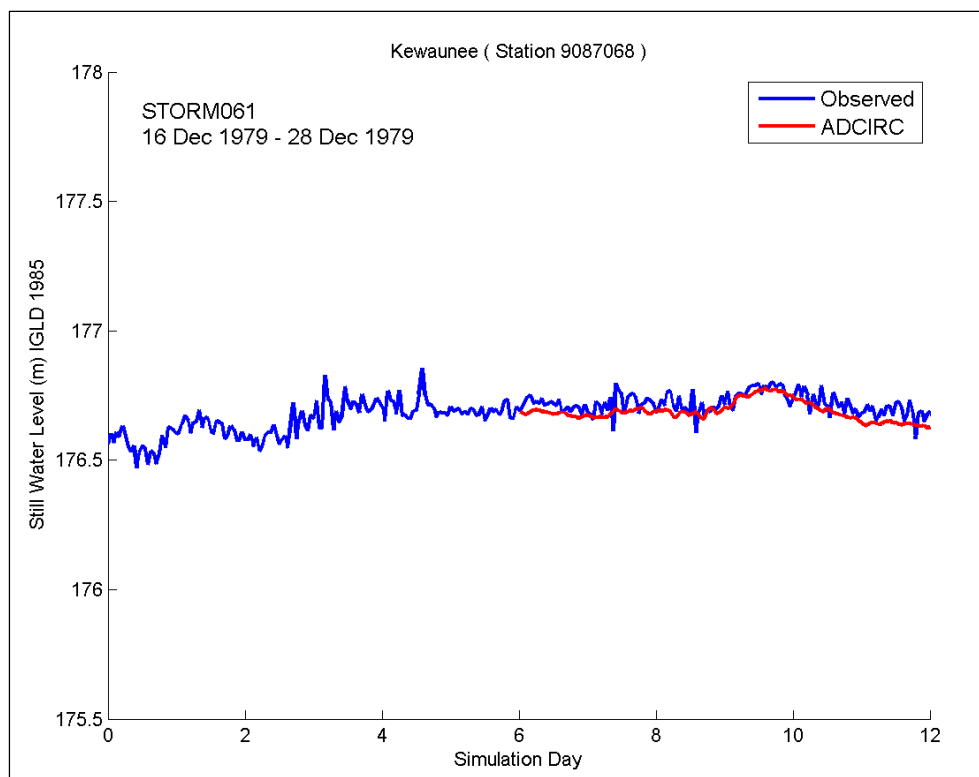


Figure 6-66. Time series of water levels for Storm061 (December 1979); Kewaunee.

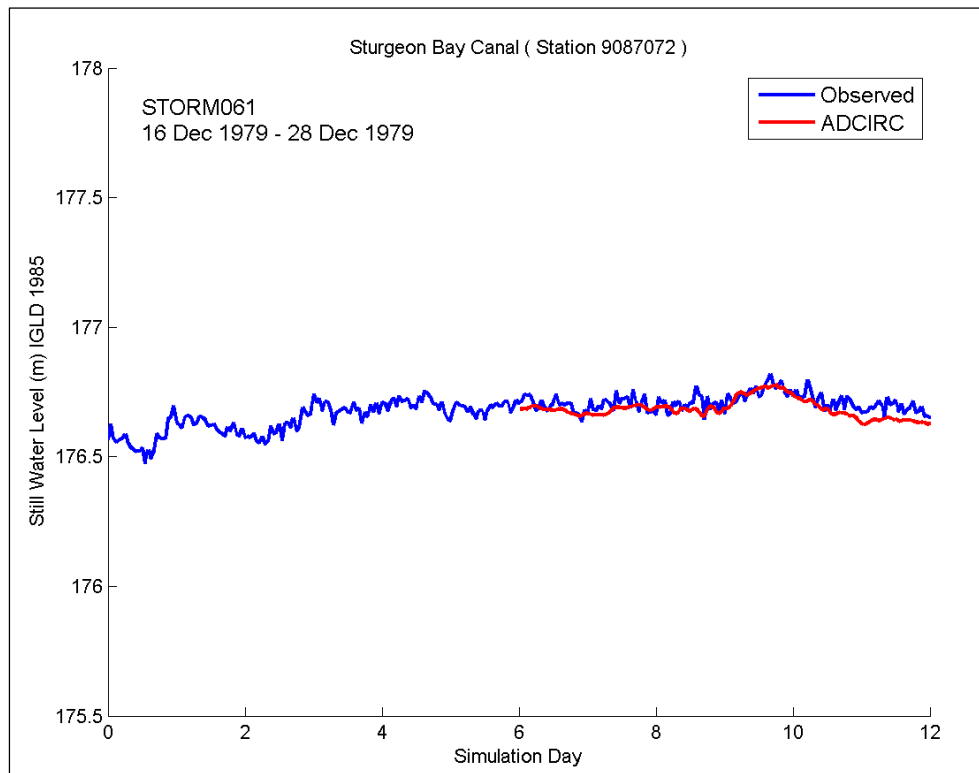


Figure 6-67. Time series of water levels for Storm061 (December 1979); Sturgeon Bay Canal.

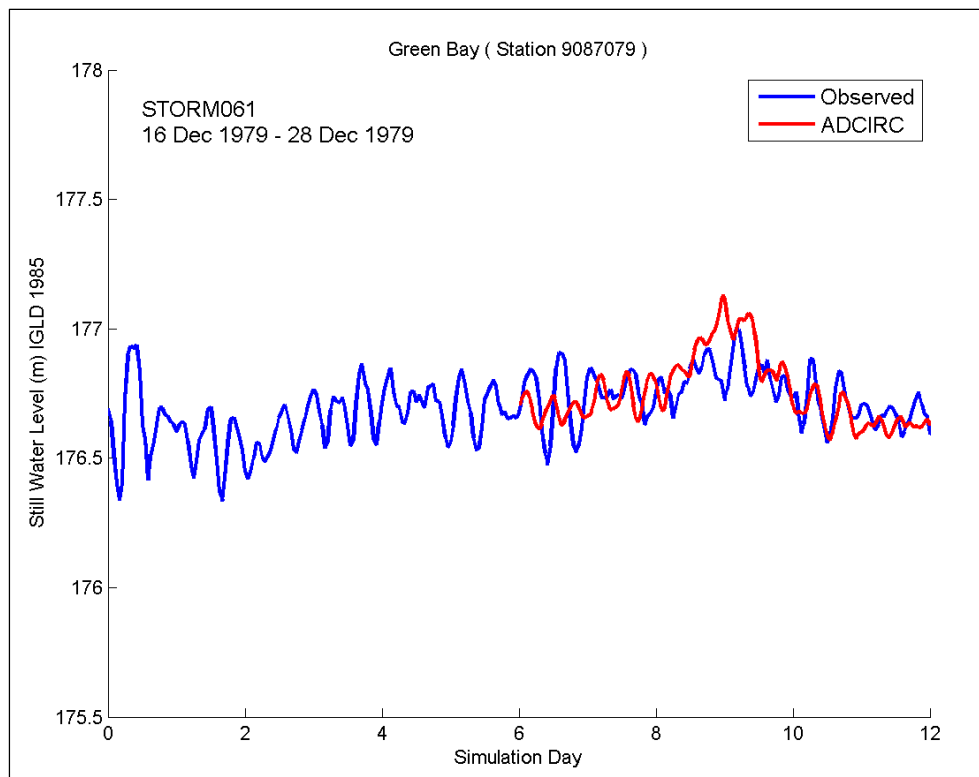


Figure 6-68. Time series of water levels for Storm061 (December 1979); Green Bay.

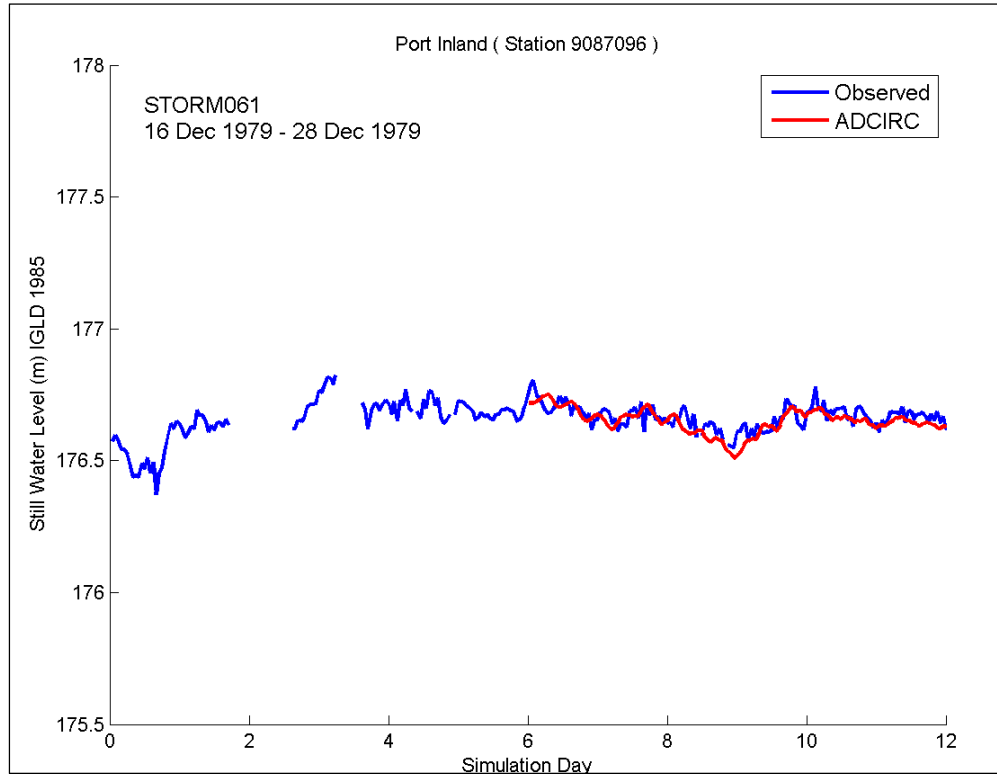


Figure 6-69. Time series of water levels for Storm061 (December 1979); Port Inland.

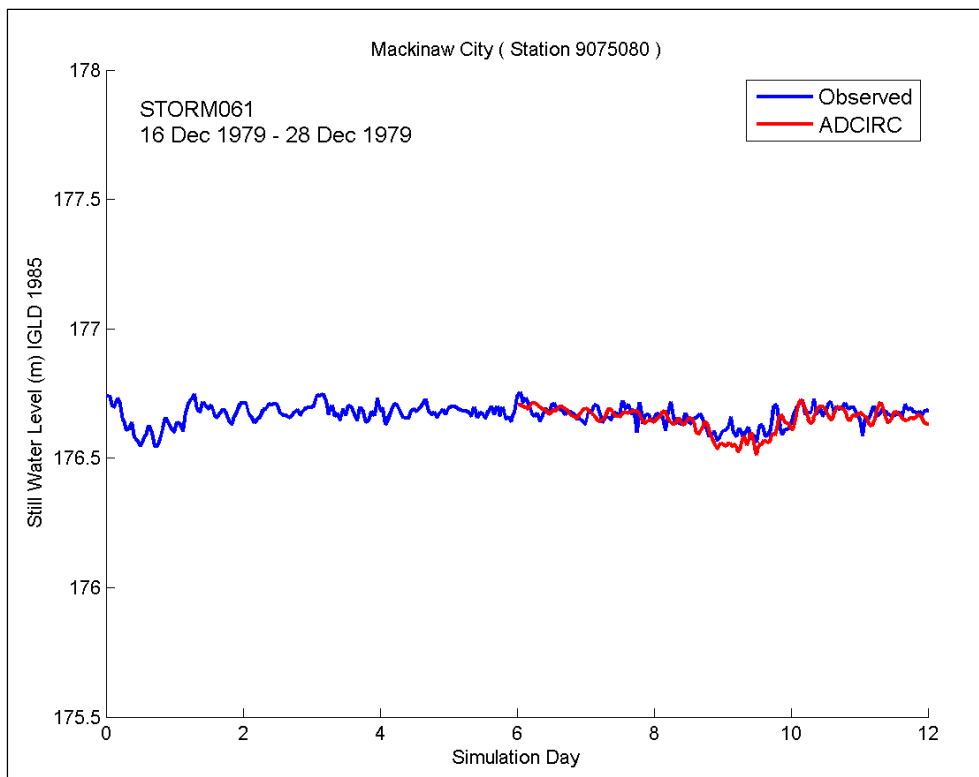


Figure 6-70. Time series of water levels for Storm061 (December 1979); Mackinaw City.

west over southern Lake Michigan and southern Lake Huron.) Time series of water levels at the mid-lake at northern lake gages at Ludington (Figure 6-62), Kewaunee (6-66), Sturgeon Bay Canal (6-67), Port Inland (6-69), and Mackinaw City (6-70) show minimal water level oscillation for this storm event. Further south, the surge response increases at Holland (Figure 6-63) and Milwaukee (6-65) to approximately 0.3 m and at Calumet (Figure 6-64) the surge response is 0.6 m. At Green Bay, model performance is fair, capturing the general trend, but not the detailed oscillations. There are several possible causes for the lower model skill at Green Bay. Because details of this wind event are not captured in the wind and pressure applied as forcing conditions at Green Bay, the model performance is weak at this location. In addition, the effect of waves on water levels is not included in the simulations, which could be significant in Green Bay for this event.

The last storm selected for discussion is Storm 129. Nine NOAA water level gages were operational during all or part of this storm event. The time series of simulated and measured water levels for this storm show a large variability in response from location to location (Figures 6-71 through 6-79). This storm was selected because of the extreme set down at Calumet and Green Bay, the well-defined, peak surge at Port Inland, and the mid-lake surge

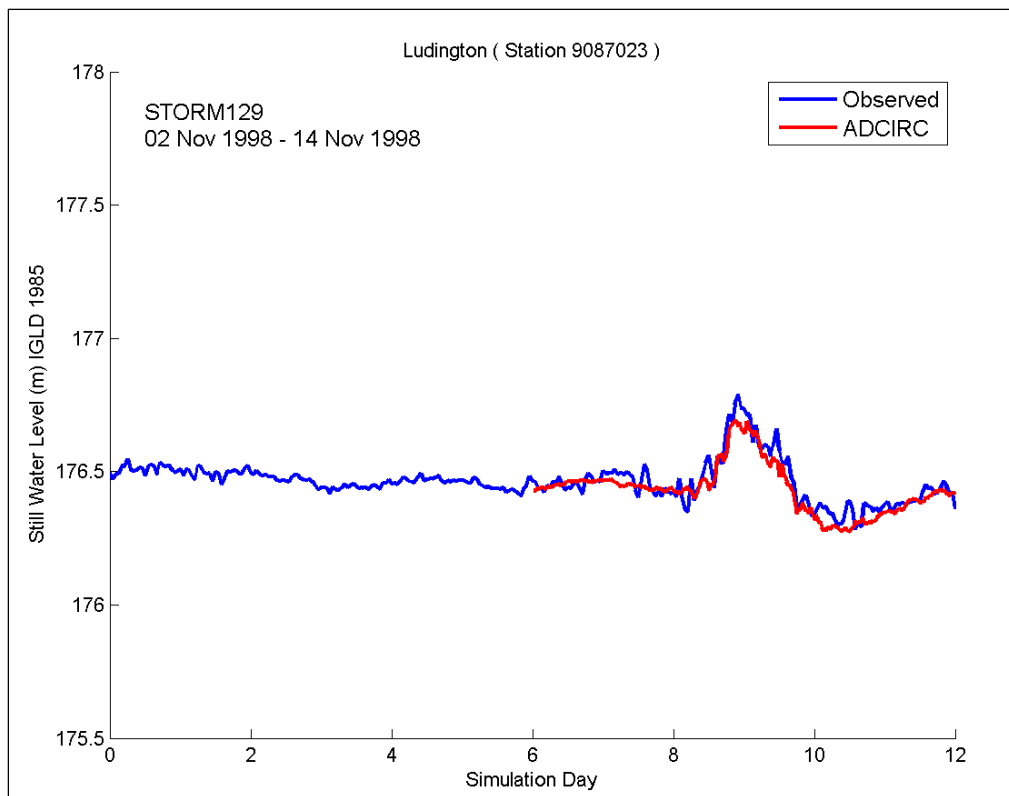


Figure 6-71. Time series of water levels for Storm129 (November 1998); Ludington.

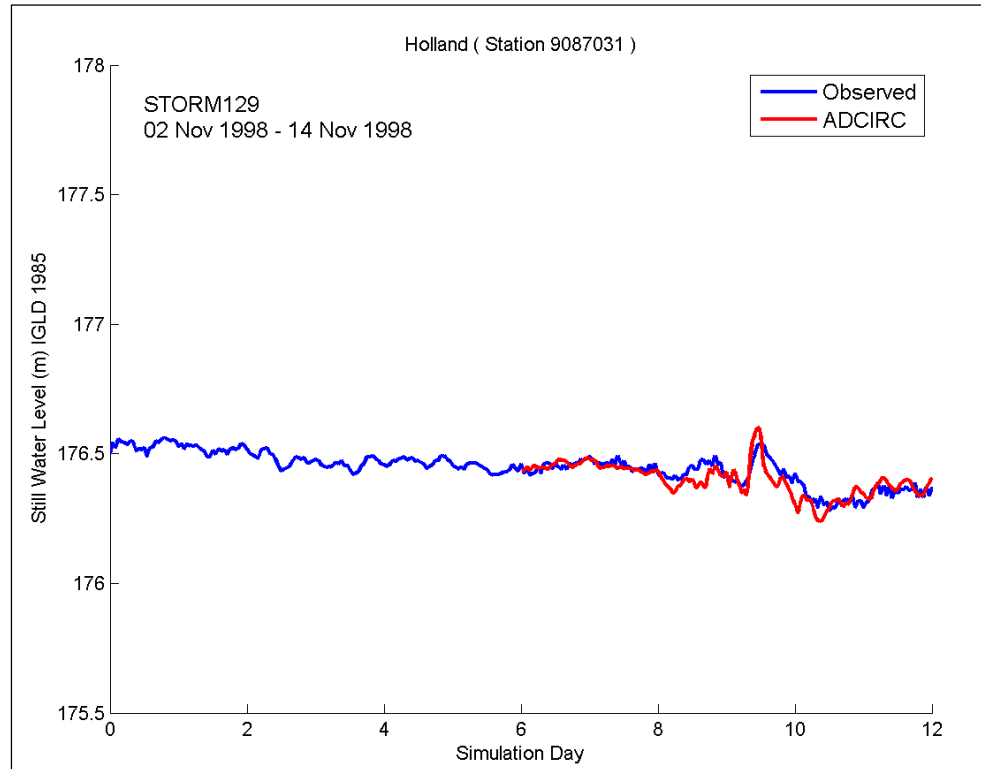


Figure 6-72. Time series of water levels for Storm129 (November 1998); Holland.

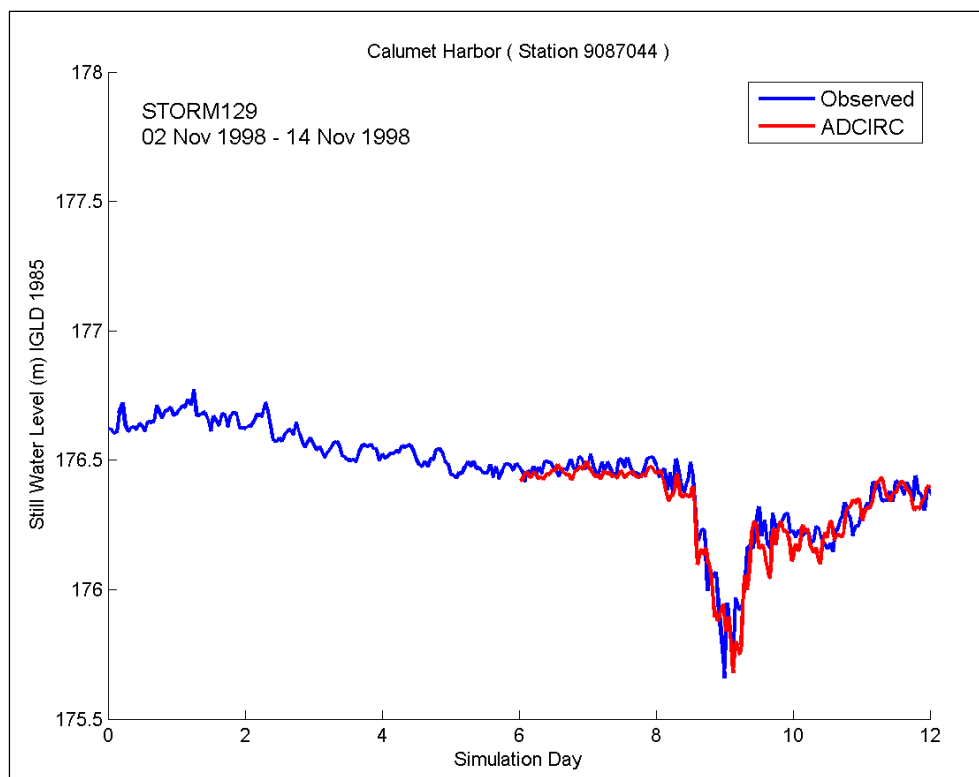


Figure 6-73. Time series of water levels for Storm129 (November 1998); Calumet Harbor.

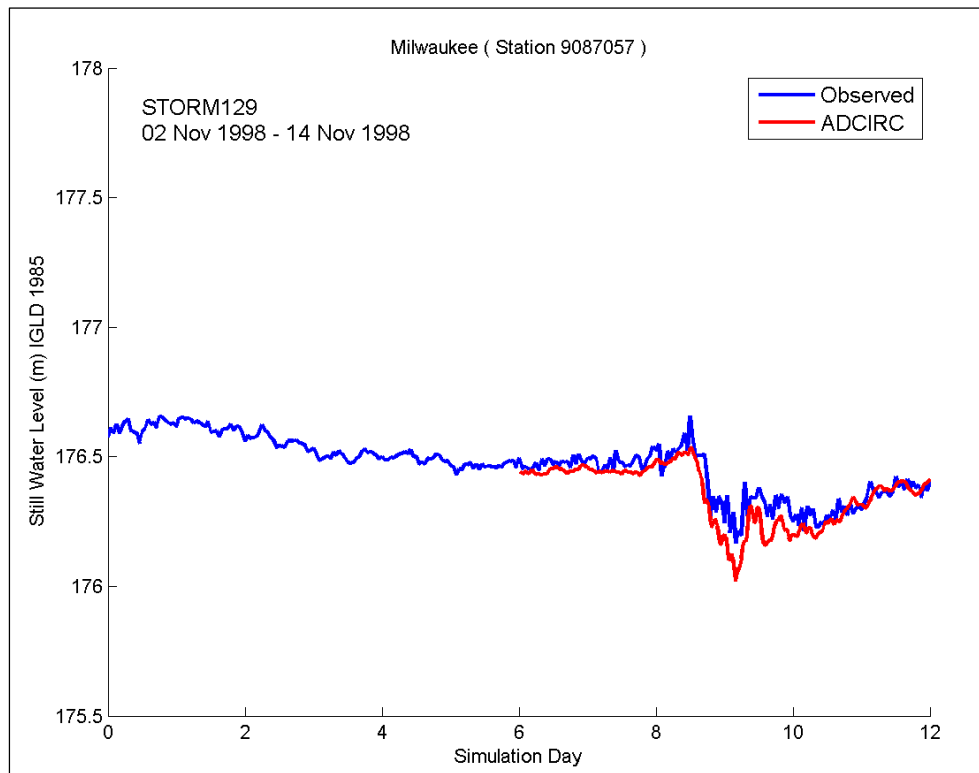


Figure 6-74. Time series of water levels for Storm129 (November 1998); Milwaukee.

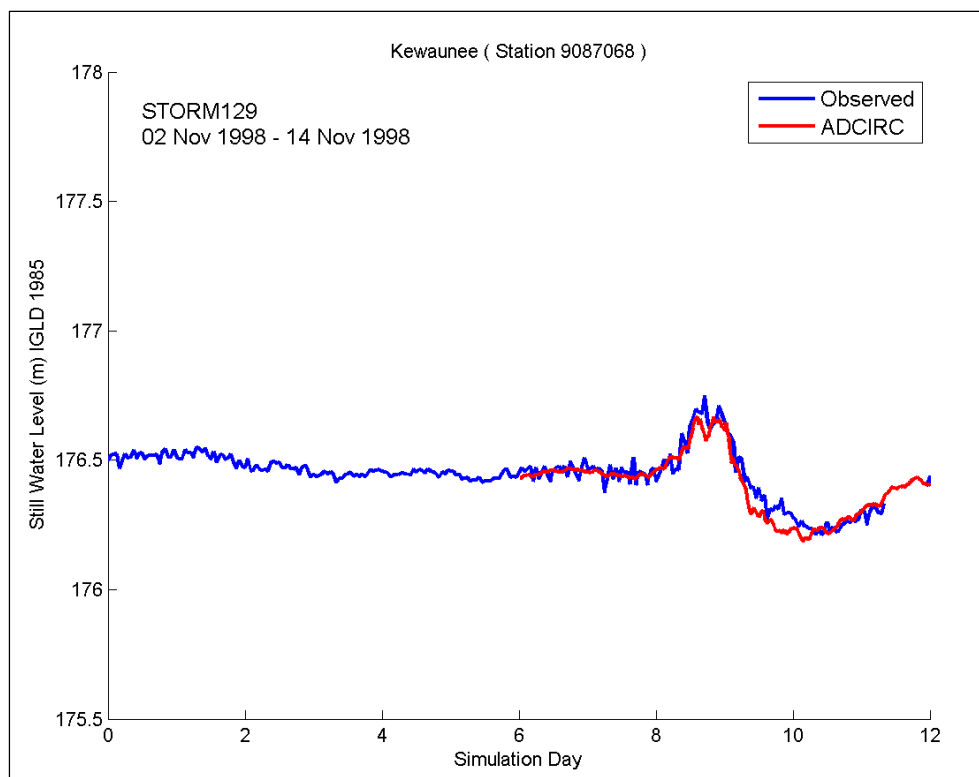


Figure 6-75. Time series of water levels for Storm129 (November 1998); Kewaunee.

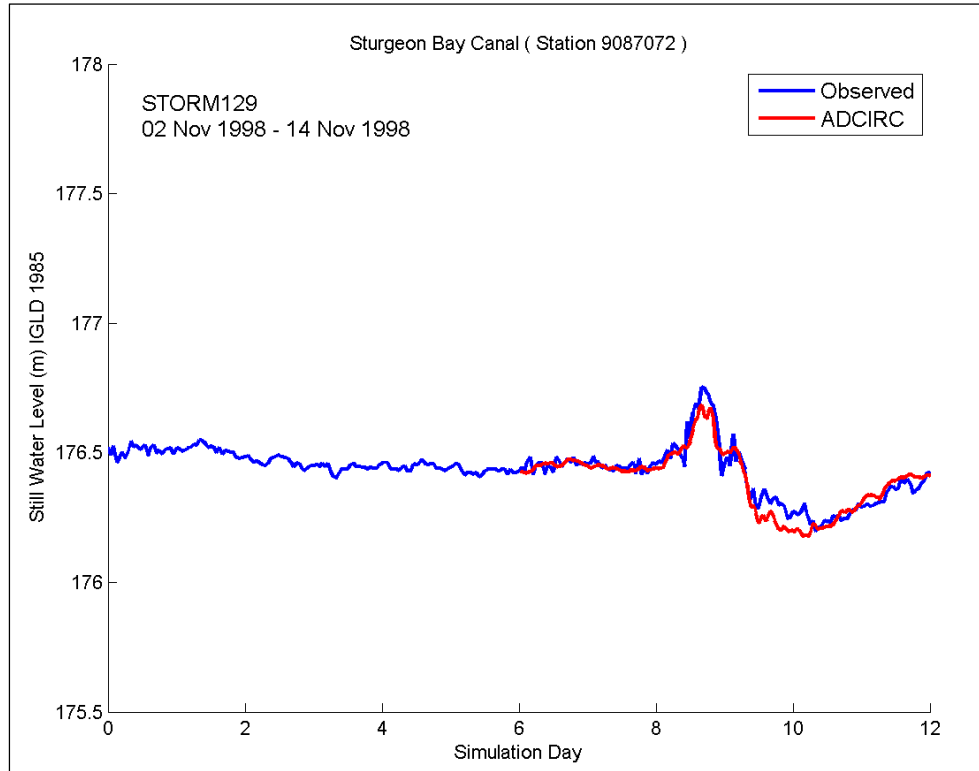


Figure 6-76. Time series of water levels for Storm129 (November 1998); Sturgeon Bay Canal.

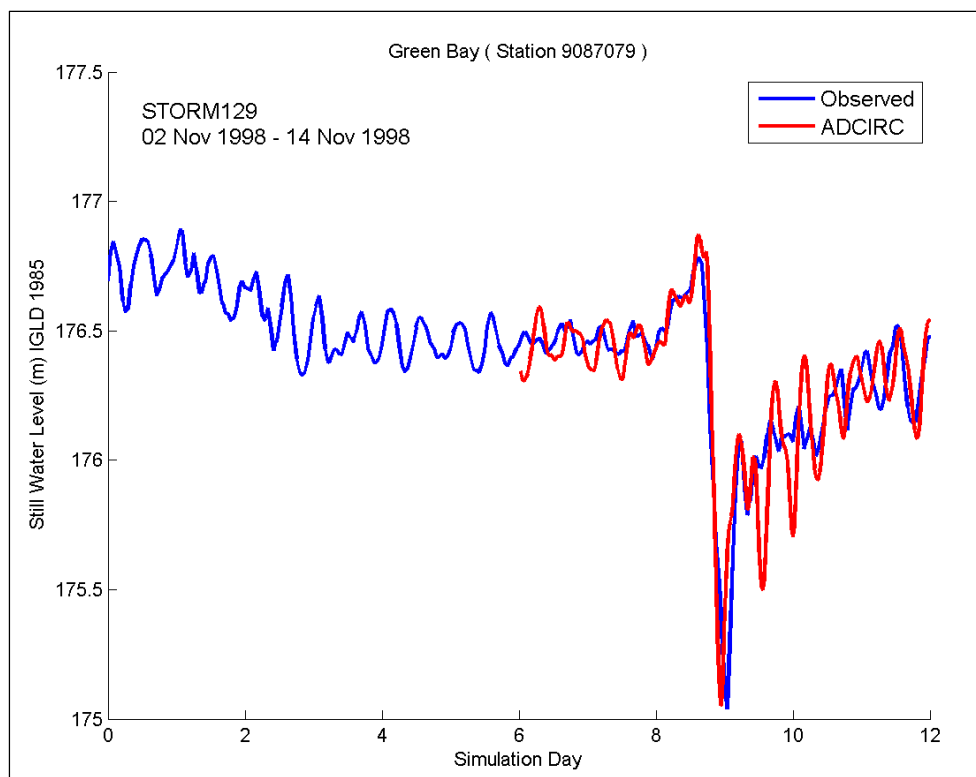


Figure 6-77. Time series of water levels for Storm129 (November 1998); Green Bay.

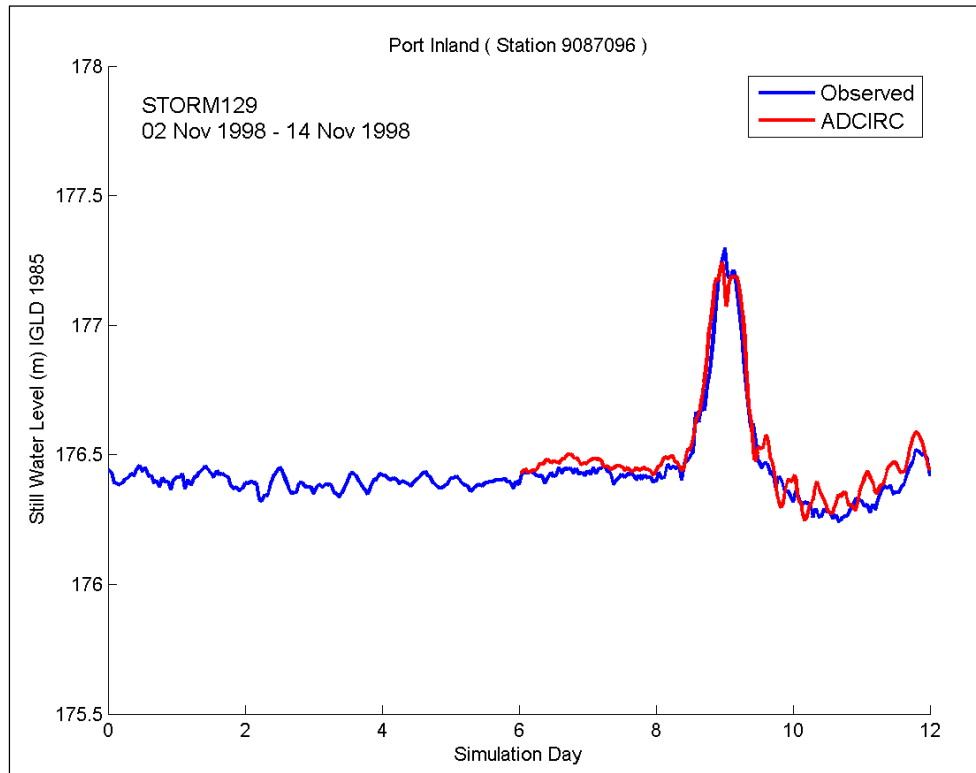


Figure 6-78. Time series of water levels for Storm129 (November 1998); Port Inland.

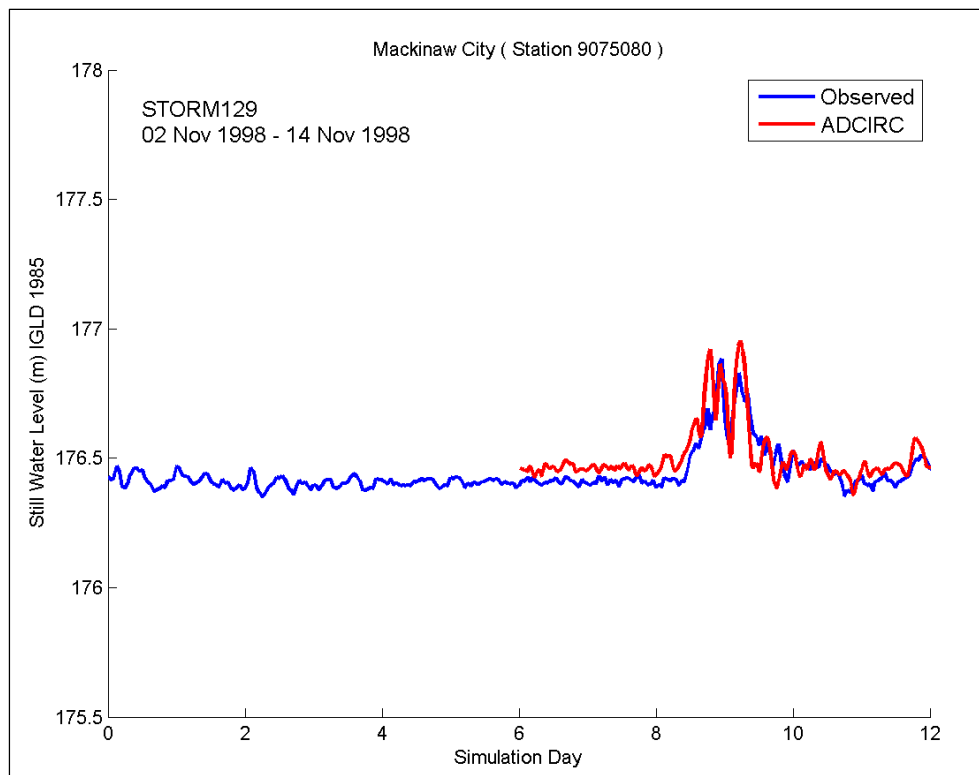


Figure 6-79. Time series of water levels for Storm129 (November 1998); Mackinaw City.

response. Storm 129 is the third ranked surge event at Port Inland and the first ranked wave event at Mackinaw City. The time-series figures that are discussed in this section are arranged to begin at Ludington and then progress clockwise around the lake. An examination of the winds and atmospheric pressure applied to represent this storm shows winds out of the southeast, south, then southwest as a low pressure system passes over Green Bay then sweeps eastward over northern Lake Michigan. The combination of low pressure and northeasterly-directed winds causes a surge response and then a large drop in water level at Green Bay (Figure 6-77). The change in wind direction from onshore to alongshore to offshore at Milwaukee causes a slight increase in water level and then a decrease in water level (Figure 6-74). Calumet does not experience onshore winds or low pressures and therefore responds to the offshore winds only. Water level at this location experiences a notable drop for this storm event (Figure 6-73). The mid-lake gages (Ludington and Holland on the east and Sturgeon Bay Canal and Kewaunee on the west) show a small surge response then a small degree of set down. The gages on the west side of the lake (Sturgeon Bay Canal and Kewaunee) first experience onshore winds and some of the lower storm pressure contributing to the increase in water level followed by offshore winds and a lowering of water level (Figures 6-76

and 6-75, respectively). On the east side Ludington experiences offshore then onshore winds as the low pressure system passes and experiences a surge response similar to what is observed at Keweenaw. However, the response at Ludington occurs later, has a longer duration, and has less set down than the gages on the west side of the mid-lake region (Figure 6-71). Further south along the eastern shoreline, Holland responds mainly to the onshore winds during the latter part of this storm event and exhibits a small increase in water level (Figure 6-72). Port Inland responds strongly to the onshore winds and low pressure system that passes directly over this location. The 0.8 m surge response is extremely well modeled in magnitude and duration by ADCIRC (Figure 6-78). The nearest gage to Port Inland is at Mackinaw City where the response is quite different than what is observed at Port Inland. The Mackinaw City gage is actually located in Lake Huron and does not experience the onshore winds along the long axis of Lake Michigan that Port Inland experiences. The Mackinaw City water level response appears to be mainly due to the passage of the low pressure system over the Straits of Mackinac. For all locations in the lake, whether near the storm center across Green Bay and the northern part of Lake Michigan or at a distance from the storm center (for example, Calumet), the model was able to capture the trend in surge response magnitude and duration as well as the notable set down at several locations. The ability to simulate set down at Calumet and Green Bay, set up at Port Inland, and the various levels of set up/set down at the central gage locations again displays the ability of ADCIRC to simulate storm surge hydrodynamics in Lake Michigan. Small scale oscillations that are finer than the temporal and spatial scales of the forcing conditions were not captured in the simulated responses.

6.7 Statistics

The ADCIRC water level time series results were evaluated and compared to measured NOAA water levels at 10 locations. The statistical comparisons tabulated for each storm and each location are the Bias (model minus measurements) (Table 6-7) and root-mean-square error (RMSE) (Table 6-8). The statistical tests are performed on the time series of water levels for the final 6 days of the storm simulation. (The first six days were considered the model spin up time period and modeled time-series were not saved during that time period.) Areas in the table marked with a dashed line indicate that measured data were not available for that gage for the particular storm time period. Storms 001 through 026 had no data available and were therefore removed from the tables.

Table 6-7. Water level bias for all storms and all gages, meters.

STORM	9075080	9087096	9087023	9087031	9087044	9087057	9087068	9087072	9087079	9087088
027	-0.04	-0.05	0	-	-0.01	0	-	-0.04	-	-
028	-0.02	-0.06	0	-0.02	-0.02	-0.01	-	-0.04	-	-
029	-0.01	-0.03	0	0	-0.02	0.01	-	0	-	-
030	-0.02	-0.05	0	-0.01	-0.02	0	-	-0.01	-	-
031	-0.01	-0.02	0	-0.01	-0.03	-0.01	-	-0.04	-	-
032	-0.04	-0.05	0.01	0.04	0.06	0.03	-	-0.01	-	-
033	-0.03	-0.04	0.01	0.02	0.02	0.01	-	-0.02	-	-
034	0.00	-0.04	0.01	0.03	0.03	0.03	-	0	-	-
035	-	-0.03	-	0.02	-0.02	-0.01	--	-0.04	-	-
036	-	-0.07	-0.03	-0.02	-0.05	-0.06	-	-0.1	-	-
037	-0.04	-0.04	0.02	0	-	0	-	-0.03	-	-
038	-0.07	-0.07	-0.01	-0.03	-	-0.04	-	-0.05	-	-
039	-0.05	-0.07	-0.01	-0.01	-	-0.01	-	-0.07	-	-
040	0.00	-0.01	-0.04	-0.05	-0.06	-0.06	-0.04	-0.04	-0.04	-
041	-0.01	0.00	0.03	-	0.03	0.03	-	0.02	-	-
042	-0.02	-0.06	-0.06	-0.05	-0.06	-0.06	-	-0.09	-	-
043	-	0.04	0.02	0.02	0.03	0.04	-	0.03	-	-
044	-	-0.01	0	-0.01	-0.01	0.01	0.04	0.04	-	-
045	-0.02	-0.03	-0.02	-0.04	-0.04	-0.02	-0.02	-0.04	-	-
046	0.02	-	0	0.01	0.02	0.03	0.04	0.01	-	-
047	0.04	0.03	0.03	0.03	0.02	0.04	0.05	0.03	-	-
048	-0.04	-0.03	-0.01	0	-0.03	0.01	-0.03	-0.04	-	-
049	0	-0.02	-0.01	-0.02	-0.03	-0.02	0	-0.03	-	-
050	-0.01	-0.04	-0.01	-0.04	-0.03	0	0.01	-0.01	-	-
051	0	-0.01	0.02	0.03	0.01	0.02	0.02	0.01	-	-
052	-0.01	-0.02	-0.02	-0.05	-0.02	-0.02	-0.03	-0.05	-	-
053	-0.01	-0.01	-0.01	-0.01	-0.02	-0.01	-0.03	-0.03	-	-
054	0.04	0.01	0.01	0.02	0.03	0.03	0	0.01	-	-
055	0.03	0.01	0.02	0.04	0.02	0.01	-0.02	0	-	-
056	0.01	0.03	0.02	0	-0.01	0.01	0.01	0.02	-	-
057	-0.03	-0.02	0	0	0	0.01	0	0.01	-	-
058	-0.02	0	-0.01	0	-0.02	-0.02	-0.02	-0.01	-	-
059	0.03	-0.01	-0.01	-0.01	-0.02	-0.01	-0.01	-0.02	-	-
060	0	-0.01	-0.03	-0.04	-0.04	-0.02	-0.02	-0.02	0	-
061	-0.01	-0.01	-0.02	-0.02	-0.02	-0.01	-0.03	-0.02	0.01	-
062	0	-0.01	-0.02	-0.03	-0.04	-0.02	-0.02	-0.02	-0.01	-

STORM	9075080	9087096	9087023	9087031	9087044	9087057	9087068	9087072	9087079	9087088
063	0.01	-0.01	0	0	0	0	0	0	-	-
064	0.03	0.02	0.01	0.02	-0.01	0	0	0	-0.01	-
065	0	-0.02	-0.01	-0.02	-0.03	-0.02	-0.03	-0.03	0	-
066	0.02	0.01	0	-0.03	-0.01	-0.01	-0.02	-0.01	0.02	-
067	0.01	-0.02	-0.04	-0.02	-0.06	-0.01	-0.05	-0.05	-0.03	-
068	-0.01	0	-0.01	-0.01	-0.02	-0.01	-0.02	-0.01	-0.01	-
069	0	0	0	0	0.01	0	-0.01	0	0.07	-
070	0.04	0.03	0.02	0.02	0.01	0.02	0.01	0.03	0.15	-
071	0.07	0.06	0.05	0.05	0.04	0.06	0.05	0.06	0.09	-
072	0.03	0.01	0	-0.02	-	-0.01	0	0	0	-
073	0.02	0.02	-	0	-0.02	-0.01	0	0	-0.04	-
074	0.04	0.04	0.04	0.04	0	0.02	0.03	0.03	-0.02	-
075	0.02	0.04	0.01	0.01	0	0	0	0.01	0.03	-
076	0.01	0	0	0	-0.02	-0.01	-0.01	0	0.09	-
077	0.03	0.03	0.03	0.03	0.03	0.04	0.03	0.04	0.05	-
078	-0.03	-0.05	-0.01	0.03	0.18	0.09	0.02	0.02	0.11	-
079	0.03	0.03	-0.01	0	-0.02	-0.05	-0.01	-0.01	0.05	-
080	0.04	0.01	0.01	0.03	0.03	-0.02	0.01	0.02	0.05	-
081	0.02	0	-0.02	-0.01	-0.02	-0.05	-0.04	-0.01	0	-
082	0.02	0	-0.01	0.02	-0.01	-0.04	-0.02	-0.01	-0.01	-
083	0.02	0	0	0.01	-0.02	-0.05	-0.03	-0.02	-0.03	-
084	0.05	0.04	0.02	0.01	0	-0.05	0	0.01	0.04	-
085	0	0	-0.01	0	-0.01	-0.02	-0.03	-0.01	0	-
086	0.01	0	-0.02	-0.02	-0.03	-0.02	-0.03	-0.02	0.03	-
087	0.01	-0.01	-0.02	-0.03	-0.02	-0.02	-0.03	-	-0.02	-
088	0.02	0.03	0	0.01	0	0	0	0	0.02	-
089	-0.02	-0.01	-0.07	-0.06	-0.07	-0.06	-0.01	-0.04	-0.03	-
090	0.01	-0.02	-0.02	-	-0.05	-0.05	-0.06	-0.04	-0.07	-
091	0.06	0.02	-0.01	0.06	0.01	-0.02	0	0	0	-
092	-0.01	-0.02	-0.03	-0.03	-0.04	-0.04	-0.01	-0.03	-0.03	-
093	-0.01	-0.02	-0.02	-0.01	-0.03	-0.04	-0.02	-0.03	-0.03	-
094	0.03	0.01	-0.02	-0.01	-0.02	-0.03	-0.01	-0.03	-0.07	-
095	0	-0.02	-0.05	-0.04	-0.08	-0.08	-0.05	-0.08	-0.19	-
096	0.04	0.01	-0.01	-0.02	-0.03	-0.04	-0.01	-0.03	-0.07	-
097	0.02	0	-0.04	-0.05	-0.08	-0.06	-0.04	-0.05	-0.12	-
098	0.01	0	-0.01	-0.02	-0.05	-0.04	-0.01	-0.02	-0.03	-
099	-0.01	0	-0.02	0.01	-0.03	-0.04	-0.04	-0.01	-0.03	-

STORM	9075080	9087096	9087023	9087031	9087044	9087057	9087068	9087072	9087079	9087088
100	0.01	0	-0.05	-0.06	-0.07	-0.07	-0.06	-0.06	-0.09	-
101	0.05	0.03	0	-0.01	-0.01	0	0.01	0.02	0.07	-
102	-0.02	-0.01	-0.05	-0.05	-0.04	-0.06	--	-0.03	-0.01	-
103	0.03	0	-0.02	0.12	-0.04	-0.05	-0.02	-0.02	0.06	-
104	0.03	0.02	-0.01	-0.02	-0.03	-0.03	-0.01	-0.01	-0.06	-
105	0.05	0.05	0.02	0.01	0.02	0	0.03	0.03	0.04	-
106	0	0	-0.03	-	-0.03	-0.06	-0.04	-0.04	-0.09	-
107	0.08	0.05	0.04	0.05	0.03	0.04	0.07	0.07	0.14	-
108	0.04	0.03	0.01	0.02	-0.03	0	0.02	0.03	-0.01	-
109	0.02	0.02	-0.03	-0.02	-0.02	-0.03	-0.01	-0.01	-0.01	-
110	0.01	0.01	-0.02	-0.02	-0.04	-0.04	-0.02	-0.02	-0.02	-
111	0.05	0.03	-0.01	0	0	0	0.01	0.02	0.12	-
112	0.02	0	-0.04	-0.05	-0.07	-0.07	-0.05	-0.05	-0.07	-
113	0.01	0.03	-0.05	-0.02	-0.02	-0.04	-0.03	-0.02	-0.03	-
114	0	-0.01	-0.09	-0.05	-0.06	-0.06	-0.04	-0.04	-0.05	-
115	0.01	0	-0.04	-0.03	-0.05	-0.06	-0.04	-0.04	-0.05	-
116	0.02	0.02	-0.06	-0.01	-0.03	-0.05	-0.02	-0.02	-0.02	-
117	0.06	0.06	-0.02	0	0	-0.02	0.01	0.02	-0.01	-
118	0.01	0	-0.02	-0.03	-0.03	-0.03	-0.03	-0.03	-0.06	-
119	0.01	0	-0.04	-0.04	-0.04	-0.05	-0.03	-0.03	-0.08	-
120	0.03	0.01	-0.02	-0.03	-0.03	-0.05	-0.03	-0.03	-0.05	-
121	0.06	0.04	0.04	0.03	0.03	0.01	0.03	0.04	0.13	-
122	0.06	0.05	0.03	0.03	0.02	0.01	0.02	0.03	0.06	-
123	0	0.01	-0.03	-0.03	-0.03	-0.05	-0.03	-0.03	-0.02	-
124	0.04	-	-0.04	-0.04	-0.05	-0.06	-	-0.04	-0.08	-
125	0.03	0.01	-0.02	-0.02	-0.03	-0.04	-	-0.02	-0.06	-
126	0.03	0.03	-0.03	-0.02	-0.01	-0.03	-0.01	0	-0.04	-
127	0.07	0.05	0.02	0.02	0.01	0	0.02	0.03	0.07	-
128	0.04	0.03	-0.02	-0.03	-0.04	-0.04	-0.01	-0.04	-0.02	-
129	0.04	0.04	-0.02	-0.01	-0.03	-0.04	-0.02	-0.01	0	-
130	0.04	0.03	-0.02	-0.01	-0.01	-0.04	-0.01	0	0.03	-
131	0.04	0.02	-0.04	-0.03	-0.05	-0.06	-0.05	-0.04	-0.15	-
132	0.06	0.05	0.01	-	0.02	0.01	-	0.03	0	-
133	0.05	0.03	-0.03	-0.02	-0.03	-0.03	-0.01	-0.01	-0.04	-
134	-0.02	-0.02	-0.07	-0.08	-0.08	-0.07	-0.05	-0.05	-0.05	-
135	0.05	0.03	-0.03	-0.02	-0.05	-0.05	-0.02	-0.03	-0.07	-
136	0.07	0.04	-0.01	0	-0.02	-0.01	0.01	0.01	0	-

STORM	9075080	9087096	9087023	9087031	9087044	9087057	9087068	9087072	9087079	9087088
137	0.04	0.03	-0.03	-0.04	-0.03	-0.04	-0.01	-0.01	-0.07	—
138	0.04	0.01	-0.04	-0.04	-0.06	-0.05	-0.01	-0.03	-0.01	—
139	0.04	0.02	-0.02	-0.02	-0.05	-0.03	-0.01	-0.02	-0.04	—
140	0.01	0	-0.07	-0.06	-0.08	-0.07	-0.05	-0.05	-0.08	—
141	0.03	0.01	-0.06	-0.04	-0.05	-0.06	-0.04	-0.04	-0.05	-0.04
142	0.08	—	0.01	0.02	0.01	0.01	0.02	0.02	-0.04	0.04
143	0.06	0.04	-0.02	-0.02	-0.04	-0.02	-0.01	0	-0.04	0
144	0.1	0.07	0.01	0	-0.01	0	0.02	0.03	0.08	0.07
145	0.05	0.03	-0.02	-0.02	-0.03	-0.02	-0.01	0	-0.04	0.01
146	0.02	0.03	-0.04	-0.04	-0.05	-0.06	—	-0.03	-0.03	-0.02
147	0.06	0.04	-0.02	-0.03	-0.04	-0.04	-0.02	-0.02	-0.07	-0.01
148	0.04	0.03	-0.04	-0.06	-0.08	-0.07	-0.05	-0.05	-0.14	-0.06
149	0.04	0.03	-0.02	-0.02	-0.02	-0.03	-0.01	-0.01	0.01	0
150	0.06	0.05	-0.01	-0.02	-0.01	-0.02	0.01	0.01	-0.01	0.02

Table 6-8. Water level root mean square error for all storms and all gages, meters.

STORM	9075080	9087096	9087023	9087031	9087044	9087057	9087068	9087072	9087079	9087088
027	0.07	0.1	0.04	—	0.1	0.07		0.08		
028	0.06	0.08	0.04	0.04	0.07	0.04		0.06		
029	0.05	0.06	0.04	0.04	0.07	0.05		0.05		
030	0.05	0.07	0.03	0.03	0.05	0.03		0.03		
031	0.04	0.05	0.04	0.04	0.06	0.04		0.06		
032	0.09	0.09	0.06	0.08	0.11	0.08		0.06		
033	0.08	0.1	0.05	0.06	0.1	0.06		0.06		
034	0.06	0.1	0.05	0.06	0.1	0.07		0.06		
035	—	0.09	—	0.05	0.08	0.06		0.07		
036	—	0.12	0.07	0.05	0.09	0.09		0.12		
037	0.07	0.06	0.05	0.04	—	0.06		0.06		
038	0.1	0.11	0.05	0.06	—	0.07		0.08		
039	0.1	0.12	0.06	0.07	—	0.08		0.12		
040	0.03	0.03	0.05	0.05	0.08	0.06	0.05	0.05	0.11	
041	0.05	0.05	0.05	—	0.07	0.06	—	0.05	—	
042	0.05	0.11	0.1	0.1	0.12	0.12	—	0.15	—	
043	—	0.06	0.04	0.04	0.06	0.05	—	0.04	—	
044	—	0.05	0.04	0.04	0.06	0.04	0.05	0.05	—	
045	0.05	0.05	0.04	0.05	0.08	0.04	0.03	0.05	—	
046	0.04	—	0.03	0.03	0.07	0.05	0.05	0.03	—	

STORM	9075080	9087096	9087023	9087031	9087044	9087057	9087068	9087072	9087079	9087088
047	0.06	0.05	0.05	0.04	0.07	0.08	0.05	0.05	-	
048	0.08	0.1	0.04	0.06	0.09	0.04	0.05	0.07	-	
049	0.03	0.05	0.04	0.04	0.06	0.05	0.03	0.05	-	
050	0.05	0.06	0.03	0.05	0.06	0.04	0.04	0.04	-	
051	0.06	0.08	0.04	0.05	0.08	0.05	0.04	0.04	-	
052	0.05	0.05	0.04	0.06	0.08	0.05	0.04	0.07	-	
053	0.06	0.04	0.03	0.04	0.06	0.05	0.05	0.05	-	
054	0.06	0.04	0.05	0.04	0.09	0.07	0.04	0.05	-	
055	0.07	0.05	0.05	0.06	0.08	0.07	0.04	0.05	-	
056	0.05	0.04	0.03	0.02	0.05	0.04	0.03	0.03	-	
057	0.06	0.06	0.03	0.02	0.06	0.04	0.04	0.04	-	
058	0.05	0.04	0.05	0.03	0.08	0.06	0.06	0.04	-	
059	0.05	0.06	0.06	0.05	0.11	0.08	0.07	0.06	-	
060	0.04	0.03	0.05	0.05	0.07	0.04	0.04	0.03	0.1	
061	0.04	0.04	0.04	0.03	0.06	0.04	0.04	0.04	0.12	
062	0.03	0.03	0.04	0.04	0.06	0.04	0.04	0.04	0.08	
063	0.03	0.03	0.03	0.02	0.03	0.03	0.03	0.03	-	
064	0.05	0.06	0.05	0.04	0.08	0.05	0.05	0.04	0.14	
065	0.07	0.06	0.05	0.05	0.08	0.05	0.05	0.05	0.21	
066	0.06	0.06	0.05	0.04	0.06	0.05	0.04	0.03	0.2	
067	0.05	0.07	0.06	0.07	0.1	0.01	0.07	0.07	0.13	
068	0.04	0.04	0.03	0.03	0.06	0.04	0.04	0.03	0.14	
069	0.05	0.04	0.03	0.03	0.06	0.03	0.03	0.02	0.17	
070	0.05	0.04	0.03	0.03	0.05	0.04	0.04	0.05	0.26	
071	0.08	0.07	0.06	0.05	0.06	0.06	0.06	0.07	0.15	
072	0.05	0.04	0.04	0.04	-	0.04	0.04	0.03	0.11	
073	0.05	0.04	-	0.03	0.05	0.03	0.03	0.03	0.14	
074	0.05	0.05	0.05	0.05	0.05	0.04	0.04	0.03	0.12	
075	0.05	0.05	0.04	0.03	0.06	0.04	0.02	0.04	0.11	
076	0.04	0.04	0.02	0.03	0.05	0.03	0.03	0.04	0.19	
077	0.05	0.05	0.04	0.04	0.06	0.05	0.05	0.05	0.1	
078	0.06	0.09	0.04	0.07	0.23	0.11	0.05	0.06	0.24	
079	0.07	0.07	0.06	0.05	0.07	0.08	0.06	0.05	0.24	
080	0.07	0.06	0.06	0.05	0.08	0.05	0.05	0.04	0.17	
081	0.06	0.06	0.05	0.03	0.06	0.07	0.06	0.04	0.13	
082	0.05	0.04	0.04	0.05	0.05	0.06	0.04	0.03	0.11	
083	0.05	0.04	0.04	0.06	0.06	0.08	0.04	0.04	0.18	

STORM	9075080	9087096	9087023	9087031	9087044	9087057	9087068	9087072	9087079	9087088
084	0.06	0.05	0.03	0.03	0.05	0.11	0.04	0.04	0.13	
085	0.05	0.04	0.04	0.04	0.06	0.07	0.05	0.05	0.1	
086	0.04	0.05	0.05	0.04	0.06	0.05	0.05	0.05	0.19	
087	0.06	0.06	0.05	0.05	0.09	0.06	0.05	-	0.18	
088	0.05	0.05	0.04	0.03	0.04	0.04	0.03	0.04	0.1	
089	0.05	0.05	0.08	0.06	0.09	0.07	0.1	0.05	0.11	
090	0.04	0.05	0.03	-	0.08	0.07	0.07	0.06	0.2	
091	0.07	0.06	0.05	0.07	0.07	0.05	0.04	0.05	0.16	
092	0.05	0.04	0.05	0.05	0.07	0.06	0.04	0.04	0.11	
093	0.05	0.04	0.04	0.04	0.07	0.05	0.04	0.04	0.12	
094	0.05	0.04	0.04	0.04	0.08	0.06	0.04	0.05	0.18	
095	0.06	0.05	0.06	0.06	0.11	0.09	0.07	0.09	0.25	
096	0.06	0.04	0.04	0.06	0.07	0.06	0.05	0.06	0.23	
097	0.04	0.05	0.06	0.06	0.1	0.08	0.07	0.07	0.18	
098	0.03	0.03	0.03	0.03	0.06	0.04	0.03	0.03	0.1	
099	0.05	0.05	0.05	0.05	0.08	0.08	0.06	0.05	0.12	
100	0.03	0.03	0.06	0.07	0.09	0.08	0.07	0.07	0.2	
101	0.06	0.05	0.03	0.03	0.05	0.03	0.03	0.04	0.18	
102	0.05	0.05	0.06	0.06	0.08	0.07	-	0.04	0.16	
103	0.04	0.04	0.05	0.15	0.08	0.07	0.05	0.04	0.12	
104	0.04	0.04	0.02	0.03	0.06	0.04	0.03	0.03	0.13	
105	0.07	0.06	0.05	0.04	0.05	0.04	0.05	0.05	0.11	
106	0.05	0.05	0.05	-	0.07	0.08	0.05	0.06	0.15	
107	0.09	0.06	0.05	0.06	0.06	0.06	0.07	0.08	0.2	
108	0.06	0.05	0.03	0.03	0.06	0.03	0.04	0.04	0.13	
109	0.04	0.04	0.04	0.03	0.05	0.04	0.02	0.03	0.11	
110	0.04	0.04	0.04	0.03	0.06	0.05	0.04	0.04	0.09	
111	0.06	0.07	0.05	0.04	0.07	0.05	0.06	0.06	0.23	
112	0.05	0.05	0.06	0.05	0.09	0.08	0.07	0.06	0.12	
113	0.04	0.05	0.07	0.04	0.08	0.06	0.05	0.04	0.1	
114	0.04	0.09	0.1	0.05	0.08	0.07	0.05	0.05	0.13	
115	0.04	0.03	0.05	0.05	0.07	0.07	0.05	0.05	0.11	
116	0.06	0.12	0.07	0.04	0.06	0.07	0.04	0.03	0.13	
117	0.08	0.09	0.07	0.03	0.11	0.08	0.07	0.05	0.1	
118	0.05	0.04	0.05	0.06	0.06	0.05	0.05	0.04	0.11	
119	0.04	0.03	0.06	0.05	0.07	0.07	0.05	0.04	0.13	
120	0.06	0.05	0.05	0.06	0.07	0.07	0.05	0.06	0.28	

STORM	9075080	9087096	9087023	9087031	9087044	9087057	9087068	9087072	9087079	9087088
121	0.07	0.05	0.06	0.05	0.05	0.03	0.05	0.07	0.24	
122	0.08	0.09	0.08	0.06	0.09	0.07	0.08	0.06	0.16	
123	0.06	0.04	0.06	0.04	0.07	0.07	0.06	0.05	0.1	
124	0.06	-	0.06	0.06	0.08	0.08	-	0.06	0.16	
125	0.05	0.04	0.05	0.03	0.06	0.05	-	0.03	0.16	
126	0.05	0.05	0.05	0.04	0.04	0.05	0.04	0.04	0.13	
127	0.08	0.06	0.04	0.03	0.05	0.04	0.04	0.05	0.14	
128	0.07	0.06	0.07	0.05	0.12	0.08	0.05	0.07	0.12	
129	0.07	0.06	0.05	0.04	0.07	0.07	0.04	0.04	0.15	
130	0.05	0.05	0.03	0.03	0.04	0.05	0.02	0.03	0.16	
131	0.05	0.05	0.06	0.04	0.08	0.07	0.07	0.06	0.21	
132	0.07	0.06	0.06	-	0.07	0.05	-	0.05	0.1	
133	0.07	0.06	0.06	0.04	0.09	0.07	0.06	0.05	0.13	
134	0.07	0.04	0.08	0.09	0.1	0.08	0.06	0.06	0.11	
135	0.07	0.05	0.05	0.04	0.08	0.07	0.04	0.05	0.21	
136	0.08	0.05	0.04	0.02	0.05	0.04	0.03	0.03	0.12	
137	0.07	0.06	0.06	0.07	0.07	0.06	0.05	0.06	0.2	
138	0.06	0.05	0.07	0.05	0.08	0.07	0.05	0.05	0.09	
139	0.05	0.05	0.07	0.04	0.09	0.06	0.06	0.05	0.12	
140	0.05	0.05	0.08	0.07	0.1	0.09	0.07	0.06	0.13	
141	0.06	0.06	0.06	0.06	0.09	0.07	0.05	0.05	0.16	0.08
142	0.09	-	0.03	0.05	0.05	0.03	0.04	0.04	0.1	0.06
143	0.06	0.05	0.04	0.03	0.06	0.04	0.02	0.02	0.08	0.03
144	0.11	0.08	0.05	0.03	0.06	0.05	0.04	0.04	0.18	0.11
145	0.05	0.04	0.03	0.03	0.04	0.03	0.02	0.02	0.1	0.04
146	0.06	0.05	0.05	0.05	0.08	0.07	-	0.04	0.11	0.05
147	0.07	0.06	0.04	0.04	0.07	0.06	0.04	0.04	0.12	0.05
148	0.06	0.06	0.06	0.07	0.11	0.08	0.07	0.07	0.23	0.1
149	0.06	0.05	0.03	0.04	0.06	0.04	0.03	0.03	0.11	0.05
150	0.08	0.06	0.04	0.04	0.05	0.04	0.03	0.03	0.12	0.05

With 124 storm simulations having 8-to-10 measurements available to compare to, there were over 1000 statistical Bias and RMSE values calculated. Figure 6-8o shows the bias values for all storms and all gages. In general the bias is within +/- 0.05 m. An examination of all 1053 comparisons shows that 89 percent of the Bias values are within +/- 0.05 m.

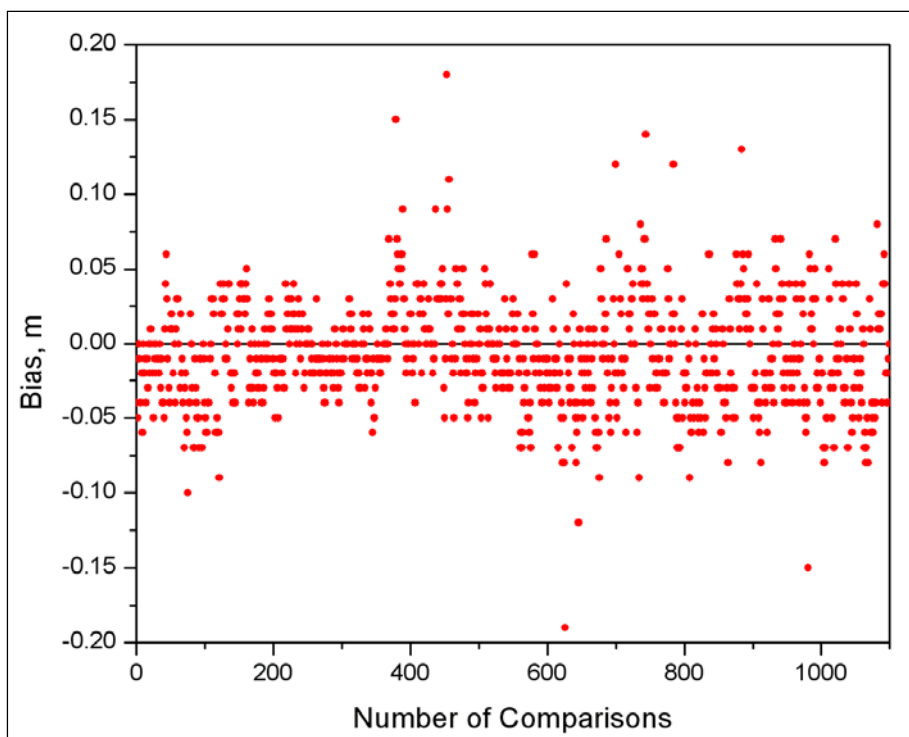


Figure 6-80. Water level bias for all storm and all gages.

Figures 6-81 through 6-90 show the Bias values for each individual station for all storms. In general, the simulated water levels compare fairly well with measured water levels. Mackinaw City and Port Inland are biased slightly high. Ludington, Holland, Calumet Harbor (with the exception of one storm), Milwaukee, Kewaunee, Sturgeon Bay Canal and Menominee are generally within $+/- 0.05$ m and have a bias of no more than 0.12 m. Green Bay shows both the lowest and nearly the highest bias values when comparing modeled and measured water levels. The most extreme low and high bias values are -0.19 m at Station 9087079 (Green Bay) for Storm 095 and 0.18 m at Station 9087044 (Calumet) for Storm 078. An examination of the time series comparison for these two cases shows that Green Bay is not simulating the trend measured at the NOAA station well for this storm. The over-prediction at Calumet shows that the simulated water levels have a surge duration that far exceeds the measured surge for this storm at this location. Figure 6-91 shows the RMSE values for all storms and all gages. In general the RMSE is within 0.10 m. An examination of all 1053 comparisons shows that 90 percent of the RMSE values are within 0.10 m. Overall, the model performs well in simulating water levels over the large spatial extent of Lake Michigan and Green Bay for a large number of storms of varying intensity, size, and location. The model's ability to predict water level at many locations under various conditions provides a strong degree of confidence in the model to predict water levels at other locations around Lake Michigan as well.

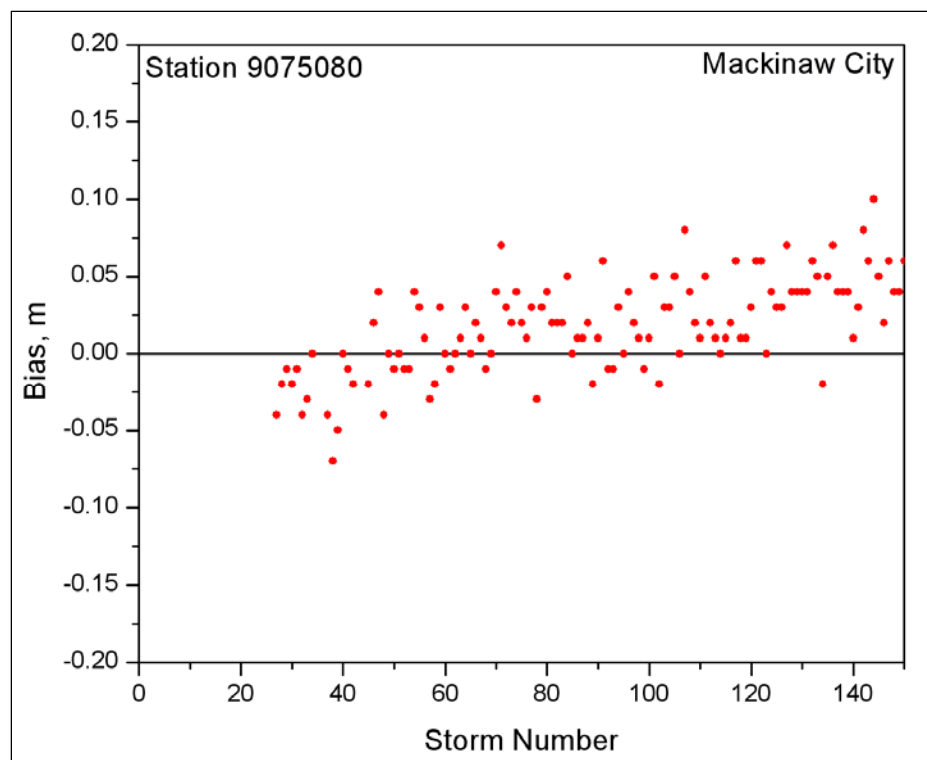


Figure 6-81. Water level bias at Station 9075080 (Mackinaw City).

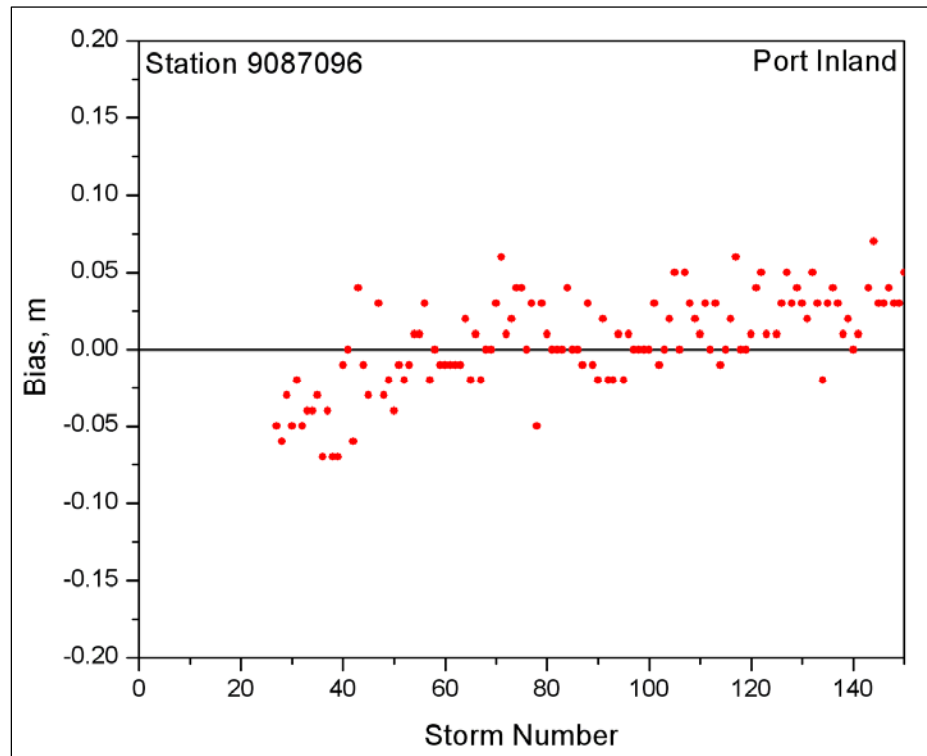


Figure 6-82. Water level bias at Station 9087096 (Port Inland).

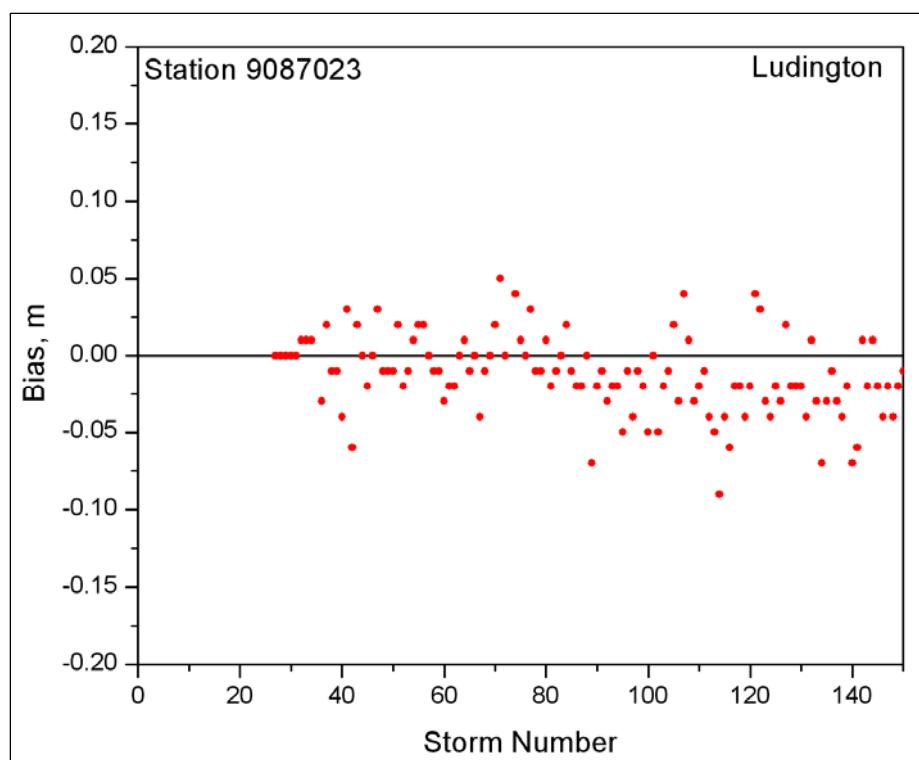


Figure 6-83. Water level bias at Station 9087023 (Ludington).

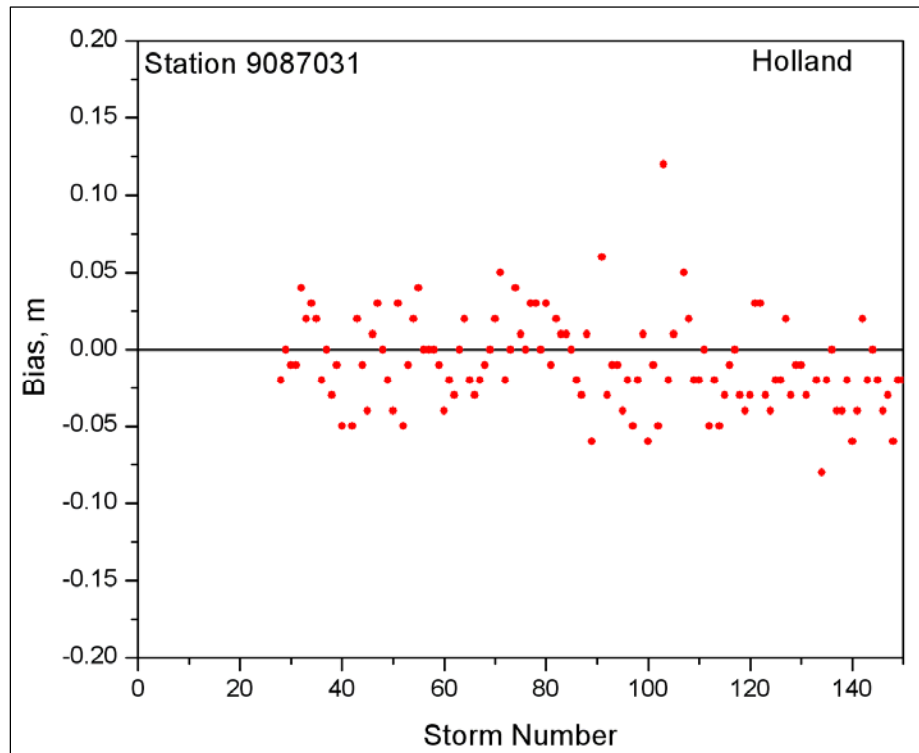


Figure 6-84. Water level bias at Station 9087031 (Holland).

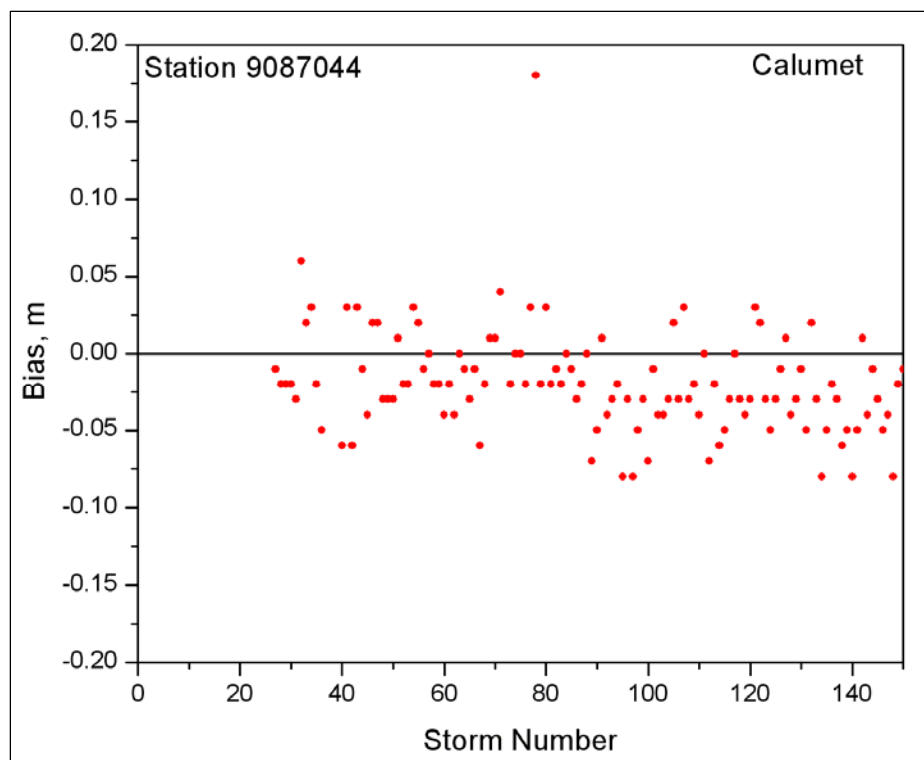


Figure 6-85. Water level bias at station 9087044 (Calumet Harbor).

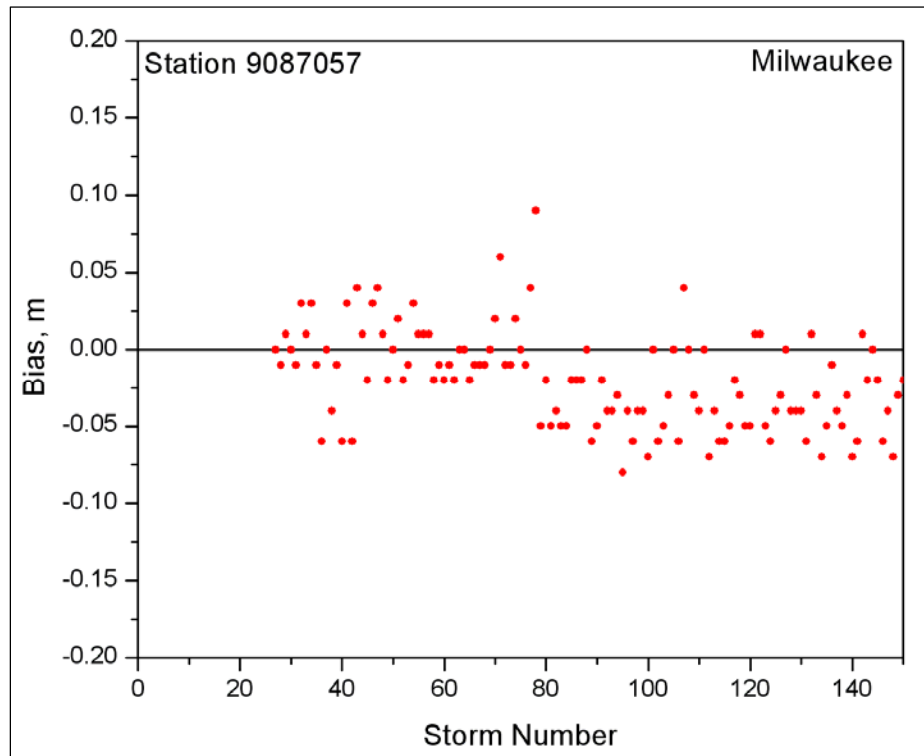


Figure 6-86. Water level bias at station 9087057 (Milwaukee).

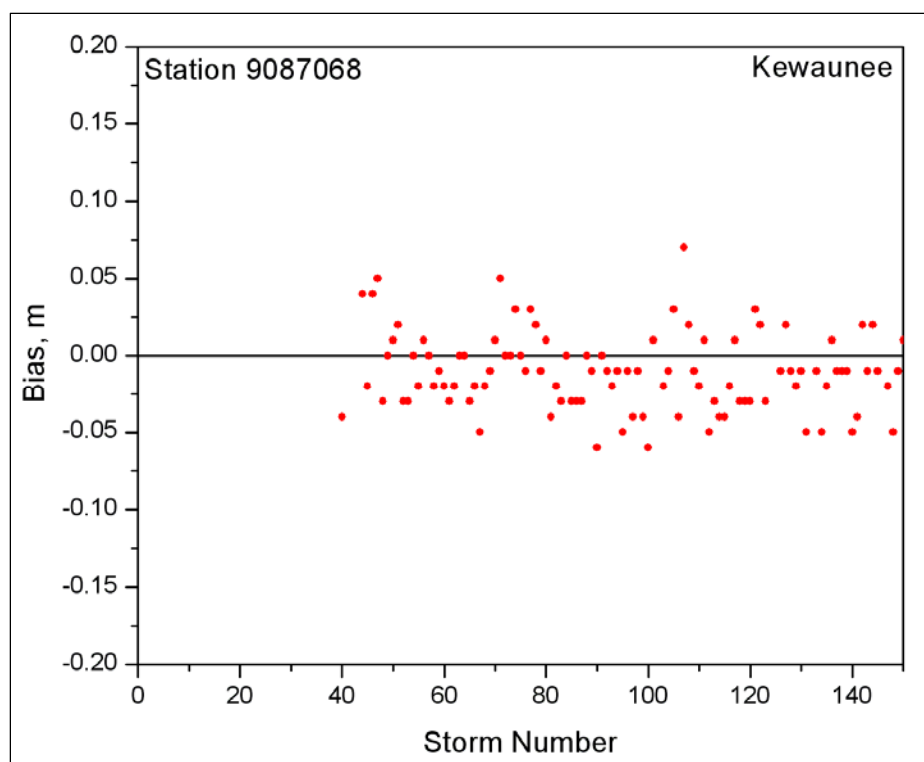


Figure 6-87. Water level bias at station 9087068 (Kewaunee).

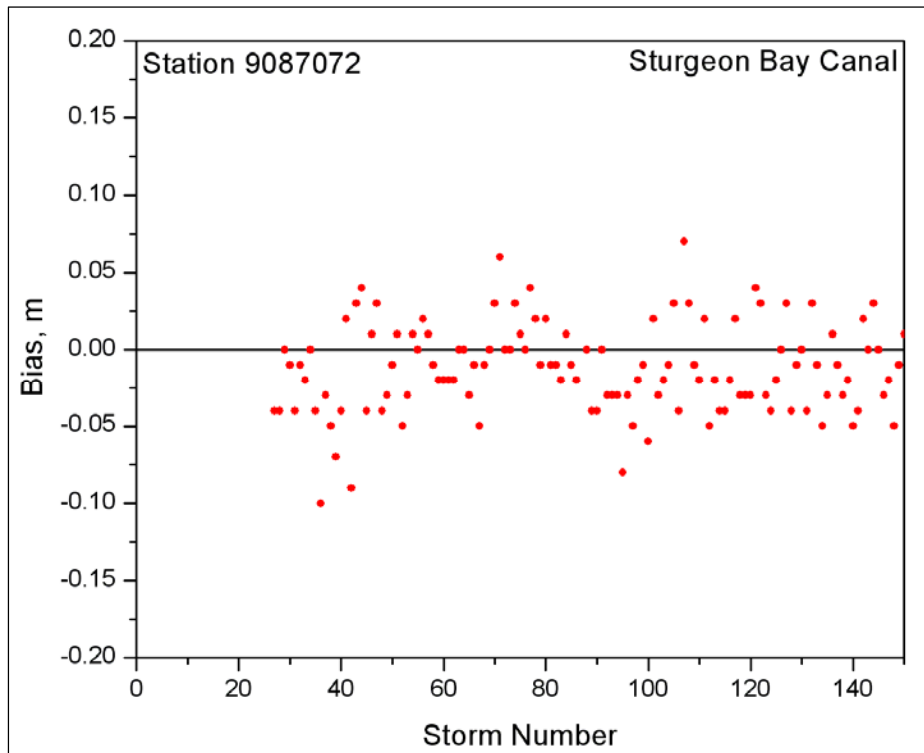


Figure 6-88. Water level bias at station 9087072 (Sturgeon Bay Canal).

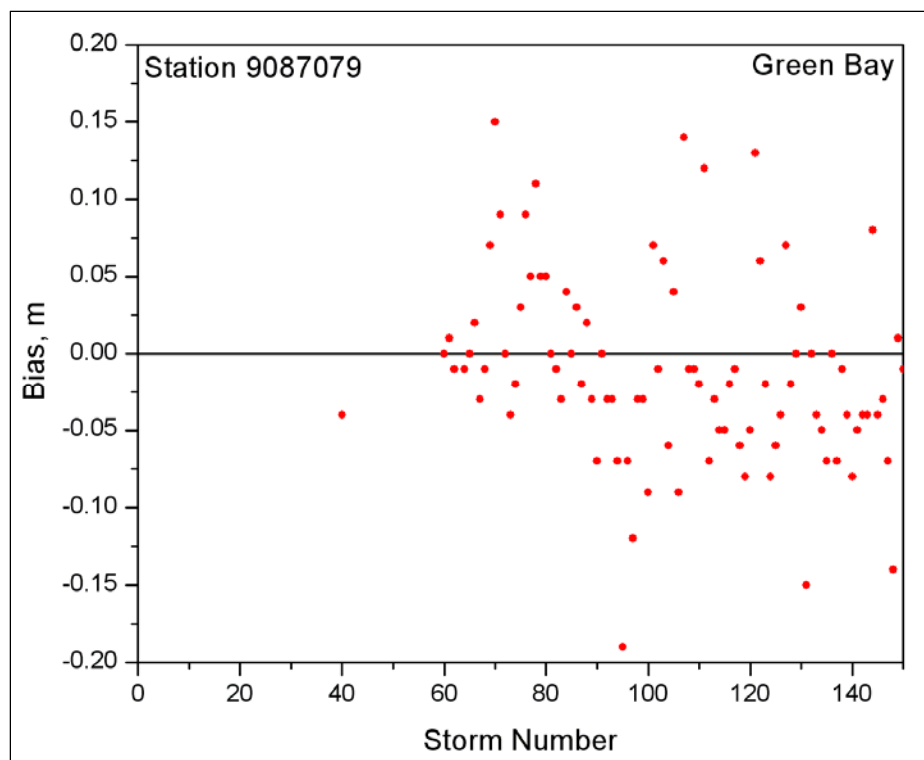


Figure 6-89. Water level bias at station 9087079 (Green Bay).

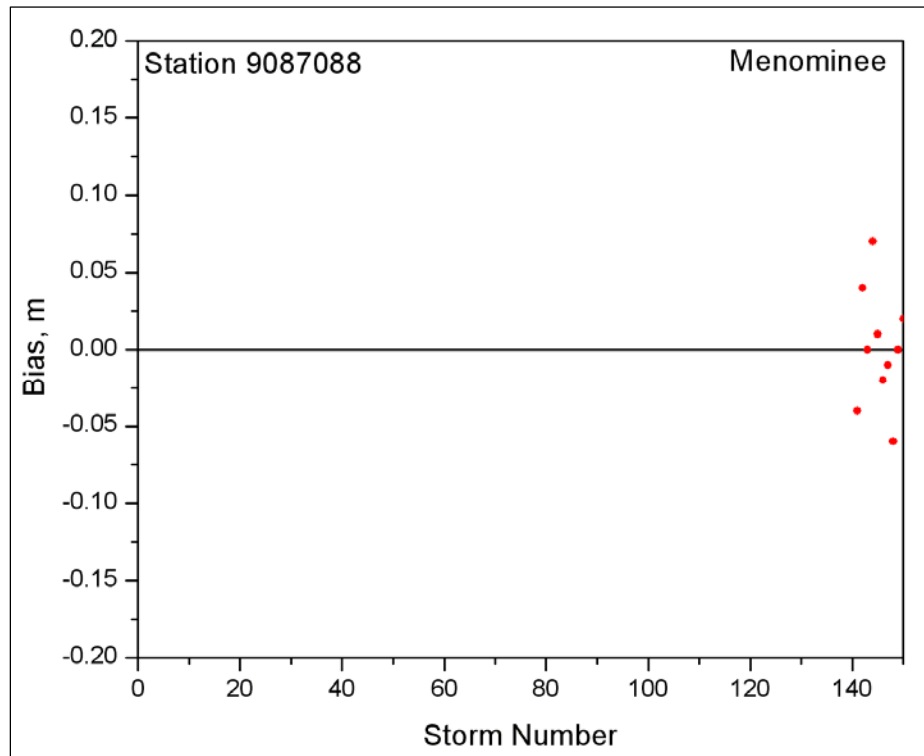


Figure 6-90. Water level bias at station 9087088 (Menominee).

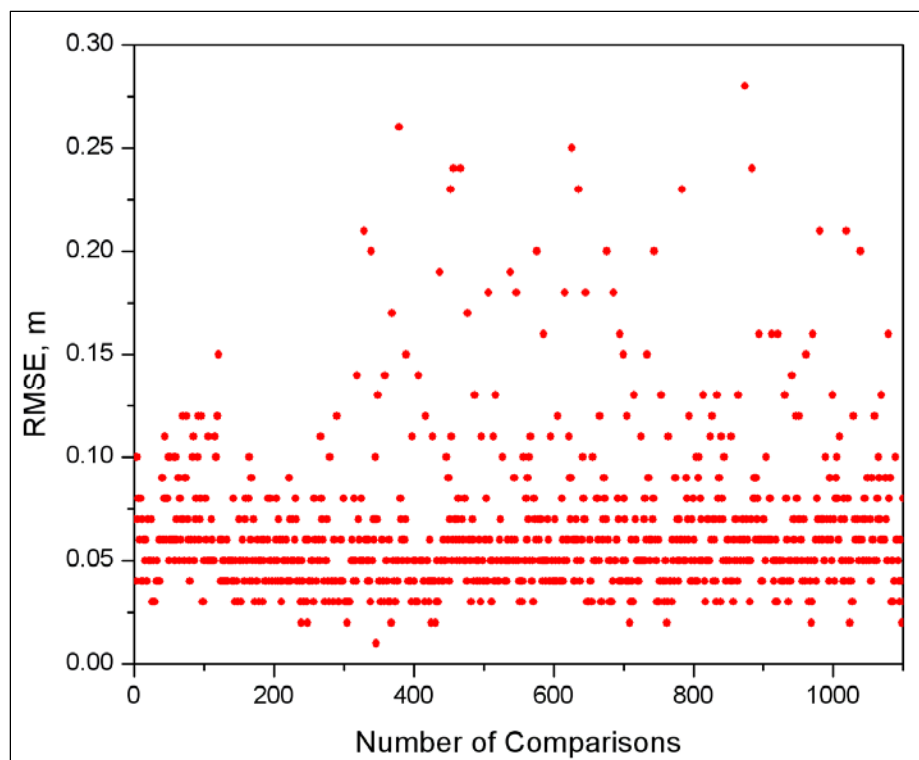


Figure 6-91. Water level RMSE for all storm and all gages.

6.8 Nearshore wave production

STWAVE was run at 30-minute time-steps for six days (three days prior to the storm peak, the peak day, and two days following the storm peak). The exported files include the save points file (containing significant wave height H_{mo} , mean wave period T_m , and mean wave direction α_m at each time-step for selected locations), the 2-D spectra file, and the field file (containing H_{mo} , T_m , and α_m at each time-step for every grid cell). Peak wave periods (T_p) for the grid were saved at each time-step to a separate file.

During the execution of the 150 extreme storm events, quality assurance and control for all 150-storms included overlaying the maximum wave height field on top of the bathymetry and reviewing final iteration criteria for solution convergence. Time series comparisons at two nearshore locations, Burns and Chicago Harbor, were completed for storms where measurements were available (36 storms from 1987-2003). However, these gages had limited deployment and in many instances were not operating during the same time period. No comparison to wave measurements was completed for Kenosha or Green Bay as there were no gages contained in these domains.

The procedure separated time paired measured and modeled wave heights by station and then concatenated these pairs across all storms where measurements were available to observe general model performance. Statistics as well as graphic analyses were conducted, which included symmetric regression, Quartile-Quartile, and peak-to-peak. Out of 150 events, 36 were during the period of wave measurements where the number of storms compared to each gage is summarized below:

- Burns Harbor: 10 Storms
- Chicago Harbor: 33 Storms

As previously mentioned, Burns and Chicago Harbor had a pre-determined threshold where periods and directions corresponding to wave heights less than 0.2 m were flagged as NO DATA. This threshold introduced a discrepancy in the evaluation as it is unknown whether the flag was caused by very low wave conditions due to low energy or due to icing in the region. As a result, the reliability of the wave measurements during these very low energy conditions is questioned.

6.8.1 QA/QC for all storms

The maximum significant wave height for each grid cell (spanning the entire simulation) was plotted over the bathymetry to identify errors and discontinuities in the wave height solution. Figures 6-92, 6-93, and 6-94 provide examples of these plots where the shown storm is the event that yielded the largest wave height in each domain. The largest event was STO127 (peak date 03/09/1998) for Chicago and Kenosha and STO099 (peak date 12/04/1990) for Green Bay.

For this particular storm, wave energy was focused in the Chicago domain as a result of the variation in the nearshore bathymetry contours (30-m and shallower), creating the streaking behavior seen in Figure 6-92. The focusing originates where the bathymetry “points” and is dependent on wave period and direction. The focusing of wave energy was absent in the Kenosha and Green Bay grids as the nearshore contours are relatively straight and parallel compared to Chicago’s.

Also, this particular storm demonstrates the complex wave climate of Green Bay as the islands along the central axis play a significant role in determining the nearshore wave climate. Waves penetrating into Green Bay attenuate very quickly due to wave-bottom energy losses (i.e., bottom

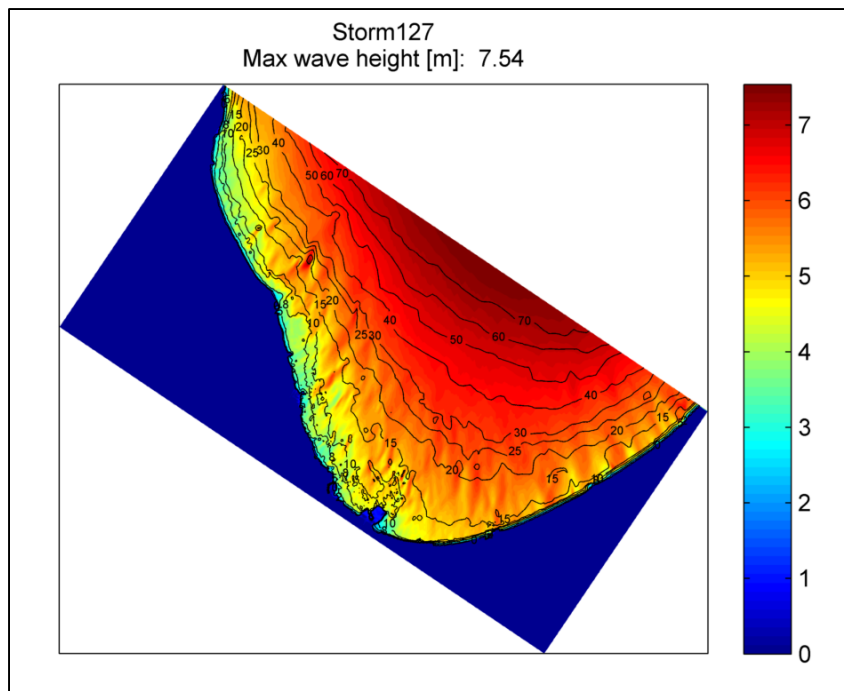


Figure 6-92. Maximum wave heights for ST0127 for Chicago.

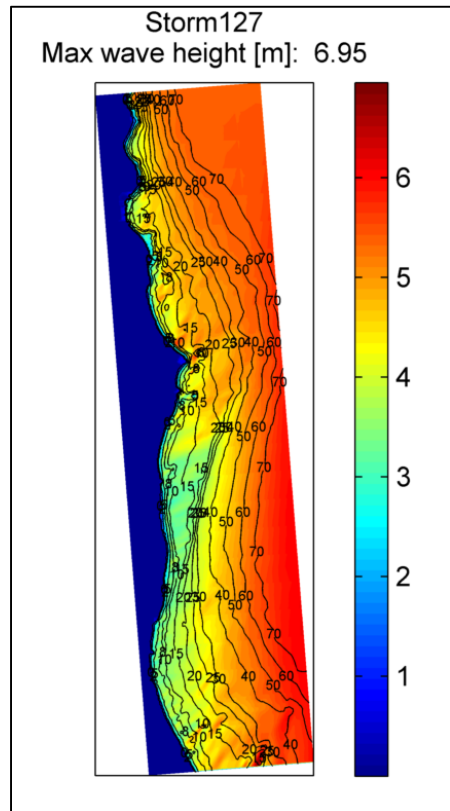


Figure 6-93. Maximum wave heights for ST0127 for Kenosha.

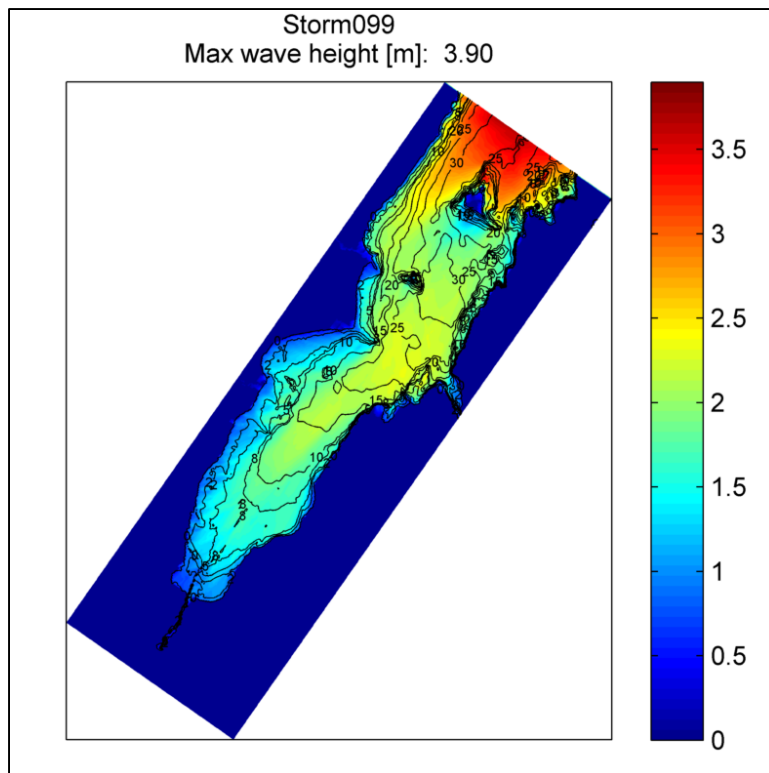


Figure 6-94. Maximum wave heights for ST0099 for Green Bay.

friction), but more importantly due to wave-sheltering. The shadow effect is demonstrated by a reduction of wave height in the region on the leeward side of the islands.

Apparitions of blocks appear in many of the wave height solutions, mainly in the Kenosha domain. This “blocking” is an artifact of the iteration scheme within STWAVE, and it occurs when the final value of individual grid partitions do not completely match the values of their neighbors’ boundaries. This artifact does not affect the integrity of the solution as the “blocking” occurs in deep water (offshore of the save points) and the difference between partitions is very small (on the order of centimeters).

The procedure for reviewing convergence was concatenating the time-steps for all 150-storm events and checking for final convergence. All three domains were ran with a final convergence criteria where at least 99.8 percent of the cells had to have a relative difference in average wave height of 0.05 m or less. In summary, non-converged time-steps accounted for less than one percent of the total final time-steps for each grid. These non-converged time-steps were not limited to one storm and occurred well before or after the storm peak. As this study is focused on extreme storm

events, these storms were not rerun as the non-converged time-steps did not affect the peak condition.

6.8.2 Evaluation to wave measurements

Wave measurements at Burns Harbor (45900) and/or Chicago Harbor (45901) were available for 36 storms from 1987-2003. 45900 and 459001 were located in the Chicago domain at cells (228, 463) and (184, 239), respectively (Figure 6-95). The STWAVE results were graphically compared to these gages in the form of time, scatter, contour, Quartile-Quartile, and peak-to-peak products. Statistics including bias, root mean square error, scatter index, skill score, and linear regression were also computed.

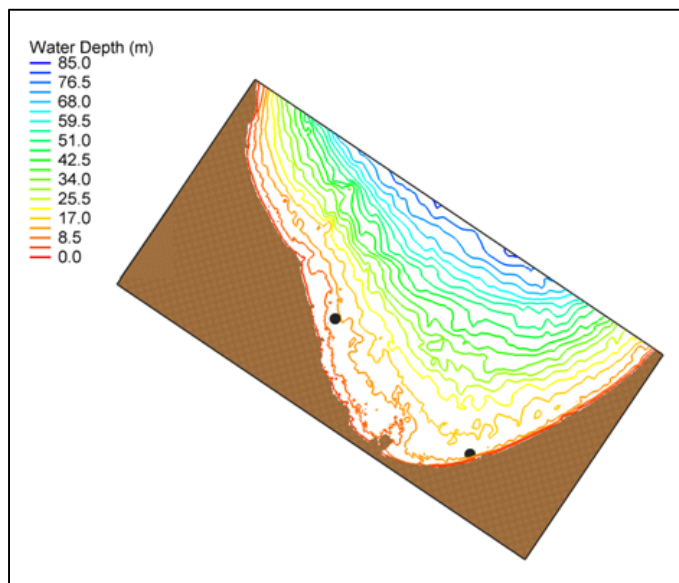


Figure 6-95. Location of Burns (45900) and Chicago Harbor (45901) indicated by filled circles.

An example of a time series comparison and calculated statistics for STO115 is shown in Figure 6-96. The top panel is a time plot of model to measurement comparison at 45900. For this event, STWAVE replicates the measurements reasonably well, capturing the growth and decay sequences of the two peaks during the simulation. STWAVE slightly underestimated the first storm peak and overestimated the second storm peak. The scatter plot (bottom panel of Figure 6-96) shows STWAVE overestimated the smallest waves (indicated by the red circle). These values correspond to measurements at the beginning and end of the STWAVE simulation where 45900 reports waves ranging from 0.02 to 0.05-m. The reliability of the gage to accurately measure waves of this small magnitude is questioned,

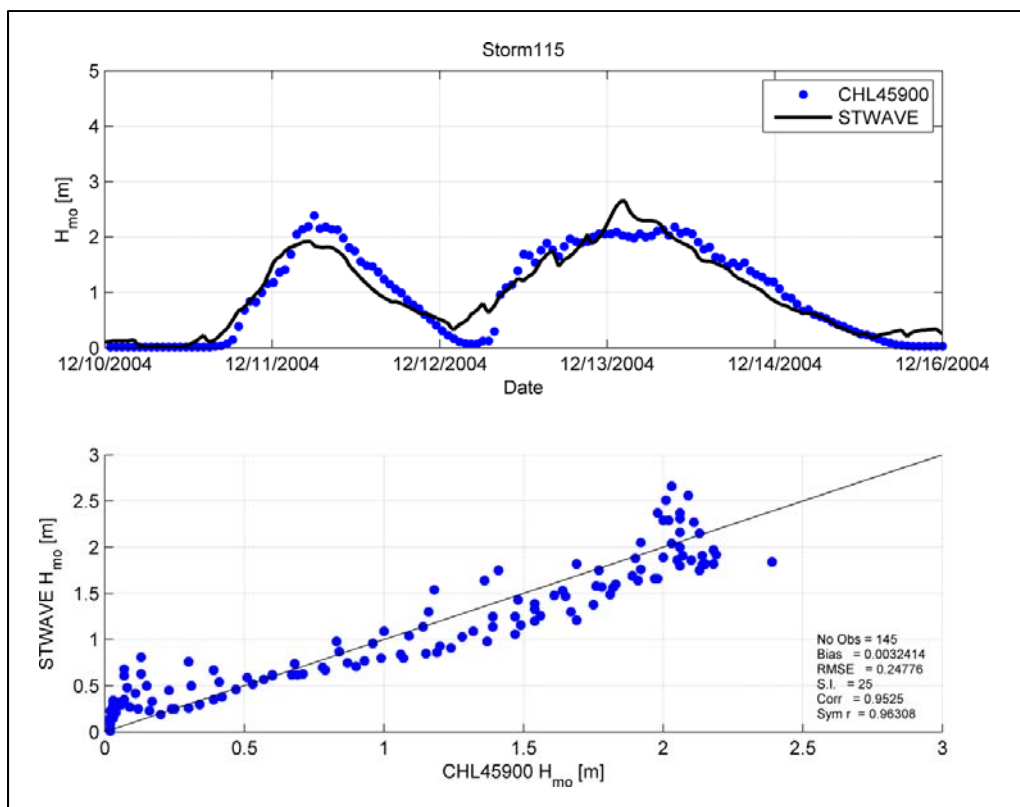


Figure 6-96. Time and scatter plot of STWAVE versus measurements at 45900 for ST0115. Top panel is the time series comparison followed by the scatter with statistics provided in the lower right corner.

and these smaller waves are not relevant to the focus of the extreme event study. There is a slight negative bias (underestimation) in the range of 0.5 to 2.0-m. The error for the maximum observed wave height is approximately 0.4 m. For this storm, STWAVE performs well with a small bias of 0.003-m, a RMSE of 0.25-m, a scatter index of 25, and a symmetric r (i.e., slope with zero intercept) of 0.963.

STWAVE results were then compared to measured data for all 36 storms to increase the sample size and evaluate general model performance as well as STWAVE's ability to capture peak wave heights. The model and measurements were paired in time, and all wave measurements were used.

Time paired color scatter plots of significant wave height for 45900 and 45901 are shown in Figures 6-97 and 6-98. For 45900, STWAVE compares favorable to wave measurements as the scatter rarely exceeds the 95-percent confidence limits. The wave climate at 45900 is generally low, with waves less than 0.5-m comprising 80-percent and above of the wave climate (e.g., red contour intervals). The relative error is six-percent above the mean. One

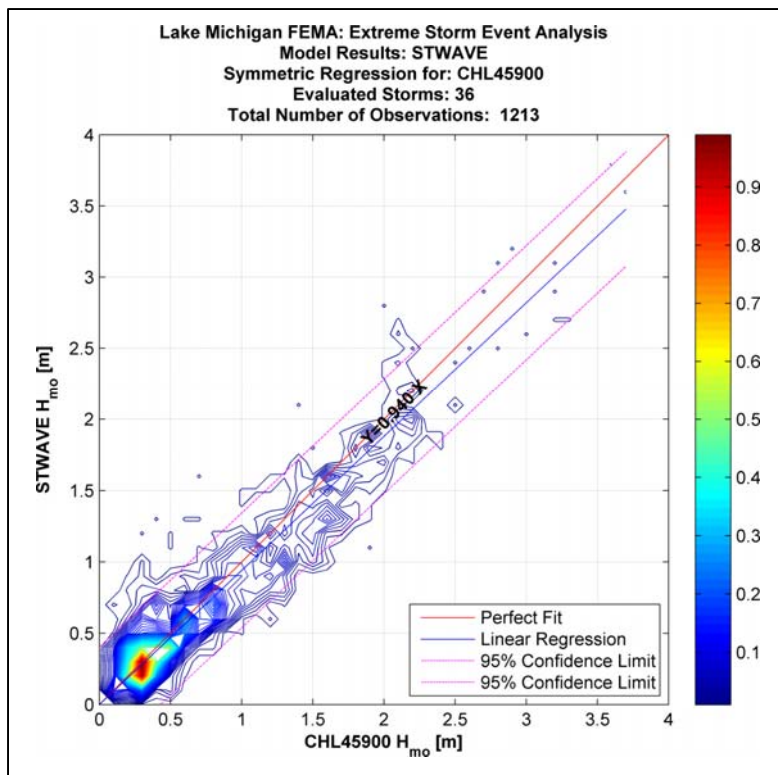


Figure 6-97. Color contour of time paired significant wave heights for 45900.

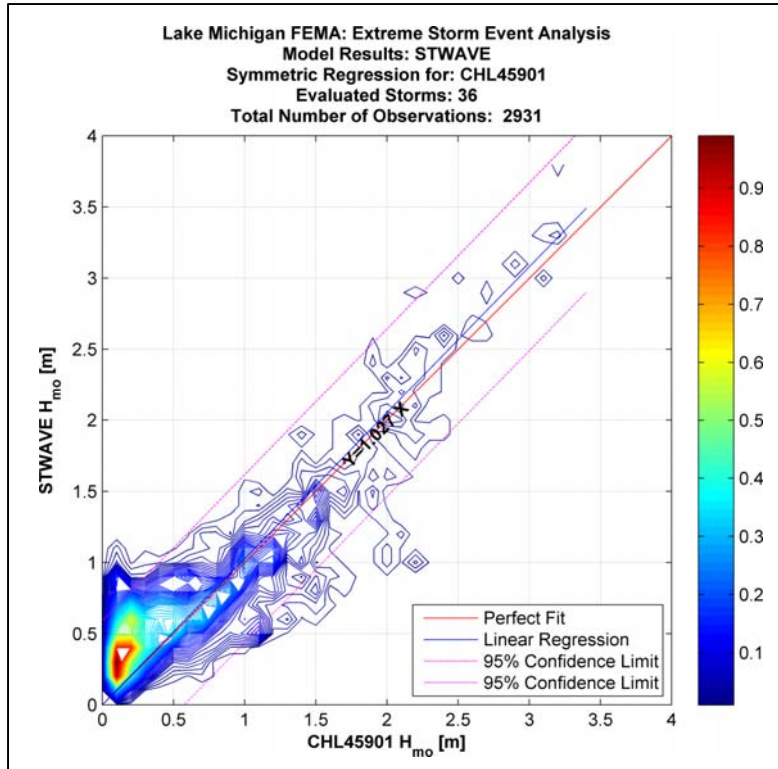


Figure 6-98. Color contour of time paired significant wave heights for 45901.

should note the error reported is an average error where overestimations of a particular range of wave heights can be offset by underestimations in a different range. For 45901, STWAVE consistently overestimates the low wave conditions or iced conditions, and the relative error is about three-percent below the mean. Again, the wave climate is mild with 80-percent and above of the waves less than 0.5 m with most ranging from 0.2 to 0.3-m. STWAVE performs well in the upper range of wave heights (greater than 1.5-m) at both locations with the majority of the extreme events contained within the 95-percent confidence limits. Additionally, note that Figures 6-97 and 6-98 are very similar to Figures 6-29 and 6-30 generated from WAM. As WAM provides the boundary information to STWAVE, underestimations or underestimations in the boundary conditions will persist in the STWAVE solution.

Quartile-Quartile graphics were also produced for 45900 and 45901. As previously mentioned, this analysis is based on recovering the cumulative distribution of the two populations and is able to analyze a unique percentile. For this study, a 0.1-percentage resolution was used to identify the 99.1 through 99.9-percentiles (blue circles). Following the line of perfect fit indicates good agreement where points above the line are overestimated by STWAVE and points below the line are underestimated by STWAVE. The quartile-quartile analysis is based on the time series for all 36 storms rather than individual storm peaks so the top percentiles identified in the following figure could be derived from a single storm event depending on its magnitude compared to the other simulations.

Figure 6-99 displays the Q-Q analysis for STWAVE results versus 45900. STWAVE performs well in the wave heights range of 0.1 to 0.6-m. STWAVE clearly underestimates the wave height distribution in the range of 0.8 to 2.3-m, and then overestimates the wave heights in the 2.3 to 2.5-m range. For the top one-percent, the STWAVE results improve and more closely follow the line of best fit. The maximum difference is about 0.3-m for both the 0.1 to 99.0-percentile and the 99.1 to 99.9-percentile.

Figure 6-100 displays the Q-Q analysis for STWAVE results versus 45901. This plot more clearly emulates the contour scatter plot (Figure 6-98) of the same location, overestimating the smallest wave heights, underestimating waves in the 0.7 to 2-m range, and then overestimating the most extreme values. Focusing on the top one-percent, the maximum difference occurs for the two largest wave heights and is about 0.5-m or 16-percent considering a 3.2-m wave. This is the same error found in the WAM Q-Q analysis at the same site.

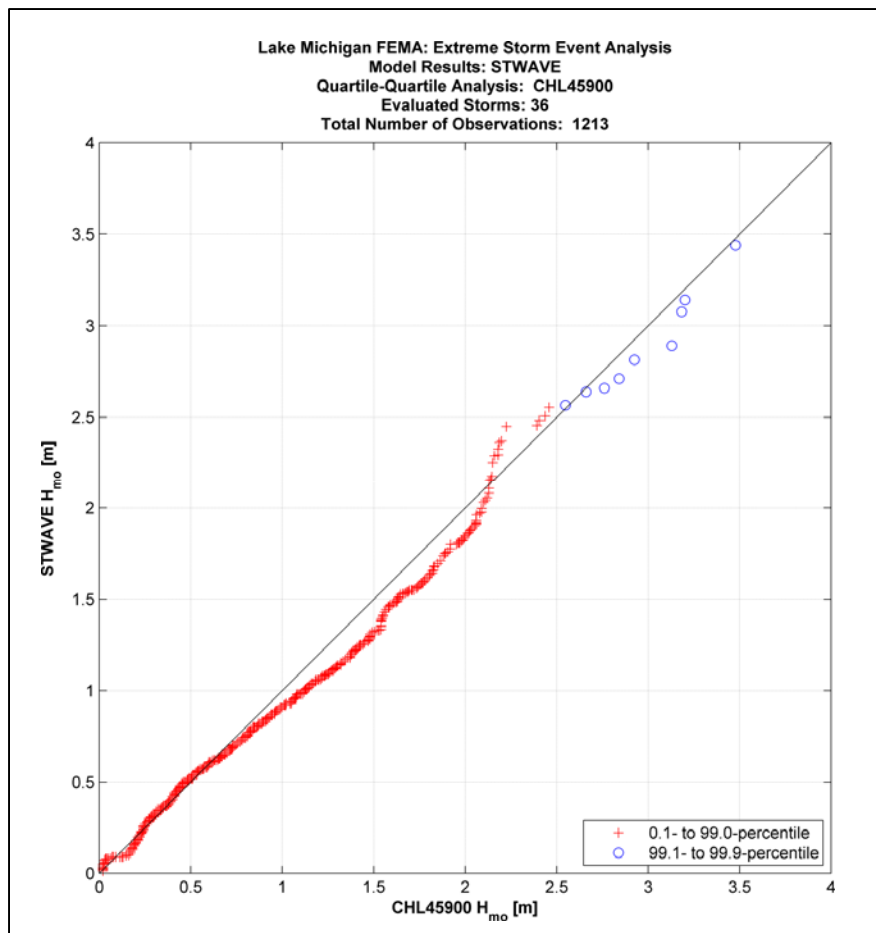


Figure 6-99. Quartile-Quartile analysis for 45900.

There is consistency in the Q-Q analysis between the two sites that merits attention. At both sites, STWAVE underestimated wave heights in the 0.7 to 2.0-m range with an abrupt overestimation occurring at about 2.0 to 2.3-m. The underestimation was also seen in WAM (Figure 6-33 and 6-34), indicating an underestimated boundary condition. Figure 6-101 closely follows the behavior of Figure 6-34 (Q-Q analysis of WAM at the same site); however, the abrupt overestimation seen in Figure 6-100 is not present in Figure 6-33, suggesting that this behavior is solely due to STWAVE. Unfortunately, the spectra at the site do not exist and a more complete evaluation of the reason could not be performed.

Following Q-Q analysis, a peak-to-peak analysis was performed to establish the trends in STWAVE results to accurately estimate extreme wave heights. Peak-to-peak identifies extreme waves using a site-specific threshold based on the sum of the mean wave height plus two times the variance (Table 6-9). The storm duration was defined as the time between first exceeding the

threshold and subsequently falling below the threshold, and the storm peak was defined as the maximum significant wave height during this storm duration. For any one given extreme storm event simulation, there could be multiple storm peaks based on the peak-to-peak analysis. As in the other analyses, the same time paired model to measurement data set was used where a total of 36 storms were considered. Data derived from the two sites may not be derived by the same storm due to differing deployment cycles.

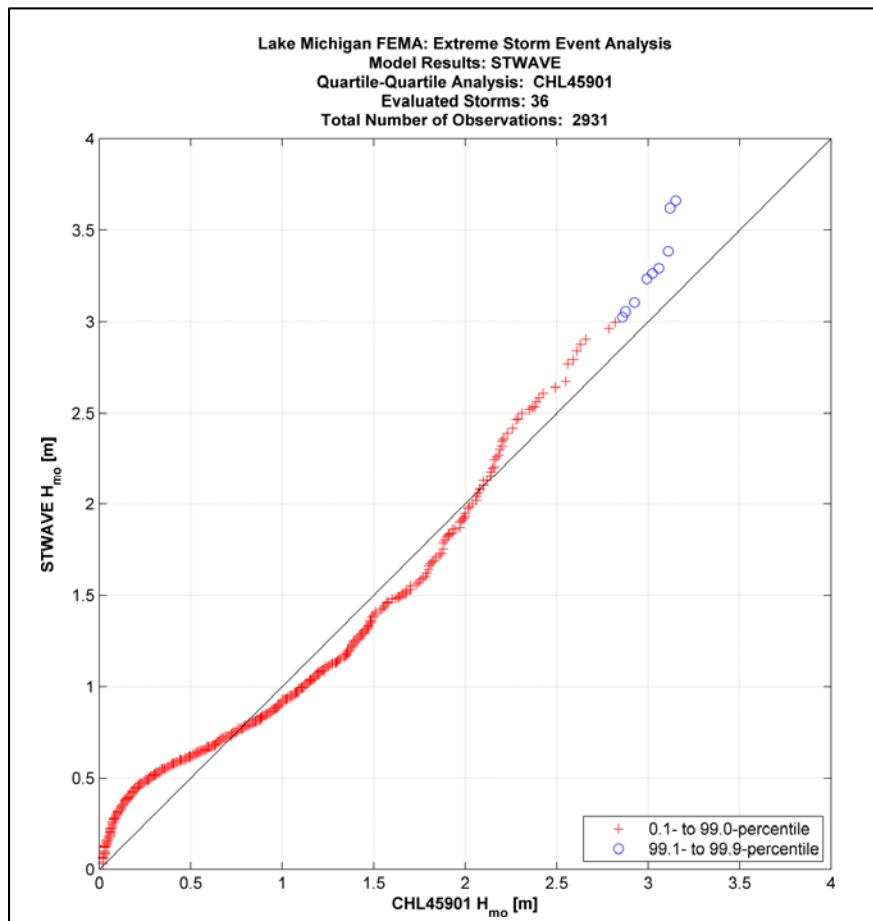


Figure 6-100. Quartile-quartile analysis for 45901.

45900 and 45901 are evaluated and graphically presented in Figures 6-101 and 6-102. The top panel shows the time series of the model results and measurements as well as identifies the threshold (blue line) and the values selected for the extreme wave heights (blue plus signs). The lower left panel presents a scatter plot of the entire population with the line of best fit (red line) and linear regression (green line) noted, and the lower right panel shows a scatter plot of the selected peak events.

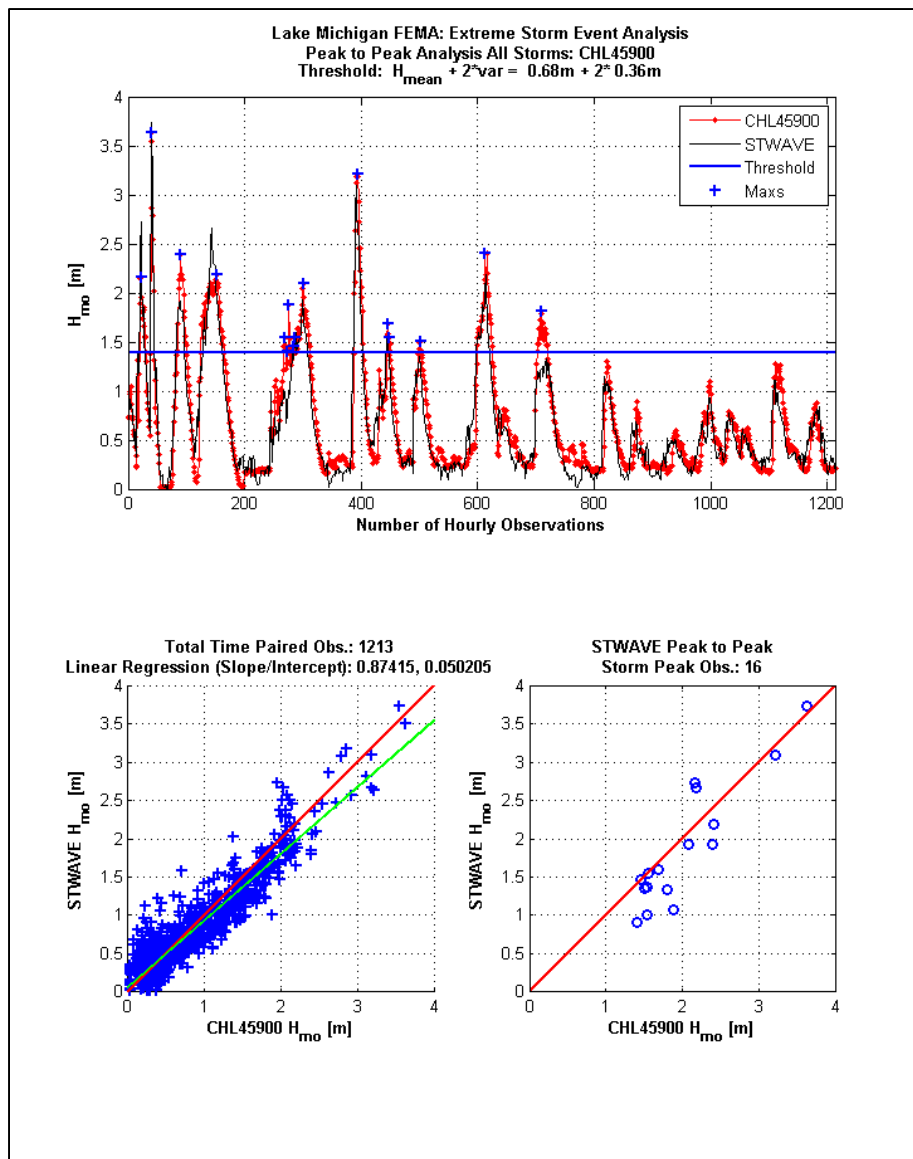


Figure 6-101. Peak-to-peak analysis at 45900. Top panel compendium of all extreme storm events containing measurements with threshold defined; lower left panel scatter plot of model and measurement data; lower right panel scatter plot of the storm peaks.

Table 6-9. Peak-to-peak analysis results

Station	No. Storms/No. Peaks	No. Obs.	Threshold (m)	Regression Results	
				Slope	Intercept
45900	10 / 16	1213	1.40	0.874	0.050
45901	33 / 33	2931	1.47	0.790	0.227

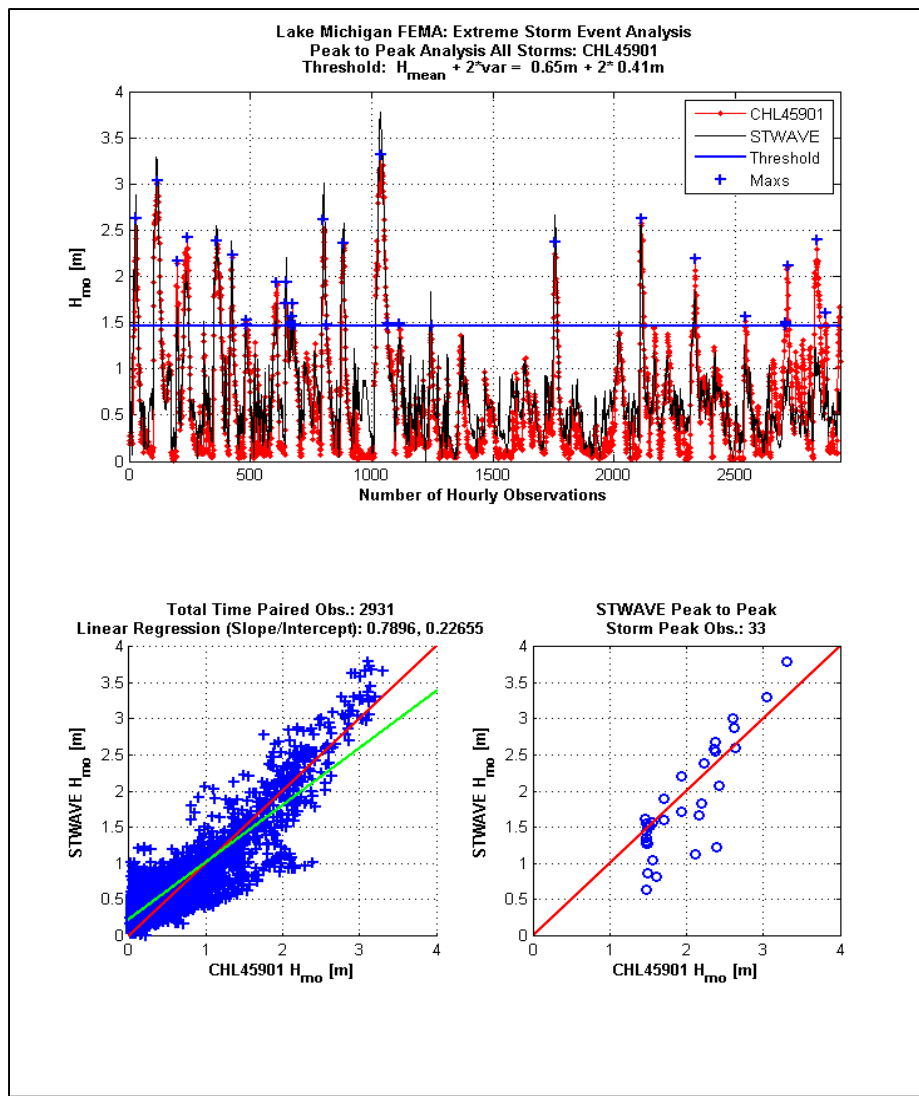


Figure 6-102. Peak-to-peak analysis at 45901. Top panel compendium of all extreme storm events containing measurements with threshold defined; lower left panel scatter plot of model and measurement data; lower right panel scatter plot of the storm peaks.

STWAVE does a good job capturing the growth and decay cycles of the selected storms at 45900 as seen in the time plot (Figure 6-101). The scatter plot roughly emulates the Q-Q plot shown in Figure 6-99, showing the overestimation of wave heights in the 2.3-m range, and indicates a slight negative bias likely due to the underestimation of 0.7 to 2-m waves. For peak wave conditions (lower right panel), STWAVE performs well for the most extreme waves (greater than 3-m) while slightly underestimating the smaller peak waves. The greatest difference between modeled and measured wave heights occurs for the smaller peaks and is approximately 0.5-m. This is likely due to underestimation of the storm peak around index 700. Note that some extreme values (one indicated by the black

circle) on the population scatter plot are missing on the peak event plot. These missing points, although large, were not the maximum that occurred during the storm duration and were not selected as a peak.

Similar results are presented in Figure 6-102 for 45901. The time plot (upper panel) demonstrates the larger population of time paired events compared to 45900. As at 45900, the STWAVE results follow the trend of the measure data, mimicking the rise and fall of the storm events.

STWAVE also behaves reasonable in low energy wave climate, supporting a suitable implementation of ice coverage into the model. The pattern of the scatter plot is similar to that of the Q-Q plot (Figure 6-100); STWAVE overestimates the low energy wave climate and slightly underestimates waves ranging from 0.7 to 2.0-m (resulting in a larger positive intercept). The greatest difference between measured and modeled wave heights is approximately 1.0-m and is due to the missed peaks occurring after index 2500. STWAVE modestly overestimates peak wave conditions.

Following the graphic analyses, statistics were computed using the time paired measurements and STWAVE results at 45900 and 45901 (Table 6-10). These statistics are the same as those used to analyze the WAM results, and they include the bias, the root-mean-square error, the scatter index, linear regression (both slope and intercept and the symmetric slope where the intercept is forced to be zero), and correlation. No time paired measurements were omitted from the analyses.

Table 6-10. Summary statistics for significant wave height (m).

Station	Mean		Bias	RSME	Scat Index	Slope	Intercept	Linear Reg.		No. Obs.
	Meas.	Model						Sym Slope	Corr.	
45900	0.68	0.65	-0.04	0.21	30	0.87	0.05	0.94	0.94	1213
45901	0.65	0.74	0.09	0.30	47	0.79	0.23	1.03	0.88	2931

The biases at both locations were very low with values of -0.04 m at 45900 and 0.09 m at 45901. The RMSE are reasonable, in the range of 0.2 to 0.3-m. The scatter indices at both sites are high, reflection the trend of values seen in the WAM results (Table 6-4). The linear regression indicates errors of negative six-percent and positive three-percent, suggesting a modest underestimation and overestimation at 45900 and 45901, with correlations of 0.94 and 0.88. These values are more than acceptable considering the environment of Lake Michigan (i.e., ice coverage) and support the estimates provided by STWAVE of the extreme storm event cycles and peak values.

7 Summary and Conclusions

The estimation of winds, pressures, waves and surge for extreme storm events along all coastlines of Lake Michigan is a daunting task. Storm systems in Lake Michigan are dominated by cyclogenesis where low pressure synoptic-scale systems rapidly move through the region. These meteorological events commonly run in a net easterly direction passing Lake Michigan in matters of hours. The resulting wind speeds can increase from near calm conditions to sustained speeds in excess of 20-m/sec, with accompanying directional wind shifts of 180-deg. The net effect on the hydrodynamics is considerable, and spatially variable. One event may only be evident in the southern section of Lake Michigan while the rest of the domain is benign. These events are further complicated by the intra-annual growth and decay of shore-fast ice. The resulting wave and surge estimates will be altered because of the spatial distribution of the ice fields. One major storm event may be co-incident with extensive shore-fast-ice coverage, blocking any major wind-generated wave estimates from reaching the coast, and a negligible surge level increase. Because the modeling effort was run for storms derived from the last 50-years the intra-annual lake level had to be considered. All totaled, the complexities in this study were great; however, selection of the appropriate wind fields (or technology), access to a consistent data archive for ice field generation, use of robust hydrodynamic models, and extensive evaluation promotes the success of the study.

Specification of the wind and pressure fields was determined from two methods. Originally the Natural Neighbor Method (NNM) was to be used for all extreme storm events selected. This method relies on land based meteorological station data (wind speed, direction, air temperature, and sea-level pressure). The winds were adjusted to a standard 10-m elevation, transformed from overland to over-water conditions, and then adjusted for stability, (air/water boundary) affecting the momentum transfer from the air to the water surface. A sophisticated interpolation method was used to translate these spatially varying locations on a fixed spherical grid defined by the domain of Lake Michigan. The number of meteorological stations in the archive (NOAA/NCDC, Integrated Surface Hourly) was not consistent from year to year. Also the number of stations decreased significantly as one approached the more historical storms (1960s).

The study originally selected the NNM based on the work of NOAA/ GLERL using wind fields for forcing conditions in the operational wave and current modeling efforts in the Great Lakes. A series of storms (seven events) were designated as test cases for an initial forensics study to determine the accuracy of the hydrodynamic models to be used in the extreme storm wave and surge estimates. WAM Cycle4.5.1C was selected for the wind-wave model, and ADCIRC was chosen to estimate the water levels. WAM and ADCIRC used the NNM wind fields. The sea-level pressure fields were a second forcing function input to ADCIRC to estimate the inverse barometer effects. The analysis of the model estimates to point source measurement of waves and water level data revealed the wind and pressure fields developed from the NNM produced fairly consistent results to the data. However, in general, it was found that the waves and water levels were biased low compared to the data. Further analysis showed that NNM results were not spatially coherent to the Lake Michigan domain, especially for north/south wind events. The isotacs did not follow the outline of Lake Michigan as one would expect. This characteristic was compensated for a better representation of local effects found in the point-source meteorological measurements applied in the method. The wind and pressure estimates derived from NNM followed the general trends in the observations, including frontal passages (180-deg wind direction shifts). The modeled wave and water level results also followed the measurements but were generally biased slightly low.

During the forensic study a new long-term re-analysis program was completed by NOAA/NCEP called the Climate Forecast System Re-analysis (CFSR). Embedded in the archive were wind and pressure fields generated on a 0.5- x 0.5-deg spherical, 1-hr intervals. Wind and pressure fields were generated for the seven storm events, derived from archive and interpolated to the WAM (0.02- x 0.02-deg spherical grid) and ADCIRC grids. Tests were run to evaluate NNM and CFSR forcing. It was determined the CFSR wind and pressure fields provided a slightly better estimate in the wave and water level conditions at the respective gage (buoy locations for waves) locations in Lake Michigan. The only drawback in using the CFSR wind and pressure fields was that the archive only spanned the time period from 1979 through 2009. For any storm selected pre-1979, NNM had to be used. From a consistency prospective, this could lead to a discontinuity in the resulting wave and water level estimates for the storm population. However, it was found in the final production runs that the maximum overall wind speed and significant wave heights were statistically uniform for the 50-yr record.

Scales represented in these wind and pressure fields are on the order of 100s of kilometers. Synoptic- and meso-scale events (low pressure centers, frontal passages) are fairly well represented. Small convective cells (thunderstorm events, land-sea breeze) are an order of magnitude smaller and cannot be rectified in the CFSR wind and pressure fields. Time scales (1-hr interval) limit the accuracy in the NNM despite using land-based meteorological information.

From the forensics study it was also determined that a portion of the low biases evident in the ADCIRC water level estimates were attributable to cross lake oscillations caused by a pressure differential between Lake Michigan and Lake Huron. It was determined that adding Lake Huron to the ADCIRC grid domain and coupling the two lakes at the Straits of Mackinac improved the overall estimates.

The last set of input fields required for the extreme storm event simulations is ice concentration fields. Extensive (high concentration levels, thickness and coverage) shore-fast-ice development acts as an impermeable boundary between open water and land. This effectively reduces the wind, wave, and storm surge impacts. However, during the spring thaw conditions change dramatically. The once fully-grounded ice barrier breaks its hold from the lake bottom. If there is an offshore storm, wind-generated surface gravity waves are able to drive the ice field landward with an increasing water level. Rafted ice leads to pressure ridges forming at the coastline. The net effect, provided continued forcing, is that ice is driven onto the land and becomes a flooding issue.

Ice implementation for WAM and ADCIRC differs. ADCIRC applies the ice concentration field information to modify the drag coefficient and roughness lengths for the momentum transfer from the air to the water. When ice concentration levels meet or exceed 50-percent, ADCIRC modifies the drag coefficient. All water points contained in the ADCIRC grid remain open water. WAM applies the ice concentration level fields as a mechanism to mask (zero out) the wave energy field. This method uses an a priori selected concentration level. The selected threshold was 70-percent. Therefore, any water point in the WAM grid with an ice concentration level of 70-percent or greater has all energy set to zero. This threshold was originally derived from work performed in multiple Western Alaska wave hindcasts. Further investigations of the simulations performed in Lake Michigan revealed that the value of 70-percent provided consistent results compared to two wave

measurement sites in southern Lake Michigan deployed during multiple ice years (December through the following May).

Three ice concentration field archives were used for the extreme storm simulations. The period of record for the most available and quality controlled data was from 1973 through 2002. There were temporal and spatial resolution differences between the two primary ice archives used but this did not impact the wave or surge level results. There was no visible discontinuity created in the storm results for 1973 through 2002 (Assel 2003) and those fields downloaded from the National Snow and Ice Center. The pre-1973 time period did become problematic in terms of the number of individual ice fields and the amount of credible estimates in each of those fields. However, for storms occurring from 1960 through 1972 the best estimate of ice was used as input conditions. Unfortunately, no wave or water level data existed prior to 1970 (approximately 26 storm simulations) so a proper evaluation of the model's performance cannot be determined.

At the conclusion of the forensics study (seven storm events), it was determined that CFSR wind and pressure fields would be applied as forcing for Lake Michigan storm simulations. Storm events prior to 1979 used the NNM. In addition, it was also determined that sea-level pressure fields must be defined for the domain containing both Lake Michigan and Lake Huron. Although the seven storm selected were for open-water conditions (non shore-fast ice field situations), the methodology for ice implementation was used and not called. During the post-processing of the storm simulations, the ice implementation for WAM was compared (graphical) to available archived graphical information for quality assurance. WAM Cycle 4.5.1C is used for all Lake Michigan wave simulations, and ADCIRC for the storm surge estimates. Output locations were defined for each model and set just offshore of land. In addition to WAM's special output locations, a series of boundary condition locations were selected to force the STWAVE simulations in the southern portion of Lake Michigan and Green Bay.

The model results of the selected storm simulations replicated the measurements well. WAM replicated the trends at multiple sites for a series of frontal passages, demonstrated rapid wind-wave growth, hitting the storm peak conditions, and decay cycle of all storms. If there is a deficiency in the WAM results, it is capturing local events near the coast (e.g. 45010, Milwaukee and 45011 South Haven) where the statistics and errors increase (-0.38-m at 45010 versus -0.10 for the offshore buoy locations). In general,

the statistics (bias, RMSE, Scatter Index, correlation) are very good in wave height and wave period estimates. There was a persistent bias in the mean wave period results that was investigated. It was determined from that investigation that the source of error was based on differences in the frequency range between the data and the model. Peak-to-peak analyses also conveyed similar results, demonstrating WAM's ability to capture the storm peaks. The CFSR forced WAM simulations did slightly better compared to the NNM.

The ADCIRC results showed a similar consistency in estimating water levels at the ten measurement sites along the Lake Michigan coast. Including Lake Huron in the model domain decreased the persistent negative biases found in the time series. There were times when ADCIRC over and under-estimated the storm peak water level event at some of the gage sites. These differences were not persistent at one site for all storm events suggesting ADCIRC and its attributes (e.g. grid resolution, bottom friction, ice field implementation) were not a specific cause. The differences were primarily a result of a deficiency in the local wind specification being too high, too low, or a slight error in the wind direction (specific to Green Bay). Overall, the quality of the ADCIRC results is considered good.

One hundred fifty extreme storm events were simulated for the Lake Michigan domain. Wind and pressure fields were developed using two different technologies. For the period from 1960 to 1979 the NNM using point-source meteorological station information constructed gridded wind and pressure fields covering the Lake Michigan and Lake Huron¹ domains. This method has been successfully used by the NOAA/GLERL in their daily wave, and circulation forecasts. From 1979 through 2009 the winds and pressure fields used the archived estimates from the NOAA/NCEP-Climate Forecast System Re-analysis (CFSR). The original wind and pressure fields were developed on a 0.5-deg spherical grid, at 1-hr intervals. These fields were subsequently interpolated on a 0.02-deg grid covering the entire Great Lakes domain.

Ice fields were used in certain storm simulations (generally storms falling in the months between December through May of the subsequent year).

¹ Sea level pressure fields were required covering the Lake Huron domain to capture the inverted barometer, and pressure differential between the two water bodies that added to the total storm surge estimates at coastal sites, (See Chapter 4 for details)..

The ice concentration level fields were derived from three data sources for the periods of:

- 1960 through 1972 (National Snow and Ice Data Center)
- 1973 through 2002 (NOAA Great Lakes Ice Atlas, Assel (2003))
- 2003 through 2009 (US Navy, NOAA and US Coast Guard: National Ice Center).

The ice fields were of different grid resolutions, and time intervals. The ice concentration estimates were spatially interpolated to the WAM grid (0.02-deg resolution), and if possible to daily ice fields. A 70-percent ice concentration threshold was used to mask all water points in the WAM domain from water to land. Additional analyses verified the 70-percent threshold based on two nearshore gage sites that were deployed over the winter months for nearly three to five years.

WAM Cycle4.5.1C was used to estimate wave conditions in Lake Michigan. The model was forced by either the NNM or CFSR wind fields, and when appropriate ice concentration fields. A constant 12-day simulation was used for all storm simulations covering nine-days prior to the storm peak conditions, and three-days after the storm peak. Output from each run consisted of integral wind and wave parameters, two-dimensional wave spectral estimates both at 649 special output locations, as well as field files containing various wave parameters defined at every grid point, on a half-hour interval. Boundary condition information (two-dimensional spectral estimates) were built for every storm simulation and used as input to STWAVE simulations for three local domains.

The results of the 150-storm simulations were summarized. The model results were analyzed based on field estimates of the mean and maximum wave parameter estimates. It was determined there was only a slight discontinuity between the wave results forced by the NNM compared to the CFSR wind fields. However, the location of the maximum wind and wave estimates derived from the two wind field forcing differed. The CFSR generally placed the wind and wave maxima along the long, north-south central axis of Lake Michigan. The NNM wind maxima were located generally at the land-based point source meteorological stations used, while the significant wave height maxima were spread along the western and eastern coasts. The central portion of Lake Michigan (from Milwaukee, WI to Ludington, MI) was generally devoid of wave height maximum

conditions. This could have been due to a limited number of easterly and westerly events, or NNM could not synthesize the north-south spatial coherency found in the CFSR winds.

Whenever possible the model estimates were evaluated at five point-source wave measurement sites in Lake Michigan. Time, scatter and Q-Q plots were generated, and a battery of statistical tests run to assure the wave estimates were of high quality. Modeled wind and wave parameters followed the measurement trends, for rapid growth, estimating the storm peak conditions, and decay cycles of the rapidly moving meteorological events. In general the modeled wind speeds were positively biased, and the significant wave height, parabolic fit peak, and mean wave periods were biased slightly low. The mean error in the winds and wave estimates were below 10-percent, and generally fell near 5-percent. For the maximum (i.e. 99.9th Percentile) the errors in significant wave heights were on the order of 0.5-m. The peak-to-peak analysis results emulated all other results, but appeared to be relatively un-biased over the top events where measurements were available.

The hydrodynamic model ADCIRC was applied in this study to estimate water levels throughout Lake Michigan and Green Bay for the set of 150 extreme storm events. The model was forced by either NNM or CFSR wind and pressure fields and, when appropriate, ice concentration fields. As with WAM, a constant 12-day simulation was used for all storm simulations covering nine-days prior to the storm peak conditions, the peak day, and two days after the storm peak. Output from each run consisted of time-series of water levels, water velocities, wind velocities, pressures, and ice concentrations at the 916 special output locations, as well as field files containing these same parameters at every computation grid node on a half-hour interval. ADCIRC water level, wind, and ice information from each storm was applied as input to each STWAVE simulation for the three STWAVE domains.

The ADCIRC model results were analyzed and compared to field measurements throughout Lake Michigan and Green Bay. Quality assurance and control for all 150 ADCIRC hydrodynamic simulations included an examination of maximum water level envelopes, a comparison of modeled and measured water level time-series at as many as 10 NOAA NOS water level gage locations, and statistical analysis of those time series. The maximum water level envelopes provided an overview of the extreme response of the

entire water body to a storm event. One storm can cause surge build-up in one portion of the domain or several locations throughout the domain. This “first-look” gives a synopsis of why and where a given event was considered significant.

At the next level of model evaluation, simulated time series are compared to measurements at diverse locations throughout the model domain. These locations are spatially varied, have different degrees of marine exposure, and diverse geographical constraints. ADCIRC’s ability to represent the model domain and its diversity was the first step in being able to capture response to storms. For all locations in the lake, whether near the storm center or at a distance from the storm center, the model was able to capture the trend in surge response magnitude and duration. The ability to simulate the significant range of responses from one end of the domain to the other, displays the skill of ADCIRC in simulating the storm surge hydrodynamics in Lake Michigan. Small scale oscillations that are finer than the temporal and spatial scales of the forcing conditions were not captured in the simulated responses.

A numerical evaluation of ADCIRC model skill in simulating water levels for storm events in Lake Michigan was performed by computing the Bias and RMSE for simulated time series compared to measured water level time series at the same 10 NOAA NOS gage sites. In general, the statistical bias results show that the simulated water levels compare well with measured water levels. An examination of all 1053 comparisons shows that 89 percent of the Bias values are within +/- 0.05 m. Most (7 of the 10) gages are generally within +/- 0.05 m and have a bias of no more than 0.12 m and two gages (Mackinaw City and Port Inland) are biased slightly high. Green Bay shows both the lowest and nearly the highest bias values when comparing modeled and measured water levels. An examination of the time series comparison for the low bias at Green Bay shows that the model is not simulating the trend measured at the NOAA station well for this storm. This is possibly due to the quality of the wind forcing or that the model did not include the contribution of waves in the ADCIRC simulations. An examination of all 1053 comparisons shows that 90 percent of the RMSE values are within 0.10 m.

Overall, the model performs well in simulating water levels over the large spatial extent of Lake Michigan and Green Bay for a large number of storms of varying intensity, size, and location. The model’s ability to predict water level at many locations under various conditions provides a

strong degree of confidence in the model to predict water levels at other locations around Lake Michigan as well.

The nearshore wave climate of Lake Michigan was modeled using full-plane STWAVE. Three 200-m resolution grids were interpolated from the ADCIRC mesh to UTM NAD 83 Zone 16. Offshore wave spectra from WAM served as the boundary conditions while water levels and ice coverage were obtained from ADCIRC via one-way coupling with CSTORM-MS. Ice was implemented into STWAVE where water cells exceeding 70 percent ice coverage were changed to land, consistent with WAM. STWAVE was run at 30-minute time-steps for six days (three days prior to the peak, the peak day, and two days following the peak). Output from each storm was generated each STWAVE timestep (half-hour intervals) and included wave parameters at 644 total save locations, two-dimensional wave spectra at the same special save locations, and field files specifying the wave parameters at every cell.

Quality assurance and control for all 150-simulations included plotting the maximum wave height field and reviewing final iteration criteria for solution convergence. The un-converged time-steps comprised a very small percent (less than one percent) of the total time-steps considering all 150 storms. Discontinuity along grid partitions, particular in the Kenosha domain, resulted in apparitions of blocks in the wave height solution. However, this artifact did not affect the integrity of the solution as these apparitions typically occur in deep water and the difference between partitions is on the order of centimeters.

Model estimates of wave height were compared to measurements at Chicago and Burns Harbor for 36 storms from 1987-2003. Measured and modeled wave heights were separated based on station and then concatenated to generate larger datasets. Visual assessments included time, contour, scatter, Quartile-Quartile, and peak-to-peak analyses. STWAVE captured the storm cycles reasonable well, following the development, the peak, and the decay of the storm events. In general, STWAVE tended to overestimate the low wave climate and slightly underestimate the 1- to 2-m wave climate at both sites, as was seen in the Q-Q plot. The most extreme events (i.e., 99.9th percentile) were modestly underestimated at Burns Harbor and overestimated at Chicago Harbor, and the maximum error in significant wave height was about 0.5-m, similar to that of WAM. The mean error in the wave estimates was six percent and three percent and Burns and Chicago Harbor, respectively.

References

Assel, R.A. (1983). "GLERL Great Lakes ice concentration data base, 1960-1979". Boulder, Colorado USA: National Snow and Ice Data Center.

Assel, R. A. (2005). "Great Lakes weekly ice cover statistics." NOAA Technical Memorandum GLERL-133. NOAA, Great Lakes Environmental Research Laboratory, Ann Arbor, MI, 27 pp.

Assel, R.A. (2003). "NOAA Atlas. An Electronic Atlas of Great Lakes Ice Cover, Winters: 1973-2002." NOAA, Great Lakes Environmental Research Laboratory, Ann Arbor, MI. (<http://www.glerl.noaa.gov/data/ice/atlas/>)

As-Salek, J.A. and D.J. Schwab. 2004. High-frequency water level fluctuations in Lake Michigan. *J. Waterway, Port, Coastal and Ocean Engineering*, pp. 45-53.

Baird and Associates, (2003)."International Joint Commission and USACE: Lake Ontario WAVAD hindcast for IJC study," Submitted to USACE, Buffalo District.

Banke, E. G. and S.D. Smith. 1973. Wind stress on Arctic Sea ice. *JGR*. Vol. 78, pp. 7871-7883.

Barnes, S.L., (1964). "A technique for maximizing details in numerical weather map analysis," *J. Appl. Metror.* **3**, 394-409.

Barnes, S.L. (1973). "Mesoscale objective analysis using weighted time-series observations," NOAA Tech. Memo. ERL NSSL-62, National Severe Storms Laboratory, Norman, OK., 60pp.

Belesky, D. and D. J. Schwab, (2001). "Modeling circulation and thermal structure in Lake Michigan: annual cycle and inter-annual variability." *Journal of Geophysical Research* 106(C9):19745-19771.

Beletsky, D., D. J. Schwab, R. P. Roebber, M. J. McCormick, G. S. Miller and J. H. Saylor, (2003). "Modeling wind-driven circulation during the March 1998 sediment resuspension event in Lake Michigan," *Journal of Geophysical Research* 108(C2):3038.

Braun, J., and Sambridge, M. S., (1995). "A numerical method for solving partial differential equations on highly irregular evolving grids," *Nature*, 376, 655-660.

Birnbaum, G. and Lupkes, C. (2002). "A new parameterization of surface drag in the marginal sea ice zone," *Tellus*, Vol. 54 A, pp. 107-123.

Bunya, S., J.C. Dietrich, J.J. Westerink, B.A. Ebersole, J.M. Smith, J.H. Atkinson, R. Jensen, D.T. Resio, R.A. Luettich, C. Dawson, V.J. Cardone, A.T. Cox, M.D. Powell, H.J. Westerink, and H.J. Roberts. (2010). "A high resolution coupled riverine flow, tide, wind, wind wave and storm surge model for southern Louisiana and Mississippi: Part I - model development and validation," *Monthly Weather Review*, Vol. 138, Issur 2, pp. 345-377.

Chapman, R. S., Mark, D. and A. Cialone (2005). "Regional tide and storm-induced water level prediction study for the West Coast Alaska." Draft Report to POA, U.S. Army Engineer Waterways Experiment Station, Vicksburg, MS.

Chapman, R. S., Kim, S-C and D. J. Mark (2009). "Storm-induced water level prediction study for the Western Coast of Alaska." Draft Report to POA, U.S. Army Engineer Waterways Experiment Station, Vicksburg, MS.

Danard, M. B., Rasmussen, M. C., Murty, T. S., Henry, R. F., Kowalik, Z., and Venkatesh, S.: 1989, Inclusion of ice cover in a storm surge model for the Beaufort Sea, *Natural Hazards* **2**, 153–171.

Driver, D. B., R.D. Reinhard, and J.M. Hubertz, (1991). "Hindcast wave information for the Great Lakes-Lake Erie," WIS Report 22, US Army Engineer Waterways Experiment Station, Vicksburg, MS.

Driver, D.B, R.D. Reinhard, and J.M. Hubertz (1992). "Hindcast wave information for the Great Lakes-Lake Superior," WIS Report 23, US Army Engineer Waterways Experiment Station, Vicksburg, MS.

Garratt, J.R., (1977). "Review of drag coefficients over oceans and continents," *Monthly Weather Review* **105**, 915-929.

Garbrecht, T., Lupkes, C., Hartmann, J. and Wolff, M. (2002), "Atmospheric drag coefficients over sea ice—validation of a parameterization concept," *Tellus*, Vol. 54 A, pp. 205-219.

Hasselmann, K., T.P. Barnett, E. Bouws, H. Carlson, D.E. Cartwright, K. Enke, J.A. Ewing, H. Gienapp, D.E. Hasselmann, P. Kruseman, A. Meerburg, P. Muller, D.J. Olbers, K. Richter, W. Sell, and H. Walden. 1973. Measurement of wind-wave growth and swell decay during the Joint North Sea Wave Project (JONSWAP). *Deutsches Hydrographisches Institut* Suppl. A, 8 (12), 1-95.

Henry, R.F. and N.S. Heaps. 1976. Storm surge in the southern Beaufort Sea. *H.J. Fish. Res. Board Canada*, Vol. 33, No. 10, pp. 2362-2376.

Herterich, K. and K. Hasselmann, (1980). A similarity relation for the nonlinear energy transfer in a finite depth gravity-wave spectrum. *J.Fluid Mech.*, **97**, 215-224.

Holthuijsen, L.H. 2007. *Waves in ocean and coastal waters*. Cambridge: Cambridge University Press.

Hubertz, J.M., D.B. Driver and R.D. Reinhard, (1991). "Hindcast wave information for the Great Lakes-Lake Michigan," WIS Report 24, US Army Engineer Waterways Experiment Station, Vicksburg, MS.

Jensen, R., N. Schneffer, S.J. Smith, D. Webb, and B. Ebersole. (2002). "Engineering studies in support of Delong Mountain Terminal Project," ERDC/CHL TR-02-26, US Army Engineer Research and Development Center, Vicksburg, MS.

Jensen, R.E. (2009). "A 20-year wind and wave hindcast for the western Alaska coast," In Preparation, US Army Engineer Research and Development Center, Vicksburg, MS.

Jensen, R.E., V.J. Cardone, and A.T. Cox, (2006). "Performance of third generation wave models in extreme hurricanes," 9th International Wave Hindcast and Forecast Workshop, September 25-29, Victoria, B.C.

Jonsson, I.G. 1990. *The sea*. Wave-current interactions. Chapter 3, Vol. 9, Part A, B. New York: John Wiley & Sons, Inc.

Kalnay, E., M. Kanamitsu, R. Kistler, W. Collins, D. Deaven, L. Gandin, M. Iredell, S. Saha, G. White, J. Woollen, Y. Zhu, M. Chelliah, W. Ebisuzaki, W. Higgins, J. Janowiak, K. C. Mo, C. Ropelewski, J. Wang, A. Leetmaa, R. Reynolds, R. Jenne, and D. Joseph, (1996). "The NCEP/NCAR 40-Year Reanalysis Project," *Bulletin of the American Meteorological Society* **77** (3): 437-471.

Kelley, J.G.W., P. Chu, A.-J. Zhang, G.A. Lang, and D.J. Schwab, (2007). "Skill assessment of NOS Lake Michigan Operational Forecast System (LMOFS)," NOAA Technical Memorandum NOS CS 8. NOAA, Office of Coast Survey, Coast Survey Development Laboratory, Silver Spring, MD, 67 pp.

Komen, G.J., L. Cavaleri, M. Donelan, K. Hasselmann, S. Hasselmann, and P.A.E.M. Janssen, (1994). "Dynamics and modeling of ocean waves," Cambridge University Press.

Kowalik, Z. (1984). "Storm surges in the Beaufort and Chukchi Seas," JGR, Vol. 89, No. C6, pp. 10,570-10578.

Lasserre, J. B., (1983). "An analytical expression and an Algorithm for the Volume of a Convex Polyhedron in Rⁿ," JOTA, vol. 39, No. 3, 363-377.

Lin, L. and D.T. Resio, (2000). "Improving wind input information for Great Lakes wave hindcast study," 6th International Workshop on Wave Hindcasting and Forecasting, Monterey, Calif. 29-43.

Lombardy, K., (2002). Great lakes storm November 9-11 1998: Edmund Fitzgerald remembered, *Mariners Weather Log*, Spring-Summer, 1-7.

Luettich, R.A., Jr., Westerink, J.J., and Scheffner, N.W., (1992). "ADCRIC: An Advanced Three-Dimensional Circulation Model for Shelves, Coasts, and Estuaries," Technical Report DRP-92-6, U.S. Army Engineer Waterways Experiment Station, Vicksburg, MS.

Lui, P.C., D.J. Schwab, and R.E. Jensen. 2002. Has wind-wave modeling reached its limit? *Ocean Engineering*, **29**. 81-98.

Macklin, S.A. 1983. Wind drag coefficients over first year ice in the Bearing Sea. *J. Geophys. Res.* 88, 2845-2852.

Massey, T.C., M.E. Anderson, J.M Smith, J. Gomez, and R. Jones. 2011. *STWAVE: Steady-state spectral wave model user's manual for STWAVE, version 6.0*. ERDC/CHL SR-11-1. Vicksburg, MS: U.S. Army Engineer Research and Development Center.

Mei, C.C. 1989. *The applied dynamics of ocean surface waves*. Singapore: World Scientific Publishing.

Melby , J. A., Nadal-Caraballo, N. C., and Ebersole, B. A. et al. (2012), "Lake Michigan: Analysis of Waves and Water Levels," U.S. Army Corps of Engineers, TR-XX-12

Miche, M. 1951. Le pouvoir reflechissant des ouvrages maritimes exposes a l'action de la houle. *Annals des Ponts et Chaussees* 121e Annee, 285-319 (translated by Lincoln and Chevron, University of California, Berkeley, Wave Research Laboratory, Series 3, Issue 363, June 1954).

Nadal-Caraballo, N. C., Melby, J. A., and Ebersole, B. A., (2012), "Lake Michigan: Storm Sampling and Statistical Analysis Approach,: U.S. Army Corps of Engineers, TR-XX-12

Padilla-Hernandez, R. and J. Monbaliu. 2001. Energy balance of wind-waves as a function of the bottom friction formulation. *Coastal Engineering* 43, 131-148.

Pease, C.H., S.A. Maccklin and S.A. Salo. 1981. Drag measurements for first-year sea ice over a shallow sea. *EOS. Transactions of the American Geophysical Union* 62, 895.

Pierson, W.J., and L. Moskowitz, (1964). "A proposed spectral form for fully developed wind seas based on the similarity theory of S. A. Kitaigorodskii," *J. Geophys. Res.* **69**, 5181.

Reinhard, R.A., D.B. Driver and J.M. Hubertz, (1991). "Hindcast wave information for the Great Lakes-Lake Ontario," WIS Report 25, US Army Engineer Waterways Experiment Station, Vicksburg, MS.

Reinhard, R.A. , D.B. Driver and J.M. Hubertz, (1991a). "Hindcast wave information for the Great Lakes-Lake Huron," WIS Report 26 US Army Engineer Waterways Experiment Station, Vicksburg, MS.

Resio, D.T. and C.L. Vincent, (1976). "Estimation of Winds Over the Great Lakes," Technical Report H-76-12, US Army Engineer Waterways Experiment Station, Vicksburg, MS.

Resio, D.T. and C.L. Vincent, (1976a). "Design Wave Information for the Great Lakes; Report 3, Lake Michigan," Technical Report H-76-1, US Army Engineer Waterways Experiment Station, Vicksburg, MS.

Resio, D.T., (1981) "The estimation of wind-wave generation in a discrete spectral model," *J. Phys. Oceanogr.* 11, 510-525.

Resio, D.T. 1987. Shallow-water waves. I: Theory. *Journal of Waterway, Port, Coastal, and Ocean Engineering* 113 (3), 264-281.

Resio, D.T. 1988. Shallow-water waves. II: Data comparisons. *Journal of Waterway, Port, Coastal, and Ocean Engineering* 114 (1), 50-65.

Resio, D.T. and W. Perrie. 1989. Implications of an f^{-4} equilibrium range for wind-generated waves. *Journal of Physical Oceanography* 19, 193-204.

Ris, R.C., (1997). "Spectral modelling of wind waves in coastal areas," Ph.D. Dissertation Delft University of Technology, Department of Civil Engineering, Communications on Hydraulic and Geotechnical Engineering, Report No. 97-4, Delft, The Netherlands.

Saha, S., S. Moorthi, Hua-Lu Pan, X. Wu, J. Wang, S. Nadiga, P. Tripp, R. Kistler, J. Woollen, D. Behringer, H. Liu, D. Stokes, R. Grumbine, G. Gayno, J. Wang, Y. Hou, H. Chuang, H. Juang, J. Sela, Mark Iredell, Russ Treadon, Daryl Kleist, P. Delst, D. Keyser, J. Derber, M. Ek, J. Meng, H. Wei, R. Yang, S. Lord, H. Dool, A. Kumar, W. Wang, C. Long, M. Chelliah, Y. Xue, B. Huang, J. Schemm, W. Ebisuzaki, R. Lin, P. Xie, M. Chen, S. Zhou, W. Higgins, C. Zou, Q. Liu, Y. Chen, Y. Han, L. Cucurull, R. Reynolds, G. Rutledge, and M. Goldberg, (2010). "The NCEP Climate Forecast System Reanalysis, Submitted to *Bulletin of the American Meteorological Society*.

Schafer, P. J. (1966). "Computation of storm surge at Barrow, Alaska," Archiv. Meteorol., Geophys. Bioklimatol. Vol. A, No. 15(3-4), pp 372-393.

Schertzer, W. M., R. A. Assel, D. Beletsky, T. E. Croley II, B. M. Lofgren, J. H. Saylor and D. J. Schwab (2008). "Lake Huron climatology, inter-lake exchange and mean circulation". Aquatic Ecosystem Health & Management, Vol. 11, No. 2, pp 144 - 152.

Schwab, D.J. (1989). "The use of analyzed wind fields from the Great Lakes Marine Observation Network in wave and storm surge forecast models," 2nd International Workshop on Wave Hindcasting and Forecasting, Vancouver, BC, April 25-29, 257-266.

Schwab, D.J. (1978). "Simulation and forecasting of Lake Erie storm surges," *Monthly Weather Review* 106(10):1476-1487.

Schwab, D.J., G.A. Meadows, J.R. Bennett, H. Schultz, P.C. Liu, J.E. Cambell, and H.H. Dannelongue, (1984). "The response of the coastal boundary layer to wind and waves: Analysis of an experiment in Lake Erie," *Journal of Geophysical Research* 89:8043-8053.

Schwab, D. J. and D. Beletsky, (1998). "Lake Michigan Mass Balance Study: Hydrodynamic modeling project." NOAA Technical Memorandum ERL GLERL-108, Great Lakes Environmental Research Laboratory, Ann Arbor, MI, 53pp.

Smith, J.M., A.R. Sherlock, and D.T. Resio. 2001. *STWAVE: Steady-state spectral wave model user's manual for STWAVE, version 3.0*. ERDC/CHL SR-01-1. Vicksburg: MS: U.S. Army Engineer Research and Development Center.

Smith, J.M. 2007. *Full-plane STWAVE with bottom friction: II. Model overview*. ERDC/CHL CHETN-I-75. Vicksburg, MS: U.S. Army Engineer Research and Development Center.

Tolman, H. L., and D. V. Chalikov, (1994). "Development of a third-generation ocean wave model at NOAA-NMC," Proc. Waves - Physical and numerical modelling , M. Isaacson and M.C. Quick Eds., Vancouver, 724-733.

Tolman, H.L. (2002) "Limiters in third-generation wind wave models," *Global Atmos. and Ocean. System*, **8**, 67-83.

REPORT DOCUMENTATION PAGE

*Form Approved
OMB No. 0704-0188*

Public reporting burden for this collection of information is estimated to average 1 hour per response, including the time for reviewing instructions, searching existing data sources, gathering and maintaining the data needed, and completing and reviewing this collection of information. Send comments regarding this burden estimate or any other aspect of this collection of information, including suggestions for reducing this burden to Department of Defense, Washington Headquarters Services, Directorate for Information Operations and Reports (0704-0188), 1215 Jefferson Davis Highway, Suite 1204, Arlington, VA 22202-4302. Respondents should be aware that notwithstanding any other provision of law, no person shall be subject to any penalty for failing to comply with a collection of information if it does not display a currently valid OMB control number. **PLEASE DO NOT RETURN YOUR FORM TO THE ABOVE ADDRESS.**

1. REPORT DATE (DD-MM-YYYY) November 2012		2. REPORT TYPE Final		3. DATES COVERED (From - To)	
4. TITLE AND SUBTITLE Modeling of Lake Michigan Storm Waves and Water Levels				5a. CONTRACT NUMBER	
				5b. GRANT NUMBER	
				5c. PROGRAM ELEMENT NUMBER	
6. AUTHOR(S) Robert E. Jensen, Mary A. Cialone, Raymond S. Chapman, Bruce A. Ebersole, Mary Anderson, and Leonette Thomas				5d. PROJECT NUMBER	
				5e. TASK NUMBER	
				5f. WORK UNIT NUMBER	
7. PERFORMING ORGANIZATION NAME(S) AND ADDRESS(ES) Coastal and Hydraulics Laboratory U.S. Army Engineer Research and Development Center 3909 Halls Ferry Road Vicksburg, MS 39180-6199				8. PERFORMING ORGANIZATION REPORT NUMBER ERDC/CHL TR-12-26	
9. SPONSORING / MONITORING AGENCY NAME(S) AND ADDRESS(ES) U.S. Army Engineer District, Detroit ATTN: CELRE-HH-E 477 Michigan Ave. Detroit, MI				10. SPONSOR/MONITOR'S ACRONYM(S)	
				11. SPONSOR/MONITOR'S REPORT NUMBER(S)	
12. DISTRIBUTION / AVAILABILITY STATEMENT Approved for public release; distribution is unlimited.					
13. SUPPLEMENTARY NOTES					
14. ABSTRACT This report documents the methodologies used, procedures followed to generate wind, wave, and storm surge estimates for 150 pre-selected extreme storm events along the Lake Michigan coastline. These simulations provide a storm climatology spanning 60-years (1960 through 2009). Two methodologies are used to generate the wind and pressure fields for the Lake Michigan region. The NOAA/NCEP Climate Forecast System Reanalysis, a 30-year (1979 through 2009) archive data set providing gridded wind speed, direction and sea level surface pressure fields. The second being the Natural Neighbor Method developing necessary fields from point source meteorological stations on a fixed grid system (1960 though 1978). Archived ice concentration fields were applied to the extreme storm events occurring during the winter months. The WAM model and STWAVE are used to describe the wave climate; ADCIRC is used to estimate the surge. The models are rigorously evaluated for a pre-selected storm population, using both wind field methodologies and compared to existing data sources (winds, waves and water levels). Upon completion of this evaluation phase, the 150-extreme storm events are simulated and evaluated at gage sites, for the entire coastline of Lake Michigan.					
15. SUBJECT TERMS Evaluation Extremes		Hindcast Ice Modeling		Surge Waves Wind	
16. SECURITY CLASSIFICATION OF:			17. LIMITATION OF ABSTRACT Unclassified	18. NUMBER OF PAGES 330	19a. NAME OF RESPONSIBLE PERSON: Ty V. Wamsley
a. REPORT Unclassified	b. ABSTRACT Unclassified	c. THIS PAGE Unclassified			19b. TELEPHONE NUMBER (include area code) (601) 634-2099